Characterisation of the Formin Protein FHOD1 in Striated Muscle

Dwyer, Joseph

Awarding institution:
King's College London

Characterisation of the Formin Protein FHOD1 in Striated Muscle

Joseph Dwyer

Thesis submitted to King's College London for the degree of Doctor of Philosophy

June 2015

“I never practice; I always play.” ~ Wanda Landowska

"The saddest aspect of life right now is that science gathers knowledge faster than society gathers wisdom." ~ Isaac Asimov

“One becomes firmly established in practice only after attending to it for a long time, without interruption and with an attitude of devotion.” ~ Yoga Sutra I.14

This thesis is dedicated to my parents:

Dr. John P. Dwyer and Mrs. Angela Micioni Dwyer

Their love and support have helped guide me through my studies and I will always be grateful to them.

Acknowledgements

I would like to thank the following people for their help and support. My first supervisor Dr. Elisabeth Ehler for her help and support throughout my research studies. Her enthusiasm and kindness have provided me much of the motivation and inspiration for my work. My second supervisor Prof. Anne Ridley for her helpful discussions and for the donation of expression constructs. Dr. Thomas Iskratsch for the donation of expression constructs and general support. Without his help in learning the relevant molecular biology techniques this project would not have been possible. Dr. Sue Perera for her invaluable help in learning GST pull-down assays, for general lab support, and for her friendship. Dr. Atsushi Fukuzawa for his support in the lab with the yeast two-hybrid technique. Dr. Ay Lin Kho for her assistance in the neonatal rat cardiomyocyte preps. I would like to extend a very warm thanks to Ms. Birgit Brandmeier for her general lab support and for her friendship. The current and previous members of Dr. Elisabeth Ehler's group for help and support in the lab: Dr. Thomas Randall, Dr. Sagair Hussain, Ms. Marlene Plüß, Ms. Nadine Gose, and Ms. Nadine Lohmann. The current and previous members of Prof. Mathias Gautel's group for their help and support in the lab: Prof. Mathias Gautel, Dr. Alexander Alexandrovich, Dr. Martin Rees, Mr. Christopher Jenkins, Dr. Mark Holt, Mr. Andrea Ghisleni, Dr. Sarah Waters, and Dr. Elena Rostkova. Dr. Daniel Soong and Dr. Peter Stevenson for their assistance with the confocal microscopes. I would also like to thank Dr. Pauline Bennett and Ms. Amanda Wilson for their helpful discussions regarding the intercalated disk. From the group of Dr. Maddy Parsons I would like to thank Dr. Asier Jayo, for advice on performing F-actin quantification in cells and Ms. Giulia Villari, for many in depth scientific discussions and for her kindness and friendship. The Randall Protein Production Facility for their assistance with cloning: Dr. Paul Brown, Mrs. Renée Tata, Dr. Mitla Garcia-Maya. I would also like to acknowledge the memory of Henrietta Lacks and her contribution to science in the creation of HeLa cells. I would like to thank all of my friends in the Randall Division for their help and support throughout my studies, especially, Ms. Ivanka Sevrieva, Ms. Maira Silva, Dr. Thomas Kampourakis, Dr. Andrea Knowles, Ms. Rumena Begum, Ms. Upamali Perera, Ms. Rachael Inglis, Mr.

Richard Downes, and Ms. Louise Moyle. I would like to give a special thanks to Dr. Sehrish Rafique, Ms. Kaye Batten, and Mrs. Stefanie Hoffart for their love and support. I would also like to thank Ms. Francesca Ludwinski for her friendship and support during all of my scientific studies. I would like to give a very warm thanks to Ms. Marie Lecomte who has provided me with a decade of friendship and the inspiration to study science. Lastly I would like to give the biggest thanks to my family: Dr. John P. Dwyer, Mrs. Angela Micioni Dwyer, Ms. Francesca Dwyer, and Jack Dwyer. I would also like to thank my grandmother Mrs. Thea Stanchieri Micioni and Dusty Dwyer who are sadly no longer with us but will remain in my heart forever. My family are my biggest inspiration and provide me the strength and will to excel in every aspect of life.

Sources of Funding:

Thank you to King's College London and the British Heart Foundation for their funding, help, and support. Thank you to the Randall Division of Cell & Molecular Biophysics and the BHF Centre of Research Excellence for their help and support.

I Abstract

Formin homology 2 domain containing protein 1 (FHOD1) is a diaphanous related formin of the FHOD subclass. In a similar manner to other formins, FHOD1 has primarily been found to regulate the polymerisation of actin-based structures in cells. In muscle, actin is a major constituent of both skeletal and cardiac myocytes, with the thin filament system of sarcomeres and the cytoskeleton being partly composed of actin. FHOD proteins have previously been highlighted as important regulators of muscle cell biology since FHOD3, a close relative of FHOD1 was shown to be essential for myofibrillar maintenance. There is little known about the regulation of actin-based structures in muscle cells. We therefore aimed to characterise FHOD1 and probe into its involvement in myofibrillar and cytoskeletal regulation. In this study of FHOD1 we addressed various aspects of the protein including its expression pattern and localisation, function, regulation, and novel interacting partners. Insight into the expression pattern of FHOD1 was gained by examining relative protein levels in different tissues, including both healthy and diseased heart. Subcellular localisation was addressed in a number of fluorescence microscopy experiments through antibody localisation studies in muscle tissue and cultured cells and through transient transfection of GFP tagged constructs. Expression of GFP tagged fragments and mutants helped to delineate the functional distribution of the FHOD1 molecule in cells. The function of the protein was further probed via molecular knockdown by RNAi and by looking at the capacity of FHOD1 to polymerise actin in cells. The role of formins in the heart was more broadly addressed by drug inhibition of their actin polymerising capacity. Previous studies have suggested that the Rho family of small GTPases as well as the Src kinases regulate FHOD1. Involvement of the GTPases and Src was shown through biochemical experiments. Finally, a number of Yeast2Hybrid assays were performed using different domains of FHOD1 to screen for novel binding partners. Our findings would suggest that FHOD1 is a crucial regulator of the myofibrillar apparatus and the cytoskeleton at the level of actin in striated muscle.

II Table of Contents

III List of Figures

IV List of Tables

V. Abbreviations

(-) end – pointed end

(+) end – barbed end

°C – the degree of Celsius

3AT – 3-amino-1,2,4-triazole

A – Alanine

a.a. – amino acid

ABD – actin binding domain

ADF – actin depolymerising factor

ADP – adenosinediphosphate

AML – acute myeloid leukaemia

ARC – adult rat cardiomyocyte

Arp – actin related protein

ATP – adenosinetriphosphate

A-zone – anisotropic zone

b.p. – base pair

bHLH - basic helix-loop-helix

BPB – bromophenol blue

BSA – bovine serum albumin

BWM – body wall muscles

C - Cysteine

CA – constitutively active

CAA – cardiac muscle actin

CACP - Camptodactyly-arthropathy-coxa-vara-pericarditis

CC – coiled coil

CD – cluster of differentiation

cDNA – complementary DNA

cGMP – cyclic guanosinemonophosphate

CHF - cardiovascular basic helix-loop-helix factor

CK – casein kinase

CMV – cytomegalovirus

C-terminus – carboxy terminus

CYA – cytoplasmic actin

CYK – cytokinesis defect

D – Aspartic Acid

DAAM – dishevelled associated activator of morphogenesis

DAD – diaphanous autoregulatory domain

DAPI - 4',6-diamidino-2-phenylindole

DCM – dilated cardiomyopathy

DD – dimerisation domain

Dia – diaphanous

DID – diaphanous inhibitory domain

DLG – discs large

DMEM – Dulbecco's Modified Eagle's Medium

DMSO - Dimethyl sulfoxide

DN – dominant negative

DNA – deoxyribonucleic acid

dNTP – deoxyribonucleotide triphosphate

DRF – diaphanous related formin

DTT – dithiothreitol

E – Glutamic acid

ECL – enhanced chemilimuinescence

ECM – extracellular matrix

EDTA - ethylenediaminetetraacetic acid

EGTA - ethylene glycol tetraacetic acid

F-actin – filamentous actin

FAK – focal adhesion kinase

FH – formin homology

FHOD – formin homology domain containing protein

FHOS – formin homology overexpressed in the spleen

FIZ - FLT3-interacting zinc finger

FMN – formin

FRL - formin related gene in leukocytes

G – Glycine

G-actin – globular actin

GAP - GTPase activating protein

GBD – GTPase binding domain

GDI - guanine nucleotide-dissociation inhibitors

GDP – guanosinediphosphate

GEF – guanine nucleotide exchange factor

GFP – green fluorescent protein

GMP-PNP - 5'-Guanylyl imidodiphosphate

GST – glutathione S-transferase

GTP – guanosinetriphosphate

H/His – Histidine

HA – haemagglutinin

HCM – hypertrophic cardiomyopathy

HEPES - 4-(2-hydroxyethyl)-1-piperazineethanesulfonic acid

HEY - hairy/enhancer-of-split related with YRPW motif

ICD – intercalated disk

INF- inverted formin

IPTG - isopropyl β-D-1-thiogalactopyranoside

IRAP - insulin-responsive aminopeptidase

I-zone – Isotropic zone

Kb – kilobases

kDa – kilodaltons

KO - knockout

L/Leu – Leucine

LARG – leukaemia associated Rho-GEF

LIMK – LIM kinase

LiOAc - Lithium acetate

MAGUK - membrane associated gyanylate kinases

mDia – mammalian diaphanous

MLL - mixed-lineage leukaemia protein

MLP – muscle lim protein

MLV – mouse leukaemia virus

MRTF – myocardin-related transcription factor

mRNA – messenger RNA

MyBP-C – myosin binding protein C

N – Asparagine

NLS – nuclear localisation signal

NP - nonyl phenoxypolyethoxylethanol

NRAP – nebulin-related anchoring protein

NRC – neonatal rat cardiomyocyte

N-terminus – amino terminus

ORF – open reading frame

P – proline

PAGE – polyacrylamide gel electrophoresis

PAK - p21-activated kinase

PBD – PAK binding domain

PBS – phosphate buffered saline

PCR – polymerase chain reaction

PFA – paraformaldehyde

PK – protein kinase

PKGI - cyclic GMP-dependent protein kinase I

PLZF - promyelocytic leukaemia zinc finger protein

PRKCBP - with protein kinase C binding protein

PVA - polyvinylalcohol

qRT-PCR – quantitative real-time polymerase chain reaction

R - Arginine

RNA – ribonucleic acid

ROCK – Rho associated protein kinase

RT – reverse transcriptase

S/Ser – Serine

SDS – sodium dodecyl sulphate

SFK – Src family kinase

SH – Src homology

shRNA – small hairpin RNA

siRNA – short interfering RNA

SKA – skeletal muscle actin

SMA – smooth muscle actin

SMC – smooth muscle cell

SMIFH2 – small molecule inhibitor of FH2 domain

SOX – SRY-box

SR – super repeat

SRE – serum response element

SRF – serum response factor

SRY - sex determining region Y

SV40 - Simian vacuolating virus 40

T/Thr - Threonine

TA – tibialis anterior

TE – Tris/EDTA

Tn – troponin

UAS - upstream activations sequences

UTR – untranslated region

V – Valine

VSMC – vascular smooth muscle cells

W/Trp – Tryptophan

WASP - Wiskott-Aldrich syndrome protein

WH2 – WASP homology 2 domain

WISH – WASP interacting SH3-domain protein

WISH/DIP1 - WASP-interacting SH3-domain protein/diaphanous-interacting protein 1

WT – wild type

XRCC - X-ray repair complementing defective repair in Chinese hamster cells

ZBTB16 - zinc finger and BTB domain containing 16

Chapter 1

Introduction

1. Introduction

1.1 Muscle

Cellular movement is brought on by the interaction between actin and myosin. Acto-myosin mediated contractions form the basis of many important cellular events, such as cell polarisation and migration (Lammermann and Sixt 2009; Mseka et al. 2009). This interaction is also crucial in mediating muscle contraction. In striated muscle, actin and myosin are arranged in a highly ordered manner as myofibrils (Dwyer et al. 2012). The basic repeating contractile unit of a myofibril is referred to as the sarcomere. A sarcomere is defined as the area between two Z-disks, the lateral borders of a single sarcomere (Figure 1.1). The Z-disks anchor the actin (thin) filaments while the myosin (thick) filaments emanate from the centre of the sarcomere (Huxley 1953; Koubassova and Tsaturyan 2011). Some of the earliest work on muscle used X-ray diffraction studies and electron microscopy to resolve this highly specialised arrangement of thick and thin filaments (Huxley and Perutz 1951; Hanson and Huxley 1953). Muscle was topologically divided into two sections (Figure 1.1). The lighter sections near the Z-disks were referred to as the I (isotropic) zones and were found to contain only thin filaments. A darker region near the centre of the sarcomere was referred to as the A (anisotropic) zone and was found to contain a mixture of both thick and thin filaments. Additionally, another lighter zone was found in the very centre of the sarcomere (the H zone) and was composed only of thick filaments (Huxley and Niedergerke 1954; Huxley and Hanson 1954). Muscle contraction was subsequently found to be mediated by the sliding of thin filaments past the thick filaments, and that this was powered by ATP hydrolysis due to the intrinsic ATPase activity of myosin (Hanson and Huxley 1953). With the advent of more advanced techniques, such as fluorescence microscopy, our understanding of the precise molecular events governing muscle contraction as well as the organisation of muscle has substantially increased.

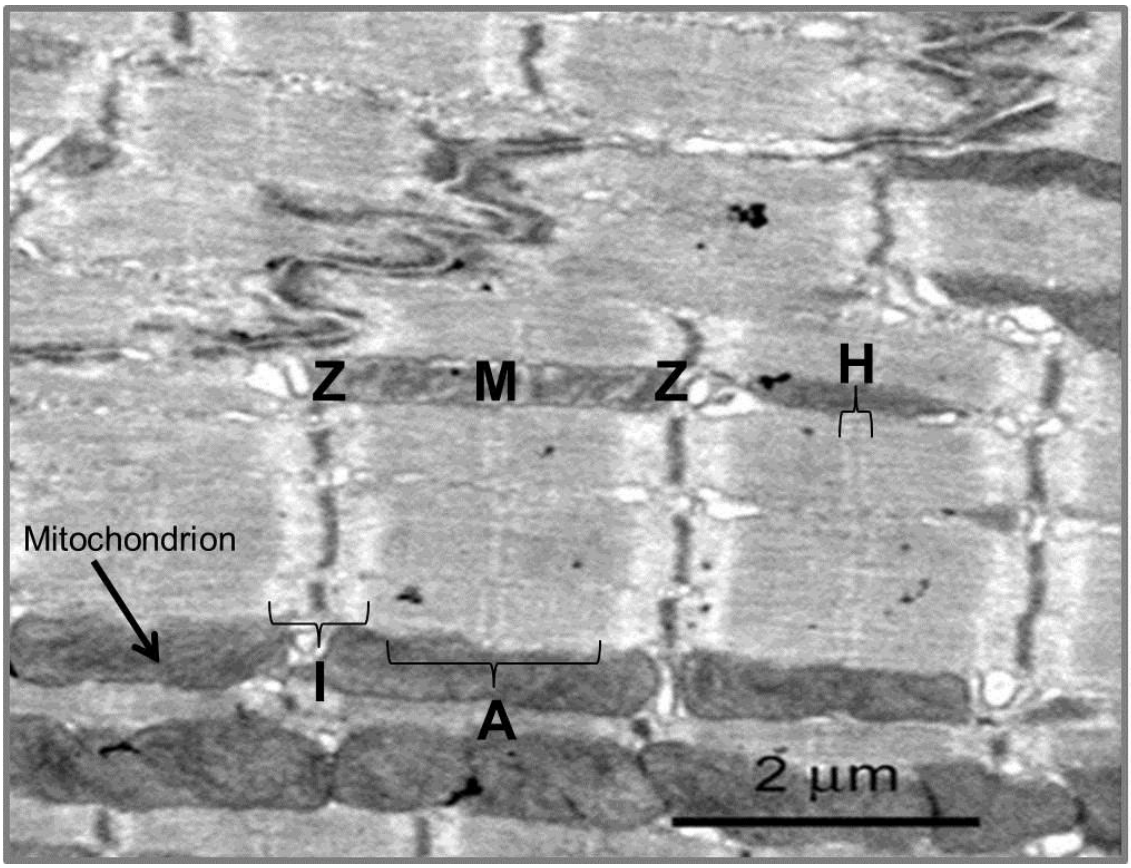

Figure 1.1: Major Regions of Striated Muscle Sarcomeres. Electron micrograph from adult mouse hearts with some of the major sarcomeric demarcations resolved and labelled. The borders of the sarcomere are the Z-disks (Z) whereas the M-band is visualised in the middle (M). The light isotropic (I) zones are visualised on either side of the Z-disks and correspond to the thin (actin) filaments. The darker staining anisotropic (A) zone is visualised either side of the M-band and contains a mixture of thin and thick (myosin) filaments. The H zone (H) is seen proximal to either side of the M-band as a region lighter than the A-zone and contains only thick filaments. Scale bar represent 2µm. Image taken from (Bennett et al. 2006)

1.1.1 Smooth Muscle

Muscle is divided into two major groups: smooth muscle and striated muscle. Smooth muscle cells (SMCs) make up the majority of the vasculature, the gastrointestinal, and the urogenitary tract (Figure 1.2 A). Control of smooth muscle is involuntary and is mediated by the autonomic nervous system and hormonal triggers (Webb 2003). The organisation and regulation of the myofilaments in smooth muscle differs substantially from that seen in striated muscle, although the basic contractile mechanism is conserved in all three muscle types. In smooth muscle, actin filaments are arranged as hexagonal arrays that form cable like bundles, with the myosin filaments interspersed around the actin filaments (Gabella 1984; Gunst and Tang 2000; Webb 2003). This results in an oblique arrangement of filaments that form a lattice like network throughout cells. A third network of intermediate filaments associate with the actin filaments, are involved in regulating cell shape and force transmission (Small and Gimona 1998) and include desmin (Paulin and Li 2004) and vimentin (Frank and Warren 1981). Dense bodies serve to anchor thin filaments in the cytoplasm and are rich in proteins such as α-actinin (Fay et al. 1983), desmin, and vimentin. The actin filaments are anchored at the membrane in regions known as dense plaques. Dense plaques serve as sites of transmission of mechanical force to the extra cellular matrix (ECM) (Figure 1.2 B). Mechanical coupling between neighbouring SMCs occurs through attachment plaques (Gunst and Tang 2000). The basic contractile mechanism in smooth muscle relies on the actin filaments sliding past the myosin filaments. Contraction is mediated by Ca^{2+} specific effects on the myosin filaments which eventually trigger phosphorylation of myosin light chain. The ATPase activity of myosin then results in induction of cross bridge cycling (Webb 2003). Thin filaments are also decorated with caldesmon and tropomyosin, which participate in contractile regulation (Marston and Smith 1985). Thus, smooth muscle differs from striated muscle in its organisation and mode of regulation.

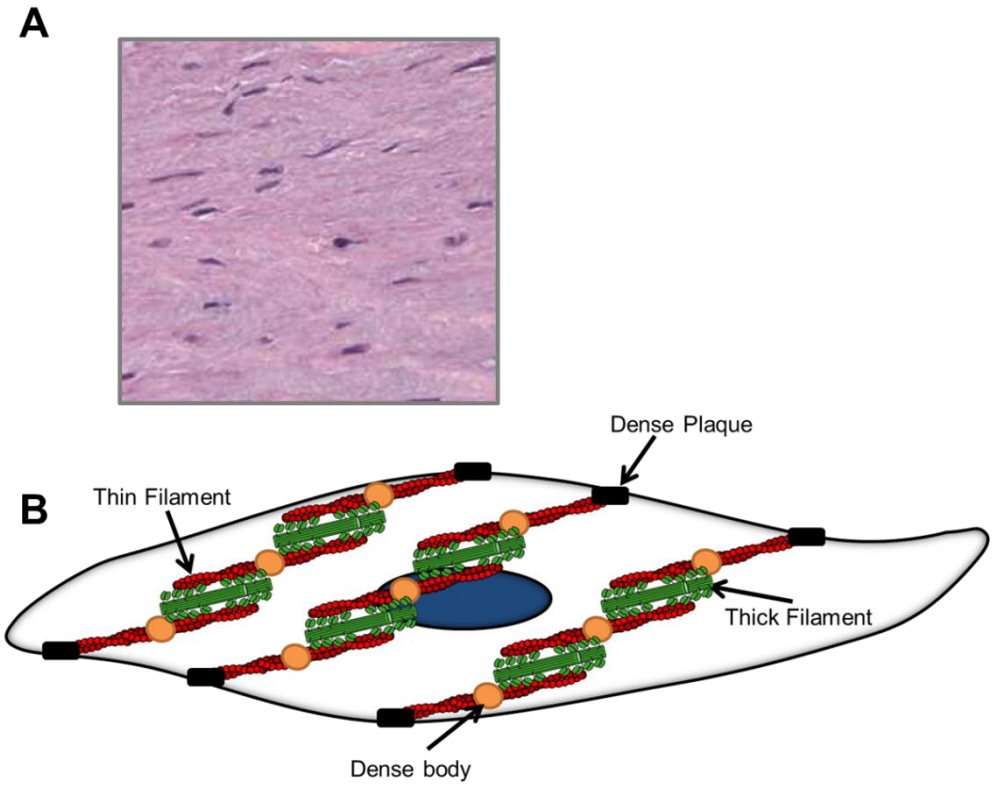

Figure 1.2: Smooth Muscle. A) Human vascular smooth muscle cells found in the arterial wall lining stained with haematoxylin and eosin. Figure taken from (Panchenko et al. 2009). **B)** Schematic of the basic contractile apparatus in a smooth muscle cell. Smooth muscle cells are long and spindle shaped. The thin (actin) filaments are anchored at the membrane by dense plaques. Dense bodies anchor the thin filaments in the cytoplasm. The thin filaments slide past the thick (myosin) filaments to produce contractile force.

1.1.2 Cardiac Muscle

As mentioned above, striated muscle differs greatly from smooth muscle in appearance and regulation. As their name suggests striated muscles are distinguished by their characteristic cross-striated/banded appearance, a feature accounted for by the presence of highly ordered sarcomeres (Figure 1.3). Striated muscle can further be divided into two groups: cardiac muscle and skeletal muscle. The structure of cardiac muscle is described below.

During embryonic development, the heart becomes the first fully functional organ in mammals (Olson and Srivastava 1996). A myogenic organ derived from the embryonic mesoderm, the primary function of the heart is to pump oxygenated blood throughout the body. Cardiac muscle occupies the walls of the heart making up a region known as the myocardium. It is composed of contractile cells, termed cardiomyocytes. Cardiomyocytes exist as branched networks of cells containing one or two centrally located nuclei (Figure 1.3 A-B). The coordinated contraction of the cardiomyocytes enables the heart to pump blood systemically. Innervation of cardiac muscle occurs involuntarily via the autonomic nervous system.

The contractile apparatus of cardiomyocytes is constituted by actin and myosin filaments arranged as myofibrils. The structural integrity of myofibrils is partly determined by an intermediate filament network comprising of desmin, which with the aid of proteins like plectin anchors myofibrils at the membrane in sites called costameres (Severs 2000; Konieczny et al. 2008). Costameres are rib-like structures rich in vinculin and are responsible for mediating force transmission to the ECM via linkages from the Z-disk to the membrane (Samarel 2005). Neighbouring cardiomyocytes are electro-mechanically linked at sites called intercalated disks. Within the intercalated disk, cells are electrically coupled by structures called gap junctions (Rohr 2004). Mechanical linkage is made possible by insertion of terminal thin filaments into the adherens junction portion of the intercalated disks (Dwyer et al. 2012). Cardiomyocytes are also characterised by sarcolemmal membrane invaginations above the Z-disks, called t-tubules (Severs 2000). Like smooth muscle, striated muscle requires the presence of Ca^{2+} to initiate contraction of myofilaments. T-tubules are rich in L-type calcium channels which allow for the entry of Ca^{2+} which further stimulate more release of Ca^{2+} from the sarcoplasmic reticulum (SR). Hence, T-tubules are involved in excitation contraction coupling in cardiomyocytes (Beuckelmann and Wier 1988; Leach et al. 2005; Orchard and Brette 2008). An incredibly complex cell with a number of specialised structures, cardiomyocytes are further stabilised by a vast cytoskeletal network (Hein et al. 2000) involving dystrophin (Klietsch et al. 1993) and integrins connecting the cytoskeleton to the ECM through the membrane, and other intercalated disk proteins like the catenins and cadherins which are involved in coupling neighbouring cells (Koch and Franke 1994).

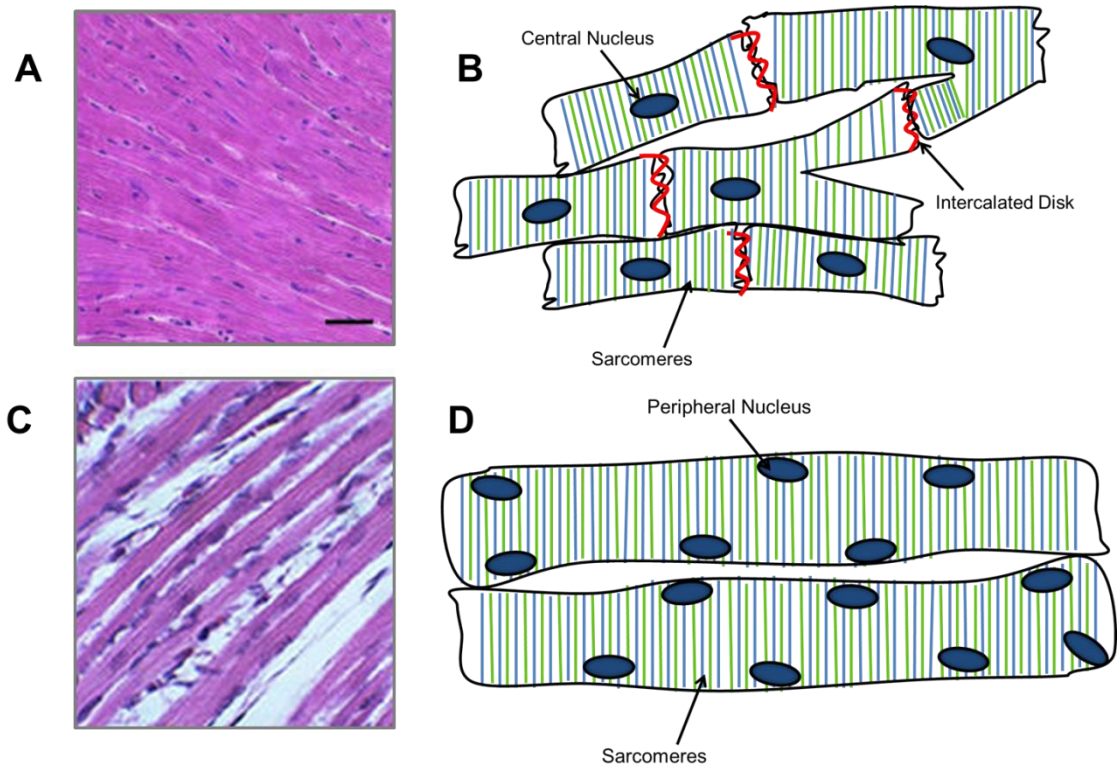

Figure 1.3: Striated Muscle. A) Longitudinal heart sections from wild type mice stained with haematoxylin and eosin. Figure taken from (Moza et al. 2007). **B)** Schematic of the ultrastructure of cardiac muscle. **C)** Longitudinal skeletal muscle sections from wild type mice stained with haematoxylin and eosin. Figure taken from (Ware et al. 2003). **D)** Schematic of the ultrastructure of skeletal muscle.

1.1.3 Skeletal Muscle

Skeletal muscle represents the other type of striated muscle found in vertebrates. It is found throughout the body attached to bones by connective tissue. Skeletal muscle is essential in the way that it allows for the generation of movement. Unlike cardiac and smooth muscle, skeletal muscle is under voluntary control via the peripheral nervous system. Skeletal muscles can be distinguished via a number of classification systems. From the most basic standpoint, skeletal muscles are either classed as fast twitch muscles or slow twitch muscles. Fast twitch muscle are often white and utilise glycolysis for more specialised motor activities. On the other hand, slow twitch muscles are red in colour due to the presence of myoglobin and utilise oxidative enzymes for more sustained motor activity (Schiaffino and Reggiani 2011). Regardless of fibre type, skeletal muscles are composed of myofibres, which are the result of fusion

of many myoblasts which then differentiate into myocytes (Abmayr and Pavlath 2012). The resulting myofibres are long and cylindrical in shape with many peripherally located nuclei (Figure 1.3 C-D). Fused cells contract in syncytium to produce force.

The basic organisation of a skeletal muscle myocyte is similar to that seen in cardiomyocytes. The contractile apparatus is composed of actin and myosin arranged as myofibrils. In skeletal muscle, myofibrils are anchored to the membrane at costameres via the Z-disk and the M-band (Pardo et al. 1983). Like in cardiac muscle, anchorage to the membrane via the Z-disk primarily occurs via the intermediate filament protein desmin (Granger and Lazarides 1979; O'Neill et al. 2002). This is also mediated via the skeletal muscle specific protein nebulin, which has been suggested to associate with desmin (Costa et al. 2004; Tonino et al. 2010). Dystrophin, a member of the spectrin superfamily, plays a particularly important role in stabilising the sarcomeric cytoskeleton in skeletal muscle (Ahn and Kunkel 1993). Dystrophin localises to the cytoplasmic face of the sarcolemma (Minetti et al. 1992) and has been found to be especially relevant in stabilising the M-band (Porter et al. 1992; Williams and Bloch 1999). One difference between skeletal and cardiac muscle is the location of the t-tubule system. In a skeletal muscle myocyte, the t-tubule system can be found above the A/I junction (Dwyer et al. 2012). Skeletal muscle myocytes also lack intercalated disks and instead have intercellular junctions as well as myotendinous junctions. Although skeletal and cardiac muscle may differ slightly in their ultrastructural organisation, the layout of their sarcomeres and the regulation of their contractile mechanism remain very similar.

1.1.4 Contractile Mechanism of Striated Muscle

Contraction of striated muscle is a markedly different process to that seen in smooth muscle. Although the process is Ca^{2+} dependent, it is the thin filaments rather than the thick filaments which are Ca^{2+} sensitive (Gordon et al. 1997). Ca^{2+} acts on the troponin-tropomyosin complex of thin filaments by binding troponin-C (TnC) (Poole et al. 2006). This leads to a conformational change of the troponin-tropomyosin complex resulting in the exposure of the myosin binding sites on actin, allowing the association of myosin and actin (Geeves and Holmes 1999). The S1 portion of the myosin heads then

reversibly bind two actin molecules and drive the sliding of the thin and thick filaments past each other, promoted by the energy produced due to the intrinsic ATPase activity of myosin (Lorenz and Holmes 2010). During contraction, the thick filaments remain centrally located within the context of the sarcomere and mediate shortening of the thin filaments along the horizontal axis of the sarcomere. Overall, contractile force in striated muscle requires the interaction between the thin actin filaments and the thick myosin filaments and is dependent on the presence of Ca^{2+} and ATP.

1.2 The Sarcomere

The basic repeating contractile unit of muscle is the sarcomere, a highly complex multiprotein assembly and defined as the area in between two Z-disks (Figure 1.4). The Z-disk anchors the thin (actin) filaments of the sarcomere. The length of the thin filaments to both sides of the Z-disk is now commonly referred to as the I-band. In the centre of each sarcomere is the M-band, which serves for tightly packing and anchoring the thick filaments, composed of myosin molecules (Auerbach et al. 1999; Boateng and Goldspink 2008; Ehler and Gautel 2008; Sanger and Sanger 2008). The length of the region containing thick filaments on either side of the M-band is referred to as the A-band. Each part of the sarcomere plays an integral role in maintaining stability and functionality of the contractile filaments.

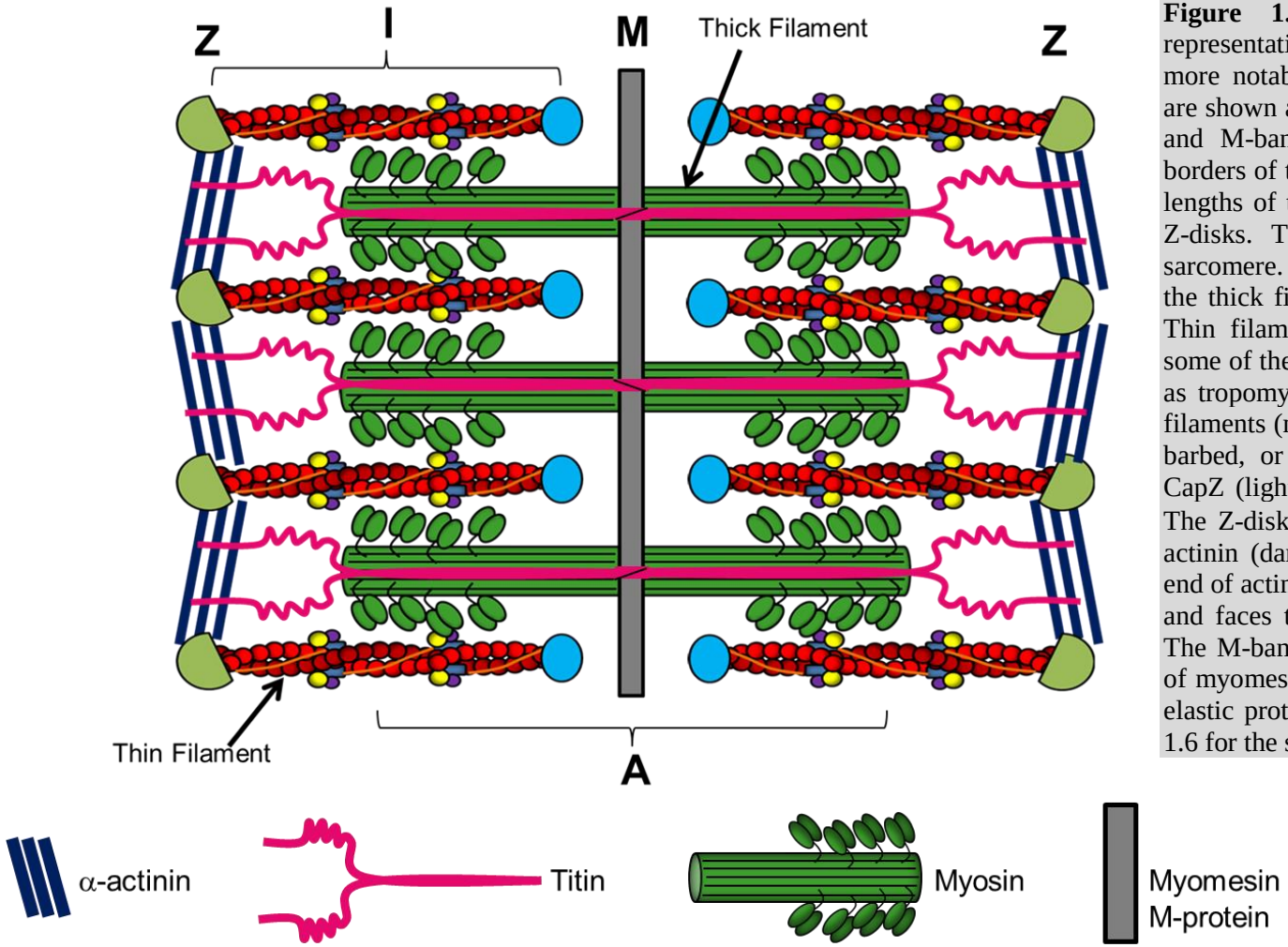

Figure 1.4: The Sarcomere. Schematic representation of the sarcomere and some of its more notable features. The major demarcations are shown and include the Z-disk, I-band, A-band, and M-band. The Z-disks represent the lateral borders of the sarcomere. The I-bands refer to the lengths of the thin filaments on either side of the Z-disks. The M-band represents the centre of the sarcomere. The A-band represents the length of the thick filaments on either side of the M-band. Thin filaments (actin) are depicted in red with some of the most relevant accessory proteins, such as tropomyosin and the troponin complex. Thick filaments (myosin) are depicted in dark green. The barbed, or growing, end of actin is capped by CapZ (light green) and is anchored at the Zdisk. The Z-disk is partly comprised of sarcomeric α-actinin (dark blue). The pointed, slow growing, end of actin is capped by tropomodulin (light blue) and faces towards the centre of each sarcomere. The M-band of the sarcomere is party comprised of myomesin and M-protein (grey). Titin, a giant elastic protein is shown in pink. Refer to Figure 1.6 for the structure of the thin filaments.

1.2.1 The Z-disk

The sarcomere is best delineated by focusing on some of the major proteins that determine its structure. The primary component of the Z-disk is α-actinin, a member of the actin binding spectrin family of proteins (Figure 1.4). α-actinin plays an important structural role within the topology of the sarcomere (Sjoblom et al. 2008). The most notable function of α-actinin is the anchorage of thin filaments via their barbed end. This occurs partly through the interaction between α-actinin and CapZ, which stabilises the barbed end of thin filaments (Papa et al. 1999). α-actinin also arranges thin filaments into cross linked arrays via its actin binding domain (ABD). This occurs through α-actinin forming symmetric anti-parallel homodimers along its length, thus exposing the ABDs at the ends of the rod domain (Djinovic-Carugo et al. 1999). The resulting network of α-actinin at the borders of the sarcomere resemble a lattice like basket weave structure, although this depends on the type of contraction exhibited on muscle (Goldstein et al. 1986), and with variable thickness depending on the type of striated muscle (Luther 2009). The Z-disks therefore serve mainly as a site for thin filaments anchorage.

1.2.2 The M-band

The M-band is situated in the centre of the sarcomere and contains a number of proteins that determine the structure and stability of the thick filaments (Figure 1.4). Some of the notable proteins include myomesin (Grove et al. 1984; Bähler et al. 1985; Auerbach et al. 1999), M-protein (Masaki and Takaiti 1974; Bähler et al. 1985), and the myomesin splice variant EH-myomesin (Price 1987; Price and Gomer 1993; Steiner et al. 1999; Agarkova et al. 2000). Particular attention has been placed on myomesin as a crucial determinant of M-band regulation. Myomesin is a member of the immunoglobulin superfamily (Bantle et al. 1996) and contains many immunoglobulin-like and fibronectin type III domains (Auerbach et al. 1999). Myomesin has also been found to be expressed in all the examined types of vertebrate striated muscle (Agarkova et al. 2000). One of the main proposed roles of myomesin is the incorporation of the thick filaments in the M-band. This occurs via myomesin forming anti-parallel dimers

via its C-terminal domain through dimerisation with its last domain (Lange et al. 2005). The thick filaments are accordingly incorporated by binding of myosin to the N-terminus of myomesin (Obermann et al. 1997). Thus, the M-band serves primarily as a site of thick filament anchorage.

1.2.3 Titin

Another notable component of the sarcomere is the giant protein titin (Figure 1.4). Titin, a very large protein with a molecular weight of 3000 kDa, makes up the third elastic filament system of sarcomeres. Titin spans the length of half a sarcomere, from the Z-disk to the M-band (Granzier and Labeit 2004). Titin has a number of proposed roles. It has been suggested that titin provides a template for sarcomere length (Agarkova and Perriard 2005). Additionally, titin plays a role in the integration of both thick (Agarkova and Perriard 2005; Lange et al. 2005) and thin filament (Kulke et al. 2001; Luther 2009) networks into the frame of the sarcomere. The N-terminus of titin binds capZ and α-actinin at the Z-disks and is cross linked in the thin filament system. The C-terminal end of titin extends into the region of the M-band where it binds myosin. It additionally binds myosin binding protein C (MyBP-C), another important component of the thick filaments (Fürst et al. 1988; Labeit et al. 1992). A number of other roles have been proposed for titin, such as the protein acting as an elastic molecular spring during sarcomeric stretching (Labeit and Kolmerer 1995), a blueprint for sarcomere assembly (Trinick 1994), and as a signalling hub for mechanosensing (Gautel 2011). A multitude of proteins make up the sarcomere and many more proteins are continuously being revealed. This paints a complex picture of a highly dynamic structure that was once viewed as static.

1.3 Actin

Actin is a ~42kDa protein that is ubiquitously expressed and conserved throughout eukaryotic evolution. The actin monomer consists of 375 residues which are the same in human and chicken and differ minimally in yeast (Luther 2009). In humans, actin exists as 6 isoforms which derive from the same ancestral gene. The actin isoforms are named according to their isoelectric point and include α-skeletal muscle actin (α-SKA),

α-cardiac muscle actin (α-CAA), α-smooth muscle actin (α-SMA), γ-smooth muscle actin (γ-SMA), β-cytoplasmic actin (β-CYA), and γ-cytoplasmic actin (γ-CYA). Actin isoforms exhibit tissue and cell-type specific expression as well as being developmentally regulated (Tondeleir et al. 2009).

Actin is polymerised into microfilaments, so named for having the smallest diameter compared to the other filament types, which make up the majority of the cytoskeleton in most cell types. The cytoskeleton is a complex three dimensional network of microfilaments, intermediate filaments, microtubules, and accessory proteins. It represents a crucial feature of cytoarchitecture as it mediates functions ranging from stability to motility. The dynamic nature of the cytoskeleton dictates that it must be able to rearrange and form discrete structures. This is crucial in order to fulfil a variety of physiologically relevant processes such as wound healing, morphogenesis, and muscle contraction (Naumanen et al. 2008).

1.3.1 Actin Polymerisation

Formation of actin filaments occurs through polymerisation (Figure 1.5). Monomeric, or globular (G) actin is polymerised into helical, or filamentous (F) actin by virtue of its ATP binding activity. G-actin can bind ATP in its ATP binding cleft in a 1:1 complex allowing a conformational change to take place so that it may be added to other monomers to create F-actin. The intrinsic ATPase activity of actin allows hydrolysis of ATP to ADP and subsequent dissociation of monomers to replenish the available pool of G-actin (Carlier and Pantaloni 1986). ATP is hydrolysed to ADP with a half time of 2sec (Blanchoin and Pollard 2002) whereas inorganic phosphate dissociates more slowly with a half time of 6min (Melki et al. 1996; Pollard 2007). The growing end of an actin filament is known as the barbed (+) end, whereas monomers are lost at the pointed (-) end. Although monomers can be added to and lost at both ends of a filament, *in vitro* kinetic studies have shown that filament growth is greatly favoured over loss since monomer addition is 5-10 times faster at the barbed end (Pollard et al. 2000; Chhabra and Higgs 2007). Continuous cycles of monomer addition and loss allow for a steady state treadmilling effect to be reached to create motile force (Pollard 1986). However, this explanation only allows a simplistic view of actin dynamics *in*

vivo. Nucleation is the rate limiting step of polymerisation (Chesarone and Goode 2009). Initial nucleation of filaments is very unfavourable and the majority of the cytosolic pool of G-actin is sequestered by profilin, further preventing spontaneous nucleation (Kaiser et al. 1999; Kovar 2006; Chhabra and Higgs 2007). Thus, there are a variety of mechanisms that regulate actin dynamics at the level of filament nucleation, elongation, stabilisation, as well as there being a vast number of determinants dictating the actin structures being formed. In other words, the presence of other regulatory and accessory proteins determine the kind of actin-based structure that is formed (Chhabra and Higgs 2007).

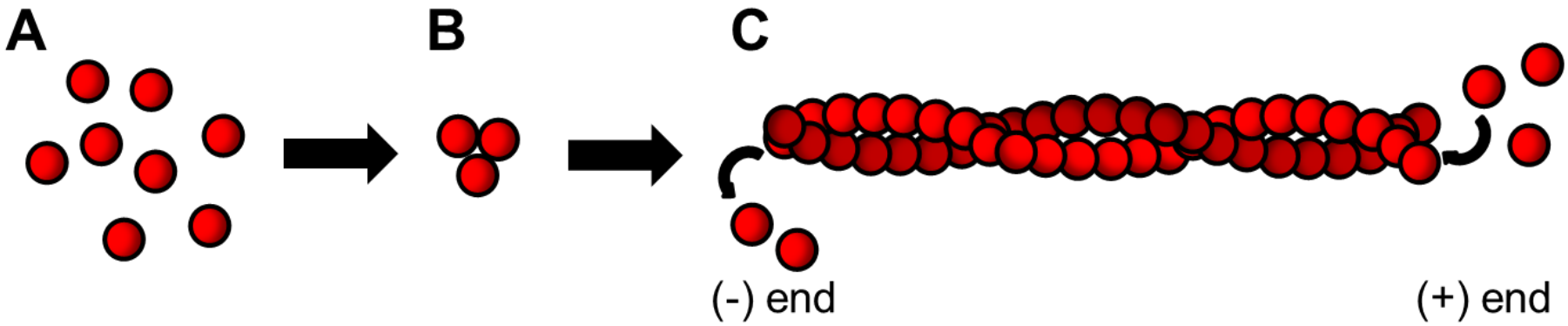

Figure 1.5: The Polymerisation of Actin. A schematic representation of the basic steps involved in the polymerisation of G-actin into F-actin. **A)** G-actin is not capable of being polymerised until it has bound ATP. **B)** ATP-bound G-actin begin to form stable trimers during initial nucleation. **C)** After the initially slow nucleation step, elongation takes place with ATP-bound G-actin monomers rapidly associating with the growing (+) end of F-actin filaments. Actin slowly hydrolyses ATP to ADP and dissociates upon doing so. Loss of G-actin takes place at the pointed (-) end and serves to replenish the pool of available actin. ATP, adenosine triphosphate; ADP, adenosine diphosphate.

1.3.2 Thin Filaments

As mentioned above, within the context of muscle, polymerised actin filaments are referred to as thin filaments (Figure 1.6). Thin filaments are not only made of actin but a variety of other proteins that regulate the length and stability of the filaments. Thin filaments do not exist in a treadmilling state, but rather represent microfilaments that have been stabilised by a number of proteins. The pointed ends of thin filaments are bound by tropomodulin (Fowler et al. 1993; Gregorio et al. 1995). Tropomodulin capping blocks elongation and depolymerisation at the barbed ends but requires the presence of tropomyosin to do so (Weber et al. 1994). The actin nucleating protein leiomodin has also been shown to regulate thin filaments at their pointed ends in a tropomyosin dependent manner (Chereau et al. 2008; Skwarek-Maruszewska et al. 2010). At the other end of the thin filaments, CapZ seems to be the major capping protein and binds with high affinity thus preventing further polymerisation and depolymerisation (Caldwell et al. 1989). CapZ also reportedly interacts with nebulin to form a structural link between thin filaments (Pappas et al. 2008). Nebulin is a giant protein, only found in skeletal muscle, that spans almost the entire length of the thin filaments but stops just short of the pointed end (Wang and Williamson 1980; Castillo et al. 2009). Initially thought to participate in myofibrillogenesis and to determine thin filament length, it is more likely that nebulin is involved in myofibrillar maintenance (Bang et al. 2006) and stabilisation of the thin filament core (Littlefield and Fowler 2008). The equivalent of nebulin in cardiac muscle is nebulette, a significantly smaller member of the nebulin family. Nebulette also plays a role maintaining thin filament stability since disruption of nebulette expression resulted in reduced thin filament length in cardiomyocytes (Moncman and Wang 2002; Pappas et al. 2011). Although a number of proteins have been implicated in regulating thin filament function, the polymerisation and regulation of thin filaments are subjects which require further elaboration.

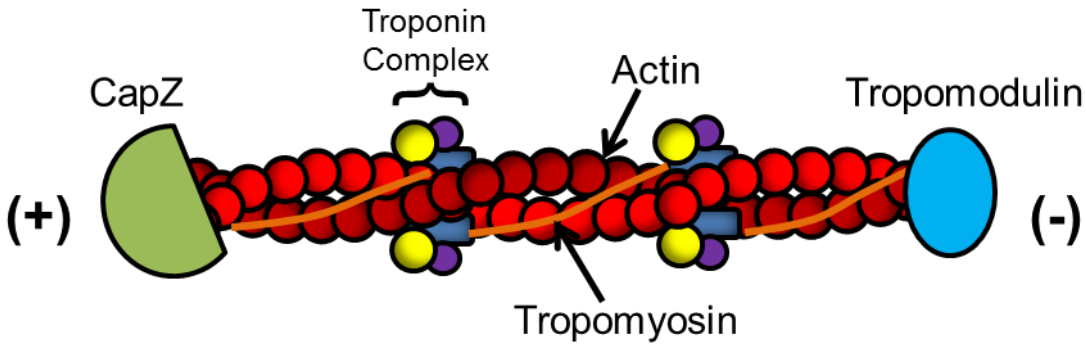

Figure 1.6: The Thin Filaments of Striated Muscle. A schematic representation of a thin filament that is found in striated muscle. Thin filaments are made of polymerised actin. The barbed ends of thin filaments are capped by CapZ and the pointed ends are capped by tropomodulin to prevent any addition or loss of monomers. Thin filaments are also decorated with the troponin complex (troponin I, C, and T) and tropomyosin, which participate in the regulation of contraction. (+), barbed end; (-), pointed end. (Dwyer et al. 2012)

1.4 Regulation of Actin Polymerisation

The polymerisation of actin is difficult for a number of reasons. Apart from spontaneous actin nucleation being a thermodynamically unfavourable process requiring energy, it has also been found that nucleation cores of actin dimers and trimers are unstable (Sept and McCammon 2001; Paul and Pollard 2009). Processes involving actin polymerisation require rapid and effective bursts at specific sites (Chesarone and Goode 2009). The existence of multiple nucleation and elongation factors allows the polymerisation of actin to be carefully regulated. A varied cellular milieu of actin interacting proteins allows the formation of different actin-based structures, such as lamellipodia, filopodia, and pseudopodia to be possible. Nucleation factors promote the formation of a filament and can initiate this from the pool of profilin-actin. They essentially regulate the timing of filament formation. Elongation factors move with the barbed ends of filaments and protect them from inactivating capping proteins. These factors control the extent of filament growth (Chesarone and Goode 2009).

1.4.1 Arp2/3

The first nucleation factor to be identified was the Arp2/3 complex (Figure 1.7 A). The Arp2/3 complex is a multiprotein assembly that nucleates pre-existing actin filaments at a 70˚ angle to promote the outgrowth of a new daughter filament (Machesky et al. 1994) and can also cross-link actin filaments (Mullins et al. 1998). The Arp2/3 complex is comprised of two actin related proteins (Arp2 and 3) and 5 regulatory subunits: ARPC1 (40-kDa subunit); ARPC2 (35-kDa subunit); ARPC3 (21-kDa subunit); ARPC4 (20-kDa subunit); and ARPC5 (16-kDa subunit) (Pollard 2007). Arp2/3 forms a nucleation core by structurally mimicking G-actin monomers (Chesarone and Goode 2009). Microscopy has shown that Arp2/3 remains associated with the pointed end of actin filaments. Arp2/3 inhibits monomer addition and loss at the pointed and increases polymerisation at the barbed end (Mullins et al. 1998). Therefore, by binding, stabilising, and inhibiting the loss of actin monomers, the Arp2/3 complex promotes the formation of branched actin filament networks. Branched networks are crucial for the formation of lamellipodia in cell migration (Naumanen et al. 2008). Dendritic networks based on Arp2/3 nucleation are also essential for the formation of focal adhesions. The highly specialised nature of Arp2/3 is really made apparent by the fact that the 70˚ outgrowth of daughter filaments maximises the potential for membrane protrusions (Chesarone and Goode 2009; Paul and Pollard 2009).

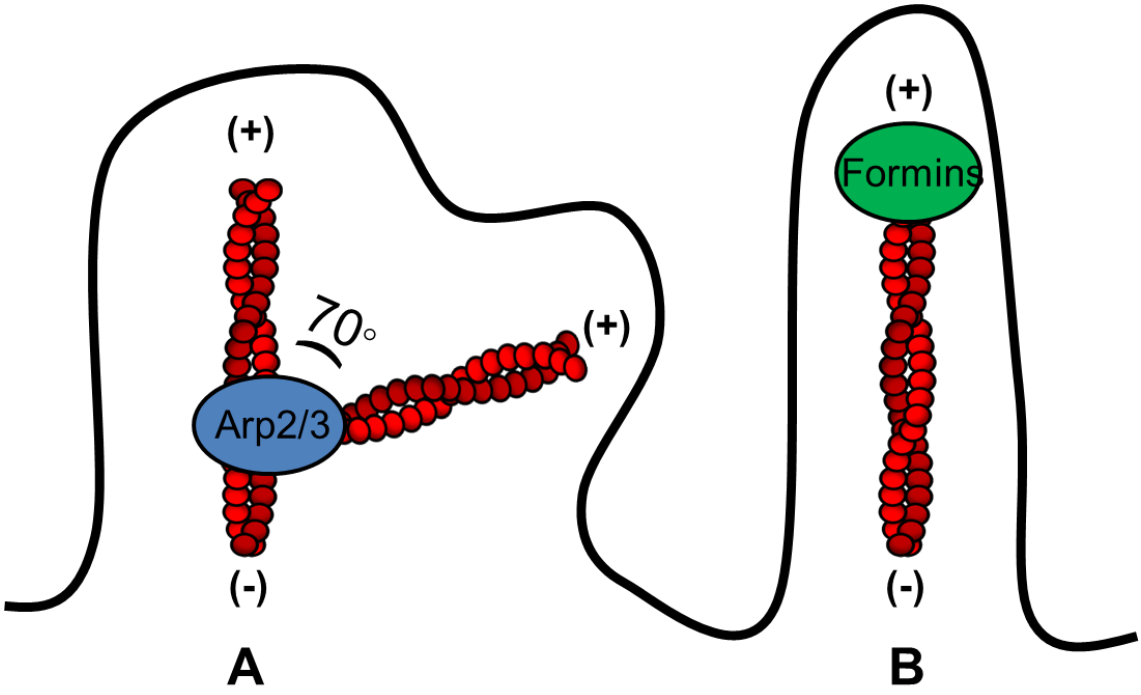

Figure 1.7: Actin Polymerisation: Arp2/3 versus Formins. Schematic diagram depicting actin polymerisation by Arp2/3 and formins as well as the structures they localise to. **A)** The Arp2/3 complex mediates the formation of dendritically branched actin filaments. It binds to the side of a pre-existing filament and nucleates a new daughter filament at a 70˚ angle from the mother filament. These structures are typically seen in the formation of lamellipodia. **B)** Formins polymerise actin into linear unbranched structures. They remain processively associated with the barbed end of filaments. These structures are essential in the formation of filopodia. (+), barbed end; (-), pointed end.

1.4.2 Other Actin Regulatory Proteins

Another more recently described actin nucleator is leiomodin (Chereau et al. 2008). Leiomodin is similar in structure to tropomodulin and contains a Wiskott-Aldrich syndrome protein (WASP) homology 2 (WH2) domain (Qualmann and Kessels 2009). Leiomodin is expressed as both a smooth muscle isoform and a striated muscle isoform, that is exclusively present in foetal and adult heart and adult skeletal muscle (Conley 2001; Conley et al. 2001). Leiomodin was found to be a strong nucleator of thin filaments in muscle cells as well as being integral in mediating sarcomeric maintenance (Chereau et al. 2008). It was also found to antagonise the effects of tropomodulin in regulating the lengths of thin filaments (Tsukada et al. 2010). Other notable proteins that regulate actin polymerisation include spire (Schuldt 2005; Sitar et al. 2011), N-

WASP (Martinez-Quiles et al. 2001; Takano et al. 2010), and cordon bleu (Qualmann and Kessels 2009; Husson et al. 2011).

1.5 Other Mechanisms of Actin Regulation

While actin filament formation occurs through nucleation and elongation, a number of other processes exist that regulate actin filaments. As mentioned above, profilin serves to sequester G-actin monomers to prevent spontaneous polymerisation. Profilin represents a major actin binding protein and also serves to facilitate actin polymerisation (Figure 1.8 A), particularly in the presence of assembly factors, by catalysing the conversion of ADP-actin to ATP-actin. Other actin binding proteins participate in the regulation of actin filaments at the level of capping (Figure 1.8 B), disassembly (Figure 1.8 C), and cross-linking (Figure 1.8 D, E).

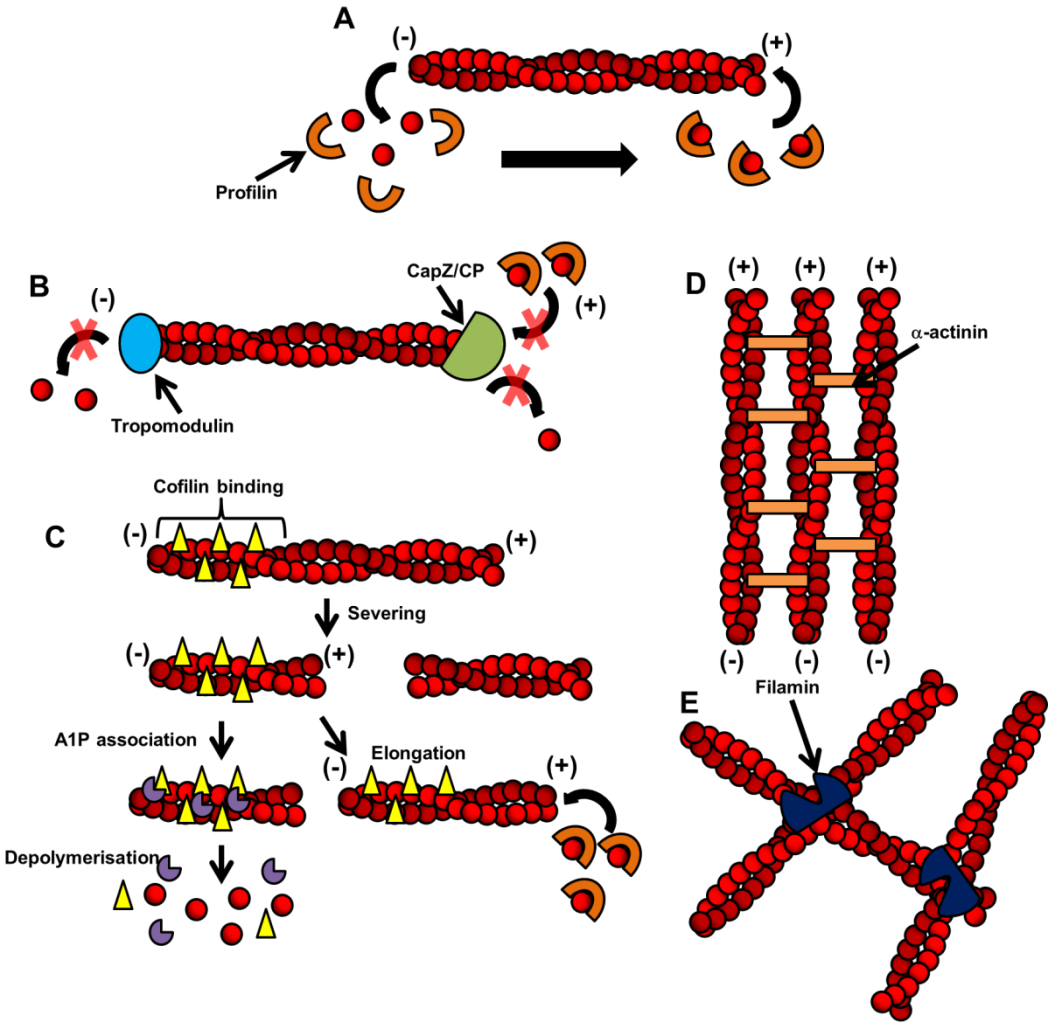

Figure 1.8: Other Mechanisms of Actin Regulation. A) Profilin serves to sequester G-actin monomers to prevent spontaneous assembly but can also facilitate polymerisation by catalysing the exchange for ADP to ATP in actin. Apart from nucleation and elongation, actin filaments are regulated via other mechanisms, such as capping, severing/disassembly, and cross-linking. **B)** An actin filament capped at its (+) end by CapZ/CP and capped at its (-) end by tropomodulin. **C)** Actin filaments can undergo severing by cofilin. The resulting actin rods/bundles can serve for further elongation or can undergo disassembly upon association of AIP1. **D)** Actin filaments can be tightly packed into parallel bundles by α-actinin. **E)** Actin filaments can be cross-linked into orthogonal networks. (+), barbed end; (-), pointed end; CP, Capping protein; AIP1, actin interacting protein1.

1.5.1 Actin Capping

Actin capping proteins bind the ends of actin filaments and play roles in the stabilisation of filaments, prevention of filament disassembly, and regulation of filament length. Capping proteins either bind the pointed end or barbed end of actin filaments in order to prevent actin monomer addition or dissociation (Figure 1.8 B).

The best characterised group of pointed end capping proteins is the tropomodulin family (Tmod 1-4). There have been four mammalian tropomodulin described, as well as three

larger variants termed the leiomodins (Lmod 1-3) (Yamashiro et al. 2012). Tropomodulins have been shown to bind both tropomyosin and actin at the ends of actin filaments in order to prevent elongation or depolymerisation (Weber et al. 1994). Furthermore, the presence of tropomyosin influences the strength of binding to the actin filament pointed end. In actin filaments lacking tropomyosin, Tmod1 was shown to be a leaky capper, in that actin monomer addition and dissociation was reduced but not completely blocked. However, the presence of tropomyosin on thin filaments resulted in tighter capping activity of Tmod1. Tropomodulins thus possess both tropomyosin-independent and tropomyosin-dependent mechanisms of pointed end capping (Figure 1.8 B). Tropomyosin-independent pointed end capping is thought to predominantly occur through binding of actin via the C-terminal LRR-Cap domain on tropomodulin (Fowler et al. 2003; Yamashiro et al. 2012). On the other hand, tropomyosin-dependent binding occurs through binding to both tropomyosin and actin via the N-terminal TM-Cap domain on tropomodulin, with two binding sites on tropomyosin and two binding sites on actin proposed. The physiological relevance of the tropomodulins has been highlighted in mouse knockout studies. Global Tmod1 knockouts have been reported to exhibit aberrant cardiac myofibril assembly, aborted cardiac morphogenesis, and embryonic lethality by E9.5 (Fritz-Six et al. 2003; Ochala et al. 2014),

Actin capping activity is not solely restricted to the tropomodulins (or pointed end capping for that matter). Another notable actin capping protein is Capping Protein (CP), aptly named for its ability to prevent growth of actin filaments from the barbed end (Figure 1.8 B) (Cooper and Sept 2008). Furthermore, CP is involved in the tethering of actin filaments (Bearer 1991). CP participates in the formation of Arp2/3-driven dendritic networks *in vitro* (Nicholson-Dykstra et al. 2005) and in cultured cells (Mejillano et al. 2004). Studies performed *in vivo* also indicated that CP plays roles in morphogenesis and differentiation. CP is also expressed in striated muscle, where it is referred to as CapZ (Figure 1.6), by virtue of its localization to the Z-disks. Notably, one molecule of CapZ is required to bind the barbed end of an actin filament (Schafer et al. 1993; Cooper and Sept 2008). In the context of striated muscle, CapZ is thought to function by anchoring actin filaments to the Z-disk and/or preventing aberrant growth of actin filaments into adjacent sarcomeres. As mentioned above, CapZ seems to require an interaction with nebulin in order to preserve the structural link between adjacent sarcomeres. Knockdown studies have indicated that nebulin depletion reduces

expression of assembled CapZ and results in misalignment of the barbed ends of actin filaments (Pappas et al. 2008). The role of CapZ in the maintenance of filament stability could also remain central to its function since CapZ was shown to prevent disassembly of actin filaments in the presence of cofilin, coronin, and Aip1 in single filament studies (Kueh et al. 2008).

1.5.2 Actin Disassembly

While actin capping primarily serves to stabilise filaments by preventing further elongation or disassembly, factors that promote disassembly of actin filaments are required to rapidly replenish the available pool of monomeric G-actin that are needed during instances of the dynamic treadmilling events that are required to promote protrusive movement of filaments (Kueh et al. 2008; Brieher 2013). Actin disassembly factors therefore contribute significantly to the highly dynamic nature of actin filaments and the cytoskeleton. A number of mechanisms of actin disassembly have been proposed, including the following: induction of loss of G-actin monomers from the filament pointed due ATP hydrolysis; severing of actin filaments; induction of loss of G-actin monomers from the barbed end in a process referred to as dynamic instability and promotion of whole filament destabilisation (Kueh et al. 2008; Brieher 2013). Notable factors involved in actin disassembly include gelsolin and actin depolymerising factor (ADF)/cofilin.

Gelsolin acts on actin by severing actin filaments in two and by capping the growing barbed end in a Ca^{2+}-dependent process (Kwiatkowski 1999). There are at least six other members of the gelsolin family that may play distinct roles in a number of cellular processes: villin, adseverin, capG, advillin, supervillin and flightless I (Silacci et al. 2004). Interestingly, the initially discovered gelsolin protein exists as both cytoplasmic and plasma isoforms. Gelsolin binds and severs actin filaments in the presence of calcium and remains bound to the barbed end of the resulting actin filament. Uncapping occurs through gelsolin binding phosphatidylinositol lipids (Silacci et al. 2004). Gelsolin has been reported to play roles in the regulation of cell motility. Studies using homozygous gelsolin knockout mice revealed that this protein was required for retraction processes but not for filopodial formation in neuronal growth cones (Lu et al. 1997; Silacci et al. 2004). Early overexpression studies in NIH 3T3 cells transfected

with gelsolin indicated that this actin disassembly factor enhanced cell migration by increasing the rate at which cells migrated through a porous filter (Cunningham et al. 1991; Silacci et al. 2004). The importance of actin severing in the regulation of processes requiring actin has been further highlighted by the fact that gelsolin is involved in processes including phagocytosis (Witke et al. 2001), apoptosis (Kothakota et al. 1997), and tissue morphogenesis (Crowley et al. 2000).

ADF/Cofilin is another well-studied family of actin disassembly factors. Cofilin, one of the more notable members of this family, preferentially binds ADP-actin to promote severing (Figure 1.8 B) of actin filaments or depolymerisation of actin filaments from the pointed ends. One mechanism by which this occurs could be by coupling ATP hydrolysis to filament turnover, therefore increasing the rate of monomer dissociation from the pointed end (Carlier et al. 1997; Kueh et al. 2008). However, cofilin's ability to promote depolymerisation of filament pointed ends is a subject of dispute (Bravo-Cordero et al. 2013); therefore its severing activity is the subject of primary focus. Cofilin's actions on actin are dependent on the concentration ratio of cofilin to actin. When the concentration of actin is higher than that of cofilin, cofilin has been shown to continuously sever actin filaments, as has been demonstrated *in vitro* (Andrianantoandro and Pollard 2006; Bamburg and Bernstein 2010). Under such instances of persistent severing, severed portions of filaments can be further elongated via their newly created barbed ends. Furthermore, G-actin monomers sequestered by cofilin serve to replenish the pool of available G-actin for further elongation once subunits are exchanged for profilin. In situations where the concentration of cofilin is higher than that of actin, cofilin will rapidly but not persistently sever actin filaments while remaining bound to actin, resulting in the generation of actin bundles/rods (Andrianantoandro and Pollard 2006; Bamburg and Bernstein 2010). Actin bundles can either be further elongated or can be depolymerised in the presence of actin interacting protein 1 (AIP1) to replenish the available pool of G-actin monomers (Figure 1.8 C). While *in vitro* work has shed light onto the mechanisms of filament depolymerisation, factors involved in actin disassembly have been found to play important roles *in vivo*. One study used transgenic mice, in which conditional knockout of ADF and cofilin were performed in the nervous system. ADF and cofilin depletion resulted in blockade of F-actin retrograde flow and irregular microtubule growth, two factors which contributed to failure of neuritogenesis in these animals (Flynn et al. 2012). Also, mice depleted of cofilin-2 die shortly after

birth by day 8 and are partly characterised by disrupted sarcomere architecture and accumulation of F-actin in skeletal muscle. These anomalies arose by postnatal day 7, thus indicating that cofilin-2 plays a role in myofibrillar maintenance rather than myogenesis (Agrawal et al. 2012).

1.5.3 Actin Cross-Linking

Actin cross-linking proteins are involved in the construction of the molecular scaffolds required for processes ranging from cellular motility to adhesion. Actin cross-linking proteins can link the actin cytoskeleton to extracellular matrix proteins (e.g., ankyrin, laminin and dystroglycan (Lee and Dominguez 2010)) and can also contribute to the formation of cross-linked or bundled networks of F-actin found in structures such as stress fibres (Wang 1984) and dorsal arcs (Heath 1981), among others (Tseng et al. 2005; Lee and Dominguez 2010). Generally speaking, actin cross-linking proteins tend to function as dimers and bind actin via multiple binding sites, the locations of which partly determine the actin network formed (Stevenson et al. 2012). Furthermore, smaller actin cross-linking proteins tend to contribute to the organization of F-actin into parallel bundles. Larger actin cross-linking proteins, on the other hand, tend to exhibit more complex behaviour in that their effects are concentration specific. Larger actin cross-linking proteins tend to organise actin filaments into networks or gels at lower cross-linking protein concentrations and they organize actin filaments into bundled networks or composite networks (a mixture of cross-linked and bundled actin filament networks) at higher cross-linking protein concentrations (Lieleg et al. 2010).

Actin cross-linking proteins that promote the formation of actin bundles, in which actin filaments are aligned along their axes by the same polarity and are tightly packed (Bartles 2000) include notable actin bundling proteins such as fascin (Jansen et al. 2011) and α-actinin (Broderick and Winder 2005). α-actinin, a member of the spectrin family of proteins, represents the archetypal actin bundling protein. *In vitro* studies have indicated that α-actinin organises actin into loose networks at low concentrations of α-actinin to actin. At higher concentrations of α-actinin to actin, α-actinin organises actin filaments into tight bundles (Figure 1.8 D) (Tseng and Wirtz 2001; Tseng et al. 2005). Apart from the actin-crosslinking activity that it possesses in the sarcomere, α-actinin also cross-links actin filaments into stress fibres. Stress fibres are arrays of bundled

actin filaments that usually interact with myosin II motors (Pellegrin and Mellor 2007; Naumanen et al. 2008). They create contractile force and are responsible for processes such as the stabilisation of the trailing edge of cells during migration and for contracting the rear end of the cell. Studies have indicated that α-actinin often plays an indispensable role in the formation of stress fibres. In U2OS human osteosarcoma cells, partial knockdown of α-actinin-1, one of the major non-muscle α-actinin isoforms, with short hairpin RNA (shRNA) resulted in reduced formation of radial stress fibres (Oakes et al. 2012). Similarly, U2OS cells depleted of α-actinin-1 displayed reduced formation of dorsal stress fibres (Kovac et al. 2013).

The filamin family of proteins has also been highlighted as important actin binding proteins. Filamin-A is the most abundant and widely expressed member of the filamin family and notably cross-links cortical actin filaments into three-dimensional orthogonal networks (Figure 1.8 E). This is mediated through the N-terminal actin binding domain on filamin-A and binding of filamin-A to actin at large angles (Yue et al. 2013). The filamin proteins have proposed roles in cell migration as has been indicated in a number of studies. For example, knockdown of filamin-A and B in Jurkat cells impaired the initiation of cell migration (Baldassarre et al. 2009). Mutations of filamin-A have also been linked to human diseases such as periventricular heterotopia, an X-linked brain malformation (Feng and Walsh 2004).

When examined in a modular fashion, actin binding proteins exhibit individually important roles. However, when viewed on a more holistic level and when the formation of complex actin-based structures is concerned, one can discern a complex interplay of many of the factors and processes described above.

1.6. Regulation and Dynamics of Actin-based Structures

There are at least 15 types of actin-based structures that have been described in metazoan cells. These actin-based structures arise from the polymerisation of G-actin to F-actin in a tightly controlled temporal and spatial process to give rise to distinct structures. Not only is actin polymerised into the helical filaments, but these filaments have the capacity to be further organised into higher order assemblies, giving rise to structures such as lamellipodia, filopodia, and stress fibres (Figure 1.9). Unlike yeast

cells, which are far less complex by virtue of the number of actin-based structures they possesses as well as their more clearly delineated spatial arrangement, actin-based structures in metazoan cells are of numerous kinds and often overlap spatially (Chhabra and Higgs 2007).

Actin-based structures that protrude from the plasma membrane can be thought of as sheet-like structures or finger-like structures. Sheet-like protrusive actin-based structures include lamellipodia, ruffles, phagocytic cups, podosomes, and invadopodia (Mattila and Lappalainen 2008). Finger-like protrusive actin-based structures describe filopodia and microvilli. The term stress fibre has been broadly adopted to describe contractile actin filaments that interact with myosin motors. The multitude of processes and actin binding proteins described above converge in a carefully timed manner at tightly regulated locations to give rise to higher order actin networks, dynamic motile processes, and adhesive processes.

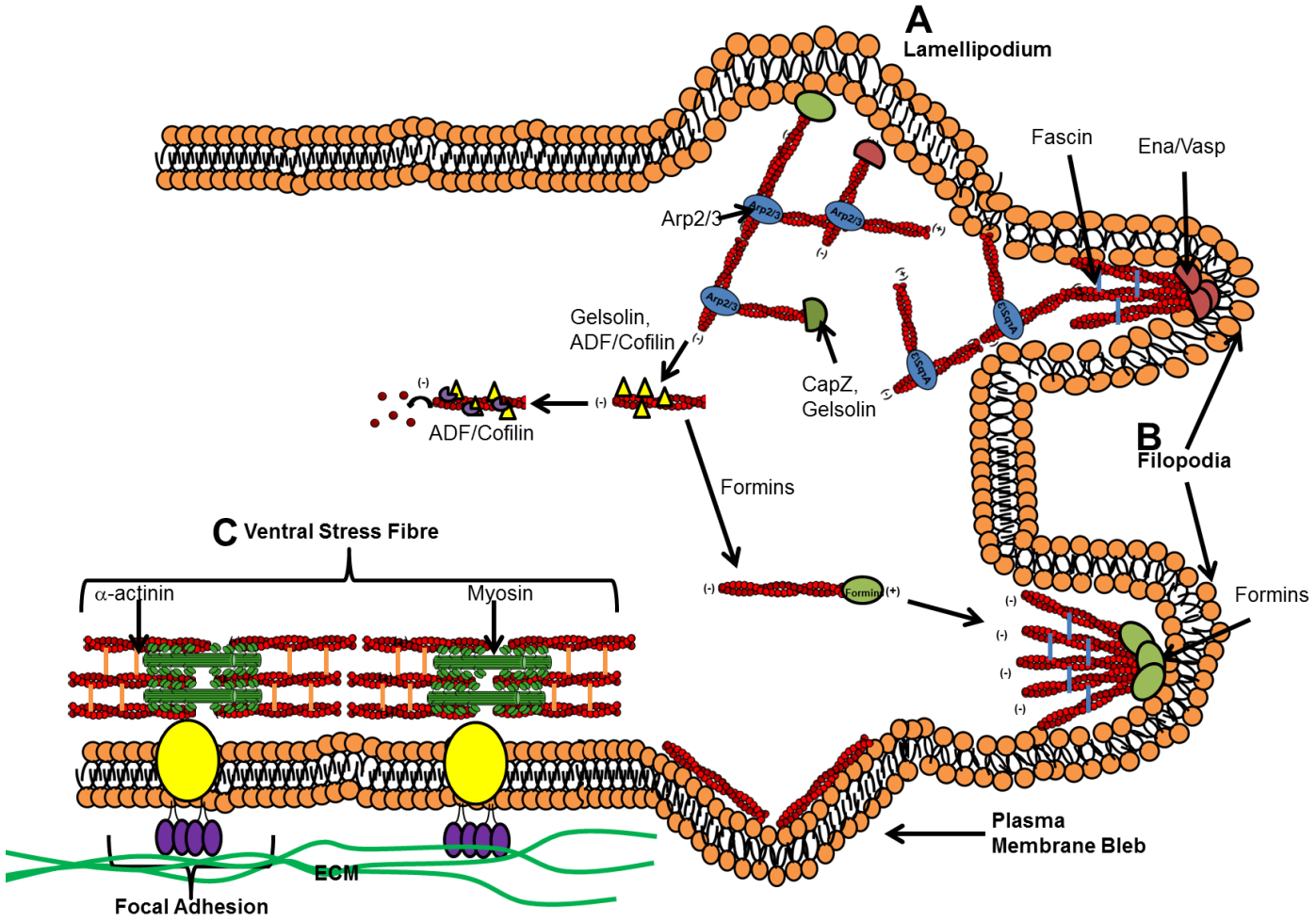

Figure 1.9: Actin-Based Structures in Cells. A) Lamellipodia are sheet-like membrane protrusions formed near the leading edge of cells. Their actin filament network is of a branched nature. Filaments are nucleated by the Arp2/3 complex and can be further elongated by Ena/Vasp or members of the formin family. The actin turnover function of proteins like cofilin, which resides beneath the lamellipodium serve to replenish the available pool of G-actin for further elongation and can provide new filaments for further elongation. **B)** Filopodia are finger-like projections composed of linear actin filaments that are polymerized by formins or Ena/Vasp and are bundled by fascin. **C)** An example of a ventral stress fibre, the most commonly observed type of stress fibre. Ventral stress fibres are composed of actin filaments bundled by α–actinin. Myosin II motors facilitate the generation of contractile force. Ventral stress fibres are anchored at each end by integrin-rich focal adhesions. (+), barbed end; (-), pointed end; ECM, extracellular matrix.

1.6.1 Lamellipodia

Lamellipodia are examples of membrane protrusions that form at the leading edge of migrating cells (Figure 1.9 A). The lamellipodium is a sheet-like actin-based structure that attaches to the extracellular substratum and can occur during crawling cell motility and during cell spreading (Vinzenz et al. 2012). The lamellipodium describes the area closest to the leading edge of a cell, whereas the larger, less dynamic, and more adhesive lamella describes the area behind the lamellipodium, which stretches towards the cell body (Delorme et al. 2007). The distribution and nature of the actin filaments (as well as the actin binding proteins that regulate them) differ between the lamellipodium and the lamella (although some overlap may occur) and is partly dependent on the level of tension exerted on the cell. The Arp2/3 complex and cofilin primarily associate with the lamellipodium and promote the nucleation/treadmilling of F-actin that it required for membrane protrusion to occur (Welch et al. 1997; Svitkina and Borisy 1999; Delorme et al. 2007). The lamella is more typically characterised by the presence of proteins involved in contraction, such as myosin II and tropomyosin (Ponti et al. 2004; Gupton et al. 2005; Delorme et al. 2007).

The dense actin networks comprising lamellipodial networks are predominantly that of an Arp2/3-mediated dendritically branched nature. It is widely accepted that Arp2/3 is the predominant actin nucleator of lamellipodial networks in most cells. Furthermore, the Arp2/3 complex is a crucial regulator of lamellipodial networks since inhibition of Arp2/3 activity has been found to disrupt lamellipodial assembly (Suraneni et al. 2012). Actin nucleation and elongation primarily occur in a confined area near the leading edge of the cell. While Arp2/3 might be primarily responsible for nucleating filaments and promoting branched networks, distinct actin binding proteins have been suggested to elongate actin filaments towards the plasma membrane, namely Ena/VASP and members of the formin family of proteins (Figure 1.9 A) (Chesarone and Goode 2009). Targeted depletion of Ena/VASP and formins in cells has been associated with the formation of lamellipodial networks comprised of shorter actin filaments and highlighted the importance of these factors for lamellipodial actin dynamics (Bear et al. 2002; Yang et al. 2007; Chesarone and Goode 2009).

As mentioned above, cofilin localises to the base of the lamellipodium. In this context, cofilin is thought to support Arp2/3-mediated nucleation of filaments through the creation of newly severed filaments (Figure 1.9). Cofilin is also thought to promote retrograde flow of filaments in order for the lamellipodium to expand. In other words, the actin severing and depolymerising activities of cofilin provide further substrate (i.e., new barbed ends on actin filaments and liberated G-actin monomers) required for the polymerisation of actin filaments within lamellipodia. Evidence for this model has come from numerous studies (Oser and Condeelis 2009; Bravo-Cordero et al. 2013). One study in Ptk1 cells found that activation of cofilin promoted actin turnover in the lamellipodia (Delorme et al. 2007). Furthermore, cofilin activation induced widening of the lamellipodia, narrowing of the area between the lamella and lamellipodium, and inhibited membrane protrusion. These findings would suggest that a balance of cofilin activity is required in order for efficient cycles of actin severing and polymerisation to occur. Indeed, regulatory mechanisms have been identified that describe the inactivation of cofilin at membrane protrusions. For example, phosphorylation of cofilin by LIM kinase results in cofilin inactivation in lamellipodia (Oser and Condeelis 2009). Cofilin is also negatively regulated by binding of cortactin, although this mechanism appears to be specific to invasive protrusions (Bravo-Cordero et al. 2013).

While cofilin regulates the actin meshwork at the base of lamellipodia, capping proteins have been found to regulate filaments at the tips of these membrane protrusions. Capping is an essential process required for the formation of lamellipodia. For example, one study found that CP is required for Arp2/3-mediated actin-based motility (Loisel et al. 1999) and a subsequent study found that depletion of CP resulted in disruption of lamellipodial formation in favour of filopodial formation (Mejillano et al. 2004). Capping proteins are thought to regulate the extent of filament formation in lamellipodia, an effect which can be antagonised by elongation factors. One study found that Ena/VASP displaces CP from the barbed ends of actin filaments in order to further elongate them (Bear et al. 2002). In this same study, Ena/VASP-mediated actin networks were less branched and filaments were longer, suggesting that an interplay between elongation factors and capping proteins occurs to regulate the geometry of the actin networks and the extent of filament growth in lamellipodia.

1.6.2 Filopodia

Filopodia are thin finger-like plasma membrane protrusions that are rich in actin (Figure 1.9 B). Within filopodial protrusions, actin filaments are organised into parallel bundles, with their barbed ends oriented towards the plasma membrane (Chesarone and Goode 2009). Furthermore, the actin network found within filopodia is characterised by long, unbranched actin filaments. The structural and molecular composition of filopodia can vary between cell types, but overall, these structures have been found to play roles in cellular sensing, cellular migration, and cell-cell interactions (Yang and Svitkina 2011).

Filopodia are formed when actin filaments push against the plasma membrane, leading to the formation of protrusions. The participation of elongation factors is crucial in this setting, with strong evidence pointing to the contribution to the formin family of proteins and Ena/VASP (Figure 1.9 B). For instance, overexpression and knockdown studies have implied that the formin mDia2 is required for the formation of filopodia (Yang et al. 2007; Block et al. 2008; Chesarone and Goode 2009). Similarly, Ena/VASP proteins have been described to be concentrated at filopodial tips and contribute to the formation of such structures (Lebrand et al. 2004; Yang and Svitkina 2011). However, while these two family of proteins have undisputed and even overlapping roles in filopodial formation, their interaction with various actin networks and cross-talk with other actin binding proteins may vary according to cell type. Consequently, two main models have been proposed for the elongation of filaments in filopodia. In the convergent elongation model, the aforementioned elongation factors polymerise actin filaments derived from Arp2/3-mediated branched networks found in lamellipodia (Svitkina et al. 2003; Mattila and Lappalainen 2008). In the alternative tip nucleation model, *de novo* formation of actin filaments occurs in the filopodial tip and is not coupled to an underlying lamelliopodial network (Mattila and Lappalainen 2008). While the second model is thought to be primarily driven by formins, the participation of the Ena/VASP proteins cannot be dismissed. For example, neuronal cells depleted of Ena/VASP were unable to form filopodia, although overexpression of Dia2 was shown to rescue filopodial formation (Dent et al. 2007; Mattila and Lappalainen 2008).

Another notable player in filopodial formation is fascin. Metazoan cells express three different isoforms of fascin (fascin-1, 2, and 3), which exhibit cell and tissue-specific

distribution. Fascin is notably overexpressed in a variety of metastatic tumors (Kureishy et al. 2002). Regardless of the model of filopodial growth, it is widely accepted that the association of fascin with formin or Ena/VASP-induced actin bundles is required for completion of filopodial formation (Figure 1.9 B). Fascin cross-links the parallel actin filaments in filopodia to form stable, rigid bundles (Mattila and Lappalainen 2008; Yang and Svitkina 2011). Fascin binds actin filaments via two major sites, the mutation of which results in disrupted filopodial formation (Yang et al. 2013). Furthermore, electron microscopy studies have shown that fascin can bundle between 10 and 30 actin filaments to form filopodia that are 60-200nm in diameter (Mattila and Lappalainen 2008). Studies in human keratinocytes would suggest that actin filaments in filopodia undergo cycles of elongation, stabilisation, and persistence, which is influenced by binding of fascin. For example, levels of fascin are reduced upon regrowth of filopodia in order for further elongation of actin filaments to occur (Schafer et al. 2011).

1.6.3 Stress Fibres

As mentioned previously, stress fibres are bundles of 10-30 actin filaments that typically interact with myosin motors and are involved in the generation of contractile force in non-muscle cells (Cramer et al. 1997; Pellegrin and Mellor 2007). Stress fibre formation is often modulated by Rho family GTPase signalling events (Ridley and Hall 1992a; Tojkander et al. 2012). Stress fibres are involved in cellular processes including the stabilisation of cell shape (Kumar et al. 2006), production of force (Guolla et al. 2012), and mechanotransduction (Hayakawa et al. 2008; Tojkander et al. 2012). Stress fibres are usually cross-linked into bundles by α-actinin, although this is not the only actin cross-linking protein that has been described at stress fibres. The predominant categories of stress fibres that have been well-described are the following: transverse arcs, dorsal stress fibres, and ventral stress fibres (Figure 1.9 C).

The different types of stress fibres are distinguished by their subcellular localization, association with focal adhesions, dynamics of their actin filaments, and function. Transverse arcs form underneath the lamella in protrusive cells (i.e., migrating cells), are not tethered on either end by a focal adhesions, and are thought to facilitate retrograde movement of actin from the leading edge of to the cell centre, near the nucleus, where dorsal stress fibres undergo disassembly (Heath 1983; Pellegrin and

Mellor 2007). Dorsal stress fibres do not exhibit periodic staining for α-actinin and myosin, are non-contractile, have uniformly aligned actin filaments in terms of polarity, and are attached at one end by a focal adhesion at the base of the cell. The non-tethered end of dorsal stress fibres emanates towards the dorsal surface of the cell and often terminates into a transverse arc at their proximal ends (Pellegrin and Mellor 2007; Naumanen et al. 2008; Tojkander et al. 2012). Dorsal stress fibres play notable roles in cell migration, such as contributing to the maturation of adhesion complexes (Vallenius 2013). Ventral stress fibres (Figure 1.9 C) are the most commonly observed stress fibres and mediate the generation of contractile force. This stress fibre type is found on the ventral side of the cell (i.e., the base of the cell) and is tethered on both sides by separate integrin-rich focal adhesions (Pellegrin and Mellor 2007). While dorsal stress fibres and transverse arcs primarily exert their functions at the leading edge of migrating cells, ventral stress fibres often play role at the trailing edge, with involvement in tail retraction as an example (Pellegrin and Mellor 2007; Tojkander et al. 2012; Vallenius 2013).

Actin dynamics also differ between stress fibre subsets, especially concerning the steps in their assembly (Hotulainen and Lappalainen 2006), although these dynamic events in different types of stress fibres can often converge. Actin filaments in transverse arcs are thought to be derived primarily from actin filaments found at the leading edge (Nemethova et al. 2008), especially Arp2/3-nucleated filaments found in lamellipodia (Hotulainen and Lappalainen 2006). Elongated filaments are bound, cross-linked, and bundled by α–actinin. Bundles of myosin II are subsequently incorporated into nascent arcs. Completion of transverse arc formation takes place through annealing of the smaller actin bundles. As these contractile bundles mature, they move away from the plasma membrane toward the centre of the cell (Hotulainen and Lappalainen 2006; Tojkander et al. 2012). Dorsal stress fibres, on the other hand, are initiated from focal adhesions, complex macromolecular protein assemblies which contribute to the generation of mechanical stability and the forces required for cell movement. Although the precise mechanisms accounting for actin growth from these structures remains elusive, elongation of actin from focal adhesions is thought to be mediated by formins during dorsal stress fibre formation (Le Clainche and Carlier 2008). Elongated filaments are subsequently cross-linked by α–actinin (Hotulainen and Lappalainen 2006). Ventral

stress fibre formation is thought to take place through the interplay between dorsal stress fibres and transverse arcs. As retrograde flow of actin in the lamellipodia drives transverse arcs towards the cell centre, these structures collide with dorsal stress fibres and become attached to their proximal ends. The fusion of dorsal stress fibres and transverse arcs subsequently gives rise to a contractile stress fibre that is anchored by a focal adhesion at each end (Hotulainen and Lappalainen 2006). Ventral stress fibres can also result from the fusion of two dorsal stress fibres (Small et al. 1998; Tojkander et al. 2012). Thus, the regulation of the numerous actin-based structures in cells take place via numerous mechanisms and involve a varied set of proteins. The participation of formins as actin regulatory proteins is often highlighted in the formation of these structures.

1.7 Formins

Where Arp2/3 is responsible for creating branched networks, the family of formin proteins polymerises actin into linear unbranched structures (Figure 1.7 B). Such structures include linear actin filaments seen in filopodia, those required for formation of the cytokinetic contractile ring, as well as filaments in lamellipodia (Wallar and Alberts 2003). Many formins are strong nucleators and can elongate actin filaments in an Arp2/3 independent manner (Pruyne et al. 2002). Unlike Arp2/3, formins act by associating with the barbed ends of actin filaments. Formins do not necessarily inhibit elongation by capping filaments, rather they regulate the rate of monomer addition. They also promote elongation by preventing the association of other capping proteins that would prevent growth otherwise (Moseley et al. 2004; Chhabra and Higgs 2007). Many formins act as dimers through association via their FH2 domains (Chhabra and Higgs 2007). Formins are said to catalyse the nucleation of actin filaments by binding and stabilising the spontaneously formed actin dimers and trimers. They elongate filaments by remaining associated with growing filaments allowing rapid addition of actin monomers (Higashida et al. 2004; Chhabra and Higgs 2007). Structurally similar, formins are not functionally redundant and exhibit different actin elongation kinetics. Coupled with the fact that they exhibit varying levels of expression according to tissue and show distinct subcellular localisation, formins can direct the formation of diverse actin-based structures (Chesarone and Goode 2009). Although formins and Arp2/3 function downstream of distinct effector signalling pathways, this is not to say that they have completely discrete or antagonistic effects. In humans, Arp2/3 and formins

cooperate for leading edge actin-based structures and filopodia formation (Yang et al. 2007). Arp2/3 and formins have been reported to work synergistically in actin polymerisation as electron micrographs have revealed Arp2/3 associated with the pointed end and formins associated with the growing barbed end of the same actin filament (Chesarone and Goode 2009).

Formins are multidomain proteins found in all eukaryotes ranging from yeast, invertebrates, plants, and mammals (Kovar 2006). They are large proteins typically over 1,000 amino acids in length (Higgs 2005). The high degree of structural homology found across all species suggests that they have been conserved throughout eukaryotic evolution. Currently there are 15 mammalian formins documented which have been divided into several groups. Phylogenetic analysis of the formin domains has revealed that they fall into 8 categories which include Diaphanous (Dia), dishevelled associated activator of morphogenesis (DAAM), formin related gene in leukocytes (FRL), formin homology domain containing (FHOD), inverted formin (INF) 1, INF 2, formin/cappuccino (FMN), and delphilin (Higgs 2005; Schulte et al. 2008). The diaphanous related formins (DRFs) mediate cytoskeletal remodelling downstream of Rho family small GTPase signalling events. Through these signalling pathways DRFs have been proposed to link G-protein coupled signals to cytoskeletal rearrangement and modulate gene expression. Formins have been found to participate in important processes requiring motility, including embryonic development and phagocytosis. In fact, the first formin identified, mouse formin 1 was encoded by the mouse limb deformity (*ld*) gene and was thought to be essential for proper limb and kidney formation (Mass et al. 1990; Woychik et al. 1990; Evangelista et al. 2003). However, such defects were eventually attributed to disruption of the gremlin gene (Zuniga et al. 2004). In humans, naturally occurring mutations in formins mDia1 and -3 have also been implicated in non-syndromic deafness and ovarian failure, respectively. Defects in formins have also been proposed to contribute to cancer progression. To date, most of our understanding of formins is derived from research on mDia and Bni1 (Higgs 2005; Kovar 2006).

1.7.1 Formins as Actin Nucleators and Elongators

Formins have been implicated in rearranging both the actin and microtubule cytoskeletons (Bartolini et al. 2008). They have been found to participate in a wide range of cellular roles during cell division, migration, adhesion, and intracellular trafficking (Goode and Eck 2007). During such processes, formins have been found to create a wide array of actin-based structures in cells. Both FMN1 (Kobielak et al. 2004) and mDia1 were found to mediate cell-cell adhesion by assembling radial actin cables and actin rich contacts, respectively (Goode and Eck 2007). mDia1 also participated in the formation of Rho-induced stress fibres (Nakano et al. 1999). Stress fibres are bipolar arrays of bundled actin filaments that interact with myosin II motors, as described above (Naumanen et al. 2008). They create contractile force and are responsible for stabilising the trailing edge of cells during migration and for contracting the rear end of the cell. Although very similar in structure, formins direct the formation of different actin-based structures. For example, the mouse formin mDia2 has been implicated in formation of lamellar filament assembly (Chhabra and Higgs 2007), since lamellipodial formation was inhibited when mDia2 was knocked down by short interfering RNAs (siRNAs) (Yang et al. 2007). Furthermore, in fission yeast (*Schizosaccharomyces pombe)*, formins display very specialised roles in the way that particular formins are required for formation of a given structure which cannot be substituted for by the action of another formin. For example, Cdc12p is responsible for formation of the contractile ring (Chang et al. 1997), For3p is required for actin cable assembly (Chang et al. 1997), and Fus1p is required for conjugation (yeast mating) (Petersen et al. 1998). Similarly in budding yeast (*Saccharomyces cerevesiae*), formins are responsible for the formation of actin cables around the cleavage site during division (Evangelista et al. 2002). Also in yeast, Bni1p and Bnr1p work together to make actin filaments for cell polarisation (Sagot et al. 2002). Formins are continuously being shown to play a number of essential roles in regulation of actin polymerisation in a vast array of cell types.

1.8 DRF Domain Structure

Formin function is best understood by dissecting their structure. Most DRFs characterised so far have been found to share many of the same modular domains (Higgs 2005). DRFs are characterised by formin homology (FH) domains, a GTPase binding domain (GBD), a diaphanous inhibitory domain (DID), and a diaphanous autoregulatory domain (DAD). The structure of a typical DRF is usually GBD-DID-FH1-FH2-DAD (Figure 1.10 A). Formins share most similarity in their carboxy-termini (C-termini) with the highest degree of homology in the FH2 domain and the DAD, both of which contain core consensus sequences. Sequence divergence is more apparent in the amino-termini (N-termini), which contain the GBD and the DID domain. The N-termini of formins usually mediate their subcellular localisation and sequence divergence may confer distinct compartmental targeting to each formin. DRFs can essentially be divided in two halves, with the C-terminal half being the actin polymerisation apparatus and the N-terminus being the regulatory portion of the protein (Goode and Eck 2007). A substantial proportion of information regarding the structure and function of each domain has come from overexpression studies using cell lines and crystallisation studies of mDia1 (Li and Higgs 2003; Li and Higgs 2005; Otomo et al. 2005a; Rose et al. 2005b).

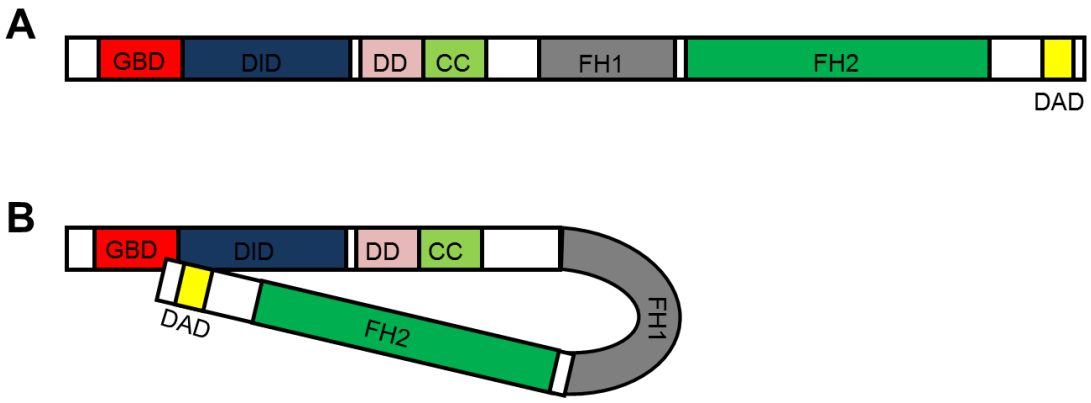

Figure 1.10: Domain Structure of Formins. Schematic representation of the domain structure seen in diaphanous related formins, namely mDia1. **A)** The major domains in the N-terminus include the GBD, DID, as well as a DD and CC. The C-terminus contains the FH1, FH2, and DAD. **B)** mDia in its autoinhibited closed confirmation. The protein is maintained in an inactive state via an autoinhibitory intramolecular interaction via its N-terminal DID and its C-terminal DAD until binding by a Rho family small GTPase in the GBD, which alleviates the interaction. GBD, GTPase binding domain; DID, diaphanous inhibitory domain; DD, dimerization domain; CC, coiled coil motif; FH, formin homology; DAD, diaphanous autoregulatory domain.

1.8.1 The FH2 Domain

The formin homology (FH) 2 domain is the most highly conserved among DRFs (Figure 1.10 A). Although originally thought to span ~100 amino acids, sequence comparison among formins has revealed that the FH2 domain actually spans ~500 amino acids. It normally lies downstream of the FH1 domain towards the C-terminus and is the largest domain, containing many bundles of α-helices (Paul and Pollard 2009). The FH2 domain is the actin interacting portion of formins. More importantly, it drives actin nucleation as it has been found that recombinant FH2 domains alone were enough to create actin filaments (Pruyne et al. 2002; Chhabra and Higgs 2007). In mammalian cells the FH2 domain of mDia was sufficient to induce accumulation of polymerised actin (Copeland and Treisman 2002). The FH2 domain also associates with the barbed end of actin as has been made evident in fluorescent microscopy studies in *Xenopus* fibroblasts, using the GFP-tagged FH2 domain from mDia1 and 2 (Higashida et al. 2004). The precise mechanism by which the FH2 domain interacts with actin and polymerises it is still somewhat disputed but crystallisation studies have provided some insight. Co-crystal structures of formin FH2 domains and actin have revealed that the FH2 domains form flexible but stable doughnut shaped dimeric rings around actin (Kovar 2006). Each side contacts with actin, with up to 4 total contacts proposed. It is also apparent that each side only has one contact with actin at any time. Dimerisation of the FH2 domain is essential for formin function. Crystal structures have revealed that an FH2 hemidimer bridges two actin subunits, hence it can contribute to the stabilisation of nucleation seeds (Chesarone and Goode 2009). The FH2 domain is thus interacting with actin in a dynamic equilibrium involving rapid cycles of association and dissociation. This would make processive movement possible as formins remain associated with the growing end of actin filaments. Different models of processive association have been proposed. Most evidence points to formins processively moving with filaments via a stairstep mechanism (Zigmond et al. 2003; Xu et al. 2004). This involves the addition of a new actin monomer followed by the dissociation of the FH2 domain from the previous monomer and re-association with the new one (Chesarone and Goode 2009) (Figure 1.11). However there are reports of other models such as the stepping second mechanism (Paul and Pollard 2009). Overall, the

FH2 domains dimerise to form head-to-tail dimers that are thought to wrap around the barbed ends of actin filaments like a sleeve (Xu et al. 2004; Otomo et al. 2005b). The FH2 domain can influence actin dynamics by increasing rate of nucleation, altering elongation rate, and preventing barbed end capping (Higgs 2005).

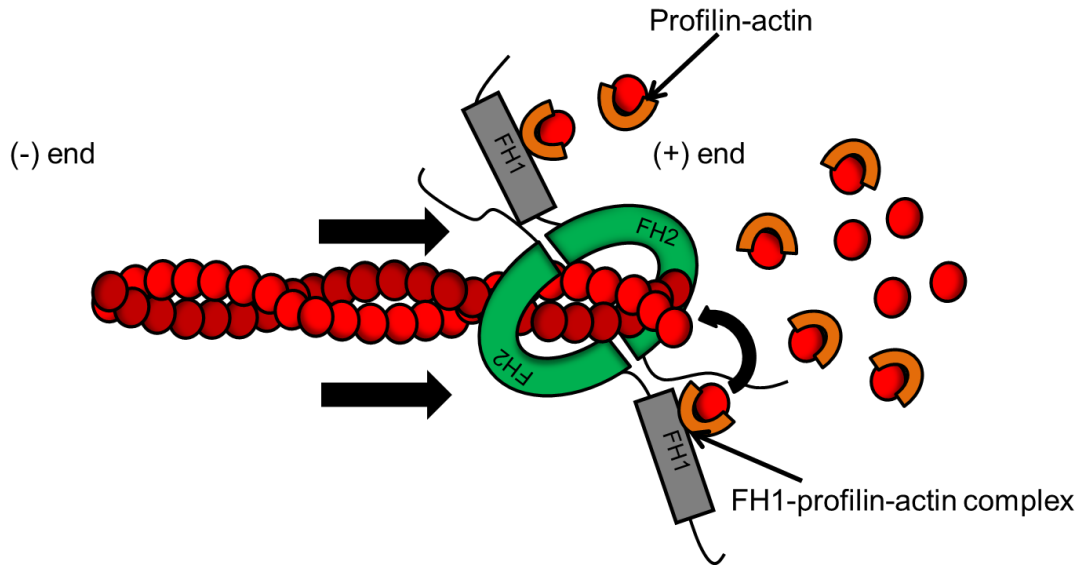

Figure 1.11: Formin Mediated Actin Assembly. Schematic representation of formin mediated actin assembly. Formins dimerise via their FH2 domains, which create doughnut shaped antiparallel dimers. The FH2 domains bind actin and polymerise filaments by remaining processively associated with their growing barbed ends and facilitating the addition of profilin-actin monomers. The FH1 domain functions by binding profilin-actin monomers and concentrating them at the growing ends of filaments. Profilin is seen in orange, actin in red, the FH1 domains in grey, and the FH2 domains in green. (+), barbed end; (-), pointed end).

1.8.2 The FH1 Domain

N-terminally to the FH2 domain lies the FH1 domain (Figure 1.10 A). The FH1 domain of DRFs contains varying numbers of stretches of polyproline residues and is less conserved than the FH2 domain. These polyproline tracks (PPPPP) are predicted to form type II polyproline helices (Rivero et al. 2005). This results in FH1 domains that are much less structured, rope-like domains capable of mediating a number of protein interactions (Chhabra and Higgs 2007; Chesarone and Goode 2009). In terms of protein interactions, FH1 domains have been found to bind Src homology (SH) and Wasp homology (WH) domains (Young and Copeland 2010). For instance, the FH1 domain

of the yeast formin Bnr1p binds the SH3 domain of Hof1p in a Rho dependent manner to regulate cytokinesis (Vallen et al. 2000). More notably yet, the FH1 domain binds profilin with high affinity through its polyproline motifs as shown by co-immunoprecipitation experiments (Watanabe et al. 1997). Binding on profilin occurs on a groove with a stretch of highly conserved aromatic amino acids (Schutt et al. 1993). As mentioned previously, profilin is an actin binding protein that sequesters G-actin. It prevents spontaneous nucleation of actin filaments but facilitates the elongation of F-actin by rapidly mobilising them to the barbed end (Higgs 2005; Chhabra and Higgs 2007). The interaction between the FH1 domain and profilin-actin has been found to be central to the actin polymerisation activity of formins. Profilin greatly accelerates elongation of filaments associated with FH1 and FH2 domains (Kovar et al. 2003; Romero et al. 2004) and profilin-actin binding to the FH1 domain has been shown to be the rate limiting step in formin mediated actin polymerisation (Paul and Pollard 2008). It has been proposed that the FH1 domains concentrate profilin-actin monomers near the barbed end of an actin filament (Figure 1.11). Experiments also suggest that the FH1 domain functions by passing profilin-actin monomers to the FH2 domain in the correct orientation for addition (Higgs 2005). The FH1-profilin-actin complex may form a transient ring like structure by interacting with the FH2 domain by virtue of the flexibility that the FH1 domains possess. The actin monomer binds the FH2 domain and is then added to the growing filament followed by dissociation of the FH1-profilin-actin-FH2 ring (Vavylonis et al. 2006). Together, the FH1 and FH2 domains have been shown to remain processively associated with the growing ends of actin filaments (Kovar and Pollard 2004). Overall, the FH1 domain is required for the actin polymerising activity of formins by facilitating the addition of profilin-actin at the growing ends of actin filaments (Chang et al. 1997).

1.8.3 The DID and DAD

Formins are held in an inactive conformation through an interaction between the N-terminal DID and the C-terminal DAD (Figure 1.10 B). The DAD is not necessarily a domain but really only a stretch of 20-30 amino acids found downstream of the FH2 domain (Higgs 2005). The intramolecular interaction masks the FH1 and FH2 domain, preventing their association with actin and other accessory proteins. Evidence for this

autoinhibitory mechanism first came from experiments using constructs of mDia1 and mDia2 (Watanabe et al. 1999). Truncation mutations lacking the DAD or N-terminal region resulted in activation (Higgs 2005). Activation is commonly achieved by binding of a Rho family small GTPase in the GBD, which is usually N-terminal to the DID. It has also been shown that Rho GTPases have to be activated in order to bind the GBD of formins (Tominaga et al. 2000). This partly alleviates the intramolecular interaction by displacing the DID from the DAD. However, activation may not be merely due to steric displacement and could be the result of a more complex process. Overall, formins are self-regulated by this autoinhibitory mechanism to prevent aberrant actin polymerisation.

1.9 Regulation of DRFs by Rho Family Small GTPases

Rho family small GTPases are a subgroup of the Ras superfamily of GTP-dependent enzymes. They link extracellular stimuli to intracellular signalling cascades that induce cytoskeletal rearrangements (Heasman and Ridley 2008; Naumanen et al. 2008). This partly occurs through binding and modulating the effector proteins that dictate cytoskeletal structure. As their name partly suggests, Rho GTPases are GTP binding proteins. They become activated upon binding GTP and become inactive upon hydrolysis of GTP to GDP, by virtue of their intrinsic GTPase capability (Figure 1.12). Regulation of Rho GTPases takes place through guanine nucleotide exchange factors (GEFs), GTPase activating proteins (GAPs), and guanine nucleotide-dissociation inhibitors (GDIs) (Heasman and Ridley 2008). Rho GTPases are central in regulating many processes including the cell cycle, cell morphology (Braga 2000), and cell adhesion (Lozano et al. 2008).

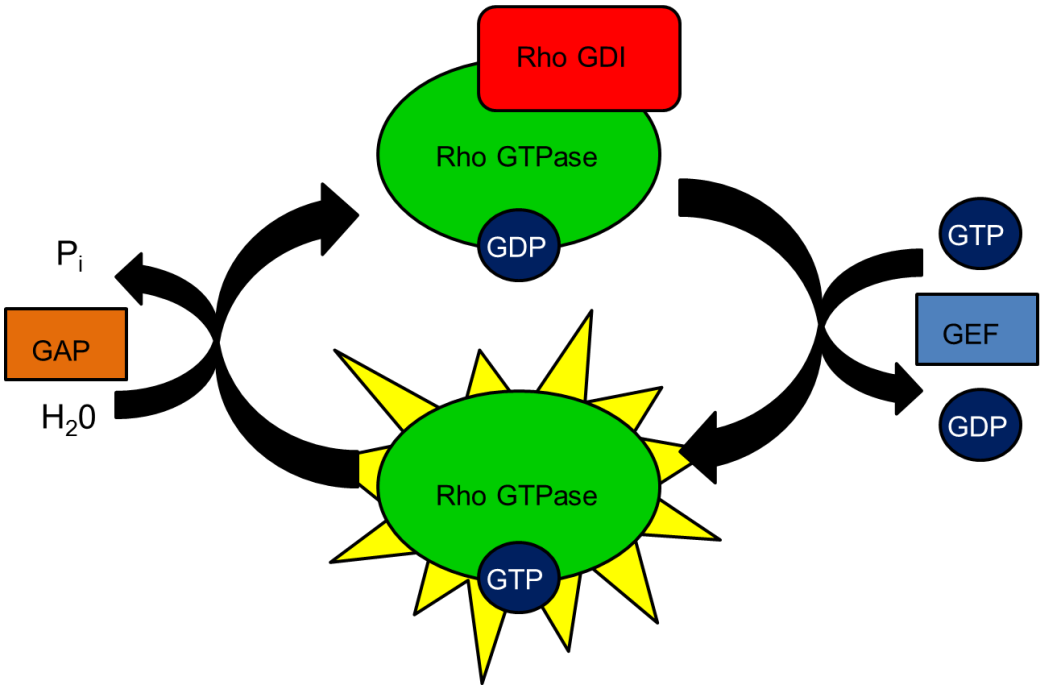

Figure 1.12: The GTPase Cycle. Schematic diagram showing the mechanism underlying the regulation of Rho GTPases. In their GDP bound state, Rho GTPases are inactive. Rho GDP dissociation inhibitor (GDI) prevents dissociation of GDP. Activation is achieved upon binding GTP, which is facilitated by interactions with guanine nucleotide exchange factors (GEFs). Subsequent deactivation is achieved through hydrolysis of GTP to GDP, which is stimulated through an interaction with a GTPase activating protein (GAP). GTP, guanosine triphosphate; GDP, guanosine diphosphate.

Mammalian Rho GTPases include over 20 intracellular signalling molecules, the most extensively studied being RhoA, Rac, and Cdc42 (Heasman and Ridley 2008). Rho GTPases signal the formation of a variety of actin-based structures. For example, all three Rho isoforms have been shown to induce the formation of stress fibres (Wheeler and Ridley 2004). Rho isoforms also play roles in a number of cellular processes such as endosomal trafficking (Ellis and Mellor 2000) and regulation of cell-cell contact formation (Braga et al. 1997). RhoA was one of the first of the small GTPases to be identified (Ridley and Hall 1992b). Its role in cytoskeletal organisation has been frequently highlighted and it is generally thought to participate in the formation of stress fibres (Ridley and Hall 1992a). RhoA has a number of downstream targets that mediate cytoskeletal regulation. One well characterised pathway involves the kinase ROCK. GTP-bound RhoA binds and activates Rho associated protein kinase (ROCK) I and II (Alberts et al. 1998; Ridley 2006). ROCK then phosphorylates and activates LIMK

(Ohashi et al. 2000) which subsequently phosphorylates and inactivates the actin filament severing protein cofilin (Yang et al. 1998). This has the effect of stabilising actin-based structures in cells. ROCK-I is one of the major effector molecules that lies downstream the RhoA pathway (Ridley 2006). ROCK-I participates in the signalling events that link G-protein mediated signals, such as thrombin activation in vascular cells, to cytoskeletal remodelling (Takeya et al. 2008). ROCK-I is classically associated with mediating the formation of stress fibres (Pellegrin and Mellor 2007).

Rac stimulate formation of lamellipodia and membrane ruffling (Ridley et al. 1992; Ridley and Hall 1992b) and have been demonstrated to be involved in processes such as mediating axonal guidance in the brain (Chen et al. 2007). The effects of Rac are sometimes thought to be antagonistic to the action of Rho although the Rho/ROCK pathway and Rac signalling can both converge at the level of cofilin inhibition. However, instead of acting on ROCK, activated Rac acts on the kinase PAK (Knaus et al. 1998). PAK then phosphorylates LIMK which then inactivates cofilin (Edwards et al. 1999; Ridley 2006). Rac acts via numerous signalling pathways and can play diverse roles therefore the above description is by no means exhaustive. For example, Rac is a component of the Nox2-dependent NADPH oxidase complex in cardiac cells. In this context, Rac has been shown to be essential in promoting the association of the cytosolic components with the membrane bound components of the complex (Satoh et al. 2006).

Another well studied member of the Rho family small GTPases, Cdc42 has been primarily implicated in the formation of filopodia (Zamudio-Meza et al. 2009). Cdc42 has been shown to participate in processes like regulation of cell polarity and was found to do so via the polarity protein partitioning-defective-6 (PAR6) complex (Etienne-Manneville and Hall 2003). Cdc42 can also bind to WASP and N-WASP (Rohatgi et al. 2000) to stimulate actin polymerisation via the Arp2/3 complex (Ridley 2006). The wide array of structures formed by members of the Rho family small GTPases thus vary between cell type and depend on their interacting partners.

DRFs are regulated by multiple GTPases. They were found to be activated by Rho family members including Rho, Rac, Cdc42, and Rif (Pellegrin and Mellor 2005; Kovar 2006; Goh et al. 2011). The interaction between a given Rho family GTPase and a

formin have been shown to drive specific cellular processes. For example, the interaction between RhoB and mDia2 was shown to drive the events required for endosomal trafficking (Wallar et al. 2007), whereas the interaction between Rac and mDia2 was required for contractile actin ring formation during erythroblast enucleation (Ji et al. 2008). Conversely, formins have also been found to regulate Rho GTPase activity. The FH2 domain of mDia1 was found to bind Rho-GEF LARG, which lead to activation of RhoA (Kitzing et al. 2007). Although the basic consensus regarding DRF activation is that activation is achieved by binding of a Rho family member within the N-terminus of the formins, the mechanism may be more complicated than previously thought. This has been illustrated by the fact that RhoA was shown to bind the N-terminus of mDia1 with high affinity, but this only resulted in minimal activation of the DRF (Li and Higgs 2003; Goode and Eck 2007). However, regulation of formins is not restricted to direct interactions with GTPases. A number of formins, including Bni1p (Evangelista et al. 2003), FHOD1 (Takeya et al. 2008), and FHOD3 (Iskratsch et al. 2013a) have been found to be regulated by phosphorylation. Nevertheless, the dominant mechanism by which formin activity and localisation is regulated seems to be Rho family small GTPase mediated.

1.10 Formins and Cell Signalling

Formins have also been found to initiate signalling to mediate cytoskeletal rearrangements and to regulate gene expression in the nucleus. A number of studies have indicated that such signalling may be bridged by Src. Src is a member of the Src family of non-receptor tyrosine kinases. Src activity is often associated with cancer biology, namely metastasis, as it participates in regulation of cell motility and gene transcription (Summy and Gallick 2003). Src regulates adhesive structures and integrin-cytoskeletal interactions (Felsenfeld et al. 1999) through the phosphorylation of key focal adhesion proteins. One notable function of this kinase is that it phosphorylates focal adhesion kinase (FAK) to promote turnover of focal adhesions (Parsons 2003). Interestingly, Src also participates in Rho mediated signalling that culminates in events like phosphorylation of important cytoskeletal regulators or transcription from the SRE.

Src activity has been found to lie downstream of many formins (Tominaga et al. 2000). Src regulates a number of processes ranging from cell differentiation, migration, but its role is most frequently highlighted in oncogenesis and tumour metastasis since it was found in the Rous sarcoma virus (Guarino 2010). The cross talk between formins and Src appears to be rather complex. In one instance, mDia1 was found to indirectly regulate focal adhesion turnover by regulating the targeting of Src to focal adhesions in a cancer cell line (Yamana et al. 2006). Src has also been shown to bind DRFs via its SH3 domain. The mDia-Src interaction mediates signalling to the serum response element (SRE) (Tominaga et al. 2000; Evangelista et al. 2003). The SRE is a short gene regulatory sequence that controls transcription of immediate early genes like c-fos and β-actin upon growth factor stimulation. It involves activation of the serum response factor (SRF) transcription factor which stimulates transcription after binding to promoter regions (Westendorf 2001; Miano et al. 2007). It was found that mDia1 and 2 along with Src signalled downstream of Rho and activated transcription from the SRE independently of ROCK and profilin (Tominaga et al. 2000). FHOD1 was also found to be a potent stimulator of gene expression from the SRE (Westendorf 2001) and may directly involve its proposed actin regulatory activities as well as cross-talk with well-established cytoskeletal regulators, such as Src, which are discussed below. SRF activation appears to be a common target of formins, but especially of formin homology proteins.

1.11 Other Activities of Formins

Formins are classically viewed as actin nucleators and elongators. These notions have predominantly stemmed from *in vitro* experiments using purified formin proteins. Such studies have described how formins nucleate actin filaments, exhibit processive movement along actin filaments while protecting the filament from capping proteins, and have described the interplay between formins and profilin in accelerating the rate of actin filament elongation (Harris and Higgs 2006; Breitsprecher and Goode 2013). However, numerous studies have emerged describing other roles of formins, which has led to views regarding canonical formin activities to further include other cytoskeletal related processes, aside from actin polymerisation. Other activities of formins that have

been described include actin bundling, actin severing, actin depolymerisation, and, more-notably, the regulation of microtubules.

1.11.1 Formins as Actin Bundlers

The bundling activity of formins has been explored in a number of studies. One study found that FRL1 and mDia2 were capable of bundling filaments, whereas mDia1 was not (Harris et al. 2006). Furthermore the FH2 domain was sufficient to induce the bundling associated with these formins. Fluorescence and electron microscopy experiments revealed that FRL1 and mDia2 did not result in a cross-linked morphology of their actin networks, but rather induced the formation of thick actin bundles. In the same experiment, it was found that FRL1 associated with its bundled network and that this was purported to be mediated by its previously reported actin side binding activity (Harris et al. 2004; Harris et al. 2006). Similarly, FRL2 and 3 have also been documented to possess actin bundling activity *in vitro*, as measured by F-actin pelleting assays (Vaillant et al. 2008). The exact contribution of formin-induced actin bundling with respect to the formation of cellular structures is not always clear, however. While FRL2 and mDia2 both possess actin bundling activity and induce the formation of filopodia, which require bundled actin filaments, it is unclear which function of these formins (i.e., nucleation, elongation, or bundling) contributed to filopodial formation (Harris et al. 2010). While bundling activity at the filopodial tip could be a possibility, an elongation function seems more appropriate since elongators are likely to exert their function at the tips of filopodia according to the more-accepted models of actin filament elongation within these structures. More-recent efforts, which have tried to resolve the gap between this formin function and its effect on actin-based structures, have identified DAAM-1 as playing a crucial role in maintaining filopodial integrity via its actin bundling activity. One study found that DAAM-1 is a potent actin bundler that is bound and stably recruited by fascin along the filopodial shaft, where it binds to the sides of fascin-bundled filaments (Jaiswal et al. 2013). Furthermore, silencing of DAAM-1 resulted in perturbed filopodial structure and reduced filopodial density, thereby suggesting that its actin bundling activity is crucial for the maintenance of filopodia. FHOD1, which is further discussed below, also possess bundling activity (Schonichen et al. 2013) and has been found to play a role in the formation of bundled actin structures, particularly stress fibres (Takeya et al. 2008; Schulze et al. 2014).

1.11.2 Formins as Actin Severing and Actin Depolymerisation Factors

The abilities of formins to nucleate and elongate filaments also extend to a seemingly converse function, with reports of formins severing actin filaments and accelerating their depolymerisation (Breitsprecher and Goode 2013). This was the particular case in a study which examined the mouse formin INF2. A construct containing the functional domains and C-terminus of INF2 was found to behave similarly to other formins in that it inhibited the elongation of filaments in the absence of profilin, and accelerated the elongation kinetics in the presence of profilin-bound actin monomers (Chhabra and Higgs 2006). Interestingly, at higher concentrations, this construct was also found to have a biphasic effect on actin kinetics in that it first stimulated polymerisation followed by depolymerisation. This effect was not present in experiments utilizing mDia1 and FRL1. Furthermore, addition of P_i (inorganic phosphate) abolished INF2's depolymerisation activity but had no effect on its ability to polymerise filaments, thereby suggesting that release of P_i during the ATP hydrolysis event that takes place during actin polymerisation could be a stimulator of INF2's depolymerising activity. INF2's ability to depolymerise filaments was partly attributed to its C-terminal portion, which was found to sequester actin monomers and prevent elongation from the barbed end. However, it was also found that the FH regions were required along with the C-terminus, and that these portions bound to the side of actin filaments and resulted in their severing, an activity that more-likely contributed to the enhanced depolymerisation rates noted rather than just monomer sequestration by the C-terminus alone. Furthermore, a WH2 motif was also found to partly mediate the depolymerisation activities of INF2, although it could conceivably have contributed less to the severing activity of the protein (Chhabra and Higgs 2006). Actin filament severing has not been limited to INF2 since FRL1 has also been reported to sever actin filaments in order to create new barbed ends for subsequent elongation (Harris et al. 2004).

1.11.3 Formins and the Regulation of Microtubules

More-substantial evidence has also emerged implicating formins in the regulation of microtubules than in the aforementioned supplementary functions (Bartolini and Gundersen 2010). Microtubules, essential components of the cytoskeleton, are dynamic structures composed of polymers of 12-15 protofilaments, made of α/β tubulin heterodimers (Bartolini and Gundersen 2010). Microtubules play a number of essential roles within the cell ranging from vesicular transport and cell division to cell motility and polarity. Formins have generally been shown to regulate microtubule dynamics by binding and stabilising microtubules directly, by affecting microtubule dynamics via an interaction with an accessory protein, and/or affecting the post-translational state of microtubules (Breitsprecher and Goode 2013). One study found that the functional FH domains of mDia2 were sufficient to directly bind and stabilise microtubules under disassembly conditions (Bartolini et al. 2008). mDia was also reported to associate with EB1 and APC, two microtubule-end binding proteins, and through the cooperation of this complex of proteins, contributed to microtubule stability and the promotion of cell migration (Wen et al. 2004). Formins can also promote stabilisation of microtubules by inducing their acetylation. One study implemented active constructs of nearly every mammalian formin and revealed that the induction of microtubule acetylation was a function common to many formins, albeit to varying degrees (Thurston et al. 2012). Furthermore, constructs solely comprised of the functional FH domains were sufficient to induce acetylation for most formins.

While the description of formin activities that extend beyond their actin nucleation and elongation activities pose fundamental questions about the involvement of these processes in regulating higher order cytoskeletal structures as well as their involvement in broader cellular functions, this area of research requires further investigation. Indeed, the regulation of microtubules by formins could be a function more common among the class, since not every formin that has been tested has necessarily been found to possess bundling, severing, and disassembly activity.

1.12 FHOD1

1.12.1 The Formin Homology Protein, FHOD1

Formin homology proteins are a subfamily of DRFs and Rho family dependent effectors. Like other formins, they are actin regulators, and also play important roles in organogenesis, tissue homeostasis, and cancer cell division (Katoh 2004). In humans the FHOD protein that has been best characterised thus far is the formin homology 2 domain containing protein 1 (FHOD1) (Figure 1.13). FHOD1 was first discovered as a binding partner for the acute myeloid leukaemia (AML1β) transcription factor in the littoral cells of the spleen (Westendorf et al. 1999). Formerly known as formin homology overexpressed in the spleen (FHOS), its name was changed to FHOD1 to meet the criteria on Guidelines for Human Gene Nomenclature. The originally described FHOD1 isoform is a 1,165 amino acid protein with a molecular weight of ~128kDa. It is translated from a 4kb mRNA transcript which is transcribed from the *FHOD1* gene (Gene ID: 29109) found on human chromosome 16q22.1. The gene is comprised of a 3,495bp open reading frame (ORF) with an 18bp stretch in the 5' untranslated region (UTR) and a 260bp 3' UTR containing polyU termination signals. The gene contains an inframe STOP codon at position 18 (Westendorf et al. 1999)

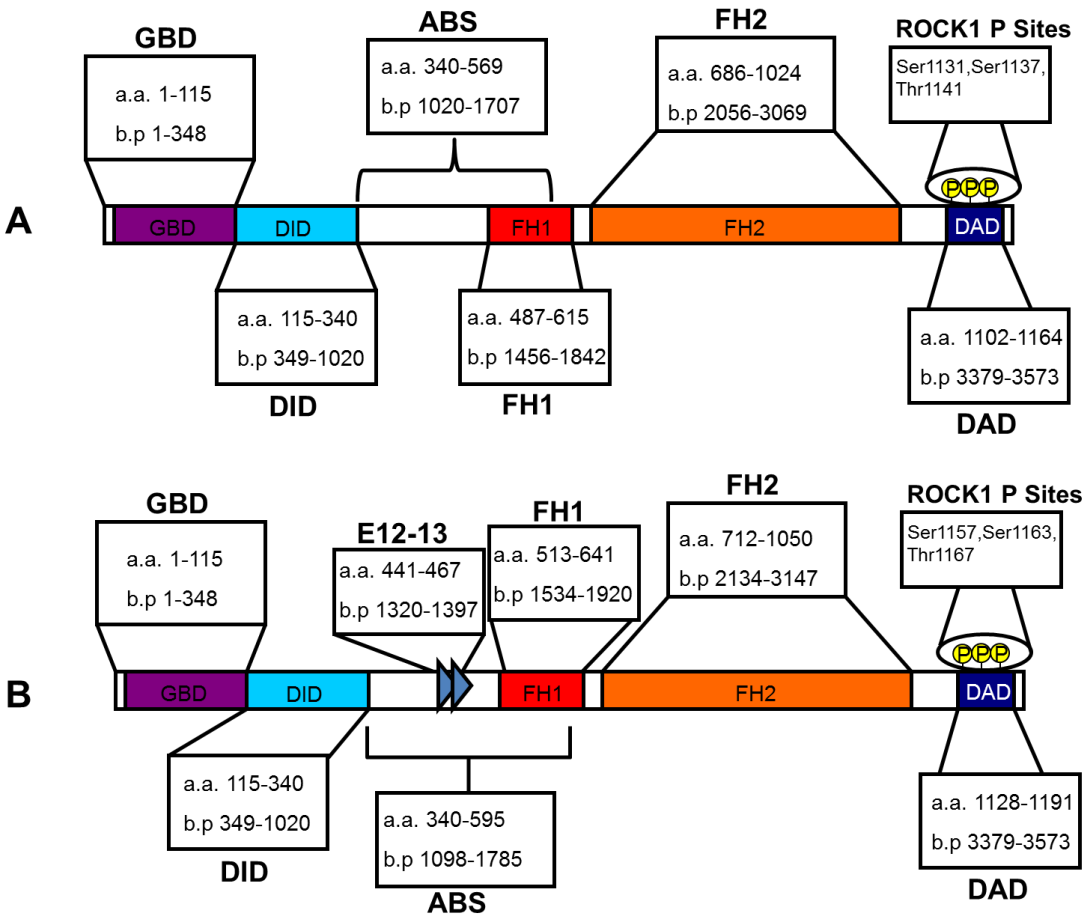

Figure 1.13: Domain Map of FHOD1. A) Schematic representation of the full length short variant of human FHOD1. **B)** Schematic representation of the full length long variant of human FHOD1. The major FHOD1 domains are shown including the alternatively spliced exons (E12-13) found in the larger FHOD1 isoform. The ROCKI phosphorylation sites are also highlighted in the DAD. Domain borders are highlighted and include the amino acid (a.a.) lengths and their corresponding base pair (b.p.) sequence on the *FHOD1* DNA sequence. The domains downstream of the alternatively spliced exons are labelled with respect to the long FHOD1 amino acid and base pair sequence. GBD, GTPase binding domain; DID, diaphanous inhibitory domain; FH, formin homology; DAD, diaphanous autoregulatory domain; ABS, actin binding site

Initial sequence comparison of FHOD1 revealed that it was homologous to other DRFs within its C-terminus, namely between amino acids 716-1070. Characterisation initially revealed a relatively small FH1 domain of 42 amino acids containing only 3 polyproline stretches, although this region is actually larger. The FH2 domain was found downstream of the FH1 domain and was within the region spanning amino acids 716-1070. The N-terminus of FHOD1 bears the lowest homology to other formins (Westendorf et al. 1999). FHOD1 was also found to have a DID, also referred to as the FH3 domain. The DID of FHOD1 has been reported to span amino acids 115-340. Crystal structures have shown it is composed of repeat bundles of 14 α-helices followed

by 4 armadillo repeats to form an elongated superhelical domain (Schulte et al. 2008). Other features of the protein included a coiled-coil motif, a Glycine-Proline rich collagen like domain, a potential bipartite nuclear localisation signal (NLS), a basic NLS, and a number of putative phosphorylation sites for kinases like PKA and PKC (Westendorf et al. 1999). The coiled-coil motif, found C-terminal to the core FH2 domain but within the boundaries of the larger FH2 domain, is central to the function of FHOD1. It mediates self-association of the protein, a prerequisite for its actin regulating activity (Madrid et al. 2005). The layout of FHOD1 is very similar to other DRFs and has allowed studies to extrapolate on the function of this formin.

Analysis of expression patterns showed that FHOD1 was expressed in many haematopoietic cell lines and it was first thought to be involved in antigen internalisation, B cell or erythrocyte maturation, as well as splenic development (Westendorf et al. 1999). FHOD1 mRNA was found to be transcribed in the spleen, lymph nodes, bone marrow, peripheral blood lymphocytes, and liver. Fainter expression was observed in muscle, lung, heart, kidney, and colon. Expression is absent from the central nervous system (Gill et al. 2004). Another study noted substantial expression of FHOD1 in vascular smooth muscle cells (VSMCs) and vascular endothelial cells in the aortic and coronary vasculature (Wang et al. 2004). More recent studies also found that FHOD1 is the most abundantly expressed formin in mouse megakaryocytes and is also expressed in platelets (Thomas et al. 2011). Furthermore, expression of FHOD1 protein was confirmed in SMCs, aorta, bladder, brain, lung, skeletal muscle, stomach and testis by Staus et al. 2011. However, this study did not note any FHOD1 protein expression in the heart (Staus et al. 2011a) which would contradict previous work that found FHOD1 mRNA in heart (Gill et al. 2004). These differences could be explained due to antibody specificity or species-specific differences in FHOD1 expression. Although widely expressed, FHOD1 has been found to undergo differential alternative splicing. Tojo et al. 2003 described two different splice variants of the FHOD1 mRNA transcripts. One contained a 78bp insertion (exon 12-13) and was found to be mainly expressed in skeletal muscle and faintly in the heart and was 1,191 amino acids in length (Figure 1.13). The second variant had a 24bp insertion which encoded a STOP codon to form a truncated protein. This variant was found to be expressed in all tissue except skeletal muscle (Tojo et al. 2003).

A more-recent study took an immunohistochemical approach in the hopes of delineating FHOD1's expression pattern in 26 human tissues and found that FHOD1 was widely expressed in a variety of tissues, but was restricted to certain cell types. The most intense staining for FHOD1, using a polyclonal rabbit anti-FHOD1 antibody generated by the Human Protein Atlas (HPA) programme, was seen in the small blood vessels of the spleen, endometrium, ovary, and in peritoneal vessels below the mesothelium (Gardberg et al. 2013). Another study looking at expression level of all 15 formins in 22 different human cell and tissue types using quantitative real-time polymerase chain reaction (qRT-PCR) found that FHOD1 was the most abundantly expressed formin across the different samples that were tested. Interestingly, FHOD1's sister homolog, FHOD3, was found to display the lowest expression levels as well as contrasting expression pattern to FHOD1 in muscle. FHOD1 expression was higher in cardiac muscle than in skeletal muscle, whereas expression of FHOD3 was higher in skeletal muscle than in cardiac muscle (Krainer et al. 2013). Furthermore, these findings were also confirmed by Western blotting, thus strengthening their validity.

1.12.2 Cellular Roles of FHOD1

The capacity of FHOD1 to regulate the actin cytoskeleton has been thoroughly explored in a number of studies. Koka et al. 2003 found that FHOD1 enhances cell migration in an integrin dependent manner using transfection studies. FHOD1 overexpressing cells were found to have elongated morphology. It was found that activated FHOD1 was targeted to actin and stabilised stress fibre formation and that this was dependent on the presence of the FH1 and FH2 domains. The FH1 domain is required for actin reorganisation whereas the FH2 domain is needed for self-association of FHOD1 (Koka et al. 2003; Takeya and Sumimoto 2003). Further to these early studies, the mechanisms of FHOD1 mediated cell elongation were clarified when it was shown that FHOD1 also coordinated microtubules by causing them to align along the long axis of the cell and overlap with stress fibres (Gasteier et al. 2005). N-terminal FHOD1 constructs also revealed that the first 421 residues are crucial to mediating its subcellular targeting to cell peripheries (Koka et al. 2003). This was in agreement with previous studies that found FHOD1 localising to membrane edges and cell extensions (Westendorf 2001). Another study found that the N-terminus of FHOD1 is responsible

for its F-actin binding activity. Using active FHOD1 mutants lacking the N or C-termini it was also noted that in COS-7 cells FHOD1 formed thick actin stress fibres and localised to these structures (Takeya and Sumimoto 2003). It was also shown that stress fibre induction upon FHOD1 activation was dependent on the association of FHOD1 with the actin-based structures and that these effects were independent of Arp2/3 (Gasteier et al. 2003). The upstream signalling events that dictated stress fibre formation were also concluded to be a product of Rho-ROCK signalling and were Src-independent (Koka et al. 2005).

While it has become well established that activation of FHOD1 predominantly results in a stress fibre phenotype, this has begged the question as to whether FHOD1 is mediating stress fibre formation through actin reorganisation rather than promoting nucleation/elongation of actin filaments. One study tested FHOD1 using *in vitro* actin polymerisation assays and found that it inhibited actin polymerisation and that this inhibition was intensified upon FHOD1 activation. Even in the presence of profilin, FHOD1 only possessed a weak capacity to elongate actin filaments compared to mDia1 (Schonichen et al. 2013). Instead, *in vitro* actin bundling assays, performed by way of centrifugation assays and electron microscopy analysis, revealed that FHOD1 bundles pre-existing actin filaments and that its bundling activity was increased upon activation. Furthermore, while the barbed end capping activity of FHOD1 was mediated by the FH2 domain, its actin bundling activity was dependent on the presence of the N-terminal actin binding domain. This notion was confirmed in localization studies using neuroblastoma cells expressing constitutively active Rac1 and in COS7 cells. Wild-type FHOD1 and an N-terminal construct of FHOD1 (amino acids 1-573; FHOD1 short variant) co-localised with actin arcs and stress fibres whereas a truncation mutant of FHOD1, lacking the N-terminus but retaining the FH2 domain, did not (Schonichen et al. 2013). The observation that FHOD1 N-terminus is required for its stress fibre bundling activity was consistent with previous reports of the actin binding activity of this region (Takeya and Sumimoto 2003). A subsequent study attempted to elucidate the mechanisms by which FHOD1 regulates stress fibre formation and revealed that FHOD1 stimulated the formation/organization of and is preferentially associated with transverse arcs and ventral stress fibres but actually inhibited dorsal stress fibre growth (Schulze et al. 2014). The involvement of the FHOD1 N-terminus was once again probed and it was found that the GBD-DID portion of FHOD1 mediated its targeting to

stress fibres and co-localisation with myosin II. However, this is in sight contrast to previous studies which identified the linker region and helical domain of FHOD1 as the actin binding site that lies outside the FH2 domain (Figure 1.13) (Schonichen et al. 2013). Regardless of the position of any additional actin binding sites/activity found outside of the FH2 domain, it has become clear that FHOD1 is involved in regulating the dynamics of specific stress fibre types and that this activity could extend beyond the archetypal actin nucleation/elongation functions that are readily ascribed to formin proteins.

Although *in vitro* studies suggest that FHOD1 preferentially caps the barbed ends of actin filaments rather than elongating them, the involvement of this formin in the formation of cell-matrix adhesions (i.e. focal adhesions) in the context of cell spreading have indicated its potential capacity to polymerise actin (Iskratsch et al. 2013b). The initiation of focal adhesion formation takes place through receptor-matrix binding along the cell periphery, and namely involves the integrins, a family of heterodimeric transmembrane ECM receptor proteins (Campbell and Humphries 2011). Integrin binding to ECM ligands results in clustering and the propagation of a number of signalling events that contribute to focal adhesion growth. The activation and recruitment of Src is one of the earliest events in focal adhesion initiation (Hamadi et al. 2009) and is important in driving the recruitment and activation of focal adhesion components via phosphorylation of key proteins such as FAK, which in turn phosphorylates other adhesive components and further contributes to focal adhesion formation (Parsons 2003). Furthermore, integrin clustering results in initiation of the Src family kinase (SFK)-dependent actin polymerisation events that are required for cell spreading (Yu et al. 2011), although the precise actin polymerisation machinery has yet to be identified. Iskratsch et al. 2013 found that FHOD1 was recruited to early integrin clusters in a SFK-dependent manner and this occurred upstream of ROCK activation. FHOD1 depletion was also found to reduce actin polymerisation at integrin clusters, to cause impaired cell spreading, and impaired early adhesion maturation into focal adhesions (Iskratsch et al. 2013b). These findings occurred in contrast to FHOD1's proposed capping activity (Schonichen et al. 2013) but asserted previous claims that FHOD1 can enhance actin polymerisation *in cyto* (Watanabe et al. 1999; Gasteier et al. 2003; Gasteier et al. 2005; Koka et al. 2005). One possibility could be that FHOD1

could elongate pre-existing filaments and this could be a tightly spatio-temporally regulated process that is controlled by effector molecules like the SFKs.

As with other DRFs, initial efforts found that FHOD1 was a potent transcriptional activator of the SRE. These data were ascertained using N and C-terminal FHOD1 truncation mutants which rendered the protein active, thus having caused it to stimulate transcription from the SRE (Westendorf 2001; Gasteier et al. 2003). Gene expression from the SRE was found to be dependent on ERK/MAPK activation and the native skeletal actin promoter was activated through FHOD1 via the SRF binding site (Boehm et al. 2005). Furthermore, FHOD1 was shown to directly interact with components of ERK/MAPK pathway by co-immunoprecipitation: FHOD1 directly interacted with MEK and Raf-1 and associated with these signalling effectors at stress fibres and lamellipodia, respectively. Self-association of FHOD1 was also found to be required for its transcriptional activity, since deletion of the coiled-coil motif prevented SRE transcription (Madrid et al. 2005). Subsequent work then noted that transcriptional activity of FHOD1 was dependent on Src activity (Koka et al. 2005). FHOD1 thus drives transcription from the SRE as well as participating in the formation of stress fibres.

Most studies have reported FHOD1 as a cytoplasmic protein although it has been found to have a potential role in the nucleus (Menard et al. 2006). It has been described how caspase can cleave FHOD1 during apoptosis. This lead to the exposure of the two NLS in the resulting two FHOD1 fragments that were targeted to the nucleus. The FHOD1 617-1164 fragment in particular localised to nucleoli where it inhibited transcription by RNA polymerase I (Menard et al. 2006). This highlights the possibility of FHOD1 participating in apoptosis, but whether this is physiologically relevant or just an artefact of cell culture is an issue that remains to be determined. Experiments thus far have implicated FHOD1 predominantly as an actin regulatory protein although it may also have a role in regulating microtubule dynamics.

1.12.3 FHOD1 and the Regulation of Microtubules

While the interplay between formins and microtubules is still a comparatively budding area of research, some work has also indicated that FHOD1 could be a regulator of microtubule dynamics. Initial evidence for the possible role of FHOD1 in regulating microtubules came from an observation that the overexpression of constitutively active FHOD1 led to the formation of stress fibres and the concomitant alignment of microtubules (Gasteier et al. 2005). Another study attempted to characterise the microtubule regulating activity of nearly every formin by implementing constructs comprised of their function FH domains (FH1-FH2). While Dia1,2,&3, DAAM-1&2, FMNL1, and INF1 were found to be strong acetylators of microtubules and FMNL2&3 and INF2 were found to be weak acetylators, FHOD1, FHOD3, and Fmn1 were not found to induce acetylation of microtubules via their isolated FH domains (Thurston et al. 2012). Furthermore, the FH1-FH2 domains of FHOD1 and FHOD3 were unable to induce the formation of stress fibres nor were they able to stimulate SRF reporter gene activation, while other formin constructs were able to do so. On the other hand, truncation mutants of FHOD1 and FHOD3 comprised of longer versions of the protein (FHOD1ΔDAD or FHOD3ΔN) were able to induce the formation of stress fibres and microtubule coalignment in HeLa cells. Furthermore, FHOD3ΔN induced microtubule acetylation and activation of the SRF reporter gene, indicating that other modules of this protein, apart from the FH1-FH2 portion, are required for its actin and microtubule modulating activity. Unfortunately, this study was unable to recapitulate all of these experiments with FHOD1ΔDAD, citing inadequate levels of expression for this construct (Thurston et al. 2012). Another study silenced FHOD1 in U2OS cells and found that FHOD1 depletion in post mitotic cells resulted in perturbations in the microtubule and stress fibre network, although this phenotype was subsequently rescued by overexpression of siRNA-resistant HA-tagged full-length FHOD1 (Floyd et al. 2013). While the coordination of the microtubule and actin cytoskeletons may be a central function of FHOD1, further work will be required to elucidate the role of FHOD1 in microtubule regulation and the mechanisms involved.

1.12.4 Regulation of FHOD1

Early characterisation of FHOD1 suggested that its activation was regulated by the autoinhibitory interaction, typical to DRFs, which masked the FH1 and FH2 domains. This interaction was found to be mediated by polybasic residues between amino acids 1490 and 904-1165 (Westendorf 2001). The autoregulatory region of FHOD1 bears notable homology to the DAD regions of other DRFs, namely, mDia1, Bni1, and SepA (Takeya and Sumimoto 2003). The DAD also contains a number of conserved Serine and Threonine residues (Takeya et al. 2008). Further biochemical characterisation revealed that 60 amino acids in the DAD region specifically mediate the interaction with the N-terminus. The N-terminal DID was found to contain a functional hydrophobic autoregulatory motif, MDXLL, that contributed to the interaction (Schonichen et al. 2006). A Valine residue at position 228 was found to be central to mediating the autoinhibitory interaction since mutation to a Glutamic acid residue disrupted DAD binding (Schulte et al. 2008).

Like other formins, it has been suggested that FHOD1 is activated by binding of a Rho family small GTPase. It had first become apparent that FHOD1 interacted with Rac1 but not RhoA or Cdc42 (Gasteier et al. 2003). These first reports describing this interaction found that Rac1 and FHOD1 also co-localised in the cytoplasm of HeLa cells. The interaction was found to be mediated by the polybasic domain in the Rac1 C-terminus and a region on FHOD1 between the DID and FH1 domain between amino acids 422-717, a possible GBD. However, the interaction with Rac1 was independent of it being bound to GTP or GDP (Westendorf 2001) and is independent of the coiled-coil motif on FHOD1 (Madrid et al. 2005). A later study then revealed that activation of Rac recruits both Rac and FHOD1 to actin in membrane ruffles and lamellipodia (Gasteier et al. 2003). This same study speculated that even though FHOD1 does not interact with Rho it still acts downstream of it to form stress fibres.

Initial sequence analysis and experiments with Rac have placed the GBD in a region downstream of the DID and overlapping the FH1 domain. However, recent crystallisation studies have proven the existence of another GBD N-terminally to the DID domain. Schulte et al. 2008 have shown that amino acids 14-115 contain a

ubiquitin superfold. This region was found to bear similar sequence to the GBD of Raf, Byr2, PI3Kγ, moesin, and ubiquitin. Deletion of this region in DAD truncation mutants lead to impairment of actin regulating activity and SRE transcription. Moreover, this newly discovered GBD was purported to directly interact with Ras and not Rac, as found by isothermal titration calorimetry (ITC) (Schulte et al. 2008). Ras, another member of the small GTPases, has been highlighted in propagating signalling events via the MAPK/ERK pathway via proteins such as Raf (Jelinek et al. 1996). However, the interaction between the FHOD1 GBD and Ras is dubious considering that the FHOD1 GBD did not interact with Ras using GST pull-down assays (Table 1.1). Furthermore, the ITC experiments used in this study relied on the mutation of residues within the GBD in order to isolate possible regions of binding. Out of the three stable GBD mutants (P41K, D46R, and L61K), only the P41K mutant bound Ras. The wild-type FHOD1 GBD fragment was not addressed in ITC experiments. Ras only interacted with the GBD when GppNHp loaded, and hence in its activated state, versus the negative interaction displayed in its GDP-bound state. This would be suggestive of the specificity of the putative interaction between the GBD and Ras but the implementation of site-directed mutagenesis in order to achieve the interaction, the lack of reproducibility in binding across the FHOD1 GBD mutants, and the lack of a positive interaction in GST pull-down experiments would suggest that the interaction is merely artefactual and further analyses would be required. The FHOD1-Rac interaction also remains questionable as a study attempting to co-immunoprecipitate the two proteins was unable to do so, suggesting they do not bind (Thomas et al. 2011). So far, work has suggested that FHOD1 may have two independent GTPase binding regions, although the GBD found in the most N-terminal part of the protein is the more likely candidate. Further work will be required by way of characterising FHOD1 and possibly identifying a Rho family small GTPase that binds the more N-terminal GBD and activates FHOD1 to resolve this discrepancy.

FHOD1 Interacting Portion (amino acids)	Interacting Molecule	Interaction	Level of Evidence	Comments	Study
FHOD1 1-1165	RhoA	Negative	GST pull-down assay	N/A	(Westendorf 2001; Gasteier et al. 2003; Wang et al. 2004)
	Cdc42	Negative	GST pull-down assay	N/A	
	Rac1	Positive	GST pull-down assay	FHOD1 bound independent of GDP or GTPγS loading state	
	Rac2	Negative	GST pull-down assay	N/A	
	Rac3	Negative	GST pull-down assay	N/A	
FHOD1 1-421	Rac1	Negative	GST pull-down assay	N/A	(Westendorf 2001)
FHOD1 1-717	Rac1	Positive	GST pull-down assay	N/A	
FHOD1 469-1165	Rac1	Positive	GST pull-down assay	N/A	
FHOD1 1-115 (GBD); FHOD1 1-339	Ras	Negative	GST pull-down assay	N/A	(Schulte et al. 2008)
	Rnd3	Negative	GST pull-down assay	N/A	
	TCL	Negative	GST pull-down assay	N/A	
	RhoA	Negative	GST pull-down assay	N/A	
	Rac1	Negative	GST pull-down assay	N/A	
FHOD1 1-115 (GBD; P41K)	Ras	Positive	Isothermal titration calorimetry	GBD bound only in GppNHp loaded state of Ras	
FHOD1 1-115 (GBD; D46R)	Ras	Negative	Isothermal titration calorimetry	N/A	
FHOD1 1-115 (GBD; L61K)	Ras	Negative	Isothermal titration calorimetry	N/A	

Table 1.1: Assessing the Potential Interaction between FHOD1 and the Rho family Small GTPases. Summary of the published literature that reported attempts to find a physical interaction between FHOD1, or portions thereof (especially the N-terminus and GBD), and members of the Rho family small GTPases and related molecules. To date, the most-likely interaction to have been demonstrated took place between a central portion of FHOD1 and the C-terminus of Rac. N/A, not applicable; GBD, GTPase binding domain;

Although doubtful, there is some evidence suggesting an interaction between the FHOD1 GBD and a number of Rho family GTPases and related molecules. One study co-expressed the FHOD1 GBD with constitutively active variants of Rac1, Rac2, Rac3,

RhoA, Cdc42, and Ras in NIH3T3 cells (Schulte et al. 2008). The three Rac variants efficiently recruited the FHOD1 GBD to the plasma membrane, where the two proteins co-localised, as gauged by immunofluorescence imaging. The other GTPases that were investigated resulted in less profound recruitment of the FHOD1 GBD. However, such results cannot be taken as sufficient evidence of a direct interaction between the FHOD1 GBD and these cytoskeletal effector molecules since co-localisation of two proteins *in cyto* does not necessarily equate to their direct association. Therefore, supporting evidence from biochemical and molecular biology interaction assays would be required in order to compliment such findings and confirm if the FHOD1 GBD directly interacts with a Rho family small GTPase.

To date, none of the Rho family small GTPases have been shown to definitely bind the FHOD1 GBD using biochemical methods (Table 1.1). This is in contrast to other mammalian formins that have been shown to bind one or more member of these cytoskeletal effectors. The first formin-GTPase interaction to be described was that between mDia1 and RhoA (Kühn and Geyer 2014). GTP-bound RhoA has been shown to bind the GBD of mDia1 and to contribute to the activation of this formin (Lammers et al. 2005; Lammers et al. 2008; Kühn and Geyer 2014). Furthermore, numerous Rho family GTPases have been demonstrated to bind the N-terminal region (the GBD and FH3 domain) of mDia1, including RhoB, RhoC (Rose et al. 2005a; Rose et al. 2005b), Rac1, and Rac2 (Lammers et al. 2005; Kühn and Geyer 2014). Experiments using mDia1 and RhoC indicated that binding to the formin GBD and the proximal FH3 region (analogous to the FHOD1 DID) was mediated by the effector loop region that is conserved among Rho small GTPases (Rose et al. 2005a; Kühn and Geyer 2014). Whilst providing mechanistic insight into the steps involved in the steric displacement of the formin FH3/DID-DAD interaction, such a finding casts doubt as to the specificity of the interaction between the Rho family small GTPases and the formin GBD (Kühn and Geyer 2014). Insights into the mechanism of DRF activation have primarily stemmed from crystallographic and structural studies, which have suggested that Rho displaces the autoinhibitory DRF interaction between the FH3 and DAD domains in a two-step mechanism: first through weak binding of the GBD followed by stronger binding to the FH3 domain (Lammers et al. 2005; Kühn and Geyer 2014). RhoA binding to mDia1 has been directly attributed to activation of this formin since RhoA activated mDia1 stimulated the assembly of actin in functional experiments by way of

pyrene-actin assembly assays (Maiti et al. 2012). However, greater activation was achieved with the mDia1 variant lacking the C-terminal DAD, and even at relatively high concentrations of RhoA, only partial activation of mDia1 was achieved. Both of these factors suggest that further cues are required for full activation to occur. Regardless of the placement of the GBD of FHOD1, this also appears to be the case with the FHOD1 and Rac interaction. Although Rac has been suggested to recruit FHOD1 to the plasma membrane, the association of these two proteins did not appear to result in full FHOD1 activation as evidenced by a lack of stress fibre formation in cells (Gasteier et al. 2003; Schulte et al. 2008; Patel and Cote 2013). While some of the extra signals that contribute to the activation of mDia1 remain elusive, further insights have been gained with mDia2 and the FHOD proteins. mDia2 was shown to be phosphorylated by ROCK in two residues near the DAD, an event which resulted in activation of the formin (Staus et al. 2011b). FHOD1 and FHOD3 have also been shown to be activated by ROCK phosphorylation (Staus et al. 2011a; Iskratsch et al. 2013a).

A number of studies have found that ROCK regulates the activity of FHOD1. It has been demonstrated that ROCK directly phosphorylates Ser1131, Ser1138, and Thr1141 in the DAD of FHOD1. Site directed mutagenesis of these residues to Aspartates, which mimics phosphorylation, disrupted the intramolecular autoinhibitory interaction and activated FHOD1, as was evidenced by stress fibre formation (Takeya et al. 2008). Further experiments revealed that FHOD1 directly bound ROCK via the N-terminal part of its FH2 domain and that co-expression of the two proteins resulted in the formation of non-apoptotic plasma membrane blebs (Hannemann et al. 2008). FHOD1 was also shown to function downstream of RhoA-ROCK signalling to promote SMC differentiation. Downstream of ROCK phosphorylation, FHOD1 was shown to induce expression of SMC-specific genes. This induction of gene expression was dependent on the actin regulating activity of FHOD1, which ultimately influenced myocardin-related transcription factor (MRTF) localisation to the nucleus by altering the cytoplasmic ratio of F-actin to G-actin (Staus et al. 2011). Furthermore, FHOD1 was shown to function downstream of ROCK phosphorylation in platelets, where it might participate in the formation of thrombin induced stress fibres (Thomas et al. 2011). Phosphorylation by ROCK may represent the primary mechanism by which FHOD1 is activated, rather than binding by a Rho family small GTPase.

But where does this leave the notion of a possible physical association between Rho family small GTPases and FHOD1? None of the commonly studied Rho family GTPase members bind the GBD of FHOD1 but studies have shown they certainly could play a role in influencing the subcellular localization of FHOD1. The initial studies examining the FHOD1-Rac interaction revealed that overexpression of constitutively active Rac1 or treatment with platelet-derived growth factor (PDGF), a Rac activator, resulted in greater association of endogenous FHOD1 with F-actin in NIH3T3 cells (Gasteier et al. 2003). FHOD1 was specifically recruited to plasma membrane ruffles, lamellipodia, and actin fibres. Importantly, FHOD1 co-localised with Rac at these subcellular locations. Overexpression of constitutively active Rho or Cdc42 did not result in notable changes in the localization of endogenous FHOD1. This same study also highlighted the involvement of FHOD1 in the formation of Rac-induced lamellipodia (Gasteier et al. 2003). Rac1 has also been shown to mediate targeting of FHOD1 to actin tails, where FHOD1 participates in actin tail initiation and elongation in HeLa cells infected with the WR strain of vaccinia virus (Alvarez and Agaisse 2013). While it is questionable whether Rac1 directly contributed to the activation of FHOD1 in this study, the depletion of Rac in cells resulted in reduced targeting of FHOD1 to actin tails, suggesting that Rac1 is partly responsible for the targeting of this formin. Thus, while the extent of activation that is achieved upon association of FHOD1 and Rac is debatable, the cross-talk between these two proteins seems to contribute to the regulation of certain F-actin-based structures.

Src has also been shown to regulate FHOD1. Apart from mediating FHOD1 induced transcription from the SRE, Src has also been shown to regulate the subcellular localisation of FHOD1. Studies have found that Src activity was required to mediate FHOD1 targeting to lamellipodia (Koka et al. 2005) and to non-apoptotic plasma membrane blebs (Hannemann et al. 2008). The association of FHOD1 and ROCK was also found to be dependent on Src activity as was evidenced in co-immunoprecipitation experiments using Src inhibitors (Hannemann et al. 2008). Further work by Iskratsch et al. 2013 revealed that the direct interaction between FHOD1 and the SFKs was required for targeting of FHOD1 to early integrin clusters, where it was able to participate in actin polymerisation during cell spreading and migration. Binding of the SFKs to the polyproline motif on FHOD1 resulted in phosphorylation of FHOD1 by the SFKs at the Y99 residue and consequently increased the interaction between FHOD1 and the SFKs.

This phosphorylation event did not necessarily disrupt the autoinhibitory interaction of FHOD1 but more-likely contributed to the targeting of FHOD1 since the constitutive inactive FHOD1 3A mutant still localized to adhesions (Iskratsch et al. 2013b).

1.12.5 Additional Kinases that Phosphorylate FHOD1

Protein phosphorylation is a recognized mechanism by which cellular function can be modulated downstream of physiological stimuli. One notable example is the involvement of protein phosphorylation during myocardial contraction, namely the phosphorylation of myosin light chain and the resulting interaction between actin and myosin required for cross-bridge cycling (Rapundalo 1998). There have been examples of formins influencing the physiology of certain cell types by facilitating the propagation of signalling cascades involving phosphorylation of key proteins. For example, mDia1, which binds to the intracellular domain of the receptor for advanced glycation endproducts (RAGE), was required for RAGE induced oxidative stress generation, which culminated in Akt and glycogen synthase kinase (GSK3)β phosphorylation followed by SMC migration in a model of neoinitimal hyperplasia (Toure et al. 2012). As discussed above, it has also become apparent that certain formins, including FHOD1, are directly regulated by phosphorylation (Takeya et al. 2008; Staus et al. 2011b; Iskratsch et al. 2013a).

Another study with FHOD1 have also found through co-immunoprecipitation experiments and *in vitro* kinase assays that PKGI binds and phosphorylates FHOD1 and that this interaction is disrupted by the presence of cGMP. This raises the possibility that FHOD1 may regulate VSMC migration and vascular tone (Wang et al. 2004). Another study looked at Aurora-B, a mitotic kinase, and found that it phosphorylates FHOD1 (Floyd et al. 2013). This phosphorylation event was thought to contribute to cytoskeletal organization since a non-phoshophorylatable version of FHOD1 was impaired in its ability to organise stress fibres and microtubules. Overall, the interplay between FHOD1 and Aurora-B could implicate FHOD1 in mediating cytoskeletal rearrangements in dividing cells. Thus, FHOD1 could be phosphorylated by different kinases in various cell types but further work with these proteins will be required to learn more about the regulation and function of this formin.

1.12.6 Further Insights into FHOD1 Function from other Interacting Partners

A number of binding proteins have been described for FHOD1, with binding spanning different regions of the FHOD1 molecule. Figure 1.14 represents a comprehensive map of the different proteins that have been shown to bind FHOD1. Figure 1.15 represents a map of the cell and highlights the subcellular compartments where FHOD1 has been noted to co-localise with its binding proteins. Characterisation of some of the FHOD1's interacting proteins has also shed some light on its function. As expected, FHOD1 was found to interact with profilin, more specifically profilin IIa (Tojo et al. 2003). Subsequent studies revealed a wide array of FHOD1 binding partners. The C-terminal portion of the protein was found to interact with protein kinase C binding protein 1 (PRKCBP1), cyclophilin B, and WISHB. The interaction with WISHB revealed a possible inhibitory regulatory mechanism since its association disrupted FHOD1 induced stress fibre formation (Figure 1.15 Part II) (Westendorf and Koka 2004). FHOD1 was also found to bind insulin responsive aminopeptidase, which suggested a scaffolding role for the protein by tethering GLUT4 containing vesicles to the cytoskeleton (Figure 1.15 Part I) (Tojo et al. 2003). In human B cells lacking CD19, the interaction between FHOD1 and CD21 was found to participate in receptor aggregation (Figure 1.15 Part I) (Gill et al. 2004).

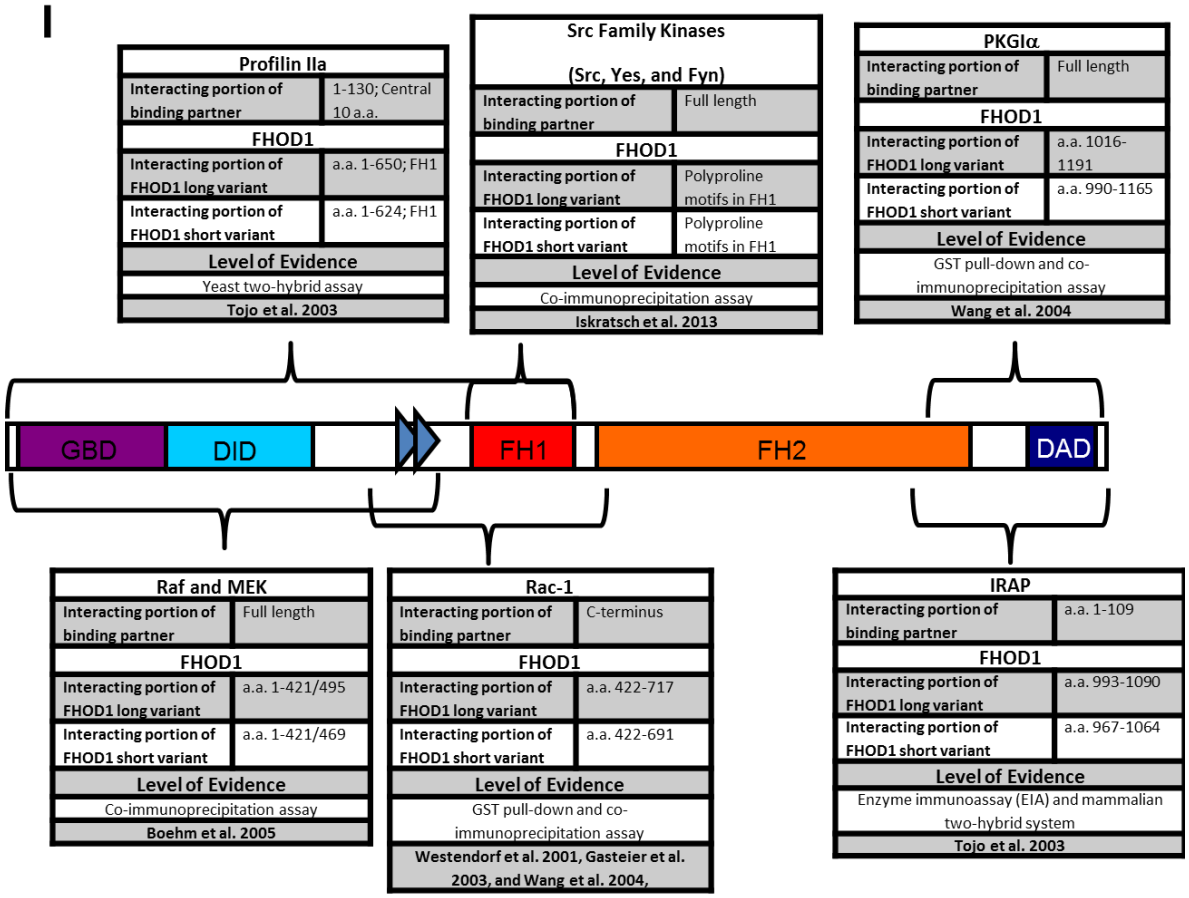

Figure 1.14: Schematic of FHOD1 Regions of Binding for Identified Interaction Partners (Part I). Schematic of FHOD1 and regions of binding by other proteins identified in the scientific literature. Tables describe the interaction by summarising the following: name of FHOD1 binding protein and region of protein involved in interaction; corresponding amino acids of FHOD1 involved in the interaction (for both the long and short FHOD1 variants); experimental procedures used to ascertain the interaction and the corresponding source of the study.

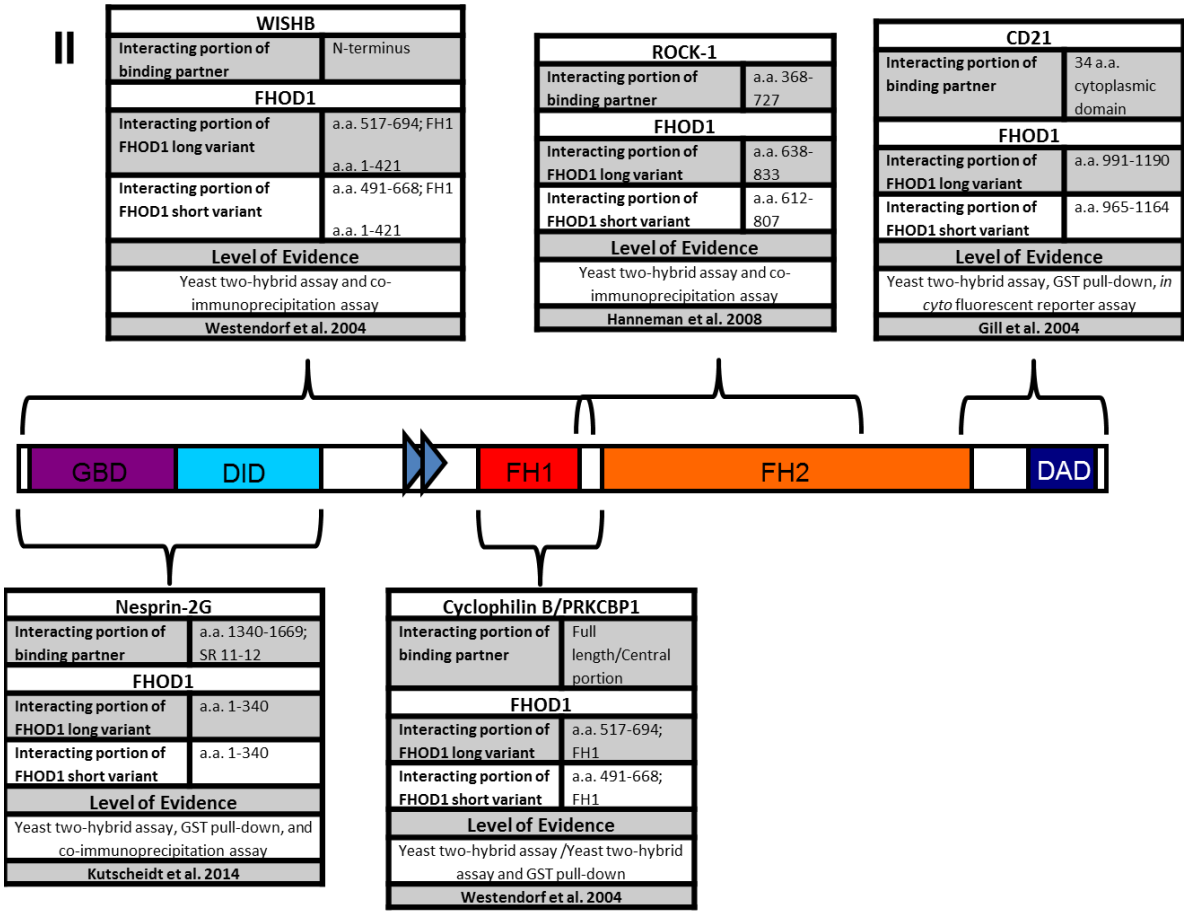

Figure 1.14: Schematic of FHOD1 Regions of Binding for Identified Interaction Partners (Part II). Schematic of FHOD1 and regions of binding by other proteins identified in the scientific literature. Tables describe the interaction by summarising the following: name of FHOD1 binding protein and region of protein involved in interaction; corresponding amino acids of FHOD1 involved in the interaction (for both the short and long FHOD1 variant); experimental procedures used to ascertain the interaction and the corresponding source of

FHOD1 was also found to interact with nesprin-2 giant (nesprin-2G) and using yeast two-hybrid, GST pull-down, and co-immunoprecipitation assays, the interaction was mapped to the FHOD1 N-terminus (GBD-DID) and to the spectrin repeats (SRs) 11-12, which are unique to nesprin-2G (Figure 1.14 Part II) (Kutscheidt et al. 2014). In this study FHOD1 was found to be required for the formation of TAN lines, arrays of nesprin and actin cables that are found across the nucleus (Figure 1.15 Part I). Actin cables are bundles of actin filaments that localize to the cell cortex which play roles in particle transport and can mediate cell polarity. TAN lines are required to position the nucleus at the rear of the cell. Rearward movement of the nucleus is achieved by coupling dorsal actin cables with nesprin-2G (outer nuclear lamina) and SUN proteins (inner nuclear lamina). In migrating fibroblasts, rearward movement of the nucleus is required for placement of the centrosome at the leading edge of the cell (Chang et al. 2013). Positioning of the centrosome at the leading edge is an important step since centrosomes dictate the arrangement of microtubules, which are required for migration (Tang and Marshall 2012). Interestingly, while FHOD1 was required for TAN line formation, it was found to be dispensable for the formation of actin cables (Kutscheidt et al. 2014). This study this highlighted the potential anchoring role of FHOD1 in linking nesprin-2G to actin cables. The function of FHOD1 may thus vary according to the cell-type and the binding partners in question.

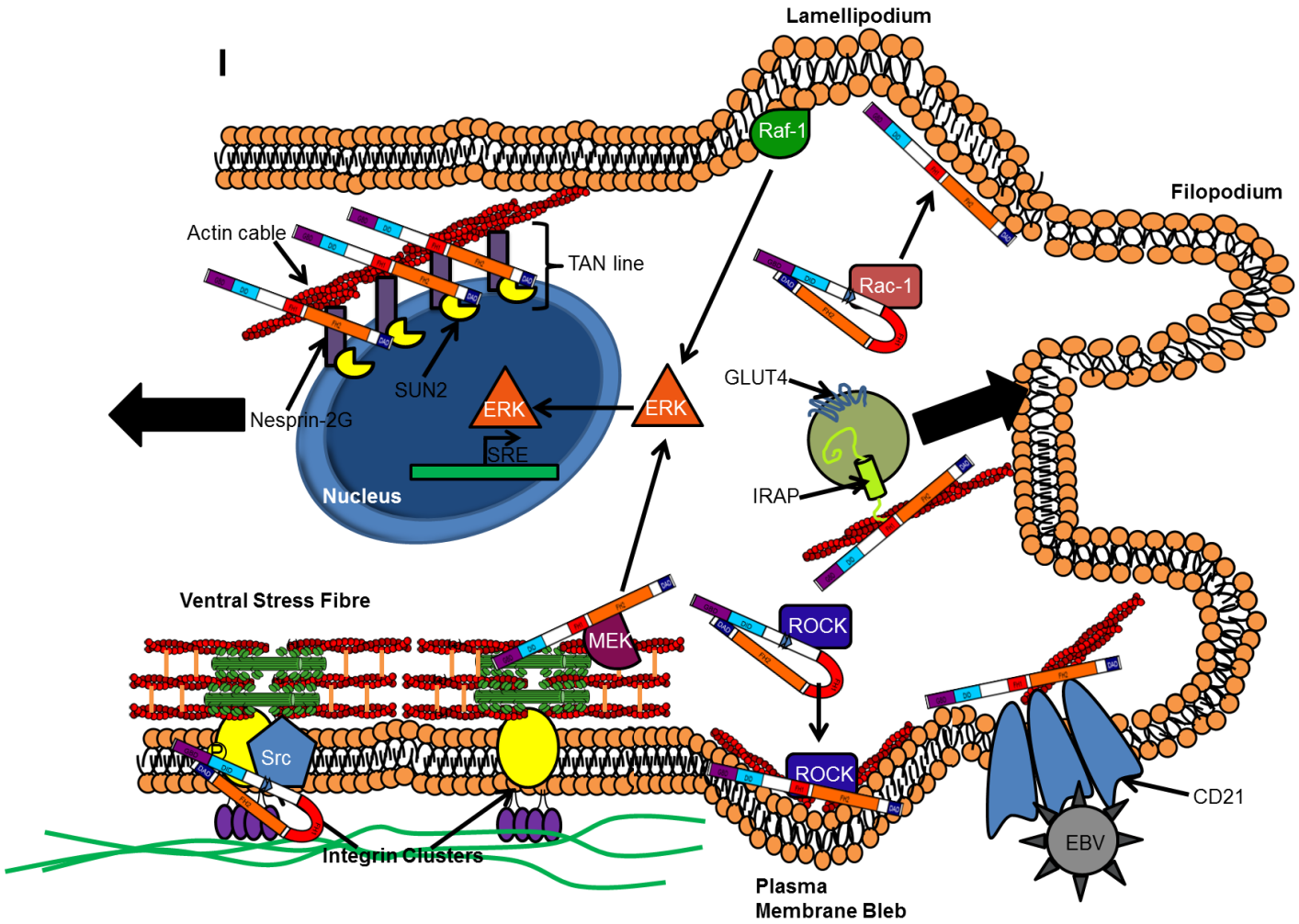

Figure 1.15: Schematic of Subcellular Localisations of FHOD1 Interactions (Part I). A multitude of interactions have been described for FHOD1. These interactions were noted to take place in specific subcellular compartments.

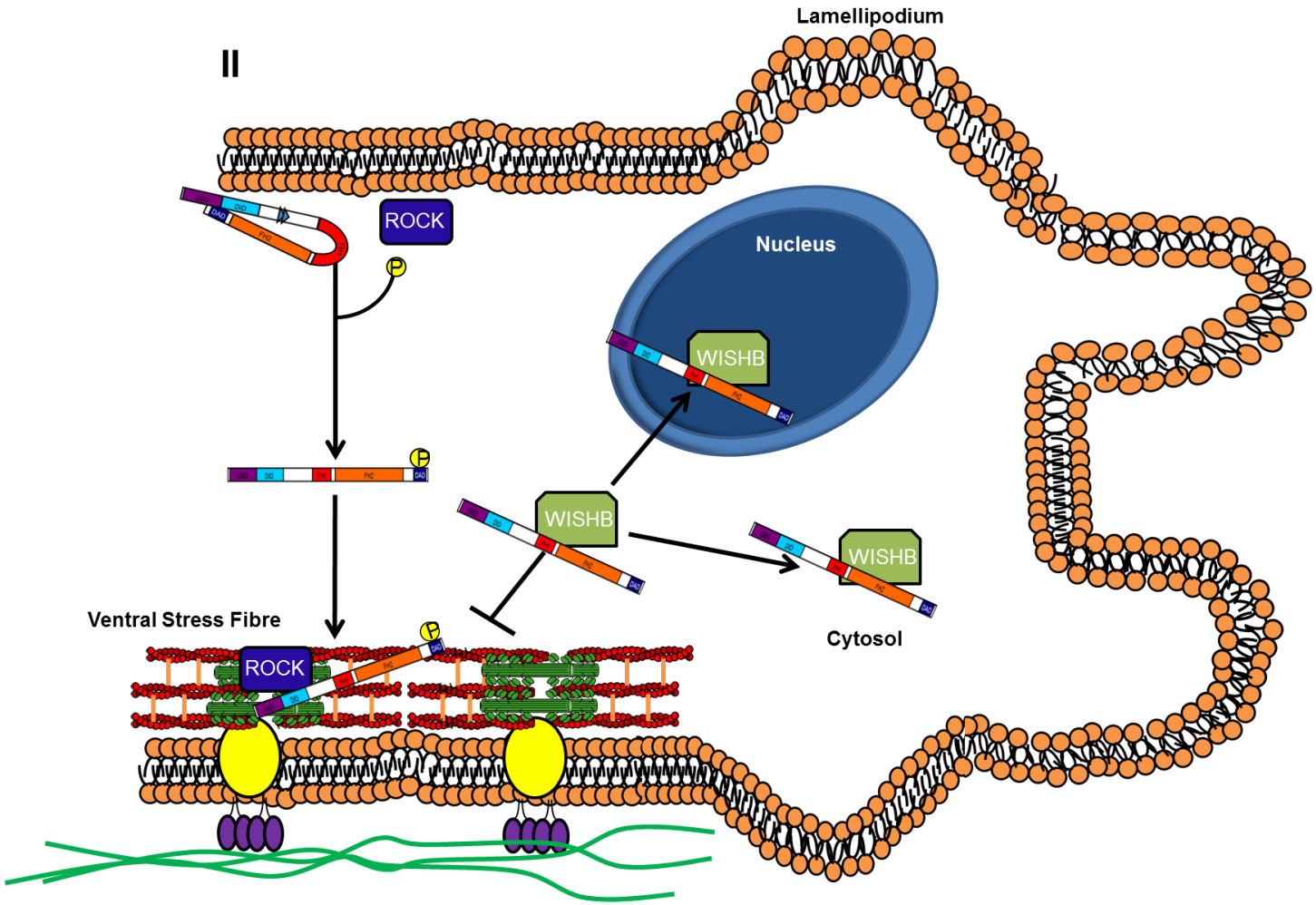

Figure 1.15: Schematic of Subcellular Localisations of FHOD1 Interactions (Part II). A multitude of interactions have been described for FHOD1. These interactions were noted to take place in specific subcellular compartments.

Although a variety of FHOD1 binding partners have been described, it is somewhat difficult to extrapolate a unified view of FHOD1's function from the available literature. This partly stems from the fact that different cell types have been used to characterise the functional significance of these interactions. Furthermore, many of the FHOD1 interacting proteins localize to distinct subcellular compartments. Consequently, the association of FHOD1 with a number of its individual interacting partners seem to play non-overlapping roles. While FHOD1 co-localises with Raf-1 and MEK at lamellipodia and stress fibres (Boehm et al. 2005), respectively (Figure 1.15 Part I), the functional significance of this co-localisation is not clear. Raf-1 and MEK may provide a link between the actin cytoskeleton and the nucleus by facilitating the transcriptional effects of FHOD1 on the SRE by signalling through ERK in NIH 3T3 cells. However, work in SMCs indicated that the transcriptional activity of FHOD1 is mediated by the actin-sensitive MRTF-SRF pathway, and occurs downstream of the Rho-ROCK pathway (Staus et al. 2011a). While there is potential for cross-talk between ROCK and MEK, given that they can be found at stress fibres with FHOD1, it is difficult to speculate as to what the functional relevance would be. A similar case can be made for Raf-1 and Rac-1. Rac-1 recruits FHOD1 to lamellipodia (Figure 1.15 Part I), which is also incidentally the site where FHOD1 associates with Raf-1. Until the relevance of the interactions between FHOD1, Raf-1, and MEK are fully elucidated, one can only speculate as to how these molecules could function together, thus, their proximity within specific cellular compartments can only be described as incidental. A similar argument can be made for the FHOD1 interactions that take place at/near the plasma membrane, as was the case with ROCK at plasma membrane blebs (Hannemann et al. 2008), the CD21 receptor aggregation event following EBV attachment (Gill et al. 2004), and the transport of GLUT4-containing vesicles towards the plasma membrane via actin cables (Tojo et al. 2003) (Figure 1.15 Part I). These interactions occur in distinct cell types; therefore it would be difficult to speculate as to how they are linked, although a theoretical example could be the possible recruitment of FHOD1 to these sites by Rac-1.

A more-likely possibility of cross-talk among the FHOD1 binding proteins could take place between the SFKs and ROCK. Not only is FHOD1 recruited to plasma membrane blebs by ROCK, but this process is also dependent on Src activity (Hannemann et al. 2008). Furthermore, FHOD1 targeting to early integrin clusters is mediated by Src and

likely occurs upstream of ROCK phosphorylation (Iskratsch et al. 2013b). Src phosphorylation and binding of FHOD1 could serve as a means to recruit FHOD1 to the plasma membrane, where FHOD1 is subsequently activated by ROCK. A similar argument can be made for Rac-mediated targeting of FHOD1 to the plasma membrane. Interestingly, Rac is activated downstream of Src during instances of integrin-mediated signalling events (Huveneers and Danen 2009) and could serve as another mediator for FHOD1 targeting to adhesion sites. Overall, the study of FHOD1's binding partners has painted a complex picture of this formin in cells, with multiple interacting partners and localisations identified. Nevertheless, FHOD1 has been shown to be an important regulator of the actin cytoskeleton in a variety of cell types, although, its role in striated muscle has yet to be examined. The role of its closest relative, the formin homology protein FHOD3 has provided some additional insight into the possible function of FHOD1 in striated muscle.

1.13 FHOD3

1.13.1 The Formin Homology Protein, FHOD3

Formin homology 2 domain containing protein 3 (FHOD3), formerly known as FHOS2, is another DRF of the FHOD subclass. It was identified as a paralogue of FHOD1, bearing 52.1% amino acid homology, and is found on chromosome 18q12.2. Initial *in silico* characterisation predicted it to be 1,439 amino acids long. The human *FHOD3* gene is comprised of a 4,964 ORF with an 119bp 5' UTR and an 525bp 3' UTR. Sequence comparison to other formins found that FHOD3 is comprised of a similar modular structure. *FHOD3* was predicted to encode at least 3 different isoforms due to alternative splicing of the exon skipping type (Katoh 2004). Bioinformatic analysis has found that it undergoes alternative splicing between exons 11-13. Studies with the mouse variant have found mFhod3 to be abundant in the heart, kidney, and to a lesser extent in the brain. More importantly, it exhibited isoform specific distribution. A larger FHOD3 1,578 amino acid isoform exhibited predominantly cardiac specific expression whereas another smaller 1,422 amino acid isoform was restricted to expression in the kidney and brain (Kanaya et al. 2005).

FHOD3 has also been found to regulate actin dynamics. Initial transfection experiments in HeLa cells found that C-terminal truncation mutants of FHOD3 lead to stress fibre formation and that FHOD3 was targeted to these actin-based structures to some extent. Fluorescence microscopy also revealed that FHOD3 associates with nestin filaments in H9C2 and COS7 cells (Kanaya et al. 2005). More recent work on FHOD3 has highlighted the importance of formins in striated muscle.

1.13.2 Preliminary Work with FHOD3 – Motivation for Work with FHOD1 in Striated Muscle

Characterisation of FHOD3 has revealed that the protein plays a crucial role in regulating cardiac muscle cell biology. It was shown that FHOD3 is required for myofibrillar maintenance in cultured cardiomyocytes by disrupting expression of the protein using siRNA (Taniguchi et al. 2009). This was concurrently confirmed by Iskratsch et al. 2010 using a more elegant vector based siRNA approach to knock down FHOD3 in cultured cardiomyocytes. Depletion of FHOD3 led to fragmentation of myofibrils thus highlighting the requirement of the formin in myofibrillar maintenance. Myofibril recovery experiments following Latrunculin B treatment also revealed that FHOD3 was able to more efficiently induce recovery of myofibrils compared to mDia1, highlighting the possibility that formin homology proteins are key players in the maintenance of the myofibrillar apparatus (Iskratsch et al. 2010; Dwyer et al. 2012).

The localisation of FHOD3 has also been studied in cardiac muscle. Cultured neonatal rat cardiomyocytes revealed that FHOD3 associated with thin filaments and also exhibited a doublet localisation for FHOD3 around the area of the A-band (Taniguchi et al. 2009; Iskratsch et al. 2010; Kan-o et al. 2012b). There are still some discrepancies regarding the localisation of FHOD3 in adult cardiac muscle. Iskratsch et al. 2010 reported FHOD3 at the Z-disk in adult heart muscle (Iskratsch et al. 2010) whereas Kan-o et al. 2012 reported that the localisation of FHOD3 in adult cardiac muscle is relatively unchanged compared to that seen in neonatal rat cardiomyocytes and can be found near the centre of the sarcomere as a pair of doublet bands (Kan-o et al. 2012b). This work was further elaborated on and it was revealed that FHOD3 is

developmentally regulated in both its expression levels and myofibrillar targeting. The likely localisation of FHOD3 in the mature myofibril is at the Z-disk (Iskratsch et al. 2013a).

Iskratsch et al. 2010 additionally cloned a novel striated muscle specific variant of FHOD3 that is phosphorylated by CK2. CK2 phosphorylation was found to govern the subcellular localisation and turnover of muscle FHOD3 (Iskratsch et al. 2010). This notion was subsequently confirmed in CK2alpha knockout mice in which FHOD3 had lost its defined myofibrillar targeting (Iskratsch et al. 2013a). Overall, FHOD3 has been found to play an important role in cardiac muscle as evidenced by experiments looking at its expression, localisation, function, and regulation. The importance of this formin homology protein indicates that FHOD1 may also play an important role in striated muscle.

1.14 Formins in Disease

As mentioned previously, a number of formins have been directly implicated in disease processes. For instance, mDia1 has been implicated in a form of non-syndromic deafness in a kindred in Costa Rica. The disease was associated with a truncated variant of mDia1 that arose from a four base pair insertion, resulting in the generation of a premature STOP codon (Lynch et al. 1997; DeWard et al. 2010). Disruptions in the gene encoding mDia3 (*DIAPH2*) have been linked to premature ovarian failure (Bione et al. 1998; DeWard et al. 2010). Other formins have been reported to be expressed at differential levels in disease states. Although it has yet to be directly linked to mediating a disease process, increased levels of FHOD1 have been reported in an oral squamous cell cancer line (Gardberg et al. 2013). Furthermore, FHOD1 was also found to enhance cell migration when overexpressed in human melanoma cells and has allowed for the proposal of a role of FHOD1 in metastasis (Koka et al. 2003). With respect to the participation of formins in cardiac disease, insights have been gained through the study of FHOD3.

1.14.1 Formins in Cardiac Disease

Among the formin homology proteins, FHOD3 has been the best documented to display altered expression levels during instances of cardiac disease. FHOD3 has been shown to be downregulated in human cardiomyopathy samples associated with heart failure (Iskratsch et al. 2010). In this study, different samples of human myocardial tissue were examined for levels of FHOD3 and covered a broad range of aetiologies of heart failure such as idiopathic dilated cardiomyopathy (DCM), ventricular DCM, familial DCM, ischemic heart disease, and perinatal DCM. Regardless of the aetiology accounting for the cardiomyopathy, levels of FHOD3 were found to be down-regulated. This notion was also supported by immunofluorescence experiments, which revealed fainter staining for FHOD3 in failing heart tissue sections (Iskratsch et al. 2010). Certain FHOD3 variants have also been found to be closely associated with hypertrophic cardiomyopathy (HCM) (Wooten et al. 2012). Although two variants were identified to be closely associated with HCM, one variant in particular, FHOD3 V1151I, displayed a stronger association with the HCM phenotype in humans. Furthermore, analysis of HCM septal myectomy samples by quantitative polymerase chain reaction (PCR) and Western blotting revealed increased levels of FHOD3 at the transcript and protein level, respectively (Wooten et al. 2012). FHOD3 could thus be downregulated during instances of DCM and upregulated during instances of HCM.

The above findings concerning FHOD3 in cardiac disease could mean this formin could play a role in pathological states that often result in heart failure in humans. Cardiac hypertrophy, an increase in heart mass, is a leading cause of mortality associated with cardiovascular disease (Wooten et al. 2012). Cardiac hypertrophy (Figure 1.16 B) can be triggered as a response to ischaemic insults or to hypertension. The increase in cardiomyocyte size associated with hypertrophy initially functions as a compensatory response to preserve cardiac function. It is even possible for the heart to remodel itself back to its previous state (Figure 1.16 A). However, it is often the case that adverse remodelling events take place with negative consequences. Increased ventricular mass often precedes the onset of heart failure, a state in which the dilated heart fails to adequately meet the energetic demands of the myocardium in order to pump blood systemically (Paul et al. 2006). Such a state is usually characterised by a heart with distended ventricular cavities and thinning walls (Figure 1.16 C). The transition to heart

failure can be explained partly by increased levels of myocyte apoptosis and necrosis due to greater levels of oxidative stress (Hingtgen et al. 2006). Cardiac hypertrophy also predisposes individuals to ischaemia and arrhythmias therefore it is also a major risk factor for sudden cardiac death (Hilfiker-Kleiner et al. 2006). The precise mechanisms underlying the remodelling events that are characteristic of cardiac hypertrophy have yet to be fully explained. In both humans and animal models, mutations in cytoskeletal regulatory proteins, such as muscle lim protein (MLP), are associated with hypertrophic and dilated cardiomyopathy (Buyandelger et al. 2011). So far there have been no FHOD1 mutations reportedly associated with heart disease in humans.

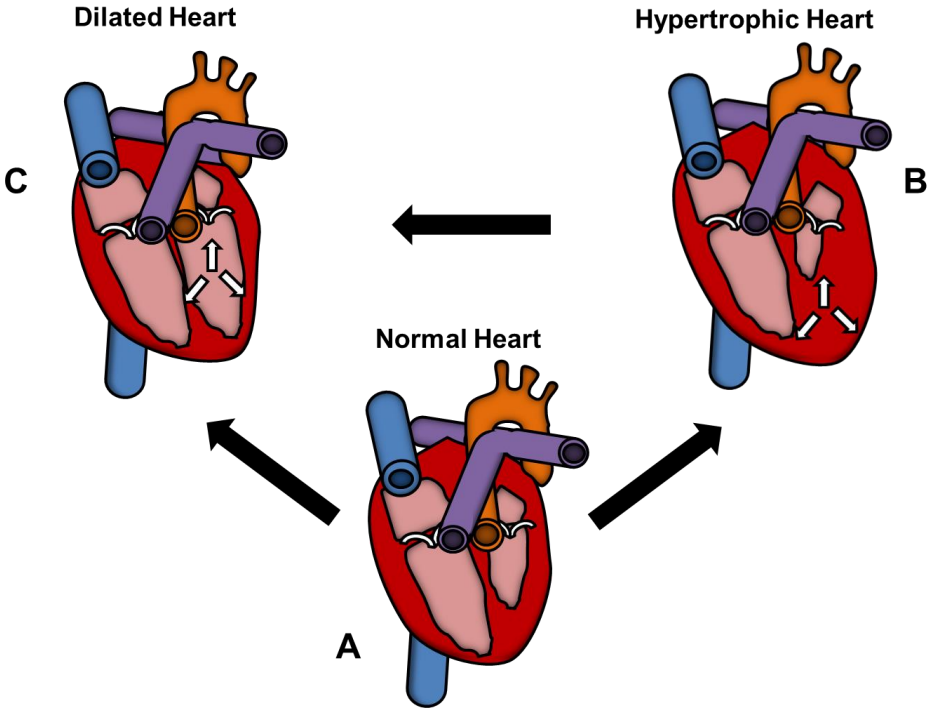

Figure 1.16: Cardiac Disease. Schematic representation of hypertrophic and dilated hearts. **A)** Normal heart. **B)** Heart exhibiting left ventricular hypertrophy, as shown by an increase in the size of the myocardium (dark red). Cardiac hypertrophy can be pathological and often progresses to a dilated phenotype followed by heart failure. Cardiac hypertrophy can result from chronic pressure overload (i.e. hypertension). This schematic is also representative of HCM, which is often inherited. **C)** Dilated heart exhibiting left ventricular dilatation and thinning of the ventricular wall. This dilated phenotype is often associated with heart failure. This schematic is also representative of the DCM phenotype, which is also often inherited. HCM, hypertrophic cardiomyopathy; DCM, dilated cardiomyopathy. White arrows indicate site of hypertrophy or dilation.

Work using an animal model of DCM, the MLP$^{-/-}$ mouse (Arber et al. 1997), has also indicated the possible involvement of FHOD3 in cardiac disease. MLP deficient mice have been reported to display a number of alterations in cardiomyocyte structure. Although overall structure of sarcomeres remains unchanged, MLP deficient mice display a number of abnormalities at the level of the intercalated disk. The most notable feature is widening of the intercalated disk, which has been attributed to greater convolution of the structure (Ehler et al. 2001). Analysis of FHOD3 expression in MLP$^{-/-}$ mice revealed that there was a downregulation in FHOD3 expression and a switch to the non-muscle FHOD3 isoform. Furthermore, the Z-disk and intercalated disk associations of FHOD3 were lost and instead the formin was found distributing as weak striations around the M-band or in p62 containing autophagosomes (Iskratsch et al. 2010).

MLP was initially identified by Arber et al. (Arber et al. 1994) and is a striated muscle specific cytoskeletal regulator that is found at the Z-disk (Knöll et al. 2010) and the nucleus (Knöll et al. 2002a; Knöll et al. 2002b; Boateng et al. 2009). It has a number of binding partners and has importantly been shown to form a ternary complex with α-actinin and nebulin related anchoring protein (NRAP), an actin binding protein that has been shown to play a role in myofibril assembly (Carroll et al. 2001; Carroll et al. 2004; Dhume et al. 2006). It is not fully understood how MLP depletion results in a hypertrophic and DCM phenotype but work using a mutant variant of MLP associated with DCM in humans has shed some light on the issue. Gehmlich et al. 2004 showed that a DCM mutant variant of MLP (C58G) is more susceptible to proteolysis due to improper zinc coordination and misfolding of one of its LIM domains. It was also shown that the MLP-α-actinin-NRAP interaction decreased with the DCM causing mutation. The decrease in MLP was thought to be partly compensated for by an increase in NRAP expression (Ehler et al. 2001), which was thought to account for the myofibrillar disarray phenotype (Gehmlich et al. 2004). However, it is not entirely clear if an upregulation in NRAP was responsible for the alterations seen in DCM mice since NRAP overexpression in mice led to right ventricular dysfunction but no perturbation of the intercalated disks (Lu et al. 2011). However, there was not substantial accumulation of NRAP at the intercalated disks of NRAP-overexpressing mice compared to wild-type mice, which may explain the lack of intercalated disk perturbation. It should also be

noted that NRAP-overexpressing mice exhibited only modest cardiac hypertrophy which may have explained why the intercalated disks had not widened.

The role of MLP in cardiomyopathy is being revealed to be increasingly complex. Work exploring a different MLP missense mutation (W4R) that is associated with DCM in humans was shown to cause hypertrophic cardiomyopathy (HCM) in knock-in mice. Decreased levels of MLP mRNA and protein were also associated with this mutation as well as a heart failure phenotype in mice (Knöll et al. 2010). These cardiomyopathic changes have been partially attributed to a decreased interaction between MLP and telethonin, resulting in impaired mechanosensing (Knöll et al. 2002a; Knöll et al. 2002b; Knöll et al. 2010). MLP seems to be relevant in both HCM and DCM. Although HCM and DCM are distinguished as separate cardiomyopathies (Figure 1.16), overlaps in features occur and 10-20% of HCM patients develop DCM later in life (Konno et al. 2003; Knöll et al. 2010). Alterations in MLP have also been noted in human heart failure samples (Zolk et al. 2000) and rats that underwent aortic banding or myocardial infarction. Increased levels of total MLP were noted in these models of heart failure but it was found that MLP accumulated in the nucleus and decreased substantially in the cytosol. Accumulation of nuclear MLP was also associated with increased synthesis of S6 ribosomal protein and may have indicated enhanced rates of protein synthesis, thus partly accounting for some of the cellular changes associated with the hypertrophic response (Boateng et al. 2007). The role of MLP thus varies depending on the pathological stimulus applied to hearts. In summary, studying the role of MLP in the heart has furthered our understanding of some of the changes involved in cardiomyopathy and insights from cardiomyopathic $MLP^{-/-}$ mice have highlighted a possible involvement of formins in this devastating group of diseases.

1.15 Conclusion

Muscle contraction is brought about by the sliding of myofilaments past each other. The basic contractile apparatus of striated muscle is organised into thin and thick filaments. The thin filaments are made of polymerised actin and are decorated and bound by a number of other proteins that confer stability and regulate their function. A number of actin regulatory proteins have been described to modulate the polymerisation of actin via a number of mechanisms including capping, severing, and processive

elongation. There is little known about the polymerisation and regulation of thin filaments in muscle but previous work has highlighted the role of diaphanous related formins in their regulation, especially the formin homology protein FHOD3. FHOD1, another formin homology protein, is a close relative of FHOD3 bearing considerable sequence homology. FHOD1 is a well-established regulator of cytoskeletal dynamics and has been shown to induce formation of actin-based structures, including stress fibres downstream of RhoA-ROCK signalling.

1.16 Hypothesis and Aims

The purpose of the present study was to investigate if FHOD1 played a role in striated muscle. Previous work suggested that FHOD3 was a crucial regulator of cardiac cell architecture and that this was due to the ability of FHOD3 to directly contribute to myofibrillar regulation at the level of actin. A growing body of evidence would indicate that FHOD1 is an important regulator of cytoskeletal dynamics, particularly at the level of actin, in a variety of cell types. Given the importance of formin homology proteins and of actin in muscle cells, we hypothesised that FHOD1 was involved in regulation of the myofibrillar apparatus and cytoskeleton in striated muscle and thus set out to characterise it. Characterisation of FHOD1 involved looking at different facets of protein biology including expression and localisation, function, regulation, and interactions with other proteins. The aims for each chapter are summarised below:

1) Expression and Localisation of FHOD1 – Since there have been conflicting reports on the expression pattern of FHOD1 in muscle, we sought to investigate the expression of FHOD1 at the protein level in cardiac and skeletal muscle samples. As has been the case for FHOD3 and other actin binding proteins in muscle, the localisation of proteins can provide insight into their roles; therefore we investigated the localisation of endogenous FHOD1 in different muscle samples using a number of commercially available anti-FHOD1 antibodies. We also attempted to complement the antibody studies with overexpression studies using full-length epitope-tagged FHOD1 constructs in order to clarify its subcellular localisation. Different modules on FHOD1 have previously been shown to contribute to its targeting, therefore we also overexpressed individual

epitope-tagged FHOD1 domains and truncation mutants to deduce how FHOD1 is targeted in cardiac muscle cells

2) Functional Characterisation of FHOD1 – Studies so far have suggested that FHOD1 is regulated by an autoinhibitory intramolecular interaction and that it primarily exerts its effects on the actin cytoskeleton after activation. Therefore, a number of gain-of-function studies were performed in cultured cardiac cells to gauge the effects of FHOD1 activation. In order to further probe the functional significance of FHOD1 in muscle cells, additional loss-of-function studies were performed, in which shRNA constructs were designed to knock down endogenous FHOD1 in cultured cardiac and skeletal muscle cells. The general role of formins was also investigated in cultured cardiomyocytes in experiments using a general inhibitor of formin mediated actin assembly.

3) Regulation of FHOD1 – With the regulation of FHOD1 by the Rho family small GTPases a possibility, a number of binding assays were performed. This work also examined the downstream effector of the Rho pathway, ROCK. While none of these effector molecules have been shown to bind the GBD of FHOD1, work with Rac and ROCK-I has suggested that binding of a Rho family small GTPase or effector molecule can occur outside of the FHOD1 GBD and can contribute to the regulation of this formin. Previous studies have only addressed the smaller FHOD1 variant, lacking the alternatively spliced exons 12-13; therefore we performed binding assays with an FHOD1 construct containing the alternatively spliced exons to test if they could mediate binding with any of the above putative regulatory proteins. Src is also being increasingly highlighted as a regulator of FHOD1; therefore we performed binding assays between FHOD1 and Src to test the possibility that regulation could occur by a direct binding.

4) Novel Protein-Protein Interactions – Many actin regulatory proteins interact with other factors that modify or enhance their activity in some way. We additionally aimed to identify new binding partners for FHOD1 by performing cDNA library screens using a yeast two-hybrid system with different FHOD1 fragments. In order to gain a view of the potential FHOD1 interacting partners that may occur in muscle, a human cardiac cDNA library was employed.

Chapter 2

Materials and Methods

2. Materials and Methods

2.1 Specimens

2.1.1 Mice

Adult male C57/BL6 wild-type and $MLP^{-/-}$ mice were used for tissues in Western Blot analysis and immunofluorescence studies. Mice were fed a normal dry chow diet and kept on a light/dark cycle (12/12h) at 22°C receiving food and water *ad libitum*. $MLP^{-/-}$ mice were described in Arber et al. 1997 and generated through targeted disruption of the *MLP* gene (Arber et al. 1997). Experiments were performed in accordance with the Guidance on the Operation of Animals (Scientific Procedures) Act, 1986 (UK). Prior to harvesting tissue, mice were sacrificed by cervical dislocation. Tissues were then kept in PBS before methylbutane treatment for 1 min. in liquid nitrogen or snap frozen in liquid nitrogen for storage at -80°C.

2.1.2 Murine Samples

Tissues samples were frozen in liquid nitrogen, pulverised, and lysed in 100µl of SDS lysis buffer (130mM Tris, 190mM SDS, 3.69M urea, 0.06% NP40, 0.17%β-mercaptoethanol, 3.85% glycerol and 0.01% bromophenol blue at pH 6.8). For immunofluorescence staining, tissues (heart) were cut on a Leica CM1950 cryostat (Leica, Wetzlar, Germany) into 12µm sections, mounted on poly-L-lysine coated microscope slides, fixed with pre-cooled acetone (-20°C) for 5min at -20°C and stained as described below (See 2.11.2), or stored at -80°C until further use.

2.1.3 COS-1 Cells

COS-1 cells were washed in PBS and lysed in 100µl of SDS lysis buffer using a rubber policeman, then boiled for 2min and stored at -20°C until further use. For pull-down assays, COS-1 cells were washed in ice cold PBS and lysed in 100µl of pull-down lysis buffer (150 mM NaCl, 20 mM Tris-HCl pH 7.6, 1 mM EDTA, 0.2% (v/v) NP-40, 1 mM Dithiothreitol DTT) and 1x protease inhibitor (complete mini, Roche applied

science, Mannheim, Germany) for 10min on ice, the lysates collected with a cell scraper, centrifuged at 16,000 x g and 4°C for 15min, the supernatant transferred to a new tube for another round of centrifugation at 16,000 x g and 4°C for 15min, and the supernatant collected and stored at -80°C until further use.

2.1.4 Yeast

For expression tests, *Saccharomyces cerevisiae* yeast (L40 strain) were transformed with the relevant FHOD1 bait constructs and cultured in 0.5ml SD-drop out medium lacking Tryptophan (MP Biomedical, Santa Ana, California) at 30°C shaking at 200rpm. Liquid cultures were spun down for 30sec at 15,000 x g for 1min. Yeast were then re-suspended in 25ml TE buffer (0.1M Tris-HCl, 10mM EDTA, pH7.5, sterile by filtration) with 1x protease inhibitor (complete mini, Roche applied science, Mannheim, Germany). Glass beads were added to the mixture which was then vortexed for 10sec. 100µl of yeast lysis buffer (8M Urea, 2% NP40, 1% TritonX100 5%, glycerol-BPB, 5% β-mercaptoethanol, 5% SDS, 0.1M Tris-HCl pH6.7) were then added to samples which were mixed by vortexing for 2min. Samples were then boiled for 5min spun down briefly and the supernatant was then transferred to a new tube. Samples were stored at -20°C until further use.

2.2 Cell Culture

2.2.1 Neonatal Rat Cardiomyocytes

Neonatal rat cardiomyocytes (NRCs) were isolated from day 1 newborn Wistar rat pups. NRCs were isolated using the Worthington Neonatal Cardiomyocyte Isolation System (Worthington Biochemical Corporation, Lakewood, NJ, USA) according to the manufacturer's instructions. The following protocol describes isolation for one litter of rat pups (approximately 10-12 rat pups per litter). All reagents/supplies were provided by Worthington Biochemical Corporation unless otherwise stated. Wister rat pups were sacrificed by decapitation with sterile straight scissors and the hearts were excised, chopped into smaller pieces and stored on ice in 30ml Hank's Balanced Salt Solution (HBSS) containing 20 mM 2,3-Butanedione monoxime (BDM). BDM, a reversible potassium and L-type calcium channel and myosin ATPase inhibitor was added to protect cells during the isolation procedure and improves cell-yield and viability (Ehler

et al. 2013). Heart pieces were transferred to a petri dish on ice in a sterile hood, HBSS was removed and the tissue pieces were minced using curved scissors. 20 ml of HBSS + 20 mM BDM containing 1 mg trypsin were then added to the petri dish. Samples were then subjected to an overnight trypsin digest at 4°C without agitation. The next morning the tissue suspension was transferred to a sterile 50ml centrifugation tube on ice. The trypsinisation reaction was subsequently stopped by the addition of 2 mg of trypsin inhibitor (reconstituted in 1 ml of HBSS + 20 mM BDM). After oxygenation of the tissue suspension by bubbling it with a pipette for 30sec, the vial was then warmed in a 37°C water bath for 15 min and then subjected to collagenase digestion. 1500 units of lyophilised Worthington Purified Collagenase, which contains less than 50 UI/mg caseinase and is composed of two separable but very similar collagenases, were reconstituted in 5 ml of 5 ml Leibovitz L-15 media + 20mM BDM. The collagenase solution was added to the centrifugation tube, which was placed in a shaking incubator (2-4 rpm) at 37°C and incubated for 30min. The tissue suspension was then triturated with a standard 10 ml plastic serological pipet about 10 times to release cells. Cells were then transferred into a new 50 ml centrifugation tube by filtering through a cell strainer that was pre-rinsed with 2 ml of Leibovitz L-15 media + 20mM BDM. After the solution containing the cells was filtered through, the cell strainer was once again rinsed with 2 ml of Leibovitz L-15 media + 20mM BDM in order to wash through residual cells. The solution was then oxygenated for 1min by bubbling it with a pipette before centrifugation at 70 x g for 5min at room temperature. Pelleted cells were suspended in 30 ml of plating medium (66% DMEM, 16.5% M199, 10% horse serum, 5% fetal calf serum, 4mM Glutamine, 1% penicillin/streptomycin), distributed between three 90mm dishes and left to incubate at 37°C for 3hrs to allow fibroblasts to attach. After this pre-plating step, cardiomyocytes, which would still be in suspension since they take much longer to attach to cell culture plastic, were rinsed off, seeded onto PureCol® purified bovine collagen solution (Advanced BioMatrix, San Diego, CA, USA) coated 30mm dishes in NRC plating medium and left at 37°C in 5% CO_2 for 24 hr. After 24 hr, cells that were to be transfected were placed into transfection medium (20% M199, 75% DBSSK, 4% horse serum, 4mM Glutamine; DBSS-K: 6.8 g/l NaCl, 0.14mM NaH2PO4, 0.2 mM CaCl2, 0.2mM MgSO4, 1mM dextrose, 2.7mM NaHCO3) . Cells not used for transfection were transferred into NRC maintenance medium (75% DMEM, 20% M199, 4% horse serum, 4 mM Glutamine, 1% penicillin/streptomycin, 0.1 mM phenylephrine, 10 μM cytosine-B-D-arabino-furanoside hydrochloride [AraC]).

2.2.2 Adult Rat Cardiomyocytes

Adult rat cardiomyocytes (ARCs) were isolated by Dr. Shiney Reji from Langendorff perfused adult male Wister rats (250-300g body weight). Cells were seeded onto PureCol® purified bovine collagen solution (Advanced BioMatrix, San Diego, CA, USA) coated 30mm dishes with COS maintenance medium (10% fetal calf serum, 1% penicillin/streptomycin and 4 mM Glutamine in DMEM) at 37°C in 5% CO_2.

2.2.3 COS-1 Cells

COS-1 cells (Gluzman 1981) were cultured in COS maintenance medium at 37°C in 5% CO_2. Cells were passaged at 70-80% confluency by trypsinisation. For passaging, cells were treated with 2ml trypsin/EDTA solution (Sigma, St. Louis, MO, USA) for 5min at 37°C, before stopping the trypsin digest by addition of COS maintenance medium. For transfection, cells were plated onto 30mm dishes and grown to 50-70% confluency.

2.2.4 C2C12 Cells

C2C12 cells (Yaffe and Saxel 1977) were cultured in C2C12 maintenance medium (20% fetal calf serum 1% penicillin/streptomycin and 4mM Glutamine in DMEM) at 37°C in 5% CO_2. Cells were passaged with standard trypsinisation (See 2.2.3) and plated at $1x10^5$ cells onto collagen coated 30mm dishes. Cells were changed into C2C12 differentiation medium (2% horse serum 1% penicillin/streptomycin and 4 mM Glutamine in DMEM) and left to differentiate over a time course of 14 days at 37°C in 5% CO_2

2.2.5 HeLa Cells

HeLa cells (Scherer et al. 1953) were cultured in COS maintenance medium at 37°C in 5% CO_2. Cells were passaged at 70-80% confluency by trypsinisation (See 2.2.3). For transfection, cells were plated onto 30mm dishes and grown to 50-70% confluency.

2.2.6 Latrunculin B Treatment

NRCs were transfected and cultured in transfection medium as described in 2.10.1. Cells were grown for 5 days in transfection medium containing 1μg/ml verapamil. Actin depolymerisation took place by treatment with 20μM latrunculin B (VWR International) in transfection medium containing verapamil (1μg/ml) overnight. The Latrunculin B was subsequently washed out and replaced with NRC maintenance medium containing verapamil (1μg/ml) for 1hr. Cells were then fixed in paraformaldehyde and stained as described below (See 2.11.1). (Iskratsch et al. 2010)

The Latrunculins bind actin monomers in a 1:1 complex thereby inhibiting actin polymerization. They are heterocyclic marine toxins that were initially derived from the Red Sea sponge *Latrunculia magnifica*. Latrunculin A is characterised by a 16-member ring and Latrunculin B is characterised by a 14-member ring. Both compounds contain a rare 2-thiazolidinone moiety. Initial experiments using these compounds revealed that they had a profound impact on cell morphology, an effect attributed to their action on actin but not on microtubules (Spector et al. 1983). While the effects of both Latrunculin A and B are reversible, Latrunculin A is the more potent of the two compounds and its effects on cell morphology are less transient than those of latrunculin B (Spector et al. 1989). The more transient effects on cell morphology noted with Latrunculin B was one of the reasons for selection of this agent over Latrunculin A, especially considering that thin filament recovery following depolymerisation was being investigated. Furthermore, Latrunculin A was not used in this assay because it has been suggested that myofibrils are stable in the presence of Latrunculin A (Wang et al. 2005; Ono 2010). Although cytochalasin, a fungal toxin that prevents actin assembly (Goddette and Frieden 1986), seemingly represented an option to induce thin filament disruption, we selected Latrunculin B over cytochalasin (i.e., cytochalasin D) for the following reason: while the thin filaments of isolated cardiomyocytes are susceptible to inhibition by cytochalasin D during plating, mature thin filaments seemingly become resistant to cytochalasin D treatment after they have adapted to culture conditions (Rothen-Rutishauser et al. 1998).

The concentration of Latrunculin B used in this experiment was previously optimised in our laboratory in similar experiments using NRCs (Iskratsch et al. 2010). The

seemingly high working concentration of Latrunculin B used may have been partially influenced by the presence of serum in the medium required to culture NRCs. It has been suggested that the effects of Latrunculin B are dampened by the presence of serum since previous studies have described how the presence of serum shifted the working range of latrunculin B concentrations upward as much as ten-fold (Wakatsuki et al. 2001). However, serum in the NRC medium was essential in order to promote cell viability and adequate expression of the transfection constructs and has been a longstanding and integral component of NRC growth mediums that have been previously described (Chlopcikova et al. 2001).

The addition of verapamil was also required for the disassembly of thin filaments in NRCs. Verapamil is an L-type calcium channel blocker that inhibits cross-bridge cycling in cardiomyocytes and is used as a rate-controlling anti-hypertensive drug in humans due to its cardiac-specific negative inotropic effects. Previous attempts to disassemble the thin filaments of NRCs with Latrunculin B were unsuccessful but the addition of verapamil facilitated disassembly of thin filaments, a side effect attributed to destabilisation of the sarcomeric Z-disks.

Previous optimization efforts in our laboratory revealed that overnight treatment with Latrunculin B was required for a complete effect to be seen (Iskratsch et al. 2010). After latrunculin B wash out, NRC maintenance medium containing phenylephrine was added to cells. Phenylephrine, an alpha-1 adrenergic agonist was included in the NRC maintenance medium to promote thin filament recovery, since phenylephrine has been shown to promote sarcomere assembly and increase cell size, although this response varies according to the substrate that cells are plated on (e.g., laminin versus collagen) (Taylor et al. 2000). Verapamil was included in the NRC maintenance medium after wash out as previously indicated (Iskratsch et al. 2010). One discrepancy that arose in this protocol regarded the antagonistic effects that phenylephrine and verapamil have on myofibrillar contractility. While phenylephrine increases intracellular Ca^{2+} concentration and stimulates cardiac contractility, verapamil blocks intracellular Ca^{2+} transients and beating. Through these antagonistic effects, verapamil has been shown to partially inhibit phenylephrine induced hypertrophy and sarcomere assembly in NRCs (Eble et al. 1998). Nevertheless, the present conditions were sufficient to induce

depolymerisation of F-actin and myofibrils, although future experiments may require optimisation in order to address the outlined discrepancies.

2.2.7 SMIFH2 Treatment

The formin inhibitor 1-(3-bromophenyl)-5-(2-furylmethylene)-2-thioxodihydro-4,6(1H,5H)-pyrimidinedione (ID#5992446, ChemBridge™), here referred to as SMIFH2 was purchased from Chembridge Corporation (San Diego, CA, USA). SMIFH2 lyophilised powder was reconstituted in DMSO as described by Rizvi et al.2009 and stored at -80°C (Rizvi et al. 2009). NRCs were treated with 30μM SMIFH2 in 2ml of culture medium over a time course of 2, 4, and 8hr.

SMIFH2, is an inhibitor of formin mediated actin assembly. It was found to inhibit actin polymerisation by formins at the level of nucleation, elongation, and association with the barbed end of filaments. The effects of the inhibitor have been attributed to its targeting the conserved FH2 domain, although binding by the small molecule has never been shown (Rizvi et al. 2009). Moreover, it was shown to specifically inhibit formins and not any other actin polymerising proteins such as Arp2/3. However, there are still a number of uncertainties regarding how it exerts its effects. While SMIFH2 is thought to inhibit formin mediated actin polymerisation by targeting the conserved FH2 domain, initial characterisation efforts have been limited to investigating only a handful of formins: mDia1, mDia2, and Cdc12. Further characterisation of SMIFH2 will be required in order to establish if it indeed acts on all members of the formin family of proteins, whether its effects on individual formins occur at specific concentrations, and whether it can inhibit other activities attributed to formins, such as actin bundling.

2.3 Antibodies

Experimental procedures involving Western blotting and immunofluorescence required the use of antibodies to identify specific proteins. An account of the primary antibodies and their appropriate dilutions is given in Table 2.1. The Polyclonal Rabbit anti-sarcomeric α-actinin was kindly donated by Prof. Dieter Fürst. The Polyclonal Rabbit anti-all Myosin Binding Protein C was produced by Prof. Mathias Gautel. The Monoclonal Mouse anti- Myomesin B4 hybridoma supernatant was produced by Dr.

Elisabeth Ehler. The Polyclonal Rabbit anti-NRAP antibody was specially generated by immunisation of rabbits with a peptide portion of NRAP by Bioscience (Göttingen, Germany) and donated by Dr. Elisabeth Ehler. All Cy conjugated secondary antibodies were purchased from Jackson Immuno Research (West Grove, PA, USA). All secondary antibodies employed in this study were of "multi-labelling" quality, i.e. had been tested for a lack of cross-reaction between the relevant species (mouse, rat and rabbit). These secondary antibodies were used in combination successfully in the past and no cross-reaction was ever seen e.g. (Nosal et al. 1992; Ehler et al. 1999; Lange et al. 2002; Ahuja et al. 2004; Ehler et al. 2004; Ahuja et al. 2006; Ahuja et al. 2007; Hirschy et al. 2010; Iskratsch et al. 2010; Iskratsch et al. 2013a; Dwyer et al. 2014). The mouse and rat HRP conjugated secondary antibodies were purchased from DAKO (Glostrup, Denmark) and the goat and rabbit HRP conjugated secondary antibodies were purchased from Chemicon (CA, USA). Counterstains were also used to visualise specific subcellular compartments. An account of the secondary antibodies, counterstains, and their appropriate dilutions is given in Table 2.2.

Primary Antibody	Source	Dilution WeB	Dilution IF
Polyclonal Goat anti-FHOD1 C14 (sc-46964), raised against internal epitope of human protein	Santa Cruz Biotechnology, Santa Cruz, CA, USA	1:500	1:50
Polyclonal Goat anti-FHOD1 C20 (sc-46965), raised against the C-terminus of the human protein	Santa Cruz Biotechnology, Santa Cruz, CA, USA	1:500	1:50
Polyclonal Mouse anti-FHOD1 (ab73443) , raised against the full-length human protein	Abcam, Cambridge, UK	1:500	1:50
Polyclonal Mouse anti-FHOD1 (FM3521), raised against the full-length human protein	ECM Biosciences, Versailles, KY, USA	1:500	1:50
Polyclonal Rabbit anti-PhosphoThreonine1141 (FP3481), raised against peptide sequence surrounding Threonine1141 in human FHOD1.	ECM Biosciences, Versailles, KY, USA	1:500	1:50
Monoclonal Rat anti-HA	Roche Applied Science, Mannheim, Germany	N/A	1:100
Monoclonal Mouse anti-GFP	Roche Applied Science, Mannheim, Germany	1:1000	N/A
Monoclonal Mouse anti-T7	Novagen/Merck, Darmstadt, Germany	1:1000	1:100
Polyclonal Rabbit anti-dsRed	Clontech/TaKaRa Bio, Shiga, Japan	1:1000	N/A
Monoclonal Mouse anti-c-myc	Roche Applied Science, Mannheim, Germany	1:1000	1:100
Monoclonal Mouse anti-FLAG M2	Sigma, St. Louis, MO, USA	1:1000	1:100
Polyclonal Goat anti-GST	GE-Healthcare, Amersham Place, UK	1:5000	N/A
Polyclonal Rabbit Anti-LexA	Abcam, Cambridge, UK	1:2000	N/A

Monoclonal Mouse anti-sarcomeric-α-actinin clone EA53	Sigma, St. Louis, MO, USA	1:500	1:250
Polyclonal Rabbit anti-α-actinin	D. Fürst	N/A	1:200
Polyclonal Rabbit anti-all Myosin Binding Protein C	M.Gautel	N/A	1:50
Monoclonal Mouse anti-Myomesin clone B4	E. Ehler	N/A	1:200
Polyclonal Rabbit anti-β-catenin	Sigma, St. Louis, MO, USA	N/A	1:250
Polyclonal Rabbit anti-NRAP	Bioscience, Göttingen, Germany	N/A	1:50
Monoclonal Mouse anti-desmin clone D33	DAKO, Glostrup, Denmark	1:1000	N/A

Table 2.1: List of Primary Antibodies used for Western Blotting and Immunofluorescence Studies. Names of primary antibodies are given with the species of animal they were raised in. The companies and individuals where antibodies were acquired from are given as the source. Dilutions for antibodies are listed for western blotting and immunofluorescence. WeB, western blotting; IF, immunofluorescence; N/A, not applicable; HA, haemagglutinin; GFP, green fluorescent protein; GST, glutathione S-transferase.

Secondary Antibody	Source	Dilution WeB	Dilution IF
Donkey Cy2 conjugated anti-Rabbit	Jackson Immuno Research, West Grove, PA, USA	N/A	1:100
Donkey Cy5 conjugated anti-Rabbit	-	N/A	1:100
Goat Cy2 conjugated anti-Mouse	-	N/A	1:100
Goat Cy3 conjugated anti-Mouse	-	N/A	1:500
Goat Cy5 conjugated anti-Mouse	-	N/A	1:100
Donkey Cy2 conjugated anti-Mouse (Rat absorbed)	-	N/A	1:100
Donkey Cy3 conjugated anti-Mouse (Rat absorbed)	-	N/A	1:100
Donkey Cy5 conjugated anti-Mouse (Rat absorbed)	-	N/A	1:100
Goat Cy2 conjugated anti-Rat (Mouse absorbed)	-	N/A	1:100
Donkey Cy2 conjugated anti-Goat	-	N/A	1:100
Donkey Cy3 conjugated anti-Goat	-	N/A	1:100
Rabbit HRP anti-Mouse	DAKO, Glostrup, Denmark	1:1000	N/A
Goat HRP anti-Rat	-	1:1000	N/A
Goat HRP anti-Rabbit	Chemicon, CA, USA	1:1000	N/A
Rabbit HRP anti-Goat	-	1:1000	N/A
Counterstain	Source	Dilution WeB	Dilution IF
DAPI	Sigma, St. Louis, MO, USA	N/A	1:100
Alexa 633 Phalloidin	Invitrogen, Renfrew, UK	N/A	1:50
Alexa 546 Phalloidin	-	N/A	1:100

Table 2.2: List of Secondary Antibodies and Counterstains used for Western Blotting and Immunofluorescence Studies. Names of HRP and fluorophore conjugated secondary antibodies are given with the species of animal they were raised in and which species they recognised. DAPI was used to visualise nuclei and Alexa fluor conjugated Phalloidin was used to visualise F-actin. The companies where antibodies and counterstains were acquired from are given as the source. Dilutions for antibodies and counterstains are listed for western blotting and immunofluorescence. WeB, western blotting; IF, immunofluorescence; Cy, cyanine fluor; HRP, horse radish peroxidase; DAPI, 4',6diamidino2phenylindole; N/A, not applicable.

2.3.1 Validation of Novel Antibodies

We attempted to characterise the specificity of the 5 commercially available anti-FHOD1 antibodies that were presently used for Western blot and Immunofluorescence studies. Validation efforts took place by testing the antibodies against human FHOD1 and FHOD3 expression constructs in Western blot and immunofluorescence studies. Validation efforts for the antibodies recognising total FHOD1 (polyclonal goat anti-FHOD1 C14 [Santa Cruz], polyclonal goat anti-FHOD1 C20 [Santa Cruz], polyclonal mouse anti-FHOD1 [Abcam], polyclonal mouse anti-FHOD1 [ECM Biosciences]) can be found in section 3.1. Validation efforts for the polyclonal rabbit anti-PhosphoThreonine1141 FHOD1 antibody can be found in section 4.2.

2.4 Preparation of Transfection Constructs

2.4.1 First Strand cDNA Synthesis with Reverse Transcriptase

Human skeletal muscle cDNA was generated for use as a template in PCR. 2µg total RNA from adult human skeletal muscle were mixed with 0.5µg d(T)18 and 0.5µg d(N)10 Primers. Nuclease free water was added to make a final volume of 15µl. The mix was incubated at 75°C for 5min and subsequently cooled on ice. Then 5µl of 5x RT buffer, 1.5µl of 10 mM dNTPs, 0.5µl RNasin (RNase Inhibitor), 2µl nuclease free water and 100U of M-MLV reverse transcriptase (Promega, Madison, WI, USA) were added to the mixture. The reaction was incubated at 42°C for 90min. Finally the reverse transcriptase enzyme was denatured by incubating at 75°C for 10min.

2.4.2 PCR

The full-length long variant of FHOD1[1-1191] was amplified from 0.5µl human skeletal muscle cDNA (See 2.4.1), using LaTaq polymerase (TaKaRa Bio, Shiga, Japan) and 0.02nmol sense and antisense primers (synthesized by Eurofins MWG Operon, Ebersberg, Germany). FHOD1 ΔDAD [1-1096] was later amplified using 0.2µl of the GFP-tagged full-length FHOD1 [1-1191] construct DNA as a template. 50µl total reaction volume contained 25µl 2x GC buffer 1, 80nmol dNTPs, and 2.5U LaTaq DNA polymerase. PCRs were performed on a Techne TC-512 thermal cycler

(Techne, Chelmsford, UK). Products were amplified using a touchdown approach (for improved product yield), implementing a denaturation temperature of 98°C for 1.5min during all cycles. For the first 5 cycles an annealing temperature of 65°C was implemented for 2min. For the next 30 cycles the annealing temperature was lowered to 62°C for 2min. The elongation temperature used throughout the touchdown procedure remained at 72°C for 1.5min.

FHOD1 domain constructs (FH2, GBD-DID, GBD, and DID) were amplified using 0.2µl of the full-length FHOD1 [1-1191] construct DNA as a template. Amplifications were performed using 20pmol sense and antisense primers (Eurofins MWG Operon, Ebersberg, Germany). 50µl total reaction volume contained 5µl 10x HF buffer, 10nmol dNTPs, and 0.8U Phusion-High Fidelity DNA polymerase (Finnzymes, Espoo, Finland). PCRs were performed on a TC-512 thermal cycler. After hot start and initial denaturation at 98°C (1.5min) fragments were amplified with touchdown procedure conditions listed above but reducing the extension time to 1min due to the smaller product sizes. Primer pairs used for amplification reactions are listed in table 2.3.

Construct	Primer Sequence	Restriction Enzyme
pEGFP C2- FHOD1$_L$ [1-1191]	FW 5'GGAATTCATGGCGGGCGGGGAAGAC3'	EcoRI
	RV 3'GGGGTACCCACCTCCAGGCCAGGACC5'	KpnI
pEGFP C2- FHOD1$_L$ ΔDAD [1-1096]	FW 5'GGAATTCATGGCGGGCGGGGAAGAC3'	EcoRI
	RV 3'GGGGTACCGGCGATTGTGTGTGGTG5'	KpnI
pEGFP C2- FHOD1 FH2 [642-1031]	FW 5'GGAATTCGACAGCTCAGCCCTCCCC3'	EcoRI
	RV 3'GGGGTACCGGCGATTGTGTGTGGTG5'	KpnI
pEGFP C2- FHOD1 GBD [1-116]	FW 5'GGAATTCATGGCGGGCGGGGAAGAC3'	EcoRI
	RV 3'GGGGTACCAAGATAGCGTTGACCCTC5'	KpnI
pEGFP C2- FHOD1 GBD-DID [1-340]	FW 5'GGAATTCATGGCGGGCGGGGAAGAC3'	EcoRI
	RV 3'GGGGTACCTTCTTCGATGTCTCCATC5'	KpnI
pEGFP C1- FHOD1 DID [117-340]	FW 5'GGAATTCTACCCAGCTCTCTGTGAGG3'	EcoRI
	RV 3'GGGGTACCTTCTTCGATGTCTCCATC5'	KpnI

Table 2.3: List of PCR Primers Used to Amplify FHOD1 Constructs. Construct names are given in the left hand column with the name of the vector used for cloning into, followed by the portion of FHOD1 that was amplified. The middle column lists the primer pairs used for PCR reactions and their orientation. 5'→3' indicates sense direction and 3'→5' indicates antisense direction. The right hand column lists the restriction enzymes used and which primer sequence they correspond to. FW, indicates forward primer; RV, indicates reverse primer; L, FHOD1 long variant; pEGFP C1, green fluorescent protein (GFP) expression vector frame1; pEGFP C1, green fluorescent protein (GFP) expression vector frame 2.

2.4.3 Cloning

DNA fragments amplified from PCR (See 2.4.2) were cloned into the pEGFP-C1 and pEGFP-C2 (Clontech/TaKaRa Bio, Shiga, Japan) vectors for eventual expression as N-terminally-tagged green fluorescent fusion proteins. Insert DNA was cloned into the vector through the EcoRI and KpnI sites. Digests were performed under standard conditions with EcoRI (12U/µl Promega, USA) and KpnI (10U/µl, Promega, USA) at

37°C with subsequent purification with the WizardR SV Gel and PCR Clean-Up System (Promega, USA). Inserts were ligated into the vector using a 3:1 insert to vector ratio using 1µl of 10x T4 DNA ligase buffer (Promega, USA), 0.5µl of T4 DNA ligase (3u/µl, Promega, Madison, WI, USA) in a 10µl reaction. Constructs were transformed into competent *Escherichia coli* (XL1 blue strain) and plated onto LB agar plates (Thermo Fisher Scientific Waltham, MA) containing 50µg/ml kanamycin. Colonies were selected, cultured overnight in 5ml LB broth liquid cultures (Thermo Fisher Scientific Waltham, MA) containing 50µg/ml kanamycin, and the plasmid constructs were subsequently purified using the PureYield™ Plasmid Miniprep System (Promega, USA). Refer to Appendix Figure 8.1 for maps of all the FHOD1 expression constructs.

2.4.4 Sequencing

All sequencing was performed with Eurofins MWG Operon (Ebersberg, Germany). 50-100ng/µl purified plasmid DNA (diluted in 12µl H20) were sequenced with 2pmol/µl of the appropriate sequencing primer. GFP-tagged constructs were sequenced with the GFP forward and SV40 reverse primers specified by MWG.

2.4.5 Constructs

The following constructs were outsourced. The GFP-FHOD1 full-length short variant [1-1164], GST-FHOD1 [1-513], GST-FHOD1 GBD-DID [1-340], LEXA-FHOD1 [340-585], and LEXA-FHOD1 GBD-DID [1-340] were cloned by the Randall Protein Production Facility. The HA-DLG [1395-1919] was cloned in our laboratory by Nadine Lohmann. GFP-FHOD3 FH1 [941-1079] and GFP-FHOD3 CTS [1065-1622] were cloned in our laboratory by Dr. Thomas Iskratsch. The TOMATO-FHOD1 [1-1191] and the GFP-FHOD1 3A, 3D, ΔGBD, and V228E constructs were kindly donated by Dr. Thomas Iskratsch (Columbia University, New York, USA). The NRAP (SR5-6, SR5-7, SR4, r01-r10, LIM) constructs were kindly donated by Dr. Katja Gehmlich (University of Oxford, Oxford, UK). The Rho family small GTPase (CA Rac1 G12V, CA Cdc42 G12V) and the ROCK (CA ROCK-I Δ1 and WT ROCK-II) constructs were kindly donated by the lab of Prof. Anne Ridley (King's College London, UK). The Src (WT, CA, DA) constructs were donated by the lab of Dr. Michael Way (LRI, London, UK).
The remainder of the constructs were made in-house by myself. These included the following constructs: GFP-FHOD1 [1-1191], GFP-FHOD1 ΔDAD [1-1128], GFP-

FHOD1 GBD [1-116], GFP-FHOD1 DID [117-340], GFP-FHOD1 GBD-DID [1-340], GFP-FHOD1 FH2 [642-1031], 1095 shRNA construct, 2375 shRNA construct, and the 2635 shRNA construct.

2.4.6 Validation of Expression Constructs

Expression constructs were validated by testing their expression in COS-1 cells. COS-1 cells were transfected (See 2.10.2), cultured to 2 days, and subsequently lysed in SDS lysis buffer. Samples were resolved on SDS-PAGE gels with subsequent Western blotting (See 2.9.1). This was performed to see if constructs expressed at the correct size in cells.

2.5 RNA Interference

A vector-based shRNA approach was used to deplete FHOD1 in cultured cells. Oligonucleotides were designed to target 22 nucleotide sequences of FHOD1 in *Rattus norvegicus* and *Mus musculus*. Three sets of sense and antisense 64mer DNA oligonucleotides were designed against separate portions of FHOD1 (Table 2.4) and were referred to by the section of the FHOD1 coding sequence they corresponded to. Oligonucleotides were obtained from Sigma-Genosys (Poole, UK) in 0.05μM scale and dissolved to a final concentration of 1mM. 2nmol of forward and reverse oligonucleotides were diluted in 50μl of annealing buffer (30 mM HEPES, 100 mM potassium acetate and 2mM magnesium acetate at pH 7.4) and incubated for 4min at 98°C, 10min at 70°C and then slowly cooled down to 4°C. Annealed oligonucleotides were ligated into the BglII and XhoI restriction sites of a modified cDNA 3.1 vector (H1GFP vector), which was constructed by Dr. Stephan Lange by inserting the H1 expression cassette from pSUPER. The vector functions under the control of the polymerase III H1-RNA gene promoter thereby transcribing small RNA transcripts which are further processed to siRNAs that target homologous cellular RNA for degradation. The vector additionally expresses GFP under control of the CMV promoter. The system is described in Brummelkamp et al. 2002 (Brummelkamp et al. 2002). The vector underwent restriction digest by BglII (10U/μl, Promega) and XhoI (10U/μl, Promega) and the unphosphorylated DNA oligonucleotides were then ligated into the vector and cloned using *Escherichia coli* (XL1 blue strain) as described above (See 2.1.3). Transformed bacteria were plated onto LB agar plates containing

ampicillin 50µg/ml. Colonies were selected, cultured overnight in 5ml LB broth liquid cultures with ampicillin 50µg/ml, and the plasmid constructs purified as described above (See 2.4.3).

RNAi Construct	Oligonucleotide Sequence
H1GFP - FHOD1 1095	FW5'GATCCCCAGGAGCCGAAGATCACTAGAAGTTCAAGAGACTTCT AGTGATCTTCGGCTCCTTTTTTGGAAC3' RV3'TCGAGTTCCAAAAAAGGAGCCGAAGATCACTAGAAGTCTCTTG AACTTCTAGTGATCTTCGGCTCCTGGG5'
H1GFP - FHOD1 2375	FW5'GATCCCCGCCACTGTTTGATCTGAAAGTGTTCAAGAGACACTT TCAGATCAAACAGTGGCTTTTTGGAAC3' RV3'TCGAGTTCCAAAAAGCCACTGTTTGATCTGAAAGTGTCTCTTG AACACTTTCAGATCAAACAGTGGCGGG5'
H1GFP - FHOD1 2635	FW5'GATCCCCGCTGTGCCAAGGTGGACTTTGATTCAAGAGATCAAA GTCCACCTTGGCACAGCTTTTTGGAAC3' RV3'TCGAGTTCCAAAAAGCTGTGCCAAGGTGGACTTTGATCTCTTG AATCAAAGTCCACCTTGGCACAGCGGG5'

Table 2.4: List of Oligonucleotides Used to Design RNAi Constructs. Construct names are given in the left hand column with the name of the vector used for cloning into. Oligonucleotide names incorporate the starting base pair of the target sequence. The right hand column lists the sequence of the 64mer oligonucleotides and their orientation. FW, indicates forward primer; RV, indicates reverse primer; H1GFP, RNAi vector functioning under the H1 promoter that additionally expressed green fluorescent protein (GFP).

2.6 Library Screens and Interactions Assays using the Yeast Two-Hybrid System

The FHOD1 GBD-DID [1-340] and FHOD1 [340-585] fragments were cloned into the pLEXA C vector (Dualsystems Biotech, Schlieren, CH) by the Randall Protein Production Facility using the EcoRI and KpnI restriction sites. For yeast transformations, plasmid DNA was mixed with denatured salmon sperm DNA (Dualsystems Biotech, Schlieren, CH) (~ 20 x plasmid DNA amount), *Saccharomyces cerevisiae* (L40 strain) (initially washed twice in yeast buffer A (10mM Tris-HCl, 1mM EDTA, and 100mM LiOAc at pH 7.5)), yeast buffer B (40% PEG 4000, 10mM Tris-

HCl, 1mM EDTA, and 100mM LiOAc at pH 7.5), and incubated for 20min at 30°C. After addition of DMSO to a final concentration of 6%, yeast were heat shocked at 42°C for 15min, spun down, re-suspended in sterile water and plated on selection plates lacking Tryptophan. For library screening, overnight cultures of yeast, already transformed with bait construct (FHOD1 GBD-DID [1-340] or FHOD1 [340-585] were transformed with pACT2 human cardiac muscle library (Clontech/TaKaRa Bio, Shiga, Japan) (kindly donated by Dr. Katja Gehmlich and amplified by Dr. Ay Lin Kho) as described above. After heat shocking, yeast were spun down, re-suspended in 2xYPD (Lab M, Lancashire, UK) medium and incubated for 90min at 30°C, spun down again and re-suspended in water. Transformants were screened by plating on selection plates lacking the amino acids Histidine, Tryptophan and Leucine. For β-galactosidase reporter assays, clones were transferred to Hybond N+ nylon membranes (GE Healthcare, Amersham Place, UK) on selection plates, lacking the amino acids Tryptophan and Leucine and grown for 3 days at 30°C. Membranes were frozen in liquid nitrogen, thawed, transferred to filter paper, pre-soaked with Z-buffer (60mM Na2HPO4, 40mM NaH2PO4, 10mM KCl, 1mM $MgSO_4$ and 50mM β-mercaptoethanol + 20µl 2% X-Gal in dimethylformamide) and incubated at 30°C for several hours. Library plasmids from positive clones were isolated using the QIAprep miniprep kit (Qiagen, Crawley, UK), following the manufacturer's instructions. Isolated plasmids were transformed into *Escherichia coli* (XL1 blue strain) for amplification. Plasmids were sequenced with a Gal4 AD sequencing primer (5' TAC CAC TAC AAT GGA TG 3'). For further verification of the interaction, identified clones were re-transformed into the yeast together with the empty pLEXA plasmid or the corresponding FHOD1 pLEXA constructs and grown on selection plates lacking Histidine, Tryptophan and Leucine and containing 2.5mM 3-amino-1,2,4-triazole. The NRAP SR5-6 and SR5-7 were cloned into the pACT2 vector by Dr. Atsushi Fukuzawa and used for the yeast two-hybrid assays.

2.7 Protein Expression

For protein expression, constructs were cloned into a pGEX-2TK vector (GE-Healthcare, Amersham Place, UK), including a GST-tag followed by a thrombin consensus sequence on the 5' end of the insert. Cloning of the FHOD1 [1-513] GST

construct and the FHOD1 GBD-DID [1-340] GST construct was performed by the Randall Protein Production Facility. After amplification of the plasmids in *Escherichia coli* (XL1 blue strain), plasmids were transformed into competent *Escherichia coli* (BL21-RIL strain), which were plated on LB-agar, containing ampicillin (100μg/ml). Colonies were picked, transferred into 50ml LB broth liquid cultures containing ampicillin (100μg/ml) and grown at 37°C while shaking at 150rpm until OD600 reached 0.6. Protein expression was then induced by addition of isopropyl β-D-1-thiogalactopyranoside (IPTG) to a final concentration of 0.4mM. Protein was expressed overnight at 18°C with cultures shaking at 150rpm. For lysis, cell suspensions were spun down and the pellet was re-suspended in pull-down lysis buffer with 1x protease inhibitor cocktail before addition of lysozyme. Cell suspensions were incubated for 1hr on ice while shaking before sonication (Jencons, Lutterworth, UK) and centrifugation at 5000 x g and 4°C for 30min. For GST-fusion proteins, glutathione sepharose 4 fast flow beads (GE Healthcare, Amersham Place, UK) at ~100μl/100ml initial culture volume were added to the lysates and incubated for 90min at 4°C on a rotating wheel. After incubation, beads were separated by centrifugation (3000 rpm, 4°C, 5min) and washed 3 times with pull-down lysis buffer. Overexpression and purification of GST-fusion proteins were confirmed by Western blotting (See 2.9.1) and Coomassie staining (2.9.2) as described below.

2.8 GST Pull-down Assay

The amount of GST-fusion protein bound to glutathione beads utilised for the GST-pull down assays was estimated by standardisation using SDS-PAGE (See 2.9.1) and Coomassie staining (See 2.9.2). Prior to commencing pull-down assays, 10% of the target protein lysates were taken as an input control. The cell lysates were incubated with the beads overnight on a rotating wheel at 4°C. Pull-down assays yielding a positive interaction were repeated by incubating cell lysates with the beads for 1 hr on a rotating wheel at 4°C. Three wash steps in pull-down lysis buffer using 10 times of the used bead volume were carried out for 1 min with gentle rotation on ice. After the first spinning at 4,000 rpm for 30 sec, 10% of the supernatant was taken as a second control. SDS lysis buffer was added to the final pellet in a ratio of 1:1 followed by boiling for 5 min, SDS-PAGE, and Western Blotting as described (See 2.9.1).

Although the pull-down lysis buffer was sufficient for extraction of the majority of the target proteins used for pull-down assays, the conditions in the buffer were not optimised for each of the interactions being tested. The lack of optimisation was reflected by the absence of positive controls for many seemingly negative interactions; therefore a number of the pull-down assays were inconclusive.

2.9 Resolution of Protein Samples by Gel Electrophoresis

2.9.1 SDS-PAGE and Western Blotting

Samples were electrophoretically separated on polyacrylamide minigels (Mini-Protean Electrophoresis System, Biorad, Hercules, Ca, USA). Tissue SDS samples were run on 7.5% SDS gels and other lysates were run on 10-12% SDS gels for Western Blotting. Gels were run at 200mV. A rainbow marker (Novex marker, Invitrogen, Carlsbad, CA, USA) was included for size standardisation. The gel containing the samples was then blotted onto a nitrocellulose membrane (Amersham, UK) in a wet Western blot apparatus and left to transfer in blotting buffer (25mM Tris-Base pH 8.3, 192mM Glycine, 0.01% SDS, and 20% methanol) overnight at 60mA. Membranes were stained with Ponceau red stain (Sigma, St. Louis, MO, USA) to confirm transfer and equal loading of protein samples. Blocking and destaining took place in 5% non-fat milk in low salt buffer (0.9% NaCl, 0.1% Tween-20, 9mM Tris Base pH7.4). Membranes were incubated with primary and secondary antibodies for 1hr at room temperature with three 5min washing steps in between. Protein bands were then visualised by enhanced chemiluminescence with 1min incubation of membranes in ECL solution (7.5ml H_2O, 1ml 10x Luminol (250 mg Luminol in 50ml H_2O), 1ml 10x Iodophenol (55mg Iodophenol in 50ml DMSO), 0.5ml 1M Tris pH 7.5, 5µl H_2O_2). Luminol was purchased from Sigma (Sigma, St. Louis, MO, USA) and Iodophenol from Fluka (Fluka, USA). Membranes were developed on X-ray film at varying exposure times.

2.9.2 Quantification of Western Blots

Quantification of the relative expression levels of FHOD1 in murine tissues on Western blots was performed with ImageJ software. The ImageJ software measurement tool was used to quantify the level of intensity within each region of interest (ROI) (i.e., band) in images converted to grayscale. The measurement tool was set to quantify mean grey value and area. The rectangle tool was used to capture each ROI and measurement areas were fitted to capture individual ROI. Background measurements of Western blots were also captured by taking measurements outside the ROI. Measurements were all adjusted to the rectangular area used around each ROI; this essentially calculated intensity per unit area of measurement. Background measurements were then subtracted from measurements of each band on the same blot. Quantification of relative FHOD1 levels in muscle tissue lysates was performed by normalising measurements to sarcomeric α-actinin levels. The present methodology is exemplified in the following flow of equations:

$$Background\ Reading = \left(\frac{Measurement\ Outside\ ROI}{Area\ of\ Rectangle\ used\ to\ Measure\ Background}\right)$$

$$FHOD1\ Measurement = \frac{Measurement\ of\ ROI}{Area\ of\ Rectangle\ used\ to\ Measure\ ROI} - Background\ Reading$$

$$\alpha - actinin\ Measurement = \frac{Measurement\ of\ ROI}{Area\ of\ rectangle\ used\ to\ measure\ ROI} - Background\ Reading$$

$$Relative\ Expression\ Level = \frac{FHOD1\ Measurement}{\alpha - actinin\ Measurement}$$

The quantification of Western blots was potentially restricted by the innate drawbacks of the technique and particularly the attainment of the linear range desired for accurate quantification. Enhanced chemiluminescence is limited by the characteristics of the X-ray film used: a minimal threshold for silver activation and the finite amount of silver grain available to detect signals can result in the non-linear response of X-ray film to weak or strong signals. Very faint signals, resulting from low light emission, may be underrepresented on X-ray films due to improper activation of the silver on the membrane. The amount of silver present on the film also represents a limiting substrate in detection of the chemiluminescence reaction. Oversaturation of the X-ray film can occur in the presence of a strong signal. In this situation, further signal cannot be

detected, the optical density of the band will plateau, and subsequent measurements will be underrepresented. The desirable linear range for quantification can thus be obtained when the density of the band on the film is proportional to the exposure time. Therefore, upon underexposure or oversaturation of protein signals on Western blots, a non-linear relationship between the amount of protein and the observed signal occurs and will skew quantification.

2.9.2.1 Statistical Analysis used for Quantification of Western Blots

The quantification of FHOD1 expression relative to α-actinin effectively compared the average levels of expression across different tissues. Three Western blots using samples from two C57/BL6 mice were quantified for this purpose and allowed for basic statistical analysis to be performed. In order to see if levels of expression were significantly different between two tissues, we employed an unpaired, two-tailed student's t-test. The student's t-test was deemed appropriate for this analysis since the means were being compared between 2 samples under the same condition (i.e., different treatment arms were not employed that would necessitate implementation of ANOVA analysis). Independent samples (e.g., murine heart, soleus, and tibialis anterior) were used for analysis of expression levels; therefore the t-test was unpaired. Since expression levels for a given sample could theoretically be higher or lower than the comparator sample, a two-tailed approach was used to test significance in both directions. A value of $P < 0.05$ was considered significant. The level of variability in expression levels was calculated using standard error of the mean (SEM)

2.9.3 Coomassie Staining

Polyacrylamide gels were stained with boiling 0.1% Coomassie Brilliant Blue R250 in 40% methanol and 10% acidic acid for 30min and subsequently destained for 30min in boiling 10% acidic acid.

2.10 Transient Expression Studies

2.10.1 Transient Transfection of Neonatal Rat Cardiomyocytes

NRCs were isolated as described above (See 2.2.1) and 1d after plating were transferred to transfection medium and transfected with approximately 1μg of plasmid DNA per 30mm plate using 3μl Escort III transfection reagent (Sigma, St. Louis, MO, USA). After 6hr, medium was replaced with NRC maintenance medium for short term transfections (up to 48hr) and subsequently replaced with transfection medium for long term transfections (> 48hr). Unless otherwise stated, cells were cultured for 48 h at 37°C in 10% CO_2.

2.10.2 Transient Transfection of COS-1 Cells

COS-1 cells were cultured as described above (See 2.2.3). Cells were transfected with approximately 1μg of plasmid DNA per 30mm plate, using Escort IV, following supplier's instructions (Sigma, St. Louis, MO, USA). After 48hr of maintenance at 37°C in 5% CO_2, cells were either fixed with 4% paraformaldehyde/PBS for 10min and examined by fluorescence microscopy, lysed with SDS lysis buffer for SDS-PAGE and western blotting, or lysed with pull-down assay lysis buffer.

2.10.3 Transient Transfection of C2C12 Cells

C2C12 cells were cultured as described above (See 2.2.4). Cells were transfected with approximately 1μg of plasmid DNA per 30mm plate, using Lipofectamine LTX with Plus reagent (Invitrogen, Carlsbad, CA, USA), following supplier's instructions. After 24hr of culture cells were then changed into C2C12 differentiation medium.

2.10.4 Transient Transfection of HeLa Cells

HeLa cells were cultured as described above (See 2.2.5). Cells were transfected with approximately 1μg of plasmid DNA per 30mm plate, using Lipofectamine LTX with Plus reagent (Invitrogen, Carlsbad, CA, USA), following supplier's instructions. After 24hr in maintenance medium at 37°C in 5% CO_2, cells were then changed into starvation medium (0.1% foetal calf serum, 1% penicillin–streptomycin, and 4mM Glutamine in DMEM) for 24hr prior to being fixed with paraformaldehyde.

2.11 Immunofluorescence

2.11.1 Staining of Cultured Cells

NRCs, ARCs, COS-1, C2C12, and HeLa cells were fixed prior to staining. Cells were fixed with 4% paraformaldehyde/PBS for 10min or with pre-cooled methanol (-20°C) for 5min at -20°C. When staining for endogenous FHOD1 in cells we compared paraformaldehyde and methanol fixation and their effect on the signals produced by the commercially available anti-FHOD1 antibodies. Paraformaldehyde fixation gave a consistently stronger and clearer signal for FHOD1, therefore it was used for all of the antibody localisation studies. Furthermore, localisation of the FHOD1 signal was not dependent on the fixation method. Permeabilisation took place using 0.2% Triton X-100/PBS for 2 min for COS-1, C2C12, and HeLa cells and 5min for NRCs and ARCs. Primary antibodies were diluted in Gold buffer (20 mM Tris, 155 mM NaCl, 2 mM EGTA, 2 mM MgCl2 at pH 7.5), as listed in Table 2.1. For triple-immunofluorescence staining Cy2/Alexa Fluor 488, Cy3 and Cy5/Alexa Fluor 633 conjugated secondary antibodies and Phalloidin (Invitrogen, Renfrew, UK), as well as 4',6-diamidino-2-phenylindole (DAPI, Sigma, St. Louis, MO, USA) were used. For double labelling of primary mouse antibodies together with monoclonal rat anti-HA, cross adsorbed anti-mouse and anti-rat antibodies were used. Secondary antibodies were diluted as listed in Table 2.2. Antibody incubations took place for 1hr at room temperature in a humid chamber. After each step, cells were washed 3 times for 5min with PBS. Finally, cells were mounted in Lisbeth's medium (0.1 M Tris-HCl/glycerol (3:7) and 50 mg/ml n-propylgallate at pH 9.5) with a glass coverslip (Messerli et al. 1993). Where cells where transfected with TOMATO-tagged constructs, dishes were mounted in Cherry mounting medium (See 2.13).

2.11.2 Staining of Tissue Sections

Wild-type and $MLP^{-/-}$ mouse hearts were frozen down in methylbutane, which was chilled in liquid nitrogen immediately after dissection and stored at -80°C until sectioning (See 2.1.2). Tissue sections were blocked in 5% horse or goat serum in Gold buffer for 20min. Staining took place using the same procedure with cultured cells (See 2.11.1).

2.11.3 Confocal Microscopy

All confocal microscopy was performed on a LSM510 laser scanning confocal microscope (Carl Zeiss MicroImaging GmbH, Jena, Germany) with solid state (diode) laser excitation at 405 nm and emission at 420-480 nm, Ar-laser excitation at 488 nm and emission at 505-530 nm or He-Ne-laser excitation at 546 and 633 nm and emission at 560-615 nm and > 650 nm, respectively, using a Plan-Apochromat 63x/1.4 oil objective, Plan-Neofluar 40x/0.9 oil objective, or a LCI Plan-Neofluar 25x/0.8 oil objective. An optical slice of 284 nm was used to acquire images. Sequential scans were used to acquire images in order to avoid bleedthrough. Visual inspection/cross-checking of individual channels was also performed prior to scanning images in order to partly gain a sense of bleedthrough between channels and possible background.

2.11.4 Quantification of F-actin Staining

Transfected HeLa cells were stained with Phalloidin as described above (2.11.1). Levels of F-actin were quantified from confocal images using ImageJ. 10 views were used for each construct per experiment using the Plan-Neofluar 40x/0.9oil objective. 1-5 transfected cells and 3-6 untransfected cells were present per view. In each view the Phalloidin pixel intensity was measured individually in transfected and untransfected cells. Values were obtained by normalising the average Phalloidin pixel intensities in transfected cells to untransfected cells. However, since the experiment was only performed once, it did not allow for an adequate sample size for statistical analysis to ensue. Instead, variability of the F-actin ratio measured for each construct was represented with standard deviation.

One caveat that applied to the measurement of the F-actin signal in HeLa related to the possibility that measurements may not have been captured within the desired linear range for quantification. Although fluorescence exhibits a fairly broad linear range, measurements may be skewed in the presence of a very bright signal. In this assay, the presence of F-actin stress fibres, with relatively bright staining for F-actin, may have been a source of error in the measurement of the Phalloidin pixel intensity. When

measurements are performed in the presence of an oversaturated F-actin signal, the relationship between the level of F-actin and the present signal is no longer linear.

2.11.5 Scoring of Myofibrillar Integrity for F-actin/Myofibril Depolymerisation Assay

The integrity of myofibrils was judged by looking at the distribution of α-actinin and F-actin, namely if they were incorporated into myofibrils and regained their striated appearance. Staining for F-actin was used to visualise myofibrils. Organisation at the level of the sarcomere was assessed by staining for the Z-disk marker, α-actinin. Transfected cells were counted and grouped according to whether they had poor, intermediate, or excellent myofibrillar integrity. Cells deemed to exhibit poor myofibrillar integrity were devoid of myofibrils and displayed patchy and irregular α-actinin staining. Cells deemed to exhibit intermediate myofibrillar integrity displayed evidence of filamentous F-actin-based structures with α-actinin distributing along them, although the spacing of α-actinin was irregular and hence indicated improper formation of the Z-disks. Cells deemed to have excellent myofibrillar integrity displayed well-formed myofibrils with regularly spaced Z-disks. Due to the fairly heterogeneous response seen with Latrunculin B treatments, baseline measurements were taken in untransfected cells as a comparison.

2.11.6 Calculation of Fusion Index in Differentiating C2C12 Cells

For RNAi experiments, a fusion index was calculated for day 7 C2C12 cells transfected with the shRNA constructs and the empty shRNA vector. Cells were stained with DAPI for enumeration of nuclei. Transfected cells were identified by their GFP signal, since the shRNA vectors additionally express GFP. The fusion index was calculated by taking the number of nuclei in transfected cells and dividing it by the total number of transfected cells. This essentially calculated the number of nuclei per cell. The values were represented as the average fusion index for the 70-100 cells that were counted for each construct. However, since the experiment was only performed once, it did not allow for an adequate sample size for statistical analysis to ensue. Instead, variability of the fusion indices measured for each construct was represented with standard deviation.

2.12 Sequence Alignment

2.12.1 Amino Acid Sequence Alignment

Sequence alignment was performed with clustalw2 (http://www.ebi.ac.uk/Tools/msa/clustalw2/). Alignment was performed using the amino acid sequence of FHOD1 from human (*Homo sapiens*; NCBI Reference Sequence: NP_037373.2), rat (*Rattus norvegicus*; NCBI Reference Sequence: NP_001178529.1), and mouse (*Mus musculus*; NCBI Reference Sequence: NP_808367.2). This was performed to look at the extent of sequence similarity between human and rodent FHOD1.

2.12.2 Nucleic Acid Sequence Alignment

Alignment of the shRNA target sequences used for RNAi experiments was performed with Mega5 (Tamura et al. 2011). Alignment was performed using the DNA sequence of *FHOD1* from human (*Homo sapiens*; Accession No: NM_013241.2), rat (*Rattus norvegicus*; Accession No: NM_001191600.1), and mouse (*Mus musculus*; Accession No: NM_177699.4). This was performed to confirm that the shRNA target sequences were matched to the corresponding sequence on rodent *fhod1* and to highlight mismatched base pairs on the corresponding human *FHOD1* sequence.

2.13 Buffers/Solutions/Media

Name	Contents
Annealing Buffer	30mM HEPES, 100mM potassium acetate and 2mM magnesium acetate at pH 7.4
Blotting Buffer	25mM Tris-Base pH 8.3, 192mM Glycine, 0.01% SDS, and 20% Methanol
C2C12 Differentiation Medium	2% horse serum 1% penicillin/streptomycin and 4mM Glutamine in DMEM
C2C12 Maintenance Medium	20% fetal calf serum 1% penicillin/streptomycin and 4mM Glutamine in DMEM
Cherry Mounting Medium	PVA (polyvinylalcohol) mix: 10 g Airvol 203 in 40 ml 0.14 M NaCl, 0.01 M KH_2PO_4, 0.01 M Na_2HPO_4; stir overnight, add 20 ml glycerol, stir again overnight, aliquot and store at -20°C. Before use add 1 part 10x n-propyl-gallate (250 mg/ml glycerol, mix overnight) to 9 parts PVA mix
COS Maintenance Medium	10% fetal calf serum, 1% penicillin/streptomycin and 4 mM Glutamine in DMEM
DBSS-K	6.8 g/l NaCl, 0.14mM NaH_2PO_4, 0.2mM $CaCl_2$, 0.2mM $MgSO_4$, 1mM dextrose, 2.7mM $NaHCO_3$
ECL solution	7.5ml H_2O, 1ml 10x Luminol, 1ml 10x Iodophenol, 0.5ml 1M Tris pH 7.5, 5ml H_2O_2
Gold Buffer	20mM Tris, 155mM NaCl, 2mM EGTA, 2mM $MgCl_2$ at pH 7.5
Iodophenol (10x solution)	55mg Iodophenol in 50ml DMSO
Lisbeth's Medium	0.1 M Tris-HCl/glycerol (3:7) and 50mg/ml n-propylgallate at pH 9.5
Low Salt Buffer	0.9% NaCl, 0.1% Tween-20, 9mM Tris Base pH7.4
Luminol (10x solution)	250 mg Luminol in 50ml H_2O
NRC Maintenance Medium	78% DMEM, 20% M199, 4% horse serum, 4mM Glutamine, 1% penicillin/streptomycin, 0.1mM phenylephrine, 10 µM cytosine-B-D-arabino-furanoside hydrochloride (AraC)
NRC Plating Medium	66% DMEM, 16.6% M199, 9.8% horse serum, 4.8% fetal calf serum, 4mM Glutamine, 1% penicillin/streptomycin
NRC Transfection Medium	20% M199, 75% DBSSK, 4% horse serum, 4 mM Glutamine
Pull-down Lysis Buffer	150 mM NaCl, 20 mM Tris-HCl pH 7.6, 1 mM EDTA, 0.2% (v/v) NP-40, 1 mM Dithiothreitol DTT
SDS Lysis Buffer	130mM Tris, 190mM SDS, 3.69M urea, 0.06% NP40, 0.17%β-mercaptoethanol, 3.85% glycerol and 0.01% bromophenol blue at pH 6.8
Starvation medium	0.1% fetal calf serum, 1% penicillin–streptomycin, and 4mM Glutamine in DMEM
TE Buffer	0.1M Tris-HCl, 10mM EDTA, pH7.5, sterile by filtration
Yeast Buffer A	10mM Tris-HCl, 1 mM EDTA, and 100mM LiOAc at pH 7.5
Yeast Buffer B	40% PEG 4000, 10mM Tris-HCl, 1mM EDTA, and 100mM LiOAc at pH 7.5
Yeast Lysis Buffer	8M Urea, 2% NP40, 1% TritonX1005%, glycerol-BPB, 5% β-mercaptoethanol, 5% SDS, 0.1M Tris-HCl pH6.7
Z-Buffer	60mM Na_2HPO_4, 40mM $NaH2PO_4$, 10mM KCl, 1mM $MgSO_4$ and 50mM β-mercaptoethanol + 20 µl 2% X-Gal in dimethylformamide

Table 2.5: List of Buffers, Solutions, and Media Used in all Experimental Procedures. Alphabetised list describing the contents of the buffers, solutions, and media used in all molecular, biochemical, and cell biological experimental procedures.

Chapter 3

Expression and Localisation of FHOD1

3. Expression and Localisation of FHOD1

3.1 Validation of Commercially Available Anti-FHOD1 Antibodies

In order to investigate the expression and localisation of FHOD1 at the tissue level, we performed Western blot and immunofluorescence studies with FHOD1 specific antibodies. We only used commercially available antibodies, however, due to the high levels of homology between formin family members and based on potential cross-reactivity of polyclonal antisera with other muscle proteins, we attempted to validate the specificity of our reagents. 4 different commercially available anti-FHOD1 antibodies were used to examine FHOD1. The 4 antibodies designed to recognise total levels of endogenous FHOD1 included the following: Polyclonal goat C14 anti-FHOD1 (Santa Cruz); Polyclonal goat C20 anti-FHOD1 (Santa Cruz); Polyclonal mouse anti-FHOD1 (Abcam); Polyclonal mouse anti-FHOD1 (ECM Biosciences). The polyclonal goat C14 anti-FHOD1 was raised against a peptide within an internal region of human FHOD1 whereas the C20 antibody was raised against a peptide near the C-terminus of human FHOD1. The polyclonal mouse anti-FHOD1 antibodies were raised against full-length human FHOD1.

The specificity of these 4 commercially available anti-FHOD1 antibodies was first tested against epitope tagged FHOD1 constructs, comprised of full-length variants of the protein as well as fragments. The expression constructs were transfected into COS-1 cells prior to harvest and visualization by Western blotting with the 4 anti-FHOD1 antibodies. The following constructs were used (Figure 3.1): GFP-tagged long variant of full-length FHOD1 comprising the alternatively spliced exons 12-13 [1-1191] (Figure 3.1 A); GFP-tagged short variant of FHOD1 lacking the alternatively spliced exons 12-13 [1-1164] (Figure 3.1 B); GFP-tagged truncation mutant of the long FHOD1 variant

lacking the C-terminal diaphanous autoregulatory domain (FHOD1 ΔDAD [1-1228]) (Figure 3.1 C); GFP-tagged truncation mutant of the long variant lacking the N-terminal GTPase binding domain (FHOD1 ΔGBD [117-1191]) (Figure 3.1 D); GFP-tagged FHOD1 [1-340], the N-terminus comprised of the GBD and diaphanous inhibitory domain (DID) (Figure 3.1 E); GFP-tagged GBD [1-116] (Figure 3.1 F); GFP-tagged DID (Figure 3.1 G); GFP-tagged formin homology 2 (FH2) domain [642-1031] (Figure 3.1 H); HA-tagged FHOD1 C-terminus [641-1191/616-1164] (Figure 3.1 I).

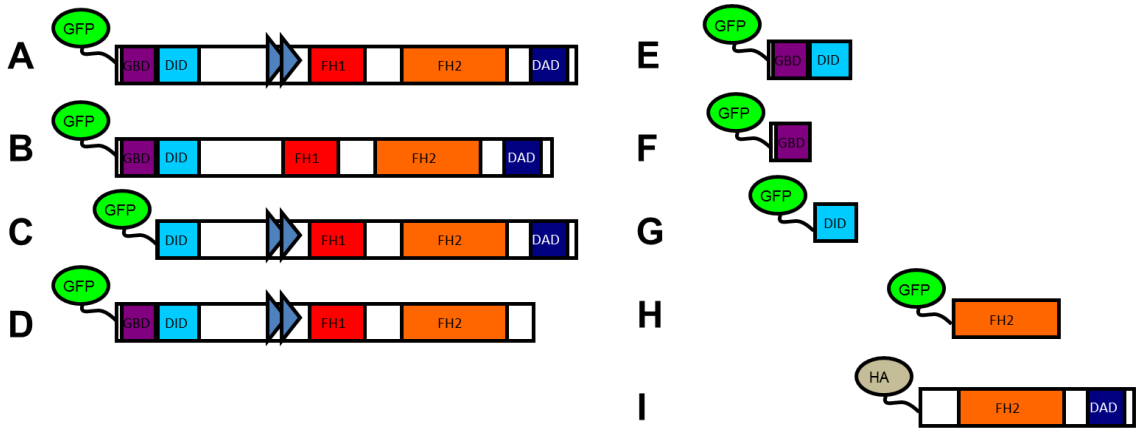

Figure 3.1: Maps of FHOD1 Expression Constructs used for Antibody Validation. Schematic representation of the different human FHOD1 expression constructs used throughout experimental procedures. **A)** GFP-tagged full-length long variant [1-1191] containing the alternatively spliced exons (E12-13). **B)** GFP-tagged full-length short variant [1-1164] lacking the alternatively spliced exons (E12-13). **C)** GFP-tagged full-length long variant truncation mutant containing the alternatively spliced exons (E12-13) and lacking the GBD [117-1191]. **D)** GFP-tagged full-length long variant truncation mutant containing the alternatively spliced exons (E12-13) and lacking the DAD [1-1128]. **E)** GFP-tagged GBD-DID [1-340]. **F)** GFP-tagged GBD [1-116]. **G)** GFP-tagged DID [117-340]. **H)** GFP-tagged FH2 [642-1031]. **I)** HA-tagged C-terminal construct of FHOD1 [641-1191/616-1164]. Amino acid length is given in brackets []. GBD, GTPase binding domain; DID, diaphanous inhibitory domain; FH, formin homology; DAD, diaphanous autoregulatory domain.

The following expression experiments describe qualitative results since the exact protein concentration was not determined before loading (Figure 3.2). In these experiments, some degradation of the longer FHOD1 constructs was apparent as evidenced by lower running faint bands. Western blot analysis revealed the portions of FHOD1 recognised by the commercially obtained antibodies. The polyclonal mouse FHOD1 antibodies from ECM Biosciences (Figure 3.2 A) and Abcam (Figure 3.3 B) recognised all of the variants and fragments of FHOD1. These antibodies therefore seemingly recognise multiple epitopes on FHOD1 within the N and C-termini. One

limitation of this experiments was that we were unable to ascertain whether the antibodies recognized portions of FHOD1 found within amino acids 341 to 641 on the long variant of FHOD1 containing the alternatively spliced exons or amino acids 341 to 615 on the short variant of FHOD1 lacking the alternatively spliced exons. These regions corresponded to the linker region and FH1 domain of FHOD1. While the seemingly indiscriminate recognition of multiple epitopes could call into question the specificity of the polyclonal mouse antibodies, this finding was in line with the fact that these antibodies were raised against the full-length FHOD1 molecule; therefore it is conceivable that they recognised multiple epitopes on the protein. The polyclonal goat antibodies recognised the full-length long and short variant of FHOD1 as well as the truncation mutants lacking either the GBD or DAD (Figure 3.2 C-D). Unlike the polyclonal mouse antibodies, the polyclonal goat antibodies specifically recognised the FH2 domain and the FHOD1 C-terminal construct, out of the FHOD1 fragments tested and did not show any reaction with GBD and/or DID. This is as expected considering that the polyclonal goat C14 and C20 antibodies were raised against an internal portion and a C-terminal portion of FHOD1, respectively. However, the caveat applies that we were unable to test for the specificity of the polyclonal goat antibodies against the portion of FHOD1 comprised of the linker region and FH1 region.

Overall, we demonstrated that the 4 antibodies could recognise human FHOD1 constructs on Western blots. In the case of the polyclonal mouse antibodies, these recognized multiple fragments of FHOD1 whereas the polyclonal goat antibodies recognized the C-terminus of FHOD1 but did not recognize the FHOD1 N-terminus, despite adequate expression of the GFP-tagged FHOD1 N-terminal fragments (Figure 3.2 E). It is unclear whether the polyclonal goat antibodies preferentially recognized the FH2 domain or the sequence of FHOD1 that lies downstream of the FH2 domain since the HA-tagged C-terminal FHOD1 construct also comprised the FH2 domain. Overall, the antibodies recognized the full-length human FHOD1 constructs and this was not mediated by the presence of the GFP tag, which was included on gels as a control.

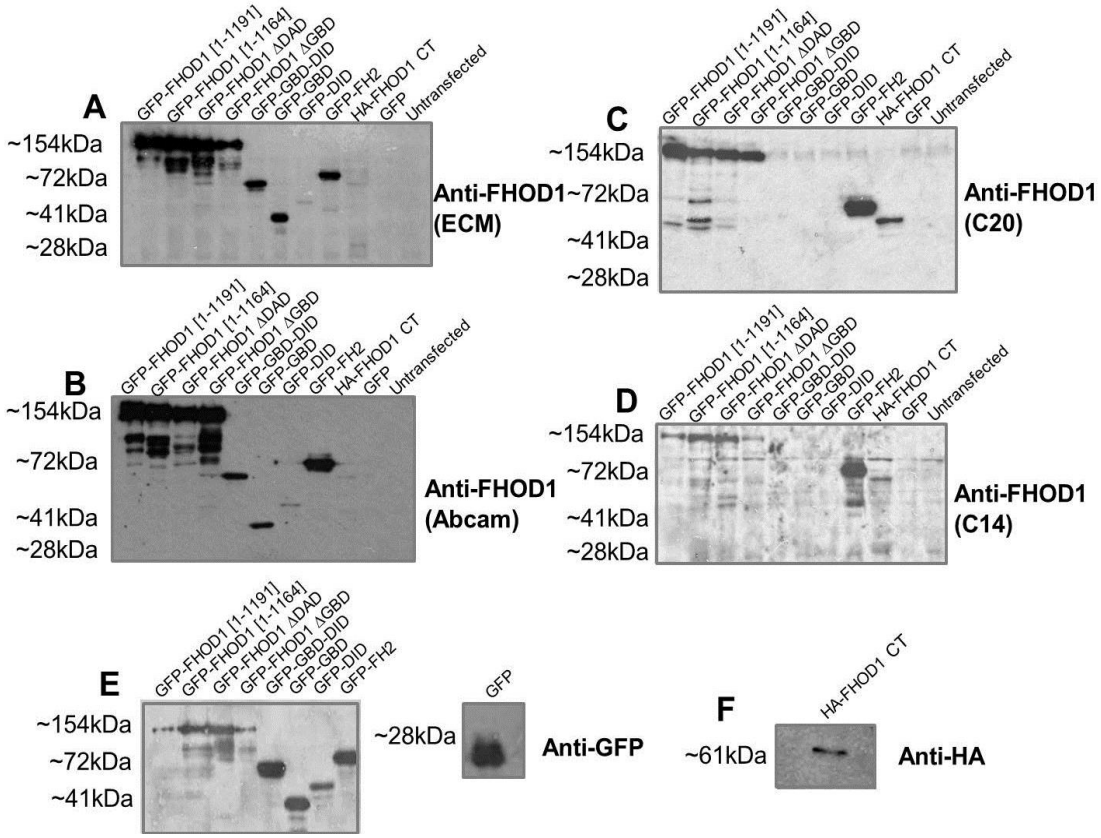

Figure 3.2: Validation of anti-FHOD1 Antibodies against FHOD1 Constructs. COS-1 cells were transfected with the following epitope tagged FHOD1 constructs: GFP-tagged full-length long variant [1-1191] containing the alternatively spliced exons (E12-13); GFP-tagged full-length short variant [1-1164] lacking the alternatively spliced exons (E12-13); GFP-tagged full-length long variant truncation mutant containing the alternatively spliced exons (E12-13) and lacking the GBD [117-1191]; GFP-tagged full-length long variant truncation mutant containing the alternatively spliced exons (E12-13) and lacking the DAD [1-1128].; GFP-tagged GBD-DID [1-340]; GFP-tagged GBD [1-116]; GFP-tagged DID [117-340]. H) GFP-tagged FH2 [642-1031]; HA-tagged C-terminal construct of FHOD1 [641-1191/616-1164]. Cells were cultured to day two prior to lysis and resolution by SDS-PAGE followed by Western blotting. Blots were tested with the commercially available anti-FHOD1 antibodies in order to gauge the specificity of each antibody. Blots were incubated with the following anti-FHOD1 antibodies: **A)** Polyclonal Mouse (ECM Biosciences); **B)** Polyclonal Mouse (abcam); **C)** Polyclonal goat C20 (Santa Cruz); **D)** Polyclonal goat C14 (Santa Cruz). **E)** Expression of the GFP-tagged constructs was confirmed by incubating blots the with the anti-GFP antibody. **F)** Expression of the HA-tagged FHOD1 C-terminal construct was confirmed using the anti-HA antibody. Relative molecular weight marker is shown on the left hand side of blots. Amino acid length is given in brackets []. Some degradation was apparent for the longer FHOD1 constructs. GBD, GTPase binding domain; DID, diaphanous inhibitory domain; FH, formin homology; DAD, diaphanous autoregulatory domain. **N=3**

In order to rule out cross-reactivity with FHOD1's sister homolog, FHOD3, we performed Western blot and immunofluorescence studies using COS-1 cells that were transiently transfected by the full-length long variant of FHOD1 [1-1191], HA-tagged FHOD3, or the empty GFP vector. Cross-reactivity with FHOD3 could have represented an issue since human FHOD1 and FHOD3 bear 52.1% amino acid similarity. While the anti-FHOD1 antibodies recognised GFP-tagged FHOD1 as a band running around 156kDa, none of the anti-FHOD1 antibodies displayed evidence of cross-reactivity with FHOD3 on Western blots (Figure 3.3 A-D) despite the presence of HA-tagged FHOD3 in the lanes (Figure 3.3 F), which resolved as a band running at approximately 160kDa. While the lower running bands in the lanes of lysates with GFP-tagged FHOD1 most likely represented degradation products, the band running near the 128kDa marker produced by the polyclonal goat anti-FHOD1 antibodies in all three lanes likely represented recognition of endogenous FHOD1 in COS-1 cells. However, in the absence of an antigen competition assay, it was not possible to determine with certainty that this band corresponded to endogenous FHOD1. Overall, the present Western blot studies indicated that the anti-FHOD1 antibodies recognised human FHOD1 and did not cross-react with human FHOD3.

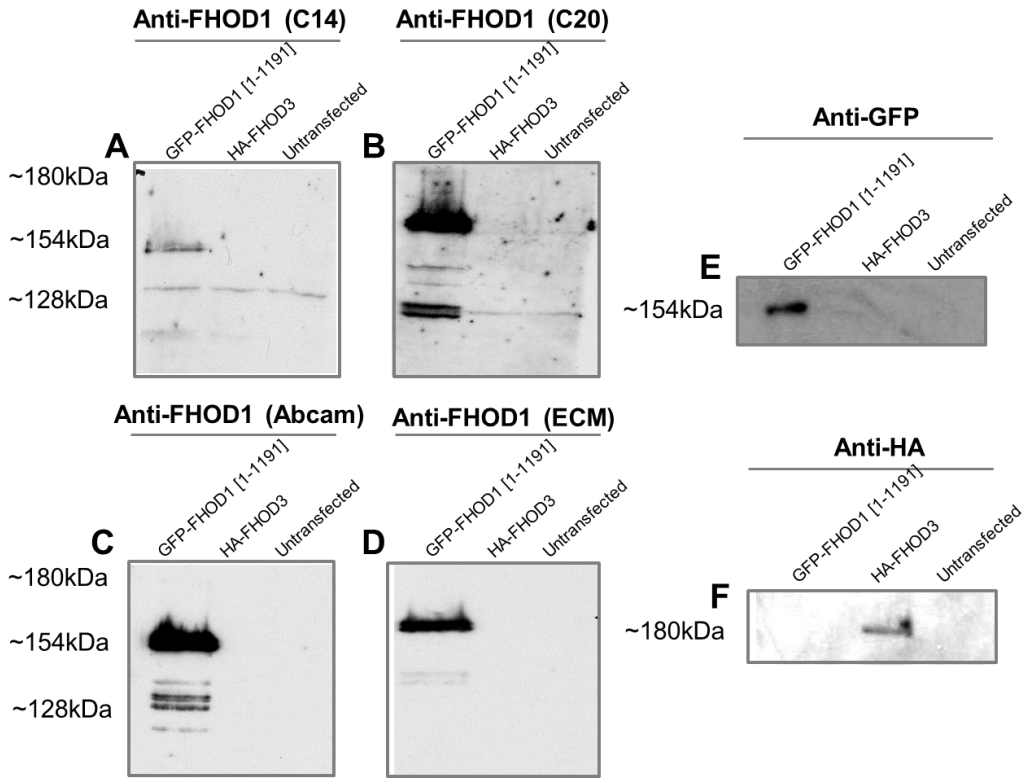

Figure 3.3: Assessment of Cross-Reactivity against FHOD3 with the anti-FHOD1 Antibodies by Western Blotting. COS-1 cells were transfected with the GFP-tagged full-length long variant of FHOD1 containing the alternatively spliced exons (E12-13) or the HA-tagged full-length long variant of FHOD3. Cells were cultured to day two prior to lysis and resolution by SDS-PAGE followed by Western blotting. Blots were tested with the commercially available anti-FHOD1 antibodies in order to gauge the specificity of each antibody and to rule out any cross-reactivity with FHOD3. Blots were incubated with the following anti-FHOD1 antibodies: **A)** Polyclonal Goat C14 (Santa Cruz), **B)** Polyclonal Goat C20 (Santa Cruz), **C)** Polyclonal Mouse (abcam), **D)** Polyclonal Mouse (ECM Biosciences), **E)** Phospho-Thr1141 (ECM Biosciences). **E)** Blots were visualised using the anti-GFP antibody to confirm the presence of GFP-tagged FHOD1. **F)** Blots were visualised with the anti-HA antibody to confirm the presence of HA-tagged FHOD3, especially in the absence of cross-reactivity with the anti-FHOD1 antibodies. Lane 1, lysates of COS-1 cells transfected with GFP-FHOD1; Lane 2, lysates of COS-1 cells transfected with HA-FHOD3; Lane 3, lysates from untransfected COS-1 cells. Relative molecular weight marker is shown on the left hand side of blots. Some degradation was apparent with the FHOD1 construct. GFP, green fluorescent protein. HA, haemagglutinin. **N=2**

Results from immunofluorescence studies resonated those found via Western blotting. The anti-FHOD1 antibodies recognised GFP-tagged FHOD1 when overexpressed in COS-1 cells (Figure 3.4). With the exception of the polyclonal goat C14 antibody, which produced a signal for FHOD1 that only displayed minimal co-localisation with GFP-tagged FHOD1 (Figure 3.4 A), the remainder of the anti-FHOD1 antibodies produced a signal that displayed abundant co-localisation with GFP-tagged FHOD1 throughout the cytoplasm of cells (Figure 3.4 B-D). Control cells, transfected with the empty GFP vector and thus expressing just the GFP tag, were also stained with the anti-FHOD1 antibodies (Figure 3.5). No substantial co-localisation was noted between the antibody signal and the GFP tag. In COS-1 cells transfected with HA-tagged FHOD3 (Figure 3.6), no co-localisation was noted between the signal produced by the anti-FHOD1 antibodies and the HA signal, indicating that the antibodies did not recognise human FHOD3. While we were able to rule out cross-reactivity of the anti-FHOD1 antibodies with human FHOD3, we were unable to do so with certainty for rodent FHOD3. However, similarly to human FHOD1 and FHOD3, which bear 52.1% amino acid similarity, human FHOD1 bears 56% amino acid similarity to rat and mouse FHOD3. This comparable level of homology was not associated with cross-reactivity of the anti-FHOD1 antibodies when human FHOD3 constructs were concerned and suggest that it would be a similar case for rodent FHOD3, however, such findings are merely suggestive that no cross-reactivity would occur and do not substitute for biochemical verification of antibody cross-reactivity against rodent FHOD3 constructs.

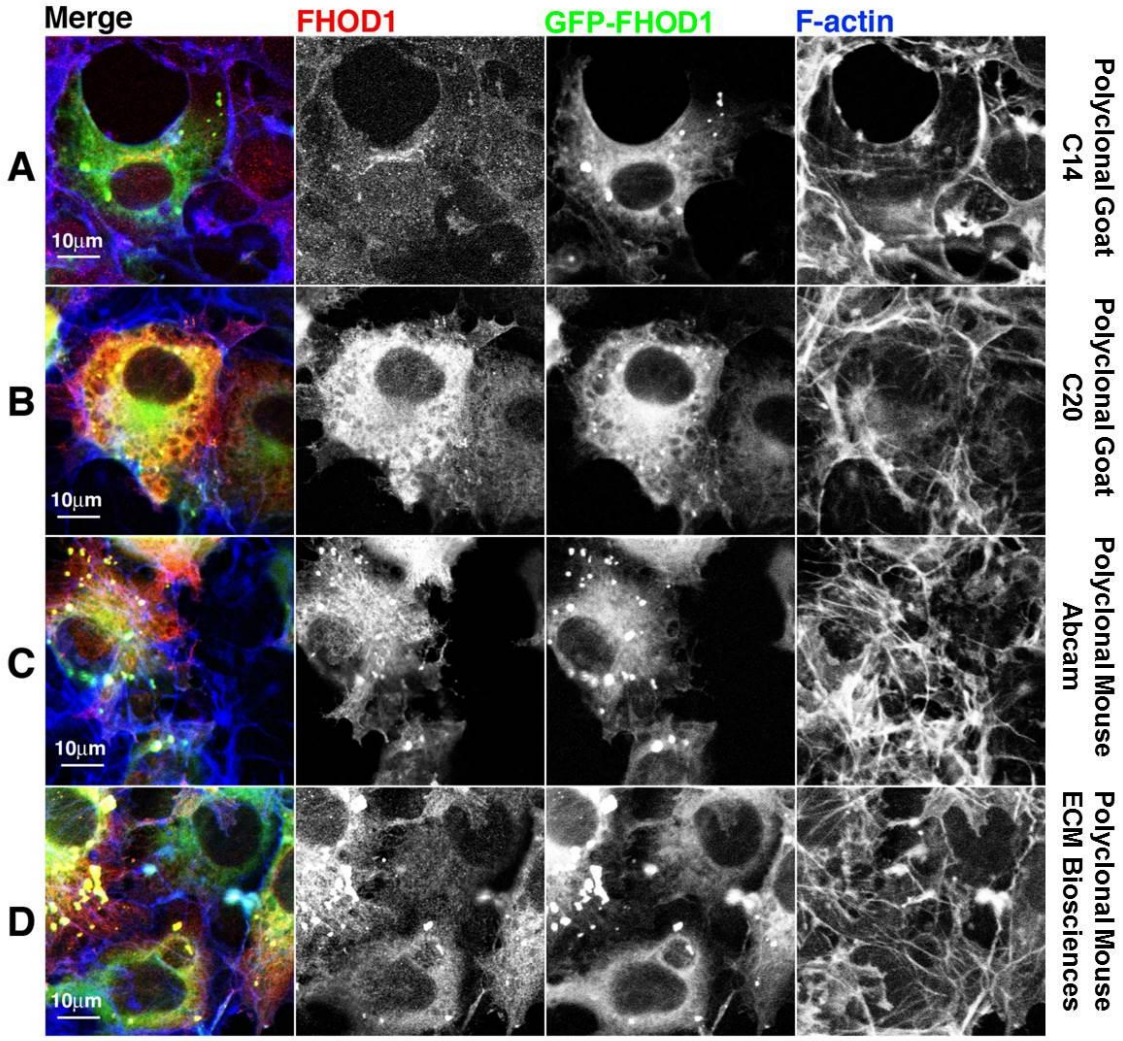

Figure 3.4: Validation of anti-FHOD1 Antibodies with Full-length FHOD1 by Fluorescence Confocal Microscopy. COS-1 cells were transfected with GFP-tagged full-length long variant of FHOD1 containing the alternatively spliced exons (E12-13), cultured to day two, fixed, and stained with the commercially available anti-FHOD1 antibodies. This was performed in order to gauge the specificity of each antibody in immunofluorescence specimens. COS-1 cells were stained with the following anti-FHOD1 antibodies: **A)** Polyclonal goat C14 (Santa Cruz), **B)** Polyclonal goat C20 (Santa Cruz), **C)** Polyclonal mouse (Abcam), **D)** Polyclonal mouse (ECM Biosciences). GFP-FHOD1 is seen in green, anti-FHOD1 antibodies in red, F-actin in blue. Scale bar represents 10μm. **N=2**

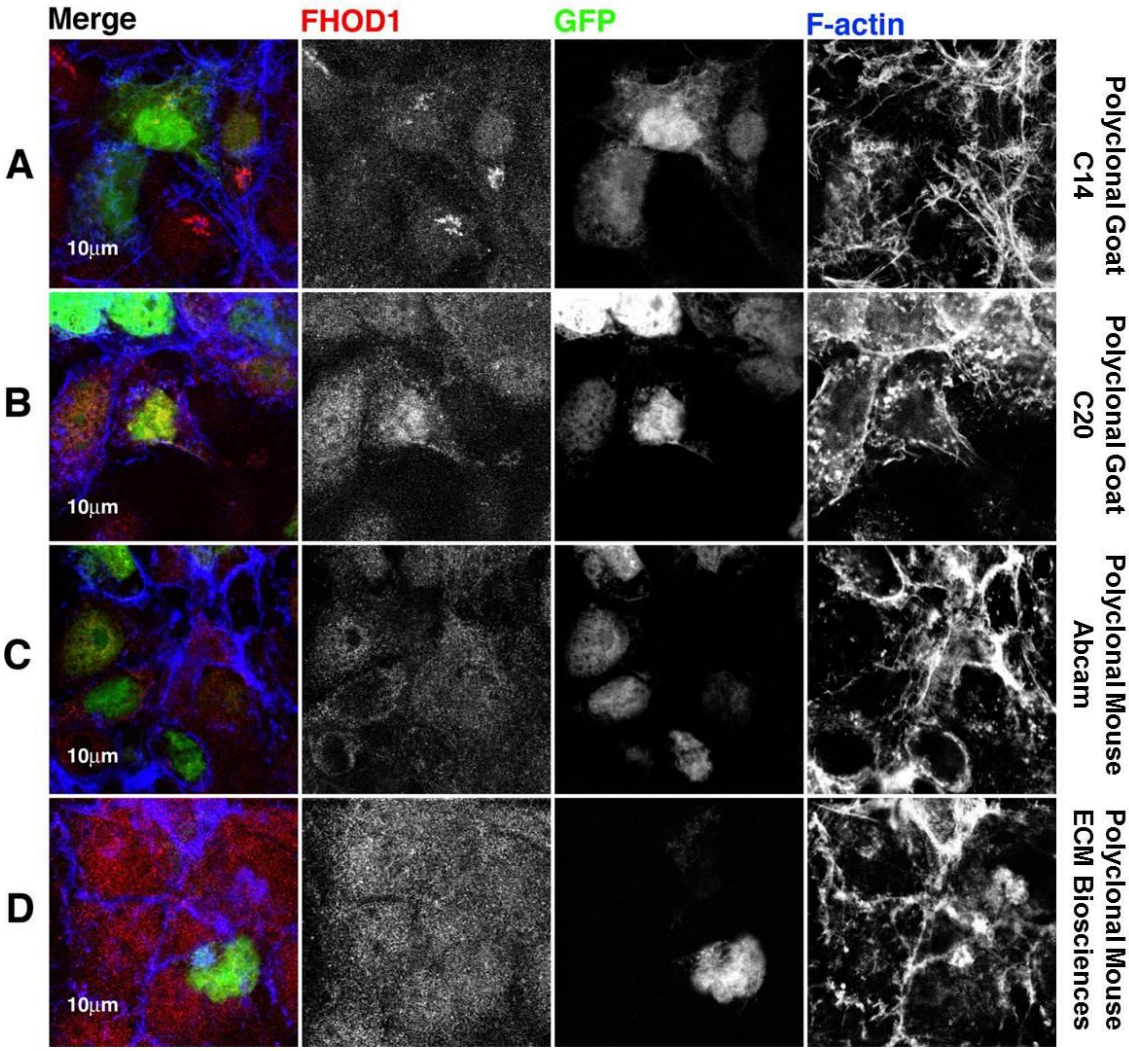

Figure 3.5: Assessing the Reactivity of the anti-FHOD1 Antibodies against GFP by Fluorescence Confocal Microscopy. COS-1 cells were transfected with the empty GFP vector, cultured to day two, fixed, and stained with the commercially available anti-FHOD1 antibodies. This was performed in order to gauge the specificity of each antibody in immunofluorescence specimens. COS-1 cells were stained with the following anti-FHOD1 antibodies: **A)** Polyclonal goat C14 (Santa Cruz), **B)** Polyclonal goat C20 (Santa Cruz), **C)** Polyclonal mouse (Abcam), **D)** Polyclonal mouse (ECM Biosciences). GFP-FHOD1 is seen in green, anti-FHOD1 antibodies in red, F-actin in blue. Scale bar represents 10µm. **N=2**

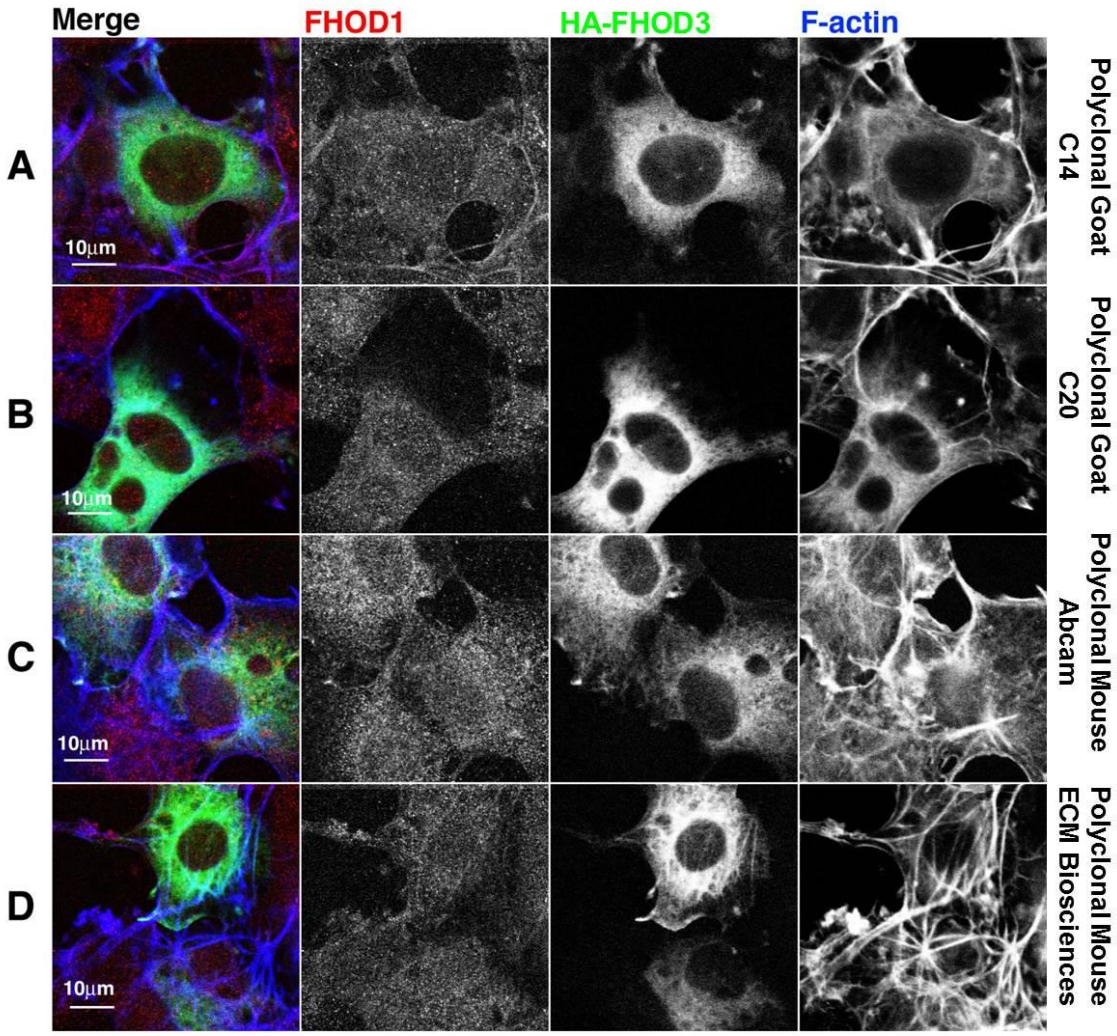

Figure 3.6: Validation of anti-FHOD1 Antibodies with Full-length FHOD3 by Fluorescence Confocal Microscopy. COS-1 cells were transfected with the HA-tagged full-length long variant of FHOD3, cultured to day two, fixed, and stained with the commercially available anti-FHOD1 antibodies. This was performed in order to gauge the specificity of each antibody in immunofluorescence specimens and to rule out any cross-reactivity with FHOD3. COS-1 cells were stained with the following anti-FHOD1 antibodies: **A)** Polyclonal goat C14 (Santa Cruz), **B)** Polyclonal goat C20 (Santa Cruz), **C)** Polyclonal mouse (Abcam), **D)** Polyclonal mouse (ECM Biosciences). HA-FHOD3 is seen in green, anti-FHOD1 antibodies in red, F-actin in blue. Scale bar represents 10µm. **N=2**

While the above studies addressed the specificity of the FHOD1 antibodies against the human FHOD1 protein, they do not clarify whether the antibodies were sensitive enough to recognise FHOD1 in mouse and rat tissues. In the absence of rodent FHOD1 constructs, we performed an amino acid sequence comparison of the short variant of human FHOD1 with rat and mouse FHOD1 (Figure 3.7). The overall sequence identity between human FHOD1 and rat FHOD1 was 86%. Homology between the human FHOD1 N-terminus [1-357] and the rat FHOD1 N-terminus [1-360] was 94%. Homology between the human FHOD1 internal portion [358-626] and the rat FHOD1 internal portion [361-619] was 73%. Homology between the human FHOD1 C-terminus [627-1164] and the rat FHOD1 C-terminus [620-1138] was 86%. The overall sequence identity between human FHOD1 and mouse FHOD1 was 91%. Homology between the human FHOD1 N-terminus [1-357] and the mouse FHOD1 N-terminus [1-360] was 94%. Homology between the human FHOD1 internal portion [358-626] and the mouse FHOD1 internal portion [361-619] was 75%. Homology between the human FHOD1 C-terminus [627-1164] and the mouse FHOD1 C-terminus [620-1138] was 91%. This sequence comparison suggested that human FHOD1 bears considerable homology to rat and mouse FHOD1, particularly within the N and C-termini. We demonstrated via Western blot analysis that the polyclonal mouse antibodies recognised portions of the FHOD1 N and C-termini. Furthermore, we demonstrated that the polyclonal goat antibodies recognised portions of the FHOD1 C-terminus. Therefore, the commercially available anti-FHOD1 antibodies could conceivably have possessed sufficient sensitivity to recognize rodent FHOD1 at the tissue and cellular level. However, such findings are only suggestive of sensitivity and do not substitute biochemical verification of antibody sensitivity against rodent FHOD1 constructs.

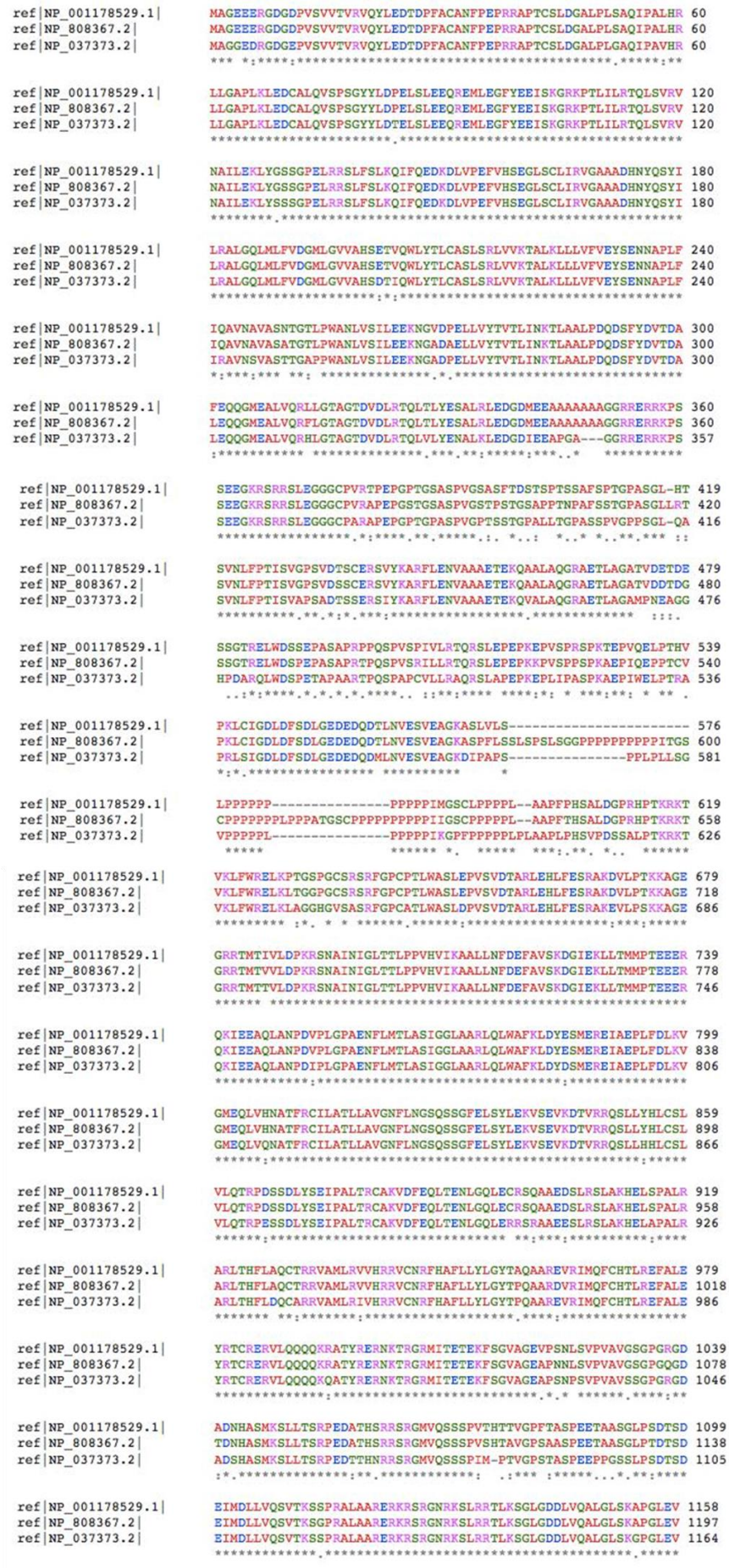

Figure 3.7: Sequence Comparison between Human and Rodent FHOD1. Alignment of the human FHOD1 amino acid sequence with the corresponding portions of mouse and rat FHOD1. The top reference sequence represents the *Rattus norvegicus* sequence (NCBI Reference Sequence: NP_001178529.1) [1-1138]. The middle reference sequence represents the *Mus musculus* sequence (NCBI Reference Sequence: NP_808367.2) [1-1197]. The bottom reference sequence represents the *Homo Sapiens* sequence (NCBI Reference Sequence: NP_037373.2) [1-1164]. Sequence alignment was performed with clustalw2 (http://www.ebi.ac.uk/Tools/msa/clustalw2/).

3.2 Expression of FHOD1 in Muscle

The characterisation of FHOD1 was initiated by examining the expression pattern of the FHOD1 protein in murine muscle samples. Currently there are few studies describing the expression of FHOD1 in muscle. FHOD1 mRNA has been found in lymphatic tissue but also in skeletal muscle, cardiac muscle, lung, kidney, and colon (Gill et al. 2004). Originally, FHOD1 was found to be abundantly expressed in the spleen (Westendorf et al. 1999). FHOD1 protein was previously described as being expressed in the aortic and coronary vasculature, bladder, lung, testis, stomach, and skeletal muscle (Wang et al. 2004). However, the protein expression profile of FHOD1 is not in complete agreement with the reported mRNA expression profile, since FHOD1 expression has been reported as absent in murine myocardial lysates (Staus et al. 2011a). However, a more-recent study reported FHOD1 expression at the mRNA transcript and protein level in human cardiac and skeletal muscle (Krainer et al. 2013). Presently, expression levels of FHOD1 were examined in mouse skeletal muscle (tibialis anterior and soleus) and mouse cardiac muscle.

Western blot analysis of FHOD1 protein was performed using lysates from murine muscle tissue and out of the 4 antibodies, only the polyclonal mouse anti-FHOD1 antibody (abcam) produced a discernible signal for the protein when visualised by enhanced chemiluminescence. While the other anti-FHOD1 antibodies should theoretically have recognised FHOD1 in murine heart lysates, they may not have done so because the method of sample preparation (i.e., subjection to denaturing conditions such as boiling), which may have comprised the epitope site they would have otherwise recognised in rodent tissue. Expression was present in the heart, tibialis anterior (TA), and soleus (Figure 3.8 A). A band for FHOD1 could be identified as running above the 123 kDa marker, which is consistent with the predicted molecular weight of murine FHOD1, approximately 129kDa. Since high FHOD1 expression has been reported in the spleen (Westendorf et al. 1999), spleen lysates were also loaded as a positive control, where a strong signal for FHOD1 could be seen at the same molecular weight. To gauge the relative expression levels of FHOD1 in the different muscle samples, densitometric analysis of Western blots was performed. The intensity of the single

FHOD1 band was measured in each sample and normalised to levels of sarcomeric α-actinin, which was used to visualise the loading of the protein samples (Figure 3.8 B-C). Highest FHOD1 expression was observed in the heart with levels in the heart 2.66 times greater than that seen in the TA (P=0.0077) and 4.9 times greater than that seen in the soleus (P=0.0023). Levels of FHOD1 in the TA were 1.85 times greater than that seen in the soleus (P=0.0417). Lowest levels of FHOD1 expression occurred in soleus samples. Overall, these results suggest that significantly greater expression of FHOD1 occurs in cardiac and fast twitch skeletal muscle, rather than slow twitch skeletal muscle. However, it is important to note that this experiment only provides information on the relative levels of expression of FHOD1 between murine tissues since the total protein concentration of the tissue lysate preparations was not measured. While the SDS lysis buffer used for all experiments was optimised for extraction of cytoskeletal proteins, the concentrations of the urea, β-mercaptoethanol, and SDS used in the buffer interfere with most protein assays (e.g., bicinchoninic acid [BCA] assay). Furthermore, in the absence of an antigen competition assay, we could not conclude with certainty that we were measuring levels of FHOD1 instead of another protein.

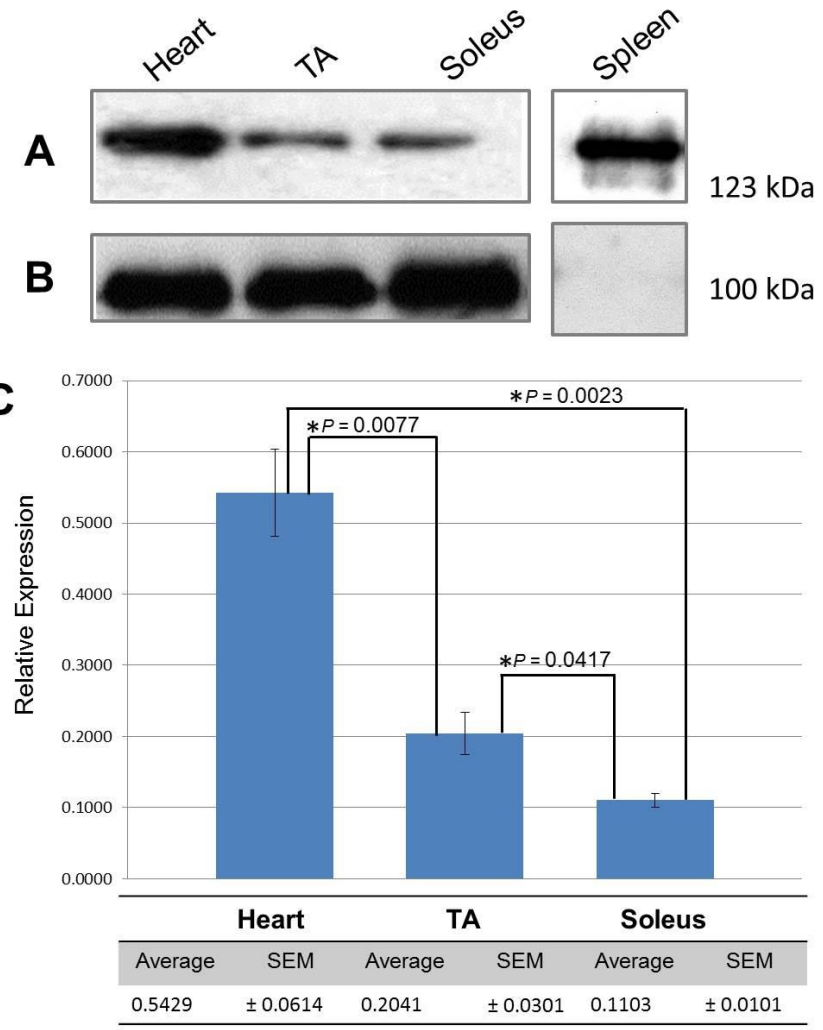

	Heart		TA		Soleus	
	Average	SEM	Average	SEM	Average	SEM
	0.5429	± 0.0614	0.2041	± 0.0301	0.1103	± 0.0101

Figure 3.8: Expression of FHOD1 in Striated Muscle. Western blot of murine tissue lysates from heart, TA, soleus, and spleen. **A)** Western blot probed with the polyclonal mouse anti-FHOD1 antibody (Abcam). Spleen samples were loaded as a positive control. **B)** Western blot probed against sarcomeric α-actinin. **C)** Bar chart displaying relative expression levels of FHOD1 in striated muscle. Relative levels were obtained by performing densitometric analysis on bands visualised by Western blotting. The relative intensity of FHOD1 bands were normalised to that of the α-actinin bands. Relative expression is expressed as arbitrary units. TA, tibialis anterior; kDa, kilodaltons. An unpaired, two-tailed student's t-test was used to test for statistical significance. **P*<0.05. Error bars represent standard error mean. **N=3** repetitions of Western blots with 2 sets of samples.

3.3 Localisation Studies in Heart Muscle

After potentially establishing that FHOD1 was expressed in striated muscle we set out to investigate the subcellular localisation of the formin protein in cardiac muscle. A number of localisations have previously been reported for FHOD1 including distribution within the cytoplasm (Westendorf et al. 1999) and at the plasma membrane (Westendorf 2001; Gill et al. 2004; Hannemann et al. 2008). FHOD1 has also been found to be targeted to a number of structures that contain actin such as stress fibres and membrane ruffles (Koka et al. 2003). It has also been suggested that the protein can translocate to the nucleus in instances of apoptosis (Menard et al. 2006). The consensus reached by most studies is that FHOD1 is targeted to F-actin based structures, especially after activation (Gasteier et al. 2003). Such studies looking at FHOD1 have mainly investigated targeting of the protein in cultured cells by overexpression studies. However, there is little published data reporting the localisation of endogenous FHOD1 protein. Localisation of endogenous FHOD1 was examined in Co396 cells (a vascular smooth muscle cell line), where the protein was found to distribute within the cytoplasm and in the perinuclear region of cells (Wang et al. 2004). A more recent study examining FHOD1 localisation in *Caenorhabditis elegans* found that FHOD1 was localised near the equivalent of the sarcomeric Z-disks in striated body wall muscles (Mi-Mi et al. 2012). We performed a number of localisation studies by staining against endogenous FHOD1 with the commercially available anti-FHOD1 antibodies. To build a picture of where FHOD1 was localised in heart muscle we stained for FHOD1 in neonatal rat cardiomyocytes (NRCs), adult rat cardiomyocytes (ARCs), and mouse heart tissue sections. Localisation was visualised by confocal microscopy.

Prior to commencing localisation studies, we sought to confirm the presence of endogenous FHOD1 at the protein level via Western blotting in NRCs and ARCs. The following experiments describe qualitative results since the exact protein concentration was not determined before loading; we merely sought to confirm the presence of endogenous FHOD1. The 4 commercially available anti-FHOD1 antibodies were tested for their reactivity against day 3 NRCs and day 0 freshly isolated ARCs lysates. The GFP-tagged long variant of FHOD1 was loaded as a positive control to demonstrate that the antibodies were functioning in the possible absence of a signal in the cultured cardiomyocyte lysates. All 4 anti-FHOD1 antibodies produced a signal for the protein

as a band migrating at approximately 128kDa in NRC lysates (Figure 3.9 A-D). Furthermore, the band for FHOD1 in ARCs as visualised by the polyclonal mouse (Abcam) antibody ran at a slightly higher molecular weight than that seen in NRCs, and could indicate the presence of a different FHOD1 isoform. However, this size shift was not apparent with the polyclonal goat C20 antibody. While the polyclonal mouse (Abcam) and the polyclonal goat C20 antibodies produced a signal in ARCs, the polyclonal mouse (ECM Biosciences) and the polyclonal goat C14 antibodies did not produce a discernible signal for FHOD1 in ARCs. Levels of α–actinin were also visualised as a loading control in order to confirm the presence of protein and the integrity of the cultured cardiomyocyte samples (Figure 3.9 E). Overall, while all 4 anti-FHOD1 antibodies were in agreement with the notion that the protein could be detected in NRCs, the possibility of detection in ARCs across the antibodies remained doubtful.

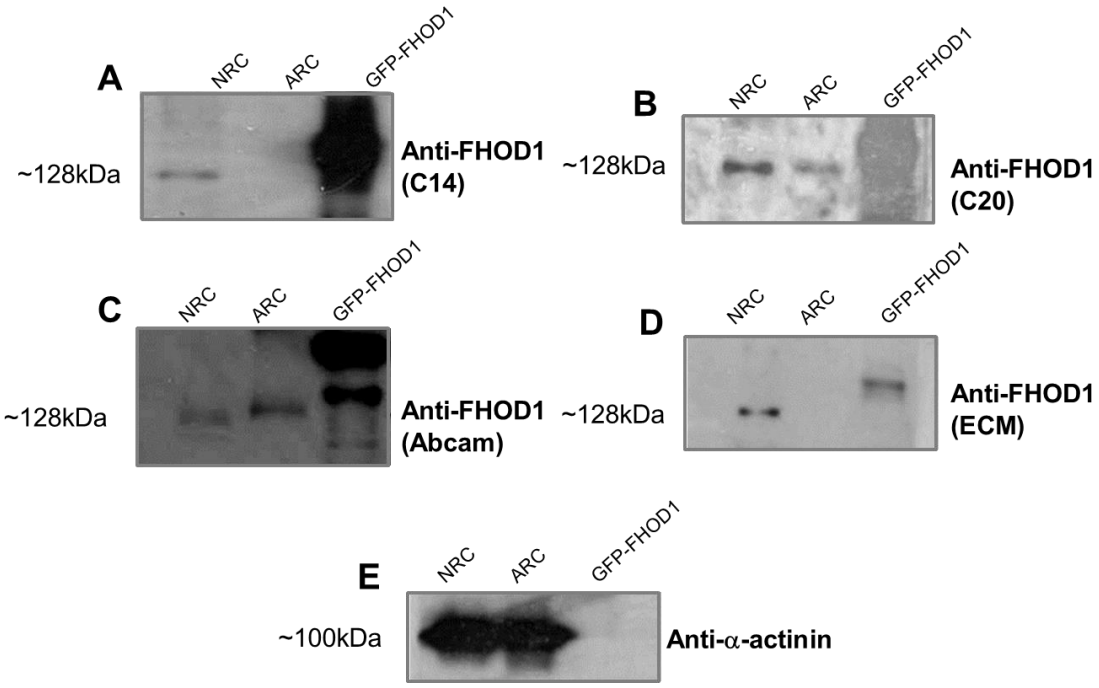

Figure 3.9: Expression of FHOD1 in Cultured Neonatal Rat and Adult Rat Cardiomyocytes. Western blot of lysates of day 3 cultured NRCs and day 0 freshly isolated ARCs to confirm the presence of rat Fhod1 at the protein level. COS-1 cells were transfected with the GFP-tagged full-length long variant of FHOD1 containing the alternatively spliced exons (E12-13); these lysates functioned as a positive control in the possible absence of a signal in the lysates of cultured cardiomyocytes. Blots were incubated with the following anti-FHOD1 antibodies: **A)** Polyclonal Goat C14 (Santa Cruz), **B)** Polyclonal Goat C20 (Santa Cruz), **C)** Polyclonal Mouse (abcam), **D)** Polyclonal Mouse (ECM Biosciences), **E** Western blot probed against sarcomeric α-actinin. **N=2**

3.3.1 Localisation of Endogenous FHOD1 in Neonatal Rat Cardiomyocytes

The relative localisation of FHOD1 in cardiac muscle samples was partially delineated by counterstaining against well-known subcellular markers as a reference. NRCs were stained with four of the commercially available anti-FHOD1 antibodies. All 4 of the anti-FHOD1 antibodies produced a signal when visualised by immunofluorescence. When staining for endogenous FHOD1, it became apparent that the protein was distributing along myofibrils and in a striated manner (Figure 3.10 A-D). Such a distribution would indicate targeting of the protein somewhere within the sarcomere. Cardiomyocytes were counterstained with the A-band protein Myosin Binding Protein C (MyBP-C) to discern the relative localisation of FHOD1 in the sarcomere.

Counterstaining with this sarcomeric marker indicated that each antibody produced a unique staining pattern for FHOD1. The polyclonal goat C14 anti-FHOD1 antibody revealed FHOD1 distributing along myofibrils (Figure 3.10 A). Prominent bands for FHOD1 were found at the lateral portions of the sarcomere, as gauged by staining for MyBP-C (Figure 3.10, Zoom). Some concentrated FHOD1 staining was also found at the peripheries of the cells, one of the proposed sites of myofibril assembly in cardiomyocytes. The polyclonal goat C20 antibody revealed FHOD1 distributing along myofibrils, but its striated appearance was dramatically different in that it consisted of thick doublet bands (Figure 3.10 B). These bands overlapped with the MyBP-C signal and seemed to extended towards the lateral portions of each sarcomere (Figure 3.10, Zoom).

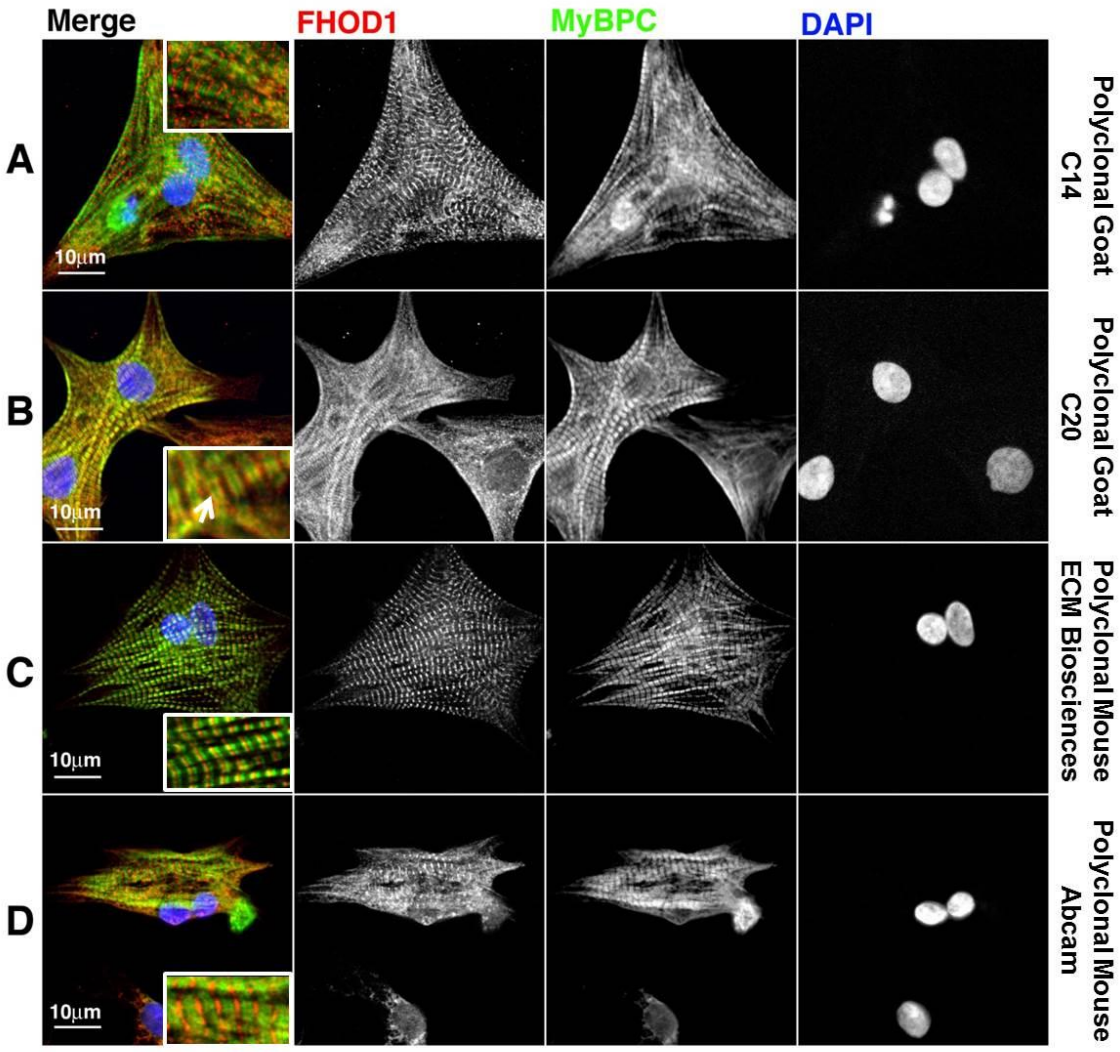

Figure 3.10: Localisation of Endogenous FHOD1 in Neonatal Rat Cardiomyocytes. Day 3 NRCs were cultured in maintenance medium. Cells were stained with the commercially available anti-FHOD1 antibodies and MyBP-C. The following anti-FHOD1 antibodies were used: **A)** Polyclonal goat C14 (Santa Cruz), **B)** Polyclonal goat C20 (Santa Cruz), **C)** Polyclonal mouse (ECM Biosciences), **D)** Polyclonal mouse (abcam). FHOD1 is seen in red, MyBP-C in green, and DAPI/nuclei in blue. NRC, neonatal rat cardiomyocytes; MyBP-C, myosin binding protein-C. White boxes show zoomed selections of merged images. Scale bars represent 10µm. **N=3**

Staining with the two polyclonal mouse anti-FHOD1 antibodies (Figure 3.10 C-D) also produced a striated pattern for FHOD1, again indicating some localisation within the sarcomere. The polyclonal mouse anti-FHOD1 antibody (ECM Biosciences) gave well defined and broadly spaced striations (Figure 3.10 C). These striations were found within the central region of the sarcomere, although there was some overlap with the

signal for MyBP-C, indicating the possibility of some distribution along the region of the thick filaments. The other polyclonal mouse anti-FHOD1 antibody (Abcam) revealed FHOD1 distributing along myofibrils, with striations also being occasionally discerned (Figure 3.10 D). FHOD1 striations were visible as alternating bright and faint bands. The brighter bands were found near the lateral portions of the sarcomere and the fainter bands near the centre.

While these staining experiments suggest that endogenous FHOD1 is targeted to myofibrils and might concentrate in particular regions of the sarcomere, such disparate results between the 4 antibodies could indicate a number of issues. One likely possibility is that the antibodies were actually detecting other sarcomeric proteins, which have been shown to be problematic in antibody studies (Wang et al. 2012). In the absence of an antigen competition assay, it was not possible to rule out cross-reactivity of the 4 anti-FHOD1 antibodies with other sarcomeric proteins. Another possibility was the potential for cross-reactivity of the fluorophore labelled secondary antibodies to the incorrect primary antibody, although we strove to avoid this issue by only employing multi-labelling quality antibodies. However, in the absence of single staining controls using just the FHOD1 antibodies, cross-reactivity between the secondary antibodies cannot be ruled out. It is therefore difficult to draw any definitive conclusions regarding the localisation of endogenous FHOD1 in NRCs until these issues are resolved..

3.3.2 Localisation of Endogenous FHOD1 in Adult Rat Cardiomyocytes

As heart muscle grows and remodels over time, the expression and localisation of certain proteins are altered. For example, the formin homology protein FHOD3 was shown to localise to the region of the A-bands in NRCs (Iskratsch et al. 2010) but was found at the Z-disk in freshly isolated ARCs (Iskratsch et al. 2013a). FHOD1 was therefore stained against in freshly isolated adult rat cardiomyocytes to look for any alterations in localisation when compared to the localisation patterns seen in NRCs. Out of the 4 commercially available antibodies recognising endogenous FHOD1, only three of the antibodies produced a signal for the protein in ARCs when visualised by immunofluorescence.

Localisation of each anti-FHOD1antibody in ARCs was similar to that seen in NRCs (Figure 3.3 A-C). Similarly to NRCs, the signal for FHOD1 was again found distributing along myofibrils and could be occasionally be visualised as striations. The polyclonal goat C14 antibody produced fairly weak staining for FHOD1 that consisted of a predominantly filamentous signal, although the signal was also occasionally visible as faint striations within the lateral regions of the sarcomeres, as gauged by an alternating pattern with the M-band marker, myomesin (Figure 3.11 A, Zoom). The polyclonal goat C20 antibody revealed a myofibrillar signal for FHOD1, which resolved as thick doublet bands that localised either side of the Z-disks, as gauged by α–actinin staining, emanating towards the centre of the sarcomere (Figure 3.11 B, Zoom). The polyclonal mouse antibody (Abcam) revealed endogenous FHOD1 distributing in a striated manner. Counterstaining with MyBP-C revealed that prominent FHOD1 bands were consistently resolved in between the A-bands, near the centre of the sarcomere (Figure 3.11 C, Zoom). Fainter targeting to lateral portions of the sarcomere could occasionally be discerned. However, the same caveats apply here as in the above antibody staining studies using NRCs. In the absence of an antigen competition assay and single staining controls for FHOD1, we cannot rule out the possibility of cross-reactivity of the anti-FHOD1 antibodies with other sarcomeric proteins and with the other antibodies used in the staining procedures. Although it was difficult to detect any dramatic alterations in FHOD1 localisation between NRCs and ARCs due to limits in resolution, results with the polyclonal mouse (Abcam) could suggest redistribution of FHOD1 from the lateral portions of the sarcomere in NRCs, where it displayed prominent striations, to the central portion of the sarcomere in ARCs. .

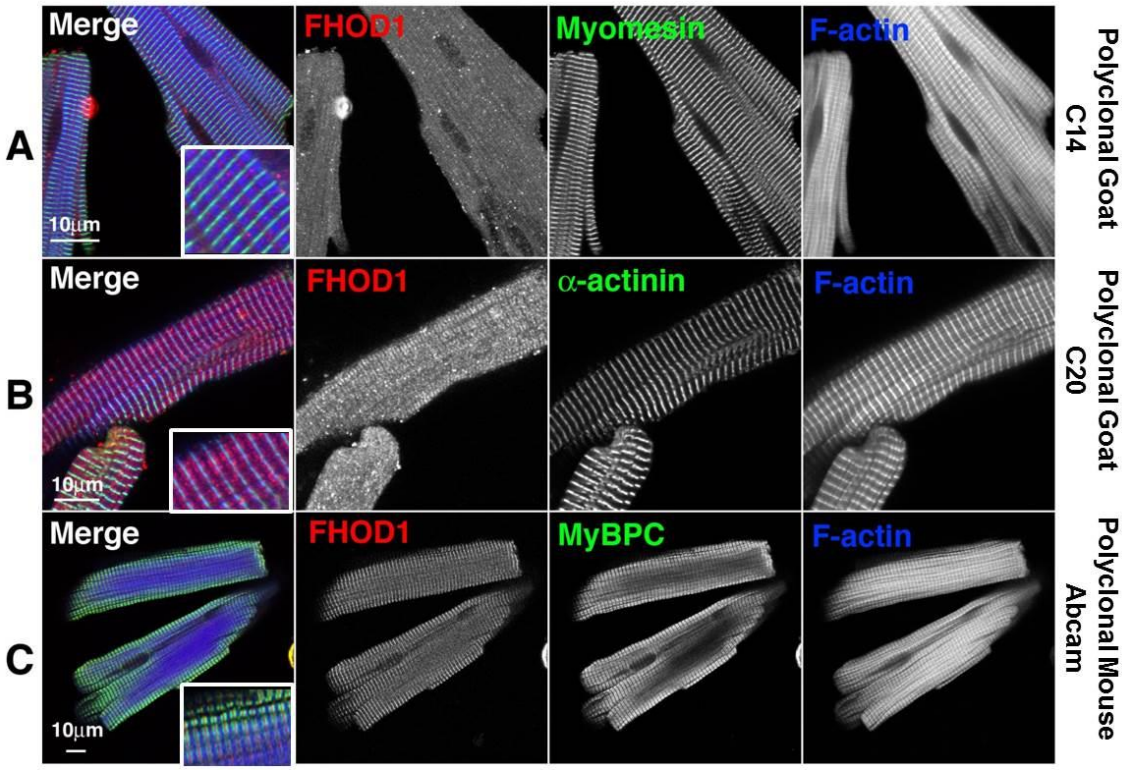

Figure 3.11: Localisation of Endogenous FHOD1 in Adult Rat Cardiomyocytes. Freshly isolated ARCs were fixed and stained with the commercially available anti-FHOD1 antibodies as well as other sarcomeric markers and F-actin, with subsequent visualisation by confocal microscopy. The following anti-FHOD1 antibodies were used: **A)** Polyclonal goat C14 (Santa Cruz), **B)** Polyclonal goat C20 (Santa Cruz), **C)** Polyclonal mouse (Abcam). FHOD1 is seen in red, myomesin/α-actinin/MyBP-C are seen in green, and F-actin seen in blue. ARC, adult rat cardiomyocytes; MyBP-C, myosin binding protein-C. Scale bars represent 10μm. White boxes show zoomed selections of merged images. **N=2**

3.3.3 Localisation of Endogenous FHOD1 in Adult Mouse Heart Tissue Sections

In order to visualise the localisation of endogenous FHOD1 *in situ*, we stained for the protein in frozen heart sections from adult mice. Proteins can alter their localisation in cultured cells under two-dimensional culture conditions therefore tissue sections allow one to study the localisation of a protein in its native environment. Out of the 4 commercial anti-FHOD1 antibodies tested in heart sections, only the two polyclonal goat anti-FHOD1 antibodies (Santa Cruz) produced a signal for the protein when visualised by immunofluorescence.

FHOD1 localisation was visualised in both transverse and longitudinal heart sections to discern whether the protein was localising to the sarcomere and/or the sarcoplasmic reticulum. Low magnification images of transverse sections taken through myofibrils with both the polyclonal goat C14 (Figure 3.12 A) and C20 (Figure 3.13 A) antibodies revealed FHOD1 distributing within myofibrils although some membrane targeting was apparent. Low magnification images of longitudinal sections also revealed FHOD1 distributing in cardiomyocytes in a filamentous manner (Figure 3.12 B, 3.13 B). Most notably, FHOD1 was also found as a bright signal at the intercalated disk, the specialised electro-mechanical junction between neighbouring cardiomyocytes.

High magnification images of longitudinal sections confirmed a strong signal for FHOD1 in cardiomyocytes and revealed that FHOD1 was concentrated at the intercalated disks. Staining also revealed that FHOD1 was occasionally distributing in a striated manner, once again indicating some sarcomeric localisation. Counterstaining with the M-band marker, myomesin revealed an alternating pattern with FHOD1 which would suggest that FHOD1 may have been present in the lateral portions of the sarcomeres, near the Z-disks (Figure 3.12 C, Zoom; Figure 3.13 C, Zoom). Some staining for FHOD1 was also noted in the interstitial spaces between cardiomyocytes, indicating that it could have also been expressed in cardiac fibroblasts, one of the more numerous cell types in the heart that play roles in maintaining the structural, electrochemical, and biochemical properties of the heart (Camelliti et al. 2005). Indeed, FHOD1 expression has been reported in fibroblasts (Iskratsch et al. 2013b) therefore it is entirely conceivable that it was also found in cardiac fibroblasts in our immunofluorescence samples. However, we were unable to confirm FHOD1 expression in this cell type. Counterstaining tissue sections against vimentin would allow for cardiac fibroblasts to be spatially delineated and would facilitate the confirmation FHOD1 expression in this cell type.

In the absence of an antigen competition assay or single staining controls with the anti-FHOD1 antibodies alone, we were unable to determine if the signal for FHOD1 was *bona fide* or a product of cross-reactivity with other myocardial proteins. However, we were able to examine the effects of the fluorophore coupled secondary antibodies on any non-specific localisation (Figure 3.14). The Cy3-coupled donkey anti-goat antibody, which was used to detect the goat anti-FHOD1 antibodies, displayed co-

localisation with myofibrils in both transverse (Figure 3.14 A) and longitudinal sections (Figure 3.14 B) but did not stain the intercalated disks nor did it produce the distinct cross striations seen with the anti-FHOD1 antibodies. The Cy2-coupled donkey anti-mouse antibody, used to detect the mouse anti-myomesin antibody, produced some background staining along myofibrils and at cell boundaries, although this background staining disappeared when staining was performed with the appropriate primary antibody. Although the caveat remained regarding the specificity of the anti-FHOD1 antibodies in these experiments, we were able to exclude the effects of any extraneous background staining with the secondary antibodies.

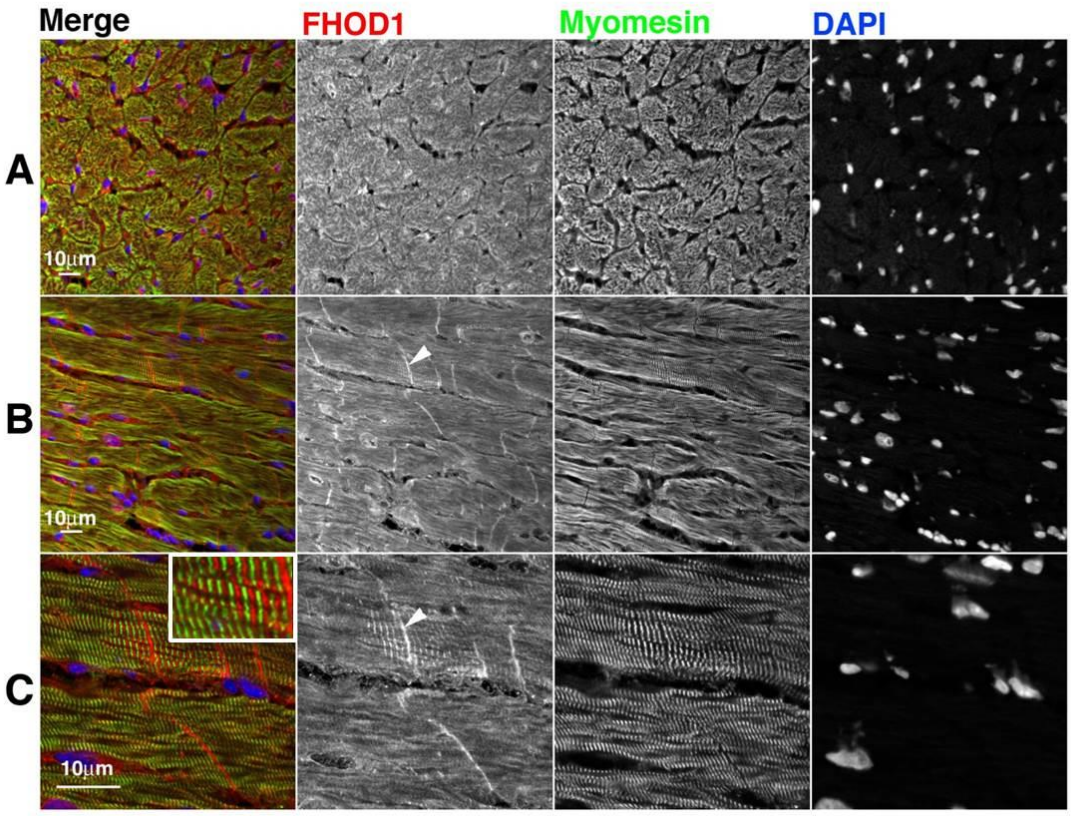

Figure 3.12: Localisation of Endogenous FHOD1 with the Polyclonal Goat C14 Antibody in Murine Hearts. Frozen heart sections of 1 year old male adult C57/BL6 mice were stained with the anti-FHOD1 goat C14 antibody (Santa Cruz), myomesin, and visualised by confocal microscopy. Images represent portions of **A)** low magnification transverse sections, **B)** low magnification longitudinal sections, and **C)** high magnification longitudinal sections. FHOD1 is seen in red, myomesin is seen in green, and DAPI/nuclei are seen in blue. Arrowheads indicate an intercalated disk. Scale bars represent 10µm. White box shows zoomed selection of merged images. **N=3**

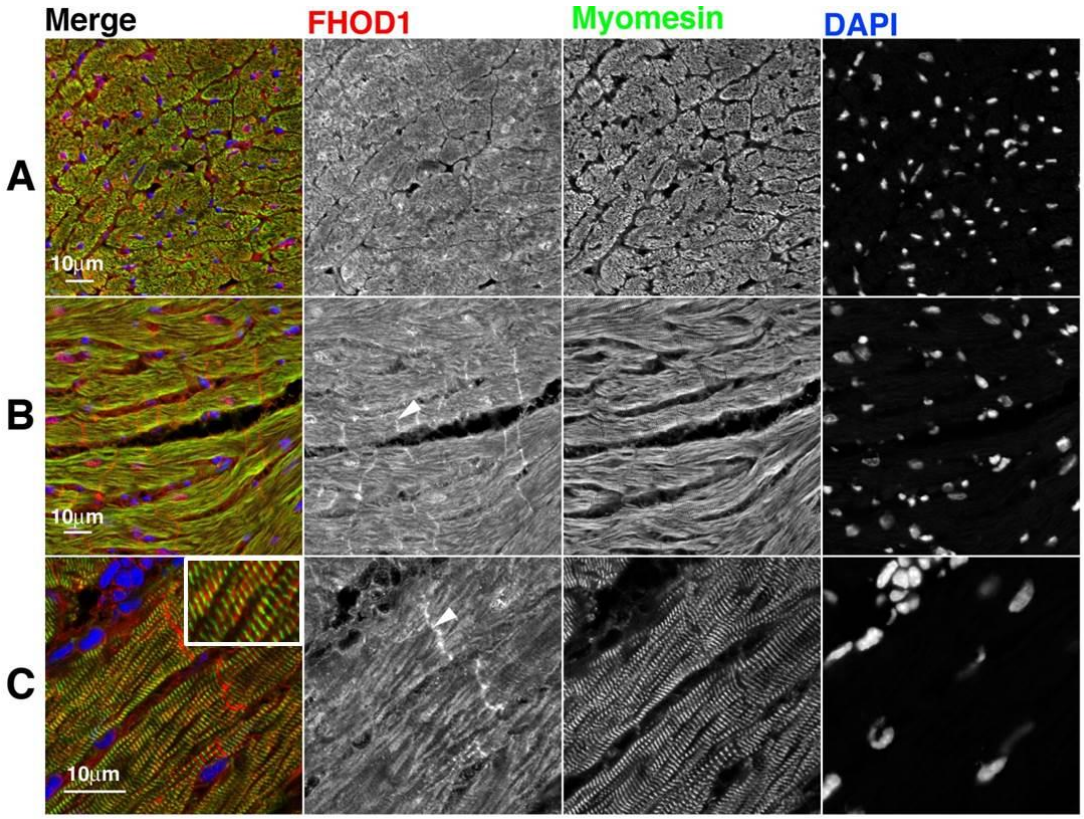

Figure 3.13: Localisation of Endogenous FHOD1 with the Polyclonal Goat C20 Antibody in Murine Hearts. Frozen heart sections of 1 year old male adult C57/BL6 mice were stained with the anti-FHOD1 goat C20 antibody (Santa Cruz) and), myomesin, and visualised by confocal microscopy. Images represent portions of **A)** low magnification transverse sections, **B)** low magnification longitudinal sections, and **C)** high magnification longitudinal sections. FHOD1 is seen in red, myomesin is seen in green, and DAPI/nuclei are seen in blue. Arrowheads indicate an intercalated disk. Scale bars represent 10µm. White box shows zoomed selection of merged images. **N=3**

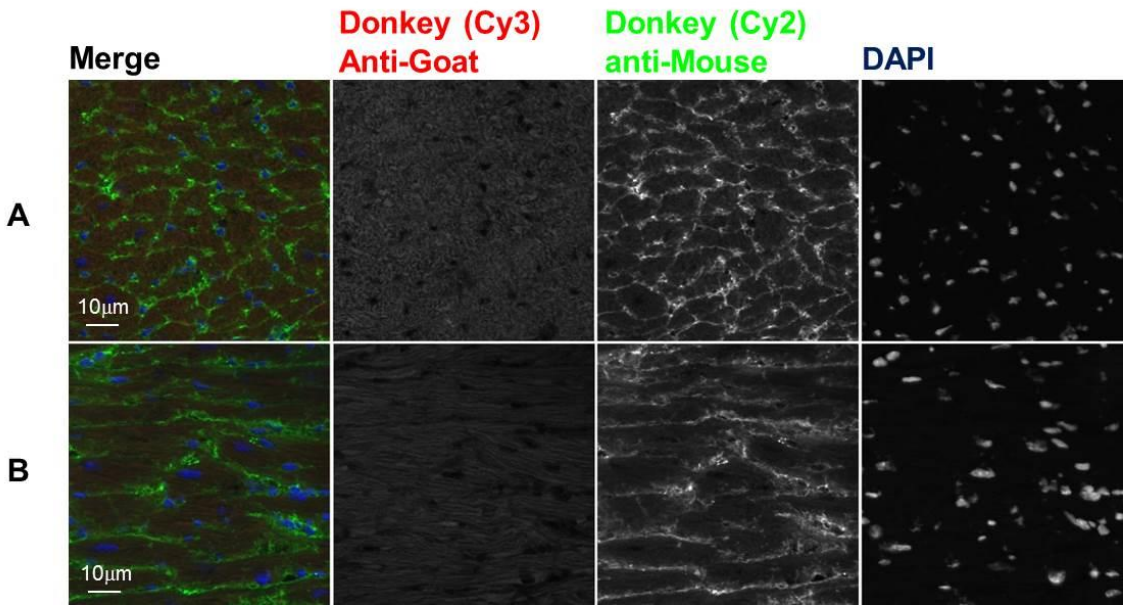

Figure 3.14: Negative Control for Fluorophore Coupled Secondary Antibodies. In order to assess the extent of background staining produced by the secondary antibodies used for localisation studies in tissue sections, frozen heart sections of 1 year old male adult C57/BL6 mice were stained with the Cy3-coupled donkey anti-goat antibody, which was used to detect the goat anti-FHOD1 antibodies and the Cy2-coupled donkey anti-mouse antibody, which was used to detect the mouse anti-myomesin antibody and visualised by confocal microscopy. Images represent portions of **A)** low magnification transverse sections and **B)** low magnification longitudinal sections. Cy3-coupled donkey anti-goat is seen in red, Cy2-coupled donkey anti-mouse is seen in green, and DAPI/nuclei are seen in blue. Scale bars represent 10µm. **N=1**

3.4 Expression and Localisation of FHOD1 in Differentiating C2C12 Myoblasts

C2C12 myoblasts are a murine cell line of skeletal muscle lineage. They represent a model that can be used to study myofibrillogenesis and myogenic differentiation under culture conditions (Berry et al. 2001), as they recapitulate some of the events in formation of skeletal muscle (Burattini et al. 2004). C2C12 cells begin as proliferative myoblasts, muscle precursor cells. When cultured under low serum conditions they begin the differentiation process into skeletal muscle cells. In the early stages of differentiation, C2C12 myoblasts will fuse with neighbouring cells. Fused cells will then elongate and become morphologically distinct myotubes. During the later stages of differentiation, fused cells complete the process of assembling their sarcomeres and eventually become skeletal muscle cells, which are sometimes seen to contract in

syncytium. C2C12 differentiation requires a number of cytoskeletal remodelling events, especially at the level of F-actin (Malone et al. 2011). We therefore chose to look at FHOD1 expression and localisation through Western blot and antibody localisation studies, respectively in differentiating C2C12 cells at different time points.

3.4.1 Expression of FHOD1 in Differentiating C2C12 Myoblasts

Prior to initiating localisation studies, we sought to confirm expression of FHOD1 at the protein level in differentiating C2C12 cells. FHOD1 expression was examined in differentiating C2C12 cells, with harvesting of protein samples occurring every two days, after culture in low serum conditions (Figure 3.15). The earliest time point was day 0, when progenitor cells were seeded into dishes coated with collagen but were kept in proliferation medium. The following expression experiments describe qualitative results since the exact protein concentration was not determined before loading. Initially, the 4 commercially available anti-FHOD1 antibodies were tested for their reactivity against C2C12 protein lysates. Out of the 4 antibodies, only the polyclonal goat C14 anti-FHOD1 antibody produced a discernible signal for the FHOD1 protein when visualised by enhanced chemiluminescence (Figure 3.15 A). Lysates were also blotted against sarcomeric α–actinin (Figure 3.15 C) and desmin (Figure 3.15 D), to confirm the differentiation status of cultured cells over time. An increased signal for α–actinin and desmin after switching cells into low serum conditions was consistent with the reported upregulation of these proteins during the differentiation process (Kislinger et al. 2005).

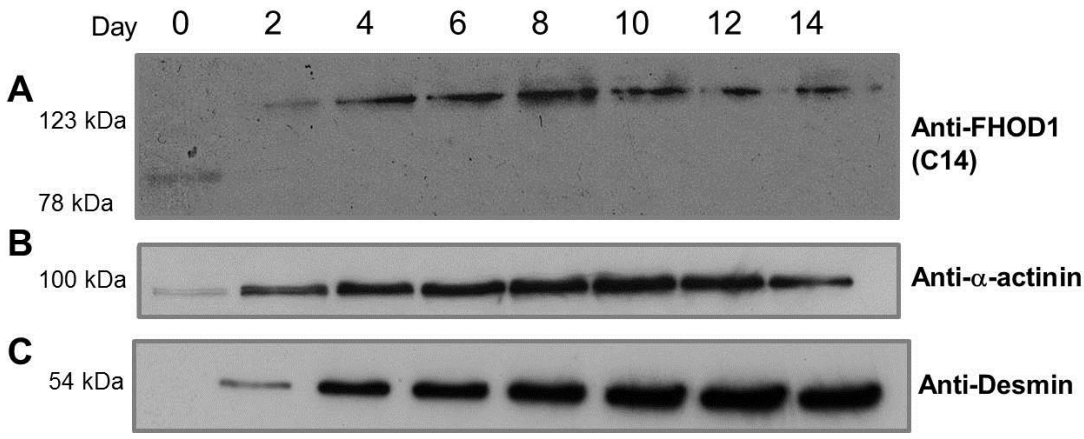

Figure 3.15: Expression of FHOD1 in Differentiating C2C12 Myoblasts. Western blots of differentiating C2C12 myoblasts at different time points **A)** Western blot probed with the polyclonal goat C14 anti-FHOD1 antibody (Santa Cruz). **B)** Western blot probed against sarcomeric α-actinin. A signal for the protein is seen as a single band around 100 kDa. **C)** Western blot probed against desmin. A signal for the protein is seen as a single band around 54 kDa. kDa, kilodaltons. **N=2** repetitions of Western blots from 2 rounds of cell culture/C2C12 differentiation.

Western Blot studies with the polyclonal goat C14 anti-FHOD1 antibody resolved one distinct band associated with FHOD1 at each time point (Figure 3.15 A). In day 0 undifferentiated C2C12 myoblasts, FHOD1 expression was visible as a faster migrating, smaller molecular weight band between the 123 kDa and 78 kDa protein markers. In all of the subsequent time points, a band for FHOD1 was resolved as a slower running, therefore higher molecular weight band just above the 123 kDa protein marker. The higher molecular weight band was consistent with the predicted molecular weight of 129kDa for mouse FHOD1. Human FHOD1 has been previously found to undergo differential splicing with a longer mRNA transcript for FHOD1 with a 78bp insert having been described by Tojo et al. 2003. From day 2 through day 14, the FHOD1 signal in differentiating cells, likely corresponded to the 1,197 amino acid variant reported in mice. Currently, there is only one definite FHOD1 isoform in mice and no smaller isoforms have been documented. In our model of differentiating C2C12 myoblasts, the band in day zero lysates may have corresponded to an unreported FHOD1 splice variant. These data may indicate an isoform switch in FHOD1 expression during skeletal muscle development. However, in the absence of an antigen competition assay, we could not rule out the possibility of the polyclonal Goat C14 antibody cross-reacting with other murine skeletal myoblast/myotube proteins, which could particularly explain the band at day 0 that was found to migrate at an unexpected

molecular weight. Further confirmation should take place by examining the expression of FHOD1 at the mRNA transcript level in differentiating C2C12 cells in order to resolve discrepancies regarding the presence of a faster migrating species in day 0 lysates.

3.4.2 Localisation of Endogenous FHOD1 in Differentiating C2C12 Myoblasts

With the possibility in mind that FHOD1 was expressed in C2C12 cells, we subsequently stained for endogenous FHOD1 in differentiating C2C12 cells to examine the localisation of FHOD1 over time. C2C12 cells were fixed at four different time points starting from freshly seeded day zero myoblasts to day 14 myotubes. Out of the 4 commercially available antibodies raised against FHOD1, only three of the antibodies produced a signal for FHOD1 when visualised by immunofluorescence. Each antibody produced a distinct localisation pattern for FHOD1 in differentiating C2C12 cells.

In day 0 myoblasts, staining for FHOD1 with the polyclonal goat C14 antibody produced a predominantly diffuse cytoplasmic signal (Figure 3.16 A). FHOD1 was also visualised as cytoplasmic speckles. There was no co-localisation with the F-actin network. At day 3, when cells began to elongate and fuse, the signal for FHOD1 became more diffuse and was sometimes concentrated along F-actin stress fibres (Figure 3.16 B). At day 7, when myotubes began to enlarge and lay down sarcomeres, the signal for FHOD1 was mostly diffuse throughout the cytoplasm of cells (Figure 3.16 C). At day 14, when myotubes had laid down mature sarcomeres, FHOD1 still distributed in a diffuse cytoplasmic manner although some localisation along myofibrils was apparent (Figure 3.16 D). However, there was little visible evidence to support that FHOD1 was distributing in a cross striated manner. Overall, the polyclonal C14 antibody primarily revealed FHOD1 distributing in a diffuse cytoplasmic manner although some myofibrillar targeting was noted in mature myotubes.

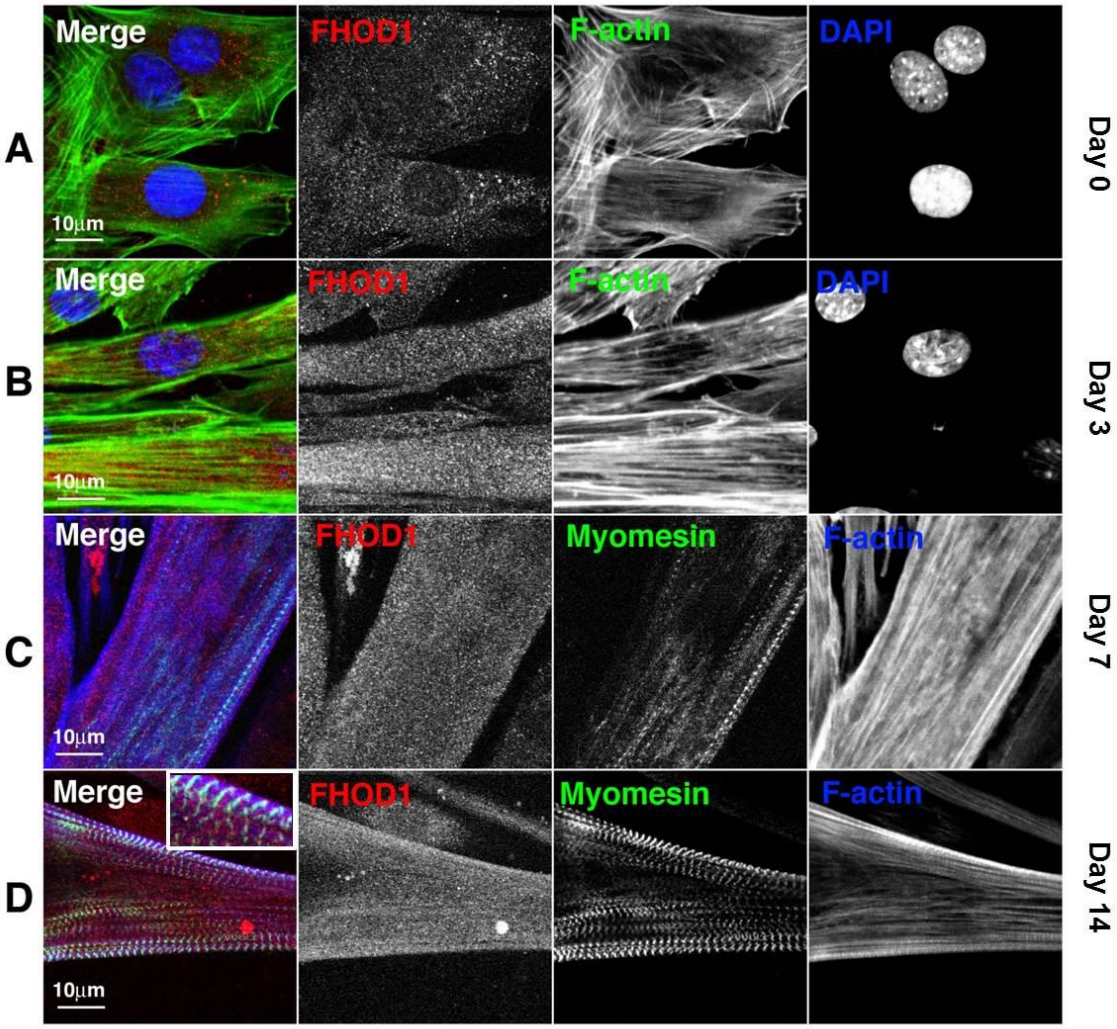

Figure 3.16: Localisation of Endogenous FHOD1 with the Polyclonal Goat C14 Antibody in Differentiating C2C12 Myoblasts. C2C12 myoblasts were differentiated from day 0 myoblasts to day 14 myotubes. Cells were fixed at multiple time points prior to staining with the anti-FHOD1 polyclonal goat C14 antibody (Santa Cruz) as well as other myofibrillar and cellular markers. Stained cells were visualised by confocal microscopy. Images represent cells at separate stages of differentiation at **A)** day 0, **B)** day 3, **C)** day 7, and **D)** day 14. FHOD1 is seen in red, F-actin/myomesin in green, and DAPI/nuclei/F-actin in blue. Scale bars represent 10μm. White box shows zoomed selection of merged images. **N=2**

When staining with the polyclonal goat C20 antibody, the signal for FHOD1 was comparatively stronger than that for the polyclonal goat C14 or polyclonal mouse antibodies (ECM Biosciences) (Figure 3.17). In day 0 myoblasts, FHOD1 was again visible as speckles, albeit distributing in a more concentrated manner within the cytoplasm (Figure 3.17 A). At day 3, the signal for FHOD1 became more diffuse with some occasional localisation along F-actin stress fibres (Figure 3.17 B). At day 7, it was apparent that FHOD1 was already distributing along newly formed myofibrils and was even producing a striated signal (Figure 3.17 C, Zoom). FHOD1 striations were present as doublet bands found either side of myomesin, and could have indicated some distribution of the endogenous protein along the length of the thick filaments. At day 14, the doublet FHOD1 striations became more prominent (Figure 3.17 D, Zoom). Unlike the staining found in NRCs and ARCs, the spacing of these doublets were narrower and there was some overlap between the FHOD1 and myomesin signals.

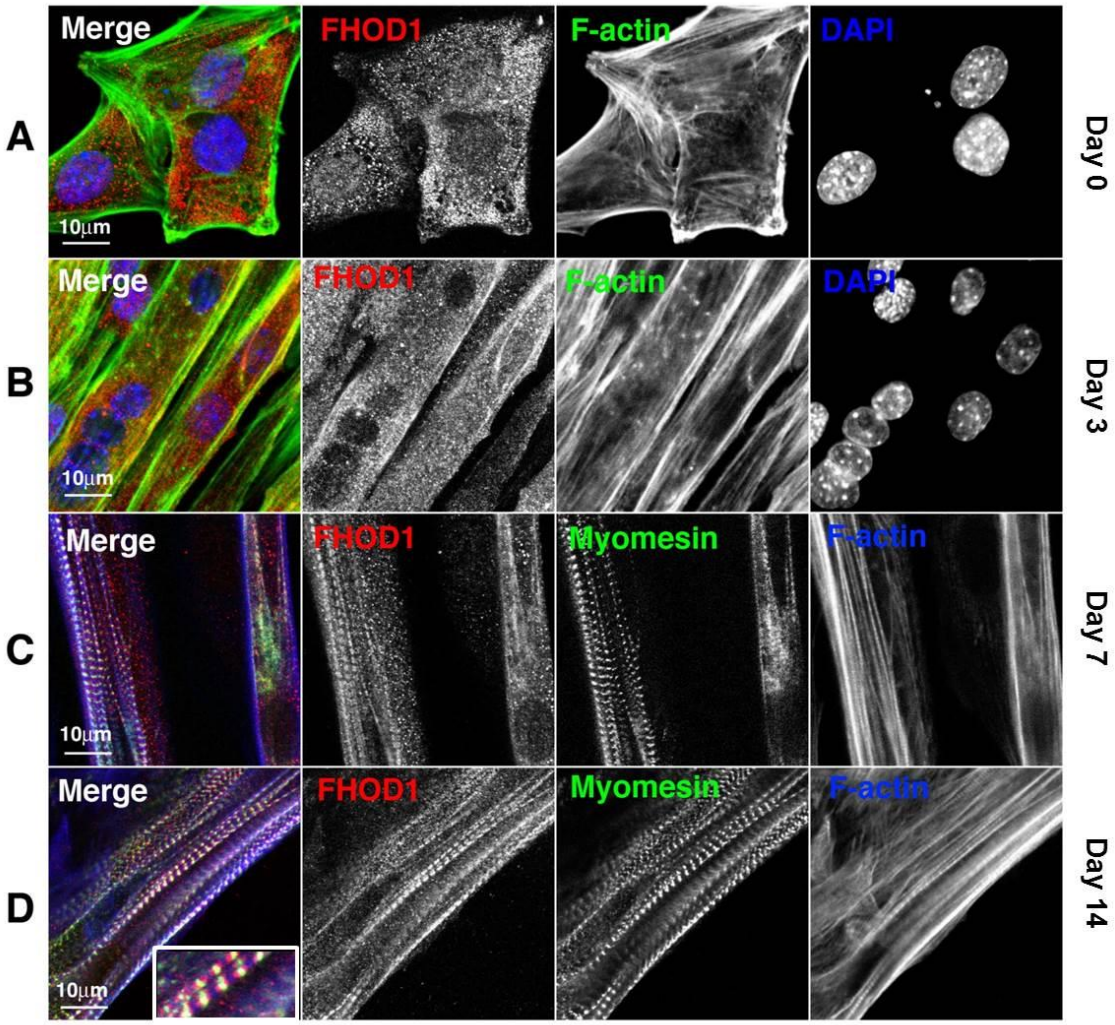

Figure 3.17: Localisation of Endogenous FHOD1 with the Polyclonal Goat C20 Antibody in Differentiating C2C12 Myoblasts. C2C12 myoblasts were differentiated from day 0 myoblasts to day 14 myotubes. Cells were fixed at multiple time points prior to staining with the anti-FHOD1 polyclonal goat C20 antibody (Santa Cruz) as well as other myofibrillar and cellular markers. Stained cells were visualised by confocal microscopy. Images represent cells at separate stages of differentiation at **A)** day 0, **B)** day 3, **C)** day 7, and **D)** day 14. FHOD1 is seen in red, F-actin/myomesin in green, and DAPI/nuclei/F-actin in blue. Scale bars represent 10μm. White box shows zoomed selection of merged images. **N=2**

The polyclonal mouse anti-FHOD1 antibody (ECM Biosciences) produced a distinct signal for FHOD1 in day 0 undifferentiated myoblasts (Figure 3.18 A) when compared to the other anti-FHOD1 antibodies. Although the signal was primarily diffuse and cytoplasmic, it was apparent that FHOD1 was occasionally distributing in a faint filamentous manner. In day 3 cells, the FHOD1 signal was diffuse throughout the cytoplasm of cells, although there were some hints of targeting along F-actin stress fibres (Figure 3.18 B). The distribution of the protein remained relatively unchanged at day 7 (Figure 3.18 C). In day 14 mature myotubes, the FHOD1 signal was predominantly diffuse throughout the cytoplasm although some targeting to myofibrils and faint striations could occasionally be discerned (Figure 3.18 D, Zoom). However, it was not possible to discern the precise spacing of the FHOD1 striations. There was some evidence that a prominent FHOD1 band alternated with the signal for MyBP-C, although the resolution currently achieved in this experiment did not allow us to gain a clear idea of FHOD1 distribution within the sarcomere.

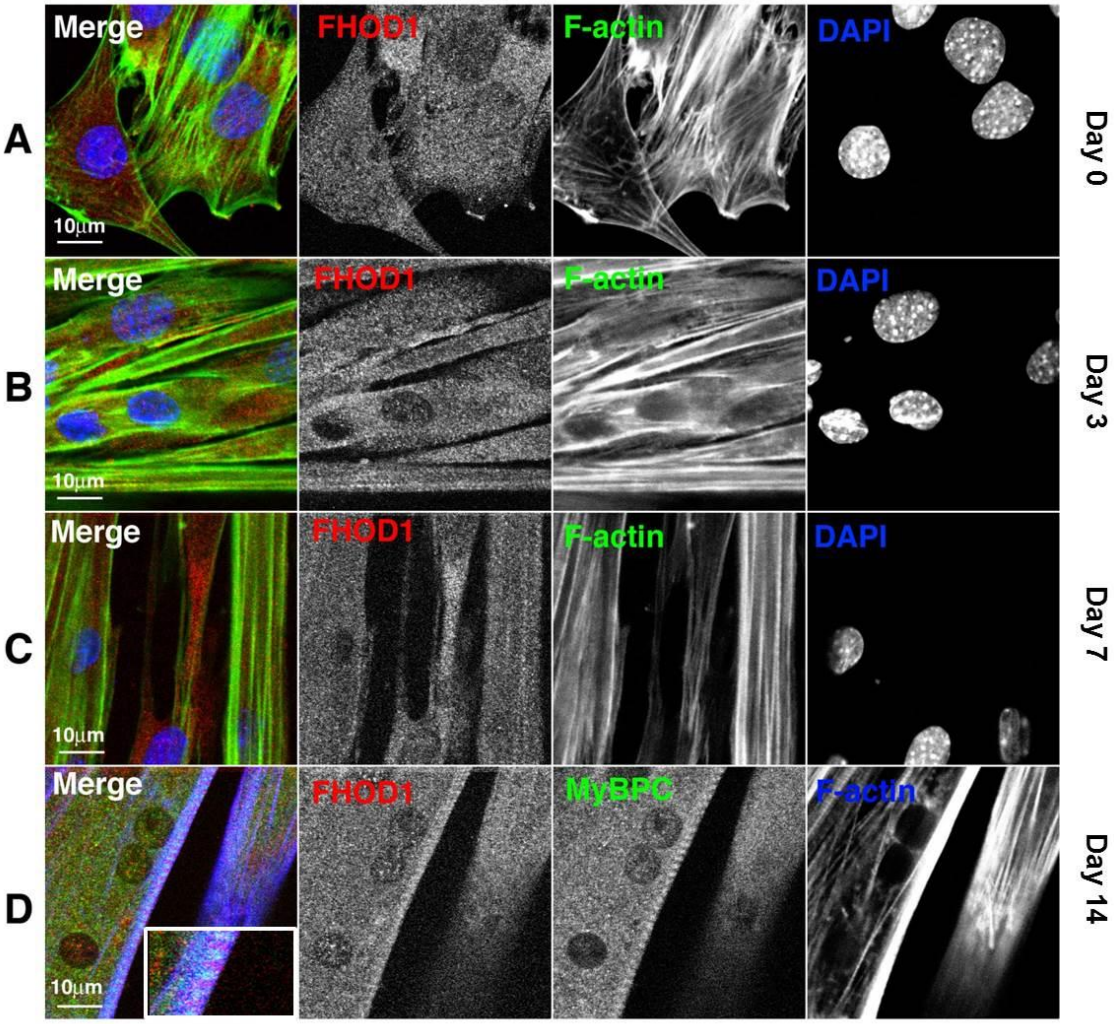

Figure 3.18: Localisation of Endogenous FHOD1 with the Polyclonal Mouse Antibody in Differentiating C2C12 Myoblasts. C2C12 myoblasts were differentiated from day 0 myoblasts to day 14 myotubes. Cells were fixed at multiple time points prior to staining with the anti-FHOD1 polyclonal mouse antibody (ECM Biosciences) as well as other myofibrillar and cellular markers. Stained cells were visualised by confocal microscopy. Images represent cells at separate stages of differentiation at **A)** day 0, **B)** day 3, **C)** day 7, and **D)** day 14. FHOD1 is seen in red, F-actin/MyBP-C in green, and DAPI/nuclei/F-actin in blue. Scale bars represent 10µm. White box shows zoomed selection of merged images. **N=2**

The localisation studies performed in C2C12 cells would indicate that endogenous FHOD1 is initially found in the cytoplasm of C2C12 cells, although it was occasionally found at the membrane edge. As cells began to elongate and fuse, the FHOD1 signal became dispersed throughout the cytoplasm of differentiating myotubes and there was some occasional co-localisation with F-actin stress fibres. In mature myotubes, while the FHOD1 signal was primarily that of a diffuse cytoplasmic nature, we did note some occasional targeting to myofibrils and concentration within the sarcomere as striations. However, a number of caveats apply when interpreting the present results. In the absence of an antigen competition assay, we were unable to determine the level of non-specific staining with the anti-FHOD1 antibodies. Furthermore, while Western blot studies suggested the presence of FHOD1 at the protein level throughout the C2C12 differentiation process (Figure 3.15 A), we were only able to do this using the polyclonal goat C14 antibody, which casted doubt as to whether we were visualising FHOD1 in C2C12 cells with the polyclonal goat C20 and polyclonal mouse (ECM Biosciences) antibodies. However, the lack of detection on Western blots could be explained by the loss of the epitope the antibodies recognise due to the denaturing conditions used in our sample preparation and for SDS-PAGE.

Overall, we described the expression and localisation of endogenous FHOD1 using 4 commercially available anti-FHOD1 antibodies in a number of tissue and cell types of cardiac and skeletal muscle origin (Table 3.1). The antibodies were not always in agreement with each other regarding the localisation of endogenous FHOD1, a factor which did not bode well for the validity of these staining experiments. However, they could likely be resolved by further characterisation of antibody specificity and sensitivity through antigen competition assays and biochemical validation using rodent FHOD1 constructs, respectively.

Antibody	Specimen	Localisation	Reactivity on Western Blots
Polyclonal goat C14 (Santa Cruz)	NRC	Myofibrillar, lateral portions of sarcomere, cell peripheries	Y
	ARC	Filamentous, lateral portions of sarcomere	N
	Mouse Heart	ICD, myofibrils, lateral/central portion of sarcomere	N
	C2C12	Cytoplasmic, myofibrillar	Y
Polyclonal goat C20 (Santa Cruz)	NRC	A-band	Y
	ARC	Doublet bands found either side of the Z-disk	Y
	Mouse Heart	ICD, myofibrils, lateral/central portion of sarcomere	N
	C2C12	Cytoplasmic, myofibrillar, doublet bands found either side of the M-band	N
Polyclonal Mouse (abcam)	NRC	Myofibrillar, lateral/central portion of sarcomere	Y
	ARC	Lateral/central portion of sarcomere	Y
	Mouse Heart	No signal	Y
	C2C12	No signal	N
Polyclonal Mouse (ECM Biosciences)	NRC	Central portion of sarcomere	Y
	ARC	No signal	N
	Mouse Heart	No signal	N
	C2C12	Cytoplasmic, myofibrillar	N

Table 3.1: Summary of Antibody Studies. Table summarising the localisation of endogenous FHOD1 using the 4 commercial antibodies recognising total FHOD1 levels in different muscle specimens. A summary of the reactivity against FHOD1 via Western blotting is also given. NRC, neonatal rat cardiomyocytes; ARC, adult rat cardiomyocytes; ICD, intercalated disk; Y, yes (reactivity was noted); N, no (reactivity was not noted).

3.5 Overexpression of Full-length FHOD1 in Neonatal Rat Cardiomyocytes

In addition to antibody localisation studies, a number of transient expression studies were performed in cultured cardiomyocytes to explore the targeting of different epitope tagged FHOD1 constructs. GFP and TOMATO-tagged variants of full-length FHOD1 were transiently transfected into NRCs to visualise the subcellular targeting of full-length FHOD1. There are currently two full-length variants of human FHOD1 that have been described. The shorter version of the protein was the variant that was described in the initial characterisation of FHOD1 (Westendorf et al. 1999) and the longer version, which contains a 78bp insertion (Tojo et al. 2003) that represent the alternatively spliced exons 12-13. We compared targeting of the short and long FHOD1 isoforms to assess if there was any differential targeting between the splice variants in cells and to see if FHOD1 overexpression induced any changes in the F-actin network or cell morphology.

Prior to commencing overexpression studies in NRCs, we sought to confirm that the GFP and TOMATO-tagged expression constructs were capable of expression in mammalian cells and that they were expressed at the expected molecular weight. COS-1 cells were used for this purpose because of the substantially higher transfection efficiency that can be achieved with this cell line. Although NRC transfection by Escort III transfection reagent resulted in comparably better transfection efficiency and cell viability than other non-viral methods of transfection (results not shown), it still resulted in a relatively low transfection efficiency (approximately <5%). While results from one cell line cannot be directly translated into a completely valid interpretation in primary cells, the low transfection efficiency with NRCs restricted their use to immunofluorescence studies when implementation of expression constructs was concerned. The following expression experiments describe qualitative results because of their extrapolation in significance to another cell type and since the exact protein concentration was not determined before loading. Expression tests of the GFP-tagged constructs in transiently transfected COS-1 cells followed by Western blotting revealed that GFP fusion proteins of the expected molecular weight were generated (Figure 3.19 A-B). The long and short variant of FHOD1 ran near the 154kDa marker, consistent

with their expected combined molecular weight with GFP (Figure 3.19 D). Although there is a slight size difference of approximately 2kDa between these two constructs, we were unable to resolve the difference in size on SDS-PAGE gels but confirmed the identity of each construct by DNA sequencing. The full-length long variant of FHOD1 tagged with TOMATO protein also ran at its expected molecular weight (Figure 3.19 D) around the 180kDa marker (Figure 3.19 B), although some degradation was present.

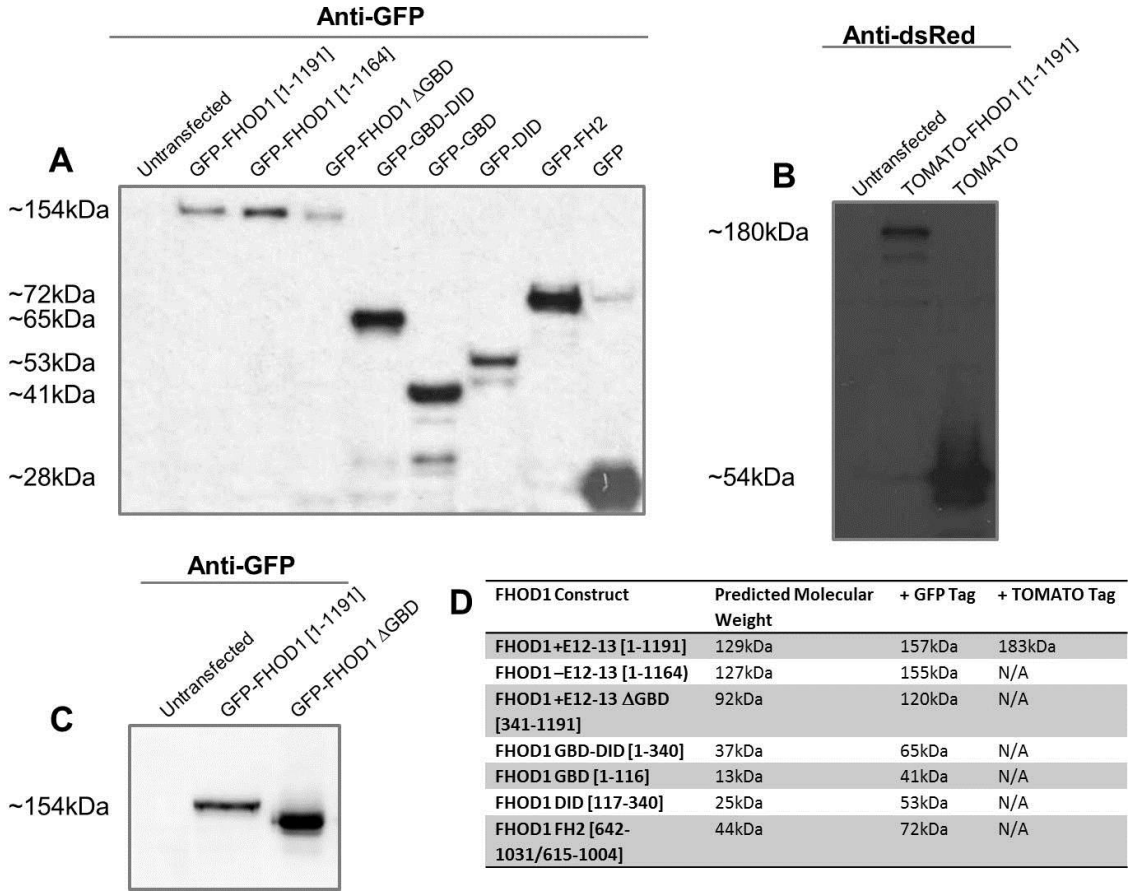

D

FHOD1 Construct	Predicted Molecular Weight	+ GFP Tag	+ TOMATO Tag
FHOD1+E12-13 [1-1191]	129kDa	157kDa	183kDa
FHOD1 –E12-13 [1-1164)	127kDa	155kDa	N/A
FHOD1+E12-13 ΔGBD [341-1191]	92kDa	120kDa	N/A
FHOD1 GBD-DID [1-340]	37kDa	65kDa	N/A
FHOD1 GBD [1-116]	13kDa	41kDa	N/A
FHOD1 DID [117-340]	25kDa	53kDa	N/A
FHOD1 FH2 [642-1031/615-1004]	44kDa	72kDa	N/A

Figure 3.19: Expression Test of Different FHOD1 Constructs in COS-1 Cells. **A)** Western blot with anti-GFP antibody of SDS samples from COS-1 cells that were transiently transfected with the different FHOD1 constructs. 12% SDS-PAGE. **B)** Western blot with anti-dsRed antibody of SDS samples from COS-1 cells that were transiently transfected with the different FHOD1 constructs. 12% SDS-PAGE. **C)** 7.5% SDS-PAGE gel with anti-GFP antibody to better resolve size difference between full-length FHOD1 and the ΔGBD construct. **D)** Table of expected molecular weights of constructs. Constructs of the expected molecular weight were observed in all samples. Untransfected COS-1 cells were used as a negative control. E12-13, alternatively spliced exons 12-13 found on the long FHOD1 splice variant. **N=3**

3.5.1 Targeting of the Full-Length FHOD1 in Neonatal Rat Cardiomyocytes

GFP-tagged version of the shorter FHOD1 variant (spanned from amino acids 1 to 1164; Figure 3.2 A), lacking exons 12-13, and the GFP-tagged longer FHOD1 variant (spanned from amino acids 1-1191; Figure 3.2 B), containing the alternatively spliced exons 12-13, were overexpressed in NRCs to compare their targeting. Both the short (Figure 3.20 C) and long (Figure 3.20 D) FHOD1 variants displayed a predominant localisation at the periphery of the cells. In addition, there was a lot of diffuse cytoplasmic signal. Counterstaining with F-actin, to visualise the I-bands of sarcomeres and the actin cytoskeleton revealed that the full-length FHOD1 construct displayed some targeting along myofibrils, but this was accompanied by little evidence of well-defined cross-striations. However, the longer construct had a slightly more striated appearance than that seen with the shorter construct. There was no considerable co-localisation between FHOD1 and F-actin in transfected cells. Furthermore, no increased signal was seen at the cell-cell contacts between NRCs. Despite FHOD1 having the reported ability to reorganise the cytoskeleton into structures like stress fibres (Takeya et al. 2008), we did not note the appearance of any new F-actin based structures or any morphological changes in transfected cells. Such an observation would be consistent with the fact that full-length FHOD1 is maintained in a closed inactive conformation. Overall, there was no marked difference in the targeting between the GFP-tagged long and short FHOD1 variants. These data would suggest that the alternatively spliced exons do not confer a specific subcellular localisation to full-length FHOD1 or govern its targeting.

As a control for both the long and short GFP-tagged full-length FHOD1 constructs, we also transfected NRCs with the empty GFP vector in order to examine if FHOD1 localisation was mediated by the GFP tag (Figure 3.20 E). Untagged GFP co-localised with F-actin throughout cells and was also found to accumulate in the nuclei of cells. While we found FHOD1 distributing along myofibrils, we did not note substantial co-localisation with F-actin. Furthermore, GFP-tagged full-length FHOD1 was excluded from the nucleus. While use of other epitope tagged constructs is required and would avoid the issue of GFP stickiness, we were fairly confident that the localisation of the GFP-tagged FHOD1 constructs were not mediated by the GFP tag.

A TOMATO-tagged version of the long variant was also transiently transfected in NRCs (Figure 3.21 A-B). Unlike cells overexpressing the GFP-tagged variants of FHOD1, FHOD1-TOMATO transfected cells had a slightly elongated morphology. Transfected cells presented with extended plasma membrane processes, to which FHOD1 localised to. In these cells, FHOD1 was occasionally found along myofibrils, although this was likely mediated by the TOMATO tag, which displayed similar co-localisation with myofibrils (Figure 3.21 C). The cellular phenotype induced by FHOD1-TOMATO might have been due to activation of the protein. This could have conceivably been due to the fact that the TOMATO tag (54 kDa) is larger than the GFP tag (28 kDa), and may have interrupted the autoinhibitory intramolecular interaction that maintains FHOD1 in a closed inactive state. Cells transfected with the empty TOMATO vector were identical to untransfected cells in their appearance (Figure 3.21 C), therefore indicated that the morphological changes noted in cells were not solely due to the TOMATO tag. Overall, results using the TOMATO tag proved to be inconclusive since the large size of the tag may have interfered with FHOD1's autoregulatory conformation and since the TOMATO tag may have mediated the subcellular targeting of FHOD1.

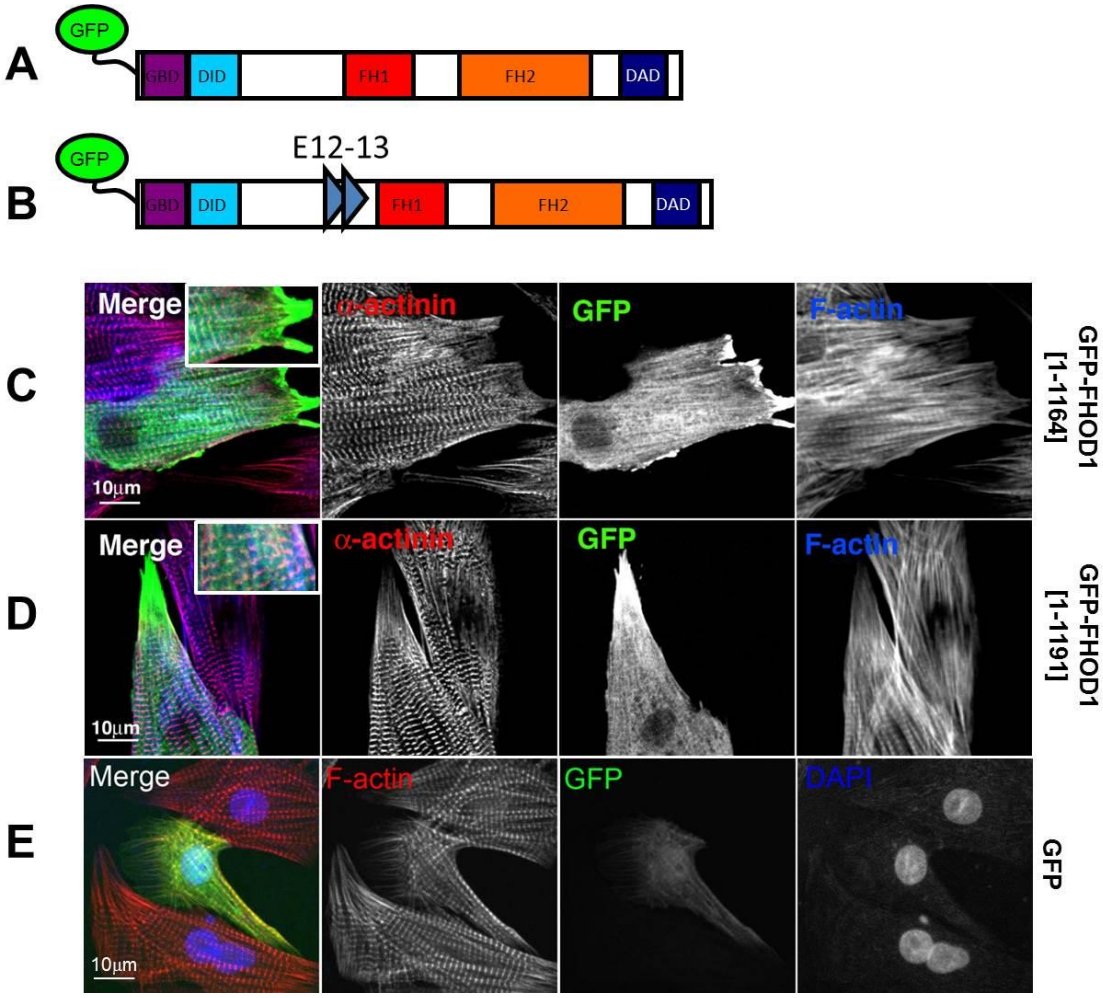

Figure 3.20: Overexpression of Full-length GFP-tagged FHOD1 in Neonatal Rat Cardiomyocytes. NRCs were transfected with different full-length fluorescent tagged FHOD1 constructs and cultured to day 4. Cells were stained against α-actinin, F-actin, and DAPI. Stained cells were visualised by confocal microscopy. GFP-tagged expression constructs were generated for **A)** the short variant of FHOD1 [1-1164], lacking the alternatively spliced exons 12-13 and **B)** the long variant of FHOD1 [1-1191], containing the alternatively spliced exons 12-13. Cells were transfected with the following constructs: **C)** the shorter variant of GFP-tagged full-length FHOD1 [1-1164], **D)** the longer variant of GFP-tagged full-length FHOD1 [1-1191], **E)** the empty GFP vector. α-actinin is seen in red, GFP-FHOD1 in green, and F-actin/DAPI in blue. GFP, green fluorescent protein. E12-13, alternatively spliced exons 12-13 found on the long FHOD1 splice variant. Scale bars represent 10μm. White boxes show zoomed selections of merged images. **N=3**

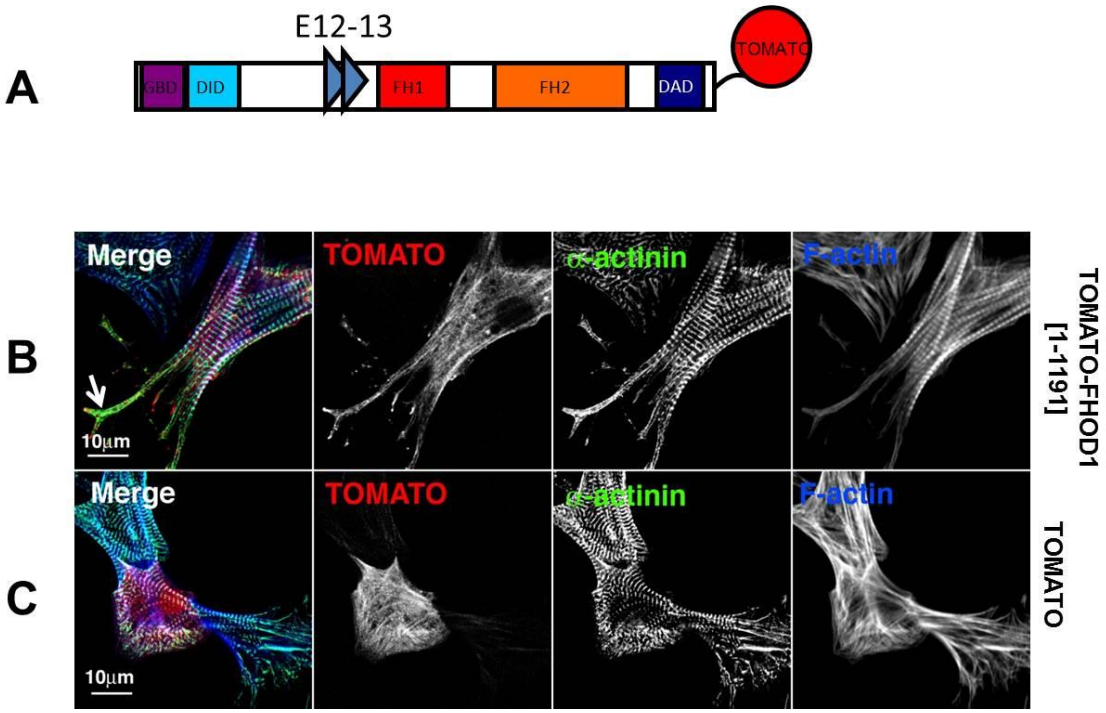

Figure 3.21: Overexpression of Full-length TOMATO-tagged FHOD1 in Neonatal Rat Cardiomyocytes. NRCs were transfected with different full-length fluorescent tagged FHOD1 constructs and cultured to day 4. Cells were stained against α-actinin and F-actin. Stained cells were visualised by confocal microscopy. **A)** A TOMATO-tagged expression construct was generated for the long variant of FHOD1, containing the alternatively spliced exons 12-13. Cells were transfected with the following constructs: **B)** the long variant of TOMATO-tagged full-length FHOD1 [1-1191], and **C)** the empty TOMATO tag vector TOMATO-FHOD1 is seen in red, α-actinin in green, and F-actin in blue. E12-13, alternatively spliced exons 12-13 found on the long FHOD1 splice variant. Scale bars represent 10μm. **N=3**

3.6 Subcellular Targeting of FHOD1 Domains in Neonatal Rat Cardiomyocytes

FHOD1 is composed of a modular domain structure typically found among the diaphanous related formins. The first half of the protein is composed of a GTPase binding domain (GBD) and a diaphanous inhibitory domain (DID). The second half is composed of two formin homology domains (FH1 and FH2) and a diaphanous autoregulatory domain (DAD). Having established the targeting of full-length FHOD1, the next step was to discern whether a particular portion of the protein was responsible for its targeting. We mapped the targeting of FHOD1 via overexpression of individual GFP-tagged fragments of the protein. The following FHOD1 constructs were examined in NRCs: the FH2 domain [642-1031]; the GBD-DID portion of the N-terminus [1-

340]; the GBD [1-116]; the DID [117-340] and a version of the long variant of FHOD1 lacking the GBD, termed FHOD1 ΔGBD [117-1191].

Prior to initiating transfection studies, we sought to confirm that the expression constructs of the individual FHOD1 domains were expressed at the correct molecular weight (Figure 3.19). COS-1 cells were used for the expression tests because of the very low transfection efficiency we were able to achieve in NRCs of approximately less than 5%. The following expression experiments describe qualitative results because of their extrapolation in significance to another cell type and because the exact protein concentration was not determined before loading. Expression tests of the GFP-tagged constructs in transiently transfected COS-1 cells followed by Western blotting revealed that the GFP fusion proteins expressed at the expected molecular weight. In order to confirm the correct size of the FHOD1 ΔGBD construct (Figure 3.19 A,C), we ran samples on lower percentage SDS-PAGE gels in order to visualise the size shift (approximately 37kDa) between the long variant of FHOD1 and the FHOD1 ΔGBD construct (Figure 3.19 C).

3.6.1 Overexpression of the FH2 Domain [642-1031]

Formin homology 2 (FH2) domains are the reported actin polymerising portion of formins (Chhabra and Higgs 2007). We overexpressed the FH2 domain of FHOD1 (amino acids 642 to 1031) on its own in NRCs (Figure 3.22 A). Transfected cells were morphologically indistinguishable from untransfected neighbours. The GFP-tagged FH2 domain distributed in a striated manner in cells. The FH2 domain produced a strong signal at the Z-disk, as indicated by co-localisation with α-actinin (Figure 3.22 B, Zoom) and an alternating signal with the M-band protein, myomesin (Figure 3.22 C). In line with the reported ability of FH2 domains to associate with F-actin (Higashida et al. 2004), co-localisation was noted between the FH2 domain of FHOD1 and F-actin at the peripheries of cells (Figure 3.22 C, Zoom). Overall, the FH2 domain of FHOD1 displayed targeting the Z-disks and F-actin in cardiomyocytes. Furthermore, in line with the capping and weak elongation activity of the FH2 domain (Schonichen et al. 2013), we observed a slight accumulation of F-actin in cells at sites where the FH2 domain and F-actin co-localised.

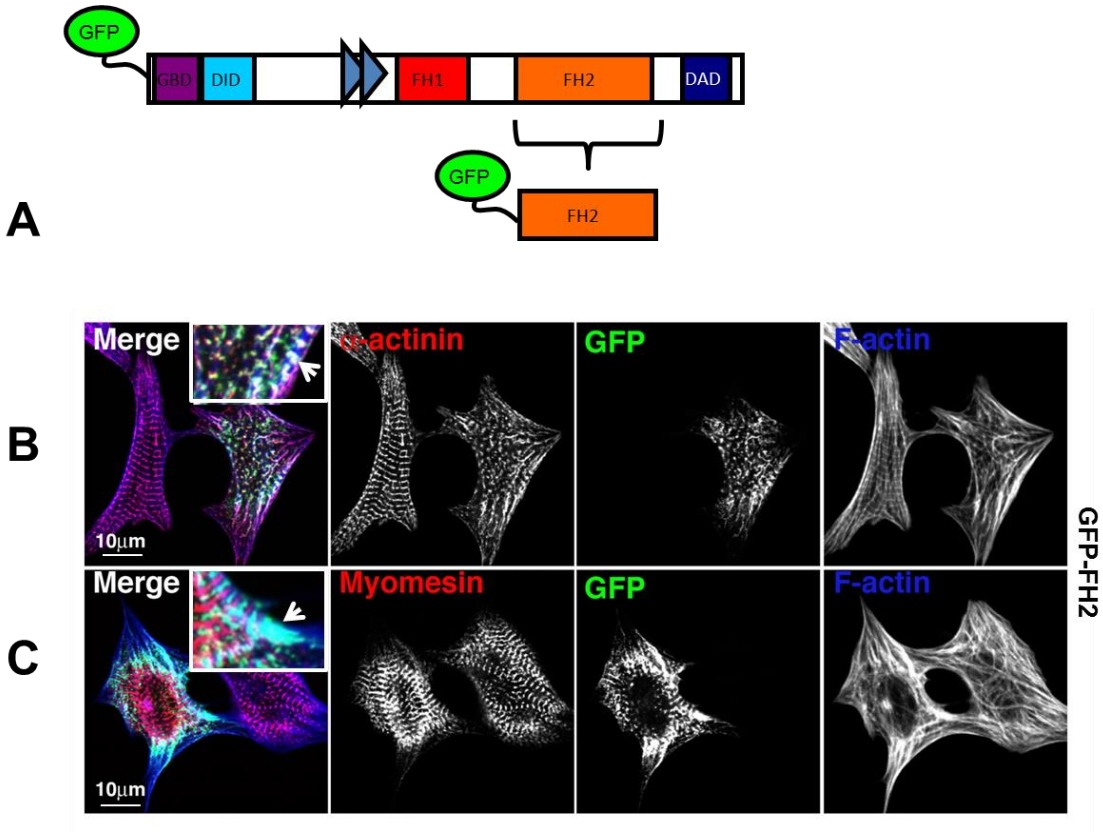

Figure 3.22: Overexpression of the FHOD1 FH2 Domain in Neonatal Rat Cardiomyocytes. **A)** An FHOD1 FH2 domain [642-1031] expression construct was generated to assess its targeting in NRCs. NRCs were transfected with the GFP-tagged expression construct and cultured to day 4. Cells were stained against **B)** sarcomeric α-actinin and F-actin or **C)** myomesin and F-actin. Stained cells were visualised by confocal microscopy. Myomesin/α-actinin are seen in red, GFP-tagged FHOD1 expression construct in green, and F-actin in blue. GFP, green fluorescent protein; FH, formin homology. White boxes show zoomed selections of merged images. Arrows denote sites of co-localisation. Scale bars represent 10μm. **N=3**

3.6.2 Overexpression of the GBD-DID [1-340]

It has previously been suggested that the distinct subcellular targeting of formin proteins is governed by their N-termini (Seth et al. 2006; Ramalingam et al. 2010). This is due partly to the fact that formins show greatest sequence and structural divergence within their N-termini (Schulte et al. 2008). We overexpressed an FHOD1 N-terminal construct comprised of the GBD and the DID and spanning amino acids 1 to 340 in NRCs (Figure 3.23 A). The GFP-tagged N-terminal fragment of FHOD1 mainly

distributed in a diffuse cytoplasmic manner, although there was some evidence of targeting to myofibrils. Occasionally, some co-localisation with F-actin could be discerned along myofibrils (Figure 3.23 B, Zoom). This would have been consistent with reports that the N-terminus of FHOD1 is required for its F-actin binding activity (Takeya and Sumimoto 2003) and targeting to actin-based structures, particularly stress fibres (Schonichen et al. 2013). Overall, the GBD-DID FHOD1 construct primarily distributed in a diffuse cytoplasmic manner although there was some evidence of myofibrillar targeting, where it sometimes co-localised with F-actin.

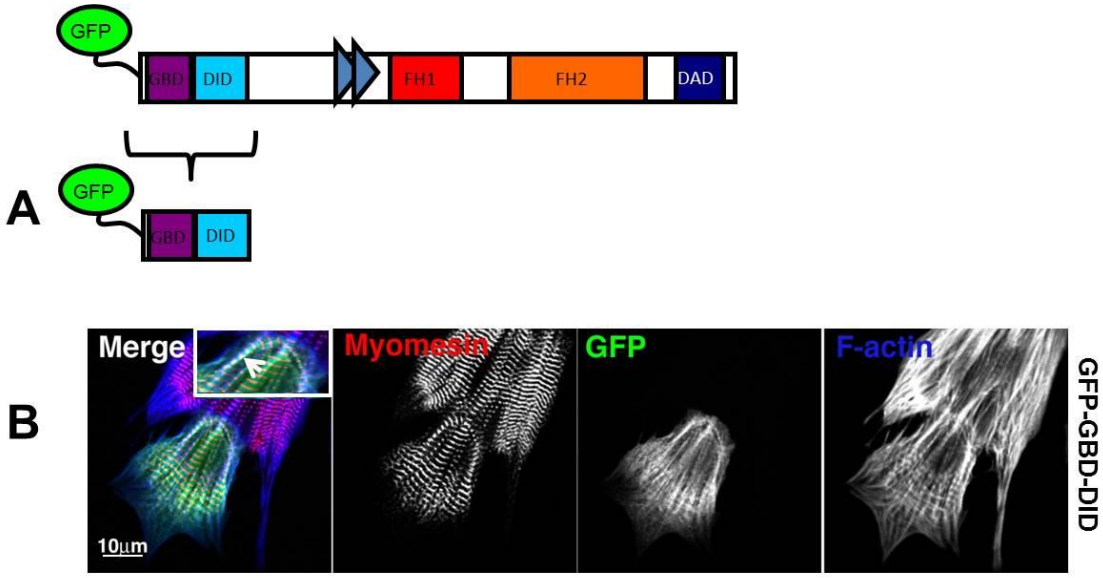

Figure 3.23: Overexpression of FHOD1 GBD-DID in Neonatal Rat Cardiomyocytes. A) An FHOD1 GBD-DID [1-340] expression construct was generated to assess its targeting in NRCs. NRCs were transfected with the GFP-tagged expression construct and cultured to day 4. Cells were stained against **B)** myomesin and F-actin. Stained cells were visualised by confocal microscopy. Myomesin is seen in red, GFP-tagged FHOD1 expression construct in green, and F-actin in blue. GFP, green fluorescent protein; GBD, GTPase binding domain; DID, diaphanous inhibitory domain. White box shows zoomed selection of merged images. Arrows denote sites of co-localisation. Scale bars represent 10µm. **N=3**

3.6.3 Overexpression of the GBD [1-116]

The GTPase binding domain (GBD) is typically thought to play a role in activation of DRFs. DRFs are normally held in a closed inactive state until binding of a Rho family small GTPase in the GBD (Tominaga et al. 2000). This partially relieves the autoinhibitory interaction between both ends of the protein and subsequently leads to activation when the functional formin homology domains are exposed. With the N-terminus of FHOD1 representing a likely portion of the protein responsible for mediating its targeting to myofibrils, we investigated the localisation of the GBD when overexpressed on its own in NRCs. A GBD construct spanning from amino acids 1 to 116 was used for this purpose (Figure 3.24 A). When overexpressed in NRCs, the GFP-tagged GBD distributed primarily in a diffuse cytoplasmic manner (Figure 3.24 B-C). There was some evidence of myofibrillar targeting and an occasional signal could be discerned at the Z-disk, as evidenced by co-localisation with α–actinin (Figure 3.24 B, Zoom) and an alternating signal with myomesin (Figure 3.24 C, Zoom). Very faint co-localisation with myomesin could occasionally be discerned, indicating the presence of the GBD at some of the M-bands. Overall, the FHOD1 GBD predominantly distributed throughout the cytoplasm of cells and was partially targeted to myofibrils..

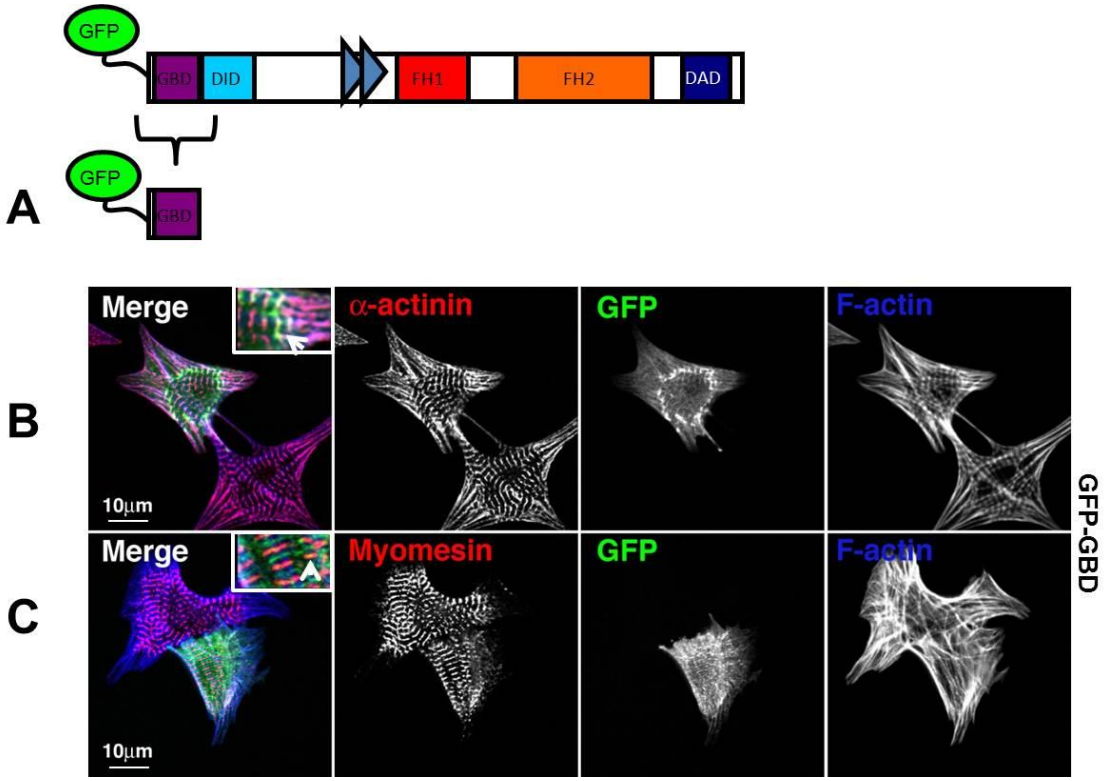

Figure 3.24: Overexpression of the FHOD1 GBD in Neonatal Rat Cardiomyocytes. A) An FHOD1 GBD [1-116] expression construct was generated to assess its targeting in NRCs. NRCs were transfected with the GFP-tagged expression construct and cultured to day 4. Cells were stained against **B)** sarcomeric α-actinin and F-actin or **C)** myomesin and F-actin. Stained cells were visualised by confocal microscopy. Myomesin/α-actinin are seen in red, GFP-tagged FHOD1 expression construct in green, and F-actin in blue. GFP, green fluorescent protein; GBD, GTPase binding domain. White boxes show zoomed selections of merged images. Arrows denote sites of co-localisation. Scale bars represent 10μm. **N=3**

3.6.4 Overexpression of the DID [117-340]

The Diaphanous inhibitory domain (DID) is involved in mediating the autoinhibitory interaction that maintains DRFs in a closed inactive state (Schonichen et al. 2006). The DID (amino acids 117 to 340) of FHOD1 was overexpressed in NRCs in order to examine its targeting (Figure 3.25 A). In contrast to the localisation of both the GBD and DID together, the GFP-tagged DID on its own distributed as aggregates or small vesicular structures throughout cells (Figure 3.25 B). The DID is likely dispensable regarding targeting of FHOD1 to the sarcomere. However, in the absence of an expression test in NRCs, we were unable to rule out whether the protein was unstable, a factor which may have accounted for its aberrant localisation.

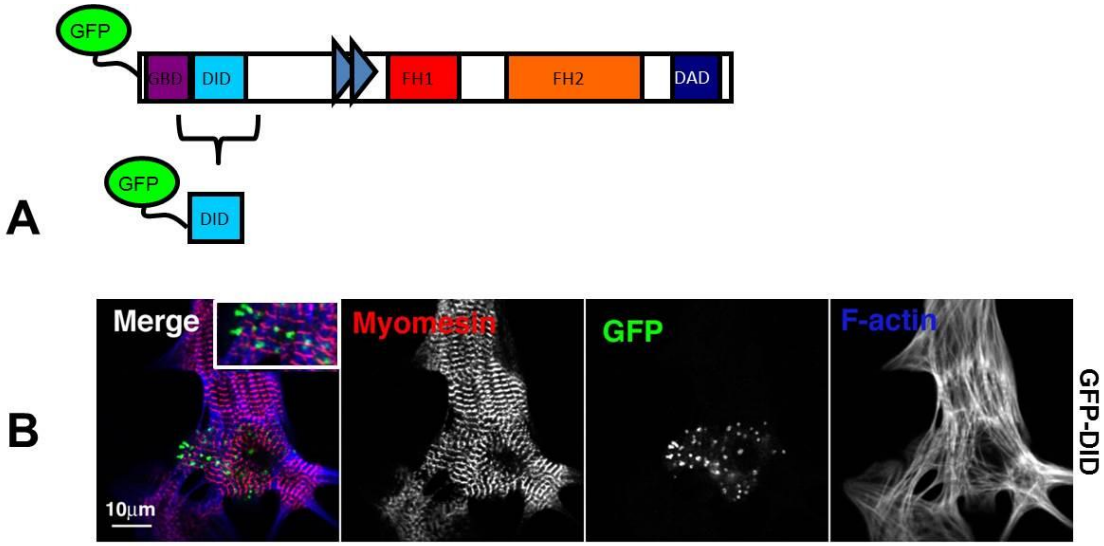

Figure 3.25: Overexpression of the FHOD1 DID in Neonatal Rat Cardiomyocytes. A) An FHOD1 DID [117-340] expression construct was generated to assess its targeting in NRCs. NRCs were transfected with the GFP-tagged expression construct and cultured to day 4. Cells were stained against **B)** myomesin and F-actin. Stained cells were visualised by confocal microscopy. Myomesin is seen in red, GFP-tagged FHOD1 expression construct in green, and F-actin in blue. GFP, green fluorescent protein; DID, diaphanous inhibitory domain. White box shows zoomed selection of merged images Scale bars represent 10µm. **N=3**

3.6.5 Overexpression of FHOD1 ΔGBD [117-1191]

In order to determine if the GBD was indeed playing a role in the targeting FHOD1 to myofibrils, we overexpressed an FHOD1 deletion construct lacking the N-terminal GBD (Figure 3.26 A). This construct spanned from amino acids 117 to 1191 and included the alternatively spliced exons, and thus represented a truncation mutant of the long FHOD1 variant. In contrast to the full-length FHOD1 construct , which accumulated in the peripheries of cells and was partially targeted to myofibrils (Figure 3.20 D), FHOD1 ΔGBD was instead distributing as aggregates or small vesicular like structures throughout cells (Figure 3.26 B). However, similarly to the DID, due to the lack of expression controls on the protein level in NRCs for the ΔGBD, we were unable to rule out if the aberrant localisation noted for the protein was merely due to its instability in NRCs. Overall, these experiments could suggest that the GBD domain of FHOD1 mediated the subcellular targeting that is observed for full-length FHOD1 in NRC.

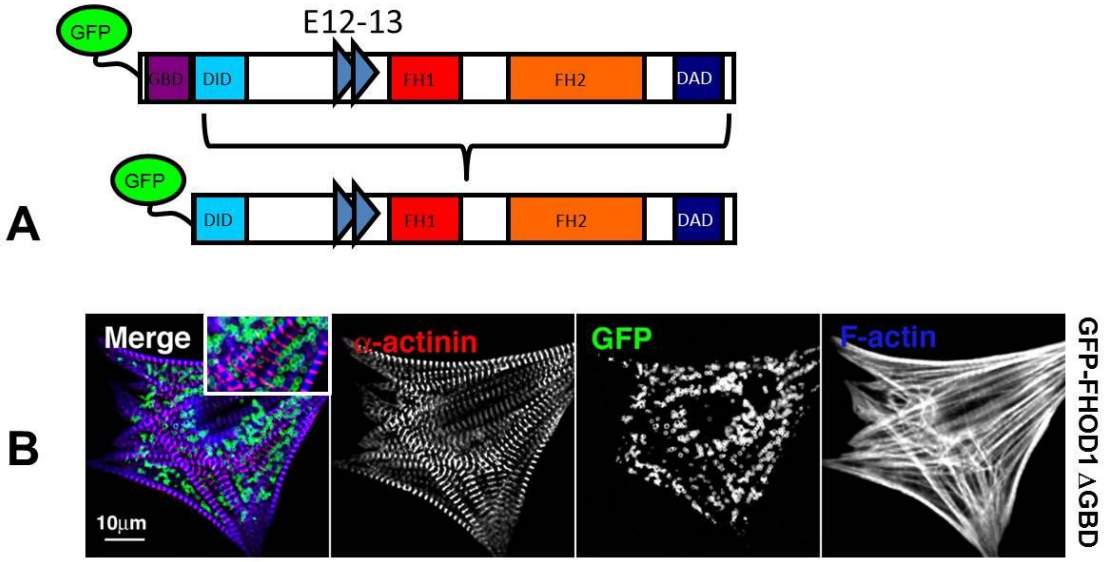

Figure 3.26: Overexpression of FHOD1 ΔGBD in Neonatal Rat Cardiomyocytes. A) An FHOD1 ΔGBD [117-1191] expression construct was generated to assess its targeting in NRCs. NRCs were transfected with the GFP-tagged expression construct and cultured to day 4. Cells were stained against **B)** myomesin and F-actin. Stained cells were visualised by confocal microscopy. Myomesin is seen in red, GFP-tagged FHOD1 expression construct in green, and F-actin in blue. GFP, green fluorescent protein; GBD, GTPase binding domain. E12-13, alternatively spliced exons 12-13 found on the long FHOD1 splice variant. White box shows zoomed selection of merged images Scale bars represent 10μm. **N=3**

3.7 Discussion

3.7.1 Expression of FHOD1 in Muscle Tissue

We initiated our characterisation of FHOD1 by seeking to confirm expression in protein lysates of murine whole muscle samples. As a positive control we loaded lysates from whole murine spleen samples where, as expected, a prominent band was seen running at the expected molecular weight of FHOD1 in *Mus musculus* (Westendorf et al. 1999; Tojo et al. 2003). Furthermore, a band of the same molecular weight was also detected in heart, as well as in fast and slow twitch skeletal muscle (Tibialis anterior, TA, and Soleus, respectively).Expression of sarcomeric α-actinin was used as a loading control for quantification, which suggested that expression of FHOD1 is significantly higher in heart and fast twitch than in slow twitch muscle. The finding suggesting that slow twitch fibres appear to express lower levels of FHOD1 than either fast twitch fibres or the heart is in contrast to many other cytoskeletal proteins, which seem to be regulated in their expression in a similar way in ventricular and slow twitch muscle (Schiaffino

and Reggiani 1996). However, although Western blots were performed three times for adequate quantification and basic statistical analysis to be performed, it must be noted that samples were derived from only two C57/BL6 mice. The results must therefore be interpreted with the caveat that they reflect findings from a relatively small sample size in an inbred strain of mice. Extrapolation of these findings to other mammalian systems, particularly to humans, must be done so with caution. However, our data in murine samples was in agreement with the expression profile of FHOD1 in human samples reported by one study that examined the expression profile of all 15 formins (Krainer et al. 2013). Here it was found that FHOD1 expression was higher in cardiac muscle than skeletal muscle on both the mRNA transcript level, as ascertained by real-time PCR, and the protein level, as confirmed by Western blotting.

Previous studies suggested expression of FHOD1 on the mRNA transcript level in both cardiac and skeletal muscle (See Table 3.2 for previous expression data) (Westendorf et al. 1999; Tojo et al. 2003; Gill et al. 2004). However, other reports implementing antibody studies suggested that FHOD1 was not expressed in hearts at the protein level (Staus et al. 2011). Staus et al. 2011 reported no expression of FHOD1 in murine hearts whereas we found a signal for FHOD1 in hearts as well as confirming expression in skeletal muscle. This discrepancy was most likely due to the fact that these profiles were ascertained using different anti-FHOD1 antibodies, since both studies were performed using C57/BL6 mice. Whereas our study was able to produce a signal for FHOD1 in the heart with the polyclonal mouse anti-FHOD1 antibody (Abcam), Staus et al. 2011 was unable to do so using the polyclonal mouse anti-FHOD1 antibody (ECM Biosciences). During our validation experiments for the polyclonal mouse anti-FHOD1 antibody (ECM Biosciences), there was no observed signal for FHOD1 in either cardiac or skeletal muscle lysates (results not shown), unlike the previous study that revealed a signal for FHOD1 in skeletal muscle (Staus et al. 2011). These conflicting results regarding the same antibody may have been accounted for by differences in sample preparation or even by the quality of different antibody batches. Taking into account microscopy data, the notion that FHOD1 protein is found in cardiac muscle was supported by the observed signal for the protein in immunofluorescence samples of cultured cardiac cells and heart sections with several different antibodies.

mRNA Expression Profile																		
Tissue																		
Study	Ovary	Thymus	Prostate	Testis	Small Intestine	Colon	Spleen	Brain	Heart	Skeletal Muscle	Kidney	Liver	Placenta	Lung	Aorta	Stomach	Cultured SMCs	Bladder
(Westendorf et al. 1999)	x	x	x	x	x	x	x	-	N/A	N/A	N/A	N/A	N/A	N/A	N/A	N/A	N/A	N/A
(Tojo et al. 2003)	N/A	x	N/A	N/A	x	x	x	x	x	x	x	x	x	x	N/A	N/A	N/A	N/A
(Gill et al. 2004)	N/A	N/A	N/A	N/A	N/A	x	x	N/A	x	x	x	x	N/A	x	N/A	N/A	N/A	N/A
(Wang et al. 2004)	N/A	N/A	N/A	N/A	N/A	N/A	N/A	N/A	N/A	N/A	N/A	N/A	N/A	N/A	N/A	N/A	x	N/A
(Krainer et al. 2013)	N/A	N/A	N/A	N/A	N/A	N/A	N/A	x	x	x	N/A	N/A	N/A	N/A	N/A	N/A	N/A	N/A
Protein Expression Profile																		
(Staus et al. 2011)	N/A	N/A	N/A	x	-	N/A	N/A	x	-	x	N/A	N/A	N/A	x	x	x	x	x
(Krainer et al. 2013)	N/A	N/A	N/A	N/A	N/A	N/A	N/A	N/A	x	x	N/A	N/A	N/A	N/A	N/A	N/A	N/A	N/A
This Study	N/A	N/A	N/A	N/A	N/A	N/A	x	N/A	x	x	N/A	N/A	N/A	N/A	N/A	N/A	N/A	N/A

Table 3.2: Expression Profile of FHOD1 in Mammalian Tissues. Summary of the expression patterns exhibited by FHOD1 in a number of tissues as described by previous studies. The mRNA expression profiles were ascertained by Northern blot experiments and Multiple Tissue Expression Arrays using human tissues. The protein expression profile was ascertained through Western blot studies using murine tissues. The studies that described each expression profile are found in the left hand column. x, denotes expression in tissue; -, denotes absence of expression in tissue; N/A, not applicable since expression was not explored in tissue.

Unlike its expression in cardiac muscle, FHOD1 expression has been confirmed in skeletal muscle by many of the relevant studies (Tojo et al. 2003; Gill et al. 2004; Staus et al. 2011a; Krainer et al. 2013), however, the present characterisation effort is the first to report differences in protein levels of this formin in fast versus slow skeletal muscle. Although weaker than that seen in cardiac muscle, a strong signal for FHOD1 was noted in samples from mouse tibialis anterior (TA). TA muscle is primarily composed of fast twitch skeletal muscle fibres. Fainter FHOD1 expression was observed in mouse soleus samples, a muscle composed primarily of slow twitch skeletal muscle fibres. The reasons behind this observed difference in protein levels can only be speculated upon but they may be explained by rates of protein turnover in these muscle types. Muscle proteins are continuously being turned over but rates vary according to the type of muscle. The average half-lives in rat adult slow twitch and fast twitch skeletal muscles are 12.1 and 18.3 days, respectively (Lewis et al. 1984; Goldspink 1991). The lower expression levels of FHOD1 in soleus could have therefore been explained by the higher rate of protein turnover, resulting in less accumulation of FHOD1 in slow twitch skeletal muscle. Different levels of FHOD1 in each tissue may have also been indicative of specific requirements for the protein in various types of striated muscle.

One discrepancy that arose in the study of FHOD1 expression in different tissues was the observation that only one antibody produced a discernible signal for FHOD1. This raised the point as to whether the polyclonal mouse anti-FHOD1 antibody (Abcam) was actually recognising FHOD1 in lysates. Antibody validation using full-length constructs and different fragments of FHOD1 suggested that all 4 of the commercial antibodies recognised the human FHOD1 constructs, albeit with varying specificity considering that the polyclonal goat antibodies seem to preferentially recognise the FHOD1 C-terminus, at least in terms of all the constructs tested. Alignment of the human and mouse FHOD1 amino acid sequences suggested relatively high levels of sequence similarity among the regions of FHOD1 that the antibodies recognised on Western blots. This would suggest that recognition of mouse FHOD1 could have been possible, although sequence alignment cannot substitute for direct biochemical verification using mouse FHOD1 constructs. We also demonstrated that the anti-FHOD1 antibodies preferentially recognised the human FHOD1 construct and did not cross-react with human FHOD3 constructs on Western blots or in immunofluorescence samples of COS

cells overexpressing FHOD1 or FHOD3. This was a particularly important point to address since human FHOD1 and FHOD3 bear 52.1% amino acid similarity. Although, direct biochemical verification was lacking in terms of cross-reactivity using a mouse FHOD3 construct, the similar level of divergence noted between human FHOD1 and mouse FHOD3 (56% sequence similarity) could have been an indicator that cross-reactivity was not occurring on blots. One likely explanation behind the lack of signal with the other anti-FHOD1 antibodies in murine tissue could be loss of the epitope the antibodies preferentially recognise, since samples are subjected to denaturing conditions. One way of addressing this potential issue could involve the use of milder sample preparation methods (e.g., lysis in RIPA buffer) and/or the inclusion of protease inhibitors in the lysis buffer.

However, one major caveat that was not addressed involved the potential of antibody cross-reactivity with other proteins. Antigen competition assays were not performed, therefore we cannot conclude with certainty that we were truly visualising FHOD1 on Western blots. Even if the observed molecular weight of the bands attributed to FHOD1 in tissue lysates were in agreement with the expected molecular weight, there are other proteins with similar molecular weight. Furthermore, a band at the correct expected molecular weight is not proof enough of protein identity since proteins can often migrate at unexpected observed molecular weights on one-dimensional gels.

3.7.2 Localisation of Endogenous FHOD1 in Muscle Samples

Aside from examining the expression of total FHOD1 protein, we looked at the localisation of the endogenous protein using the 4 commercial anti-FHOD1 antibodies in various muscle samples: NRCs, ARCs, mouse heart sections, and differentiating C2C12 skeletal muscle cells. The present localisation studies were complemented by Western blot studies, which sought to confirm reactivity against FHOD1 at the protein level. We were able to show reactivity with at least one antibody across all the different muscle samples. However, the caveat remained that we were unable to rule out non-specific recognition of other proteins in the absence of an antigen competition assay with each sample. This was the case for both Western blot and immunofluorescence studies. Furthermore, as was the case for mouse FHOD1, we were unable to confirm the

sensitivity of the commercial anti-FHOD1 antibodies in biochemical verification experiments using rat FHOD1 constructs.

Experiments in NRCs using the different antibodies revealed that FHOD1 could be found distributing along myofibrils and that it could also be visualised as striations, indicating that FHOD1 could be partly found distributing within specific compartments of the sarcomere. However, comparison between the antibodies revealed inconsistencies when the localisation of FHOD1 within the sarcomere was concerned (Table 3.1), therefore casting doubt as to the validity of these staining experiments. The multitude of FHOD1 localisations was highly suggestive that the antibodies were not recognising their designated target. A similar situation was noted for ARCs. While we noted myofibrillar targeting and some sarcomeric distribution for endogenous FHOD1 in ARCs, the results presented for the antibodies that demonstrated reactivity for FHOD1 in immunofluorescence samples produced inconsistent results when they were compared among each other. It is therefore difficult to draw meaningful conclusions regarding the precise localisation of endogenous FHOD1 in NRCs and ARCs.

We also investigated the subcellular localisation of FHOD1 in frozen sections of mouse heart. With two different FHOD1 antibodies (polyclonal goat C14 and C20) that are directed against two different epitopes along the molecule, a strong signal was seen in cardiomyocytes, which was mainly concentrated at the specific sites of cell-cell contact in heart, the intercalated discs. We also observed staining in the interstitial spaces between cardiomyocytes, which could have suggested that some FHOD1 expression occurred in cardiac fibroblasts. Occasionally a cross-striated pattern was seen in cardiomyocytes, suggesting the presence of FHOD1 within myofibrils. Counterstaining for the M-band marker myomesin revealed alternating striations and indicates that FHOD1 may be present in some of the Z-disks, although counterstaining with the Z-disk marker α–actinin must be performed in order to confirm this. Interestingly this localisation pattern may be evolutionally conserved; in *C. elegans* FHOD1 is also found as bright puncta at the muscle cell edges with faint striations at the dense bodies, the equivalent of the Z-disk (Mi-Mi et al. 2012). While we were able to rule out any background staining mediated by the secondary antibodies, we were not able to directly

demonstrate a lack of cross-reactivity of the antibody conjugates, although only multi-labelling quality antibodies were employed.

While we did not present the localisation of FHOD1 in skeletal muscle sections, we did explore its expression and localisation over the differentiation process that C2C12 cells undergo when they are subjected to low serum conditions, in concurrent Western blotting and immunofluorescence experiments. We showed reactivity with the polyclonal goat C14 antibody in C2C12 samples via Western blots throughout the entire differentiation process. However, the caveat applies that the identity of this signal was not confirmed in the absence of an antigen competition assay. We confirmed that cells were differentiating on Western blots by showing a more-prominent signal for α–actinin and desmin at day 2. The differentiation process was also confirmed visually, as cells were seen to elongate, fuse into myotubes, and occasionally twitch. At day 0 we did however note a band for FHOD1 migrating at a lower molecular weight than expected. Currently, there is only one reported FHOD1 isoform in mice, a large 1,197 amino acid variant (predicted molecular weight 128 kDa). This unidentified band may have represented non-specific recognition of another protein, although only the performance of an antigen competition assay would be able to truly clarify this.

In undifferentiated myoblasts, FHOD1 exhibited predominantly cytoplasmic distribution. Originally, FHOD1 was found to be a cytoplasmic protein as determined by immunofluorescence staining in HeLa and also since it was found in the cytoplasmic fraction in cell fractionation experiments (Westendorf et al. 1999). Furthermore, during the investigation of the localisation of endogenous FHOD1 in Co396 cells, a novel antibody was raised against FHOD1 and staining for the protein revealed that it distributed in a cytoplasmic manner and accumulated in the perinuclear region of cells (Wang et al. 2004). In C2C12 cells, FHOD1 remained diffuse throughout the cytoplasm when cells began to elongate and fuse, but FHOD1 was occasionally visualised along F-actin stress fibres. In differentiated cells that had assembled sarcomeres, FHOD1 could occasionally be discerned along myofibrils, but any evidence of sarcomeric targeting was not clear, except for the polyclonal goat C20 antibody. The goat C20 anti-FHOD1 antibody consistently produced doublet banding pattern for FHOD1 in cultured cells of myogenic origin. Once again, discrepancies in the

localisation of endogenous FHOD1 occurred between the antibodies, therefore it is difficult to draw any meaningful conclusions until we can determine with certainty that the anti-FHOD1 antibodies are only recognising their designated epitope and not another protein.

3.7.3 Overexpression of FHOD1 in NRCs

In addition to investigating the expression and localisation of endogenous FHOD1 in muscle samples, we performed transient expression studies using epitope tagged full-length FHOD1 and fragments therefore in cultured NRCs. One of the issues we sought to address was the potential for differential targeting between the short and long FHOD1 isoforms found in human. Differential splicing of FHOD1 had been previously noted when a larger FHOD1 isoform was described in skeletal muscle (Tojo et al. 2003). Apart from the 1,164 amino acid variant, two additional FHOD1 isoforms have been identified in humans: the larger skeletal muscle variant containing a 78bp (26 amino acid) insertion and a truncated variant with a 24bp insertion, containing an in-frame stop codon at the same site as the 78bp insertion. The 78 bp insertion represents two alternatively spliced exons (exons 12-13). Previous analysis of the mRNA expression pattern of the FHOD1 variants revealed that the larger variant was preferentially expressed in heart, skeletal muscle, and prostate samples whereas the original isoform exhibited a more ubiquitous expression profile. Furthermore, the larger variant was abundantly expressed in skeletal muscle and faintly in the heart whereas the original isoform was abundantly expressed in the heart and faintly expressed in skeletal muscle (Tojo et al. 2003).

Overexpression of both the long and short GFP-tagged FHOD1 constructs in NRC revealed a mainly diffuse signal with major intensities at the periphery of the cells. However, in contrast to the observed localisation for FHOD1 at the intercalated disk in heart tissue, we did not detect a consistently increased signal for GFP-tagged FHOD1 at the cell-cell contacts between NRCs. This was also the case for endogenous FHOD1, which was visualised with the commercially available anti-FHOD1 antibodies. These contacts between NRCs are often termed intercalated disk-like structures since, despite containing the classical intercalated disk components such as desmosomal proteins and gap junction proteins, one major difference is that they do not necessarily require end-

on insertion of myofibrils but can also occur in parallel to myofibrils (Hirschy et al. 2006). Analysis of FHOD1 expression during embryonic heart development and comparison of its localisation with established intercalated disk anatomy will be required to determine, whether FHOD1 is only a late addition and characterizes mature intercalated disks in the three-dimensional environment in situ.

It was noted that the GFP-tagged full-length FHOD1 constructs were well tolerated in cells and did not induce any changes in their cytoarchitecture, as gauged by staining for the Z-disk marker, α-actinin. This observation was consistent with previous overexpression studies in cultured cells that indicated full-length FHOD1 was maintained in a closed inactive state and could therefore not induce changes in cell morphology (Westendorf 2001; Gasteier et al. 2003; Koka et al. 2003; Takeya and Sumimoto 2003; Boehm et al. 2005; Gasteier et al. 2005). However, the TOMATO-tagged long variant of full-length FHOD1 induced mild cell elongation and the formation of membrane extensions, to which FHOD1 was targeted to. This would be in line with the cell elongation phenotype observed in full-length FHOD1 overexpressing NIH3T3 and WM35 cells (Koka et al. 2003). One can only speculate as to why the TOMATO-tagged FHOD1 construct induced a change in cardiomyocyte morphology whereas the full-length GFP-tagged constructs did not. We propose that the TOMATO-tagged long variant of full-length FHOD1 may have been rendered in a partially active confirmation, due to steric displacement of the formin autoinhibitory interaction by the larger size of the TOMATO tag. These potentially undesirable characteristics of the TOMATO tag highlight that it is not a suitable epitope tag for localisation studies as it could alter the native properties of the protein. Furthermore, we observed nearly identical distribution along myofibrils for the TOMATO tag on its own, indicating that the observed localisation for TOMATO-tagged FHOD1 along myofibrils may have been mediated by the tag. While stickiness of the GFP molecule posed a potential caveat in this study, we found GFP restricted to the I-bands and nuclei of NRCs while the GFP-tagged FHOD1 constructs displayed comparatively different targeting.

Interestingly, targeting of full-length FHOD1 differed from that previously noted with full-length FHOD3, which distributed along myofibrils but was found near the A-bands of sarcomeres when overexpressed in NRCs (Iskratsch et al. 2010). Perhaps distinct

subcellular localisations for the two closely related formins indicate a specialised function for each protein. However, one drawback of overexpressing human protein in rat cardiac cells is that it is not fully representative of the protein's native environment. Although the FHOD1 and FHOD3 amino acid sequences are fairly highly conserved between human and rat, further overexpression experiments using rat FHOD1 should be performed in order to see if targeting of rat and human FHOD1 differs.

The subcellular targeting of formins is often mediated by their N-terminus (Seth et al. 2006; Ramalingam et al. 2010), which also tends to be the part of the molecule with the highest divergence in its sequence and even in its structure (Schulte et al. 2008). We created GFP-tagged expression constructs that only encoded for subdomains of FHOD1 and analysed their subcellular targeting in NRC. The FH2 domain of FHOD1 on its own displayed a strong signal at the Z-disk, as indicated by its alternation with signal for the M-band protein myomesin and co-localisation with the Z-disk marker α-actinin. The FH2 domain also co-localised with F-actin near the cell peripheries and may have led to a slight increase in F-actin levels at their sites of overlap. This may have been consistent with the capping, mild elongation, or bundling activity that the FHOD1 FH2 domain may possess (Schonichen et al. 2013). Constructs encoding the GBD-DID domain or even only the GBD domain on its own showed mainly diffuse cytoplasmic localisation with some evidence for myofibrillar and sarcomeric localisation. The DID alone as well as an N-terminal deletion construct lacking the GBD domain either showed aggregates or small vesicular-like structures. These experiments would suggest that the GBD domain of FHOD1 could mediate the subcellular targeting that is observed for full-length FHOD1 in NRC.

Initial reports suggested that the C-terminus of FHOD1 was responsible for mediating its subcellular localisation (Westendorf 2001). The current work and that of others would however have indicated otherwise. The current data indicated that the GBD of FHOD1 may have mediated the targeting of the full-length GFP-tagged FHOD1construct in NRCs. This would be in line with a previous study that suggested that the GBD of FHOD1 is essential for its activity. One study overexpressed different active and inactive FHOD1 ΔGBD constructs in NIH3T3 cells to study the role of the GBD. The construct lacking the GBD but in its uninhibited confirmation (FHOD1

ΔGBDΔDAD) was unable to promote the formation of stress fibres whereas the active construct containing the GBD (FHOD1 ΔDAD) was able to promote stress fibres formation and localised to these sites (Schulte et al. 2008). It has also been noted that FHOD1 mediated stress fibre formation was dependent on the targeting of the protein to these sites (Gasteier et al. 2003). A more-recent study found that wild-type FHOD1 and an N-terminal construct of FHOD1 (amino acids 1-573; FHOD1 short variant) co-localised with actin arcs and stress fibres whereas a truncation mutant of FHOD1, lacking the N-terminus but retaining the FH2 domain, did not (Schonichen et al. 2013).The possibility that the GBD in particular is required for the targeting of FHOD1 poses interesting biological questions. Perhaps a Rho family small GTPase is required to mediate the targeting of FHOD1 by way of binding to the GBD. However, no studies have demonstrated binding of a Rho family small GTPase to the FHOD1 N-terminus (Westendorf 2001; Schulte et al. 2008). There is also currently little known about the expression pattern of the Rho family GTPases in cardiac muscle. Furthermore, while there is some evidence for the association between the Rho family GTPases and myofibrils (Ahuja et al. 2007), this remains to be fully elucidated; therefore there is little room for speculation.

However, the targeting of the FH2 domain to the Z-disks and to F-actin would suggest that the FH2 domain might also contribute to the targeting of FHOD1. Interestingly, also the FH2 domain of FHOD3 targets to Z-disks when expressed on its own (Iskratsch and Ehler, personal communication), so it may be a more general feature of FHOD formins. There are other possible explanations behind the apparent change in localisation of the FHOD1 ΔGBD construct in NRCs. This construct still contains the regulatory DID and DAD regions, therefore FHOD1 could have still been conceivably held in its autoinhibited state thus masking the FH2 domain, which could mediate targeting to the Z-disks and F-actin. The GBD could therefore mediate the subcellular targeting of FHOD1 in its autoinhibited state whereas the Z-disk targeting requires the protein in its open conformation. This notion would need to be confirmed by performing overexpression studies with FHOD1 constructs lacking the both the GBD and DID, the GBD and DAD, or the GBD, DID, and DAD. Constructs lacking the FH2 domain will also be necessary to investigate this hypothesis.

3.7.6 Conclusion

In summary, we have demonstrated possible reactivity against FHOD1 in cultured muscle cells and whole muscle samples via Western blot and immunofluorescence studies. Furthermore, we have also unearthed potentially significant differences in expression levels of FHOD1 across murine muscle samples, which were in line with the expression pattern reported in a recent study in humans (Krainer et al. 2013). Since we reported a number of localisations for endogenous FHOD1 in immunofluorescence samples, we were not able to conclude with certainty the precise subcellular localisation of the protein in rat and mouse muscle samples. This was due to the technical limitations of the study, especially the lack of antigen competition assay control experiments. We also reported the effects of full-length human FHOD1 expression in NRCs, where the protein was found to primarily concentrate in the cell peripheries and distribute within the cytoplasm. Analysis of FHOD1 subdomains suggested that the GBD domain may play a role in mediating the localisation we noted for the full-length overexpressed protein, although the FH2 domain might also influence this. We hypothesise that the influence of the GBD and FH2 on the targeting of FHOD1 might differ according to the activation status of the protein.

3.7.5 Future Directions

While we were able to demonstrate that the anti-FHOD1 antibodies specifically recognised the human FHOD1 constructs and not FHOD3, one of the major oversights in these experiments was the uncertainty as to whether FHOD1 was cross-reacting with any other proteins on Western blots and immunofluorescence samples. Antigen competition assays will be required to address this issue. The commercial anti-FHOD1 antibodies would need to be incubated with FHOD1 antigen prior to Western blotting or staining experiments in order to see if the previously noted signal for FHOD1 remains. Similarly, biochemical verification with rodent constructs will be required to prove with certainty that the antibodies recognise rodent FHOD1. Furthermore, single staining controls will be required in order to rule out any cross-reactivity with the other antibodies employed in the staining experiments, particularly if an overlapping signal was shown. Eventually, antibody studies should culminate in the generation of our own anti-FHOD1 serum from immunised rabbits.

In terms of the overexpression studies, further confirmation will be required as to whether the GBD is indeed responsible for mediating the subcellular localisation of FHOD1, using the constructs outlined above. Furthermore, it must be noted that experiments with NRCs were performed in the presence of phenylephrine, a stimulator of myocardial contraction and hypertrophy. While it is common practice to add phenylephrine to our NRC maintenance medium as it promotes greater expression of epitope tagged expression constructs, future experiments must also be done in the absence of hypertrophic stimuli as these can potentially affect the localisation of the epitope tagged and endogenous protein in question. A further oversight of the overexpression studies was a lack of presentation of overexpression data in the absence of any other antibody staining. While we strove to avoid bleedthrough in our microscopy method by capturing individual channels with sequential scans, the possibility of bleedthrough can only be ruled out by omitting the inclusion of other fluorophore containing compounds.

One important drawback relating to the analysis of FHOD1 expression concerned the methods used to quantify Western blots. Since protein assays were not performed, we were restricted to measuring levels of FHOD1 relative to the levels of α-actinin. Furthermore, the quantification of Western blots was potentially restricted by the innate drawbacks of this technique, particularly the attainment of the linear range desired for accurate quantification. Upon saturation of protein signals on Western blots, a non-linear relationship between the amount of protein and the observed signal occurs and will skew quantification. However, we strove to quantify blots within the linear range. Overall, chemiluminescence has a fairly narrow range compared to fluorescence detection systems, which have a wider linear range. Future efforts should focus on determining the levels of FHOD1 using protein assays and more-sensitive detection systems, namely fluorescence detection systems or charge-coupled device (CCD) camera-based western blot imaging setups under non saturating conditions.

Chapter 4

Functional Characterisation of FHOD1

4. Functional Characterisation of FHOD1

4.1 Overexpression of FHOD1 Mutant Constructs in Neonatal Rat Cardiomyocytes

In the current study, the localisation and expression of endogenous FHOD1 was explored in striated muscle. Although the discrepancies in the staining pattern for FHOD1 with the 4 commercially available antibodies made it difficult to draw any meaningful conclusions regarding localisation of endogenous FHOD1 in cultured cells, antibody studies in frozen sections of mouse hearts suggested concentration of FHOD1 at the intercalated disks between neighbouring cardiomyocytes, although some myofibrillar and sarcomeric localisation was also apparent. Transient expression studies in neonatal rat cardiomyocytes (NRCs) revealed that GFP-tagged full-length FHOD1 distributed in a diffuse cytoplasmic manner, although it also produced major intensities at the peripheries of cells. However, targeting of full-length FHOD1 was only explored in its supposedly inactive form. Previous work on formins has suggested that full-length formins are maintained in a closed inactive state. In the case of FHOD1, the DID has been shown to directly bind the DAD and this interaction is thought to render FHOD1 inactive (Schonichen et al. 2006). Indeed, FHOD1 constructs in their full-length inactive form have mostly been reported to distribute in a diffuse cytoplasmic manner and generally do not induce significant morphological changes in cells (Takeya and Sumimoto 2003; Gasteier et al. 2005; Menard et al. 2006). Only upon disruption of the DID-DAD interaction, such as in FHOD1 constructs lacking the DAD, is FHOD1 associated with mediating cytoskeletal changes, particularly the appearance of stress fibres (Koka et al. 2003; Takeya and Sumimoto 2003; Gasteier et al. 2005; Schulte et al. 2008; Schonichen et al. 2013). Binding of a Rho family small GTPase to the N-terminus of formins is often required for activation (Rose et al. 2005a). While no small GTPase has been found to definitively bind and activate FHOD1, it has been established that FHOD1 is rendered partially active after it undergoes phosphorylation in its C-

terminus by the Rho family effector ROCK (Takeya et al. 2008). On-going work would indicate that ROCK is a crucial regulator of FHOD1 activity (Thomas et al. 2011; Staus et al. 2011a) as well as FHOD3 activity (Iskratsch et al. 2013a). Since a number of FHOD1 truncation and phosphomimetic mutants have been reported to render FHOD1 active, they were currently implemented to explore the effects of FHOD1 activation in cultured cardiomyocytes. We embarked on our functional characterisation of FHOD1 by overexpression of inactive and constitutively active mutant and truncation constructs of the longer FHOD1 variant, containing the alternatively spliced exons, since FHOD1 mutants lacking the exons where unavailable.

Prior to initiating transfection studies, we sought to confirm that the expression constructs of the individual FHOD1 variants were expressed at the correct molecular weight (Figure 4.1). COS-1 cells were used for the expression tests because of the very low transfection efficiency we were able to achieve in NRCs of approximately less than 5%. The following expression experiments describe qualitative results because of their extrapolation in significance to another cell type and because the exact protein concentration was not determined before loading. Expression tests of the GFP-tagged constructs in transiently transfected COS cells followed by Western blotting revealed that the GFP fusion proteins expressed at the expected molecular weight (approximately 157 kDa for the full-length constructs). All of the following FHOD1 constructs were based on the long variant of FHOD1 containing the alternatively spliced exons 12-13. The FHOD1 ΔDAD represents a truncation mutant of FHOD1, with a difference in molecular weight of roughly 6kDa. A slight shift in molecular weight can be seen, with the FHOD1 ΔDAD migrating slightly faster than the full-length FHOD1 constructs. This size difference is better exemplified in Figure 4.6, A. The FHOD1 mutations for the V288E and the phosphomimetic constructs were confirmed by DNA sequencing.

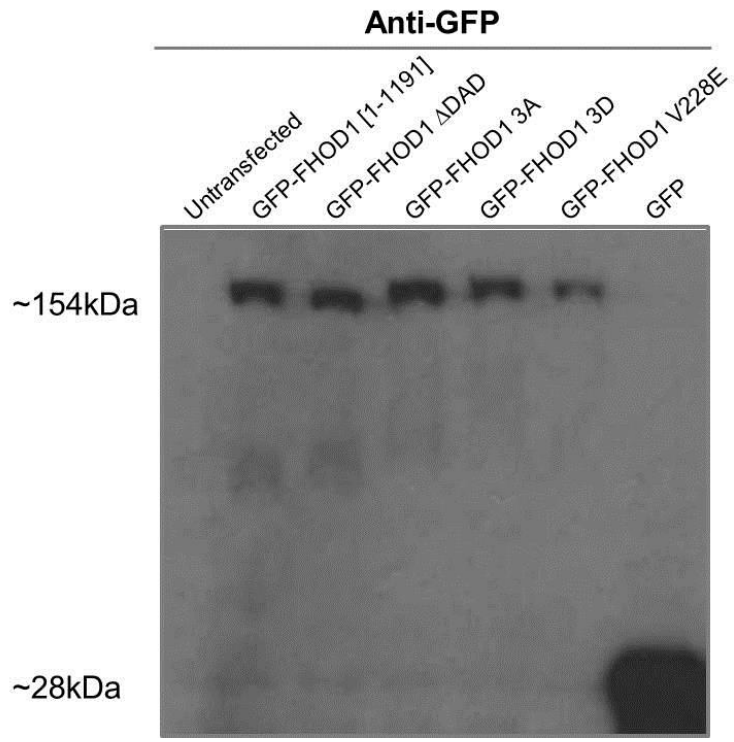

Figure 4.1: Expression Test of Different FHOD1 Constructs in COS-1 cells. A) Western blot with anti-GFP antibody of SDS samples from COS-1 cells that were transiently transfected with the different FHOD1 constructs. 12% SDS-PAGE. Cells were transfected with the following constructs: the FHOD1 ΔDAD truncation mutant lacking the C-terminal DAD [1-1128], the FHOD1 3A mutant with the three ROCK phosphorylation sites mutated to Alanine residues [1-1191], the FHOD1 3D mutant with the three ROCK phosphorylation sites mutated to Aspartic acid residues [1-1191], and the FHOD1 V228E mutant with Valine residue at position 228 mutated to a Glutamic acid residue [1-1191]. Wild-type full-length FHOD1 containing the alternatively spliced exons 12-13 [1-1191] (FL_L) was loaded as a comparator. GFP was loaded as a positive control. Untransfected COS-1 cells were used as a negative control. **N=2**.

4.1.1 Overexpression of FHOD1 3A [1-1191] and FHOD1 3D [1-1191] Phosphomutants

ROCK has been shown to phosphorylate FHOD1 at the C-terminal residues Ser1131, Ser1137, and Thr1141 on the short variant of FHOD1 lacking the alternatively spliced exons (Takeya et al. 2008; Staus et al. 2011a). Phosphorylation of these residues has been associated with activation of FHOD1, which lead to the formation of stress fibres (Takeya et al. 2008) and the promotion of vascular smooth muscle cell differentiation (Staus et al. 2011a). Two GFP-tagged FHOD1 constructs were created in which these three residues were mutated to either Alanine (FHOD1 3A) or Aspartic acid (FHOD1 3D) residues.

The FHOD1 3A construct represents a situation in which the three ROCK phosphorylation sites are unable to be phosphorylated. Thus, the protein is thought to be maintained in its closed inactive state (Figure 4.2 A). The FHOD1 3A construct was overexpressed in NRCs (Figure 4.2 B). Transfected cells were morphologically indistinguishable from their untransfected neighbours. The GFP-tagged FHOD1 3A mutant protein was found to accumulate at the peripheries of cells near the plasma membrane, as was noted previously with the GFP-tagged full-length wild-type FHOD1 constructs. The construct also distributed in a partly diffuse manner in cells. Occasionally some myofibrillar targeting was noted, since a faint cross-striated appearance could sometimes be resolved. No co-localisation was noted between FHOD1 and F-actin. The construct was also well tolerated and had no impact on the levels of organisation of α-actinin. As expected, the FHOD1 3A construct behaved similarly to the full-length wild-type constructs when overexpressed in NRCs.

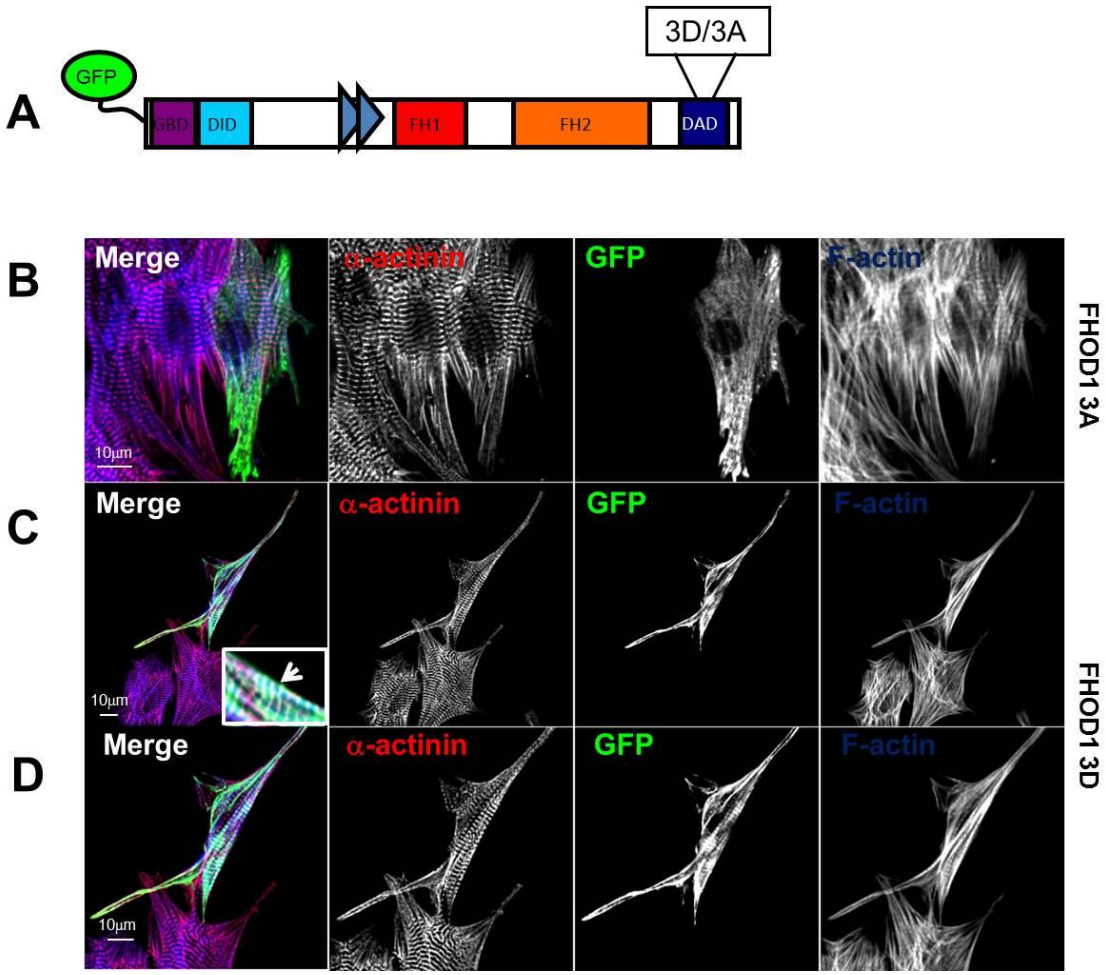

Figure 4.2: Overexpression of FHOD1 Phosphomutant Constructs in Neonatal Rat Cardiomyocytes. NRCs were transfected with different mutant variants of the longer version of GFP-tagged FHOD1 constructs and cultured to day 4. Cells were transfected with the following constructs: **A)** the FHOD1 3A mutant with the three ROCK phosphorylation sites mutated to Alanine residues [1-1191] and the FHOD1 3D mutant with the three ROCK phosphorylation sites mutated to Aspartic acid residues [1-1191]. Cells were stained against sarcomeric α-actinin, F-actin, and visualised by confocal microscopy. **B)** NRC transfected with the FHOD1 3A mutant. **C)** NRC transfected with the FHOD1 3D mutant (see **D** for zoomed image). α-actinin is seen in red, the GFP-FHOD1 mutants in green, and F-actin in blue. GFP, green fluorescent protein. Scale bars represent 10μm. White box shows zoomed selection of merged images. Arrow denotes site of co-localisation between FHOD1 and F-actin. E12-13, denotes the alternatively spliced exons 12-13. **N=2**.

The FHOD1 3D construct is a phosphomimetic variant of full-length FHOD1 designed to resonate the effects of ROCK phosphorylation in the C-terminus (Figure 4.2 A). The 3D mutation in the FHOD1 DAD thus represented a situation where FHOD1 is rendered constitutively active. The FHOD1 3D construct was overexpressed in NRCs (Figure 4.2 C) to assess the effects of constitutive FHOD1 activation in cardiomyocytes. Overexpression of the FHOD 3D construct did not seem to affect the organisation of myofibrils, as indicated by the levels and periodicity of the sarcomeric α-actinin signal.

There was some evidence for increased F-actin at the periphery of the cells and along myofibrils. Overexpression of the FHOD1 3D construct also resulted in a more elongated appearance compared to neighbouring untransfected control NRCs. Furthermore, the construct co-localised with F-actin near the plasma membrane (Figure 4.2 C, Zoom) and in within extended plasma membrane processes, an observation which we did not note with the FHOD1 3A or wild-type constructs. The FHOD1 3D construct also displayed some targeting to myofibrils, where it sometimes exhibited a faint cross-striated appearance, the spacing of which seemed to be irregular with the Z-disk marker α-actinin. The FHOD1 3D ROCK phosphomimetic mutant thus induced morphological changes and displayed some evidence of co-localisation with F-actin when compared to the FHOD1 3A inactive mutant in NRCs.

4.1.2 Overexpression of FHOD1 ΔDAD [1-1128] and FHOD1 V228E [1-1191]

The Diaphanous autoregulatory domain (DAD) is not necessarily a discrete domain but a stretch of 20-30 amino acids found downstream of the FH2 domain. It is involved in maintaining DRFs in their closed inactive state via an interaction with the N-terminal DID. In formins, DAD truncation often results in activation, as has been shown in the case of mDia1 (Maiti et al. 2012) and FHOD1 (Koka et al. 2003; Gasteier et al. 2005; Schulte et al. 2008; Staus et al. 2011a). The effects of FHOD1 activation in cardiomyocytes were further investigated by overexpressing a GFP-tagged FHOD1 mutant lacking the DAD (FHOD1 ΔDAD) (Figure 4.3 A). Overexpression of the FHOD1 ΔDAD construct resulted in a slightly elongated appearance in NRCs (Figure 4.3 B). Furthermore, FHOD1 ΔDAD also led to the formation of F-actin bundles, where FHOD1 ΔDAD was found to co-localise with F-actin (Figure 4.3 B, Zoom). Some myofibrillar targeting was also apparent, with occasional striations also resolved. However, the spacing of these striations were not always consistent. Overall, truncation of the DAD of FHOD1 induced the formation of actin bundles, where FHOD1 co-localised with F-actin, and displayed some targeting to myofibrils.

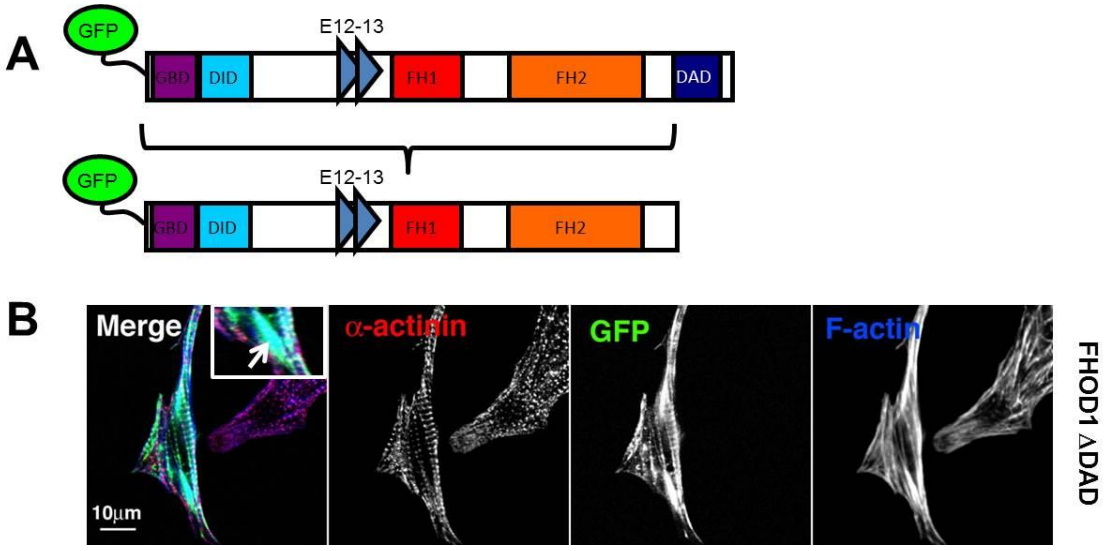

Figure 4.3: Overexpression of the FHOD1 ΔDAD Construct in Neonatal Rat Cardiomyocytes. NRCs were transfected with different mutant variants of the longer version of GFP-tagged FHOD1 constructs and cultured to day 4. Cells were transfected with the **A)** FHOD1 ΔDAD truncation mutant lacking the C-terminal DAD [1-1128]. Cells were stained against sarcomeric α-actinin, F-actin, and visualised by confocal microscopy. **B)** NRC transfected with the FHOD1 ΔDAD truncation mutant. α-actinin is seen in red, the GFP-FHOD1 mutants in green, and F-actin in blue. GFP, green fluorescent protein; DAD, diaphanous autoregulatory domain. Scale bars represent 10μm. White box shows zoomed selection of merged images. Arrow denotes site of co-localisation between FHOD1 and F-actin. E12-13, denotes the alternatively spliced exons 12-13. **N=3**.

Upon characterisation of the FHOD1 autoinhibitory mechanism it was found that the interaction between the N-terminal DID and the C-terminal DAD was dependent on the presence of a Valine residue at position 228 (Schulte et al. 2008) (Figure 4.4 A). When this residue was mutated to a Glutamic acid it led to activation of FHOD1 in NIH3T3 cells, as evidenced by formation of thick stress fibres and abrogated binding between the FHOD1 N-terminus and the DAD in GST pull-down experiments (Schulte et al. 2008). We overexpressed this constitutively active FHOD1 variant in NRCs to further investigate the effects of FHOD1 activation in cardiomyocytes (Figure 4.4 B). Overexpression of GFP-tagged FHOD1 V228E seemingly had a more-profound effect on NRC morphology than the other FHOD1 constitutively active mutant constructs. Cells displayed an elongated morphology and a number of thick stress fibres, which were arranged along the long axis of the cells. The FHOD1 V228E mutant was targeted to stress fibres where it co-localised with F-actin. Some myofibrillar targeting of the FHOD1 V228E construct was also apparent. The construct partly distributed in a faint cross-striated manner, but similarly to the other constitutively active constructs, the

spacing of these striations were irregular with respect to α-actinin. The FHOD1 V228E constitutively active mutant thus induced rearrangement of the F-actin network into thick stress fibres.

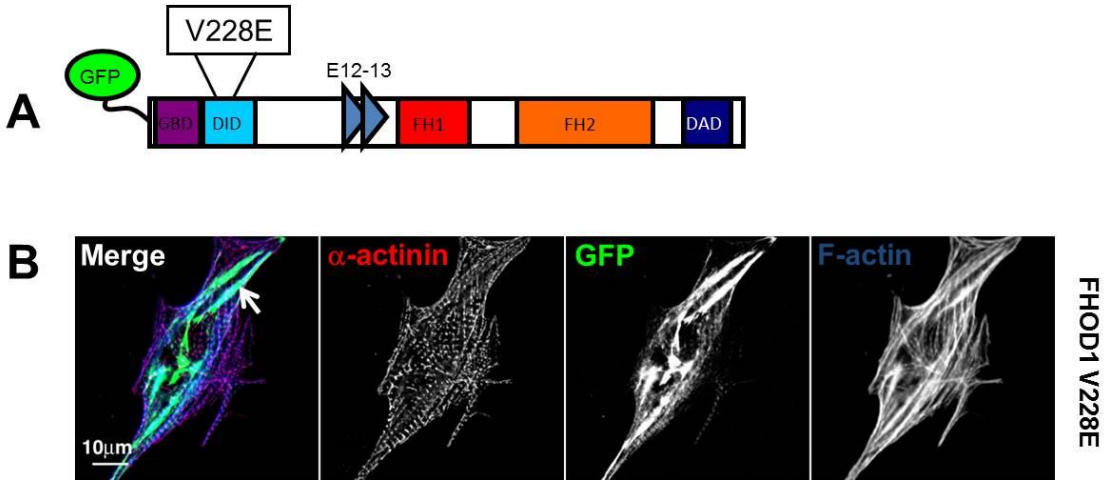

Figure 4.4: Overexpression of the FHOD1 V228E Construct in Neonatal Rat Cardiomyocytes. NRCs were transfected with different mutant variants of the longer version of GFP-tagged FHOD1 constructs and cultured to day 4. Cells were transfected with the **A)** FHOD1 V228E mutant with Valine residue at position 228 mutated to a Glutamic acid residue [1-1191].Cells were stained against sarcomeric α-actinin, F-actin, and visualised by confocal microscopy. **B)** NRC transfected with the FHOD1 V228E mutant. α-actinin is seen in red, the GFP-FHOD1 mutants in green, and F-actin in blue. GFP, green fluorescent protein. Scale bars represent 10μm. Arrow denotes site of co-localisation between FHOD1 and F-actin. E12-13, denotes the alternatively spliced exons 12-13. **N=2**.

Overall, overexpression of the constitutively active FHOD1 variants seemingly had an impact on the F-actin network of NRCs, as evidenced by increased staining for F-actin in the peripheries of cells or the appearance of F-actin bundles and stress fibres. However, constitutive FHOD1 activation had little effect on myofibrillar organisation, since the characteristic Z-disk localisation of α-actinin was mostly retained in transfected cells. Furthermore, we noted co-localisation between the constitutively active FHOD1variants and F-actin, an observation that was not seen with the full-length wild-type or the FHOD1 3A mutant. While the possible increase in F-actin staining in NRCs transfected with constitutively active FHOD1 variants may have implied greater levels of actin filament assembly, this remains to be seen, especially in light of recent reports that constitutively active FHOD1 caps actin and can only mildly elongate filaments in the presence of profilin (Schonichen et al. 2013). The present results would

also suggest that the constitutively active FHOD1 variants may have exhibited some construct specific effects, suggesting that they not might have all represented reliable reporters of FHOD1 activation. Comparable effects were noted upon expression of the FHOD1 ΔDAD and FHOD1 V228E variants, whereas we did not note substantial formation of bundled F-actin structures with the FHOD1 3D construct. Such an observation could indicate that phosphorylation in the DAD does not necessarily equate to full activation of FHOD1 when overexpressed in NRCs.

4.2 Localisation of Phosphorylated FHOD1 in Heart Sections

After addressing the function of FHOD1 in NRCs through overexpression of the different constitutively active constructs, we set out to investigate the localisation of phosphorylated endogenous FHOD1 *in situ*. For this purpose we stained frozen heart sections of adult mice with the anti-FHOD1 phospho-Threonine1141 antibody (ECM Biosciences). The anti-FHOD1 phospho-Threonine1141 antibody was raised against a synthetic peptide, which included the phosphorylated Threonine residue and corresponding amino acid residues that surround it in human FHOD1. The Threonine residue corresponds to one of the three that is phosphorylated by ROCK and therefore may represent FHOD1 in its active state (Takeya et al. 2008). The ROCK-I phosphorylation consensus motif, comprised of the two Serines and the Threonine residues, is conserved among rodent species (Figure 4.5), meaning that detection in mouse sections would be expected.

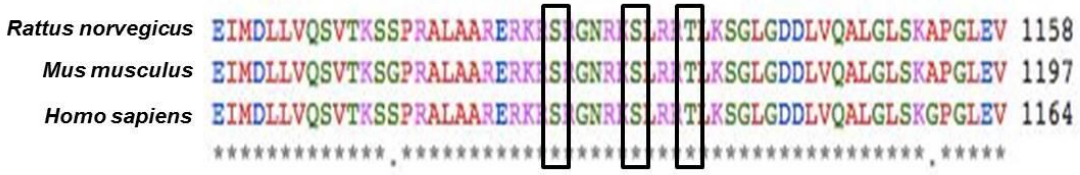

Figure 4.5: C-terminal Sequence Comparison between Human and Rodent FHOD1. Alignment of the human FHOD1 C-terminal sequence amino acid sequence with the corresponding portions of mouse and rat FHOD1. The top reference sequence represents the *Rattus norvegicus* sequence (NCBI Reference Sequence: NP_001178529.1) [1-1138]. The middle reference sequence represents the *Mus musculus sequence* (NCBI Reference Sequence: NP_808367.2) [1-1197]. The bottom reference sequence represents the *Homo sapiens* sequence (NCBI Reference Sequence: NP_037373.2) [1-1164]. Sequence alignment was performed with clustalw2 (http://www.ebi.ac.uk/Tools/msa/clustalw2/). Black boxes denote conserved serine and threonine residues.

Characterisation of the phospho-Threonine1141 antibody's specificity took place via Western blot and immunofluorescence studies. The following expression experiments describe qualitative results since the exact protein concentration was not determined before loading. Initial characterisation revealed that the phospho-Threonine1141 antibody was able to detect GFP-tagged full-length FHOD1 when overexpressed in COS-1 cells (Figure 4.6 A, GFP-FHOD1 lane), which may have indicated that some basal phosphorylation of the construct was present in COS-1 cells. However, the phospho-Threonine1141 antibody was unable to detect the GFP-tagged FHOD1 3A and FHOD1 ΔDAD constructs when overexpressed in COS-1 cells (Figure 4.6 A), despite the expression of these FHOD1 variants at comparable levels, as evidenced by detection with the anti-GFP antibody (Figure 4.6 B). These two constructs lacked the Serine and Threonine residues that are phosphorylated by ROCK-I in the DAD, therefore supporting the notion that the phospho-Threonine1141 antibody specifically recognised phosphorylation of FHOD1 within the ROCK-I consensus motif. The basal phosphorylation of the full-length FHOD1 construct may be due to serum in the culture medium.

Immunofluorescence experiments in cultured NRCs, overexpressing full-length FHOD1 and FHOD1 ΔDAD, were also in agreement with the notion of the antibody's specificity. While the phospho-Threonine1141 antibody recognised full-length FHOD1 (Figure 4.7 A), as evidenced by partial co-localisation, it did not recognise the FHOD1

ΔDAD construct. Neighbouring untransfected NRCs showed no staining with the phospho-Threonine1141 antibody above background. Lack of recognition of the FHOD1 ΔDAD construct was also evidence that recognition of the full-length construct was not due to the presence of the GFP tag since both constructs were tagged by GFP.

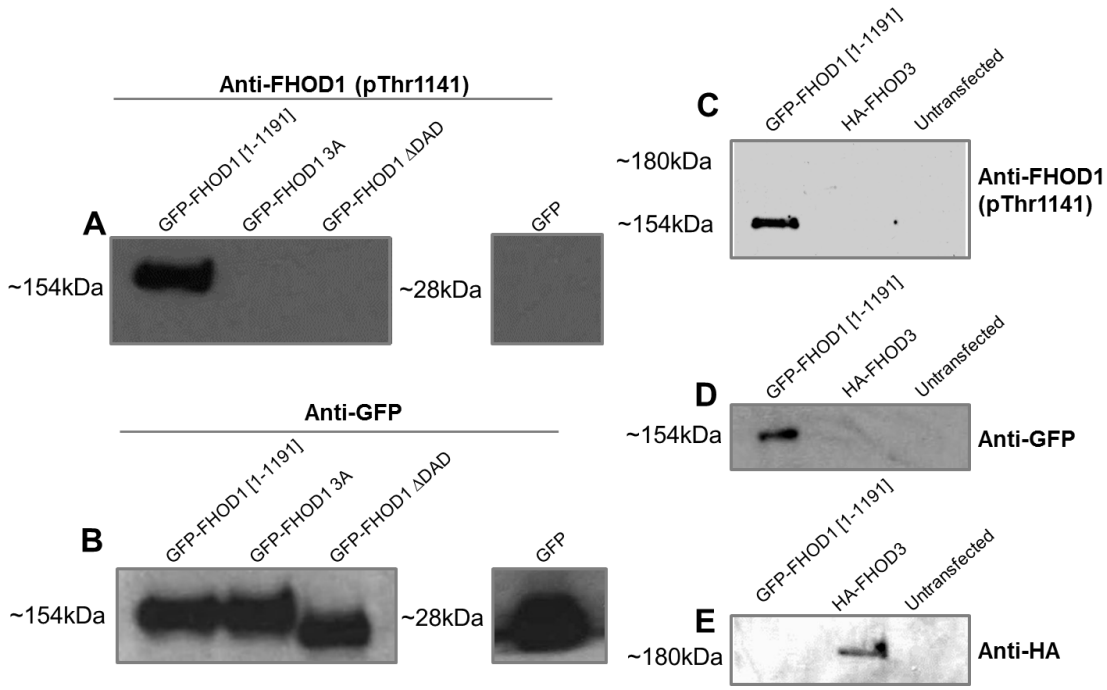

Figure 4.6: Validation of anti-FHOD1 Phospho-Threonine1141 Antibody via Western Blot Studies. A) and B) Western blot of SDS lysates of COS-1 cells transfected with one of the following GFP-tagged FHOD1 constructs: wild-type full-length FHOD1 containing the alternatively spliced exons 12-13 [1-1191], the FHOD1 3A mutant with the three ROCK phosphorylation sites mutated to Alanine residues [1-1191], and the FHOD1 ΔDAD truncation mutant lacking the C-terminal DAD [1-1128]. **A)** Western blots probed with the FHOD1 phospho-Threonine1141 antibody. **B)** Western blots probed with the anti-GFP antibody. **C), D), and E)** Western blot of SDS lysates of COS-1 cells transfected with either GFP-tagged wild-type full-length FHOD1 containing the alternatively spliced exons 12-13 [1-1191] or the HA-tagged full-length long variant of FHOD3. **C)** Western blot probed with FHOD1 phospho-Threonine1141 antibody. **D)** Western blots probed with the anti-GFP antibody. **E)** Western blot probed with the anti-HA antibody. GFP, green fluorescent protein; HA, haemagglutinin. **N=2.**

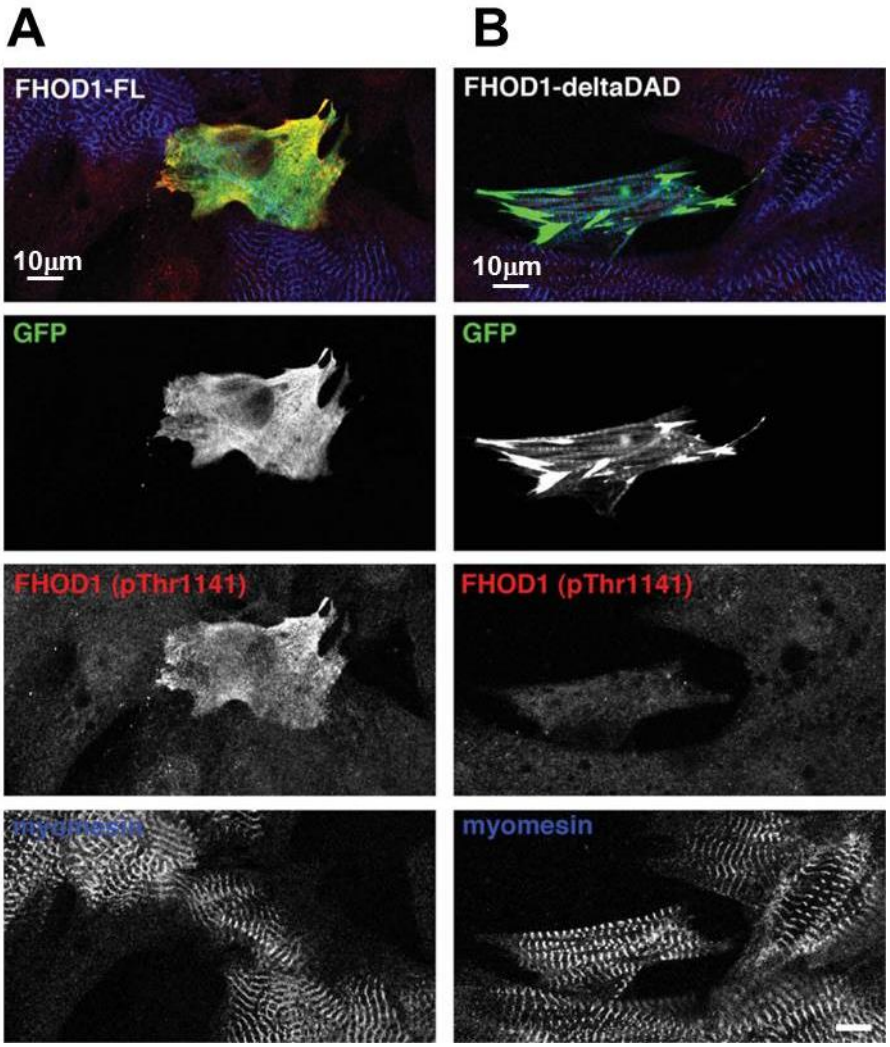

Figure 4.7: Validation of the Anti-FHOD1 PhosphoThr1141 Antibody in Neonatal Rat Cardiomyocytes by Fluorescence Microscopy. NRCs were transfected with versions of the longer GFP-tagged FHOD1 variant and cultured to day 4. Cells were stained with the anti-FHOD1 phosphoThr1141 antibody and for myomesin. Confocal micrographs of NRC transfected either with **A)** GFP-tagged full-length FHOD1 (left column) or **B)** ΔDAD FHOD1 (right column). The GFP-tagged FHOD1 constructs are seen in green, phosphoThr1141 FHOD1 is seen in red, and myomesin in blue. Scale bar is equivalent to 10 μm. GFP, green fluorescent protein. **N=3.**

Since the ROCK-I phosphorylation consensus motif is also conserved for FHOD3 (Iskratsch et al. 2013a), we looked for evidence of cross-reactivity with FHOD1's sister homolog. Western blots comparing GFP-tagged full-length FHOD1 and HA-tagged full-length FHOD3 overexpressed in COS-1 cells showed no signal with the phospho-Threonine1141 antibody at the molecular weight expected for HA-tagged FHOD3 (180 kDa; Figure 4.6 C). This observation was supported by immunofluorescence experiments in COS-1 cells expressing either full-length FHOD1 or FHOD3 which also

revealed no cross-reactivity (Figure 4.8). The phospho-Threonine1141 antibody partially recognised GFP-tagged FHOD1, as evidenced by co-localisation between the signal for the phospho-Threonine1141 antibody and the GFP-tagged FHOD1 signals within aggregates visualised throughout cells (Figure 4.8 A, Zoom), whereas there was no visual evidence of co-localisation between the phospho-Threonine1141 antibody signal and FHOD3 (Figure 4.8 C). Cells were also transfected with the empty GFP vector to rule out the possibility of the phospho-Threonine1141 antibody recognising the GFP tag on FHOD1 (Figure 4.8 B). Apart from background fluorescence in the nuclei of COS-1 cells, where the GFP tag on its own readily accumulates, we did not note co-localisation to the extent seen with FHOD1. Although the phospho-Threonine1141 antibody might detect phosphorylated FHOD3 based on sequence homology, the present validation efforts suggest that this might be minimal. However, since the extent of FHOD3 phosphorylation was not determined in these assays, we cannot totally exclude cross-reactivity. Furthermore, the present characterisation efforts were performed with human FHOD1 and FHOD3 constructs; therefore it cannot be concluded with certainty whether they can be translated fully into the context of the rodent variants thereof.

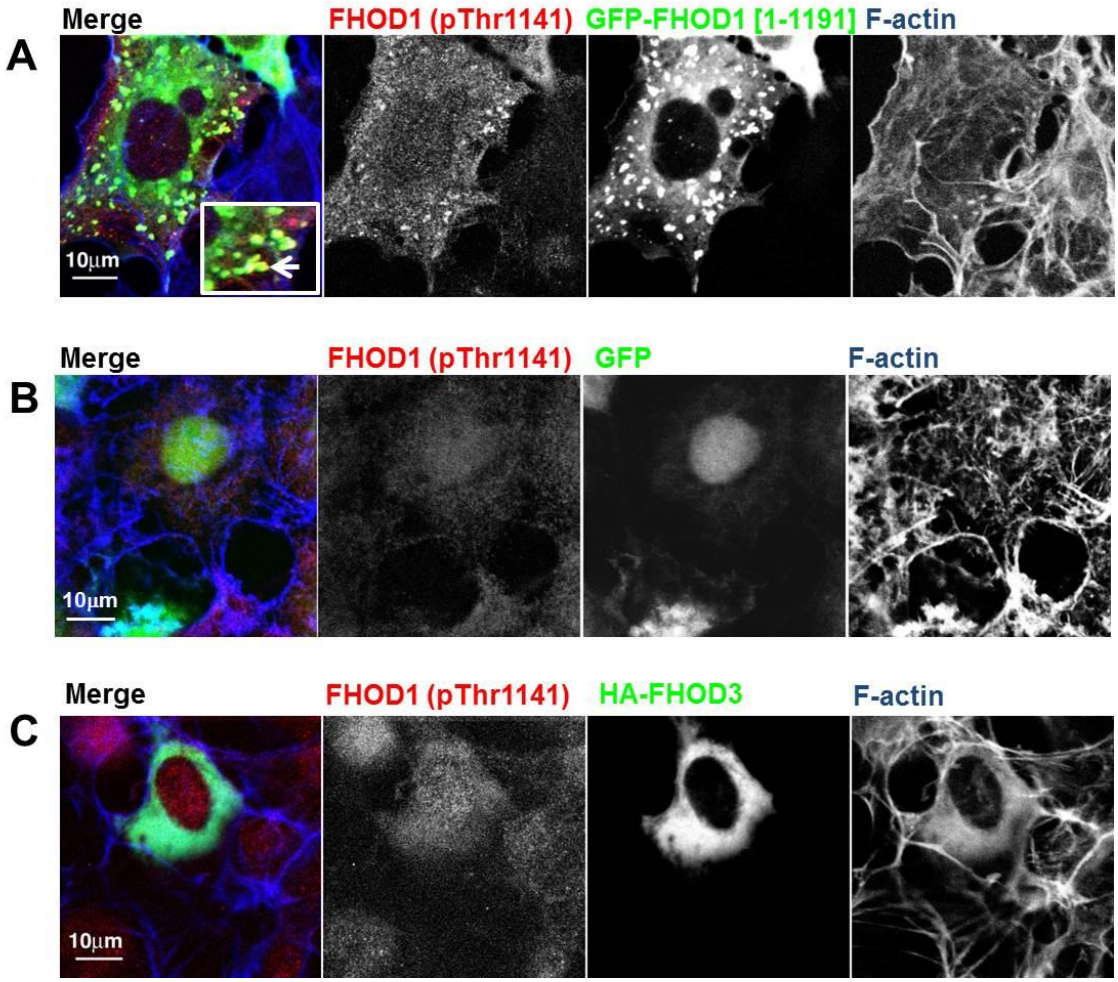

Figure 4.8: Validation of the Phospho-Thr1141 FHOD1 Antibody in COS-1 Cells by Fluorescence Microscopy. COS-1 cells were transfected with **A)** GFP-tagged full-length long variant of FHOD1 containing the alternatively spliced exons (E12-13), **B)** the empty GFP vector, **C)** and HA-tagged full-length long variant of FHOD3. Cells were cultured to day two, fixed, and stained with the phosphoThr1141 FHOD1 antibody. Cells were also counterstained with Phalloidin to visualise F-actin. This was performed in order to gauge the specificity of each antibody in immunofluorescence specimens and assess any possible cross-reactivity against FHOD3. GFP-tagged FHOD1 and HA-tagged FHOD3 are seen in green, phospho-Thr1141 FHOD1 is seen in red, and F-actin in blue. Scale bar is equivalent to 10 μm. GFP, green fluorescent protein; HA, haemagglutinin. Arrow denotes site of co-localisation. White box shows zoomed selection of merged images. **N=2.**

Nevertheless, with the caveat in mind that recognition of phosphorylated FHOD3 may have been a possibility, we stained mouse heart sections with the phospho-Threonine1141 antibody (Figure 4.9). Staining with the antibody gave a very similar staining pattern to that noted previously with the polyclonal goat C14 and C20 anti-FHOD1 antibodies, designed to recognise total levels of the protein. A strong signal was visualised at the intercalated disks. While there was a lot of diffuse staining in cells, occasional localisation along myofibrils was also noted. There was also some evidence

of the phosphorylated protein distributing in a striated manner. An alternating pattern with the M-band marker myomesin indicated that the phosphorylated FHOD1 signal was partially found at the lateral portions of the sarcomere, near the Z-disks. Although the localisation of phosphorylated endogenous FHOD1 with the phospho-Threonine1141 antibody was consistent with that seen with polyclonal goat anti-FHOD1 antibodies, in the absence of an antigen competition assay, we cannot conclude with certainty that the signal for phosphorylated FHOD1 was genuine. This is especially the case because of the potential for cross-reactivity with FHOD3, which also contains the conserved ROCK-I phosphorylation consensus motif in the DAD.

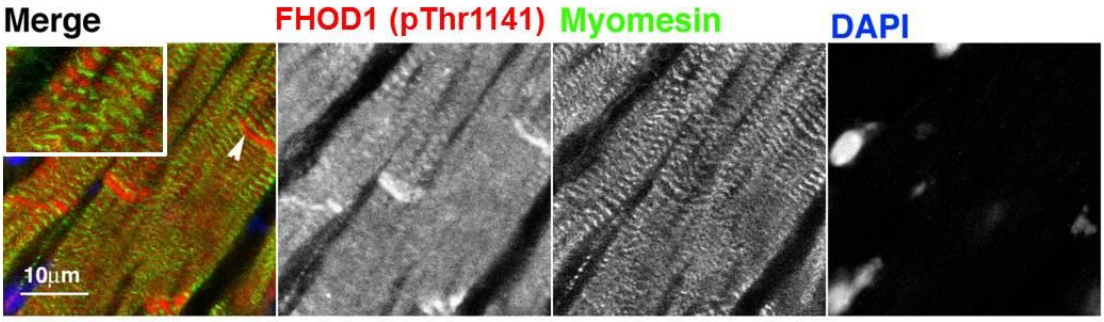

Figure 4.9: Localisation of Phosphorylated FHOD1 in Murine Hearts. Frozen heart sections of 1 year old male adult C57/BL6 mice were stained with the anti-FHOD1 Phospho-Thr1141 antibody (ECM Biosciences), myomesin, and visualised by confocal microscopy. Images represent portions of high magnification longitudinal sections. FHOD1 is seen in red, myomesin is seen in green, and DAPI/nuclei seen in blue. Arrowhead indicates an intercalated disk. Scale bar represents 10µm. White boxes show zoomed selections of merged images. **N=2.**

4.3 F-actin Regulating Activity of FHOD1

Overexpression of the constitutively active FHOD1 mutants in NRCs indicated the capacity of FHOD1 to rearrange the F-actin cytoskeleton and induce the appearance of F-actin based structures such as stress fibres and bundles. We attempted to quantify the extent of formation of F-actin based structures with some of our available FHOD1 constructs by performing *in cyto* F-actin formation assays. Due to the poor transfection efficiency we consistently achieved in NRCs, we opted to use HeLa cells as was done previously in the characterisation of the F-actin regulatory activity of FHOD3 in our laboratory (Iskratsch et al. 2010). We selected HeLa over COS-1 cells since HeLa cells

have an F-actin cytoskeleton that is better organised and hence more-amenable to imaging/quantification. HeLa cells were transfected with the wild-type, constitutively inactive, and constitutively active mutant FHOD1 constructs. Transiently transfected HeLa cells were subsequently stained with Phalloidin to measure the intensity of F-actin staining. The Phalloidin pixel intensity was measured in both transfected and neighbouring untransfected cells and the ratio taken between them was used to measure differences in F-actin staining associated with the FHOD1 expression constructs (Figure 4.10). The activities of the empty GFP and TOMATO vectors were also quantified and provided baseline measurements, as they functioned as controls. Both vectors did not have substantial actin polymerising activity since overexpression of the empty GFP vector resulted in an average Phalloidin pixel intensity ratio of 0.930 and the empty TOMATO vector produced a slightly elevated average ratio of 1.16. A Phalloidin pixel intensity ratio of 1 would indicate equal amounts of F-actin in transfected and untransfected cells. Cells expressing the GFP tag alone (Figure 4.11 A) and the TOMATO tag alone (Figure 4.11 I) were also morphologically indistinguishable from their untransfected neighbours. The tags also distributed within the cytoplasm and nuclei of HeLa cells. The negligible increases in Phalloidin pixel intensities suggested that the tags used for the assay were not responsible for any changes in F-actin staining.

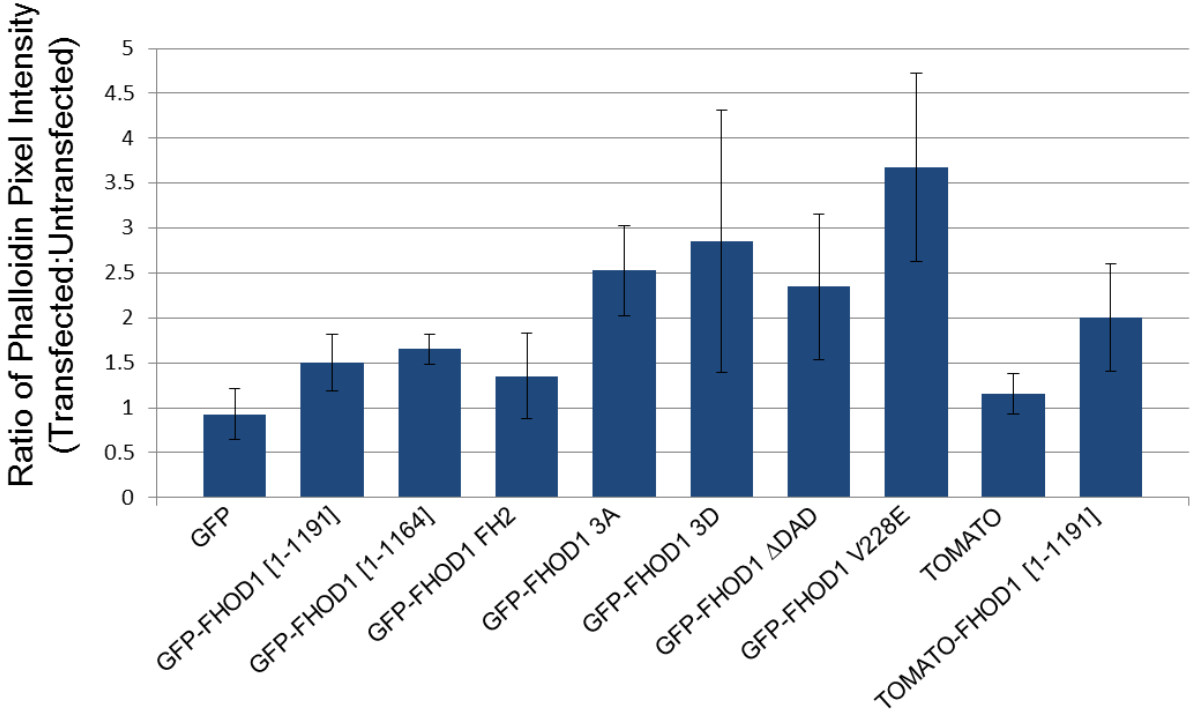

Expression Construct	F-actin ratio	STDEV
GFP	0.9297	0.2844
GFP-FHOD1 [1-1191]	1.4994	0.3177
GFP-FHOD1 [1-1164]	1.6510	0.1728
GFP-FHOD1 FH2	1.3532	0.4751
GFP-FHOD1 3A	2.5269	0.4986
GFP-FHOD1 3D	2.8509	1.4606
GFP-FHOD1 ΔDAD	2.3456	0.8050
GFP-FHOD1 V228E	3.6773	1.0477
TOMATO	1.1556	0.2299
TOMATO-FHOD1 [1-1191]	2.0102	0.5982

Figure 4.10: Quantification of the Actin Regulating Activity of FHOD1 in HeLa Cells. Bar chart depicting F-actin content in the presence of the FHOD1 constructs. HeLa cells were transfected with different FHOD1 constructs and were subsequently fixed and stained for F-actin with Phalloidin. The Phalloidin pixel intensity was measured in all cells and the ratio taken between transfected and untransfected cells. The ratios of Phalloidin pixel intensities are expressed as arbitrary units. GFP, green fluorescent protein empty vector; GFP-tagged long variant of full-length FHOD1[1-1191]; GFP-tagged short variant of full-length FHOD1 [1-1164]; FH2, GFP-tagged formin homology 2 domain [642-1031]; 3A, GFP-tagged FHOD1 ROCK consensus site triple Alanine mutant [1-1191]; 3D, GFP-tagged FHOD1 ROCK consensus site triple Aspartic acid mutant [1-1191]; DAD, GFP-tagged FHOD1 truncation mutant lacking the diaphanous autoinhibitory domain [1-1128]; VE, GFP-tagged FHOD1 Valine 228 to Glutamic acid mutant [1-1191]; TOMATO empty vector; TOMATO-tagged long variant of full-length FHOD1[1-1191]. Values represent cells seen in 10 views per dish: 1-5 transfected cells per view and 3-6 untransfected cells per view. Error bars represent standard deviation (STDEV). Values are provided in the accompanying table. **N=1.**

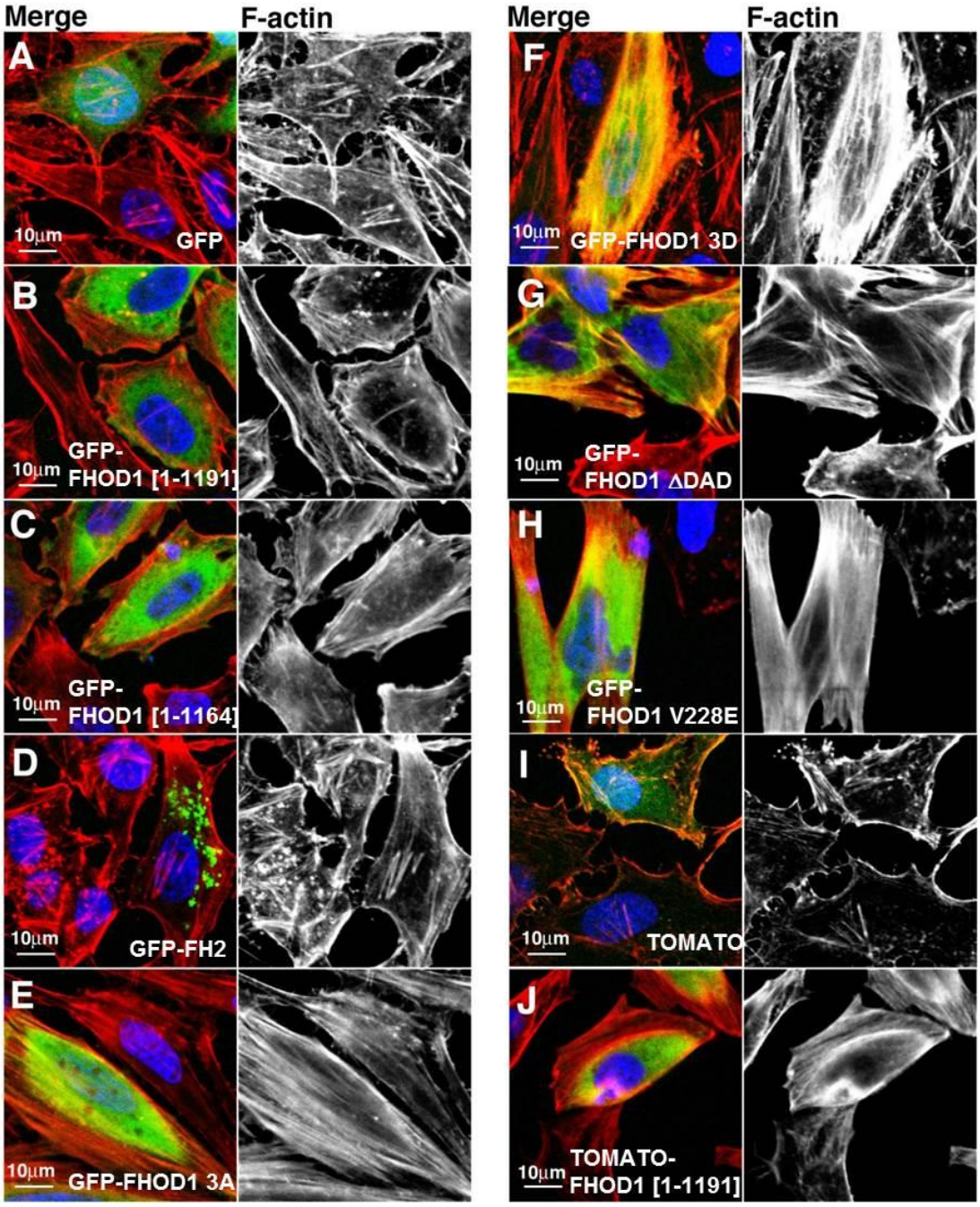

Figure 4.11: Actin Regulating Activity of FHOD1 in HeLa Cells. Representative images of HeLa cells transfected with the FHOD1 constructs. HeLa cells were transfected with the FHOD1 constructs, fixed, and stained for F-actin, using Phalloidin. Cells were transfected with the following constructs: **A)** The empty GFP tag vector, **B)** GFP-tagged long variant of full-length FHOD1 [1-1191], **C)** GFP-tagged short variant of full-length FHOD [1-1164], **D)** GFP-tagged FH2 domain [642-1031] **E)** GFP-tagged FHOD1 ROCK consensus site triple Alanine mutant (3A) [1-1191], **F)** GFP-tagged FHOD1 ROCK consensus site triple Aspartic acid mutant (3D) [1-1191], **G)** GFP-tagged FHOD1 truncation mutant lacking the diaphanous autoinhibitory domain (ΔDAD) [1-1128], **H)** GFP-tagged FHOD1 Valine 228 to Glutamic acid mutant (V228E) [1-1191], **I)** TOMATO tag empty vector, **J)** TOMATO-tagged long variant of full-length FHOD1 [1-1191]. GFP, green fluorescent protein; FH, formin homology. The FHOD1 constructs and their associated epitope tags are seen in green and F-actin in red. DAPI/nuclei are seen in blue. Scale bars represent 10μm. **N=1.**

significant co-localisation with the F-actin network in HeLa cells and distributed in a diffuse cytoplasmic manner (Figure 4.11 B-C). The full-length TOMATO-tagged FHOD1 construct (Figure 4.11 J) was associated with more F-actin staining in transfected cells than the empty TOMATO vector, although the full-length TOMATO-tagged FHOD1 construct exhibited a notable degree of variability in its capacity to alter F-actin staining (Figure 4.10). TOMATO-tagged FHOD1 was also associated with the appearance of stress fibres in some cells, indicating that it might have been partially rendered active.

The F-actin regulating activity of the FHOD1 FH2 domain was also explored since the FH2 domains of formins have been shown to be sufficient to create actin filaments, as was exemplified with Bni1p (Pruyne et al. 2002). Overexpression of the GFP-tagged FHOD1 FH2 domain on its own displayed a variable response in its capacity to alter staining for F-actin; therefore it was not possible to conclude whether the FH2 domain had an effect on the F-actin content of cells (Figure 4.10). The formation of stress fibres was not noted and transfected cells were indistinguishable from untransfected neighbours. Furthermore, the FH2 domain did not exhibit substantial co-localisation with the F-actin network and was targeted to cytoplasmic blebs (Figure 4 11.D).

When the FHOD1 mutants were overexpressed in HeLa cells they were associated with greater staining for F-actin than the wild-type FHOD1 constructs (Figure 4.10). This was strangely the case also with the supposedly inactive GFP-tagged FHOD1 3A construct, which exhibited a strong response: the average level of F-actin staining in transfected versus untransfected cells was greater than the GFP-tagged wild-type FHOD1 constructs. While the FHOD1 3D construct was associated with increases in F-actin staining above the wild-type constructs, it did so to extremely varying degrees. The GFP-tagged FHOD1 ΔDAD construct also increased F-actin staining in transfected cells, although it too exhibited a considerably variable response. The GFP-tagged FHOD1 V228E construct seemingly increased F-actin staining in transfected cells to the greatest extent among the constitutively active constructs, but similarly to the other constitutively active construct, it also exhibited a variable response. Cells transfected with the FHOD1 mutant constructs often displayed numerous stress fibres, to which they were partially targeted to (Figure 4.11 E-H).

The present experiment suggested that FHOD1 possessed the ability to induce the reorganisation and/or the accumulation of F-actin in HeLa cells. This may have occurred to a greater extent under instances of constitutive activation of FHOD1. However, it is difficult to speculate as to why the FHOD1 3A construct resulted in greater F-actin staining in transfected cells versus their untransfected neighbours, but it could indicate that phosphorylation in the DAD may not be a reliable reporter for activation. Furthermore, we noted a high degree of variability in the responses of the constitutively active FHOD1 constructs. While this is a reflection that further experiments will be required to validate these findings, it could also be indicative of other factors. We did not check levels of expression of the FHOD1 constructs in HeLa cells by Western blotting; therefore we could not rule out the possibility that certain constructs exhibited differential degrees of stability within HeLa cells. Furthermore, measurements may have been skewed in the presence of saturated F-actin signals found at stress fibres. While fluorescence has a wider linear range than chemiluminescence, very bright staining for F-actin could have resulted in measurements that were not performed in the linear range and may partly account for the variability in the responses we observed for many of the constructs. While the present experiment did not distinguish between the ability of FHOD1 to polymerise or reorganise actin, recent studies have indicated the latter. Even in its constitutively active confirmation, FHOD1 was shown to cap actin filaments rather than elongate them and was also shown to possess a potent actin bundling activity (Schonichen et al. 2013). In addition, a region N-terminal to the FH1 domain of FHOD1 was characterised, which binds F-actin and mediates bundling (Schonichen et al. 2013). It is therefore possible, that the results that were seen for the FHOD1 3A construct reflect not so much an activation of polymerisation activity but more a bundling activity of FHOD1.

4.4 Myofibril/F-actin Depolymerisation Assay

Upon overexpression, activation of FHOD1 was partly associated with reorganisation of the F-actin network in cardiomyocytes and potential increases in F-actin staining in HeLa cells. Transient expression studies were then performed to see if FHOD1 was involved in the regulation of thin filaments in cardiomyocytes. FHOD1 constructs were overexpressed in NRCs, which were subjected to depolymerisation of their myofibrils and all cellular F-actin through overnight Latrunculin B treatment. FHOD1 transfected

NRCs were subsequently allowed to recover in wash-out experiments. Transiently transfected cells were then scored on the integrity of their myofibrils and compared to cells transfected with the empty GFP and TOMATO vectors (Table 4.1). The integrity of myofibrils was judged by looking at the distribution of α-actinin and F-actin, namely if they were incorporated into myofibrils and regained their striated appearance. Staining for F-actin was used to visualise myofibrils. Organisation at the level of the sarcomere was assessed by staining of the Z-disk marker, α-actinin. Transfected cells were counted and grouped according to whether they had poor, intermediate, or excellent myofibrillar integrity. Cells deemed to exhibit poor myofibrillar integrity were devoid of myofibrils and displayed patchy and irregular α-actinin staining. Cells deemed to exhibit intermediate myofibrillar integrity displayed evidence of filamentous F-actin-based structures, although the spacing of the α-actinin signal was irregular and hence indicated improper formation of the Z-disks. Cells deemed to have excellent myofibrillar integrity displayed well-formed myofibrils with regularly spaced Z-disks. Due to the fairly heterogeneous response seen with Latrunculin B treatment, baseline measurements were taken in untransfected cells. At baseline, the majority of untransfected cells (64%) displayed poor myofibrillar integrity. However, approximately a third of untransfected cells still displayed a moderate or excellent degree of myofibrillar integrity, indicating that the conditions may have required further optimisation.

	Myofibrillar Integrity		
Construct	+	++	+++
GFP	48%	32%	20%
GFP-FHOD1 [1-1191]	13%	25%	62%
GFP-FHOD1 [1-1164]	14%	39%	47%
GFP-FH2	82%	12%	6%
GFP-FHOD1 3A	28%	36%	36%
GFP-FHOD1 3D	17%	37%	46%
GFP FHOD1 ΔDAD	25%	54%	21%
GFP FHOD1 V228E	19%	35%	46%
TOMATO	33%	49%	18%
TOMATO-FHOD1 [1-1191]	19%	47%	34%
Baseline Untransfected	64%	26%	10%

Table 4.1: Quantification of Myofibril Integrity in FHOD1 Transfected Neonatal Rat Cardiomyocytes. NRCs were transfected with the different FHOD1 constructs prior to overnight treatment with Latrunculin B. Promotion of myofibril recovery was promoted by washing out the Latrunculin B and replacing it with maintenance medium. Cells were stained for α-actinin, F-actin, visualised by confocal microscopy, and scored on their ability to recover their myofibrils. Cells were grouped as having poor (+), intermediate (++), or excellent (+++) myofibrillar integrity. The following constructs were tested: GFP, green fluorescent protein empty vector; GFP-tagged long variant of full-length FHOD1 [1-1191]; GFP-tagged short variant of full-length FHOD1 [1-1164]; GFP-tagged formin homology 2 (FH2) domain [642-1031]; GFP-tagged FHOD1 ROCK consensus site triple Alanine (3A) mutant [1-1191]; GFP-tagged FHOD1 ROCK consensus site triple Aspartic acid (3D) mutant [1-1191]; GFP-tagged FHOD1 truncation mutant lacking the diaphanous autoinhibitory domain (ΔDAD) [1-1128]; GFP-tagged FHOD1 Valine 228 to Glutamic acid (V228E) mutant [1-1191]; TOMATO empty vector; TOMATO-tagged long variant of full-length FHOD1 [1-1191]; NRC, neonatal rat cardiomyocytes. **N=1.**

Both the GFP and TOMATO empty vectors were transfected into NRCs as negative controls and to test if they had any ability to influence the integrity of myofibrils after latrunculin B treatment with subsequent wash-out. The GFP tag on its own was enough to promote myofibrillar integrity above baseline measurements, but the majority of cells (48%) still displayed poor myofibrillar integrity (Table 4.1). Most cells displayed with a lacerated appearance and lacked organised myofibrils with sarcomeres (Figure 4.12 A). On the other hand, the TOMATO tag was enough to confer a notable degree of myofibrillar integrity in most cells, since 49% of transfected cells displayed intermediate myofibrillar integrity (Table 4.1). The majority of TOMATO transfected cells had well-defined myofibrils, although they were not fully mature since the striated appearance of α-actinin was not regular (Figure 4.12 E). Both the GFP and TOMATO

tags displayed diffuse cytoplasmic signals and nuclear targeting. Although the GFP and TOMATO tags displayed the capacity to increase myofibrillar integrity with respect to untransfected cells after latrunculin B treatment, they did so to a lesser extent than most of the FHOD1 constructs.

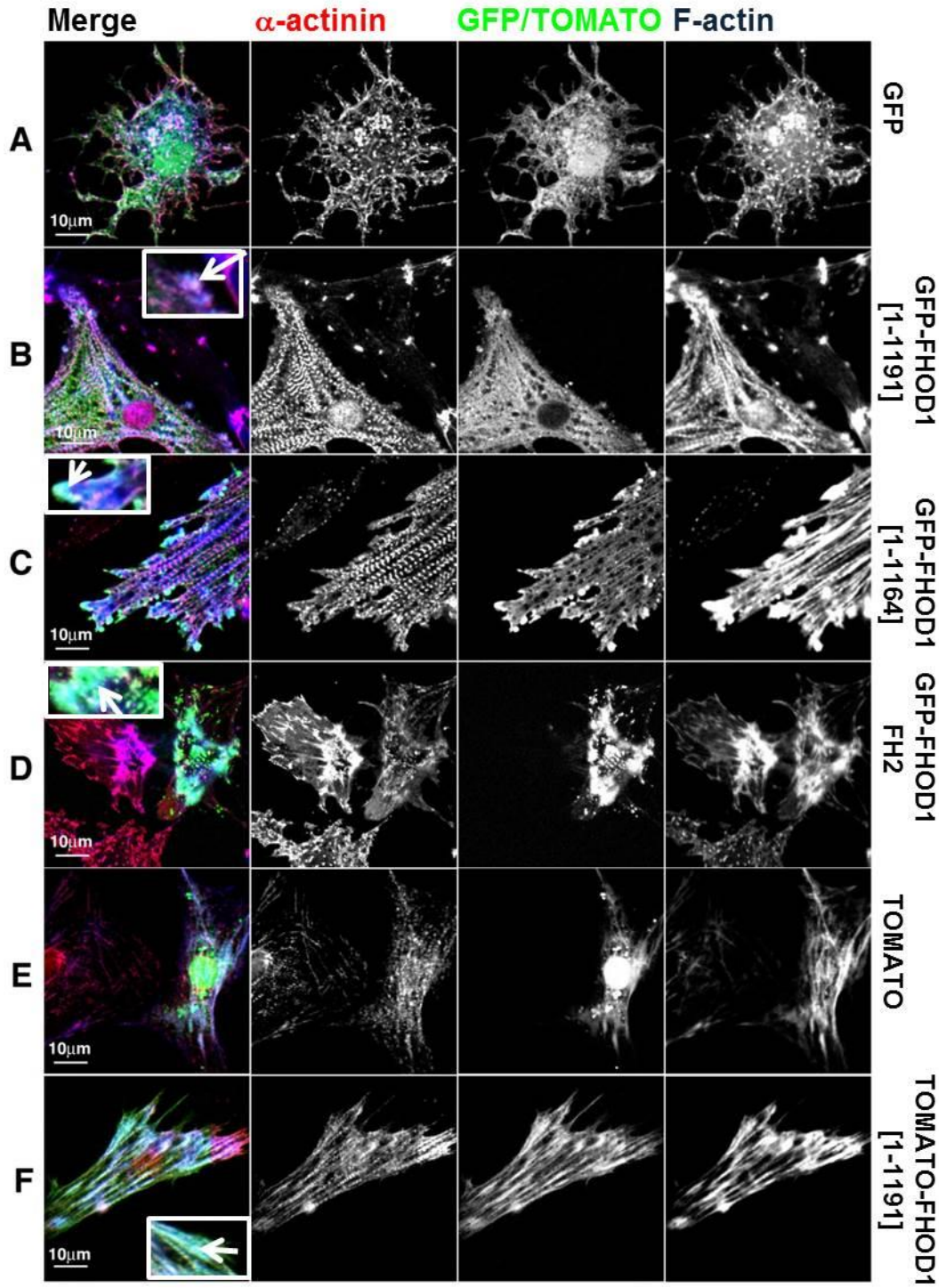

Figure 4.12: Myofibril Recovery Assay in FHOD1-Transfected Neonatal Rat Cardiomyocytes. Representative images of transfected NRCs subjected to Latrunculin B treatment with subsequent myofibril recovery. Cells were stained with α-actinin and F-actin to visualise the extent of recovery. Cells were transfected with the following constructs: **A)** the empty GFP tag vector, **B)** GFP-tagged long variant of full-length FHOD1 [1-1191], **C)** GFP-tagged short variant of full-length FHOD [1-1164], **D)** GFP-tagged FH2 domain [642-1031], **E)** TOMATO tag empty vector, **F)** TOMATO-tagged long variant of full-length FHOD1 [1-1191]. In the GFP transfected cells FHOD1 is seen as green and α-actinin in red. In the TOMATO transfected cells FHOD1 is seen as red and α-actinin in green. F-actin is seen in blue. NRC, neonatal rat cardiomyocytes; GFP, green fluorescent protein; FH, formin homology. Scale bars represent 10μm. White boxes show zoomed selections of merged images. Arrows denote sites of co-localisation with F-actin. **N=1.**

NRCs, a large proportion of transfected cells displayed excellent myofibrillar integrity when compared to the empty GFP vector. The longer variant displayed a greater response with 62% of cells displaying well-formed myofibrils with regular α–actinin staining (Figure 4.12 B). 47% of cells expressing the shorter variant displayed excellent myofibrillar integrity (Table 4.1) and presented with a similar appearance to cells transfected with the long GFP-tagged FHOD1 variant (Figure 4.12 C). The full-length FHOD1 constructs distributed along myofibrils but was sometimes found to concentrate with F-actin in round foci near the plasma membrane and at the ends of myofibrils, although the latter mainly applied to the shorter FHOD1 variant (Figure 4.12 B-C, Zoom). The TOMATO-tagged long variant of full-length FHOD1 was also overexpressed in NRCs. This construct promoted excellent myofibrillar integrity in more cells than the empty TOMATO vector. However, in a similar manner to the empty TOMATO vector, the majority of cells (47%) only displayed intermediate myofibrillar integrity (Table 4.1). TOMATO-tagged FHOD1 predominantly distributed along myofibrils where it sometimes co-localised with both α-actinin and F-actin (Figure 4.12 F, Zoom). The FH2 domain on its own was also overexpressed in NRCs and was found to have an inhibitory effect on myofibril integrity when compared to the full-length FHOD1 variants. NRCs overexpressing the GFP-tagged FHOD1 FH2 domain promoted poor myofibrillar integrity, with 82% of transfected cells essentially devoid of any discernible myofibrils (Table 4.1). Like the majority of untransfected cells, FH2 domain-transfected cells had a poorly organised F-actin network (Figure 4.12 D). The FHOD1 FH2 domain was also noted to co-localise with F-actin (Figure 4.12 D, Zoom). Thus, experiments employing overexpression of full-length wild-type FHOD1 suggested that it promoted myofibrillar integrity in the majority of NRCs after Latrunculin B treatment whereas the isolated FH2 domain seemed to have a negative effect on myofibrillar integrity.

The FHOD1 mutant constructs were also tested for their capacity to regulate myofibrillar integrity in cardiomyocytes that were subjected to Latrunculin B treatment. The GFP-tagged FHOD1 3A construct promoted a relatively high degree of myofibrillar integrity, with 37% of cells displaying well-formed myofibrils with mature Z-disks (Table 4.1). In these cells, FHOD1 3A distributed along myofibrils and occasionally co-localised with F-actin and α-actinin (Figure 4.13 A, Zoom). On the other hand, the

phosphomimetic FHOD1 3D construct enhanced myofibrillar integrity to a greater extent than the 3A construct, with 46% of cells displaying excellent myofibrillar integrity (Table 4.1). In these cells FHOD1 also distributed along myofibrils, where it sometimes co-localised with F-actin and α-actinin (Figure 4.13 B, Zoom), and exhibited some plasma membrane targeting.

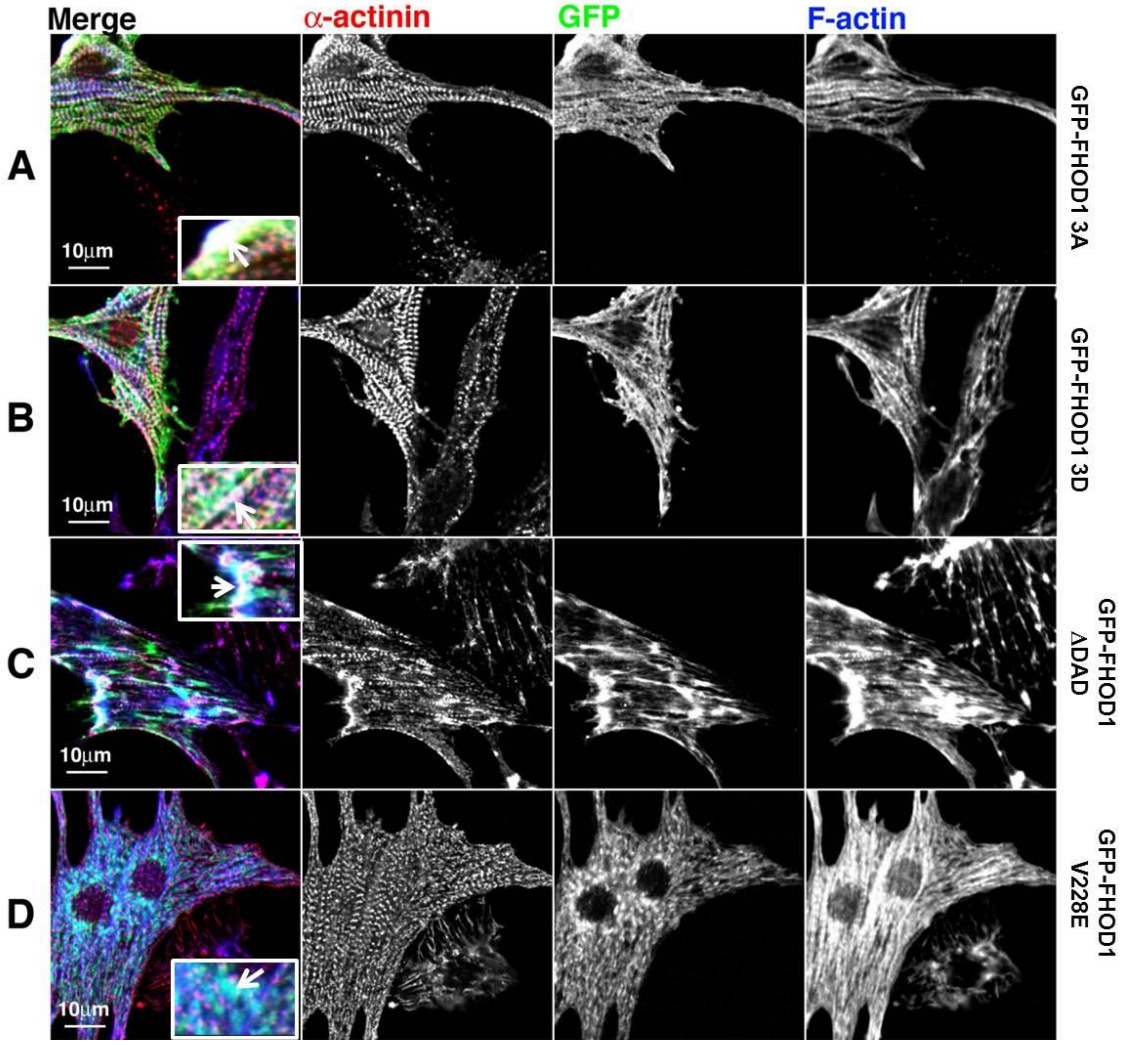

Figure 4.13: Myofibril Recovery Assay in Mutant FHOD1-Transfected Neonatal Rat Cardiomyocytes. Representative images of transfected NRCs subjected to Latrunculin B treatment with subsequent myofibril recovery. Cells were stained with α-actinin and F-actin to visualise the extent of recovery. Cells were transfected with the following FHOD1 mutant constructs: **A)** GFP-tagged FHOD1 ROCK consensus site triple Alanine mutant (3A) [1-1191], **B)** GFP-tagged FHOD1 ROCK consensus site triple Aspartic acid mutant (3D) [1-1191], **C)** GFP-tagged FHOD1 truncation mutant lacking the diaphanous autoinhibitory domain (ΔDAD) [1-1128], **D)** GFP-tagged FHOD1 Valine 228 to Glutamic acid mutant (V228E) [1-1191]. GFP-tagged FHOD1 mutant constructs are seen in green, α-actinin in red, and F-actin in blue. NRC, neonatal rat cardiomyocytes; GFP, green fluorescent protein. Scale bars represent 10μm. White boxes show zoomed selections of merged images. Arrows denote sites of co-localisation with F-actin. **N=1.**

The GFP-tagged FHOD1 ΔDAD construct seemed to have a modest effect on the integrity of myofibrils compared to other constructs, with 54% of cells displaying

intermediate myofibrillar integrity (Table 4.1). The construct distributed along less mature myofibrils where it co-localised with F-actin and α-actinin (Figure 4.6 C, Zoom). The GFP-tagged FHOD1 V228E mutant had a profound effect on myofibrillar integrity, with 46% of cells displaying well-formed myofibrils (Table 4.1). This construct exhibited a unique localisation pattern compared to the other FHOD1 constructs (Figure 4.6 D). The FHOD1 V228E construct was found as small blebs that distributed along myofibrils. Perinuclear accumulation of the construct was also present. The FHOD1 V228E construct exhibited some co-localisation with F-actin throughout transfected cells (Figure 4.6 D, Zoom).

Although myofibril/F-actin depolymerisation experiments suggested that FHOD1 may have a role in the regulation of myofibrillar integrity, it was impossible to distinguish between the FHOD1 expression constructs facilitating recovery of myofibrils (i.e., promoting *de novo* myofibrillogenesis) or preventing disassembly of myofibrils. Comparison of the wild-type and mutant FHOD1 constructs indicated that myofibrillar integrity was generally increased regardless of the activation status of FHOD1. Taken together these observations might point at slightly different subcellular roles for the closely related FHOD3 and FHOD1 in cardiomyocytes. While results for FHOD3 were clear-cut and related to its activation status (Iskratsch et al., 2010), results for FHOD1 were more ambiguous. FHOD3 is consistently associated with myofibrils, at least in its muscle isoform, while FHOD1 may mainly be localised in the cellular periphery, meaning that it may aid myofibrils integrity but not as strongly and consistently as FHOD3. Interestingly, the FH2 domain of FHOD1 seemed to reduce myofibrillar integrity in this assay, suggesting that it may have facilitated disassembly of myofibrils and/or inhibited the assembly of thin filaments after Latrunculin B wash-out. While the FH2 domains of some formins have been shown to be sufficient for thin filament assembly, this does not seem to be the case for FHOD1. FH2 domain-containing FHOD1 constructs have been shown to preferentially cap filaments rather than elongate them (Schonichen et al. 2013). If the isolated FHOD1 FH2 domain possessed any actin polymerising activity, we may have expected a greater degree of myofibrillar integrity than that seen in untransfected NRCs. The GFP-tagged full-length FHOD1 constructs containing the FH2 domain did however promote myofibrillar integrity, which could mean that elements that lie outside of the FH2 domain were partly responsible. The

FHOD1 N-terminus has been shown to possess actin bundling activity (Schonichen et al. 2013) and could conceivably play a role in promoting myofibrillar stability in the presence of Latrunculin B. These factors would suggest that the full-length and active FHOD1 constructs prevented myofibrillar/F-actin disassembly rather than promoted *de novo* filament assembly. However, this remains to be confirmed by performing this assay with other FHOD1 subunits and deletion constructs.

4.5 RNAi Mediated Knockdown Studies

In addition to the transient expression studies with the FHOD1 expression constructs, a number of loss-of-function experiments were also performed. These took place through vector based RNAi mediated knockdown of FHOD1 in cultured cells. Vector based RNAi approaches have certain advantages over direct treatment with naked siRNA. Direct addition of siRNA to cells is associated with increased toxicity. Furthermore, vector based shRNA approaches have been found to have fewer off-target effects (Rao et al. 2009). The RNA interference approach used in this study functions on the basis that the H1 RNA polymerase III promoter stimulates the transcription of a RNA strand from the cloned target coding sequence of the gene in question (Brummelkamp et al. 2002). The vector produces short hairpin RNAs (shRNAs) which are further processed into small inhibitory RNAs (siRNAs) by the enzyme Dicer. The resulting siRNAs target the specified portion of mRNA for eventual degradation. The siRNA and the complementary mRNA are then incorporated into the RNA-induced silencing complex (RISC), a multi-enzyme complex with an RNAase component responsible for cleaving the target sequence (Rao et al. 2009). Since our initial analysis of FHOD1's expression pattern through Western blot studies suggested that there were reasonably high levels of FHOD1 in both cardiac and skeletal muscle, it was decided to knock down FHOD1 in cultured NRCs and differentiating C2C12 cells. Three shRNA constructs were designed to deplete FHOD1 in mouse and rat cells. Constructs were named according to the coding sequence of rat FHOD1 that they were designed to target: 1095, 2375, and 2635. The shRNA vector, which is based on pSUPER, also separately expresses GFP and confers the additional advantage over naked siRNA molecules of allowing transfected cells to be visualised.

4.5.1 Design and Validation of shRNA Constructs

The three shRNA constructs were designed to knockdown FHOD1 in rat and mouse cells (Figure 4.14). The 2635 shRNA was also designed to target the human FHOD1 sequence, whereas the 1095 shRNA and the 2375 shRNA contained 3 and 1 mismatched base pairs with respect to the corresponding sequence on human FHOD1, respectively. The three constructs were designed to target all of the reported FHOD1 isoforms in rat and mice. Basic Local Alignment Search Tool (BLAST) queries were performed to confirm the constructs would specifically target FHOD1 and no other genes with similar sequences.

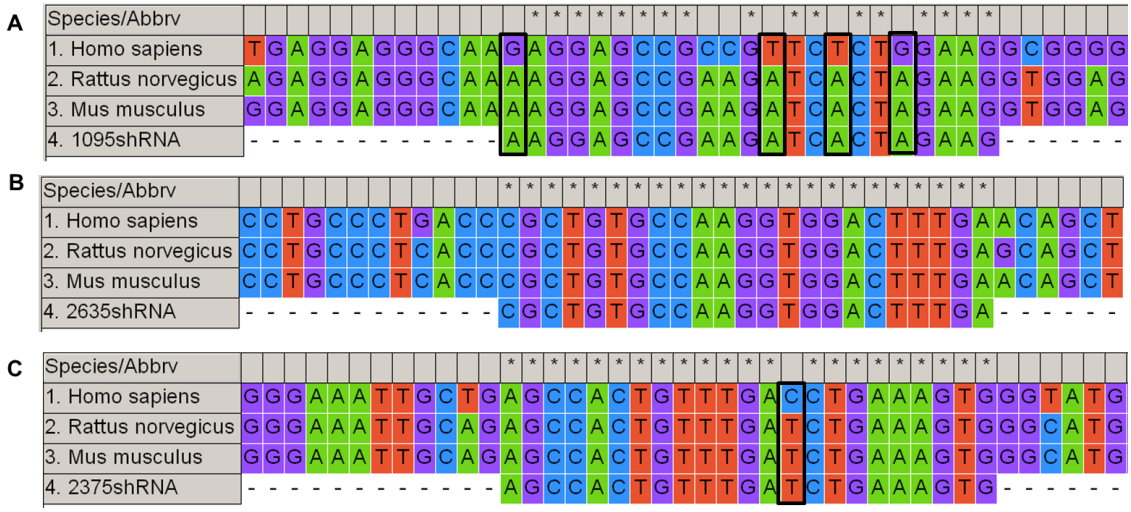

Figure 4.14: Sequence Alignment of the FHOD1 shRNA Constructs with Human and Rodent FHOD1 DNA Sequence. Target DNA sequence of the three shRNA constructs designed to disrupt expression of FHOD1. **A)** Alignment for the 1095 shRNA construct. **B)** Alignment for the 2635 shRNA construct. **C)** Alignment for the 2375 shRNA construct. Alignments were included for the *Homo sapiens* (Accession No: NM_013241.2), *Rattus norvegicus* (Accession No: NM_001191600.1) and *Mus musculus* (Accession No: NM_177699.4) sequences. Black boxes denote areas of base pair mismatch with the human sequence. Alignment was performed with Mega5 (Tamura et al. 2011).

Prior to performing knockdown studies in cultured cells, the RNAi system was first assessed for its ability to inhibit FHOD1 expression. As mentioned above, the 2635 shRNA construct was not only designed to target the rodent sequence of FHOD1, but also the human sequence. Via transfection studies in COS-1 cells, we looked at the extent of knockdown of the human FHOD1 construct by the 2635 shRNA construct. COS-1 cells were co-transfected with the long variant of TOMATO-tagged human

FHOD1 as well as the 2635 shRNA construct. Cells were lysed and protein levels were visualised by Western blotting (Figure 4.15 A). TOMATO-tagged FHOD1, with an expected molecular weight of 182 kDa, expressed as a high running band above the 128 kDa marker. In cells cotransfected with the 2635 shRNA construct and TOMATO-tagged FHOD1, the band associated with TOMATO-tagged FHOD1 was reduced to undetectable levels. This indicated that expression of the human FHOD1 construct was efficiently being disrupted. The empty shRNA vector did not have an effect on levels of the FHOD1 construct and, similarly, the 2635 shRNA construct was unable to knock down the expression of the TOMATO tag. Lysates were also blotted for GFP as a loading control (Figure 4.15 B), indicating that loading was similar between the samples in direct comparison to each other (e.g., lane of COS-1 cells co-transfected with the empty shRNA vector and TOMATO-tagged FHOD1 versus lane of COS-1 cells co-transfected with the 2635 shRNA construct and TOMATO-tagged FHOD1) and thus assuring that the FHOD1 construct was indeed knocked down by the 2635 shRNA construct.

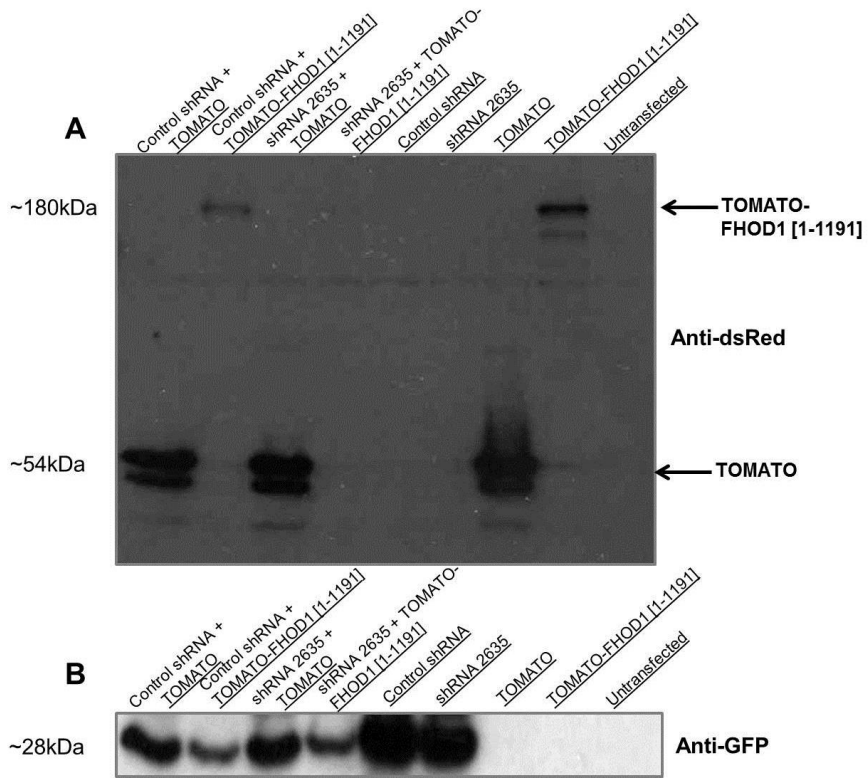

Figure 4.15: Validation of RNAi Technique by Western Blotting. Western blots from lysates of COS-1 cells. Cells were transfected with a combination of constructs to assess the ability of the 2635 shRNA construct to knock down FHOD1 expression. In the first lane on the left hand side, cells were double transfected with the empty shRNA vector (H1 GFP) and the empty TOMATO vector (TOM). In the second lane cells were double transfected with the empty shRNA vector and the TOMATO-tagged long variant of full-length FHOD1 (FlL TOM) [1-1191]. In the third lane cells were double transfected with the 2635 shRNA construct and the empty TOMATO vector. In the fourth lane on the right, cells were double transfected with the 2635 shRNA construct and TOMATO-tagged long variant of full-length FHOD1 [1-1191]. Single transfected samples of each construct are also shown on the gel. Untransfected COS-1 lysates were loaded as a negative control. **A)** COS-1 lysates probed with the dsRed antibody to visualise the TOMATO signal. **B)** COS-1 lysates probed with the GFP antibody. Arrow indicates band corresponding to the TOMATO-tagged long variant of full-length FHOD1 and to TOMATO. GFP, green fluorescent protein. **N=3.**

Further validation of the RNAi approach took place via immunofluorescence experiments to confirm the disruption of expression of the FHOD1 construct that was seen in Western blot experiments. COS-1 cells were co-transfected with TOMATO-tagged FHOD1 and the 2635 shRNA construct. If the previous experiment using Western blot analysis to visualise knockdown of FHOD1 proved accurate, an attenuated signal for TOMATO FHOD1 would be noted in double transfected cells. The resulting data resonated that seen with the Western blot studies. The empty shRNA vector was unable to knock down the expression of the TOMATO tag (Figure 4.16 A) and neither was the 2635 shRNA construct (Figure 4.16 B). The empty shRNA vector was also

unable to knock down TOMATO FHOD1 (Figure 4.16 C). The 2635 shRNA construct disrupted expression of TOMATO-tagged FHOD1 since co-transfected cells displayed a weak signal for TOMATO-tagged FHOD1 (Figure 4.16 D). These data would indicate that the RNAi approach used in this study could be specific for FHOD1 and was capable of disrupting expression of the human construct. However, while these results provide proof-of-concept evidence for the RNAi approach used, they cannot be fully extrapolated as evidence for the capacity to disrupt expression of endogenous FHOD1. This was especially the case since these experiments were limited to validation of only one shRNA construct. Better proof-of-concept may have been gained by testing the capacity of the shRNA constructs to disrupt expression of rat and mouse FHOD1 constructs while concurrently demonstrating knockdown of endogenous FHOD1 in the cell types used.

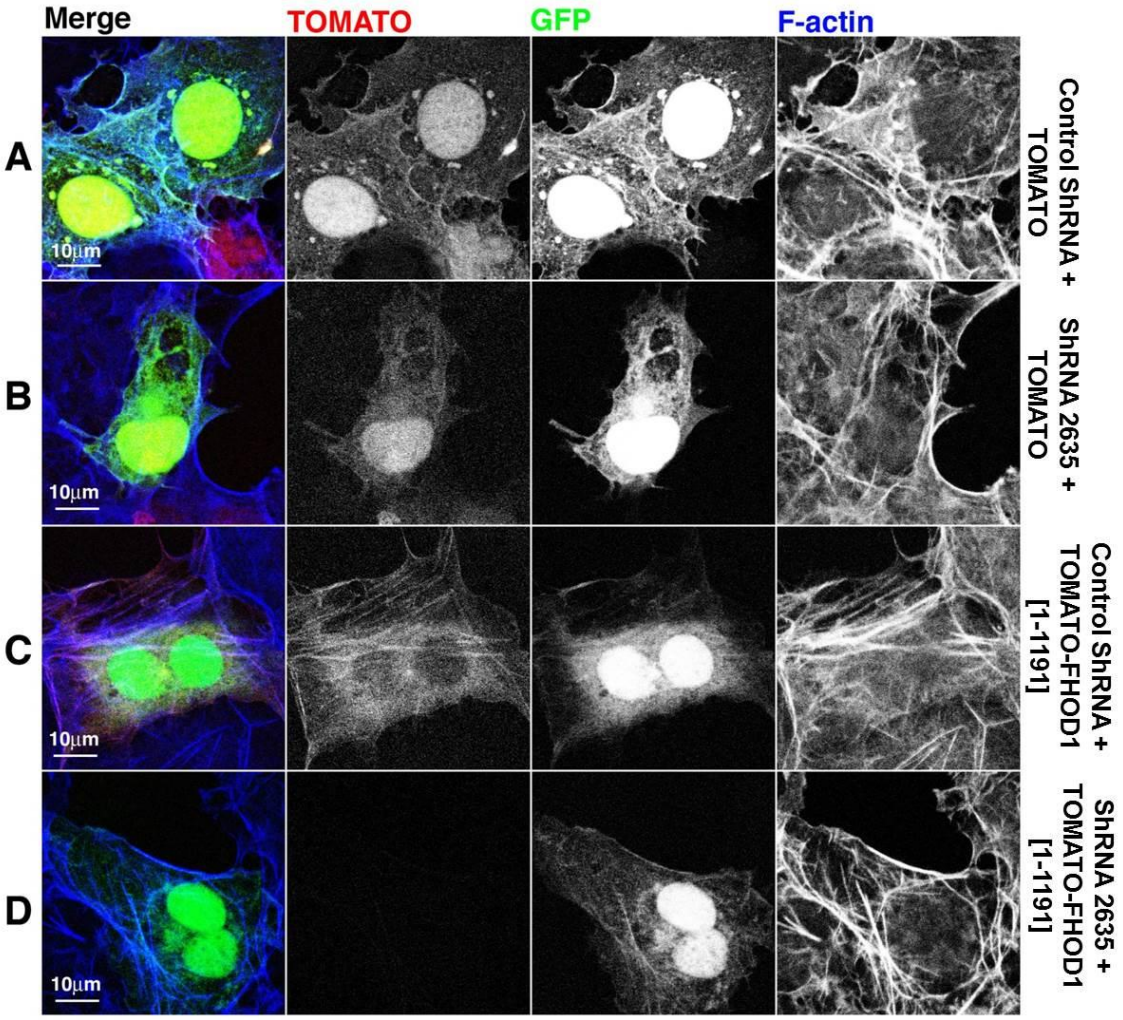

Figure 4.16: Validation of RNAi Technique by Fluorescence Confocal Microscopy. COS-1 cells were transfected with different combinations of constructs to validate knockdown of FHOD1 by RNAi. COS-1 cells were stained for F-actin prior to visualisation by confocal microscopy. Cells were transfected with a combination of constructs to assess knockdown of FHOD1 expression: **A)** cells were double transfected with the empty shRNA vector and the empty TOMATO vector, **B)** cells were double transfected with the empty shRNA vector and the TOMATO-tagged long variant of full-length FHOD1 [1-1191], **C)** cells were double transfected with the 2635 shRNA construct and the empty TOMATO vector, **D)** cells were double transfected with the 2635 shRNA construct and TOMATO-tagged long variant of full-length FHOD1 [1-1191]. GFP is seen in green, TOMATO in red, and F-actin in blue. GFP, green fluorescent protein. Scale bars represent 10μm. **N=1.**

4.5.2 Knockdown of FHOD1 in Neonatal Rat Cardiomyocytes

The three different shRNA constructs designed to target the rodent *fhod1* mRNA were transfected into cultured NRCs. The effects of the shRNA constructs were examined at different time points to assess the potentially cumulative effects of knockdown. Cells were fixed at days 3, 5 and 8. In the absence of a means to definitively show that expression of endogenous FHOD1 was disrupted at the transcript level, we qualitatively assessed the possibility of FHOD1 knockdown by staining for well-established myofibrillar, sarcomeric, and cell-cell contact markers. In the hopes of visualising knockdown of FHOD1 the protein level, we stained NRCs with the polyclonal mouse anti-FHOD1 antibody (Abcam).

Day 3 (Figure 4.17) and day 5 (Figure 4.18) FHOD1 shRNA-transfected NRCs were indistinguishable from NRCs transfected with the empty shRNA vector. A phenotype associated with the transfection of the shRNA constructs designed to knock down endogenous rat FHOD1 was not seen until day 8. In the case of the gene paralogue of *FHOD1*, *FHOD3*, the full effects of RNAi mediated knockdown were also not seen until day 8 (Iskratsch et al. 2010) and might reflect slow turnover of these proteins in myofibrils.

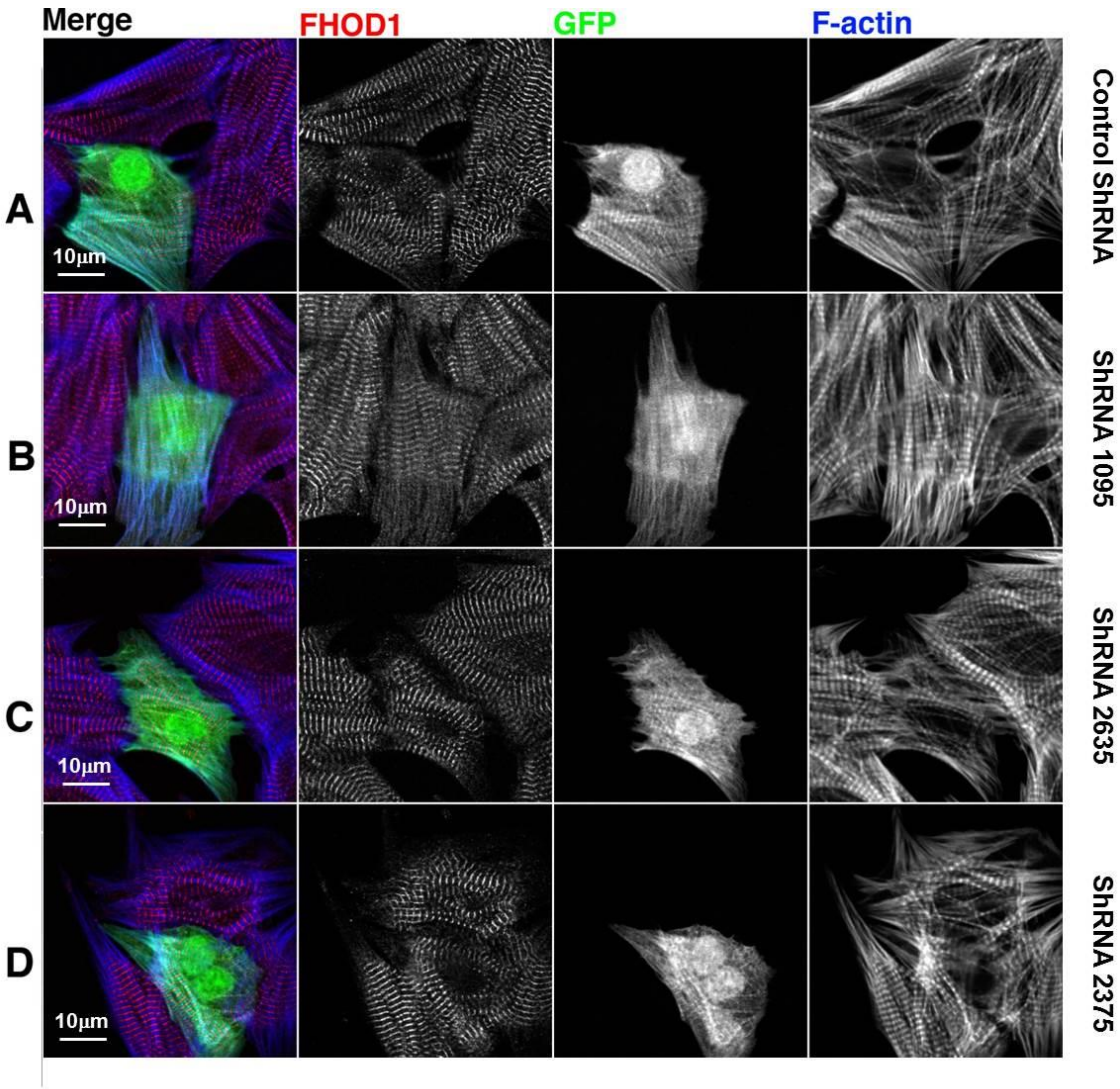

Figure 4.17: The Effects of the FHOD1 shRNAs in Neonatal Rat Cardiomyocytes at Day 3. NRCs were transfected with three different shRNA constructs designed to knockdown FHOD1. NRCs were cultured until day 3 in long term/transfection medium. Cells were stained for FHOD1, F-actin, and visualised by confocal microscopy. Transfected cells are seen in green since the shRNA vector separately expresses GFP. NRCs were transfected with the following constructs: **A)** the empty shRNA vector, **B)** the 1095 shRNA construct, **C)** the 2375 shRNA construct, **D)** the 2635 shRNA construct. GFP is seen in green, FHOD1 in red, and F-actin in blue. GFP, green fluorescent protein. Scale bars represent 10μm. **N=3.**

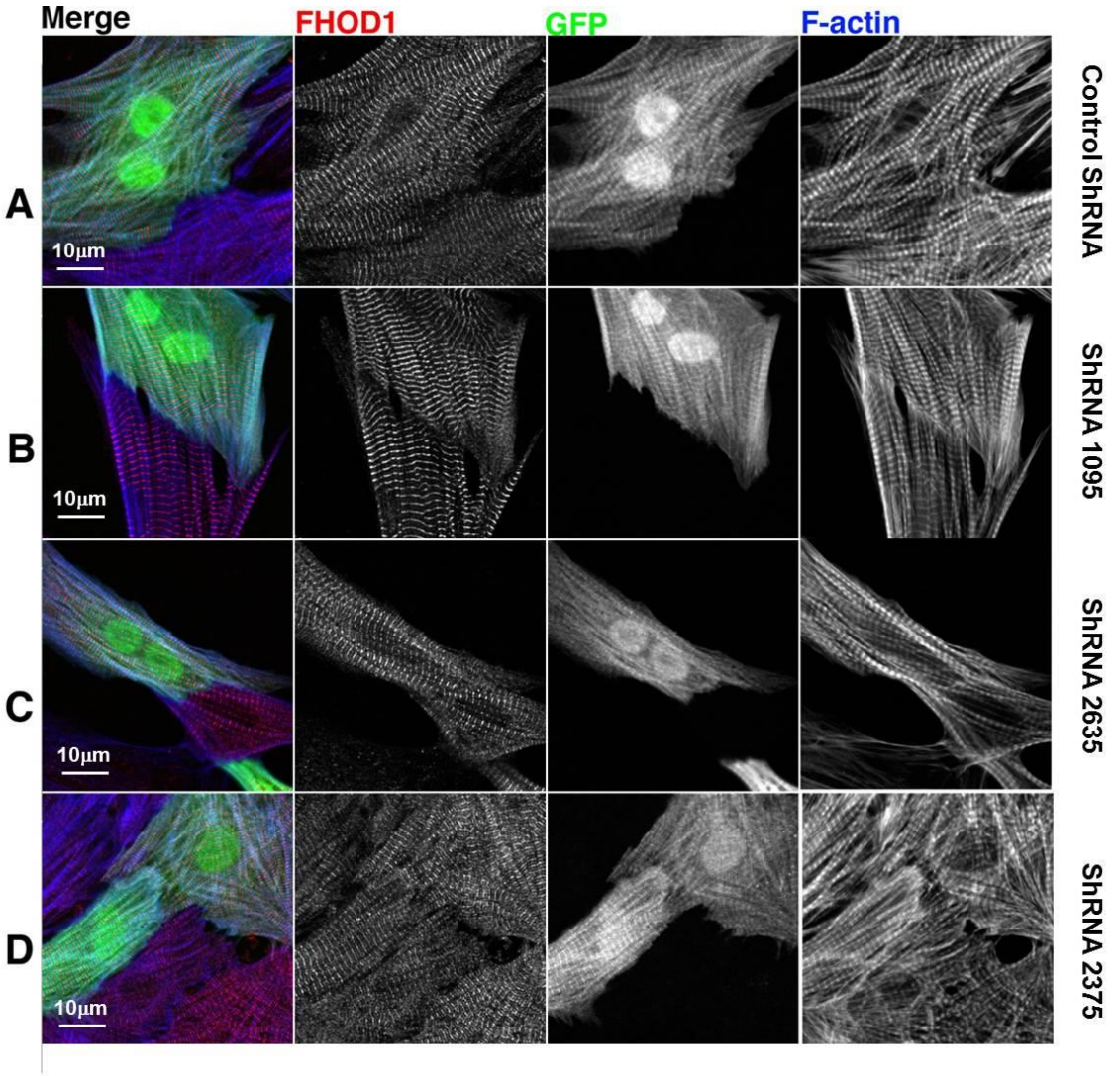

Figure 4.18: The Effects of the FHOD1 shRNAs in Neonatal Rat Cardiomyocytes at Day 5. NRCs were transfected with three different shRNA constructs designed to knockdown FHOD1. NRCs were cultured until day 5 in long term/transfection medium. Cells were stained for FHOD1, F-actin, and visualised by confocal microscopy. Transfected cells are seen in green since the shRNA vector separately expresses GFP. NRCs were transfected with the following constructs: **A)** the empty shRNA vector, **B)** the 1095 shRNA construct, **C)** the 2375 shRNA construct, **D)** the 2635 shRNA construct. GFP is seen in green, FHOD1 in red, and F-actin in blue. GFP, green fluorescent protein. Scale bars represent 10μm. **N=3.**

In control and untransfected cells, FHOD1 distributed in the manner seen previously in earlier cultures of NRCs at day 3 (Figure 4.19 A). Cells transfected with the shRNA constructs displayed a decrease in FHOD1 staining (Figure 4.19 B-D). Counterstaining with Phalloidin initially revealed that transfection with the shRNA constructs resulted in fragmentation of myofibrils. In control and untransfected cells, F-actin was seen to distribute along myofibrils at the level of the I-bands (Figure 4.19 A). Also in the shRNA transfected cells, there was a seemingly attenuated signal for F-actin, as suggested by weaker staining (Figure 4.19 B-D). In knockdown cells, F-actin often distributed in a diffuse cytoplasmic manner. This was especially the case with the 2635 shRNA construct (Figure 4.9 D), which seemed to have the most profound effect on the F-actin network and cardiomyocyte morphology as a whole.

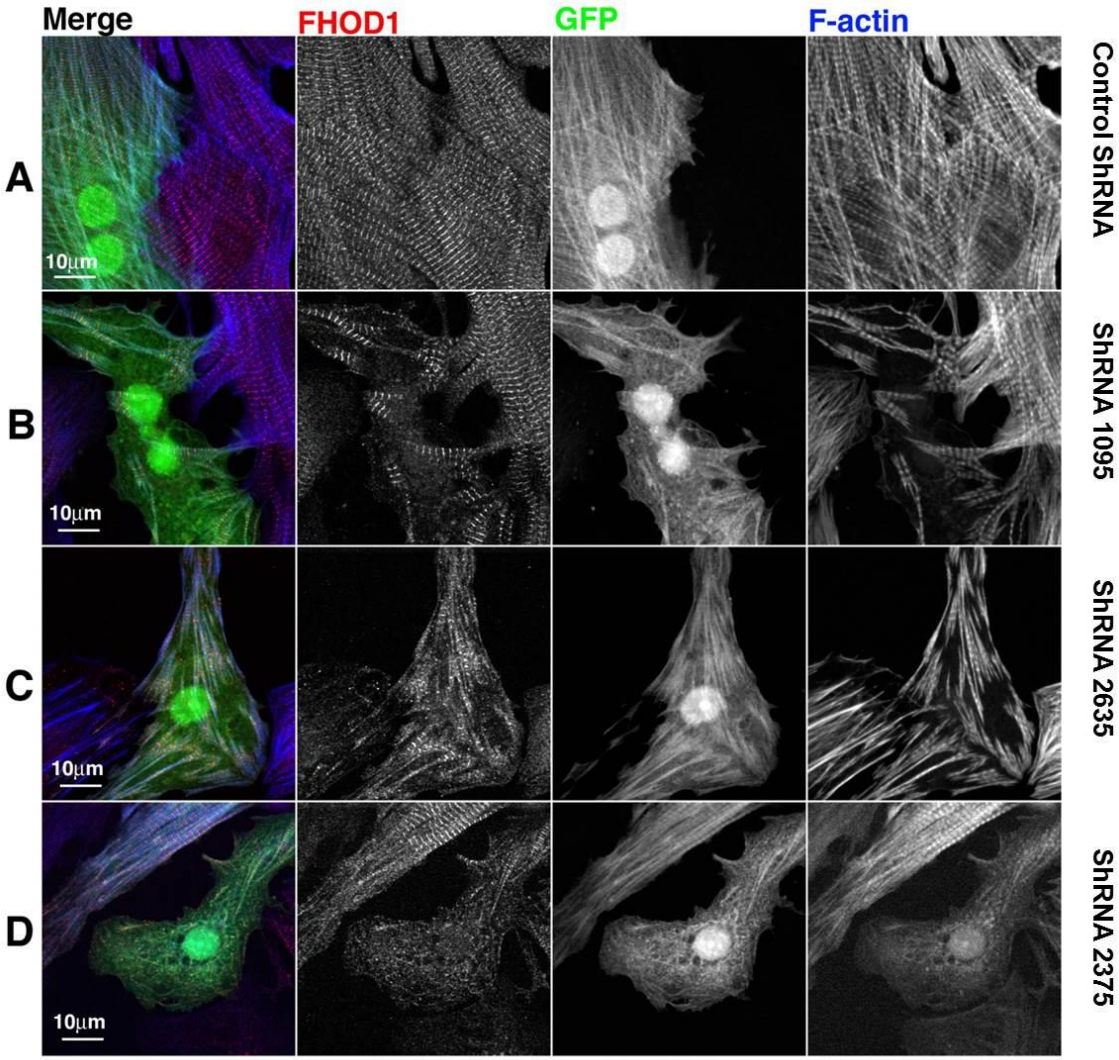

Figure 4.19: The Effects of the FHOD1 shRNAs in Neonatal Rat Cardiomyocytes at Day 8. NRCs were transfected with three different shRNA constructs designed to knockdown FHOD1. NRCs were cultured until day 8 in long term/transfection medium. Cells were stained for FHOD1, F-actin, and visualised by confocal microscopy. Transfected cells are seen in green since the shRNA vector separately expresses GFP. NRCs were transfected with the following constructs: **A)** the empty shRNA vector, **B)** the 1095 shRNA construct, **C)** the 2375 shRNA construct, **D)** the 2635 shRNA construct. GFP is seen in green, FHOD1 in red, and F-actin in blue. GFP, green fluorescent protein. Scale bars represent 10μm. **N=3.**

The effects of the shRNA constructs were further investigated by staining cardiomyocytes against other myofibrillar markers. Control and untransfected cells retained a normal flattened morphology as characterised by regular membrane edges and longitudinal myofibrils that ran along the edge of cells and emanated from within the cell peripheries (Figure 4.20 A). In cells transfected with the shRNAs designed to knock down FHOD1, it became apparent that myofibrils were absent or had been disrupted (Figure 4.20 B-D). It was also noted that FHOD1 shRNA-transfected cells displayed with irregular plasma membrane edges and appeared to have a more lacerated morphology. In control and untransfected cells α-actinin distributed in its typical pattern at the Z-disk (Figure 4.20 A). In cells transfected with the FHOD1 shRNAs, the distribution of α-actinin became more patchy, although it was still seen to localise to the Z-disk on the truncated portions of myofibrils (Figure 4.20 B-D). In the case of MyBP-C, the protein was seen to localise to the A-bands in control and untransfected cells. In knockdown cells, MyBP-C became diffusely distributed throughout cells, although it was still found to be partially targeted to the remaining portions of myofibrils (Figure 4.20 B-D). In the case of myomesin, the protein was found at the M-band in control and untransfected cells (Figure 4.21 A) but staining for the protein was seemingly reduced in shRNA-transfected cells, as suggested by fewer M-band striations and an overall attenuation in the myomesin signal (Figure 4.21 B-D).

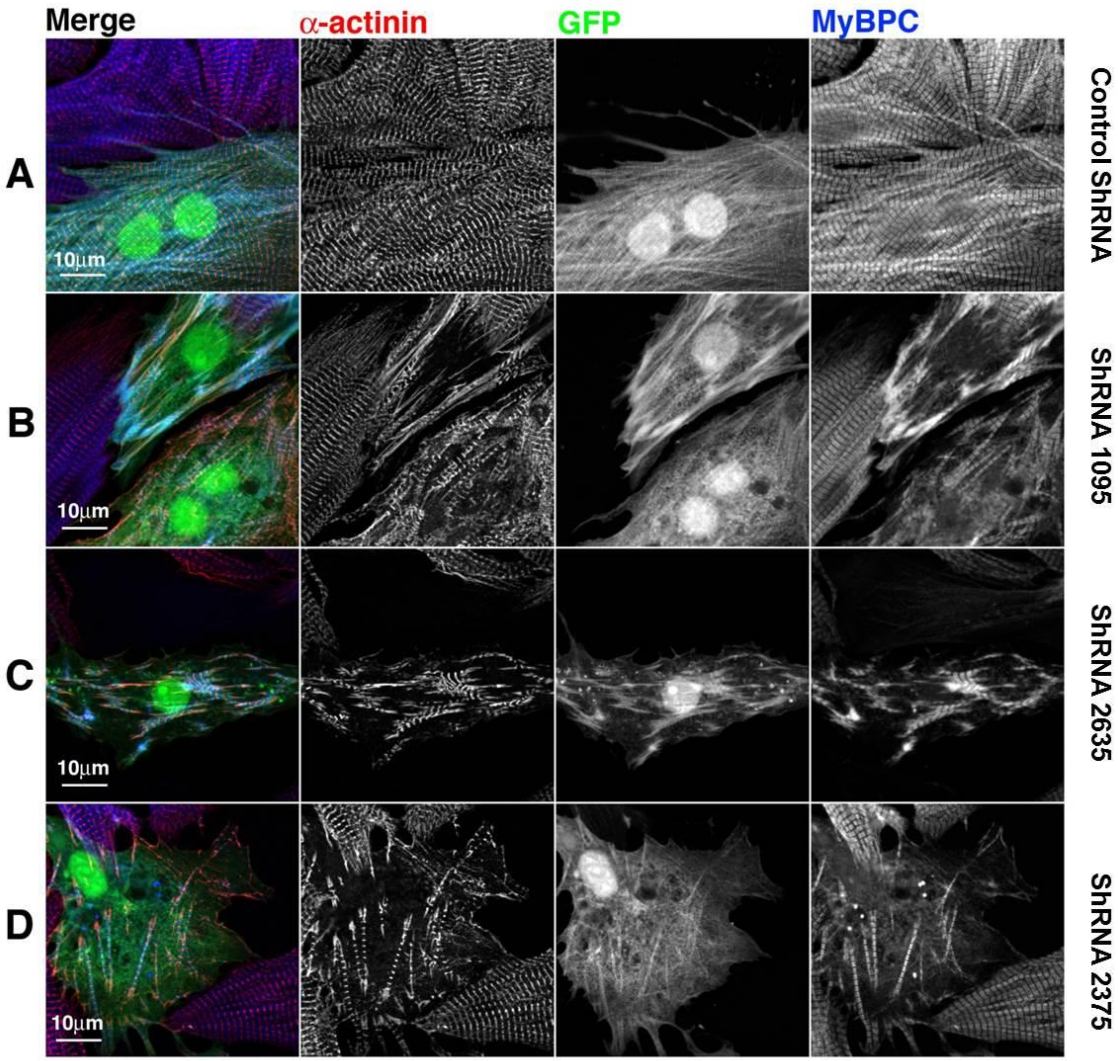

Figure 4.20: The Effects of the FHOD1 shRNAs on the Z-disk and the A-band. NRCs were transfected with three different shRNA constructs designed to knockdown FHOD1. NRCs were cultured until day 8 in long term/transfection medium. Cells were stained for α-actinin and MyBP-C to visualise the effect of knockdown on myofibrils and visualised by confocal microscopy. Transfected cells are seen in green since the shRNA vector separately expresses GFP. NRCs were transfected with the following constructs: **A)** the empty shRNA vector, **B)** the 1095 shRNA construct, **C)** the 2375 shRNA construct, **D)** the 2635 shRNA construct. GFP is seen in green, α-actinin in red, and MyBP-C in blue. MyBP-C, myosin binding protein C; GFP, green fluorescent protein. Scale bars represent 10μm. **N=3.**

Transfection with the shRNA constructs was also associated with a number of alterations at the level of the intercalated disk. Control and untransfected cells displayed normal cell-cell contacts with β-catenin distributing along the intercalated disk (Figure 4.21 A). Normally, β-catenin forms part of the cadherin-catenin complex involved in mediating cell-cell adhesion at the intercalated disk (Masuelli et al. 2003). FHOD1 shRNA-transfected cells displayed an increase in the numbers of cell-cell contacts, which were present as thin plasma membrane projections. Fluorescent staining for β-catenin in transfected cells revealed a decreased signal for the protein at the intercalated disk (Figure 4.21 B-D). Instead, it was often found concentrated throughout the cytoplasm in a punctate manner (Figure 4.21 B and D).

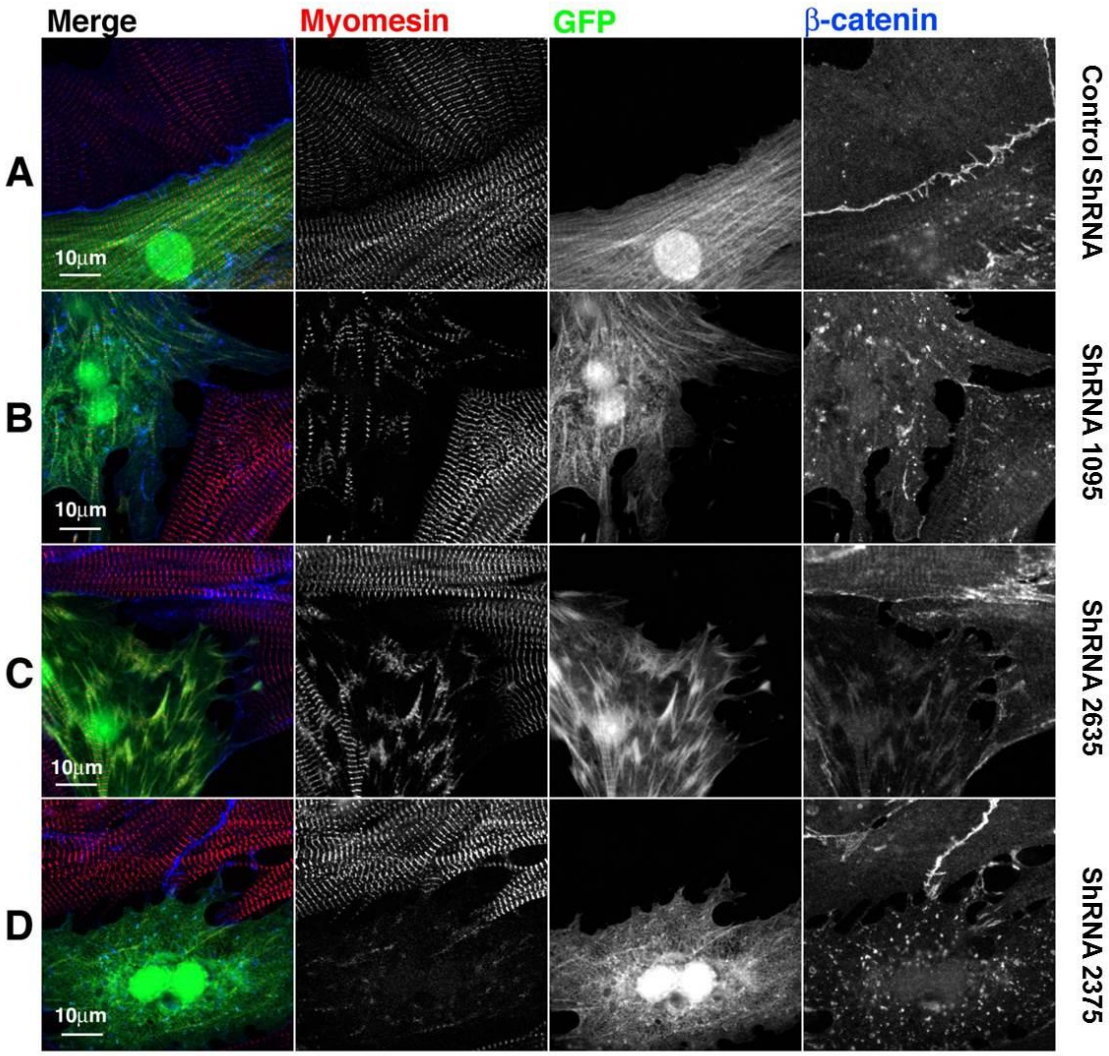

Figure 4.21: The Effects of the FHOD1 shRNAs on the M-band and the Intercalated Disk. NRCs were transfected with three different shRNA constructs designed to knockdown FHOD1. NRCs were cultured until day 8 in long term/transfection medium. Cells were stained for the intercalated disk protein β-catenin and the sarcomeric protein myomesin to visualise the effect of knockdown on the cell-cell contacts and myofibrils. Cells were visualised by confocal microscopy. Transfected cells are seen in green since the shRNA vector separately expresses GFP. NRCs were transfected with the following constructs: **A)** the empty shRNA vector, **B)** the 1095 shRNA construct, **C)** the 2375 shRNA construct, **D)** the 2635 shRNA construct. GFP is seen in green, myomesin in red, and β-catenin in blue. GFP, green fluorescent protein. Scale bars represent 10μm. **N=3.**

Overall, transfection with the shRNA constructs designed to knock down endogenous FHOD1 was associated with alterations in cardiomyocyte morphology, particularly at the level of myofibrillar organisation/integrity and the appearance of cell-cell contacts. However, we were not able to fully attribute this phenotype to depletion of FHOD1, since this was neither confirmed at the mRNA transcript or protein level. A reduction in FHOD1 at the mRNA transcript level could not be demonstrated for any of the shRNA constructs because of the low transfection efficiency we achieved in cultured NRCs. While staining of NRCs with the polyclonal mouse anti-FHOD1 antibody (Abcam) may have suggested reduced staining for FHOD1, this notion was only tested using one antibody. Furthermore, in the absence of an antigen competition assay, we could not be certain of the specificity, and hence utility, of the presently employed polyclonal mouse anti-FHOD1 antibody. Furthermore, although we demonstrated that the 2635 shRNA construct could disrupt expression of the human FHOD1 construct in COS-1 cells, such proof-of-concept data cannot be extended to the other shRNA constructs or knockdown of rodent FHOD1. Therefore, it cannot be concluded with certainty that the observed phenotypes were not due to off-target effects rather than FHOD1 depletion.

4.5.3 RNAi Rescue Experiments in Neonatal Rat Cardiomyocytes

As an additional control for the knockdown experiments in cultured cardiomyocytes, rescue experiments were performed to begin to address if the effects of the shRNA constructs were due to depletion of FHOD1 (Figure 4.22). NRCs were co-transfected with the TOMATO-tagged long variant of full-length FHOD1 and the 1095 shRNA construct. The rescue experiment functioned on the basis that the 1095 shRNA construct could not knock down the TOMATO FHOD1 construct: it was not designed for targeted degradation of any portion of the human *FHOD1* gene since it contained three mismatched base pairs with respect to its corresponding sequence on the human gene (Figure 4.14). Instead, overexpression of the TOMATO-tagged FHOD1 construct would restore normal cardiomyocyte morphology. When the empty TOMATO vector and the empty shRNA vector were co-transfected, there was no change in cardiomyocyte morphology or the appearance of myofibrils at day 8 (Figure 4.22 A). When the TOMATO-tagged FHOD1 construct was co-transfected with the empty shRNA vector, cells displayed an elongated morphology, with FHOD1 distributing along myofibrils and at the peripheries of cells (Figure 4.22 B). When co-transfected

with the empty TOMATO vector, the 1095 shRNA construct resulted in disrupted cardiomyocyte morphology and compromised myofibrillar integrity (Figure 4.22 C). When co-transfected with TOMATO-tagged FHOD1, the effects of the 1095 shRNA vector were no longer visible (Figure 4.22 D). Under these conditions, cardiomyocytes retained their normal morphology, with fully formed myofibrils and mature sarcomeres. Overexpression of FHOD1 in shRNA knockdown cells therefore seemingly rescued the phenotype associated with transfection of the 1095 shRNA construct. These data would indicate that the effects of the 1095 shRNA may have been due to FHOD1 depletion and not due to off-target effects. However, the same cannot be said for the other two shRNA constructs. In order to extrapolate these conclusions to the other shRNA constructs, definitive knockdown of FHOD1 must be demonstrated.

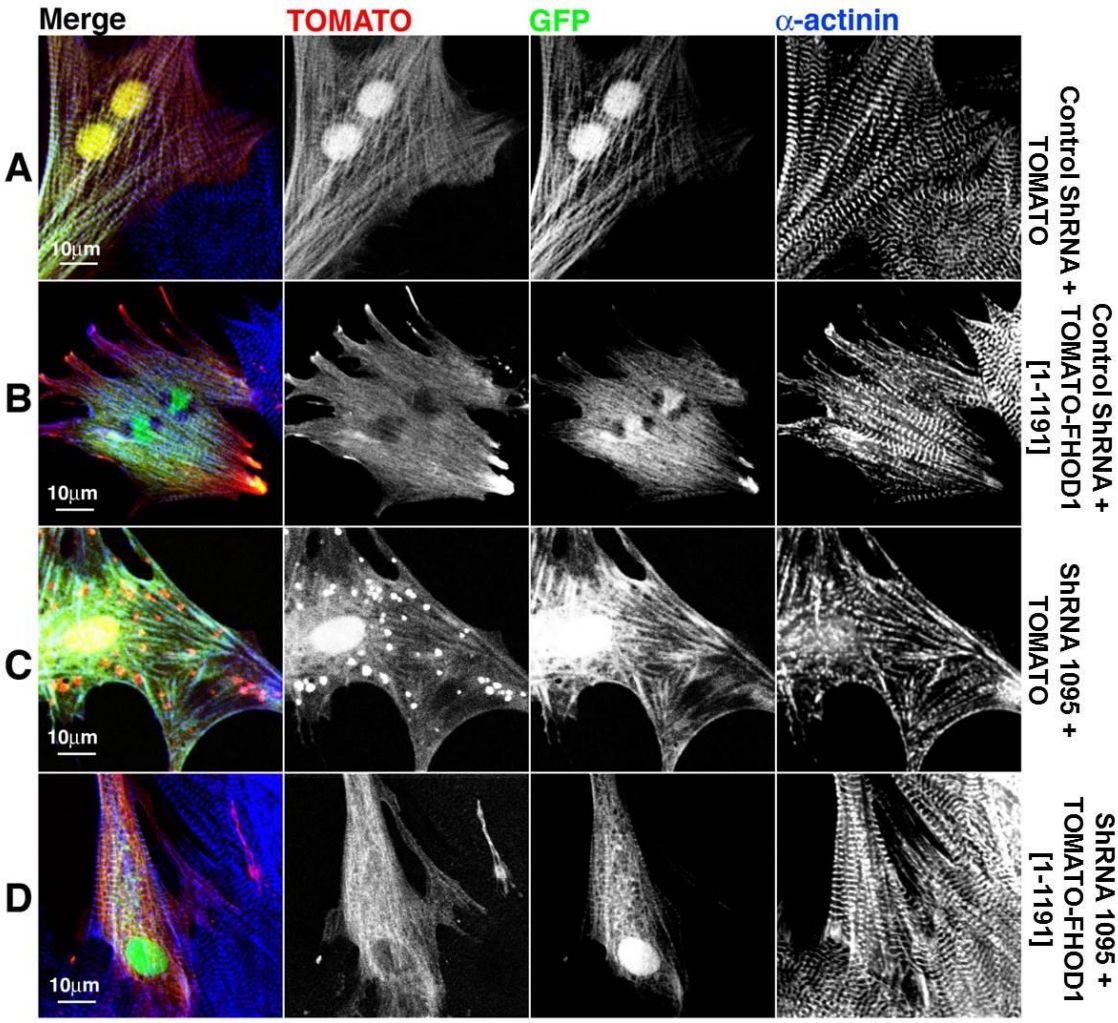

Figure 4.22: Rescue of RNAi Mediated Effects by FHOD1 Overexpression. NRCs were transfected with different combinations of constructs to assess if the effects associated with the RNAI mediated knockdown could be rescued by FHOD1 overexpression. NRCs were cultured to day 8 and stained for α-actinin prior to visualisation by confocal microscopy. shRNA transfected cells are seen in green since the shRNA vector also expresses GFP. Cells were transfected with a combination of constructs: **A)** cells were double transfected with the empty shRNA vector and the empty TOMATO vector, **B)** cells were double transfected with the empty shRNA vector and the TOMATO-tagged long variant of full-length FHOD1 [1-1191], **C)** cells were double transfected with the 1095 shRNA construct and the empty TOMATO vector, **D)** cells were double transfected with the 1095 shRNA construct and TOMATO-tagged long variant of full-length FHOD1 [1-1191]. GFP is seen in green, TOMATO in red, and α-actinin in blue. GFP, green fluorescent protein. Scale bars represent 10μm. **N=1.**

4.5.4 Knockdown of FHOD1 in Day 3 C2C12 Cells

In addition to knockdown experiments in cardiac cells, RNAi experiments were performed in differentiating C2C12 skeletal muscle myoblasts, a murine cell line. C2C12 cells were transfected with the three FHOD1 shRNA constructs and the empty shRNA vector. Cells were then induced to differentiate and were visualised by confocal microscopy at days 3 and 7. At day 3, a phenotype associated with transfection of the shRNA constructs designed to knock down FHOD1 was noted (Figure 4.23). Cells transfected with the empty shRNA vector retained their normal morphology (Figure 4.23 A). At this time point, control and untransfected cells exhibited an elongated appearance and displayed numerous stress fibres, as visualised by Phalloidin staining for F-actin. Transfection with the three shRNA constructs was associated with disruption of the F-actin network. In examining the three different shRNA constructs it became apparent that there were a number of construct-specific effects. In the case of the 1095 shRNA construct, cells had lost the stress fibres associated with this time point. Instead, they displayed a perturbed F-actin cytoskeleton consisting of diffuse staining for F-actin (Figure 4.23 B). Cells transfected with the 2375 shRNA construct displayed seemingly reduced levels of F-actin as suggested by a weaker signal. These cells also displayed a less organised F-actin cytoskeleton compared to untransfected neighbours (Figure 4.23 C). Transfection with the 2635 shRNA construct also resulted in disruption of the F-actin cytoskeleton, with complete absence of stress fibres and F-actin distributing in a punctate manner throughout cells (Figure 4.23 D). The different effects produced by the three constructs may have reflected different degrees of FHOD1 knockdown. However, we were unable to confirm knockdown of endogenous FHOD1 in C2C12 cells at the mRNA transcript or the protein level, therefore the differences between the constructs could have indicated the presence of off-target effects (i.e. knockdown of another gene). Alternatively, the construct-specific effects may have been due to transfection toxicity. While staining for DAPI did not reveal fragmented nuclei, and therefore suggested against the possibility of cell toxicity by potentially ruling out apoptosis, the performance of cytotoxicity assays by other methods (e.g. TUNEL or caspase-3 staining) might better resolve this issue,

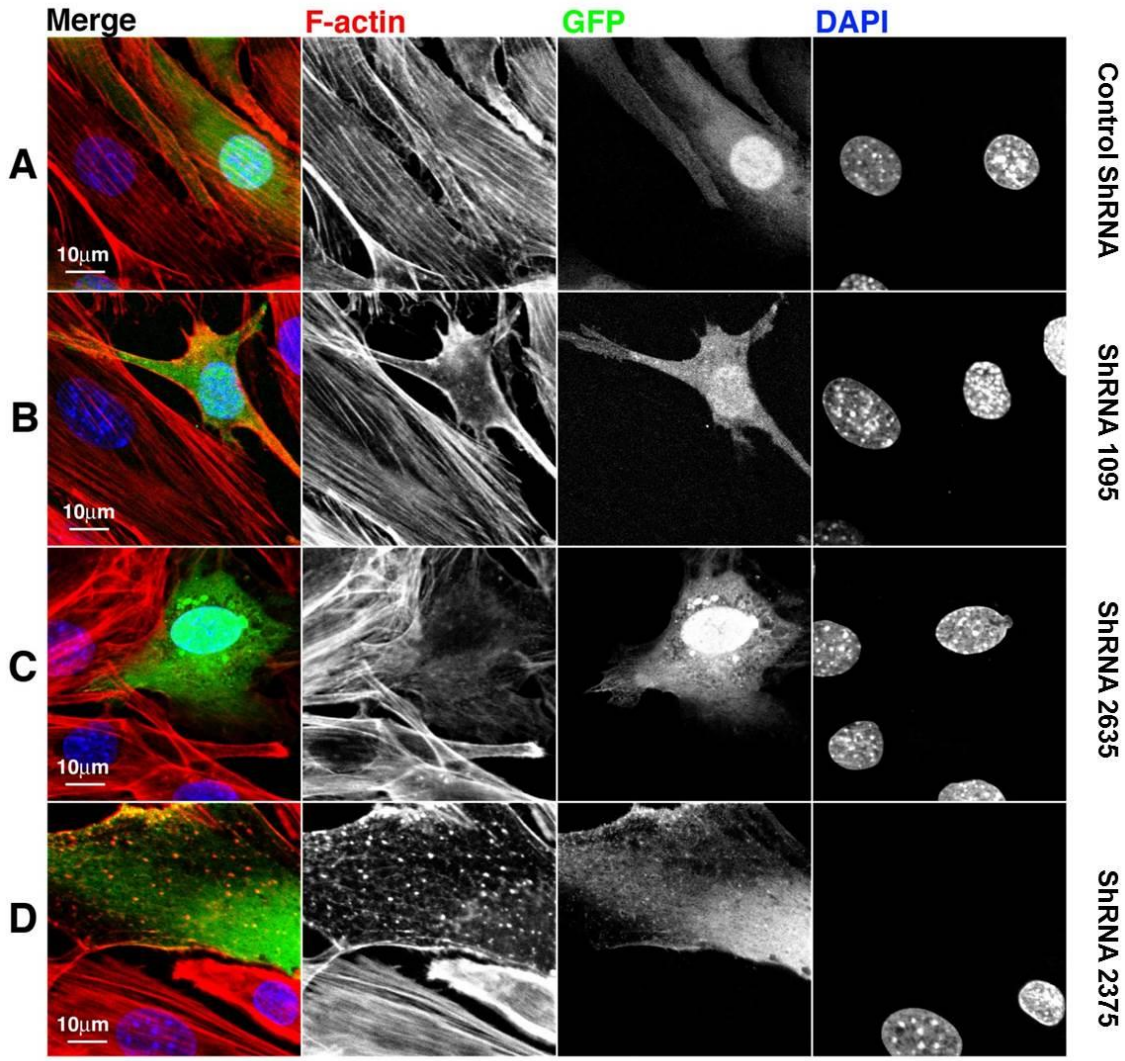

Figure 4.23: The Effects of the FHOD1 shRNAs in Day 3 C2C12 Cells. C2C12 cells were transfected with the three shRNA constructs designed to knockdown FHOD1. C2C12 cells were cultured until day 3 in differentiation medium, stained for F-actin, and were visualised by confocal microscopy. Transfected cells are seen in green since the shRNA vector separately expresses GFP. C2C12 cells were transfected with the following constructs: **A)** the empty shRNA vector, **B)** the 1095 shRNA construct, **C)** the 2375 shRNA construct, **D)** the 2635 shRNA construct. GFP is seen in green, F-actin in red, and DAPI/nuclei in blue. GFP, green fluorescent protein. Scale bars represent 10μm. **N=2.**

The effects of the shRNA constructs designed to knock down endogenous FHOD1 were also examined in day 7 differentiating C2C12 cells (Figure 4.24). Control cells, transfected with the empty shRNA vector, had a normal elongated morphology and were present as multi-nucleate myotubes (Figure 4.24 A). shRNA-transfected myotubes were indistinguishable from control cells and untransfected neighbours (Figure 4.24 B-D). We also looked to see if there were alterations in the rates of myoblast cell fusion into myotubes. A fusion index was calculated for cells transfected with the shRNA constructs and the empty vector (Figure 4.25) by taking the number of nuclei in the transfected cells and dividing it by the total number of transfected cells. This essentially calculated the number of nuclei per cell. The average cell fusion index was comparable across the constructs and the control vector. However, substantial variability in fusion indices was noted with the FHOD1 shRNA constructs and may have indicated that further experiments were required in order to see if they had an impact on C2C12 fusion. Overall, results with the FHOD1 shRNAs suggested there was no disruption of the F-actin cytoskeleton, morphological ultrastructure, or the cell fusion index in day 7 shRNA transfected C2C12 cells. However, as was the case with day 3 C2C12 cells, confirmation of reduced FHOD1 expression was not performed in day 7 C2C12 cells. The lack of treatment effect at this time point could therefore have been the result of a lack of knockdown. It may also be due to a dilution of the plasmid following the fusion of the myoblasts to myotubes and thus a decreased efficacy.

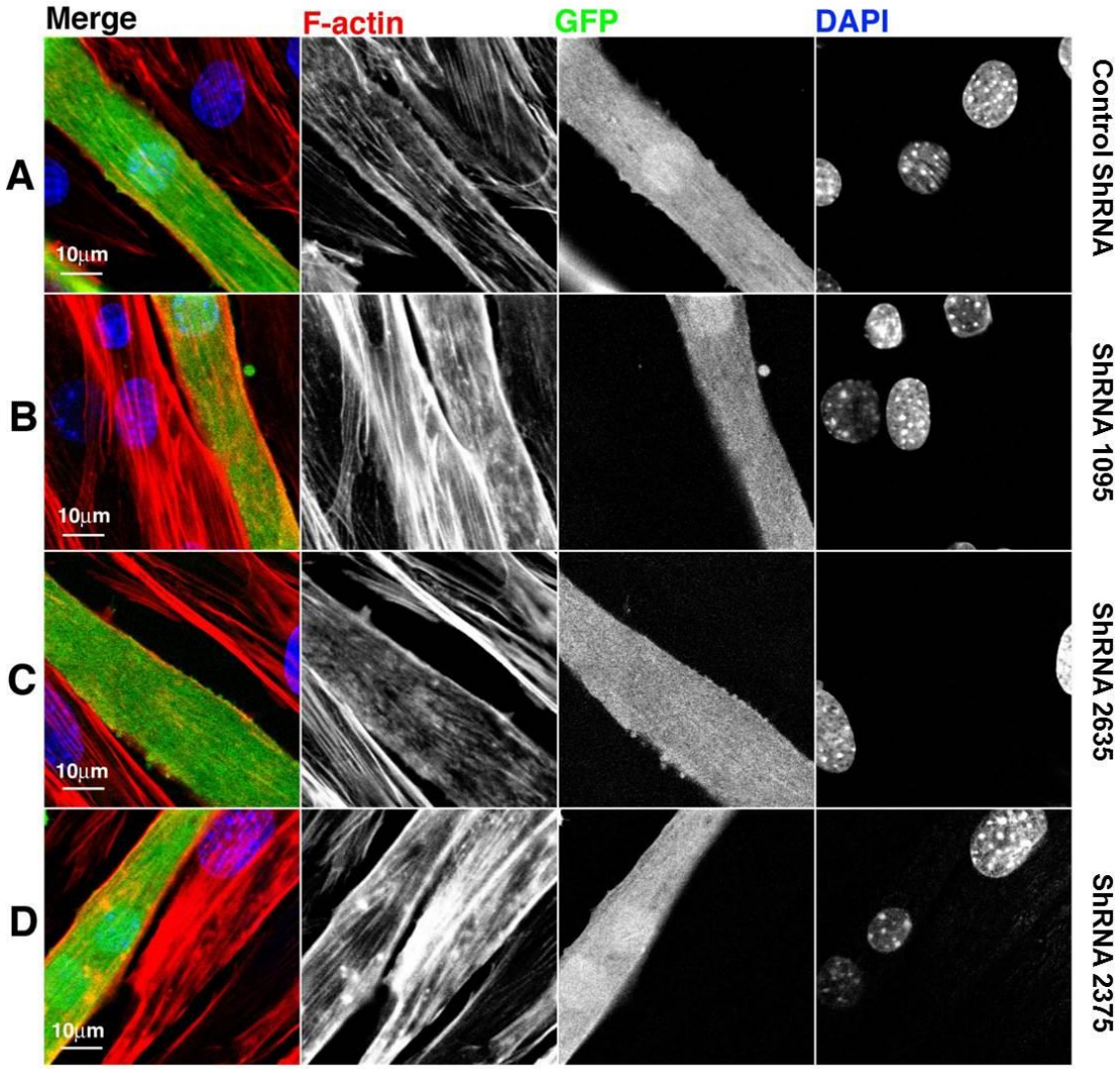

Figure 4.24: The Effects of the FHOD1 shRNAs in Day 7 C2C12 Cells. C2C12 cells were transfected with the three different shRNA constructs designed to knockdown FHOD1. C2C12 cells were cultured until day 7 in differentiation medium, stained for F-actin, and visualised by confocal microscopy. Transfected cells are seen in green since the shRNA vector separately expresses GFP. C2C12 cells were transfected with the following constructs: **A)** the empty shRNA vector, **B)** the 1095 shRNA construct, **C)** the 2375 shRNA construct, **D)** the 2635 shRNA construct. GFP is seen in green, F-actin in red, and DAPI/nuclei in blue. GFP, green fluorescent protein. Scale bars represent 10μm. **N=2.**

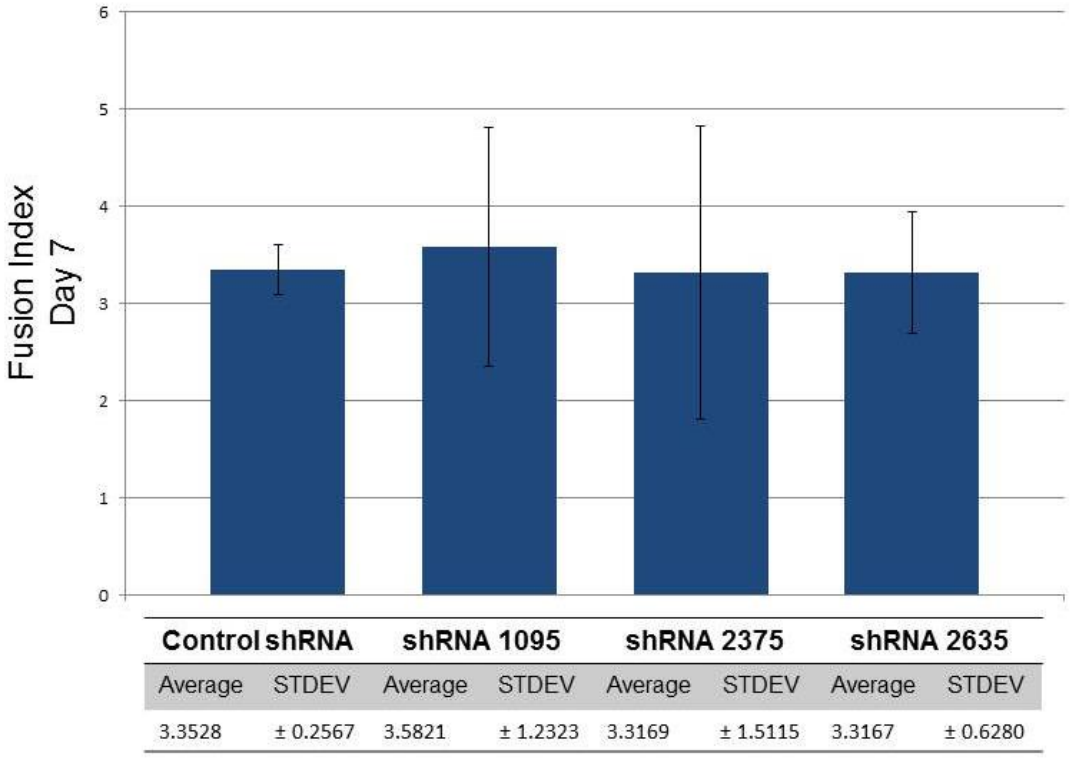

Control shRNA		shRNA 1095		shRNA 2375		shRNA 2635	
Average	STDEV	Average	STDEV	Average	STDEV	Average	STDEV
3.3528	± 0.2567	3.5821	± 1.2323	3.3169	± 1.5115	3.3167	± 0.6280

Figure 4.25: Fusion Index in Day 7 FHOD1 shRNA-transfected C2C12 Cells. Bar chart displaying fusion index values in day 7 C2C12 cells transfected with the different shRNA constructs. Cells were stained for DAPI to identify nuclei and were visualised by confocal microscopy for counting. The fusion index was calculated by counting the number of nuclei in transfected cells in one view and dividing that number by the amount of transfected cells. The fusion index represents an average of nuclei per cell. The first column on the left rep*-resents the value for the empty shRNA vector (H1 GFP). The three different shRNA constructs are shown in the following columns. Results represent average values for 70-100 cells for each construct. Error bars represent standard deviation (STDEV). **N=1.**

4.6 Treatment with the Formin Inhibitor SMIFH2

In order to more generally dissect the function of formins in the heart, NRCs were treated with a general formin inhibitor. SMIFH2, is an inhibitor of formin mediated actin assembly. It was found to inhibit actin polymerisation by formins at the level of nucleation, elongation, and association with the barbed end of filaments. The effects of the inhibitor have been attributed to its targeting the conserved FH2 domain, although binding by the small molecule has never been shown (Rizvi et al. 2009). Cells were treated with 30μM SMIFH2 for 2, 4, and 8 hours and then stained for a number of

myofibrillar proteins and subcellular markers to visualise the effects of formin inhibition.

The effects of formin inhibition on cardiomyocytes resulted in a number of cellular abnormalities. Treatment with the vehicle control, DMSO, had no effect on the appearance of NRCs during either of the time points (Figure 4.26 A and Figure 4.27 A), and therefore excluded any off-target effects of the vehicle. The effects of treatment with SMIFH2 could be seen after 2 hours (Figure 4.26 and 4.27). Affected cells had decreased staining for F-actin and Z-disk striations became less defined, as visualised by α-actinin staining. MyBP-C displayed somewhat weaker staining than DMSO-treated cells and was sometimes found to distribute in a diffuse cytoplasmic manner, although it was still predominantly found at the A-bands (Figure 4.26 B). Also at 2 hours, it was noted that myomesin staining was sometimes visualised as irregular in its spacing and patchy in its appearance. Staining for the intercalated disk protein, β-catenin revealed that there was a small degree of intercalated disk retraction, as cell-cell contacts appeared to be stretched (Figure 4.27 B). At 4 hours, the effects of the inhibitor intensified, with many cells presenting with myofibrillar disruption and weaker staining for F-actin and MyBP-C (Figure 4.26 C). Cell-cell contacts became even more stretched, suggesting further damage to the intercalated disk (Figure 4.27 C). At 8 hours, the myocardial cytoskeleton and myofibrils appeared to recover to an extent since α-actinin and MyBP-C redistributed in their characteristic striated pattern, although some diffuse cytoplasmic staining of MyBP-C was still noted. Many cells displayed numerous cell-cell contacts that were present as extended membrane protrusions, with an increased signal for α-actinin and F-actin at these sites (Figure 4.26 D). Whereas the effects of the inhibitor on myofibrils seemed to be transient, the effects on the intercalated disk appeared to be cumulative. By 8 hours, the intercalated disks appeared broader and more convoluted (Figure 4.27 D). Overall, inhibition of formin mediated actin regulation in NRCs resulted in a number of abnormalities at the level of myofibrillar maintenance and the intercalated disk.

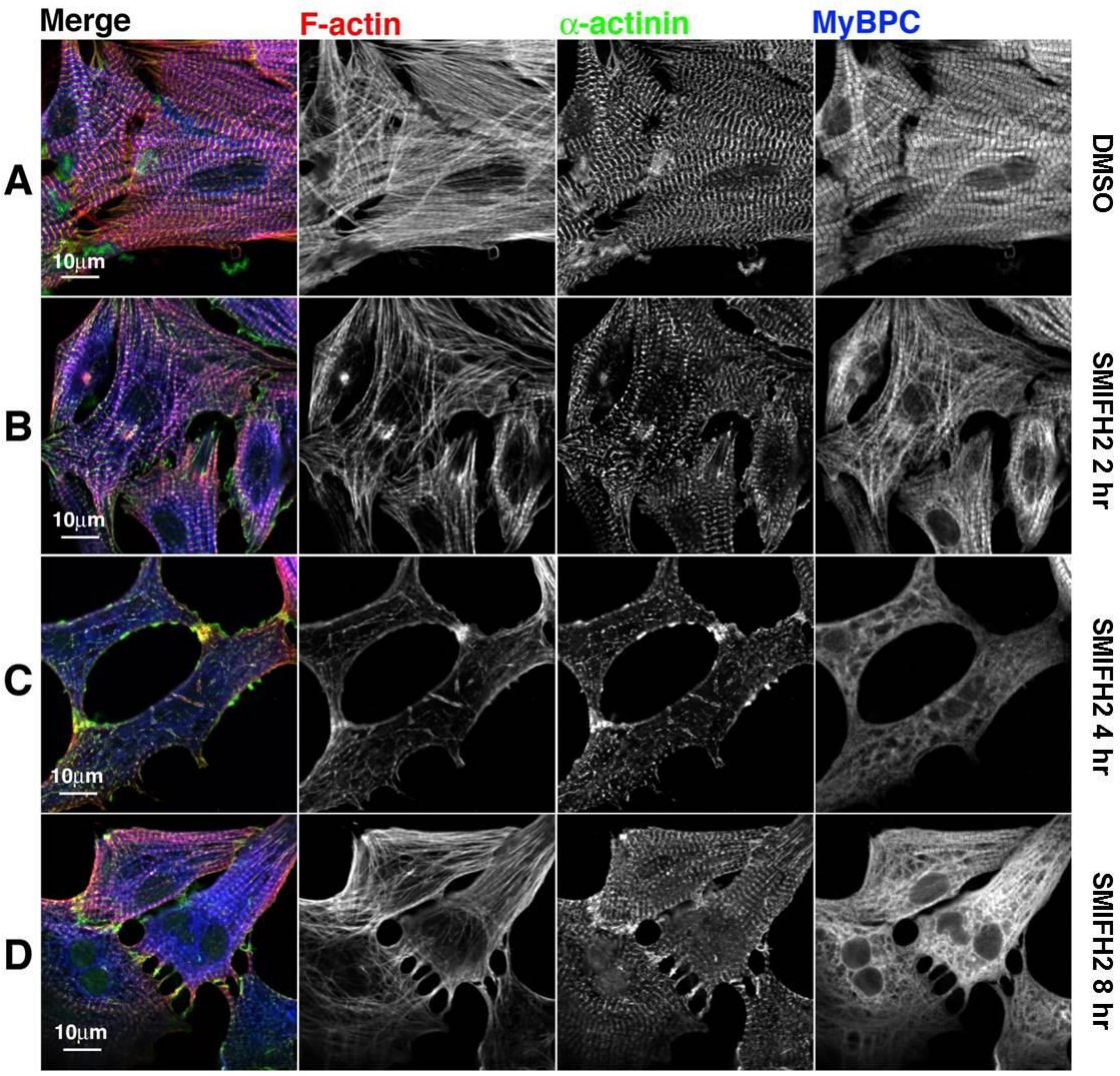

Figure 4.26: Effects of the Formin Inhibitor SMIFH2 on Myofibrils and the Sarcomere. Day 4 NRCs were cultured in maintenance medium prior to treatment with 30μM SMIFH2 or DMSO vehicle control. Cells were treated for 2, 4, and 8 hours and stained for α-actinin and MyBP-C prior to visualisation by confocal microscopy. Images represent: **A)** DMSO treated NRCs at 8 hours and SMIFH2 treated NRCs at **B)** 2, **C)** 4, and **D)** 8 hours. F-actin is seen in red, α-actinin in green, and MyBP-C in blue. NRC, neonatal rat cardiomyocytes; MyBP-C, myosin binding protein C. Scale bars represent 10μm. **N=2.**

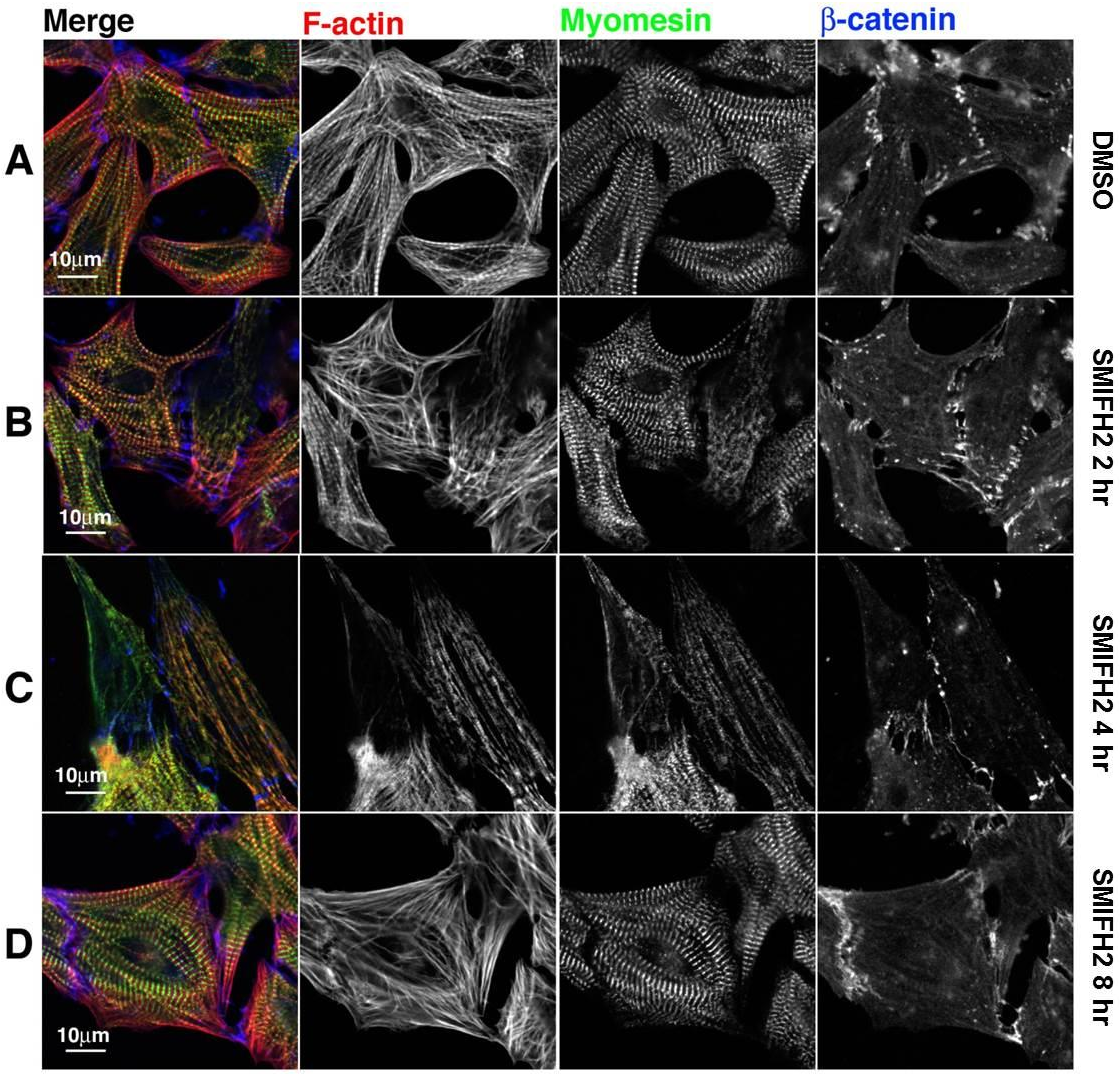

Figure 4.27: Effects of the Formin Inhibitor SMIFH2 on the M-band and the Intercalated Disk. Day 4 NRCs were cultured in maintenance medium prior to treatment with 30μM SMIFH2 or DMSO vehicle control. Cells were treated for 2, 4, and 8 hours and stained for myomesin and β-catenin prior to visualisation by confocal microscopy. Images represent: **A)** DMSO treated NRCs at 8 hours and SMIFH2 treated NRCs at **B)** 2, **C)** 4, and **D)** 8 hours. F-actin is seen in red, Myomesin in green, and β-catenin in blue. NRC, neonatal rat cardiomyocytes; MyBP-C, myosin binding protein C. Scale bars represent 10μm. **N=2.**

4.7 Discussion

4.7.1 Mapping the Functional Layout of FHOD1 in Cardiomyocytes

Presently, we explored the functional implications of FHOD1 overexpression by transiently expressing a number of inactive and constitutively active FHOD1 mutant constructs in NRCs. Overexpression studies using the different constitutively active FHOD1 mutants revealed that FHOD1 induced rearrangement of the F-actin cytoskeleton in NRCs. While all of the constitutively active mutant constructs induced cell elongation and F-actin rearrangement, they did so to varying degrees.

Overexpression of the FHOD1 3D ROCK phosphomimetic mutant induced an elongated cell phenotype. NRCs were shown to extend long processes. There was also some enrichment of FHOD1 and F-actin at the plasma membrane and along myofibrils, although not to the extent seen with the FHOD1 ΔDAD and V228E constructs. The FHOD1 3A construct, containing the kinase insensitive Alanine mutations, exhibited similar behaviour to the wild-type FHOD1 constructs when overexpressed in NRCs. The FHOD1 3A construct was found to accumulate in the peripheries of cells and did not result in any significant changes in cell morphology. This finding would be consistent with previous work indicating that phosphorylation of the Serine and Threonine residues in the FHOD1 DAD relieves the autoinhibitory interaction between the FHOD1 N-terminus and C-terminus (Takeya et al. 2008). GST pull-down assays between the FHOD1 N-terminus and a DAD fragment containing the triple Aspartate mutations abrogated binding between these two regions, whereas the DAD containing the triple Alanine mutations had no effect. Work exploring the functional effects of ROCK phosphorylation on FHOD1 had previously noted the formation of stress fibres and an elongated phenotype in HeLa cells (Takeya et al. 2008). The FHOD1 3D construct was also previously found to stimulate expression of vascular smooth muscle cell (VSMC)-specific genes to a greater capacity than the full-length construct (Staus et al. 2011a). Furthermore, this was attributed to FHOD1's capacity to regulate F-actin, since treatment with Latrunculin B inhibited the capacity of the FHOD1 3D construct to stimulate SM22 promoter activity.

The FHOD1 ΔDAD truncation mutant also induced cell elongation and displayed strong targeting to newly formed actin bundles. Studies first using FHOD1 C-terminal truncation mutants observed formation of stress fibres in NIH3T3 (Gasteier et al. 2003; Gasteier et al. 2005) and WM35 cells (Koka et al. 2003). Cell elongation and stress fibre formation was also induced in a similar manner to that seen with mDia by overexpressing a C-terminal truncation mutant in HeLa cells (Takeya and Sumimoto 2003). Overexpression of the FHOD1 V228E mutant had the most profound effect on the morphology of NRCs, which displayed an elongated appearance and thick stress fibres oriented along the long axis of the cell. The Valine at position 228 in the FHOD1 DID was previously found to be a crucial residue mediating the autoinhibitory interaction between the DID and DAD of FHOD1. When this mutant variant (FHOD1 V228E) was overexpressed in NIH3T3 cells it led to the formation of stress fibres in a similar manner to a C-terminal truncation mutant (Schulte et al. 2008). The differences between the FHOD1 ΔDAD and FHOD1 V228E constructs in NRCs could be explained by the fact that FHOD1 may have required the DAD for its biological activity.

While the FHOD1 ΔDAD and FHOD1 V228E mutants were associated with the appearance of actin bundles and stress fibres, respectively, we did not note the appearance of such structures with the FHOD1 3D construct. This may indicate that other cues beside phosphorylation in the DAD are needed for full activation of the protein to occur in NRCs. Indeed, previous comparison of the FHOD1 3D and the FHOD1 ΔDAD mutant revealed that the FHOD1 3D mutant did not stimulate VSMC-specific transcription as strongly (Staus et al. 2011a). Therefore, phosphorylation in the FHOD1 DAD might not represent a reliable marker of full FHOD1 activation.

Overall, overexpression data in NRCs would be in line with previous observations of FHOD1 activation inducing cell elongation (Koka et al. 2003; Takeya and Sumimoto 2003). More importantly, our findings are in agreement with the notion that FHOD1 has the capacity to reorganise F-actin into different structures, namely bundle them into stress fibres (Schonichen et al. 2013). Similar reorganisation of the F-actin cytoskeleton was also noted after overexpression of different FHOD3 mutants in cardiomyocytes. An FHOD3 3D ROCK phosphomimetic mutant and an FHOD3 ΔDAD truncation mutant were overexpressed in NRCs and led to the formation of small actin bundles

(referred to as actin cables) (Iskratsch et al. 2013a). Although the effects of overexpression of the FHOD3 active mutants were not as profound as those produced by FHOD1, FHOD3 was found to increase staining for F-actin in FHOD3 overexpressing NRCs (Iskratsch et al. 2013a), a possible indicator that F-actin assembly was increased.

However, the present study attempted to extrapolate the function of human FHOD1 constructs in rat cardiomyocytes, therefore the relevance of such experiments remains to be determined until similar experiments are performed with constitutively active rat FHOD1 constructs. While the human and rat FHOD1 variants bear high sequence similarity, comparison with constitutively active rat FHOD1 in NRCs will be necessary to establish whether the effects of human FHOD1 are conserved in NRCs or whether the present findings only represent an artefact of ectopically overexpressing a human protein in its non-native environment.

While the functional implications of ΔDAD truncation and the equivalent V228E mutation have not been explored with the rodent FHOD1 variants, phosphorylation in the DAD could be a common feature between human and rodent FHOD1. Indeed, the Serine and Threonine residues that are associated with phosphorylation by ROCK are conserved between human and rodent FHOD1. The antibody that recognises the phosphorylated Threonine1141 antibody on human FHOD1 was used to stain mouse heart sections and revealed similar staining to that seen previously with the antibodies designed to recognise total FHOD1. A strong signal for phosphorylated FHOD1 was noted at the intercalated disks as well as some myofibrillar and possible Z-disk localisation. The similarity in staining between phosphorylated and total FHOD1 could be taken as an indicator that the previously noted localisation of endogenous FHOD1 may be representative of its activated or partially activated state. Co-staining of total and phosphorylated FHOD1 would be required to confirm this. However, the full-length wild-type FHOD1 construct, which did not result in overt effects on NRC morphology, was recognised by the anti-FHOD1 phospho-Threonine1141 antibody in NRCs, suggesting that phosphorylation of the construct was present. While these observations could be explained by incomplete phosphorylation of all three of the relevant residues in the DAD, it could be indicative that further cues are required for full activation of

FHOD1 to occur. The full extent of phosphorylation in the FHOD1 DAD in mouse sections also needs clarification: the other two Serine residues in cells may not have been phosphorylated. Therefore the relevance of phosphorylated FHOD1 *in situ* remains to be explored.

While validation experiments using the FHOD1 3A and FHOD1 ΔDAD constructs indicated that the antibody specifically recognised the phosphorylated residue in the FHOD1 DAD, we were not able to definitively rule out cross-reactivity with FHOD3 or other proteins. Western blot studies and immunofluorescence studies in COS-1 suggested minimal levels of cross-reactivity. However, the extent of phosphorylation of the FHOD3 construct in COS-1 cells was not determined; therefore it cannot be excluded that there is some cross-reactivity between the phospho-Threonine1141 antibody and FHOD3. Indeed, cross-reactivity with FHOD3 in this instance may have been a possibility since the ROCK-I phosphorylation consensus motif is highly conserved between FHOD1 and FHOD3 (Iskratsch et al. 2013a) and because total FHOD3 has been noted to exhibit a similar localisation pattern in wild-type C57/BL6 mice (Iskratsch et al. 2010). In the absence of an antigen competition assay, it was also not possible to rule out cross-reactivity with other proteins.

4.7.2 The F-actin Regulatory Activity of FHOD1

Work in HeLa cells provided further insight into the potential actin regulating activity of FHOD1 by examining the effects of different FHOD1 constructs. While all studies, including the current one, support the idea that FHOD1 stimulates the formation of F-actin bundles and stress fibres, it has been debated as to whether this is merely due to the ability of FHOD1 to reorganise F-actin or to polymerise it as well. We attempted to quantify changes in Phalloidin pixel intensity in FHOD1-overexpressing HeLa cells in order to further dissect the protein's F-actin regulatory activity. Results suggested that FHOD1 increased staining for F-actin. The long and short GFP-tagged wild-type FHOD1 variants were able to increase levels of F-actin above the levels produced by the empty vector in a manner reminiscent of the full-length wild-type FHOD3 long and short variants in HeLa cells (Iskratsch et al. 2010). As expected, the localisations of the full-length inactive constructs were predominantly diffuse and cytoplasmic and they did

induce the formation of stress fibres or other actin-based structures. The TOMATO-tagged long FHOD1 variant may have displayed the capacity to increase F-actin staining above the GFP-tagged full-length FHOD1 variants, although its response was substantially variable. Overall, HeLa cells transfected with TOMATO-tagged FHOD1 displayed some degree of stress fibre formation and this may have been explained by partial activation of the construct due to the large size of the TOMATO tag. This phenomenon regarding the TOMATO tag was observed earlier in NRCs and may have indicated that this construct was not suitable for studies looking at the function or targeting of full-length wild-type FHOD1.

Examination of the effects of the FHOD1 FH2 domain in HeLa cells revealed no discernible effect on the F-actin content of cells. This was in contrast to a study which looked at the FH2 domain of mDia1, which was overexpressed in NIH3T3 cells and was enough to promote accumulation of F-actin (Copeland and Treisman 2002). However, previous reports suggested that FHOD1 caps actin filaments via its FH2 domain (Schonichen et al. 2013). While the FH2 domain of mDia induced actin polymerisation in *in vitro* pyrene assays, constitutively active FHOD1 FH2-domain containing constructs inhibited actin polymerisation, suggesting a capping activity for FHOD1. Presently, the FH2 domain distributed throughout cells as small blebs. This may have been indicative of the ability of the FHOD1 FH2 domain to self-associate (Takeya and Sumimoto 2003) hence concentrate as blebs within the cytoplasm of cells or may have just reflected the inactive nature of the construct in HeLa cells. The functional contribution of the FH2 domain to F-actin content *in cyto* remains to be determined using FHOD1 constructs lacking the FH2 domain.

Overexpression of the constitutively active FHOD1 variants suggested increases in F-actin staining greater than that seen with the GFP-tagged wild-type FHOD1 constructs in HeLa cells. Cells transfected with the constitutively active FHOD1 constructs were also associated with the appearance of more-prominent F-actin stress fibres. Furthermore, the constitutively active FHOD1 variants were found to partially co-localise with stress fibres, consistent with previous work performed in HeLa cells (Takeya and Sumimoto 2003; Gasteier et al. 2005). However, a discrepancy arose in this assay regarding the FHOD1 3A construct. FHOD1 3A-overexpressing HeLa cells displayed an increase in F-actin staining when compared to the full-length FHOD1

wild-type constructs. FHOD1 3A transfected cells were also associated with the appearance of stress fibres. This finding contrasted greatly to the effects of overexpression of the FHOD1 3A construct in NRCs. In NRCs, the FHOD1 3A construct behaved in a similar manner to the wild-type FHOD1 constructs: it accumulated in the peripheries of cells, did not co-localise with F-actin, and it did not result in changes in cell morphology. The present results are also in contrast to similar experiments performed with FHOD3. In HeLa cells, overexpression of the FHOD3 3D and 3A mutants resulted in similar F-actin staining as the wild-type FHOD3 construct (Iskratsch et al. 2010). However, the FHOD3 ΔDAD construct was associated with greater F-actin staining than the wild-type constructs. While the present results may suggest a divergence in function between FHOD1 and FHOD3, they raise questions as to what may be the most reliable marker of FHOD1 activation. However, these findings may stem from improper characterisation of the different FHOD1 constructs in HeLa cells; therefore, further experiments are required to determine if these construct-specific effects were extraneous occurrences or issues that merit further investigation.

In order to further investigate the activity of FHOD1, experiments were performed in primary cultures of cardiomyocytes to probe the involvement of FHOD1 in the regulation of thin filaments. We subjected FHOD1-overexpressing NRCs to Latrunculin B treatment. Latrunculin B treatment depolymerises all cellular F-actin and results in the disruption of the thin filaments of cardiomyocytes (McElhinny et al. 2005), which can subsequently recover their myofibrils after removal of Latrunculin B (Iskratsch et al. 2010). Overexpression of full-length FHOD1 and the constitutively active FHOD1 variants partially rescued the phenotype produced by Latrunculin B treatment, with FHOD1 transfected cells displaying a greater degree of myofibrillar integrity compared to GFP-transfected or untransfected cells. Interestingly, the GFP-tagged full-length wild-type variants of FHOD1 were associated with the greatest degree of myofibrillar integrity. Previously, overexpression of full-length FHOD3 in cardiomyocytes was also found to rescue the phenotype produced by Latrunculin B treatment (Iskratsch et al. 2010). The FHOD1 ΔDAD construct only exhibited an intermediate response in terms of myofibril recovery and this may have reflected the fact that the DAD could be required for the full biological activity of FHOD1. Whereas the remaining constitutively active FHOD1 constructs promoted thin filament recovery, they did so to a similar or

lower extent than that induced by the GFP-tagged wild-type FHOD1 constructs. Although further experiments are required for confirmation of this effect, the present data indicated that the promotion of myofibril integrity may have occurred irrespective of FHOD1's activation status.

While the present experiment may have indicated a role for FHOD1 in regulation of the cardiac thin filaments, it did not differentiate between FHOD1 promoting *de novo* myofibrillogenesis or preventing thin filament disassembly. Further studies will be required to investigate the mechanism by which FHOD1 exerts its effect on myofibrils in the context of Latrunculin B treatment with subsequent wash-out. Furthermore, the present methodology used to characterise the extent of myofibril integrity will likely require optimisation in order to dissect the effects of the different FHOD1 constructs in a more granular fashion. A more reliable approach to quantify the extent of myofibril integrity could involve counting of sarcomeres in NRCs. However, such an approach would create a bias towards measuring a response in the cells which were deemed to exhibit a higher degree of myofibrillar integrity after Latrunculin B treatment. A combination of the qualitative assessment presently employed and sarcomere counting may be able to further elucidate the effects of FHOD1's activation status on thin filament integrity after Latrunculin B treatment.

With the present experiments looking at FHOD1's actin regulatory activity in HeLa cells and NRCs in mind, the question remains: does FHOD1 merely reorganise F-actin into stress fibres or does it exhibit a degree of functionally relevant actin polymerisation? As discussed above, one line of thinking regarding FHOD1's actin regulatory activity is that it caps actin filaments via its dimeric FH2 domain, thus preventing both polymerisation and depolymerisation, whereas the region N-terminal to the FH1 is thought to be responsible for its bundling activity (Schonichen et al. 2013; Kühn and Geyer 2014; Schulze et al. 2014). However, other studies have suggested that the actin polymerising activity of FHOD1 may be central to some of its functions in cells. One study exploring the events following early adhesion formation in cells highlighted FHOD1 as a potential actin nucleation/elongation factor (Iskratsch et al. 2013b). Knockdown of FHOD1 in mouse embryonic fibroblasts (MEFs) on RGD-supported membranes was associated with reduced actin polymerisation from RGD-integrin clusters and reduced cluster growth. The notion that FHOD1 possesses

bundling activity was also supported in this study because FHOD1 was required for organisation of actin.

Other studies have suggested that FHOD1 displayed the capacity to polymerise actin *in cyto* (Watanabe et al. 1999; Gasteier et al. 2003; Koka et al. 2003; Gasteier et al. 2005). In one study using NIH3T3 cells, overexpression of wild-type FHOD1 did not result in an increase in F-actin staining, whereas a constitutively active FHOD1 construct lacking the C-terminus resulted in an approximate two-fold increase in F-actin staining (Gasteier et al. 2003). Regardless of the appearance of stress fibres, an increase in actin polymerisation was still claimed. Taken with the present data, it is conceivable that FHOD1 partly exhibits its effects in cells by polymerising actin. After activation, FHOD1 may associate with pre-existing actin filaments or may induce the formation of new filaments *de novo*. The association of FHOD1 and actin is reportedly increased after activation and this is likely due to direct binding. FHOD1 has been suggested to directly bind actin via a number of biochemical experiments. HA-tagged full-length FHOD1 was shown to co-immunoprecipitate with G-actin (Koka et al. 2003) and the actin binding portion of FHOD1 was subsequently mapped to the N-terminus of the protein, since an N-terminal FHOD1 construct was shown to bind F-actin in co-sedimentation assays (Takeya and Sumimoto 2003). The current findings supported the data from previous studies since co-localisation between FHOD1 and F-actin may have increased after activation of this formin in both cardiomyocytes and HeLa cells. Nevertheless, co-localisation does not necessarily equate to association between two proteins. This issue would require clarification through the implementation of actin binding deficient FHOD1 constructs, one possible example being an FHOD1 construct lacking the FH2 domain.

4.7.3 Loss-of-Function Studies in Muscle Cells

The role of FHOD1 in striated muscle was further investigated by performing a number of loss-of-function studies. Three shRNAs were designed to knock down FHOD1 in rodent cells. In cultured cardiomyocytes, transfection with the shRNA constructs resulted in disruption of myofibrils. Transfected NRCs were either completely devoid of myofibrils or presented with truncated myofibrils. Those myofibrils that were

present were also misaligned. Cells were characterised by reduced staining for F-actin and irregular distribution of other sarcomeric proteins such as α-actinin, MyBP-C, and myomesin. shRNA-transfected cardiomyocytes also exhibited a distorted morphology as they presented with an irregular plasma membrane edge, perhaps indicating disruption of the plasma membrane cytoskeleton. Interestingly, transfection with the shRNA constructs designed to knock down endogenous FHOD1 also resulted in perturbation of the intercalated disks. Under these circumstances, these specialised junctions between cells were reduced to multiple thin projections. It was also apparent that the distribution of β-catenin had been altered. Instead of distributing along the intercalated disk, β-catenin had become mislocalised and redistributed within the cytoplasm in a punctate or diffuse manner, although some β-catenin staining was still present at cell-cell contacts. This was somewhat reminiscent of what had been previously noted in NRCs depleted of emerin, another cytoskeletal regulator. Knockdown of emerin in NRCs led to mislocalisation of β-catenin, which redistributed to sites that did not participate in cell-cell adhesion (Wheeler et al. 2010). Similar perturbation of cell-cell junctions were also seen in embryonic cardiomyocytes isolated from mice that had undergone targeted disruption of the formin Dishevelled-associated activator of morphogenesis 1 (DAAM-1). DAAM-1 depleted cardiomyocytes displayed aberrant adherens junctions with prominent plaques and misalignment along the plasma membrane. Furthermore, α-catenin and N-cadherin became mislocalised from the plasma membrane, despite normal levels of expression (Li et al. 2011).

Transfection of the shRNA constructs designed to knock down endogenous FHOD1 in C2C12 cells also resulted in cytoskeletal abnormalities. In a manner similar to NRCs, Day 3 C2C12 cells transfected with the FHOD1 shRNA constructs displayed what seemed to be a reduction in staining for F-actin. Control cells and untransfected neighbours had an elongated appearance with numerous stress fibres whereas shRNA-transfected cells presented with an irregular morphology and disrupted F-actin cytoskeleton. Interestingly, there were no cellular defects associated with shRNA constructs in later time points of C2C12 differentiation as determined by cellular morphology and calculation of the cell fusion index. If FHOD1 depletion was indeed achieved in cells, perhaps FHOD1 is crucial in day 3 C2C12 cells for the formation and/or alignment of stress fibres. Any cytoskeletal defects in day 7 cells may have also

been compensated for by other actin regulatory proteins. Overall, previous work exploring knockdown of FHOD1 would be in excellent agreement with the above findings. Knockdown of FHOD1 blocked the formation of stress fibres in in Human Pulmonary Artery Endothelial Cells (HPAEC) (Takeya et al. 2008) and smooth muscle cells (Staus et al. 2011a). Knockdown of FHOD1 was also associated with altered levels of G-actin to F-actin, suggesting decreased levels of F-actin hence, possibly less actin polymerisation or stabilisation of F-actin filaments (Staus et al. 2011a). Furthermore, silencing of FHOD1 in breast cancer cells also led to a loss of stress fibres, less cell elongation, and a diminished metastatic potential (Jurmeister et al. 2012).

Although we presently report phenotypes associated with the shRNA constructs designed to knock down endogenous FHOD1 in rodent cells, we were not able to definitively show that this was the result of FHOD1 depletion. The differences between the shRNA constructs also raises doubt as to the specificity of the RNAi approach used, although these may have been due to varying degrees of FHOD1 knockdown. The time point-specific effects of the shRNA constructs in different cell types is also an issue that requires elucidation. While we noted a phenotype associated with the shRNA constructs at day 8 in NRCs, a phenotype was only seen in C2C12 cells at day 3 and not at day 7. There is the possibility that the amounts of available shRNA construct were diluted when the transfected C2C12 myoblasts fused with untransfected C2C12 myoblasts to myotubes. While we did not see dramatic differences in the GFP intensity between d3 and d7 C2C12 cells, this is not a quantitative way to assess availability of shRNA. If the effects were indeed due to FHOD1 disruption, they may reflect differences in turnover of FHOD1 in cardiac versus skeletal muscle or due to differences in maturation status. NRCs possess mature myofibrils at the time of isolation and it was shown previously that the dynamics of actin and its associated proteins is much lower in mature myofibrils than in assembling premyofibrils (Wang et al. 2014). Recently fused C2C12 myotubes are only starting to assemble their myofibrils (i.e. at premyofibril stage) and a more mobile actin cytoskeleton can be expected. Closer investigations on the time course of expression and localisation of FHOD1 in differentiating C2C12 cells, potentially accompanied by FRAP experiments to assess protein dynamics will be required before conclusions of an effect of the shRNAs can be drawn.

Although we demonstrated the capacity of the 2375 construct to disrupt expression of the human FHOD1 construct in COS-1 cells, this does not substitute for verification of FHOD1 knockdown at the transcript and protein level with all three shRNA constructs in NRCs and C2C12 cells. While we noted a decreased signal for FHOD1 with the polyclonal mouse anti-FHOD1 antibody in NRCs transfected with the shRNAs, this was not sufficient to confirm knockdown of FHOD1 since the extent of potential cross-reactivity against other proteins with the antibody has not been explored via antigen competition assays. Furthermore, we could not definitively confirm the presence of FHOD1 protein at the different time points due to improper characterisation of the anti-FHOD1 antibodies. In the case of the 1095 shRNA construct in NRCs, however, the phenotype associated with this construct was apparently rescued by overexpression of TOMATO-tagged FHOD1, which was theoretically resistant to the effects of this shRNA construct. This could be perceived as evidence that the construct's effect was due to FHOD1 depletion. However, the possibility of off-target effects with the present methodology remains.

If the effects of the FHOD1 shRNA constructs were indeed due to disruption of endogenous FHOD1, could they have been attributed to reductions in actin polymerisation? In the present functional characterisation of FHOD1, we highlighted the possibility of this protein's involvement in influencing the integrity of thin filaments, reorganisation of the myocardial cytoskeleton in NRCs, as well as the possible induction of accumulation of F-actin in the form of stress fibres in HeLa cells. Transfection of muscle cells with the FHOD1 shRNA constructs resulted in visibly less staining for F-actin and disruption of myofibrils and the cytoskeleton, possibly indicating that the actin polymerisation activity of FHOD1 may have been required for the maintenance of these structures. Previous work with FHOD3 indicated that its effects in cardiomyocytes (i.e. myofibrillar maintenance and sarcomere organisation) were partly mediated by its actin polymerisation activity since an actin binding defective variant of FHOD3 was unable to promote sarcomere organisation (Taniguchi et al. 2009). The requirement for FHOD1 in myofibrillar and cytoskeletal maintenance could therefore have been explained by the actin polymerising ability of this formin. Nevertheless, the reported capping activity of these formins *in vitro* (Taniguchi et al. 2009; Schonichen et al. 2013) would argue against a polymerisation mechanism and the well-characterised bundling activities of FHOD1 (Schonichen et al. 2013; Schulze et al.

2014) could mean that the present results may be explained by its ability to regulate the organisation of actin-based structures.

However, we cannot rule out the previously reported role of FHOD1 in mediating gene expression. FHOD1 has been implicated in signalling gene expression to the serum response element (SRE) via serum response factor (SRF) binding to the skeletal actin promoter (Boehm et al. 2005), factors which are also important in skeletal muscle differentiation (Kim et al. 2009) and the maintenance of the myofibrillar apparatus in cardiomyocytes (Balza and Misra 2006). Studies in smooth muscle revealed that FHOD1 was involved in the regulation of differentiation and that high levels of expression were required to maintain the expression of smooth muscle marker proteins (Staus et al. 2011a): knockdown of FHOD1 was associated with attenuation of markers of VSMC differentiation, including skeletal actin (Staus et al. 2011a). In VSMCs, the involvement of FHOD1 in the differentiation process may have also involved its actin polymerising or stabilising activity, which regulated the translocation of myocardin-related transcription factor (MRTF) to the nucleus. Thus, FHOD1's actin regulatory activity and/or its capacity to stimulate gene expression could be factors accounting for the phenotype observed in muscle cells transfected with the shRNA constructs designed to knock down FHOD1,

If the observed phenotypes associated with the FHOD1 shRNA constructs were indeed due to FHOD1 depletion, the results from the current loss-of-function studies in cells would be in agreement with previous work looking at FHOD1 and other formins in muscle. In *Caenorhabditis elegans*, overexpression of mutant variants of FHOD1 and CYK-1 resulted in defects relating to the development of the contractile lattice in the body wall muscles (BWM) of larvae (Mi-Mi et al. 2012). Developing larvae overexpressing the mutant formin variants had smaller BWM compared to wild-type specimens. These regions also displayed decreased staining for F-actin. Sarcomere organisation was also adversely impacted in terms of the spacing and number of striations. These defects were also recapitulated by disrupting expression of endogenous FHOD1. Knockdown of FHOD3 in cultured cardiomyocytes has also resulted in a severe myofibrillar phenotype (Taniguchi et al. 2009; Iskratsch et al. 2010). Iskratsch et al. 2010 noted defects in myofibrils by day 5 of FHOD3 knockdown. At this time point, FHOD3 depleted NRCs presented with shortened myofibrils and fewer mature sarcomeres. By day 8, FHOD3 depletion resulted in exacerbation of the myofibrillar

phenotype (Iskratsch et al. 2010) and resembled that associated with the FHOD1 shRNA constructs. Overall, these data can be taken as evidence for formin homology proteins as crucial players in myofibrillar maintenance.

4.7.4 Involvement of Formins in Regulation of the Myofibrillar Apparatus

After having highlighted a potential role for FHOD1 in myofibrillar maintenance we aimed to further investigate the role of formins more generally in cardiomyocytes. SMIFH2 is an inhibitor of formin mediated actin assembly (Rizvi et al. 2009). It was found to inhibit actin polymerisation by formins at the level of nucleation, elongation, and association with the barbed ends of filaments. These effects were attributed to SMIFH2 targeting the conserved FH2 domain, although direct binding of the small molecule has never been shown. Moreover, it was shown to specifically inhibit formins and not any other actin polymerising proteins such as Arp2/3. In NIH-3T3 cells, treatment with SMIFH2 resulted in a reduction in the number of F-actin bundles and a reduction in the size of focal adhesion plaques (Rizvi et al. 2009). In MEFs, treatment with SMIFH2 resulted in impaired cell spreading similarly to that seen in FHOD1 depleted MEFs (Iskratsch et al. 2013b). Whereas the previous study demonstrated SMIFH2 to disrupt actin-based structures in yeast and cell lines, our study is the first to use the inhibitor in primary cells.

Consistent with its reported effects, SMIFH2 disrupted the myocardial actin cytoskeleton and sarcomeric organisation. In contrast to our RNAi experiments, membrane deformation was far less than that seen in shRNA transfected cells. Overall, inhibition of formin mediated actin assembly resulted in disruption of thin filaments and mislocalisation of sarcomeric proteins, which would be in agreement with previous studies that found that some formins are required for myofibrillar formation, maintenance, and organisation (Taniguchi et al. 2009; Iskratsch et al. 2010; Iskratsch and Ehler 2011; Li et al. 2011; Dwyer et al. 2012; Mi-Mi et al. 2012; Kan-o et al. 2012a). The effects of the inhibitor also seemed to be transient since cardiomyocytes exhibited a certain degree of recovery in terms of reintegration of their myofibrils. Reintegration of the cytoskeleton and sarcomere could partly be explained by the fact that there are other actin nucleators in muscle. One potential nucleator accounting for

reintegration of myofibrils during treatment with SMIFH2 could have been Leiomodin-2, an assembly factor competes with tropomodulin for binding at the pointed ends of thin filaments to promote elongation (Tsukada et al. 2010). N-WASP could also be another potential nucleator/elongator in striated muscle. N-WASP and nebulin were shown to form a complex at the Z-disk and contribute to the formation of unbranched actin filaments in response to IGF-1 stimulation in skeletal muscle cells (Takano et al. 2010), but whether their effects on thin filament assembly extend to cardiac muscle remains to be seen. The presence of other actin polymerising proteins such as leiomodin or N-WASP may have thus accounted for the transient effect seen with the formin inhibitor.

Treatment with the formin inhibitor seemed to have an irreversible impact on the intercalated disks. SMIFH2 seemed to have a cumulative effect on cell-cell junctions which became increasingly widened and convoluted. Could formins be indispensable in the integration of the F-actin network between neighbouring cells? Transfection of NRCs with the shRNA designed to knock down endogenous FHOD1 resulted in disruption of the intercalated disk in cultured cardiomyocytes and DAAM (Li et al. 2011) along with Formin1 (Zigmond 2004) were also found to be required for proper formation of adherens junctions. The potential localisation of FHOD1 and the confirmed localisation of FHOD3 (Iskratsch et al. 2010) at the intercalated disks in frozen sections of cardiomyocytes could also point to a role for formin homology proteins at this particular site in cardiomyocytes. It is likely that formins and other actin regulatory proteins are required in specific muscle subcellular compartments at different times; therefore it would be of interest to establish a spatio-temporal expression profile of each formin in striated muscle.

While the effects of treatment with SMIFH2 partly resonated with the findings seen in NRCs transfected with the FHOD1 shRNA constructs, they were very disparate to those noted with the FHOD1 3A construct. While the FHOD1 3A construct represents a kinase insensitive FHOD1 construct, this does not necessarily mean that it possesses a dominant-negative effect. In NRCs, the FHOD1 3A mutant behaved in a similar manner to the GFP-tagged wild-type FHOD1 constructs. Surprisingly, in HeLa cells, it became apparent that the FHOD3 3A construct was associated with the formation of stress fibres. However, it remains to be seen if this was an extraneous occurrence or if it is an

effect of the construct that is specific to HeLa cells. Overexpression studies with the FHOD1 constitutively active mutants in NRCs would also suggest that phosphorylation in the FHOD1 DAD may not necessarily be a full marker of activation. Furthermore, the different full-length FHOD1 constructs, including the FHOD1 3A construct, were able to promote myofibrillar integrity after Latrunculin B treatment and wash-out regardless of activation status. Previous *in vitro* work has also demonstrated how full-length, supposedly inactive FHOD1 can both cap and bind the sides of actin filaments (Schonichen et al. 2013). These factors could account for the disparity in the effects of the FHOD1 3A construct and the SMIFH2 inhibitor. However, the differences between FHOD1 3A and SMIFH2 could also suggest that different formins might make individual contributions to the maintenance of the cardiac cytoskeleton.

While both the presently and previously reported effects of the pan-formin inhibitor SMIFH2 are somewhat in line with the canonical role of formin proteins (i.e., regulation of F-actin), there are still a number of uncertainties regarding how it exerts its effects. While SMIFH2 is thought to inhibit formin mediated actin polymerisation by targeting the conserved FH2 domain, initial characterisation efforts have been limited to investigating only a handful of formins: mDia1, mDia2, and Cdc12 (Rizvi et al. 2009). Further characterisation of SMIFH2 will be required in order to establish if it indeed acts on all members of the formin family of proteins and whether its effects on individual formins occur at specific concentrations. It also remains to be seen if SMIFH2 disrupts the other reported abilities of formins, such as actin bundling, since experiments have been restricted to looking at its effects on actin polymerisation in *in vitro* assays. If SMIFH2 does indeed inhibit actin assembly by formins via their FH2 domain, one interesting experiment could involve treating constitutively active FHOD1-overexpressing NRCs with the inhibitor to begin and dissect the contribution of FHOD1's potential actin polymerising activity.

4.7.5 Conclusion

In summary, we attempted to gain insight into the functional relevance of FHOD1 with a mixture of gain-of-function and loss-of-function studies. Gain-of-function studies using constitutively active FHOD1 mutants suggested that this formin has the capacity to reorganise the F-actin cytoskeleton in cardiomyocytes, although the discrepancies

noted between the different constructs raised questions regarding the most-appropriate reporter of FHOD1 activation. Immunofluorescence samples of mouse heart sections stained with the antibody that recognises the phosphorylated Threonine-1141 residue on FHOD1 also may have indicated the localisation of endogenous FHOD1 may represent the formin in its active state, since near-identical staining was previously noted for endogenous FHOD1, although the full extent of phosphorylation could not be probed. However, in the absence of proper characterisation of the antibody, we were unable to rule out the possibility of cross-reactivity with other proteins, particularly FHOD3. We also attempted to highlight FHOD1's actin regulatory activity with experiments in HeLa cells with multiple constructs, although discrepancies arose relating to the FHOD1 3A construct and an overall high degree of variability. Experiments in NRCs which were subjected to depolymerisation of F-actin and their myofibrils suggested that FHOD1 possessed the capacity to confer myofibrillar integrity irrespective of its activation status. However, we were unable to differentiate between FHOD1 preventing depolymerisation and FHOD1 promoting *de novo* myofibrillogenesis. Loss-of-function experiments, by way of RNAi, revealed a phenotype in NRCs and C2C12 cells transfected with the shRNA constructs designed to knock down endogenous FHOD1. This phenotype was seemingly characterised by defects in myofibrillar and cytoskeletal maintenance. However, we were not able to definitively prove that this phenotype was due to FHOD1 depletion. Finally, treatment with the general formin inhibitor, SMIFH2, also resulted in perturbation of the myofibrillar apparatus and highlighted the potential importance of formin proteins in cardiac cells.

4.7.6 Future Directions

While overexpression of the constitutively active FHOD1 variants in NRCs may have provided some insight into the function of FHOD1, this was limited to the long variant of FHOD1, which contained the alternatively spliced exons 12-13. Similar experiments should be performed with the shorter variant of FHOD1 in order to probe the possibility of divergence in function between the different FHOD1 isoforms. Furthermore, the present overexpression experiments were performed in the presence of phenylephrine. Future studies examining the effects of constitutive activation of FHOD1 in NRCs should be performed in the presence and absence of hypertrophic stimuli, which could conceivably influence the function of the protein.

Staining for phosphorylated FHOD1 in mouse heart sections suggested a similar localisation pattern for phosphorylated FHOD1 and total FHOD1. However, we were not able to rule out cross-reactivity between the FHOD1 phospho-Threonine1141 antibody and other proteins, particularly FHOD3. Antigen competition assays using both phosphorylated C-terminal fragments of FHOD1 and FHOD3 will be required to assess the extent of cross-reactivity with this antibody.

While we reported a phenotype associated with cells transfected with the FHOD1 shRNA constructs, future work should make it a priority to confirm that this was indeed due to depletion of endogenous FHOD1. In the absence of a well-characterised antibody that has been shown to definitively detect endogenous FHOD1 in the cells used in this study, it was not possible to definitively confirm knockdown on a single cell basis. Furthermore, due to the low transfection efficiency in both NRCs and C2C12 cells, it was not possible to confirm knockdown at the mRNA transcript level by RT-PCR. This could potentially be addressed by implementing a virally mediated gene transduction approach in order to achieve higher efficiency of gene transfer into cells. Furthermore, the phenotype associated with the FHOD1 shRNAs will require further characterisation via quantification of the extent of myofibrillar and cytoskeletal disruption.

Since experiments using Latrunculin B in NRCs could not differentiate between FHOD1 preventing depolymerisation of myofibrils versus FHOD1 promoting *de novo* myofibrillogenesis, further experiments will be required. One approach could involve treating FHOD1-depleted cells with Latrunculin B with subsequent wash-out and myofibril recovery. Visualising the effects of FHOD1 overexpression in Latrunculin B-treated NRCs at different time points could also provide insight into how FHOD1 exerts its effects on myofibrils. It will also be of interest to see if the effects of FHOD1 can be substituted for by other formins, especially its closest relative FHOD3.

One caveat that applied to the experiments in HeLa cells related to the possibility that differences between the F-actin bundling activity and the potential actin polymerising activities of FHOD1 could not necessarily be dissected. Although an increase in total levels of F-actin would be suggestive of actin polymerisation, the more-concentrated staining for F-actin on resulting stress fibres may have offset measurements of the Phalloidin pixel intensity, therefore accurate measurements within the linear range of

intensity may not have been captured. Such experiments need to be complimented by biochemical analysis in order to see if total levels of F-actin or if the ratio of G-actin to F-actin was altered in cells. While this would be feasible in HeLa cells, which exhibited a greater transfection efficiency, subsequent studies attempting to measure the F-actin regulatory activity of FHOD1 in NRCs may require the use of virally mediated gene transduction in order to achieve higher efficacy of gene transfer for biochemical analysis to ensue.

Chapter 5

Regulation of FHOD1

5. Regulation of FHOD1

5.1 Regulation of FHOD1 by the Rho Family Small GTPases and their Effectors

Rho family small GTPases represent a subset of the Ras superfamily of GTP-dependent enzymes. Their ability to mediate cytoskeletal rearrangements and influence actin dynamics has been well documented (Hall 1998). The Rho family small GTPases play important roles in a number of processes requiring cell polarisation (Fukata et al. 2003) such as division (Yoshizaki et al. 2003), spreading (Price et al. 1998), migration (Ridley 2001), and adhesion (Braga 2002). Most studies concerning this family of enzymes have focused on characterisation of three of around 22 members, RhoA, Rac1, and Cdc42. The Rho GTPases regulate actin assembly via activation of the WASP proteins or the diaphanous related formins (DRFs) (Ridley 2006). Activation of WASP proteins stimulates actin polymerisation via the Arp2/3 complex (Zalevsky et al. 2001). Rho family GTPases are thought to activate formins by displacing the interaction between the N-terminal Diaphanous inhibitory domain (DID) and the C-terminal Diaphanous autoregulatory domain (DAD). The small GTPases are thought to bind the N-terminal GTPase binding domain (GBD) therefore causing steric displacement of the interaction between the two ends of a DRF, hence resulting in exposure of the actin polymerising FH2 domains (Tominaga et al. 2000). GTPases have been shown to regulate aspects of formin biology including activation and localisation. We explored the potential interactions between the N-terminus of FHOD1 and some of the Rho family small GTPases and their effector molecules by GST pull-down assays.

5.1.1 Validation of the N-Terminal GST-tagged FHOD1 Construct

The presently employed GST-tagged FHOD1 construct spanned from amino acids 1 to 513. This construct was comprised of the GBD, DID, and contained the linker region which stopped just short of the FH1 domain (Figure 5.1 A). The FH1 domain was not included as this represents a region with a different subset of already specified interactions, including profilin. The novel aspect about the FHOD1 construct used in the studies here is that it included the alternatively spliced exons 12 and 13, which were described to be mainly expressed in striated muscle (Tojo et al. 2003). Interactions between FHOD1 and the Rho family small GTPases were not yet studied in the context of the alternatively spliced exons found in the longer FHOD1 variant (exons 12-13). Prior to commencing the GST pull-down studies, levels of expression and the size of the GST-tagged FHOD1 N-terminal construct were checked by SDS-PAGE followed by Western blotting. The N-terminal fragment of FHOD1 without the GST tag had a predicted molecular weight of 55kDa (Figure 5.1 B).

Western blots probed with the anti-GST antibody revealed that the FHOD N-terminal construct was expressed at sufficient levels for biochemical experiments to be performed, although some degradation was present (Figure 5.1 C). Two prominent bands were resolved for the GST-tagged FHOD1 construct on SDS-PAGE gels: a larger species migrating beneath the 123kDa marker and a smaller species migrating around the 78kDa marker. The size of the smaller band was in agreement with the expected molecular weight of the GST-tagged FHOD1 construct (81 kDa) (Figure 5.1 B). One possible explanation behind the larger species could be that it was a product of protein oligomerisation; in this case a possible aggregate of the GST-tagged FHOD1 construct and a lighter peptide resulting from degradation. However, the denaturing conditions used for the SDS-PAGE make this highly unlikely. Alternatively, the unexplained band could have represented a contaminant in the protein preparation. The unwanted influence of another protein species would call into question the validity of any GST pull-down experiments performed. This would especially be the case in the context of a positive interaction; since it would not be clear which GST-tagged species was responsible for mediating the interaction. One method of validating the protein preparation in question would involve probing blots with an anti-FHOD1 antibody that

recognises the N-terminal region of the protein. Should the larger species prove not to be reactive to the anti-FHOD1 antibodies, one method of identifying it would be to excise the unidentified band, trypsinise it, and subject it to mass spectrometry. If the unidentified band did indeed represent a contaminating species, an extra purification step could be employed (e.g., size exclusion chromatography) in order to obtain the desired GST-tagged protein for biochemical assays. Nevertheless, GST pull down assays were performed using the protein preparations containing the multiple bands. Relative levels of loading between untagged GST protein and GST-tagged FHOD1 were visually gauged on gels and subsequently adjusted to reflect comparable levels of protein in GST pull-down assays (Figure 5.1 D)..

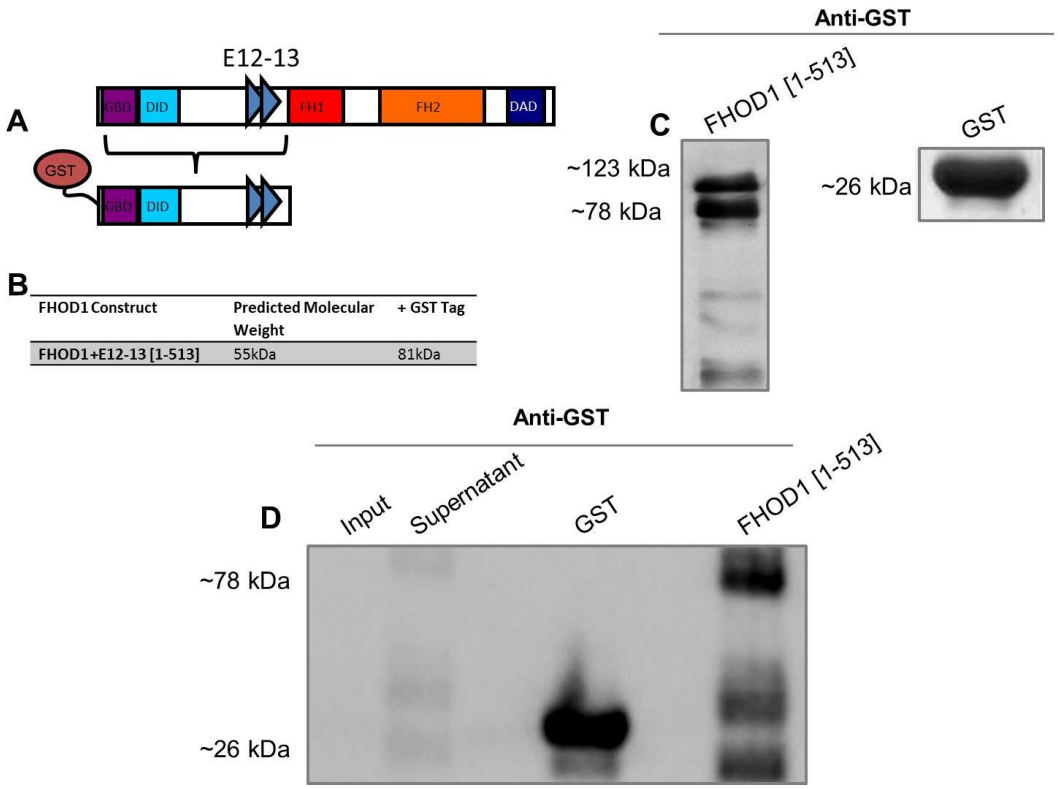

Figure 5.1: Expression Test for GST-FHOD1 [1-513]. **A)** The GST-tagged N-terminal fragment of FHOD1 spanning from amino acid 1 to 513 and containing the alternatively spliced exons 12-13 was presently employed for interaction studies since the potential interactions with the Rho family small GTPases and their effector molecules have never been studied in this context of the alternatively spliced exons. **B)** The N-terminal FHOD1 fragment had an expected molecular weight of 55kDa. Combined with the molecular weight of the GST tag (26kDa), the GST-tagged FHOD1 construct has an expected molecular weight of 81kDa. **C)** The GST-tagged FHOD1 construct and the GST tag alone were purified from bacterial lysates, resolved by SDS-PAGE, and visualised by enhanced chemiluminescence on Western blots incubated with the anti-GST antibody. This was performed to gauge the relative size and expression levels of the protein. **D)** Representative blot from GST pull-down assays that shows the relative loading of the GST tag in the negative control lanes and of the GST-tagged FHOD1 construct in the lanes testing for an interaction. Western blot was probed with the anti-GST antibody to visualise unmodified GST and the GST-tagged N-terminal FHOD1 fragment. GST, glutathione S-transferase. **N=2.**

5.1.2 Conditions used for GST Pull-Down Assays

For the GST pull-down assays the following buffer was used for lysis, washing, and incubation of the GST-tagged and target proteins: 150 mM NaCl, 20 mM Tris-HCl pH 7.6, 1 mM Ethylenediaminetetraacetic acid (EDTA), 0.2% (v/v) NP-40, 1 mM Dithiothreitol (DTT), and 1x protease inhibitor cocktail. The buffer used for GST pull-downs was designed to partly mimic the conditions within a cellular environment whilst

maximising yield and promoting stability of the extracted target proteins. Addition of 150 mM NaCl promoted an isotonic environment for cell lysis and corresponded to the ionic concentrations found in physiological conditions. Tris-HCl was added because it acts as a buffer that stabilises the pH within a narrow range. This is important because the lysis procedure can introduce rapid changes in pH, which could affect the stability of the target proteins. The 20mM Tris-HCl solution was titrated to pH 7.6, which is near to the intracellular cytosolic pH and should therefore have prevented pH dependent denaturation of the target proteins. EDTA, a metal chelator, was added to prevent oxidative damage of proteins and to prevent degradation by divalent cation dependent proteases. NP-40, a non-ionic and non-denaturing detergent, was added to improve solubilisation of cell membranes and improve lysis. We found that 0.2% (v/v) NP-40 was sufficient to promote lysis of cells as gauged by a sufficient yield of target protein. 1mM DTT, a reducing agent, was added to prevent oxidative damage of the proteins. The addition of protease inhibitors was necessary in order to prevent degradation of target proteins by proteases liberated/activated during lysis. The above buffer sufficed for isolation of all the target proteins, which were soluble and expressed to levels sufficient for biochemical experiments.

COS-1 cells were used as a means to overexpress the target proteins due to the poor transfection efficiency we obtained with neonatal rat cardiomyocytes (NRCs). The use of COS-1 cells represented a drawback to this study since proteins could undergo diverse post-translational modifications in different cell types. Therefore, the present binding assays are not entirely representative of what could occur in muscle cells. While overnight incubation at 4°C between the GST-tagged FHOD1 protein and target proteins was initially performed for all experiments, experiments yielding a positive interaction were repeated with an incubation time of 1 hr at 4°C in order to rule out the potential of non-specific binding. A temperature of 4°C was selected for experiments in order to reduce the possibility of protein degradation.

5.1.3 Assessment of Binding of FHOD1 with the Rho family small GTPases and their Effectors

In the current study we investigated the possibility of binding of the FHOD1 N-terminus with Rac1, Cdc42, and Rho associated protein kinase (ROCK) I and II. Rac1 is a member of the Rho family small GTPases (Ridley and Hall 1992b) and has previously been shown to interact with FHOD1. The FHOD1-Rac interaction has previously been mapped to the more C-terminal half of FHOD1, where the GBD was initially thought to lie (Gasteier et al. 2003). However, It has become apparent that like other DRFs, the GBD of FHOD1 lies in the N-terminus of the protein just upstream of the DID which questions the function of Rac binding in the FHOD1 C-terminus (Schulte et al. 2008). Nevertheless, Rac1 may contribute the targeting of FHOD1 in cells (Gasteier et al. 2003; Alvarez and Agaisse 2013).

Like the other GTPases, Cdc42 has been found to induce formation of membrane protrusions, namely filopodia (Nobes and Hall 1995). Although the interaction between Cdc42 and FHOD1 has not been thoroughly explored, it has been shown that Cdc42 is sometimes required for formin-mediated actin assembly. In the absence of Cdc42, formin-dependent actin cable formation was not properly executed in yeast (Dong et al. 2003). Previous work indicated that neither full length FHOD1 nor a C-terminal truncation mutant of FHOD1 bound Cdc42 in GST pull-down assay analysis (Gasteier et al. 2003).

ROCK-I is one of the major effector molecules that lies downstream the RhoA pathway (Ridley 2006). It has been shown that ROCK-I phosphorylates FHOD1 in the DAD to contribute to activation of this formin (Takeya et al. 2008). Yeast two-hybrid studies also suggested that ROCK-I interacts with the N-terminal part of the FH2 domain (Hannemann et al. 2008). ROCK-II, which is closely related to ROCK-I (65% amino acid similarity) (Riento et al. 2005), has not previously been linked to formin activity. Since regulation of FHOD1 by ROCK-I has been previously demonstrated, we also screened for the potential of an interaction between FHOD1 and ROCK-II.

While previous work has suggested that these effector molecules do not bind the FHOD1 N-terminus, they have not been studied in the context of the alternatively spliced exons 12-13 found on the long FHOD1 variant. Therefore we performed GST pull-down experiments with the FHOD1 construct described above. A pull-down with FLAG-tagged constitutively active Rac1 (Figure 5.2 A) was performed alongside a pull-down with constitutively active Rac1 and the PBD portion of PAK (Figure 5.2 B). The PBD portion of PAK has been shown to bind both active Rac1 and Cdc42 (Sells et al. 1997); this pull-down functioned as a positive control. Pull-downs were also performed with FLAG-tagged constitutively active Cdc42 (Figure 5.2 C), myc-tagged ROCK-I (Figure 5.3 A), and myc-tagged wild-type ROCK-II (Figure 5.3 B). The constitutively active Rac1 and Cdc42 constructs were created by mutating a Glycine residue at position 12 to a Valine (Ridley et al. 1992; Suzuki et al. 2000). The constitutively active ROCK-I Δ1 truncation mutant construct spanned amino acids 1-1080 (Chang et al. 2006).

The GST-tagged FHOD1 N-terminus was unable to pull down any of the currently addressed Rho family small GTPases (Figure 5.2) or ROCK-I and II (Figure 5.3) since there was no signal in the pellet portion for any of the pull-down assays. However, we could only conclude with some certainty that this was due to lack of binding in the case of Rac1, since a positive interaction in the control pull-down with PAK-PBD suggested optimised conditions for binding between FHOD1 and Rac1. The same cannot be said for the other proteins since no binding control was provided. Therefore, until positive binding controls are provided, the negative results seen in the pull-downs with Cdc42, ROCK-I, and ROCK-II cannot be concluded to hold any validity as they may have reflected lack of optimisation of binding conditions.

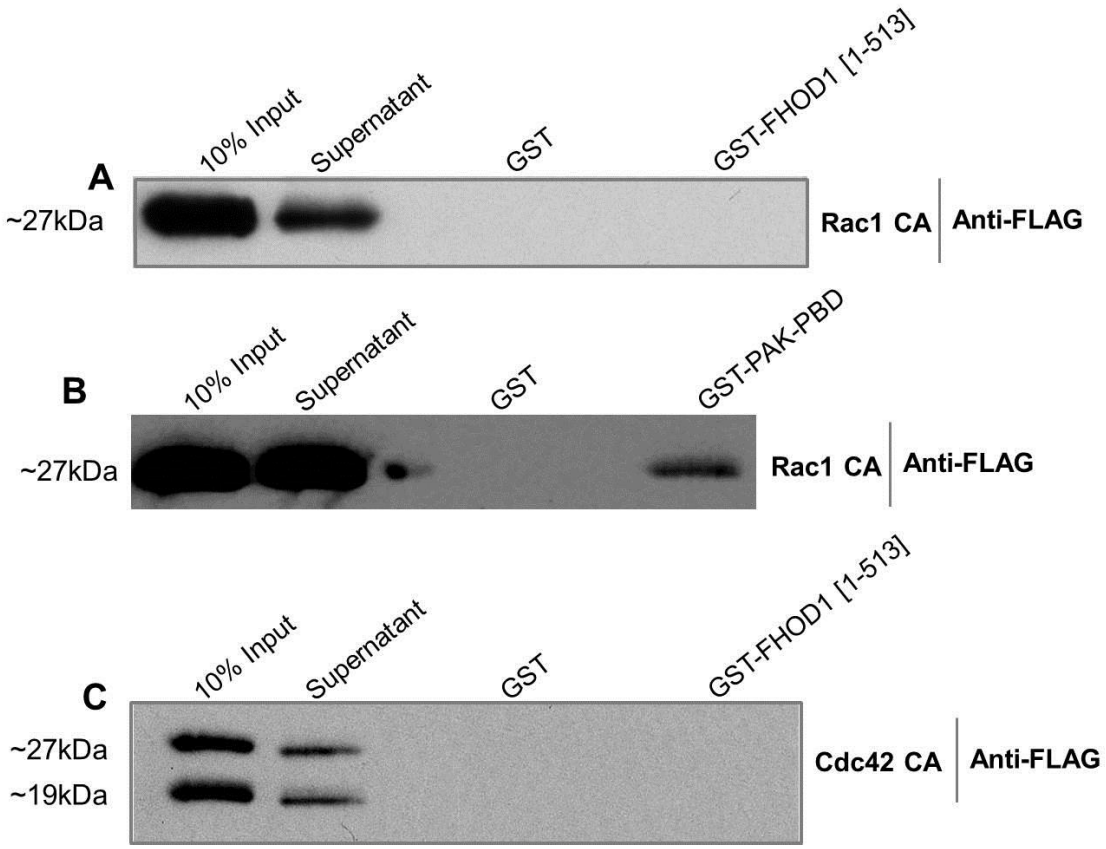

Figure 5.2: Assessing the Interaction between the FHOD1 N-terminus with Members of the Rho Family Small GTPases. Western blots depicting the results from GST pull-down assays. The GST tagged N-terminus of FHOD1 [1-513] was used to pull down FLAG-tagged constitutively active variants of **A)** Rac1 and **C)** Cdc42 from COS-1 cell lysates. Blots were probed with anti-FLAG antibody to visualise FLAG tagged constitutively active Rac1 and Cdc42. **B)** A positive control GST pull-down assay was performed for constitutively active Rac1. The GST-tagged PBD portion of PAK was used to pull down FLAG-tagged constitutively active Rac1 from COS-1 cell lysates. CA, constitutively active; GST, glutathione S-transferase. **N=2.**

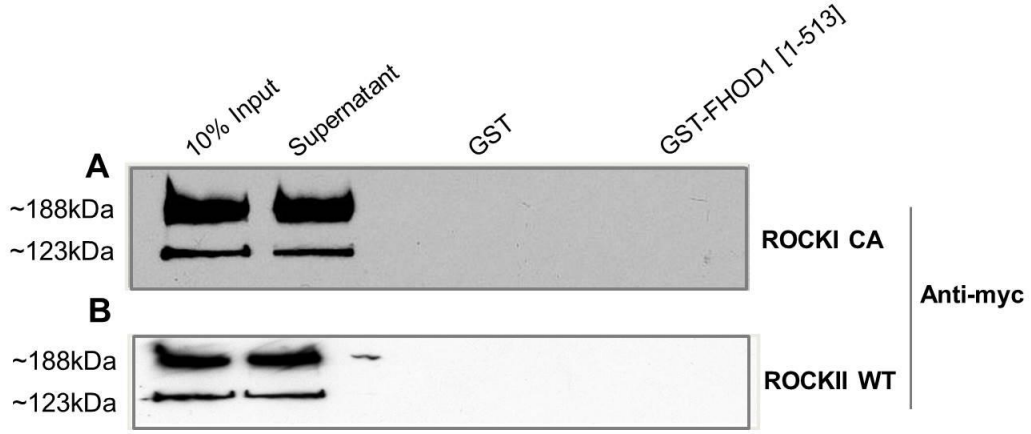

Figure 5.3: Assessing the Interaction between the FHOD1 N-terminus with Effectors of the Rho Family Small GTPases. Western blots depicting the results from GST pull-down assays. The GST tagged N-terminus of FHOD1 [1-513] was used to pull down myc-tagged constitutively active **A)** ROCK-I (ROCK-I Δ1) and **B)** wild type ROCK-II (full length) from COS-1 cell lysates. Blots were probed with anti-myc antibody to visualise myc-tagged constitutively active ROCK-I and wild type ROCK-II. CA, constitutively active; WT, wild type; GST, glutathione S-transferase. **N=2.**

5.2 Regulation of FHOD1 by Src Kinase

Src is a member of the Src family of non-receptor tyrosine kinases which has been shown to regulate FHOD1 activity. Src was suggested to mediate targeting of FHOD1 to lamellipodia and to bridge FHOD1 stimulated transcription from the SRE (Koka et al. 2005). Src activity was also found to be crucial in mediating the association of FHOD1 with ROCK-I at the plasma membrane (Hannemann et al. 2008). During the time of the present study, Iskratsch et al. 2013b elaborated on the interaction between FHOD1 and the Src family kinases (SFKs). They demonstrated that the SFKs phosphorylated a conserved YEEI motif in the FHOD1 GBD (^{99}YEEI) and that this was dependent on the SFKs binding the polyproline motifs in the FHOD1 FH1 domain (Iskratsch et al. 2013b). Overall, it was found that the direct interaction between FHOD1 and the SFKs was required for targeting of FHOD1 to early integrin clusters, where it was able to participate in actin polymerisation during cell spreading and migration. Prior to publication of the study by Iskratsch et al. 2013b, cross-talk between FHOD1 and Src had been well established but no direct binding between the two proteins had ever been shown. We had previously entertained the notion of a possible

interaction between the FHOD1 N-terminus and Src and performed GST pull-down assays.

5.2.1 Assessment of Binding of FHOD1 with Src

GST pull-down assays were performed to assess whether there was any direct binding between the GST-tagged FHOD1 N-terminus (See Figure 5.1 for characterisation of construct) and Src (Figure 5.4). We also explored the possibility of binding in the context of the activation status of Src. For this purpose we used three GFP-tagged variants of Src: wild-type Src, constitutively active Src, and dominant-negative Src. The constitutively active Src construct represents a kinase active Src mutant. The dominant-negative Src construct represents a kinase inactive variant of Src. Both constructs represent full-length variants of Src.

GST-tagged FHOD1 fragment bound GFP-tagged wild-type Src, overexpressed in COS-1 cells, in this assay as there was a signal in the pellet portion of the pull-down (Figure 5.4 A). However, the GST-tagged FHOD1 fragment was unable to bind GFP-tagged constitutively active Src (Figure 5.4 B) or dominant-negative Src (Figure 5.4 C). No signal was present in the pellet portion of the GST pull-down for constitutively active or dominant-negative Src, suggestive that the proteins do not bind. These findings would suggest that the FHOD1 N-terminus binds Src, but that this is could be dependent on the activation status of Src. However, due to the lack of positive binding controls performed with the constitutively active and dominant-negative Src constructs, we cannot conclude with certainty that this was the case. On the other hand, we were able to conclude with more certainty that FHOD1 could have at least bound wild-type Src, since we also demonstrated that the interaction was not mediated by the GFP tag (Figure 5.4 D). A GST pull-down assay was performed with the GST-tagged N-terminal fragment of FHOD1 and the GFP tag. There was no binding between the N-terminus of FHOD1 and GFP or between GST and GFP. Such a finding would be indicative of the specificity of binding between FHOD1 and wild-type Src. However, we cannot rule out that the unidentified species found in the protein preparation for the GST-tagged FHOD1 N-terminus (Figure 5.1 C) was responsible for the pull down and for a conclusive result the identity of this species has to be established first, respectively a

construct of the expected size after enrichment by size exclusion chromatography has to be employed.

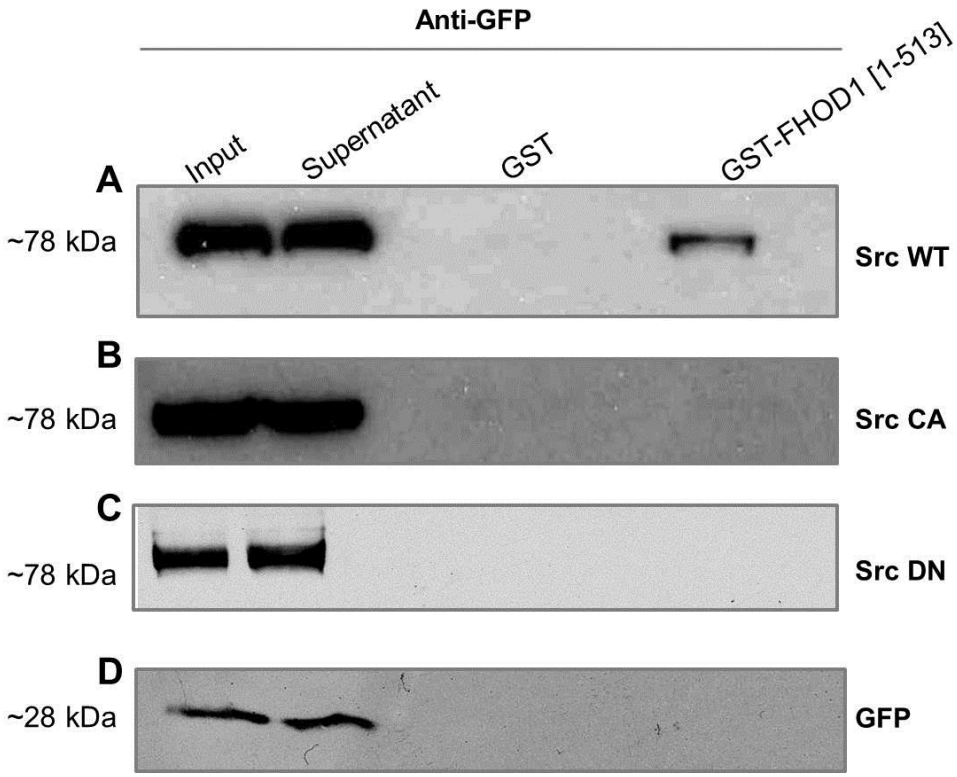

Figure 5.4: Assessing the Interaction between FHOD1 and Src. Western blots depicting the results from GST pull-down assays. The GST-tagged N-terminus of FHOD1 [1-513] containing the alternatively spliced exons 12-13was used to pull down GFP-tagged variants of Src from COS-1 cell lysates. Blots were probed with anti-GFP antibody to visualise GFP tagged Src variants. The following constructs were used for GST pull-down assays with the FHOD1 N-terminus: **A)** wild type (WT) Src, **B)** constitutively active (CA) Src, **C)** dominant-negative (DN) Src. **D)** A GST pull-down assay using untagged GFP was performed as a control to assess the potential for unspecific binding mediated by the GFP tag. GST, glutathione S-transferase; NRC, neonatal rat cardiomyocytes; GFP, green fluorescent protein. **N=3**.

5.3 Discussion

5.3.1 Interaction between the FHOD1 N-terminus, the Rho Family Small GTPases, and their Effector Molecules

DRF proteins are typically characterised as being regulated by the Rho family small GTPases. In the assessment of the regulation of FHOD1, we looked at some of the common Rho family small GTPases and their effector molecules that have been previously shown to regulate DRFs. Our study used an N-terminal fragment of the longer variant of FHOD1 containing the alternatively spliced exons 12-13, which could have influenced potential binding to GTPases and had not been included in previous characterisation efforts.

GST pull-down assays suggested that none of the currently addressed Rho family small GTPases, constitutively active variants of Rac1 and Cdc42, bound the FHOD1 N-terminus including exons 12-13. However, this could only be concluded with a degree of certainty for the GST pull-downs with constitutively active Rac1. Consistent with previous reports, constitutively active Rac1 bound the PBD portion of PAK (Sells et al. 1997). This positive control served as a means to confirm that constitutively active Rac1 was being studied in a context in which it could possibly bind our GST-tagged FHOD1 construct. Since no positive control was demonstrated for constitutively active Cdc42, we cannot conclude with certainty that the absence of interaction between the FHOD1 N-terminus and Cdc42 was genuine or merely due to a lack of optimisation of the conditions required for binding.

Previous characterisation efforts indicated that FHOD1 interacted directly with Rac. It was shown that the full length short variant of FHOD1 interacted with Rac1 but not Cdc42, RhoA, Rac2, or Rac3 (Westendorf 2001; Gasteier et al. 2003). Binding was also confirmed *in vivo* by co-immunoprecipitation assays using lysates from a breast carcinoma cell line (MDA-231 cells). Rac1 and FHOD1 were also shown to co-localise in HeLa cells. The interaction between FHOD1 and Rac1 was subsequently mapped between amino acids 422-717 of FHOD1 and the C-terminus of Rac1 (Gasteier et al. 2003). However, the FHOD1-Rac interaction has been questioned for a number of

reasons. Firstly, Rac has not been shown to bind the FHOD1 GBD, the quintessential GTPase interacting domain of formins. Secondly, Thomas et al. 2011 were unable to recapitulate binding between FHOD1 and Rac in co-immunoprecipitation experiments, although this may have just indicated that the proteins did not interact in platelets. While studies have found that Rac does not bind the FHOD1 GBD and therefore does not represent a possible means of activation like those noted previously with other formins, such as RhoA activation of mDia (Lammers et al. 2005; Lammers et al. 2008; Kühn and Geyer 2014), Rac could still influence the subcellular localisation and function of FHOD1. For example, Rac1 was shown to mediate targeting of FHOD1 to actin tails, where FHOD1 participates in actin tail initiation and elongation in HeLa cells infected with the WR strain of vaccinia virus (Alvarez and Agaisse 2013). Rac overexpression also promoted FHOD1 targeting to F-actin, membrane ruffles and the plasma membrane (Gasteier et al. 2003). Other studies involving the FHOD1-Rac interaction also implied that Rac1 not only regulates the localisation of FHOD1 but also represses FHOD1 mediated transcription from the SRE (Westendorf 2001). Future efforts should also see if Rac represents a means of mediating the targeting of FHOD1 in muscle cells.

GST pull-down assays suggested that none of the currently addressed effector molecules that act downstream of Rho, constitutively active ROCK-I and wild-type ROCK-II, bound the FHOD1 N-terminus. However, we could not conclude with certainty that this was the case in the absence of positive binding controls for these proteins. Until binding is demonstrated between these target proteins and a previously reported interacting partner using the same conditions as in our GST pull-down assays with the FHOD1 N-terminus, we cannot rule out the possibility that our conditions were not optimised for binding. Conditions may vary for binding between different sets of proteins to occur; therefore our one-buffer-fits-all approach may not have been an appropriate method for the present binding experiments.

Although FHOD1 regulation by Rac has become fairly well established, mounting evidence would suggest that a large part of FHOD1 regulation actually occurs downstream of RhoA signalling through the effector molecule ROCK. ROCK has been shown to directly affect the activity of FHOD1 by phosphorylation. Phosphorylation of FHOD1 by ROCK in three residues (Ser1131, Ser1137, and Thr1141) within the DAD

disrupted the diaphanous autoregulatory interaction and rendered FHOD1 active (Takeya et al. 2008). Furthermore, FHOD1 has been shown to bind the central region of ROCK-I via the N-terminal part of its FH2 domain (Hannemann et al. 2008). The functional importance of the Rho-ROCK cascade was further highlighted in experiments that demonstrated that ROCK phosphorylation of FHOD1 was essential in promoting smooth muscle differentiation (Staus et al. 2011a). Interestingly, activation by ROCK may be a conserved feature among DRFs, and especially formin homology proteins. mDia2 was shown to be phosphorylated by ROCK in two residues near the DAD, an event which resulted in activation of the formin (Staus et al. 2011b). FHOD3 has also been shown to be activated by ROCK phosphorylation within the DAD (Staus et al. 2011a; Iskratsch et al. 2013a).

5.3.2 Interaction between the FHOD1 N-terminus and Src

In addition to the Rho family small GTPases and ROCK, Src has also been implicated in regulating the activity of FHOD1. Src is frequently described as an important effector molecule in the context of cancer and tumour metastasis (Summy and Gallick 2003). One notable function of this kinase is that it phosphorylates focal adhesion kinase (FAK) to promote turnover of focal adhesions (Parsons 2003). Src has been shown to regulate FHOD1 in a number of studies. It was initially found to regulate the localisation of FHOD1 in fibroblasts, since Src depletion resulted in mislocalisation of FHOD1 from lamellipodia. However, Src was not required for FHOD1-induced stress fibres, which are more likely to be Rho-ROCK mediated. Furthermore, Src was found to regulate the transcriptional activity of FHOD1 since Src inhibition blocked FHOD1 induced transcription from the SRE (Koka et al. 2005). Further work looking at the cross-talk between FHOD1 and Src revealed that Src activity was required for the formation of FHOD1-ROCK-I induced plasma membrane blebs. Total and active Src also localised to plasma membrane blebs where FHOD1 and ROCK-I also co-localised (Hannemann et al. 2008). This same study also found that binding between FHOD1 and ROCK-I was dependent on Src activity, since binding was reduced in co-immunoprecipitation experiments using Src inhibitors. Generally, Src activity is required to mediate the transcriptional activity of FHOD1 and to promote its targeting to the plasma membrane (Koka et al. 2005; Hannemann et al. 2008).

The concept of Src interacting with formins is not entirely new. Src has been shown to bind the product of the *limb deformity* gene (Uetz et al. 1996) and mDia2 (Tominaga et al. 2000). Although cross-talk between FHOD1 and Src has been well established, binding assays between the two proteins had never previously been performed until publication of a study by Iskratsch et al. 2013, which was performed concurrently to the present study. The study by Iskratsch et al. 2013b suggested that a direct interaction between FHOD1 and the SFKs was required for targeting of FHOD1 to early integrin clusters, where FHOD1 was able to participate in actin regulation during cell spreading and migration. Binding of the SFKs to the polyproline motif in the FHOD1 FH1 domain resulted in phosphorylation of FHOD1 by the SFKs at the Y99 residue and consequently increased the interaction between FHOD1 and the SFKs.

The present characterisation explored the possibility of binding between Src and the N-terminus of FHOD1. GST pull-down assays suggested that wild-type Src bound the FHOD1 N-terminus, whereas the constitutively active and dominant-negative variants of Src did not. We also demonstrated that binding between FHOD1 and wild-type Src was not mediated by the GFP tag on Src or the GST tag on FHOD1. However, in the absence of a positive binding control for the constitutively active and dominant-negative Src mutants, we were unable to conclude with certainty that they did not bind the FHOD1 N-terminus.

Iskratsch et al. 2013b demonstrated that the polyproline motifs in the FHOD1 FH1 domain were required for the SFKs to be co-immunoprecipitated with FHOD1. Src has also been shown to bind the Proline rich FH1 domain of mDia2 (Tominaga et al. 2000). However, the present experiments suggested that wild-type Src could bind the FHOD1 N-terminus in the absence of the FH1 domain. There are a number of possible explanations behind this discrepancy. Our GST-tagged N-terminal FHOD1 construct retained the conserved YEEI motif in the GBD. This motif, when phosphorylated, constitutes a potential homology 2 (domain) (SH2) binding motif (Songyang et al. 1993; Iskratsch et al. 2013b). While the work by Iskratsch et al. 2013b suggested that binding of the SFKs preceded phosphorylation of the Y99 residue, the interaction between FHOD1 and the SFKs increased after phosphorylation of this motif (Iskratsch et al. 2013b), suggesting some binding of the phosphorylated motif by the SFKs. We did not

investigate the phosphorylation status of the FHOD1 N-terminal construct, therefore it remains to be seen if phosphorylation of the Y99 residue was promoting any binding with wild-type Src. An alternative explanation could be that Src bound the FHOD1 N-terminus via a region that was not previously addressed.

Another discrepancy with the observed interaction with Src is related to its activation status. It is difficult to speculate as to why the wild-type form of Src bound the FHOD1 N-terminus whereas the constitutively active and dominant-negative forms did not. Phosphorylation of the FHOD1 N-terminus by the SFKs enhances the interaction between these proteins (Iskratsch et al. 2013b), thereby suggesting that the kinase activity of the SFKs is essential in promoting their association. One might therefore expect an interaction between the FHOD1 N-terminus and constitutively active Src, but this was not the case in the present findings. Therefore the binding noted between FHOD1 and wild-type Src might be an extraneous occurrence. Indeed, the binding we noted with wild-type Src could have been mediated by the potentially contaminating high molecular weight protein species of unclear identity that we resolved in our protein preparations for the GST-tagged FHOD1 N-terminal construct. Nevertheless, the possibility of a physical interaction between FHOD1 and Src remains and could represent the means by which Src regulates FHOD1.

5.3.3 Conclusion

In summary, we assessed possible binding between the FHOD1 N-terminus with a number of known regulators of formin and FHOD1 function. The efforts were focused on an isoform of FHOD1 that contained the alternatively spliced exons 12-13 as previously described for striated muscle (Tojo et al. 2003) and which had not been included in previous studies. Although the binding experiments were not conclusive due to lack of positive binding controls for most of the putative interactions in question, they would suggest that that the constitutively active Rac1, constitutively active Cdc42, constitutively active ROCK-I, and wild-type ROCK-II do not bind to the FHOD1 N-terminus containing the alternatively spliced exons. Furthermore we investigated binding between the FHOD1 N-terminus and Src. We found binding between FHOD1 and wild-type Src but no binding with the constitutively active or dominant-negative

variants of Src. However, due to lack of a positive binding control for the constitutively active and dominant-negative Src constructs, we are unable to answer whether this result is indicative of a lack of interaction with the FHOD1 N-terminus.

5.3.4 Future Directions

In order to draw definitive conclusions from the present binding assays, positive binding controls will need to be performed for the experiments suggestive of a lack of binding with the FHOD1 N-terminus. This will be essential in order to confirm that the present results were not due to a lack of optimisation of the conditions required for binding with the target proteins in question.

The potential binding between the FHOD1 N-terminus and Src will particularly have to be looked at more closely. It remains to be seen if binding was mediated by background phosphorylation of the Y99 residue, by an additional Src binding site, or if the binding was altogether an extraneous occurrence. The purity of the GST FHOD1 protein preparation must also be determined in order to rule out the possibility of any contaminating protein species, which could conceivably have been responsible for binding Src. It also remains to be seen if binding is influenced by the activation status of Src. This can partly be addressed by repeating the GST pull-downs between FHOD1 and wild-type Src in the presence of well-established Src inhibitor, PP2. If the binding proves to be a plausible occurrence, further verification of the interaction should be performed by way of co-immunoprecipitation experiments and co-localisation studies using epitope-tagged Src and N-terminal FHOD1 constructs.

In order to gain a more-complete picture of the potential cross-talk between FHOD1 and its established regulatory proteins in cardiac muscle, co-expression studies should be performed in cultured neonatal rat cardiomyocytes (NRCs). This would allow one to study where these proteins potentially interact in heart cells and to see if they have an impact on cardiac cytoarchitecture. This is also important to perform for proteins that might not directly bind FHOD1 since proteins that do not necessarily interact directly *in vitro* could cross-talk *in vivo*.

Chapter 6

Novel Protein-Protein Interactions

6. Novel Protein-Protein Interactions

6.1 Yeast Two-Hybrid Screens with FHOD1

Yeast two-hybrid assays provide a means by which novel protein-protein interactions can be screened for. The functional basis underlying a yeast two-hybrid study is the confirmation of an interaction between two proteins via the activation of a reporter gene through a transcription factor (Figure 6.1). The transcription factor is almost invariably split into two parts, made up of a DNA binding domain and an activation domain. The 'bait' protein used to perform the screen is usually tagged with the DNA binding domain of the transcription factor. The 'prey' protein is usually tagged with the activation domain. If the bait and prey protein interact this allows for association of the two parts of the hybrid transcription factor, resulting in activation of the chosen reporter gene. This system can be used to directly test the interaction between two specified proteins or can alternatively be used to perform indiscriminate protein interaction screens against entire cDNA libraries. In this study we performed interaction screens against a cDNA library using different portions of FHOD1 (Figure 6.2). The yeast two-hybrid platform used in this study utilised the LexA system, a binary transcription factor paradigm (Van Criekinge and Beyaert 1999). LexA is based on a bacterial transcription factor that binds specific LexA operator systems to promote gene expression (Yagi et al. 2010). The different FHOD1 'bait' constructs were cloned into the pLEXC vector and were therefore expressed with the LexA tag after transformation in yeast. In this system, LexA functioned as the DNA binding domain of the hybrid transcription factor. The pLEXC vector also expressed the *TRP1* gene for selection of transformed yeast growing on medium lacking Tryptophan. The Gal4 activation domain portion of the transcription factor was expressed by the pACT2 vector. Gal4 is a yeast transcriptional activator protein that binds upstream activation sequences (UAS) to stimulate gene transcription (Gietz 2006; Yagi et al. 2010). The pACT2 vector also contains the *LEU2* gene which allows for selection of transformed yeast growing on medium lacking Leucine. A human cardiac cDNA library was cloned into the pACT2 vector and was used for the novel protein interaction screens. The FHOD1 bait constructs and the

cardiac cDNA library were transformed into the *Saccharomyces cerevisiae* strain L40. The L40 yeast strain contains two LexA inducible reporter genes, *HIS3* and *LacZ*. The *HIS3* gene in yeast encodes for the protein Imidazoleglycerol-phosphate dehydratase, which is involved in Histidine biosynthesis. The *LacZ* gene encodes for β-galactosidase, an enzyme involved in lactose metabolism. Thus, a protein-protein interaction allowing for association of the hybrid transcription factor under the LexA system in L40 yeast would permit growth of yeast on medium lacking Histidine (Struhl and Davis 1981) and because of the activity of β-galactosidase, would also produce blue yeast colonies upon incubation with the substrate X-gal (Essers and Kunze 1996) (Figure 6.1).

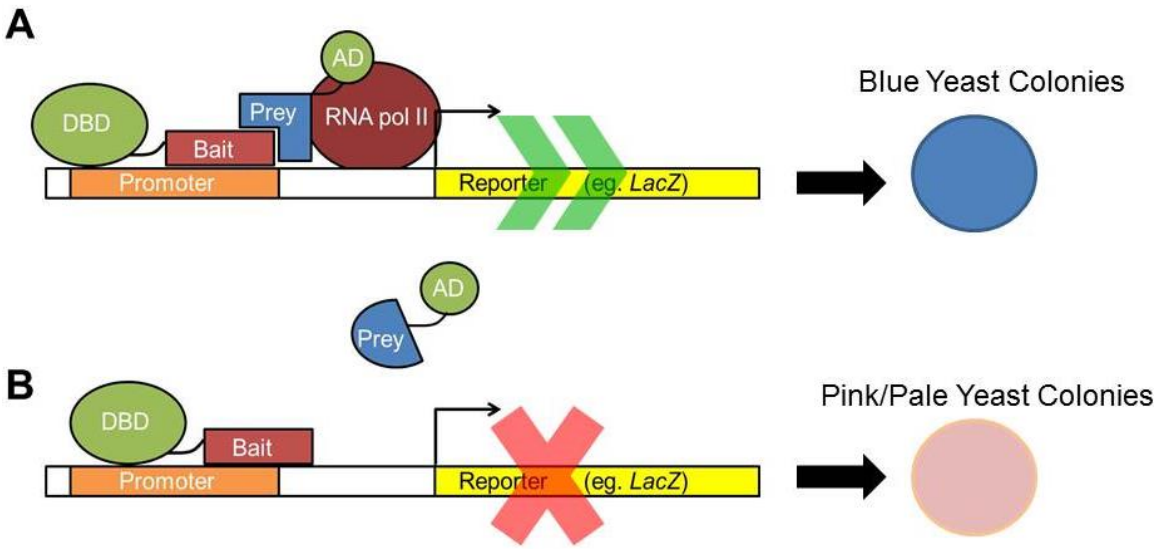

Figure 6.1: Schematic Representation of the LexA/Gal4 Yeast Two-Hybrid System. In the LexA/Gal4 yeast two-hybrid system the 'bait' protein is tagged with the LexA DNA binding domain and the 'prey' protein is tagged with the activation domain. **A)** In the case of an interaction between the 'bait' and 'prey' protein, association of LexA and Gal4 will result in formation of a functional 'hybrid' transcription factor. The LexA DNA binding domain binds the appropriate LexA inducible upstream promoter region of the relevant reporter gene. The Gal4 activation domain on the 'bait' protein participates in the induction of gene transcription by recruiting RNA polymerase II. Thus, transcription of the reporter gene is stimulated. In the illustrated example, transcription is stimulated from the *LacZ* reporter gene resulting in production of β-galactosidase. Upon incubation of yeast with X-gal, β-galactosidase will break down this substrate and result in the formation of blue yeast colonies. **B)** In the case of a lack of interaction (i.e. no binding/association of the bait and prey proteins), the LexA DNA binding domain will still bind the appropriate promoter region but the unbound Gal4 activation will be unable recruit RNA polymerase II. Therefore no transcription of *LacZ* will take place, resulting in no β-galactosidase. In this situation, treatment with X-gal will result in pale/pink yeast colonies. (Van Criekinge and Beyaert 1999)

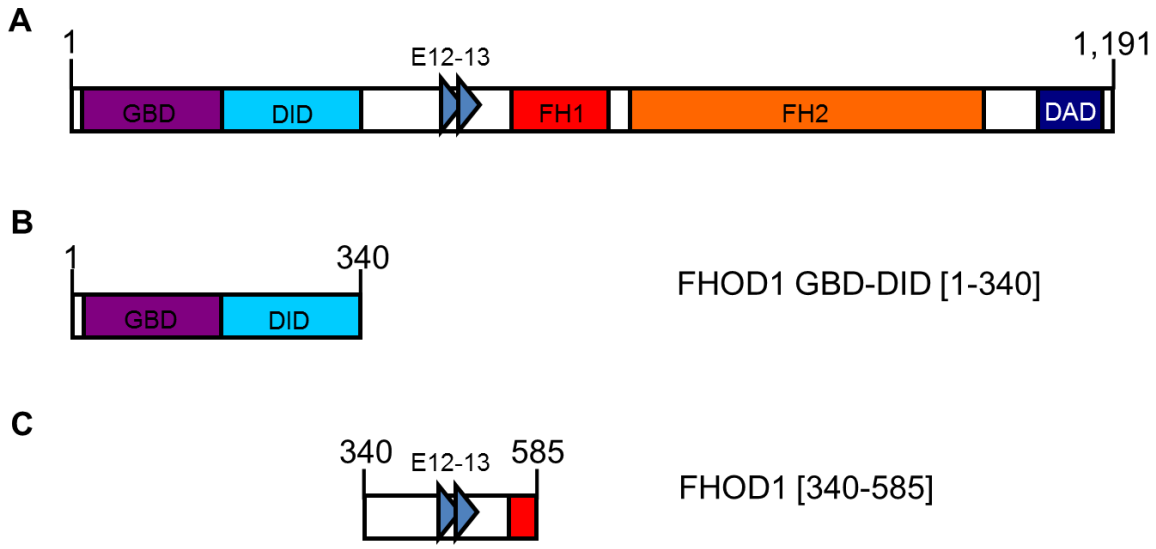

Figure 6.2: Map of FHOD1 Bait Constructs. Schematic representations of the portions of FHOD1 used as 'bait' in the yeast two-hybrid assays. Fragments of FHOD1 are shown with respect to A) the full length long variant of FHOD1, amino acids 1 to 1,1191. B) The FHOD1 GBD-DID bait construct, spanned from amino acids 1 to 340. C) An internal portion of FHOD1 after the DID and stopped in the N-terminal portion of the FH2 domain was used as bait and spanned from amino acids 340 to 585. GBD, GTPase binding domain; DID, diaphanous inhibitory domain; FH, formin homology; DAD, diaphanous autoregulatory domain; E12-13, the alternatively spliced exons 12-13 found in the long FHOD1 variant.

The purpose of the cDNA library screens was to identify novel interacting partners of FHOD1. Many actin regulatory proteins interact with other factors that modify or enhance their activity in some way. For instance N-WASP and Arp2/3 interact to enhance nucleation of actin filaments (Rohatgi et al. 1999; Suetsugu et al. 2001). Previous studies have performed yeast two-hybrid screens with different portions of FHOD1 and identified a variety of interacting proteins. Some of these included protein kinase C binding protein 1 (PRKCBP1), cyclophilin B, an isoform of WASP-interacting SH3-domain protein/diaphanous-interacting protein 1 (WISH/DIP1), named WISH-B (Westendorf and Koka 2004), insulin-responsive aminopeptidase (IRAP), profilinIIa (Tojo et al. 2003), Cyclic GMP-dependent protein kinase I (PKGI) (Wang et al. 2004), and nesprin-2G (Kutscheidt et al. 2014). These interactions have shed light onto some of the cellular functions of FHOD1. While a number of FHOD1's interacting partners have been mapped to interact with the more N-terminal part of the protein, the majority of studies have focused on interactions in the more C-terminal part of FHOD1. Formins are most divergent within their N-termini (Schulte et al. 2008). It has been speculated that the N-termini of formins may confer targeting of formins to distinct subcellular compartments and this may be mediated through unique protein interactions. We

therefore performed cDNA library screens via a yeast two-hybrid system with two different FHOD1 constructs that together covered the entirety of the FHOD1 N-terminus.

6.2 cDNA Library Screen with FHOD1 GBD-DID [1-340]

The first FHOD1 bait construct comprised of the GTPase binding domain (GBD) and the Diaphanous inhibitory domain (DID) and spanned from amino acids 1 to 340 (Figure 6.2 B). Prior to performing the library screen, an expression test was done with the FHOD1 GBD-DID construct. The construct was transformed into yeast, which were subsequently grown in culture and lysed. Expression of the GBD-DID construct was checked by looking at the size of the protein product by Western blotting (Figure 6.3). Western blotting revealed a discrete band between the 78 kDa and the 54 kDa markers. The predicted molecular weight of the FHOD1 GBD-DID was calculated to be 37 kDa. The combined weight of the bait protein and LexA equalled 61 kDa. Therefore the band visualised by Western blotting most likely corresponded to the bait protein and LexA tag combined. However, an equally prominent band was seen running near the 27 kDa marker, which could not be accounted for. This may have represented a contaminating protein species, which could have potentially compromised the results from the screen performed in yeast. Other faint bands were also noted and possibly indicated some degradation of the bait protein. Alternatively, the extra bands may have represented a non-specific background signal produced by the anti-LexA antibody. In order to test this, the expression of the bait construct would need to be compared to untransfected yeast lysates.

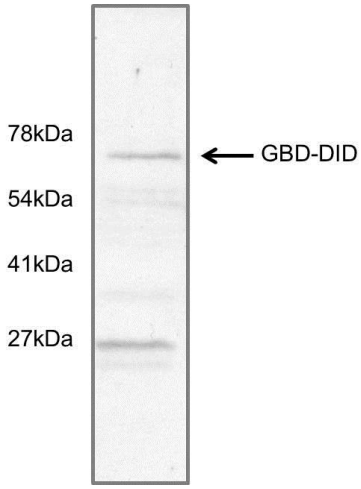

Figure 6.3: Validation of the FHOD1 GBD-DID [1-340] Bait Construct. Western blot showing expression of the FHOD1 GBD-DID bait protein [1-340]. The FHOD1 GBD-DID pLEXC bait construct was transformed into L40 yeast, which were then grown in culture and lysed. Protein lysates were resolved on SDS-PAGE gels with subsequent visualisation by Western blotting. The signal for the bait protein was visualised using the LexA antibody. **N=1.**

The FHOD1 GBD-DID construct was transformed into yeast with the pACT2 human cardiac cDNA library, resulting in a good transformation efficiency on SD-agar medium lacking Leucine, Tryptophan, and Histidine (-LWH) and on medium lacking Leucine and Tryptophan (-LW). Initially, 200 clones were picked and were more stringently screened by checking for *HIS3* and *LacZ* reporter gene activity (Results not shown). 25 clones were subsequently selected for propagation. The plasmids were isolated from the cultured yeast and then transformed into bacteria. 22 of the isolated plasmids were efficiently transformed into bacteria and grew well on plates containing ampicillin, to select for the pACT2 prey plasmids. The prey construct plasmids were then isolated from the cultured bacteria and the clones were subsequently identified by DNA sequencing (Table 6.1).

Acc.No	Gene	Reading Frame	Additional Comments
NM_001018011.1	Homo sapiens zinc finger and BTB domain containing 16 (ZBTB16), transcript variant 2 or 1	In Frame	Last 20 amino acids incorrect
NM_001018011.1	Homo sapiens zinc finger and BTB domain containing 16 (ZBTB16), transcript variant 2 or 1	In Frame	Last 10 amino acids incorrect
NM_013241.2	Homo sapiens formin homology 2 domain containing 1 (FHOD1)	In Frame	
NM_001018011.1	Homo sapiens zinc finger and BTB domain containing 16 (ZBTB16), transcript variant 2	In Frame	Last 30 amino acids incorrect
NM_004747.3	Homo sapiens discs, large homolog 5 (Drosophila) (DLG5)	In Frame	
NM_025135.2	Homo sapiens formin homology 2 domain containing 3 (FHOD3)	In Frame	
NM_001197104.1	Homo sapiens myeloid/lymphoid or mixed-lineage leukemia (trithorax homolog, Drosophila) (MLL), transcript variant 1 or 2	In Frame	Last 20 amino acids incorrect
NM_001127710.1	Homo sapiens proteoglycan 4 (PRG4), transcript variant D (C,B,A)	In Frame	Last 10 amino acids incorrect
NM_020382.3	Homo sapiens SET domain containing (lysine methyltransferase) 8 (SETD8)	In Frame	
NM_003609.3	Homo sapiens HIRA interacting protein 3 (HIRIP3)	In Frame	
NM_012259.2	Homo sapiens hairy/enhancer-of-split related with YRPW motif 2 (HEY2)	In Frame	Last 10 amino acids incorrect

Table 6.1: Results of cDNA Library Screen with FHOD1 GBD-DID [1-340]. The appropriate isolated yeast plasmid clones were transformed into bacteria prior to another round of plasmid isolation and identification by sequencing. Table lists the NCBI accession number, name of gene found for protein in question, reading frame of isolated pACT2 prey construct, and any additional comments. Highlighted entries represent potential interacting partners that were further investigated.

6.2.1 Novel Interaction Partners with FHOD1 GBD-DID [1-340]

The cDNA library screen performed with the FHOD1 GBD-DID construct yielded nine unique potential interacting partners (Table 6.1). After sequencing, these interacting partners were found to be in the correct frame in the pACT2 vector and their sequence corresponded to the coding sequence of a specific gene. The screen picked up a number of transcription factors: zinc finger and BTB domain containing 16 (ZBTB16), myeloid/lymphoid or mixed-lineage leukaemia protein (MLL), and hairy/enhancer-of-split related with YRPW motif 2 (HEY2). Other proteins included the nuclear histone binding protein HIRIP3, the cell cycle regulator mono-methylase SETD8, and the

proteoglycan PRG4. Although the potential interactions between FHOD1 and these proteins may have posed crucial biological implications, they would have been beyond the scope of this study namely due to the fact that they were mostly transcription factors. Although, FHOD1 has been found to possess transcriptional activity (Westendorf 2001), the mechanism by which it stimulated transcription from elements like the SRE was more likely due to having altered the cellular ratio of G-actin to F-actin (Staus et al. 2011a), rather than directly associating with a transcription factor. Furthermore, FHOD1 is not necessarily a nuclear protein; therefore association with transcription factors in the nucleus would be unlikely. Transcription factor proteins have been implicated in producing false positives in yeast two-hybrid screens since they often induce a high degree of auto-activation (Gietz 2006; Bruckner et al. 2009). Zinc finger proteins are also reportedly notorious for their stickiness (Schmeichel and Beckerle 1994) and could create false hits in screens such as the present one. PRG4 was not further investigated due to lack of expression in the myocardium.

The screen did however yield three potentially interesting interacting partners. The cDNA library screen with the FHOD1 GBD-DID region revealed a potential interaction with another region of FHOD1. The portion of FHOD1 identified by the screen corresponded to the C-terminal part of FHOD1, between amino acids 1018 to 1091 of the longer FHOD1 variant. This region was comprised of part of the core FH2 domain and the DAD. This interacting portion of FHOD1 that was picked up by sequencing may have represented the region that participates in the auto-inhibitory autoregulatory interaction between the N-terminus and the C-terminus of FHOD1 (Schonichen et al. 2006). Although not entirely novel, this interaction has never been previously picked up by a cDNA library screen using a yeast two-hybrid system.

The screen also identified the closest relative of FHOD1, FHOD3. Results from the screen indicated that FHOD1 GBD-DID interacted with amino acids 969 to 1253 of FHOD3. This portion of FHOD3 corresponded to a region just upstream of the FH1 domain and spanned towards the middle of the core FH2 domain. The potential interaction between FHOD1 and FHOD3 may have been important from the perspective that the proteins could heterodimerise. This would not be the first time formins have been suggested to work together since mDia1 and mDia2 have also been found to heterodimerise (Copeland et al. 2007). FHOD3 expression has been confirmed in the

heart (Kanaya et al. 2005; Taniguchi et al. 2009) where it was found to participate in myofibrillar maintenance (Iskratsch et al. 2010) therefore an FHOD1-FHOD3 interaction could pose noteworthy biological implications.

The final potential interacting partner that was found in this screen was Discs large homolog 5 (DLG5). DLG5 is a member of the membrane associated gyanylate kinases (MAGUKs) (Shah et al. 2002), which are thought to act as scaffold proteins in signal transduction networks (Nakamura et al. 1998). The structure of DLG5 is characterized by an N-terminal coiled-coil-like domain, as well as four PDZ domains, a Src homology (SH) 3 domain, and a gyanylate kinase domain, which are conserved among the MAGUKs (Wakabayashi et al. 2003). The sequencing results from the screen with FHOD1 revealed that FHOD1 GBD-DID was interacting with the C-terminal part of the DLG5 protein, namely from amino acids 1362 to 1568. This region of DLG5 comprises a PDZ and a SH3 domain. Such modular domains have been known to contribute to protein interactions (Weng et al. 1994; Lee and Zheng 2010), therefore it is interesting that this portion of DLG5 surfaced in our cDNA library screen. During initial characterization, the *DLG5* gene was found to be expressed in both skeletal and cardiac muscle (Shah et al. 2002). Apart from its expression profile in muscle, the possible interaction with DLG5 and FHOD1 may have been potentially interesting from the perspective that DLG5 may be a cytoskeletal regulator. DLG5 has been proposed to mediate membrane trafficking of cadherins (Nechiporuk et al. 2007) and regulate expression of E-cadherin (Sezaki et al. 2012). DLG5 has also been reported to interact with the microtubule binding protein cornetto (Bulgheresi et al. 2001; Giot et al. 2003). More-notably yet, DLG5 has been suggested a scaffolding role by interacting with vinexin and β-catenin to form a ternary complex, which may play a role at cell-cell contacts (Wakabayashi et al. 2003).

From the multiple potential interacting partners that came up in our screen, FHOD1, FHOD3, and DLG5 particularly caught our attention due to their expression in cardiac muscle and their reported roles as cytoskeletal regulators. These potential interactions were further investigated by yeast two-hybrid assay analysis with the isolated prey plasmids.

6.2.2 Yeast Two-Hybrid assays with FHOD1 GBD-DID [1-340]

Three of the interactions that came up in the screen with FHOD1 GBD-DID were selected for further investigation by performing additional yeast two-hybrid assays (Figure 6.4). Yeast two-hybrid assays using the isolated prey plasmids allow one to confirm an interaction between two proteins found in an initial screen. This was achieved by re-transforming the plasmid constructs isolated from the yeast and performing the gene reporter assays initially used for the library screen. In these yeast two-hybrid assays, the FHOD1 GBD-DID pLEXC bait construct was co-transformed with the FHOD1, FHOD3, and DLG5 pACT2 prey constructs. To test the specificity of the interactions for the bait construct, the prey constructs were also co-transformed with the empty pLEXC vector. An additional control for auto-activation was performed by co-transforming the FHOD1 GBD-DID bait construct and the empty bait (pLEXC) with the prey plasmid (pACT2). As expected, all of the combinations of co-transformations grew on SD-agar –LW (Figure 6.4 A). A β-galactosidase assay was performed to test for activation of the *LacZ* reporter gene. Strong interactions were confirmed by bright blue yeast colonies co-transformed with the FHOD1 GBD-DID bait along with the FHOD1 and FHOD3 prey constructs (Figure 6.4 B). Weak *LacZ* reporter gene activity was noted in yeast colonies co-transformed with the FHOD1 GBD-DID bait construct and the DLG5 prey construct, which was evidenced by very faint blue yeast colonies. In order to test for *HIS3* reporter gene activity the co-transformed yeast were grown on SD-agar –LWH (Figure 6.4 C). Colonies co-transformed with the FHOD1 GBD-DID bait and the three potential interacting prey constructs all grew on –LWH medium. To test the strength of the interactions, co-transformed yeast were also grown on SD-agar –LWH with 2.5mM 3-amino-1,2,4-triazole (3AT) (Figure 6.4 D). 3AT is a competitive inhibitor of the *HIS3* gene product, imidazoleglycerol-phosphate dehydratase and can therefore be used to measure the strength of an interaction (Joung et al. 2000). The yeast colonies co-transformed with the FHOD1 GBD-DID bait construct and all of the potential interacting prey constructs all grew on SD-agar –LWH + 3AT plates, indicating that the interactions were potentially strong. However, this was only performed with one concentration of 3AT. Future experiments should be performed with increasing concentrations of 3AT to further test the strength of the potential interactions. Furthermore, these interactions should have been tested in the context of

controls representative of previously reported positive and negative interactions in order to confirm the validity of the method.

Nevertheless, the yeast two-hybrid assay indicated that the potential interactions between the FHOD1 GBD-DID bait and the relevant preys were specific since the prey constructs did not stimulate reporter gene activity when co-transformed with the empty bait plasmid. No reporter gene activity was noted in colonies co-transformed with the FHOD1 GBD-DID bait construct and the empty pACT2 prey plasmid, therefore indicating that no auto-activation by the bait construct was present. In this instance, the yeast two-hybrid assay supported the notion of an interaction between the FHOD1 GBD-DID bait and the FHOD1 and FHOD3 prey. Regarding the interaction between the FHOD1 GBD-DID bait and DLG5, an interaction between the proteins was either less likely or weaker due to poor reporter gene activity in the β-galactosidase assay.

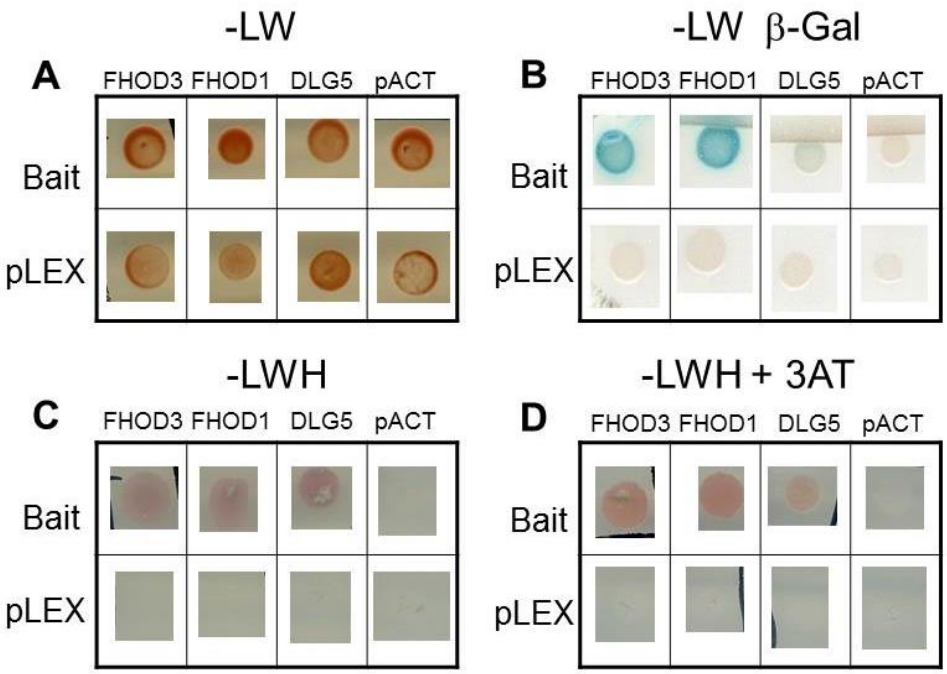

Figure 6.4: Yeast Two-Hybrid Assay with the FHOD1 GBD-DID [1-340] Bait Construct. Photographs of co-transformed L40 yeast colonies in different reporter gene assays. The FHOD1 GBD-DID bait was co-transformed with the three candidate prey interacting partners found in the initial screen. The three prey proteins included FHOD1, FHOD3, and DLG5. Co-transformation between the prey proteins and the empty bait vector (pLEXC) were performed to ensure that the interactions were specific for FHOD1 GBD-DID and not the LexA tag. Co-transformation of the FHOD1 GBD-DID bait and the empty pACT2 vector was performed to screen for autoactivation by the bait construct. **A)** Yeast were grown on SD-agar –LW to ensure the co-transformations had been performed successfully. **B)** Yeast were grown on nitrocellulose membranes placed on SD-agar –LW medium prior to incubation with X-gal for a β-galactosidase assay to test for *LacZ* reporter gene activity. Yeast were grown on SD-agar –LWH medium in the presence of **C)** no 3AT or **D)** 2.5mM 3AT to test for *HIS3* reporter gene activity. Bait, FHOD1 GBD-DID [1-340]; pLEX, empty pLEXC plasmid; pACT, empty pACT2 plasmid; L, Leucine; W, Tryptophan; H, Histidine; 3AT, 3-amino-1,2,4-triazole. **N=2.**

6.2.3 Validation of GST-tagged FHOD1 GBD-DID Construct

The yeast two-hybrid assays highlighted a number of potential interactions with the FHOD1 GBD-DID region. In order to see if these interactions were the result of direct binding between the bait and prey proteins, we performed binding assays via GST pull-down assays. For this purpose we used a GST-tagged FHOD1 GBD-DID construct.
The presently employed GST-tagged construct spanned from amino acids 1 to 340. This construct was comprised of the GBD and DID (Figure 6.5 A). Prior to commencing the GST pull-down studies, levels of expression and the size of the GST-tagged FHOD1 GBD-DID construct were checked by SDS-PAGE followed by Western blotting. The FHOD1 GBD-DID fragment without the GST tag had a predicted molecular weight of approximately 38kDa (Figure 6.5 B). The combined weight of the GST tag and the GBD-DID region was approximately 64kDa.

Western blots probed with the anti-GST antibody revealed that the FHOD N-terminal GBD-DID construct was expressed at the correct size and at sufficient levels for biochemical experiments to be performed, although some degradation was present, as evidenced by faint lower running bands (Figure 6.5 C). Relative levels of loading between unmodified GST protein and GST-tagged FHOD1 were visually gauged on gels and subsequently adjusted to reflect comparable levels of protein for GST pull-down assays (Figure 5.1 D).

For the GST pull-down assay COS-1 cells were used as a means to overexpress the target proteins due to the poor transfection efficiency we obtained with neonatal rat cardiomyocytes (NRCs). The use of COS-1 cells represented a drawback of this study since proteins could undergo diverse post-translational modifications in different cell types. Therefore, the present binding assays are not entirely representative of what could occur in muscle cells. The conditions used for GST pull-down assays are described in section 5.1.2.

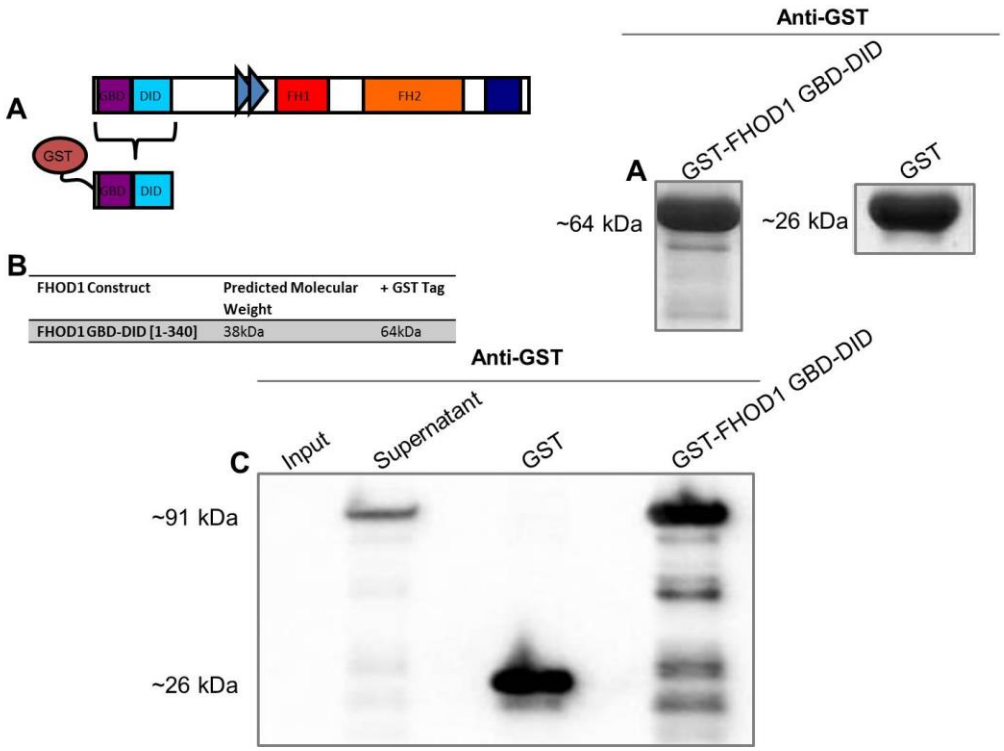

Figure 6.5: Expression Test for GST-FHOD1 GBD-DID [1-340]. A) The GST-tagged GBD-DID fragment of FHOD1 spanning from amino acid 1 to 340 was presently employed to validate the potential interactions found in the yeast two-hybrid assay using the FHOD1 GBD-DID fragment. **B)** The FHOD1 GBD-DID fragment had an expected molecular weight of 38kDa. Combined with the molecular weight of the GST tag (26kDa), the GST-tagged FHOD1 construct has an expected molecular weight of 64kDa. **C)** The GST-tagged FHOD1 construct and the GST tag alone were purified from bacterial lysates, resolved by SDS-PAGE, and visualised by enhanced chemiluminescence on Western blots incubated with the anti-GST antibody. This was performed to gauge the relative size and expression levels of the protein. **D)** Representative blot from GST pull-down assays that shows the relative loading of the GST tag in the negative control lanes and of the GST-tagged FHOD1 construct in the lanes testing for an interaction. Western blot was probed with the anti-GST antibody to visualise unmodified GST and the GST-tagged FHOD1 GBD-DID fragment. GST, glutathione S-transferase. **N=2.**

6.2.4 GST Pull-downs with FHOD1 GBD-DID [1-340]

Results from the yeast two-hybrid assay indicated that FHOD1 GBD-DID interacted with amino acids 969 to 1253 of FHOD3. This portion of FHOD3 corresponded to a region just upstream of the FH1 domain and spanned towards the middle of the core FH2 domain. We assessed binding between the FHOD1 GBD-DID region and two fragments of FHOD3 that fell within the portion of FHOD3 identified in the screen: the

FH1 domain [941-1079] and the C-terminus of the short FHOD3 variant comprised of the FH2 domain and DAD [1065-1622]. This was performed in the hopes of mapping the interaction to a specific portion of FHOD3. The GST-tagged FHOD1 GBD-DID construct pulled down both the GFP-tagged FHOD3 C-terminus (Figure 6.6, A) and the GFP-tagged FHOD3 FH1 domain (Figure 6.6, B), as evidenced by a signal in the pellet portion of the pull-down assays. As a negative control, a pull-down was performed between the GST-tagged FHOD1 GBD-DID fragment and the GFP-tagged FHOD1 ΔDAD construct (Figure 6.6, C). As expected, no binding was noted between these portions of FHOD1, since it has been previously shown that the DAD is required for binding between the FHOD1 N and C-termini (Westendorf 2001). The lack of binding in the negative control experiment can also be taken as evidence that the positive interactions with FHOD3 were not mediated by the GFP tag, since the FHOD1 ΔDAD construct was also GFP-tagged. A pull-down with the HA-tagged fragment of DLG5 and GST-tagged FHOD1 GBD-DID suggested a lack of binding between these proteins. However, in the absence of a positive binding control for the DLG5 fragment, we were not able to conclude with certainty that the negative interaction was not due to insufficient optimisation of the conditions for the present binding assay. While we sought to validate the interaction with the FHOD1 C-terminus found in the library screen, the currently available HA-tagged FHOD1 C-terminal construct [641-1191] was not expressed at sufficient levels in COS-1 cells for GST pull-down assays to be performed.

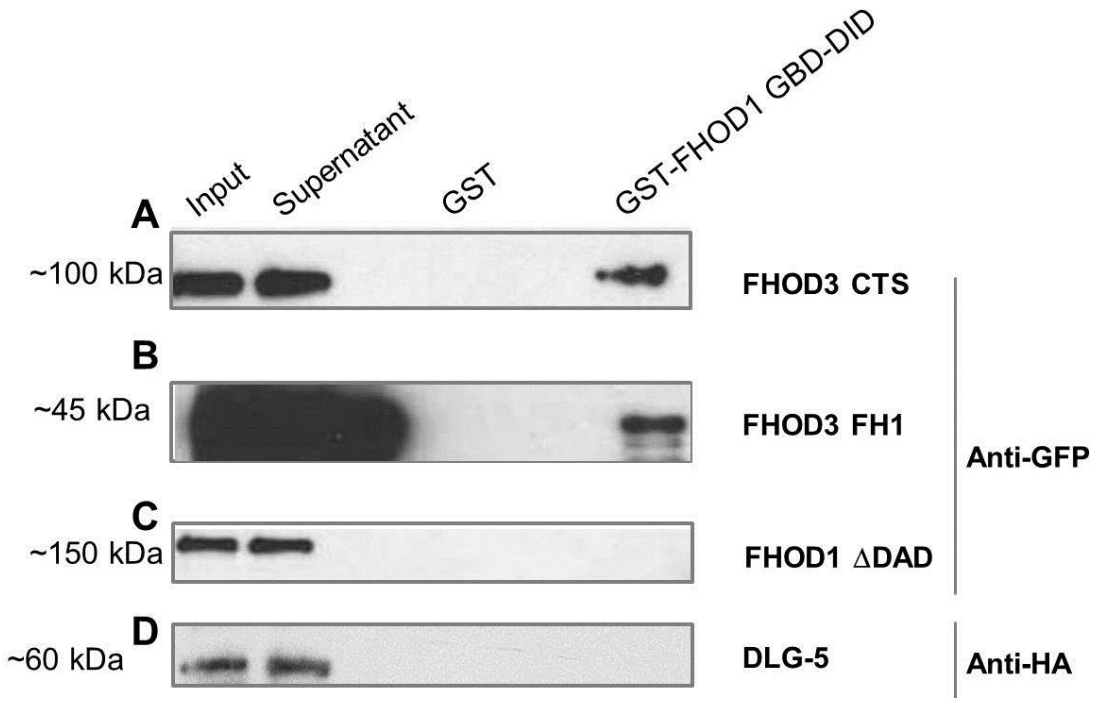

Figure 6.6: Assessing the Interaction between the FHOD1 GBD-DID fragment and Potential Interacting Partners. Western blots depicting the results from GST pull-down assays. The GST-tagged FHOD1 GBD-DID fragment [1-340] was used to pull down **A)** the GFP-tagged C-terminus of the short variant of FHOD3 [1065-1622], **B)** the GFP-tagged FH1 domain of FHOD3 [941-1079], and **C)** the HA-tagged DLG-5 fragment [1395-1919] found in the library screen. The target proteins were overexpressed in COS-1 cell. **D)** A negative control GST pull-down assay was performed using the GFP-tagged FHOD1 ΔDAD construct. Blots were probed with anti-GFP and anti-HA antibodies to visualise GFP-tagged and HA-tagged proteins, respectively. GST, glutathione S-transferase; HA, haemagglutinin; FH, formin homology. **N=2.**

Overall, a cDNA library screen performed in yeast with the FHOD1 GBD-DID region highlighted FHOD3 and DLG5 as possible interacting partners of FHOD1. Yeast two-hybrid assays hinted at a potentially strong interaction between FHOD1 and FHOD3. Binding studies by way of GST pull-down assays suggested that FHOD1 bound the FH1 domain and the C-terminus of FHOD3. However, binding to multiple regions on FHOD3 may have indicated that the interaction was not specific, although this can only be confirmed by further testing via co-immunoprecipitation assays and co-localisation studies. Nevertheless, the possible FHOD1-FHOD3 binding interaction may have indicated the potential for these two formins to heterodimerise, as has been shown for other formins (Copeland et al. 2007). The possibility of an interaction between FHOD1 and DLG5 was seemingly less likely than that for FHOD1 and FHOD3. Yeast two-

hybrid analysis provided less convincing evidence in support of an interaction between FHOD1 and DLG5. Furthermore, GST pull-down assays suggested that the FHOD1 GBD-DID region did not bind the DLG5 fragment found in the cDNA library screen. However, in the absence of a binding control for the DLG5 fragment we could not conclude with certainty that the proteins did not bind.

6.3 cDNA Library Screen with FHOD1 [340-585]

Having covered the first part of the FHOD1 N-terminus (GBD-DID), another cDNA library screen was performed in yeast with a second part of the FHOD1 N-terminus. The second FHOD1 bait construct began at the end of the DID and ended in the region of the FH1 domain just upstream of the polyproline motifs. This construct spanned from amino acids 340 to 585 (Figure 6.2 C). This construct represented an internal fragment of the N-terminal half of the long variant of FHOD1, containing the alternatively spliced exons, exons 12 and 13. Prior to performing the cDNA library screen, an expression test was done with the FHOD1 [340-585] construct. The construct was transformed into yeast, which were subsequently grown in culture and lysed. Expression of the FHOD1 [340-585] construct was checked by looking at the size of the protein product by Western blotting (Figure 6.7). Western blotting revealed multiple bands running below the 78 kDa marker and around the level of the 54 kDa marker. The predicted molecular weight of FHOD1 [340-585] was calculated to be 25 kDa. The molecular weight of the LexA tag is approximately 24 kDa. The combined weight of the bait protein and LexA equalled 49 kDa. A strong band was seen just below the 54 kDa marker and may have corresponded to FHOD1 [340-585]. However, in the presence of multiple bands of similar intensity, we could not definitively identify the band which corresponded to FHOD1. With the low probability that oligomerisation of the bait protein had occurred in the presence of denaturing conditions, the bands of unidentified origin may have represented contaminating protein species. If this was indeed the case, the validity of the present cDNA library screen may have been severely compromised, since potentially contaminating protein species could have mediated the interactions detected in the screen. An alternative explanation for the extra bands could be that the higher band actually represented the bait construct, possibly migrating at a higher molecular weight than expected, and the lower running bands represented

degradation products. This theory could be tested by repeating the experiment by including protease inhibitor in the yeast lysis buffer. The lysates could be tested for reactivity against an FHOD1 antibody to investigate the identity of the bands. Alternatively, the extra bands may have represented a non-specific background signal produced by the anti-LexA antibody. In order to test this, the expression of the bait construct would need to be compared to untransfected yeast lysates. Nevertheless, with these caveats in mind we performed a cDNA library screen with the FHOD1 [340-585] bait construct.

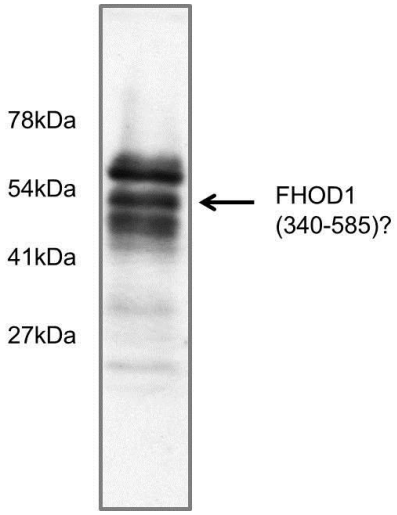

Figure 6.7: Validation of the FHOD1 [340-585] Bait Construct. Western blot showing expression of the FHOD1 [340-585] bait protein. The FHOD1 [340-585] pLEXC bait construct was transformed into L40 yeast, which were then grown in culture and lysed. Protein lysates were resolved on SDS-PAGE gels with subsequent visualisation by Western blotting. The signal for the bait protein was visualised using the LexA antibody. **N=1**

FHOD1 [340-585] was transformed into yeast with the human cardiac cDNA library, resulting in a good transformation efficiency on SD-agar medium lacking Leucine, Tryptophan, and Histidine (-LWH) and on medium lacking Leucine and Tryptophan (-LW). Initially, 50 clones were picked and were more stringently screened by checking for *HIS3* and *LacZ* reporter gene activity (Results not shown). 32 clones were subsequently selected for propagation. The plasmids were isolated from the cultured yeast and then transformed into bacteria. Only 19 of the isolated plasmids were efficiently transformed into bacteria and grew well on plates containing ampicillin, to select for the pACT2 prey plasmids. The prey construct plasmids were then isolated from the cultured bacteria and clones were subsequently identified by DNA sequencing (Table 6.2).

Acc.No	Gene	Reading Frame	Additional Comments
NM_001469.3	Homo sapiens X-ray repair complementing defective repair in Chinese hamster cells 6 (XRCC6)	In Frame	
NM_006175.3	Homo sapiens nebulin-related anchoring protein (NRAP), transcript variant 1	In Frame	Full-length protein
NM_032836.2	Homo sapiens FLT3-interacting zinc finger 1 (FIZ1)	In Frame	
NM_006941.3	Homo sapiens SRY (sex determining region Y)-box 10 (SOX10	In Frame	

Table 6.2: Results of cDNA Library Screen with FHOD1 [340-585]. The appropriate isolated yeast plasmid clones were transformed into bacteria prior to another round of plasmid isolation and identification by sequencing. Table lists the NCBI accession number, name of gene found for protein in question, reading frame of isolated pACT2 prey construct, and any additional comments. Highlighted entries represent potential interacting partners that were further investigated.

6.3.1 Novel Interaction Partners with FHOD1 [340-585]

In comparison to the previous screen, the screen performed with the FHOD1 [340-585] construct revealed fewer potential interacting partners and a higher number of identifications corresponding to genomic DNA. There were, however, four unique interacting partners that were in frame and corresponded to the coding sequence of a specific gene. One of the potential interacting partners identified in the screen was the DNA binding protein X-ray repair complementing defective repair in Chinese hamster cells 6 (XRCC6). The screen also identified two transcription factors: FLT3-interacting zinc finger 1 (FIZ1) and SRY (sex determining region Y)-box 10 (SOX10). Ku70, FIZ1, and SOX10 were not further investigated due to their roles as DNA binding proteins and transcription factors for the reasons outlined above.

The other protein that came up in the screen was Nebulin-related anchoring protein (NRAP), transcript variant 1. NRAP is an acting binding protein that was found to be exclusively expressed in striated muscle (Luo et al. 1997a; Luo et al. 1997b). It was found to be associated with the terminal ends of myofibrils and localised to the myotendinous junction in skeletal muscle and the intercalated disk in cardiac muscle

(Zhang et al. 2001). Furthermore, NRAP has been shown to play a role in myofibril assembly (Carroll et al. 2001; Carroll et al. 2004; Dhume et al. 2006). Due to the reported roles of NRAP in myofibril assembly and a shared localisation at the intercalated disk, the potential interaction between FHOD1 and NRAP was further investigated.

6.3.2 Binding between FHOD1 and NRAP

With a number of NRAP fragment constructs available, GST pull-down assays were performed to see if there was any direct binding between FHOD1 and NRAP. NRAP is composed of a LIM domain, a linker region (termed r01-r10), and 5 nebulin like super repeats (SRs) (Luo et al. 1997a; Gehmlich et al. 2004). The following T7-tagged NRAP constructs were used: a short variant of SR5 (SR5-6); a long variant of SR5 (SR5-7); SR4; r01-r10; LIM domain (Figure 6.8). The GST-tagged N-terminal fragment of FHOD1 was used for pull-down studies. This construct spanned from amino acids 1 to 513 and included the alternatively spliced exons, which were also included for the yeast two-hybrid screen (Refer to Figure 5.1 for FHOD1 GST [1-513] construct characterisation).

Figure 6.8: Domain Map of NRAP. Schematic representation of NRAP and its domains. SR, super repeats.

GST pull-down assays were performed with the N-terminal fragment of FHOD1 and the available T7-tagged NRAP fragments (Figure 6.9). Obtaining reasonable expression levels for the NRAP constructs was sometimes an issue during pull-down studies. The LIM domain in particular achieved poor expression levels and was difficult to detect via Western blotting, therefore it was excluded from this study (results not shown). Pull-downs suggested the GST-tagged N-terminal fragment of FHOD1 was able to bind the T7-tagged SR5-6 construct when overexpressed in the lysates of COS-1 cells, as evidenced by a faint band detected in the pellet portion of the pull-down (Figure 6.9 A). The faint band may be indicative of a weak interaction between SR5-6 and FHOD1. Binding between FHOD1 and SR5-6 was consistently seen upon repetition of the pull-

down. Surprisingly, the GST-tagged FHOD1 N-terminal fragment was unable to pull down the T7-tagged SR5-7 fragment (Figure 6.9 B). This fragment represents a longer version of SR5-6 therefore it theoretically should have bound FHOD1. However, there is the possibility that the additional amino acid stretch in SR5-7 may have masked the interaction domain. The FHOD1 construct was also unable to pull down the SR4 (Figure 6.9 C), and r01-r10 (Figure 6.9 D) fragments, as there was no detectable signals in the pellet portions of the pull-down assays. Therefore, it seemed that FHOD1 preferentially bound the SR5-6 fragment. However, we could not conclude a lack of binding with the other NRAP fragments in the absence of a positive control for each fragment. Therefore we could not rule out that the absence of binding was due to lack of optimisation of the conditions used for the pull-downs. Furthermore, there were concerns about the validity of the protein preparations of the GST-tagged FHOD1 [1-513] construct, which contained a higher molecular weight band of unidentified origin (See 5.1.1 for discussion of issues regarding the construct).

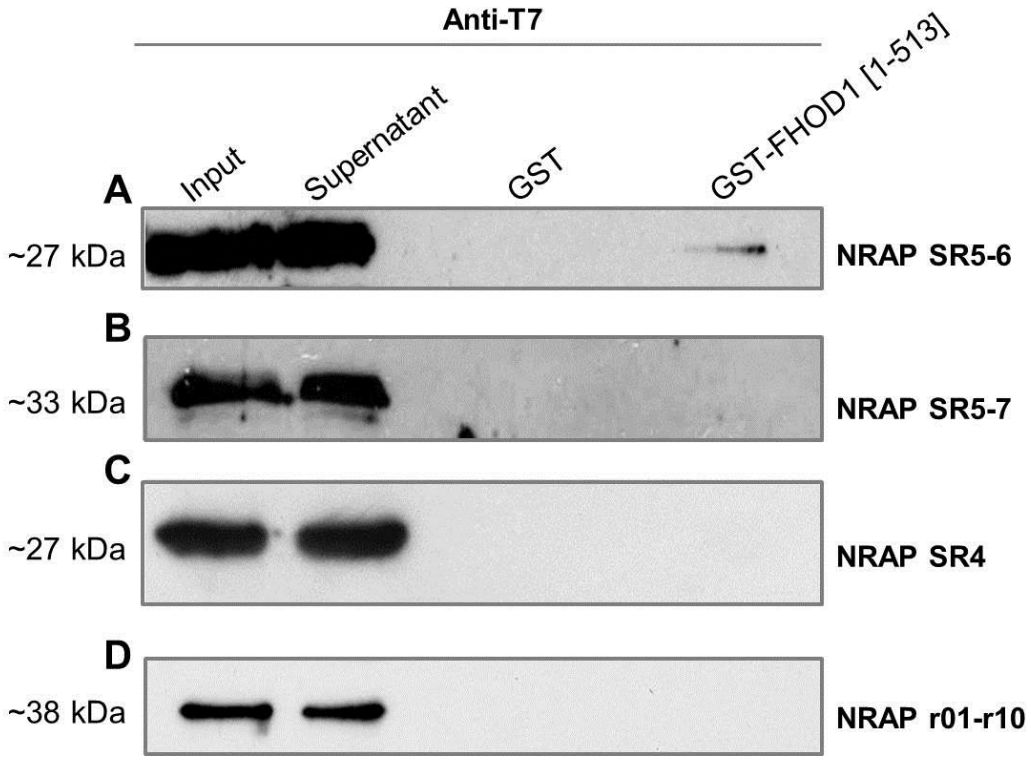

Figure 6.9: Binding between FHOD1 and NRAP. Western blots depicting the results from GST pull-down assays. The GST-tagged N-terminus of FHOD1 [1-513] was used to pull down the following T7-tagged NRAP fragments: **A)** SR5-6; **B)** SR5-7; **C)** SR4; **D)** r01-r10. Blots were probed with anti-T7 antibody to visualise the T7-tagged NRAP constructs. **N=3.**

6.3.3 Yeast Two-Hybrid Assays with FHOD1 [340-585]

With the SR5 repeat a possible candidate for binding FHOD1, the potential interaction between FHOD1 and NRAP was further investigated by performing yeast two-hybrid assays (Figure 6.10). The SR5-6 and SR5-7 constructs were obtained in the pACT2 vector and co-transformed with the FHOD1 [340-585] bait construct in yeast to test for reporter gene activation. The SR5 constructs were also co-transformed with the empty pLEXC plasmid to check the specificity of the interaction. The FHOD1 [340-585] bait was also co-transformed with the empty pACT2 plasmid to check for auto-activation of reporter gene activity by the bait construct. No activation of reporter gene activity was previously noted in yeast co-transformed with the empty pLEXC and empty pACT2 plasmids (Figure 6.4). As expected all the combinations of construct co-transformations in yeast grew on SD-agar –LW medium (Figure 6.10 A). A β-galactosidase assay to

test *LacZ* reporter gene activity confirmed positive interactions between the FHOD1 [340-585] bait and both SR5 constructs, as evidenced by blue yeast colonies (Figure 6.10 B). However, *LacZ* reporter gene activation was also seen in yeast co-transformed with the FHOD1 [340-585] bait and the empty pACT2 plasmid, which indicated that expression of the bait construct may have led to auto-activation of the reporter gene. *HIS3* reporter gene activity was tested by growing the co-transformed yeast on SD-agar –LWH medium (Figure 6.10 C). In this instance, yeast co-transformed with the FHOD1 [340-585] bait and the SR5-6 construct exhibited the most growth. Notable growth was noted in yeast co-transformed with the FHOD1 [340-585] bait and the SR5-7 construct. A degree of auto-activation by the FHOD1 [340-585] bait was again noted in this assay as there was some growth in yeast co-transformed with the FHOD1 [340-585] bait and the empty pACT2 plasmid. The strength of the observed interactions was then tested by growing yeast on SD-agar –LWH + 2.5 mM 3AT (Figure 6.10 D). Upon 3AT treatment, the auto-activation previously observed with the FHOD1 [340-585] bait and the empty pACT2 plasmid disappeared. Growth in yeast colonies co-transformed with the FHOD1 [340-585] bait and the SR5-7 construct was significantly reduced to almost undetectable levels. Yeast co-transformed with the FHOD1 [340-585] bait and the SR5-6 construct were able to grow well on SD-agar + 2.5mM 3AT plates, therefore indicated a strong interaction between these two bait and prey protein fragments. Co-transformations of the SR5 constructs and the empty pLEXC vector yielded no reporter gene activity for *LacZ* (Figure 6.7 B) or *HIS3* (Figure 6.7 C) and thus indicated that the interactions were specific for the FHOD1 [340-585] bait. In line with the results seen in the GST pull-down assays, forced yeast two-hybrid analysis indicated that the FHOD1 [340-585] interaction with the SR5-6 fragment of NRAP was stronger than the interaction with the SR5-7 fragment, although these data were somewhat inconclusive due to the presence of some autoactivation by the FHOD1 bait construct. Furthermore, these interactions should have been tested in the context of controls representative of previously reported positive and negative interactions in order to confirm the validity of the method.

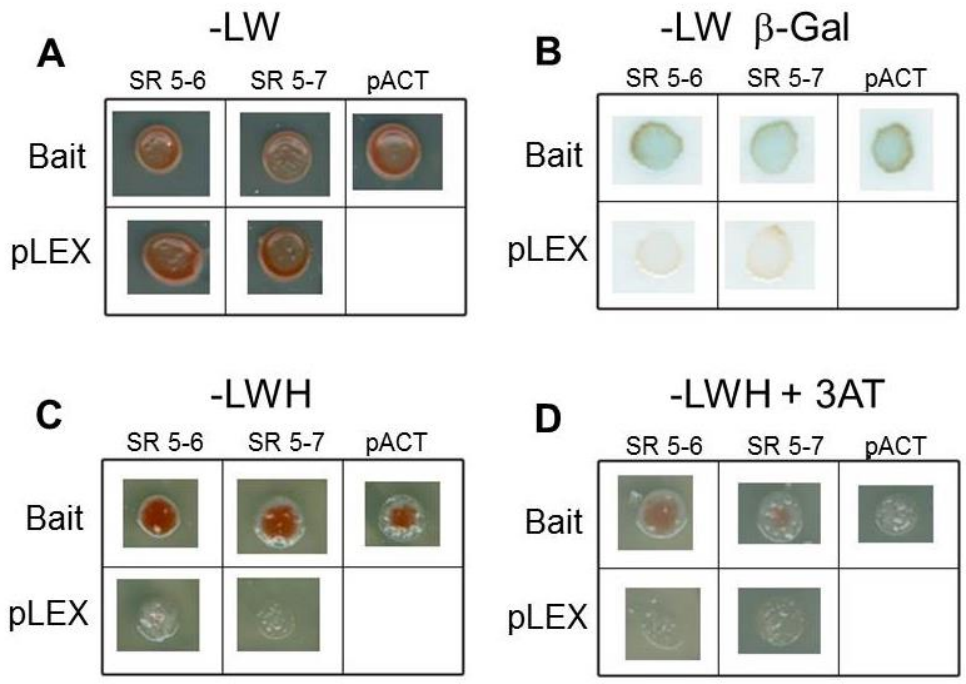

Figure 6.10: Yeast Two-Hybrid Assay with the FHOD1 [340-585] Bait Construct. Photographs of co-transformed L40 yeast colonies in different reporter assays. The FHOD1 [340-585] bait was co-transformed with the prey SR5-6 and SR5-7 pACT2 fragments of NRAP. Co-transformation between the prey proteins and the empty bait vector (pLEXC) were performed to ensure that the interactions were specific for FHOD1 [340-585]and not the LexA tag. Co-transformation of the FHOD1 [340-585] bait and the empty pACT2 vector was performed to screen for autoactivation by the bait construct. **A)** Yeast were grown on SD-agar –LW to ensure the co-transformations had been performed successfully. **B)** Yeast were grown on nitrocellulose membranes placed on SD-agar –LW medium prior to incubation with X-gal for a β-galactosidase assay to test for *LacZ* reporter gene activity. Yeast were grown on SD-agar –LWH medium in the presence of **C)** no 3AT or **D)** 2.5mM 3AT to test for *HIS3* reporter gene activity. Bait, FHOD1 [340-585] [1-340]; pLEX, empty pLEXC plasmid; pACT, empty pACT2 plasmid; L, Leucine; W, Tryptophan; H, Histidine; 3AT, 3-amino-1,2,4-triazole. **N=2.**

Overall, due to issues relating to the validity of the FHOD1 [340-585] bait construct and the purity of the GST-FHOD1 [1-513] protein preparation, we were unable to conclude with certainty that FHOD1 and NRAP represented *bona fide* interacting partners. While the potential of an interaction between FHOD1 and NRAP may pose interesting biological implications, further biochemical and molecular biology experiments will be required to validate this. Nevertheless, in the hopes of seeking further validation, we performed co-localisation studies by staining for FHOD1 and NRAP in mouse heart sections.

6.3.4 Co-localisation Studies with FHOD1 and NRAP

Interactions found in yeast two-hybrid assays require validation by multiple methods. One such method involves assessing the co-localisation of the proteins in question by confocal microscopy (Bruckner et al. 2009). The interaction between FHOD1 with NRAP was further explored by performing *in situ* co-localisation studies. Endogenous FHOD1 and NRAP were stained against in frozen sections of wild-type adult mouse hearts (Figure 6.11 A). The anti-FHOD1 polyclonal goat C20 antibody (Santa Cruz) was used for visualisation of FHOD1 in hearts. Images of longitudinal regions of heart sections revealed an overlapping signal for FHOD1 and NRAP at the intercalated disk.

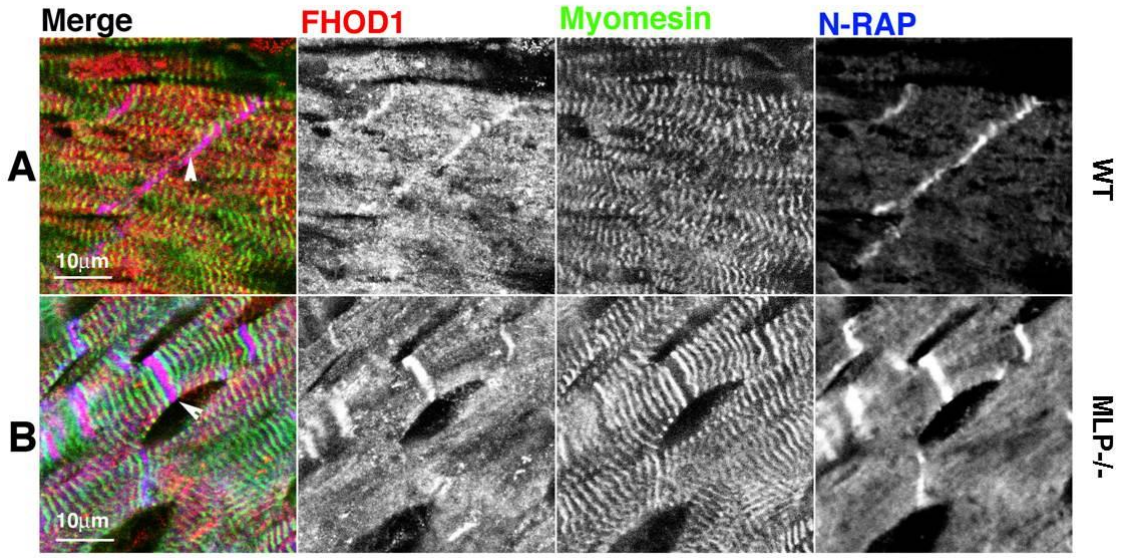

Figure 6.11: Co-Localisation of FHOD1 and NRAP in Murine Hearts. Frozen heart sections of 1 year old male adult mice were stained with the anti-FHOD1 polyclonal goat C20 antibody (Santa Cruz) and against NRAP prior to visualisation by confocal microscopy. Sections were stained for myomesin to visualise the M-bands of sarcomeres. Images represent high magnification longitudinal sections. Staining was performed in sections of **A)** wild-type (WT) C57/BL6 mouse hearts and **B)** $MLP^{-/-}$ mouse hearts. FHOD1 is seen in red, myomesin is seen in green, and NRAP seen in blue. Arrowheads indicate an intercalated disk, the subcellular structure where co-localisation between FHOD1 and NRAP was seen. Scale bars represent 10μm. **N=2.**

During instances of cardiac disease, cytoskeletal proteins can undergo changes in their expression pattern and distribution. Altered stoichiometry of proteins found at the intercalated disk was suggested to be one of the defining characteristics of dilated cardiomyopathy (DCM) (Perriard et al. 2003) and other proteins have been shown to exhibit alterations in their expression (Estigoy et al. 2009). Formins may exhibit alterations in localisation during instances of DCM, as has been suggested by previous work in our laboratory with FHOD3 in a mouse model of DCM, the $MLP^{-/-}$ mouse (Arber et al. 1997; Iskratsch et al. 2010). $MLP^{-/-}$ mice have been reported to display a number of alterations in cardiomyocyte structure. Although overall structure of sarcomeres remains unchanged, $MLP^{-/-}$ mice display a number of abnormalities at the level of the intercalated disk. The most notable feature is widening of the intercalated disk, which has been attributed to greater convolution of the structure (Ehler et al. 2001). MLP has a number of reported binding partners, including NRAP (Gehmlich et al. 2004). An increase in NRAP expression has also been reported in $MLP^{-/-}$ mice, where it redistributes over the widened intercalated disks (Ehler et al. 2001). With these factors in mind, we investigated the localisation of FHOD1 and NRAP in heart sections from $MLP^{-/-}$ mice. As expected, our study revealed staining for NRAP as a broad signal over the intercalated disk (Figure 6.11 B). Staining for FHOD1 revealed that it had also redistributed across the apparently widened intercalated disks, producing a bright signal at the structure. Both the FHOD1 and NRAP signals co-localised at the intercalated disks of $MLP^{-/-}$ mice. Co-localisation studies performed between FHOD1 and NRAP in adult mouse hearts would support the idea of an interaction between the two proteins.

In the absence of single staining controls with the anti-FHOD1 and anti-NRAP antibodies alone, we were unable to determine with absolute certainty if the overlapping signals for FHOD1 and NRAP were due to cross-reactivity between the antibody conjugates. However, all secondary antibodies employed in this study were of "multi-labelling" quality, i.e. had been tested for a lack of cross-reaction between the relevant species (mouse, rat, rabbit, and goat). These secondary antibodies were used in combination successfully in the past and no cross-reaction was ever seen. Nevertheless, in the absence of an antigen competition assay we could not conclude with certainty that the anti-FHOD1 antibody was not recognising other myocardial proteins.

We were however able to examine any potential non-specific reactivity of the secondary, fluorochrome-conjugated antibodies on their own with the heart tissue sections (Figure 6.12). The Cy3-coupled donkey anti-goat antibody, which was used to detect the goat anti-FHOD1 antibodies, displayed homogeneous background fluorescence over the entire tissue in longitudinal sections, which was at much lower intensity using the same imaging conditions that the detected signal in the experiment (Figure 6.12). The signal of the secondary antibody on its own was not associated with the intercalated disks nor did it produce the distinct cross striations seen with the anti-FHOD1 antibodies. The Cy2-coupled donkey anti-mouse antibody, used to detect the mouse anti-myomesin antibody, produced similar homogeneous background staining along myofibrils and a somewhat more intense signal at cell boundaries, potentially due to reactivity with the extracellular matrix. This background staining was not observed when staining was performed with the appropriate primary antibody. The Cy5-coupled donkey anti-rabbit antibody, used to detect the rabbit anti-NRAP produced also diffuse background fluorescence over the entire cardiac tissue. Although the caveat remained regarding the specificity of the anti-FHOD1 antibodies in these experiments, we were therefore able to exclude that the detected signal in the experiment is due to non-specific background staining of the secondary antibodies when used in conjunction with the relevant primary antibodies. However, we only presently report on the background signal produced by the secondary antibodies in wild-type mice, therefore the extent of background staining may have been different in MLP-deficient mice.

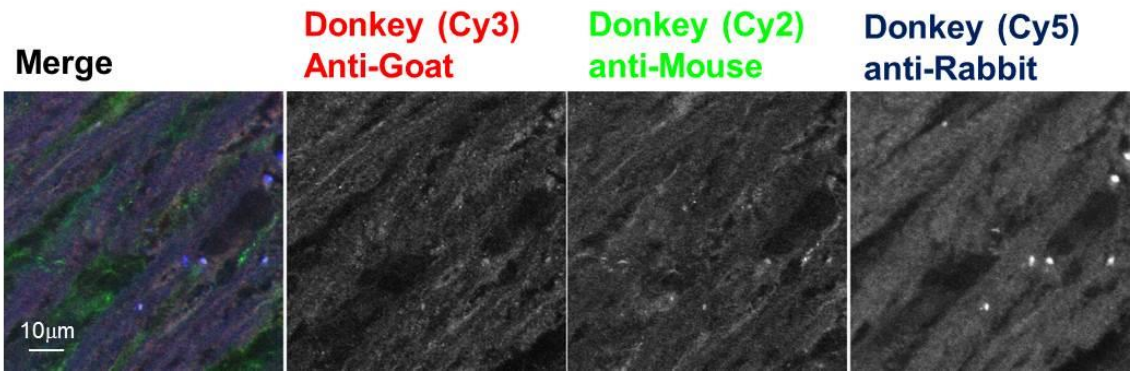

Figure 6.12: Negative Control for Fluorophore-Coupled Secondary Antibodies. In order to assess the extent of background staining produced by the secondary antibodies used for localisation studies in tissue sections, frozen heart sections of 1 year old male adult C57/BL6 mice were stained with the following antibodies: the Cy3-coupled donkey anti-goat antibody, which was used to detect the goat anti-FHOD1 antibody; the Cy2-coupled donkey anti-mouse antibody, which was used to detect the mouse anti-myomesin antibody; the Cy5-coupled donkey anti-rabbit antibody, which was used to detect the anti-NRAP antibody. Samples were visualised by confocal microscopy. Images represent portions of high magnification longitudinal sections. Cy3-coupled donkey anti-goat is seen in red, Cy2-coupled donkey anti-mouse is seen in green, and the Cy5-coupled donkey anti-rabbit antibody is seen in blue. Scale bars represent 10μm. **N=1.**

6.4 FHOD1 in MLP$^{-/-}$ Hearts

Initial staining for endogenous FHOD1 in MLP$^{-/-}$ mouse hearts revealed that the protein displayed a broad signal over the widened intercalated disks (Figure 6.11 B), which are a hallmark of this DCM model. Alterations in levels and localisation of FHOD3 have also been reported in MLP$^{-/-}$ mouse hearts (Iskratsch et al. 2010): FHOD3 was found to be downregulated in this mouse model of DCM. With initial staining for FHOD1 suggesting a possible increase in its signal in MLP$^{-/-}$ mice in comparison to wild-type mice, the possibility arose that FHOD1 may exhibit differential expression during instances of DCM. Therefore, the localisation and expression of FHOD1 was further examined in MLP$^{-/-}$ hearts by staining with other anti-FHOD1 antibodies and by checking total FHOD1 protein levels via Western blotting.

6.4.1 Localisation of FHOD1 in MLP$^{-/-}$ Hearts

In order to visualise the subcellular localisation of FHOD1 in DCM mouse hearts, staining was performed with the commercially available FHOD1 antibodies. Frozen

sections of $MLP^{-/-}$ hearts were stained with the following antibodies: polyclonal goat anti-FHOD1 C14 (Santa Cruz); polyclonal goat anti-FHOD1 C20; polyclonal rabbit anti-FHOD1 phospho-Threonine1141 antibody (Figure 6.13). The remaining anti-FHOD1 antibodies were excluded from this study as they did not produce a signal in frozen heart sections. Staining with all three antibodies revealed a strong signal for FHOD1 at the intercalated disks (Figure 6.13 A-C). Furthermore, the signal for FHOD1 across the intercalated disks appeared broader than previously noted in wild-type mice. FHOD1 was also found to sometimes distribute in a striated manner. This was especially the case with the polyclonal goat anti-FHOD1 C14 (Figure 6.13 A, Zoom) and the polyclonal rabbit anti-FHOD1 phospho-Threonine1141 antibody (Figure 6.13 C, Zoom) An alternating pattern with myomesin indicated that the FHOD1 signal may have been present in some of the Z-disks of sarcomeres. While a similar striated pattern was present with the polyclonal goat anti-FHOD1 C20 antibody (Figure 6.13 B, Zoom), it was not as strong as that seen with the other two antibodies.

Although we have demonstrated the capacity of the polyclonal goat antibodies to recognise FHOD1 and not FHOD3 using epitope-tagged recombinant human protein (See Figures 3.2-3.6), we could not rule out the possibility of cross-reactivity with other myocardial proteins. $MLP^{-/-}$ mice undergo alterations in the expression profiles of a number of proteins, therefore an antigen competition assay would be required in heart sections of both wild-type and $MLP^{-/-}$ mice to rule out the possibility of cross-reactivity in these separate samples.

We previously attempted to characterise the specificity of the polyclonal rabbit anti-FHOD1 phospho-Threonine1141 antibody and found that it specifically recognises phosphorylation in the FHOD1 DAD and due to conservation of the ROCK phosphorylation motif across human and rodents, that it could conceivably have recognised phosphorylated FHOD1 in mouse tissue (See Figures 4.5-4.8). We found no evidence of cross-reactivity with FHOD3, although we could not determine the actual extent of FHOD3 phosphorylation *in vitro*. While FHOD3 was previously shown to distribute in a similar manner as FHOD1 in wild-type mouse heart sections, FHOD3 exhibited a dramatically different localisation pattern in $MLP^{-/-}$ mice (Iskratsch et al. 2010). In wild-type mice, FHOD3 concentrates along the intercalated disks and distributes in a striated manner along the Z-disks. In $MLP^{-/-}$ mice, a decrease in total

FHOD3 was recorded at the protein level. Furthermore FHOD3 lost its characteristic staining pattern and instead distributed in a weak striated manner, where it tended to overlap with the signal for myomesin. Although staining for FHOD3 was not performed concurrently with that for phosphorylated FHOD1, the dramatically different staining pattern recorded for these two proteins can be taken as evidence that the polyclonal rabbit anti-FHOD1 phospho-Threonine1141 antibody was not recognising FHOD3, at least in $MLP^{-/-}$ mice.

Overall, the intensities at the intercalated disk and the striated appearance of FHOD1 may have been greater in $MLP^{-/-}$ mouse hearts than previously seen in wild-type mouse hearts (See Figures 3.12 and 3.13). These changes could have reflected altered levels of FHOD1 expression, therefore FHOD1 protein levels were compared in wild-type and $MLP^{-/-}$ mice via Western blotting.

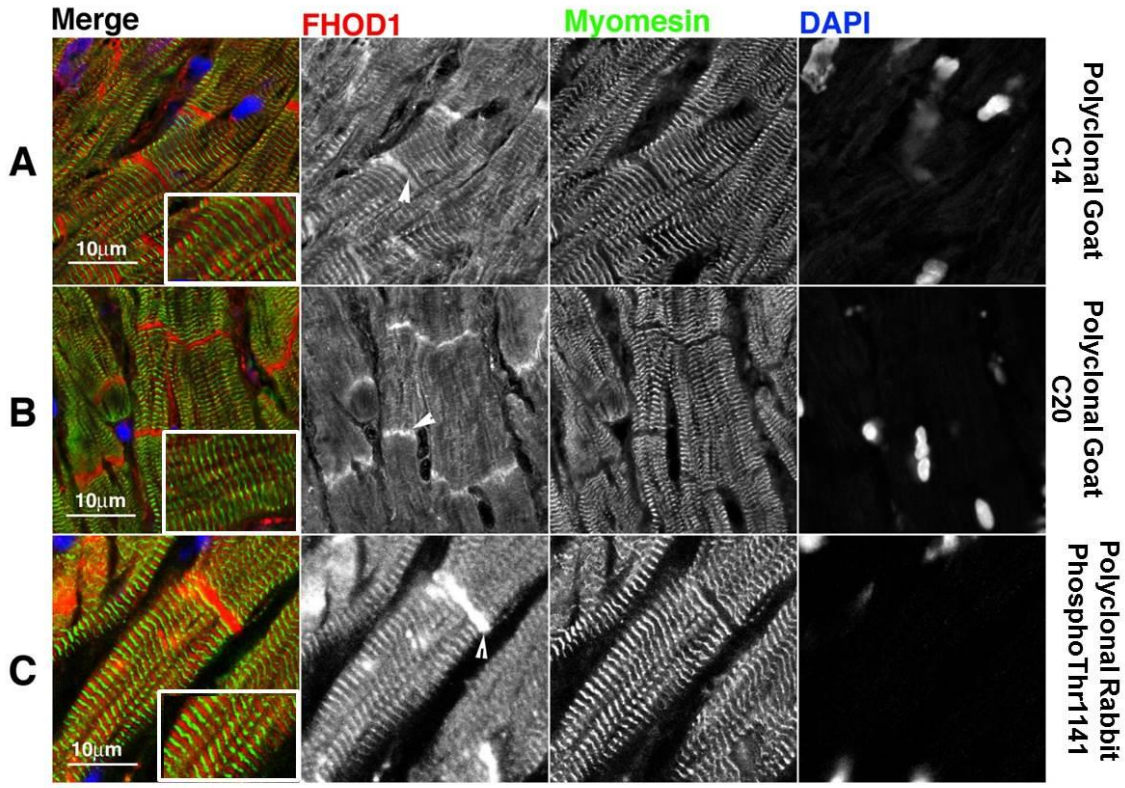

Figure 6.13: Localisation of FHOD1 in MLP$^{-/-}$ Murine Hearts. Frozen heart sections of 1 year old male adult MLP$^{-/-}$ mice were stained with the available anti-FHOD1 antibodies that produced a signal in heart sections. Sections were stained against myomesin to visualise the M-bands of sarcomeres and counterstained with DAPI to visualise nuclei. Sections were fixed in acetone prior to antibody staining and visualisation by confocal microscopy. Images represent high magnification longitudinal sections. The following antibodies were used: **A)** Polyclonal goat C14 anti-FHOD1 (Santa Cruz); **B)** Polyclonal goat C20 anti-FHOD1 (Santa Cruz); **C)** Polyclonal rabbit anti-phosphoThr1141 FHOD1 (ECM Biosciences). FHOD1 is seen in red, myomesin is seen in green, and DAPI seen in blue. Arrowheads indicate an intercalated disk. Scale bars represent 10μm. White boxes show zoomed selections of merged images. **N=2.**

6.4.2 Expression of FHOD1 in MLP$^{-/-}$ Hearts

In order to see if the levels of FHOD1 were altered in DCM mouse hearts, we compared levels of FHOD1 protein in wild-type and MLP$^{-/-}$ mouse hearts. Levels of FHOD1 were visualised using the polyclonal mouse anti-FHOD1 antibody (Abcam) (Figure 6.14 A) as it was the only commercially available antibody that produced a detectable signal on Western blots. A single band for FHOD1 was seen running just above the 123 kDa marker in the lanes for both wild-type and MLP$^{-/-}$ mouse hearts. Levels of α-actinin were also visualised to normalise protein levels for subsequent quantification (Figure 6.14 B). Relative expression levels of FHOD1 were determined by measuring the intensity of the FHOD1 bands and normalising to the intensity of the α-actinin bands

(Figure 6.14 C). Levels of FHOD1 in MLP$^{-/-}$ hearts were nearly two times greater than those seen in wild-type hearts (P = 0.0321), a result which reached statistical significance. We thus report a possible increase in cardiac FHOD1 expression in the hearts of MLP$^{-/-}$ mice. However, the caveat remained that the polyclonal mouse anti-FHOD1 antibody was not fully characterised since an antigen competition assay was not performed for Western blot studies. Therefore, we could not rule out the possibility that we were actually reporting relative expression levels of another protein in the present experiment.

While the present finding would be in line with the notion that MLP$^{-/-}$ hearts exhibited greater staining for FHOD1 at the intercalated disk and at the sarcomere, we were unable to demonstrate any changes in FHOD1 phosphorylation on Western blots. In order to detect such changes, one would need to quantify the signal for phosphorylated FHOD1 with respect to levels of total FHOD1. The apparently brighter signal for phosphorylated FHOD1 in MLP$^{-/-}$ hearts might only have reflected the total increase in FHOD1, with the ratio of phosphorylated FHOD1 to total FHOD1 remaining as it was in wild-type hearts. We attempted to detect phosphorylation in wild-type and MLP$^{-/-}$ cardiac tissue but were unable to obtain a signal using the polyclonal rabbit anti-FHOD1 phospho-Threonine1141 antibody (Results not shown). This could reflect that further optimisation of our lysis buffer is required in order to capture the signal for FHOD1 phosphorylation in the DAD on blots. This might include use of milder sample preparation methods (e.g., lysis in RIPA buffer) and/or the inclusion of phosphatase inhibitors in the lysis buffer.

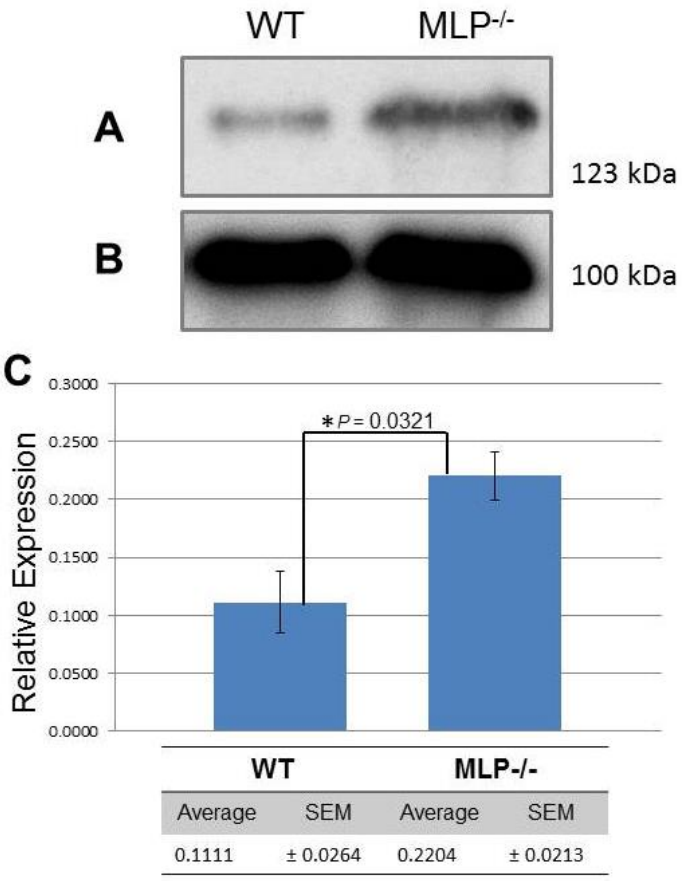

Figure 6.14: Expression of FHOD1 in MLP$^{-/-}$ Murine Hearts. Western blots of murine heart lysates. Expression was examined in 1 year old male wild-type C57/BL6 mouse hearts and in MLP$^{-/-}$ mouse hearts. **A)** Expression of FHOD1 was visualised with the polyclonal mouse anti-FHOD1 antibody (Abcam). **B)** Expression of sarcomeric α-actinin. **C)** Bar chart displaying relative expression levels of FHOD1 in wild-type versus MLP$^{-/-}$ mouse hearts. Relative levels were obtained by performing densitometric analysis on bands visualised by Western blotting. The relative intensity of FHOD1 bands were normalised to that of the α-actinin bands. WT, wild-type. Statistical significance was determined by performing an unpaired, two-tailed student's t-test *P<0.05 Error bars represent standard error mean. **N**=3 repetitions of Western blots with samples from 2 wild-type and 2 MLP$^{-/-}$ mouse hearts.

6.5 Discussion

6.5.1 Interactions with the FHOD1 GBD-DID Region

In the characterisation of FHOD1, two cDNA library screens were performed with different fragments of the FHOD1 N-terminus in the hope of finding novel binding partners. The screens utilised a human cardiac muscle cDNA library to search for interacting partners of FHOD1 in striated muscle. A yeast two-hybrid screen performed with the GBD-DID region of FHOD1 revealed three potential interacting partners.

A C-terminal fragment which contained the DAD of FHOD1 [1018-1091 on the long FHOD1 variant] was one of the protein regions identified in the screen. This interaction may have represented the autoinhibitory interaction between the FHOD1 DID and DAD which has already been extensively characterised (Schonichen et al. 2006). This result thus independently confirmed the FHOD1 autoinhibitory interactions through an indiscriminate interaction screen. However, we were unable to recapitulate binding between the FHOD1 N-terminus and the C-terminus since our C-terminal FHOD1 construct did not express to adequate levels for biochemical studies to be performed
The same screen also identified DLG5 as another potential interacting partner of FHOD1 but this interaction remained questionable since it was almost undetectable in the *LacZ* reporter gene assay. Furthermore, we were unable to show binding between the FHOD1 GBD-DID region and the C-terminal fragment of DLG5 [1362-1568] that was identified in our cDNA library screen in GST pull-down assays. However, we unable to exclude the possibility that this was due to lack of optimisation of the buffer conditions used for the GST pull-down assays. It remains to be seen by way of further biochemical and molecular biology experiments if there is indeed an interaction between FHOD1 and DLG5.

One of the proteins identified in the cDNA library screen with FHOD1 GBD-DID was a region of FHOD3 [969-1253] partly comprising the FH1 and FH2 domains. The interaction was partially validated during yeast two-hybrid assays, which supported the notion of a strong interaction between the specified portions of FHOD1 and FHOD3. This interaction could have indicated that FHOD1 and FHOD3 may form heterodimers. This would not be the first report of heterodimerisation between two different DRFs. mDia1 has been reported to dimerise with mDia2 as the full-length variants of both proteins bound each other in co-immunoprecipitation assays (Copeland et al. 2007). However, this interaction was ascribed to inhibitory cross-regulation of these formins. Binding was dependent on the presence of the DAD regions and it was also found that the DID of mDia2 inhibited the activity of mDia1. Furthermore, cross-regulation did not extend to the formin DAAM-1, implying that this mechanism was restricted to closely related members (Copeland et al. 2007). The portion of FHOD3 that was identified in the interaction screen, which did not contain the DAD, would argue against a cross-regulatory mechanism like the one seen between mDia1 and mDia2.

In the absence of functional data we can only speculate as to the consequences that this interaction could entail. Perhaps FHOD1 could sterically block association between FHOD3 and actin by binding part of its actin polymerising module (FH1-FH2), thus providing a new means of negative regulation of FHOD3 besides autoinhibitory regulation. This interaction could also be indicative of a new mechanism of activation for FHOD1. Perhaps the exposed FH1-FH2 region of activated FHOD3 could bind the N-terminus of FHOD1 to sterically displace the FHOD1 autoinhibitory interaction. Alternatively, the present results could potentially have represented a binding artefact since the FHOD1 GBD-DID region seemed to indiscriminately bind both the FH1 domain and the C-terminal fragment of FHOD3 in GST pull-down assays.

One potentially confounding factor relating to the cDNA library screen with the FHOD1 GBD-DID region related to the quality of the LexA-tagged bait protein. An equally prominent and faster migrating band was noted on Western blots testing for expression of the bait construct. Such an occurrence could indicate the presence of a contaminating protein species, which could have adversely affected the interpretation of any of the interactions studied in yeast. However, the interactions were further investigated using the GST-tagged FHOD1 GBD-DID construct, which exhibited some degradation on Western blots but did not give the same cause for concern in terms of a potentially contaminated protein preparation.

6.5.2 Interactions with FHOD1 [340-585]

During the screens to search for novel interacting proteins of FHOD1, NRAP was identified as a potential binding partner with a central portion of FHOD1 comprising the alternatively spliced exons (exons 12-13) found in the long FHOD1 variant. Although validation efforts were limited to a few NRAP fragments, we were able to show binding between the SR5-6 repeat and the N-terminus of FHOD1 [1-513] in GST pull-down experiments, although the binding appeared to be weak. The notion of an interaction between these regions was partly supported by yeast two-hybrid experiments which suggested that FHOD1 preferentially interacted with the shorter variant of SR5 (SR5-6) rather than the long variant (SR5-7). Co-staining for endogenous FHOD1 and NRAP in frozen sections of adult mouse hearts also revealed that both proteins co-localised at the intercalated disks.

However, results from the yeast two-hybrid assays remained somewhat questionable since there was some autoactivation by the FHOD1 bait construct, although incubation with 3AT could abolish this. The fact that FHOD1 preferentially interacted with the SR5-6 fragment and not the SR5-7 and SR4 fragments also raises doubt as to the specificity of the interaction since the SR5-7 fragment represents a longer variant of the SR5-6 fragment and because the SR repeats exhibit a considerable degree of homology (Mohiddin et al. 2003). However, we could not completely rule out the absence of binding for all of the currently addressed regions of NRAP due to lack of a positive binding control for each fragment. The potential issues relating to the validity of the LexA-tagged FHOD1 [340-585] bait construct and the GST-tagged FHOD1 N-terminal construct [1-513] could have influenced the present results, therefore future efforts will need to recapitulate these findings in the context of trustworthy FHOD1 preparations.
While the possibility of co-localisation of NRAP and FHOD1 at the intercalated disk suggested by immunofluorescence experiments would support the notion of an interaction between these two proteins, co-localisation does not necessarily equate to the association of two proteins *in situ*. Since we were unable to definitively show that FHOD1 and NRAP interact, their association at the intercalated disk can therefore only be concluded to be coincidental. Furthermore, we cannot conclude with certainty that the co-localisation of the two proteins at the intercalated disk was not mediated by cross-reaction of the antibody conjugates in the absence of single staining controls and controls in which the primary antibody is incubated with the secondary antibody of the other primary antibody used. Nevertheless, the use of multi-labelling quality antibodies likely reduced the chance of cross-reacting occurring.

The potential interaction between FHOD1 and NRAP may pose a number of exciting implications regarding the regulation of certain striated muscle subcellular structures, namely thin filaments and the intercalated disk. NRAP was originally identified as a striated muscle specific protein that was found to concentrate within the myotendinous junction in skeletal muscle and the intercalated disk in cardiac muscle (Luo et al. 1997a). Initial analysis of the C-terminus of NRAP revealed that it possessed 45% sequence similarity to the actin binding portion of the thin filament protein nebulin and that these nebulin SRs bound with high affinity to actin (Luo et al. 1997a; Luo et al. 1999). NRAP has also been shown to associate with the terminal ends of actin filaments (Herrera et al. 2000; Zhang et al. 2001). Analysis of NRAP within

preparations of the intercalated disk revealed that it was associated with the adherens junctions, that this association was likely mediated through the cadherin system (Zhang et al. 2001), and that it may serve to link the terminal ends of myofibrils to the cell membrane.

Aside from actin (Luo et al. 1997a), talin, vinculin (Luo et al. 1999), MLP (Ehler et al. 2001),filamin, and krp1, NRAP has also been shown to bind α-actinin (Zhang et al. 2001; Lu et al. 2003). The NRAP-α-actinin interaction initially implicated NRAP in participating in myofibrillogenesis, since both proteins co-localised in myofibril precursors near the membrane and in nascent myofibrils in cultured chick cardiomyocytes (Lu et al. 2003). Further work looking at the localisation of NRAP in embryonic mouse cardiomyocytes confirmed the association between NRAP and developing premyofibrillar structures containing α-actinin. In more-mature myofibrils, NRAP was found at the level of the Z-disk and the M-band. However, the myofibrillar association of NRAP is lost in the adult heart where it becomes preferentially associated with the intercalated disks (Lu et al. 2005). Depletion of NRAP in embryonic mouse cardiomyocytes resulted in decreased myofibril assembly thus confirming that NRAP plays a role in the regulation of the myofibrillar apparatus. Given the importance of NRAP in the regulation of muscle cytoarchitecture, If FHOD1 and NRAP indeed represent interacting partners, they could cooperate in the regulation of actin in myofibrils and at the intercalated disk.

6.5.3 Alterations in FHOD1 in MLP$^{-/-}$ Mice

Exploration of the potential FHOD1-NRAP interaction also revealed that there were possible alterations in FHOD1 expression and localisation in a mouse model of DCM, the MLP$^{-/-}$ mouse (Arber et al. 1997; Ehler et al. 2001). Co-localisation studies looking at endogenous FHOD1 and NRAP revealed that both of the proteins displayed a broader signal at the intercalated disks than previously noted in wild-type mice. Furthermore, it appeared as if their signals had increased. Staining with the other anti-FHOD1 antibodies also revealed what seemed to be a stronger signal at the intercalated disk for FHOD1.

Early observations regarding the ultrastructural changes at the intercalated disk in MLP$^{-/-}$ mice suggested that their intercalated disks undergo widening, and this was purported to be due to greater convolution of the plicate regions of the intercalated disks (Arber et al. 1997; Ehler et al. 2001), similar to observations made in the aged heart (Forbes and Sperelakis 1985). However, earlier efforts did not perform quantitative measures of the amplitude or lateral width of the plicate region of the intercalated disks in these animals; therefore the apparent widening of this structure was based on consensus. Nevertheless, recent efforts have shed light on this issue. Wilson et al. 2014 scrupulously measured the amplitude and lateral width of intercalated disks in a number of DCM samples, which included heart sections of MLP$^{-/-}$ mice, cΔex3 mice (overexpress a cardiac-specific β-catenin mutant), and idiopathic DCM human samples. Here it was found that DCM samples were consistently associated with intercalated disks of higher amplitude (Wilson et al. 2014). The broader signal that FHOD1 exhibited along the intercalated disk of MLP$^{-/-}$ mice could therefore have reflected redistribution of the formin along the widened intercalated disks (i.e., intercalated disks with greater amplitude). Alternatively, the brighter FHOD1 signal at the intercalated disks in DCM mice may have been due to enhanced access of the anti-FHOD1 antibodies to these sites. Gross ultrastructural alterations can potentially result in changes in accessibility of an antibody to a specific subcellular compartment. However, analysis of intercalated disk proteins by immunostaining semithin cryosections prepared according to the Tokuyasu method (Tokuyasu 1989), which have a thickness of 0.2 micrometres, as done in the work by Ehler et al., 2001, should prevent potential antibody penetration or access problems. In this study it was shown that in DCM a duplication of the signal for NRAP could be observed, which is consistent with the interpretation that the plasma membranes get more convoluted and that NRAP actually is located at the tips of the intercalated disk membrane, analogous to spectrin and not at the base, where the adherens junctions would be found (Bennett et al. 2006). So far stainings for FHOD1 have only be carried out on conventional cryosections with a thickness of 10μm, so it remains to be seen whether a duplication of the FHOD1 signal can also be resolved in DCM hearts using the Tokuyasu methodology and its improved resolution.

When compared to wild-type mouse hearts, the striated appearance of endogenous FHOD1 in MLP$^{-/-}$ mice was found to be more prominent. This was more so the case

with the polyclonal goat C14 anti-FHOD1 antibody and the antibody that recognised phosphorylated FHOD1, which revealed strong signals for FHOD1 at the intercalated disks and at the lateral portions of sarcomeres, suggesting some Z-disk localisation. Furthermore, we demonstrated that FHOD1 protein levels were significantly higher in $MLP^{-/-}$ mice than wild-type mice. We presently report a nearly two-fold increase in FHOD1 expression in this mouse model of DCM.

These results were a complete reversal to that seen previously with FHOD3. Analysis of FHOD3 expression in $MLP^{-/-}$ mice revealed that there was a downregulation in FHOD3 expression and a switch to the non-muscle FHOD3 isoform. Furthermore, the Z-disk and intercalated disk localisations of FHOD3 were lost and instead the formin was found distributing as weak striations around the M-band or in p62 containing autophagosomes (Iskratsch et al. 2010). $MLP^{-/-}$ mice may thus partly be characterised by an upregulation of FHOD1 expression with a concomitant decrease in FHOD3 expression.

Work in our laboratory has also suggested that the possible alterations in FHOD1 localisation and expression in the present mouse model of DCM may also be characteristic of the changes seen in human DCM. In comparison to control samples, staining for phosphorylated FHOD1 appeared to be more intense in human DCM samples, where the formin also appeared to redistribute across the widened intercalated disks (Dwyer et al. 2014). Once again, this was in contrast to the expression and localisation of FHOD3 in human DCM. Under these circumstances, FHOD3 expression is reduced and it loses its intercalated disk and Z-disk localisations (Iskratsch et al. 2010).

However, due to a number of caveats and oversights, it was not possible to definitively confirm the notions presented with respect to FHOD1 in DCM mice in the present study. The anti-FHOD1 antibodies presently employed require validation in both wild-type and MLP-deficient mice by way of antigen competition assays. Therefore we were not able to conclude with certainty that we were actually detecting FHOD1 in immunofluorescence samples and Western blots. Single staining controls and assessment of antibody cross-reactivity will also be required to confirm that the overlapping FHOD1-NRAP signal was genuine. Also, while we did not confirm loss of

MLP in the knockout mice on the protein level via Western blotting in the particular sample used for the analysis here, it is extremely unlikely that the hearts used were not from MLP knockout mice. The hearts were isolated from mice that were bred as a homozygous line for generations, so are most likely MLP knockouts. In addition, the mice have the characteristics that their light coat colour is linked to the MLP knockout phenotype making mix-ups with wild-type extremely unlikely (Elisabeth Ehler, personal communication). The MLP knockout mice are routinely checked for genotype and absence of MLP expression by Western blots and also their pronounced DCM phenotype, which was observed in the samples used for this study, indicates that we did indeed compare MLP knockout samples with wild-type..

6.5.4 Insights into DCM Phenotype

Initial characterisation of MLP-deficient mice revealed a disorganised myofibrillar phenotype with no evident changes in total protein composition (Arber et al. 1997). A number of genes, including atrial natriuretic factor and muscle ankyrin repeat protein (MARP), were elevated, in line with induction of a hypertrophic response. Further characterisation efforts of MLP-deficient mice subsequently revealed that, while overall sarcomeric ultrastructure remained intact, there were a number of alterations in cytoskeletal proteins, particularly those involved in cell-matrix and cell-cell adhesion (Ehler et al. 2001). Comparison of freshly isolated cardiomyocytes from wild-type and MLP-/- mice revealed an altered distribution of vinculin in MLP-/- mice. Vinculin was found to accumulate at the intercalated disks of cardiomyocytes and displayed aberrant distribution along the surface of cells, possibly indicating comprised costamere organisation in terms of the latter observation. Investigation of levels of a number of intercalated disk proteins also revealed trends in alterations of proteins within specific compartments of the intercalated disk. All of the adherens junction proteins that were investigated exhibit increased levels of expression. These proteins included the following: cadherin, β-catenin, plakoglobin, α-catenin, vinculin, and NRAP. The expression of the desmosomal proteins, desmoglobin and desmoplakin were seemingly unaffected. The gap junction protein, connexin-43 was downregulated.

Do the alterations in cytoskeletal proteins, including the potential increase in FHOD1 levels, account for some of the compensatory mechanisms that eventually result in

DCM in MLP$^{-/-}$ mice, or are they just artefacts resulting from perturbation of the signalling network which MLP forms a part of (Boateng et al. 2009)? MLP could bind and modulate transcription factors like GATA-4 or serum response factor (SRF) (Buyandelger et al. 2011) and disruption of MLP perturbs gene expression in muscle (e.g. reduced BNP expression) (Knöll et al. 2010) thus accounting for some of the changes noted in the knock-out mice. However, a multitude of roles have been proposed for MLP, including mechanosensing and maintenance of cardiac cytoarchitecture, therefore the compromise in cardiac cell structure plays an undeniable role in the progression to DCM (Buyandelger et al. 2011). Indeed, insights from other models of DCM, such as the tropomodulin-overexpressing transgenic (TOT) mouse, suggested that many of the previously observed alterations are conserved across DCM phenotypes. TOT mice similarly develop DCM and are characterised by an upregulation of adherens junction proteins, downregulation of gap junction proteins, and little or no change in desmosomal proteins (Ehler et al. 2001). However, MLP is downregulated in adult TOT mouse hearts; therefore it is difficult to dissect away all the perpetuating factors leading to a phenotype in these mice with respect to MLP$^{-/-}$ mice. Nevertheless, while the initial pathological insult and perpetuating factors may differ between experimental models and real-world cases of DCM, the end results can be similar.

One might also ask, why do these compensatory changes occur? In the case of adult MLP-deficient mice, alterations in the hemodynamic work load placed on the heart may necessitate many of the changes noted at the intercalated disk. As the animals age, dilatation progresses (Costandi et al. 2006; Buyandelger et al. 2011) it becomes increasingly difficult for the heart to pump blood systemically. It can be speculated that the greater convolution of the intercalated disk in such an instance may facilitate insertion of more terminal myofibrils in order for more efficient contractions to occur. However, it must be noted that the progression to the phenotype in MLP$^{-/-}$ mice is a gradual one. In fact, younger MLP$^{-/-}$ mice exhibit a hypertrophic phase before progressing onto a DCM phenotype (Arber et al. 1997; Costandi et al. 2006). We therefore captured a snapshot of a particular time point in MLP$^{-/-}$ mice in which they have already progressed to a DCM phenotype, although did not necessarily become globally decompensated. It remains to be seen how FHOD1 levels might change throughout the progression to DCM and finally heart failure. Nevertheless, the possible

increase in FHOD1 at the intercalated disk in DCM may have a number of interesting functional implications, given the actin regulatory role proposed for this formin.

6.5.5 Conclusion

Overall, we identified a novel set of potential interactions with the N-terminus of FHOD1. Some of the interacting proteins identified included FHOD3 and NRAP, which may have also bound the N-terminus of FHOD1, as suggested by GST pull-down assays. Although these interactions require extensive validation by way of biochemical means and functional assays, they may pose interesting biological implications. Furthermore, we report possible alterations in the localisation and expression pattern of FHOD1 in a mouse model of DCM.

6.5.6 Future Directions

The potential interaction between FHOD1 and FHOD3 represents an interesting finding in that it might suggest that these formins heterodimerise, a concept that is not completely foreign in the realm of formin biology (Copeland et al. 2007). However, GST pull-down assays suggested that FHOD1 bound multiple regions of FHOD3 and may have implied that binding between these two proteins was not specific. Further validation by co-immunoprecipitation assays will be essential in order to see if these formins can interact in a cellular environment. More importantly, interaction assays should also be performed in the context of a muscle cell background, although this might be difficult due to the lower transfection efficiency in primary muscle cells. This could be overcome with adenoviral mediated gene transfer however. Once there is reasonable grounds to claim an interaction (GST pull-down assays, co-immunoprecipitation assays, and co-localisation studies), functional assays should be performed in muscle cells to assess the significance of this potential interaction.

In the current experiments with FHOD1-NRAP it was difficult to definitively claim an interaction or binding between these two proteins. This stemmed from a number of factors. A questionable bait construct and a possibly contaminated GST-FHOD1 protein preparation made it difficult to conclude if the interactions were actually mediated by FHOD1. Future efforts should validate these constructs to confirm the identity of the unidentified protein species, which did not run at the expected molecular weight of the

FHOD1 constructs on gels. This could potentially be addressed by performing Western blots with the anti-FHOD1 antibodies. The FHOD1-NRAP interaction also remains doubtful since the GST-tagged N-terminal FHOD1 construct bound the shorter SR5 fragment but not the longer SR-5 fragment. This might have reflected that the conditions used for the GST pull-downs were not optimised for binding to occur with both constructs. Future efforts should be directed towards confirming binding of FHOD1 to full-length NRAP before trying to map the interaction to a specific domain. Subsequent experiments should confirm the interaction by way of co-immunoprecipitation assays and co-localisation studies. Further biophysical methods to characterise the possible interaction could also include isothermal titration calorimetry (ITC) and Biacore. The implementation of proximity ligation assays could subsequently help paint a picture of the FHOD-NRAP interaction *in situ*. The use of semithin cryosections will also help to better-delineate the relative localisations of NRAP and FHOD1 at the intercalated disk. Also, it will be of interest to see if the putative FHOD1-NRAP interaction is dependent on the alternatively spliced exons in FHOD1.

The present study and work in our laboratory suggested that the signal for phosphorylated FHOD1 was increased in DCM samples (Dwyer et al. 2014). However, the potential increase in total FHOD1 may have accounted for this change. Western blot studies may shed some light on this issue by quantifying relative levels of FHOD1 phosphorylation to total FHOD1 levels. However, we were not able to demonstrate a signal for phosphorylated FHOD1 on blots. Milder sample preparation methods and inclusion of phosphatase inhibitor could represent potential avenues to address this issue. However, antigen competition assays will be required on both Western blots and immunofluorescence samples in order to conclude that the antibody designed to recognise phosphorylated FHOD1 recognises its designated epitope.

The potential increase in FHOD1 levels found in the presently explored mouse model of DCM raises questions as to the role of FHOD1 in instances of cardiac disease and may imply diverging function with respect to FHOD3, which is downregulated in DCM. While pending antigen competition assays will be required to confirm the identity of FHOD1 in wild-type and DCM mice, it would be of interest to track FHOD1 protein levels and localisation throughout the progression to DCM in $MLP^{-/-}$ mice. It will also be of interest to explore FHOD1 expression and localisation in other models of DCM,

such as the TOT mouse, and eventually perform more-extensive studies using human samples.

Chapter 7

Discussion

7. Discussion

In the present characterisation effort, the role of FHOD1 in striated muscle was explored on a number of levels. The expression and localisation of FHOD1 was examined in cardiac and skeletal muscle. A number of gain-of-function and loss-of-function studies were also performed in the hope of elucidating the cellular roles of FHOD1 in cultured striated muscle cells. The characterisation effort was also extended to investigating possible regulatory mechanisms for FHOD1 through binding assays with various members of the Rho family small GTPases, their effectors, and Src. Finally, yeast two-hybrid assays were performed to screen for novel interacting partners of FHOD1. Overall, the present data implicated FHOD1 in the regulation of the myofibrillar apparatus and the cytoskeleton at the level of actin in striated muscle.

7.1 Expression of FHOD1

In the present study we attempted to elucidate the expression pattern of FHOD1 in striated muscle. Although pending validation by antigen competition assays, Western blot studies of whole muscle lysates indicated that FHOD1 was expressed in both cardiac and skeletal muscle. Closer analysis of FHOD1 expression in whole muscle lysates suggested that expression of FHOD1 was significantly higher in cardiac muscle than in skeletal muscle. This finding was in agreement with previous reports which also described higher expression of FHOD1 in cardiac versus skeletal muscle on both the mRNA transcript and protein level (Krainer et al. 2013). When expression of FHOD1 was compared between samples of slow twitch (soleus) and fast twitch (tibialis anterior) muscle, expression seemed to be higher in fast twitch skeletal muscle. This was in contrast to many other cytoskeletal proteins, which seem to be regulated in their expression in a similar way in ventricular and slow twitch muscle (Schiaffino and Reggiani 1996). However, this may have also reflected differential rates of protein turnover in each type of skeletal muscle: muscle proteins are continuously being turned over but rates vary according to the type of muscle. The average half-lives in rat adult slow twitch and fast twitch skeletal muscles are 12.1 and 18.3 days, respectively (Lewis et al. 1984; Goldspink 1991).The lower expression levels of FHOD1 in soleus could

have therefore been explained by the higher rate of protein turnover, resulting in less accumulation of FHOD1 in slow twitch skeletal muscle. However, different levels of FHOD1 in each tissue may have also been indicative of specific requirements for the protein, such as varying degrees of actin regulation, which is the main function ascribed to FHOD1.

The expression profiles of the different formin family members in striated muscle are also beginning to take shape. Analysis of the expression profiles of all 15 mammalian formins in striated muscle by quantitative real-time polymerase chain reaction (qRT-PCR) revealed interesting differences in the levels of each formin (Krainer et al. 2013). All 15 formins exhibited some level of expression in adult human skeletal muscle; with Dia3 and FHOD3 being the most highly expressed and DAAM-2 exhibiting comparatively low expression levels. In adult human cardiac muscle, FMN-1, FHOD1, and FHOD3 exhibited the highest expression whereas many other formins exhibited comparatively low expression levels. Expression of Delphilin was absent in cardiac muscle. Interestingly, FHOD1 may have exhibited the highest expression levels when considered across all cell and tissue types (Krainer et al. 2013), indicating that expression is not solely limited to muscle, but whether it plays a ubiquitous role in all these cell types remains to be determined.

Another study examined the expression profiles of all 15 mammalian formins at different stages of postnatal murine heart development, ranging from day 0 newborn mice to postnatal day 60 mice (Rosado et al. 2014). It was found that 13 of the 15 formins were expressed in at least one time point during postnatal heart development, with many formins exhibiting differential expression levels according to the stage of heart development. FHOD1 was found to exhibit consistent levels of expression throughout the hyperplastic and hypertrophic growth phases as well as the phase in which cardiomyocytes transition from hypertrophic growth to their mature state. Interestingly, FHOD1 levels fell at postnatal day 60, which correlates to the maintenance phase in cardiac cells. While such data may point to distinct roles for each formin and FHOD1 within separate stages of postnatal heart development, interpretation of qRT-PCR studies require caution since mRNA and protein expression profiles do not always fully correlate with each other, especially when considering that proteins may exhibit differential levels of stability in cells that may result in their

enhanced accumulation or degradation (Langley et al. 2012). The drop in FHOD1 expression in postnatal day 60 mouse hearts (Rosado et al. 2014) is somewhat inconsistent with the expression pattern of FHOD1 that we observed in cardiac specimens. Although detection of FHOD1 varied according to the anti-FHOD1 antibody that was employed, the present study suggested that FHOD1expression could be detected in neonatal rat cardiomyocytes (NRCs), adult rat cardiomyocytes (ARCs), and adult mouse whole heart lysates. However, quantification of changes in FHOD1 protein expression will be required in order to determine if FHOD1 levels are maintained at later stages of postnatal heart development.

7.2 Localisation of FHOD1

In addition to the expression pattern of FHOD1 we attempted to elucidate the subcellular localisation of this formin in different muscle specimens. Staining for endogenous FHOD1 with the commercially available anti-FHOD1 antibodies in cultured NRCs, freshly isolated ARCs, and differentiating C2C12 cells revealed inconsistent results regarding the localisation of this formin. This stemmed from improper characterisation of the antibodies in the absence of blocking peptides that would have been required to perform antigen competition assays at the time of the study. However, the antibodies highlighted the possibility of FHOD1 localising to the sarcomere in cultured cardiomyocytes. Staining for FHOD1 in sections of adult mouse heart tissue sections revealed more consistent results in that the three antibodies that displayed reactivity in tissue sections suggested similar localisation patterns for FHOD1. In tissue sections, staining for FHOD1 revealed notable intensities at the intercalated disks between neighbouring cardiomyocytes. Staining for FHOD1 was also visible throughout cardiomyocytes and could be occasionally be resolved as striations around the area of the Z-disks. Interestingly this localization pattern may be evolutionally conserved; in *Caenorhabditis elegans* FHOD1 is also found as bright puncta at the muscle cell edges with faint striations at the dense bodies, the equivalent of the Z-disk (Mi-Mi et al. 2012). In the present study, some staining for FHOD1 was also noted in the interstitial spaces between neighbouring cardiomyocytes and may have suggested expression of this formin in resident cardiac fibroblasts. Indeed, the heterogeneity of cells found within the heart may have called into question the precise cellular source accounting for FHOD1 expression in whole muscle samples, but a signal

visible throughout cardiomyocytes in heart sections suggested that they could have been an abundant source of FHOD1 expression in the heart.

Interestingly, FHOD1's closest relative, FHOD3, may exhibit a similar localisation pattern in healthy adult mouse hearts. Although there have been some discrepancies as to the precise localisation of FHOD3 in adult cardiac specimens, with initial reports placing it near the A-bands of sarcomeres (Kan-o et al. 2012b), work in our laboratory and data from another study suggested that FHOD3 is found at the Z-disks (Iskratsch et al. 2010; Iskratsch et al. 2013a; Rosado et al. 2014) and the intercalated disks (Iskratsch et al. 2010; Iskratsch et al. 2013a). Similar localisation in adult heart specimens may imply some level of conservation in the roles of FHOD formins in cardiomyocytes. However, in NRCs, both endogenous and ectopically expressed FHOD3 were shown to exhibit a broader localisation pattern across myofibrils, which may have been consistent with a more dynamic role in myofibrillar maintenance when cardiomyocytes are actively remodelling their myofibrils in response to adapting to cell culture conditions (Iskratsch et al. 2010; Iskratsch and Ehler 2011; Iskratsch et al. 2013a). Furthermore, epitope-tagged full-length FHOD1 distributed in a predominantly diffuse cytoplasmic manner with strong intensities near the peripheries of cells and some myofibrillar targeting in NRCs, suggesting that if FHOD formins exert their functions in distinct subcellular compartments, that this may vary according to specific stages of heart development.

The subcellular localisation of other formins has also been studied in cardiomyocytes. DAAM-1, which has been implicated in having an actin bundling role critical for filopodial organisation (Jaiswal et al. 2013), was found to localise to the cell peripheries in early myofibrillogenesis and to the Z-disks in mature myofibrils (Rosado et al. 2014). mDia2, which has been shown to possess actin polymerising (Pellegrin and Mellor 2005), stress fibre organising (Tojkander et al. 2011; Tojkander et al. 2012), and bundling activities (Harris and Higgs 2006) was shown to localise to the cell peripheries during early myofibrillogenesis and to the Z-disks and M-band in mature myofibrils (Rosado et al. 2014). The lesser studied FMNL formins, which have been implicated in actin polymerising events downstream of Rac and Cdc42 (Yayoshi-Yamamoto et al. 2000; Block et al. 2012), were also found to exhibit myofibrillar localisation in cardiomyocytes (Rosado et al. 2014). FMNL1 co-localised with assembling myofibrils

at the plasma membrane during myofibrillogenesis and was found near the region of the I-bands in mature myofibrils. FMNL2 exhibited localisation throughout the sarcomere, apart from the Z-disks. However, not all formins are necessarily found at a given sarcomeric compartment or even at myofibrils. For instance, FMNL3 and mDia1 are localised in puncta throughout cultured cardiomyocytes (Rosado et al. 2014). Thus, a number of formins with diverse sets of actin regulating activities have been found to be targeted within distinct compartments of cardiac cells at specific time points. However, localisations of the formins studied in Rosado et al. 2014 will require confirmation: This study employed only partially characterised antibodies from commercial studies so it remains to be confirmed by absorption studies that the signal seen for these formins during myofibrillogenesis and in mature myofibrils was indeed *bona fide*.

Although a larger part of our data presently described related to the localisation of FHOD1 in terminally differentiated cardiomyocytes, we may have gained some insight into the localisation FHOD1 during the skeletal muscle differentiation process. C2C12 cells can be used to study the cues and changes involved in myogenic differentiation, a process that is central to the development of skeletal muscle. Myogenesis occurs during embryonic development and in post-natal skeletal muscle. During embryogenesis, the first skeletal muscle fibres are derived from the embryonic mesoderm, and these are thought to serve as a template for further generation of muscle fibres. Adult skeletal muscle still has a requirement for generation of skeletal muscle fibres, although this is mainly in response to damage, hence skeletal muscle regeneration occurs from a residing pool of satellite cells (Bentzinger et al. 2012). C2C12 cells recapitulate the events involving the formation of skeletal muscle when they fuse and create newly formed myofibrils and sarcomeres. Although these events occur within the context of two-dimensional culture conditions, the advantage of the C2C12 model is that it permits specific stages of muscle differentiation to be studied. Apart from day 0 undifferentiated myoblasts, where there may have been expression of an unreported FHOD1 variant, expression of FHOD1 was noted throughout the differentiation process from skeletal myoblasts to myotubes in C2C12 cells. However, future efforts should make it a priority to see if differential levels of FHOD1 expression and activation occur throughout skeletal muscle differentiation. Antibody staining in cells revealed a predominantly diffuse localisation for FHOD1 throughout the differentiation process. Some co-localisation with F-actin stress fibres was noted in elongating cells. Some myofibrillar

and sarcomeric targeting were also noted in the later stages of differentiation, after the initiation of sarcomerogenesis (Burattini et al. 2004), although this varied between the anti-FHOD1 antibody that was used. Presently it is difficult to integrate the localisation of FHOD1 with the results from our knockdown studies, which suggested that FHOD1 may be crucial in maintaining the F-actin cytoskeleton in day 3 C2C12 cells. Due to the potential technical issues relating to shRNA plasmid dilution in C2C12 cells, it remains to be determined if FHOD1 plays roles in myoblast fusion and sarcomere assembly by investigating the function of this formin at later time points.

7.3 Potential Mechanisms Guiding FHOD1 Localisation

In the present study we attempted to dissect the contribution of some of the individual FHOD1 domains. The subcellular targeting of GFP-tagged expression constructs that only encoded for individual domains of FHOD1 were explored in NRC. The FH2 domain of FHOD1 on its own displays a strong signal at the Z-disks, as indicated by co-localisation with α-actinin, and with F-actin at the peripheries of cells. Constructs encoding the GBD-DID or GBD primarily displayed diffuse cytoplasmic localization with some evidence for myofibril targeting, which was similarly noted for full-length FHOD1 construct. The DID alone as well as the N-terminal deletion construct lacking the GBD domain (FHOD1 ΔGBD) distributed as aggregates or small vesicular-like structures. This may have indicated that the GBD influenced the targeting of the full-length wild-type FHOD1 construct in NRCs. However, the targeting of FHOD1 ΔGBD may have been a result of instability of the construct in NRCs. Nevertheless, the notion of the FHOD1 GBD contributing to the targeting of this formin is partly supported by other work with this formin.

The N-termini of formin proteins have been suggested to mediate their subcellular localisation (Seth et al. 2006; Ramalingam et al. 2010) and are coincidentally the regions of highest divergence amongst formins. Indeed, the importance of the FHOD1 N-terminus has been highlighted by other studies (Schonichen et al. 2013; Schulze et al. 2014). The N-terminal half of FHOD1 [1-568; short FHOD1 variant] was found to mediate targeting of this formin to transverse arcs and stress fibres (Schonichen et al. 2013). Further mapping of the possible mechanism governing targeting of FHOD1 revealed that it was the GBD-DID region that precisely mediated targeting of FHOD1 to

transverse arcs and stress fibres (Schulze et al. 2014). However, in terms of FHOD1 targeting to stress fibres, the GBD on its own was suggested to have a limited contribution, which would be in contrast to the present interpretation of our domain overexpression data in NRCs. Nevertheless, these differences in results could be accounted for by the use of different cell types used to explore the targeting of FHOD1 (human U2OS osteosarcoma cells in Schulze et al. 2014, COS-7 cells in Schonichen et al. 2013, and NRCs in the present study) and could suggest that cell-type specific interacting proteins may influence targeting of FHOD1 via its N-terminus.

It is tempting to speculate into the additional factors that may govern the localisation of FHOD1 in muscle cells. The notion of the GBD mediating the localisation of FHOD1 raises the possibility that recruitment of this formin could be guided by a Rho family small GTPase. However, no studies have demonstrated binding of a Rho family small GTPase to the FHOD1 N-terminus (Westendorf 2001; Schulte et al. 2008). There is also currently little known about the expression pattern of the Rho family GTPases in cardiac muscle. Furthermore, while there is some evidence for the association between the Rho family GTPases and myofibrils (Ahuja et al. 2007), this remains to be fully elucidated; therefore there is little room for speculation. Nevertheless, while previous efforts have failed to show that a Rho family small GTPase binds the FHOD1 GBD (Schulte et al. 2008) and the present study failed to show binding of a handful of GTPases and their effectors to the FHOD1 N-terminus, comprising the alternatively spliced exons, cooperation with these proteins in regulating the localisation in muscle still remains a possibility. Rac has been shown to mediate targeting of FHOD1 in a number of instances (Gasteier et al. 2003; Alvarez and Agaisse 2013) and this could be a consequence of the physical association of both proteins, since Rac has been shown to bind the central portion of FHOD1 near the FH1 domain (Westendorf 2001; Gasteier et al. 2003; Wang et al. 2004). Nevertheless, binding may vary according to cell type and other interacting partners since co-immunoprecipitation studies in platelets suggested that FHOD1 and Rac did not interact (Thomas et al. 2011). We cannot however dismiss other mechanisms potentially guiding the targeting of FHOD1. In the case of FHOD3, targeting of this formin to sarcomeres relies on a phosphorylation dependent process in which CK2 phosphorylates the sequence encoded by the T(D/E)5XE exon found in the FH2 domain of the muscle-specific variant of FHOD3 (Iskratsch et al. 2010).

7.4 Effects of FHOD1 Activation in Cardiomyocytes

In addition to addressing the expression and localisation of FHOD1, the present study also investigated the functional consequences of FHOD1 activation in cardiomyocytes. Overexpression of constitutively active FHOD1 has previously been associated with the appearance of stress fibres in cells (Gasteier et al. 2003; Koka et al. 2003; Gasteier et al. 2005; Takeya et al. 2008). We overexpressed three different FHOD1 mutants that have previously been described as models for constitutive activation of this formin. Introduction of the V228E mutation in the FHOD1 GBD, which has been previously shown to disrupt the autoinhibitory interaction between the FHOD1 N and C-termini (Schulte et al. 2008), resulted in the formation of ventral stress fibres in NRCs. Truncation of the DAD, which also results in release of the autoinhibitory interaction that supposedly retains FHOD1 in an inactive state (Koka et al. 2003; Schonichen et al. 2006), was associated with the formation of F-actin bundles. Introduction of three phosphomimetic Aspartate residues in the DAD, designed to mimic the effects of activation by ROCK-I phosphorylation (Takeya et al. 2008; Staus et al. 2011a), resulted in an elongated morphology in cells and may have resulted in increased staining for F-actin. Although the phenotypes associated with these three FHOD1 mutants were slightly incongruous, they would generally suggest that upon activation FHOD1 might co-localise with F-actin and contribute to the reorganisation of the cardiac F-actin cytoskeleton via its actin bundling capabilities (Schonichen et al. 2013) or another of its proposed actin regulating roles (e.g., actin polymerisation) (Iskratsch et al. 2013b).

The differences between the FHOD1 ΔDAD and V228E mutants could be explained by the possibility that DAD is required for full biological activity of FHOD1 in cells. A previous study noted that the FHOD1 V228E mutant was able to more potently induce the formation of stress fibres than the FHOD1 ΔDAD construct (Schulze et al. 2014). The DAD of FHOD1 could therefore play other roles besides mediating autoinhibition of the protein. This has also been noted for mDia1, whose DAD has been suggested a role in filament nucleation (Gould et al. 2011). As for the ROCK-I phosphomimetic FHOD1 mutant, one possible explanation behind the difference with this construct is that it does not represent a marker for full activation of the protein. Indeed, the full-

length wild-type FHOD1 construct, which did not result in overt effects on NRC morphology, was recognised by the anti-FHOD1 phospho-Threonine1141 antibody in NRCs, suggesting that phosphorylation of the construct was present. While this could be explained by incomplete phosphorylation of all three of the relevant residues in the DAD, it could be indicative that further cues are required for full activation of FHOD1 to occur.

However, the relevance of full FHOD1 activation in cardiomyocytes should be taken into consideration. The phenotype associated with the V228E construct could be considered to be that of an extreme nature in a physiological context, especially when considering the potential role of FHOD1 in myofibrillar maintenance. In terminally differentiated cardiomyocytes, myofibrillar maintenance seems to primarily take place through addition of new monomers at the ends of myofibrils (Ono 2010). Although *de novo* nucleation/polymerisation of filaments has been described (Skwarek-Maruszewska et al. 2009), neither of these processes seem to involve the formation of stress fibres. The stress fibre forming activity of FHOD1 may have been more relevant in the day 3 C2C12 model since transfection with the FHOD1 shRNAs was associated with the disappearance of the characteristic stress fibres noted in cells at this time point. In striated muscle, the formation of stress fibres might have some relevance during myofibrillogenesis. One of the proposed models of myofibrillogenesis, namely the template model, describes the participation of stress fibres (Sanger et al. 2005). In this model, different components of myofibrils are recruited to surface of stress fibres or stress fibre-like structures at the plasma membrane. These include dense components of the Z-disk as well as the thin and thick filaments. Stress fibres disappear after assembly takes place and then reassemble for the new myofibril to be pieced together. Regardless of the potential of FHOD1's stress fibre activity contributing to muscle development or maintenance, regulation by ROCK-I is currently the most accepted mechanism governing FHOD1 activation, therefore results gained using the V228E mutation in NRCs might not be entirely translatable to the context of terminally differentiated cardiomyocytes.

Further insight into the functional activity of FHOD1 has previously been gained through the study of its FH2 domain. Not only is the FH2 domain required for the direct actin regulating activity of FHOD1 (Schulze et al. 2014), previous work with FHOD1

also suggested that its activity in cells was dependent on oligomerisation via the FH2 domain (Takeya and Sumimoto 2003; Madrid et al. 2005). A coiled-coil motif found C-terminal of the core FH2 domain, but still found within the presently accepted boundaries of the FH2 domain, was found to be essential for the self-association of FHOD1 as supported by yeast two-hybrid and co-immunoprecipitation studies. Furthermore, the presence of the coiled-coil motif was required for the targeting of FHOD1 to stress fibres in its constitutively active state, induced by truncation of the DAD (Madrid et al. 2005). These findings supported a previous study which suggested that FHOD1 self-associates via its FH2 domain (Takeya and Sumimoto 2003).

In the present study, the FH2 domain of FHOD1 was targeted to the Z-disks and displayed co-localisation with F-actin at the peripheries of cardiomyocytes. As a component of the quintessential actin regulating module of formins, one might ask if the targeting of the FH2 domain in cardiomyocytes represents the functional localisation of FHOD1. Targeting of full-length inactive and constitutively active FHOD1 differed somewhat from the targeting of its isolated FH2 domain in NRCs. In cardiomyocytes, full-length FHOD1 displayed a diffuse cytoplasmic signal with strong intensities at the peripheries of cells with little co-localisation with myofibrils was noted in this instance. Upon activation, FHOD1 displayed targeting to F-actin, myofibrils, and the sarcomere. However, localisation of the constitutively active FHOD1 variants was not restricted to the Z-disks since their targeting within the sarcomere was often irregular with respect to the spacing of α-actinin. Regardless of its localisation within the sarcomere, the FH2 domain could still participate in targeting of active FHOD1 to F-actin. Unmasking of the functional FH domains following activation of FHOD1 could result in dimerisation of two FHOD1 molecules via their FH2 domains. Therefore, dimerisation via the FH2 domain may have been an important factor governing the activity of constitutively active FHOD1 in NRCs. However, we cannot dismiss the notion that FHOD1 possesses biologically relevant activity in its monomeric inactive state, since the GFP-tagged full-length wild-type FHOD1 constructs may have resulted in increases in the F-actin content in HeLa cells. However, the function of FHOD1 could vary considerably between cell types as previous studies investigating FHOD1's multiple interacting partners have suggested (Gill et al. 2004; Kutscheidt et al. 2014). Nevertheless, the full extent by which the FH2 domain contributes to FHOD1's function in cardiomyocytes

can only be fully dissected by employing variants lacking the FH2 domain in both inhibited and uninhibited conformations.

7.5 Role of FHOD1 and Formins in the Regulation of Muscle Cytoarchitecture

One of the more important findings in the present study related to the possibility that FHOD1 may play a crucial role in the maintenance of the myofibrillar apparatus and the F-actin network in muscle cells. Although pending validation by confirming actual disruption of endogenous FHOD1 expression, transfection of NRCs and C2C12 cells with the shRNAs designed to knock down FHOD1 was associated with a number of cellular defects. In day 8 NRCs, these effects included disruption of myofibrils at the level of F-actin and sarcomeric proteins, distortion of cell shape, and disruption of cell-cell contacts at the level of the intercalated disk. In day 3 C2C12 cells, effects included disruption of the F-actin cytoskeleton. Previous studies which looked at FHOD1 disruption also reported disruption of F-actin in cells and would be in agreement with the present findings. Knockdown of FHOD1 blocked the formation of stress fibres in in Human Pulmonary Artery Endothelial Cells (HPAEC) (Takeya et al. 2008) and smooth muscle cells (Staus et al. 2011a). Knockdown of FHOD1 was also associated with higher levels of G-actin compared to F-actin, possibly suggesting less actin polymerisation or destabilisation of F-actin filaments (Staus et al. 2011a). Furthermore, silencing of FHOD1 in breast cancer cells also led to a loss of stress fibres, less cell elongation, and a diminished metastatic potential (Jurmeister et al. 2012). FHOD1 was also shown to contribute to development of the myofibrillar apparatus in *Caenorhabditis elegans (Mi-Mi et al. 2012). Overexpression of two mutant variants of FHOD1, one* eliminating part of an intron and a DID-encoding exon and the other eliminating part of the FH2 domain, resulted in defects in development of body wall muscles (BWM) of larvae at the level of contractile lattice development, sarcomere organisation, and F-actin deposition. Interestingly, the FHOD1 mutant with the disrupted FH2 domain was associated with a more severe phenotype and may be explained by the ability of the FH2 domain to mediate self-association of FHOD1 and to directly regulate F-actin based structures. Furthermore, these defects were recapitulated with knockdown of endogenous FHOD1. The present data and the observations in *Caenorhabditis elegans larvae in particular highlight the potentially*

crucial role FHOD1 could play in the regulation of the F-actin network and the myofibrillar apparatus in muscle cells.

In terms of the FHOD proteins, FHOD3 has been shown to play a role in regulation of cardiac cytoarchitecture. Knockdown of FHOD3 also resulted in myofibrillar disruption in NRCs (Taniguchi et al. 2009; Iskratsch et al. 2010). Iskratsch et al. 2010 noted defects in myofibrils by day 5 of FHOD3 knockdown. At this time point, FHOD3 depleted NRCs presented with shortened myofibrils and fewer mature sarcomeres. By day 8, FHOD3 depletion resulted in exacerbation of the myofibrillar phenotype (Iskratsch et al. 2010) similarly noted with the FHOD1 shRNA constructs. The contribution of the FH2 domain of FHOD3 was found to be crucial in mediating its effects on myofibrillar maintenance: introduction of mutations into the FH2 domain in an siRNA resistant form of FHOD3 was unable to restore sarcomere organisation in NRCs depleted of endogenous FHOD3 (Taniguchi et al. 2009). The residues mutated in FHOD3 (I1127A and K1273D) corresponded to those found in yeast formin Bni1p, that when mutated disrupted the actin nucleating activity of Bni1p (Xu et al. 2004; Otomo et al. 2005b). The precise mechanism by which FHOD3 regulates myofibrillar and sarcomeric organisation via its FH2 domain remains to be determined however. While actin polymerisation remains a possibility, *in vitro* experiments suggested that FHOD3 prevented actin polymerisation in both the presence and absence of profilin and that it specifically prevented elongation from the barbed end of filaments (Taniguchi et al. 2009). Indeed, the multitude of actin regulatory functions that have been described for formins, ranging from actin bundling to severing (Breitsprecher and Goode 2013), could indicate roles for FHOD3 that go beyond actin polymerisation. However, the presence of actin assembly cofactors in cells could facilitate the potential actin polymerising activity of FHOD3. The effects of FHOD3 on the barbed ends of filaments and its localisation at the Z-disk in adult muscle has resulted in a 'leaky' capper role being proposed for FHOD3, in which FHOD3 could transiently associate with the barbed ends of actin filaments in myofibrils to contribute to their maintenance, possibly by addition of actin monomers at the barbed end (Iskratsch and Ehler 2011; Dwyer et al. 2012). Overall, these data can be taken as evidence for formin homology proteins as highly relevant factors that contribute to myofibrillar maintenance.

Insights into the role of formins in muscle have also been gained from studies using knock-out mice, specifically the FHOD3$^{-/-}$ (Kan-o et al. 2012a) and DAAM-1$^{-/-}$ (Li et al. 2011) mice. Homozygous null FHOD3 mice died during embryonic development due to a number of cardiac defects including improper cardiac looping and perturbed myocardial development. The cardiomyocytes of homozygous null FHOD3 mice were able to assemble premyofibrils similarly to wild-type and heterozygous null FHOD3 mouse littermates; however, mature myofibrils were never fully formed. Defects were only rescued upon re-expression of the wild-type FHOD3 variant and not with the actin binding defective FHOD3 mutant (Kan-o et al. 2012a). DAAM-1 was similarly required for proper heart development. Homozygous null DAAM-1 mice also died during embryonic development due to a number of cardiac defects, including ventricular non-compaction and ventricular septal defects. Cardiomyocytes from homozygous null DAAM-1 mice also displayed a perturbed myocardial cytoskeleton and presented with randomly oriented and aggregated striated F-actin. Cells also showed decreased staining for F-actin and fewer sarcomeric striations. Compromised sarcomeric maturation was also made evident by the fact that there was diffuse staining for actin and sarcomeric α-actinin (Li et al. 2011). These defects in myofibrillar and cytoskeletal organisation partly resonated the effects associated with the FHOD1 shRNA constructs in NRCs. The effects of DAAM-1 depletion were first speculated to be due to disruption of the plasma membrane cytoskeleton, where DAAM-1 was thought to primarily localise to (Iskratsch and Ehler 2011; Li et al. 2011). However, recent reports of DAAM-1 additionally localising to the Z-disks in neonatal mouse cardiomyocytes also makes regulation of this cellular compartment a possibility (Rosado et al. 2014). In the current study, the effects associated with FHOD1 depletion may have been due to impaired maintenance of multiple structures in cardiomyocytes, such as the myofibrils and the intercalated disks. Overall, formins would seem to play an important role in the formation and maintenance of the myofibrillar apparatus and the cytoskeleton in the muscle cells. This notion would also be in agreement with our experiments employing the pan-formin inhibitor SMIFH2, which was associated with disruption of the F-actin network, myofibrils, sarcomere organisation, and the intercalated disk in cultured NRCs. However, not all formins might play an indispensable role in the muscle since no cardiac defects were observed in homozygous null mDia1 knockout mice (Peng et al.

2007). Thus, formins may not be redundant in their effects despite sharing a conserved actin regulating module (i.e., the FH1 and FH2 domains).

Our current understanding of myofibrillar regulation describes a number of proteins that regulate the length and stability of myofibrils. For instance, CapZ is thought to cap and stabilise the barbed ends of filaments (Schafer et al. 1995; Papa et al. 1999), contribute to thin filament organisation (Hart and Cooper 1999), and prevent aberrant filament elongation from the barbed end (Ono 2010). Tropomodulin, which appears to be the main pointed end capping protein, has well-established roles in regulating thin filament lengths (Gregorio et al. 1995) and its importance has been resonated by gain-of-function and loss-of-function animals, which develop cardiac abnormalities (Sussman et al. 1998; Fritz-Six et al. 2003). The actin side binding protein, tropomyosin contributes to thin filament stability and plays roles in the regulation of muscle contractility (Ono 2010). However, many of the other mechanisms that govern regulation of myofibrils at the level of formation, maintenance, and turnover have yet to be fully elucidated. More-recent efforts have suggested a number of actin regulatory proteins to participate in some of the processes. In terms of actin nucleation at the barbed ends of filaments in terminally differentiated muscle cells, the nebulin-NWASP complex was shown to stimulate formation of unbranched actin filaments downstream of IGF-1 and could represent a mode of sarcomeric actin filament formation during hypertrophic growth (Takano et al. 2010). The pointed end associated protein leiomodin has been suggested to have actin assembly activity by promoting addition of actin monomers at the pointed ends of filaments and may also serve as a means to regulate the lengths of sarcomeric actin filaments (Tsukada et al. 2010). Indeed, the reported roles of formins make them good candidates for myofibrillar regulation: the evidenced reviewed for DAAM-1 and FHOD3 in regulating cardiac cytoarchitecture (Iskratsch et al. 2010; Li et al. 2011; Kan-o et al. 2012a; Kan-o et al. 2012b; Iskratsch et al. 2013a) as well as the present data presented for FHOD1 would support the addition of these proteins to the growing list of factors that regulate myofibrils (Ono 2010; Dwyer et al. 2012).

While FHOD3, DAAM-1, and even FHOD1 may contribute to the maintenance of myofibrils in terminally differentiated muscle cells (i.e., postnatal NRCs in the case of FHOD1), their role in myofibrillogenesis remain to be clarified. It would appear that FHOD3 and DAAM-1 are not crucial for the initial nucleation/elongation of myofibrils

but are still essential for maintenance of the myofibrillar apparatus (Li et al. 2011; Kano et al. 2012a; Rosado et al. 2014). However, experiments in mouse cardiomyocytes implicated the importance of a number of formins in *de novo* myofibril formation (Rosado et al. 2014). Day 0-3 neonatal mouse cardiomyocytes were isolated and transfected with siRNA to disrupt expression of specific formins before plating. Cardiomyocytes temporarily disassemble their myofibrils before readapting to culture conditions, therefore disruption of expression of specific formins at this time could have potentially identified whether they play a role in myofibril formation. A particularly severe phenotype was associated with knockdown of FMNL2 in this setting, and may have been due to its ability to contribute to the formation/organisation of actin filaments in the early stages of myofibril formation (Rosado et al. 2014). The role of FHOD1 in *de novo* myofibril formation and myofibrillogenesis has yet to be demonstrated but its presently suggested role in myofibrillar maintenance and possible expression throughout the C2C12 differentiation process also makes it a candidate.

Similarly to other formins and actin regulating proteins, the present study would indicate an important role for FHOD1 in striated muscle cells. However, the multitude of proposed actin regulating activities for FHOD1 highlights a number of possibilities by which it could regulate myofibrils and the F-actin network in muscle cells. FHOD1 could be mediating its effects via its proposed function as an actin polymerising protein (Iskratsch et al. 2013b), actin capping protein, actin side binding, actin bundling protein (Schonichen et al. 2013; Schulze et al. 2014), signalling effector (Westendorf 2001; Gasteier et al. 2003; Staus et al. 2011a), or a mixture of these functions. The potential contributions of each of these putative FHOD1 functions are discussed below.

7.5.1 FHOD1 as an Actin Polymerising Protein in Muscle

There are a number of observations in the present study which may have suggested that FHOD1 exerted some of its effects in cells through the polymerisation of actin. Overexpression of constitutively active FHOD1 ΔDAD and V228E mutants in NRCs seemingly resulted in an increased signal for F-actin along newly formed actin bundles and stress fibres, respectively. Overexpression of full-length FHOD1 was associated with an increased signal for F-actin in HeLa cells, possibly suggesting that the total F-actin content in cells was increased. An even greater increase in the signal for F-actin

was observed when FHOD1 was overexpressed in its constitutively active forms, which also resulted in the formation of stress fibres. Furthermore, NRCs and C2C12 cells transfected with the FHOD1 shRNA constructs were associated with disruption of the F-actin network at days 8 and 3, respectively.

Previous studies investigating the role of FHOD1 have also highlighted the possibility of an actin polymerising role for this formin. Iskratsch et al. 2013b suggested that FHOD1 partly contributed to the formation of early focal adhesions through the polymerisation of actin filaments. When knocked down in mouse embryonic fibroblasts (MEFs), polymerisation of actin filaments was reduced. Furthermore, an FHOD1 mutant lacking the polyproline motifs in the FH1 domain was also associated with reduced actin assembly at early adhesion sites (Iskratsch et al. 2013b). While this may have been due to reduced recruitment of FHOD1 by Src at these sites, we cannot rule out the possibility that actin assembly was impaired due to a reduced interaction with profilin. Previous yeast-two-hybrid analysis suggested that FHOD1 and profilin IIa, the major profilin isoform in vertebrates, represented interacting partners (Tojo et al. 2003). Profilin is required for the actin filament elongation activities of formins (Romero et al. 2004), thus an interaction between FHOD1 and profilin may point to a canonical actin polymerising role for FHOD1 in cells.

As the classical mediator of formin-mediated actin assembly, the FH2 domain of FHOD1 represents a good candidate for mediating the potential actin polymerising role of FHOD1 in cardiomyocytes. When overexpressed in cardiomyocytes, the FH2 domain of FHOD1 displayed targeting to the Z-disks, the site of anchorage of the barbed ends of the cardiac thin filaments within the sarcomere. Furthermore, the FH2 domain co-localised with F-actin in cardiomyocytes and may have induced its localised accumulation. The latter observation may have reflected that the FH2 domain of FHOD1 may have possessed the capacity to induce polymerisation of actin filaments in a similar manner to the isolated FH2 domain of mDia1, which was shown to be sufficient for inducing the accumulation of F-actin in cells (Copeland and Treisman 2002). While the extent of polymerisation that occurs at the Z-disks of striated muscle remains to be elucidated, reports of N-WASP and nebulin forming a complex at the Z-disk to stimulate actin assembly in response to IGF-1 stimulation in skeletal muscle cells (Takano et al. 2010) could indicate a similar role for FHOD1.

Thus, a number of situations can be envisaged for FHOD1 as an actin polymerising protein in muscle. One line of thinking behind how myofibrils are maintained in terminally differentiated muscle cells describes the rapid incorporation of actin monomers into mature myofibrils that are stabilised by CapZ, tropomodulin, and tropomyosin (Ono 2010; Dwyer et al. 2012). This occurs without altering the overall stoichiometry of the thin filaments and is not driven by the treadmilling of actin filaments from the Z-disks (Littlefield and Fowler 2008). The site of actin monomer addition has been a subject of dispute (Ono 2010) although many studies report that incorporation of monomers primarily occurs at the pointed ends of filaments (Littlefield et al. 2001; Ono 2010). However, the site of actin monomer addition may be subject to culture conditions and cell type, therefore filament growth could conceivably occur at the barbed end, pointed end, or both ends (Ono 2010). If FHOD1 is indeed partly found at the Z-disk, as suggested by antibody staining in mouse heart sections, it could transiently associate with the barbed ends of actin filaments. This model would imply that active FHOD1, dimerised via its FH2 domain, could facilitate the incorporation of actin monomers at the barbed ends of filaments. However, this might not be the only mechanism by which FHOD1 contributes to myofibrillar maintenance by actin polymerisation. Other efforts have described more-dynamic populations of actin filaments in cardiomyocytes: FRAP experiments in NRCs have suggested that contractility-dependent actin nucleation and polymerisation occurs during sarcomere maturation. Furthermore, this population of actin filaments is inhibited by cytochalasin D, suggesting that new filament growth is driven by barbed end elongation (Skwarek-Maruszewska et al. 2009). Barbed end elongators, potentially including FHOD1, could perhaps be responsible for creation of new, more-dynamic filament populations, whereas pointed end elongators, such as leiomodin could help regulate the lengths of mature myofibrils (Dwyer et al. 2012).

7.5.2 FHOD1 as a Capping Protein in Muscle

While regulation of myofibrils via actin assembly represents an interesting possibility for FHOD1, the actin polymerising function associated with many formins has been disputed in the case of FHOD1. FHOD1 was found to inhibit actin polymerisation in *in vitro* pyrene assays in its full-length, inactive form and the inhibition of polymerisation was potentiated when FHOD1 was rendered in its active conformation, by

implementing the FHOD1 ΔDAD mutant (Schonichen et al. 2013). Experiments employing lower concentrations of G-actin suggested that FHOD1 did not possess filament nucleating activity either. F-actin dilution assays revealed that both full-length FHOD1 and the FHOD1 ΔDAD prevented actin depolymerisation. The full-length protein showed weaker inhibition of depolymerisation thereby suggesting that association with the filament barbed end is partly dependent on the autoinhibition status of FHOD1. However, such *in vitro* observations may not be completely applicable to situations *in cyto*. Indeed, it has been described how the actin polymerising activities of certain formins in cells require the participation of a cofactor. For example, in *Drosophila melanogaster* oocytes, the formin Cappuccino and the actin regulatory protein Spire form a complex to enhance actin nucleation (Quinlan et al. 2007). A similar situation for FHOD1 might not be completely out of the question, with one potential actin assembly cofactor that was highlighted in the present study even being FHOD3. Nevertheless, the potential capping activity of FHOD1 in muscle remains a strong possibility.

A number of the present findings may have reflected the reported ability of FHOD1 to cap the barbed ends of actin filaments via its FH2 domain. The noted effects of the FH2 domain in NRCs (i.e., co-localisation with F-actin and possible localised accumulation of F-actin) might not be explained only by actin assembly but rather by stabilisation and reduced degradation of F-actin. The capping behaviour of the FH2 domain of FHOD1 may have also been reflected in the Latrunculin B experiments in NRCs. In this instance, the full-length FHOD1 constructs rescued the phenotype associated with Latrunculin B but the overexpressed FH2 domain on its own seemingly inhibited recovery of myofibrils and co-localised intensely with patches of F-actin throughout cells. In this instance it may have been the case that the capping activity of the FH2 domain on its own was insufficient to stabilise myofibrils in the presence of Latrunculin B treatment but, upon wash-out, the FH2 domain was able to cap actin filaments to prevent their elongation.

FHOD1's putative capping role is somewhat more difficult to integrate into our current understanding of myofibrillar regulation. A role for stabilisation of myofibrils or regulation of thin filament length via barbed end capping by FHOD1 is less probable in

mature myofibrils since CapZ is likely fulfilling this role (Dwyer et al. 2012). One possible mechanism by which FHOD1's capping activity contributes to regulation of the myofibrillar apparatus could involve the stabilisation of a pool of actin filaments which are subsequently elongated by other actin assembly factors. This could theoretically be extended to instances of *de novo* actin filament assembly during myofibrillogenesis and assembly of more-dynamic filament populations during myofibrillar maintenance.

7.5.3 FHOD1 as an Actin Side Binding Protein/Actin Bundler in Muscle

Further explanations by which FHOD1 exerts its effects in muscle cells could involve the actin side binding and bundling activity of this formin. In the present study this notion was supported by a number of observations. Overexpression of the FHOD1 ΔDAD and V228E mutant constructs in NRCs resulted in the formation of actin bundles and stress fibres, respectively. In Latrunculin B-treated NRCs, overexpression of FHOD1 was able to rescue the phenotype associated with myofibrillar depolymerisation. This occurred irrespective of FHOD1's activation status and could have suggested that even in FHOD1's inactive confirmation, in which its functional FH domains are thought to be masked, this formin could have stabilised myofibrils in the presence of Latrunculin B to prevent their depolymerisation.

Growing evidence from the scientific literature would suggest that FHOD1 possesses functionally relevant actin side binding and bundling activity. F-actin pelleting assays suggested that FHOD1 binds actin via two independent sites (Schonichen et al. 2013). The N-terminus of the protein may mediate binding to the side of actin filaments, whereas barbed end binding or dimerization via the FH2 domain could contribute to the efficiency of actin binding. Indeed, the pivotal study by Schonichen et al. 2013 suggested that both regions work synergistically to increase F-actin binding efficiency. The F-actin bundling activity of FHOD1 was also tested through low speed centrifugation sedimentation assays: FHOD1 required both of its independent actin binding domains (the helical actin side binding region and the FH2 domain) in order to bundle F-actin. The N-terminus may thus possess actin side binding activity and the FH2 domain could be required for the formation of higher order structures (e.g., stress

fibres, actin cables, etc.). TIRF microscopy experiments supported the results seen with the sedimentation assays: while both full-length and FHOD1 ΔDAD promoted the formation of thick actin bundles when added to polymerizing actin filaments, the effect of the FHOD1 ΔDAD construct was much stronger in promoting bundle formation. Electron microscopy also suggested greater bundling activity for FHOD1 ΔDAD but also revealed that FHOD1 could also bundle filaments stabilized in the presence of tropomyosin, the actin side binding protein which stabilises actin filaments in myofibrils.

One mechanism by which FHOD1's actin side binding/bundling activity could directly contribute to myofibrillar maintenance in cardiac cells could involve a similar role proposed for FHOD1 in the regulation of transverse arcs and ventral stress fibres (Schulze et al. 2014). FHOD1 could mediate the end-to-end annealing of shorter actin filaments or myofibrillar fragments to contribute to assembly of myofibrils. While this mechanism could fit well in the context of *de novo* myofibril formation, end-to-end annealing of myofibrils in the context of maintenance is unlikely since mature myofibrils have been suggested to retain their lengths during myofibrillar turnover (Ono 2010). However, binding alongside mature myofibrils could serve as a means to further stabilise them. In this context FHOD1 may act similarly to tropomyosin, which has been shown to antagonise the effects of actin depolymerising proteins such as ADF/cofilin to promote thin filament stability and sarcomeric organisation (Ono and Ono 2002; Ono 2010).

7.5.4 FHOD1 as a Signalling Effector in Muscle

While a growing body of evidence suggests that FHOD1 contributes to the regulation of cytoarchitecture by directly acting on F-actin, the role of this formin in signalling to the nucleus is also a factor that merits consideration. Multiple studies have documented the involvement of FHOD1 in mediating signalling to the serum response element (SRE), a short gene regulatory sequence that controls transcription of immediate early genes like c-fos and β-actin upon growth factor stimulation. It involves activation of the serum response factor (SRF) transcription factor which stimulates transcription after binding to specific promoter regions (Westendorf 2001; Gasteier et al. 2003; Koka et al. 2003; Madrid et al. 2005; Staus et al. 2011a). The precise mechanism by which FHOD1

stimulates gene expression from the SRE remains to be elucidated, but a mechanism involving myocardin-related transcription factors (MRTFs) represents a viable explanation, especially in the context of muscle. MRTFs are coactivators of SRF and represent crucial mediators of muscle differentiation and cytoskeletal organisation (Parmacek 2007). They are bound and sequestered by G-actin outside of the nucleus. Upon reduction of the available pool of G-actin (e.g., by polymerisation into F-actin), MRTFs are liberated and can subsequently translocate to the nucleus where they directly interact with SRF and other MADS box transcription factors. FHOD1 was shown to regulate translocation of MRTF to the nucleus during vascular smooth muscle cell differentiation and this may have been due to FHOD1's actin regulating activity, as suggested by experiments with Latrunculin B (Staus et al. 2011a). Furthermore, ability to mediate gene expression is not only restricted to FHOD1 and may be a result of the actin regulating activities of multiple formin proteins (Tominaga et al. 2000).

The presently noted phenotypes associated with muscle cells transfected with the FHOD1 shRNAs may not have solely been a result from FHOD1's direct effects on cytoarchitecture but may have also been a downstream product of disruption of the signalling events required to maintain muscle differentiation via promotion of expression of key myofibrillar proteins (e.g., actin) and assembly factors. In muscle, SRF regulates the expression of a number of contractile and cytoskeletal proteins including α-skeletal muscle actin (SKA), α-cardiac muscle actin (CAA), β-myosin heavy chain (β-MHC), myosin light chain-2 (MLC-2v), and dystrophin (Nelson et al. 2005). Previous work employing SRF-null mice revealed that the cardiomyocytes of these animals were associated with a number of abnormalities that were comparable to those of the FHOD1 shRNAs, ranging from impaired organisation of the myofibrillar apparatus to suggestions that cell-cell contacts were disrupted (Balza and Misra 2006). Whether the effects associated with the FHOD1 shRNAs in NRCs and C2C12 cells resulted in reduced gene expression via the SRE remains to be seen, but the previously documented involvement of this pathway with FHOD1 could explain some of FHOD1's effects in cardiomyocytes.

7.5.6 Functional Significance of FHOD1 at the Intercalated Disk

Another interesting notion that arose in this study was that FHOD1 may have played a role at the intercalated disk. The intercalated disks of cardiomyocytes represent a highly specialised junction that serves to electro-mechanically couple neighbouring cells. The intercalated disk is characterised by a step-like structure, with the membrane at the transverse regions of the steps taking on a folded appearance, resulting in it being referred to as plicate (Forbes and Sperelakis 1985; Wilson et al. 2014). Cells are electro-chemically linked by gap junctions. Mechanical coupling occurs through adherens junctions, the major structural component of the intercalated disks. Adherens junctions tether terminal myofibrils through the catenin system and link neighbouring cells via the cadherin system. Staining for endogenous FHOD1 suggested that the intercalated disk may be a major site of FHOD1 localisation in adult mouse cardiomyocytes; however, its precise localisation within the intercalated disk has yet to be fully elucidated. Transfection of NRCs with the shRNA constructs designed to target depletion of FHOD1 resulted in disruption the appearance of the intercalated disks and led to mislocalisation of β-catenin. Treatment with the formin inhibitor also had an irreversible impact on the intercalated disks: SMIFH2 seemed to have a cumulative effect on cell-cell junctions which appeared increasingly widened and convoluted. Interestingly DAAM (Li et al. 2011) along with Formin1 (Zigmond 2004) were also found to be required for proper formation of adherens junctions and might suggest that multiple formins may play a role in regulating cell-cell contacts in both muscle and non-muscle cells.

There are a number of possible mechanisms by which FHOD1 could contribute to the regulation of the intercalated disks in cardiomyocytes. Previous studies and the present work suggested that FHOD1 may exert its effects by directly acting on F-actin; therefore regulation at the level of the thin filaments found at the intercalated disks remains a strong possibility. While the exact mechanisms responsible for the insertion of actin filaments into the intercalated disk remain to be elucidated, it would appear that they are elongated filaments that originate from the terminal sarcomeres most proximal to the intercalated disks. These undecorated actin filaments are thought to comprise the area, between the terminal sarcomeres and the intercalated disk membrane, referred to as the transitional junction (Bennett et al. 2006; Bennett 2012). Given the potential

FHOD1 functions discussed above, FHOD1 could function as a nucleator and/or elongator of actin filaments in the transitional junction. Alternatively, as a capping protein, FHOD1 could stabilise a pool of available actin filaments for further elongation by other assembly factors. As an actin side binding protein, FHOD1 could serve to stabilise the actin network found at the intercalated disks. This would not be the first report of an actin side binding protein playing a role at the intercalated disks. Xin, a muscle-specific actin side binding/bundling protein, concentrates at the intercalated disks between cardiomyocytes and at the myotendinous junction in skeletal muscle (Pacholsky et al. 2004; Cherepanova et al. 2006; Choi et al. 2007; Ono 2010). Disruption of Xin in mice was associated with perturbation of intercalated disks at the ultrastructural level and at the level of the composition of the adherens and desmosomal proteins (Gustafson-Wagner et al. 2007; Otten et al. 2010; Wang et al. 2010). However, it is unknown if the effects of Xin depletion were due to its direct actin regulating capabilities or if they were due to compromised integrity of the cadherin-catenin system, since Xin also interacts with β-catenin (Choi et al. 2007). Based on the results with Xin, it would be of interest to see if FHOD1 depletion in mice is also associated with similar intercalated disk defects given that both proteins possess actin side binding/bundling activity and localise to the intercalated disks.

7.5.7 Unified View of Potential FHOD1 Functions in Muscle Cells

Focusing on the contribution of individual FHOD1 domains may not give a complete picture of the function of this protein in cells. For instance, the sole contribution of the FHOD1 FH2 domain is likely modified by the other modules present on FHOD1. This was exemplified in experiments in which NRCs were subjected to treatment with Latrunculin B to promote disassembly of all cellular F-actin and their myofibrils. While the FH2 domain seemingly inhibited recovery of myofibrils, the full-length wild-type and constitutively active FHOD1 variants rescued the phenotype associated with Latrunculin B treatment, although it was not possible to discern if these effects were due to prevention of depolymerisation of F-actin and myofibrils, if re-assembly of these components were enhanced in the recovery phase when Latrunculin B was washed out, or both. Also, the localisation of the FH2 domain does not seem to be entirely representative of the localisation of constitutively active FHOD1 in NRCs. Overexpression studies in NRCs also support the notion of an important contribution of

the other FHOD1 domains. N-terminal modules, such as the GBD, might participate in the targeting of FHOD1, and those in the C-terminus, such as the DAD, might not be solely restricted to regulating the inactive conformation of FHOD1 but might also directly contribute to FHOD1's actin regulating activity. Ultimately, the role of FHOD1 may be subject to tight spatio-temporal regulation which could involve its number of different actin regulating activities, therefore individual domains could contribute different functions in specific instances (i.e., in an activated state vs. inactive state of the full-length molecule), at different time points, and may be modulated by different sets of interacting partners. Further insight into these issues could be gained by establishing a profile of endogenous FHOD1 localisation during instances where there are different requirements for actin regulation (e.g., during myofibrillogenesis vs. myofibrillar maintenance) and assessing the extent of FHOD1 activation at these time points, possibly by gauging the extent of phosphorylation in the DAD, although the robustness of this model for activation needs to be further explored.

Previous studies supported the notion of similarly important contributions of the individual FHOD1 domains that we observed in NRCs, especially through the description of multiple actin interacting domains. It seems that the GBD-DID region mediates targeting to stress fibres, but persistent association of FHOD1 with stress fibres was not required for induction of their formation (Schulze et al. 2014). On the other hand, deletion of the helical domain, the actin side binding domain of FHOD1 (Schonichen et al. 2013), abrogated FHOD1 stimulated stress fibre formation in U2OS osteosarcoma cells (Schulze et al. 2014). However, the FH2 domain is still required for the actin bundling activity of FHOD1 (Schonichen et al. 2013). Therefore, the helical, FH modules, and C-terminal portion of FHOD1 were found to be required for both formation of transverse arcs and their maturation into ventral stress fibres (Schulze et al. 2014). The central and C-terminal domain might be the actin organizing portions of FHOD1 whereas the N-terminal region could facilitate targeting and more subtly modify FHOD1's function. In instances of stress fibre formation, FHOD1 might enrich a pool of short actin filaments by permanent or slow processive capping or even rapid polymerisation. It could then subsequently bundle those filaments. In muscle cells, FHOD1 could also mediate its effects through a combination of its activities. Further studies employing mutations and domain deletions of FHOD1 may be able to further

elucidate how each of FHOD1's possible functions contribute to its effects in muscle cells.

The mechanisms by which FHOD1 exerts its functions in muscle cells could therefore be very complex. But regulation of actin in muscle cells is not solely restricted to capping, bundling, and polymerisation. For instance, actin severing and depolymerising proteins also play a role in the maintenance of muscle cytoarchitecture, particularly at the level of degradation of actin-based structures (Ono 2010). In a human context, this has been exemplified by mutations in cofilin, which have been associated with nemaline myopathy, a disease in which nemaline rods (partly composed of actin) accumulate in muscle (Yamaguchi et al. 1982; Agrawal et al. 2007). Although processes such as actin severing and depolymerisation are of physiological relevance, the results of the present study and those of previous research efforts did not indicate that they would necessarily be associated with FHOD1.

The contribution of FHOD1 at the subcellular sites discussed above, myofibrils and the intercalated disk, might only offer a narrow view of the functional relevance of this formin in muscle cells. While muscle actins represent the predominant actin isoforms of the myofibrils in cardiac and striated muscle cells (Tondeleir et al. 2009), the role of cytoplasmic actins cannot be dismissed (Kee et al. 2009). In muscle, cytoplasmic actins, namely β-actin and γ-actin, could play roles involving membrane anchorage with the costameres (Dwyer et al. 2012). This may involve dystrophin and the dystrophin associated protein complex and different regions of the sarcoplasmic reticulum. The precise roles of cytoplasmic actins remain to be fully determined in muscle cells. Although knockout animals have indicated little importance of the cytoplasmic actins in myofibrillogenesis (Sonnemann et al. 2006; Prins et al. 2011), cytoplasmic actins seem to follow a function akin to their localisation and indeed seem to regulate membranous compartments, although this has only been shown in skeletal muscle so far (Gokhin and Fowler 2011; Dwyer et al. 2012). Whether FHOD1 plays a role in the regulation of the cytoplasmic actins at membranous compartments in muscle cells remains to be determined, although regulation of β-actin is a possibility, since this has been suggested to be the predominant actin isoform found in the undecorated thin filaments that link the

transitional junction to the intercalated disk (Bennett et al. 2006; Dwyer et al. 2012; Benz et al. 2013).

Although not addressed in the present study, the potential ability of FHOD1 to regulate the microtubule network in muscle cells could represent a means by which this formin exerts some its effects. Indeed, previous reports of FHOD1 regulating microtubule dynamics (Gasteier et al. 2003; Floyd et al. 2013) as well as the growing evidence for formins as regulators of the microtubule cytoskeleton (Breitsprecher and Goode 2013) make this a possibility. The role of microtubules is slightly underrepresented in striated muscle research. While roles in muscle cell hyperplasia and differentiation have been suggested (Li et al. 1996; Mian et al. 2012), their role in postmitotic muscle cells requires further investigation (Ehler and Perriard 2000). Nevertheless, the role of FHOD1 and formins on the microtubule network in striated muscle could represent a future avenue worth exploring.

7.6 FHOD1 in Cardiac Disease

Another interesting finding in the present study related to the expression and localisation of FHOD1 in a mouse model of dilated cardiomyopathy (DCM), the $MLP^{-/-}$ mouse. We presently report a possible upregulation in FHOD1 expression in adult $MLP^{-/-}$ mouse hearts. This may have also reflected the increased signal we saw for FHOD1 along myofibrils, but especially at the intercalated disks. $MLP^{-/-}$ mice represent a model of cardiac disease in which there is a mixture of cardiac hypertrophy and dilatation which can eventually progress to heart failure (Arber et al. 1997; Buyandelger et al. 2011). $MLP^{-/-}$ mice, and DCM phenotypes in general, are characterised by ultrastructural abnormalities in cardiomyocyte architecture, myofibrillar disarray, and fibrosis (Machackova et al. 2006; Wilson et al. 2014). It is not always clear which of these factors perpetuate the disease or represent the end result of disease progression. Nevertheless, it is interesting to speculate as to the reasons behind FHOD1 upregulation in this model of DCM.

Both cardiac hypertrophy and dilatation are characterised by alterations in a variety of subcellular compartments (e.g., mitochondria, nuclei, and sarcoplasmic reticulum) but also impact myofibrillar assembly. Although fetal gene expression is more classically

associated with hypertrophic cardiomyopathy (HCM), some of the abnormalities that arise in cardiac hypertrophy associated with DCM are the expression of fetal genes, such as α-SKA (Suurmeijer et al. 2003), which is thought to contribute to greater myofibrillar contractility (Machackova et al. 2006), although the increase in α-SKA may depend on the extent of hypertrophy (Adachi et al. 1998). Other adaptive changes in response to hypertrophy include expression of atrial myosin light chain 1 (ALC_1), which is also thought to contribute to increased cardiac contractility (Schaub et al. 1998). Actin polymerisation has also been suggested to be required for mediating hypertrophic growth of cultured cardiomyocytes in response to phenylephrine treatment (Yanazume et al. 2002). Overall, alterations in composition of myofibrils, their remodelling, and their increased assembly may contribute to the compensatory remodelling mechanisms seen in cardiac hypertrophy and DCM. Given the potential roles of FHOD1 in myofibrillar regulation in the present study, the increase in FHOD1 expression may alleviate the greater demand for myofibrillar assembly and maintenance via one or more of its different actin regulating activities.

FHOD1's proposed ability to stimulate SRF-mediated gene expression is also intriguing from a cardiac disease perspective. SRF has been suggested to be one the factors driving expression of the characteristic fetal gene expression signature noted in instances of cardiac hypertrophy and DCM. For instance, cardiac-specific overexpression of the human SRF gene in mice resulted in cardiomyopathy and a switch to fetal reprogramming (e.g., downregulation of α-CAA and upregulation of α-SKA) (Zhang et al. 2001). Furthermore, increased SRF expression has been noted in the hypertrophied hearts of ageing rats (Lu et al. 1998). Whether or not increased FHOD1 expression and/or activity could drive SRF activity during cardiac remodelling in instances of disease remains to be determined but FHOD1 upregulation could represent a perpetuating factor in compensatory and pathological remodelling responses not only on the level of direct cytoarchitectural regulation but also on the gene expression level.

The potential role of FHOD1 in regulating cell-cell contacts in NRCs, its localisation at the intercalated disk in adult mouse hearts, and its upregulation in DCM are very interesting when considering the role of the intercalated disk in cardiomyocyte growth. Altered stoichiometry of proteins found at the intercalated disk was suggested to be one

of the defining characteristics of DCM (Perriard et al. 2003) and other proteins have been shown to exhibit alterations in their expression (Estigoy et al. 2009). Generally speaking, adherens junction proteins tend to increase in expression whereas gap junction proteins are downregulated in their expression. The functional relevance of the upregulation of adherens junctions proteins may be of particular importance, since some these proteins (e.g., β-catenin) are involved in anchoring the actin filaments at the intercalated disk (Ehler et al. 2001). Interestingly, there is also an upregulation of β-actin, the supposedly predominant actin isoform at the intercalated disk (Balasubramanian et al. 2010), during some instances of cardiac remodelling (e.g., hypertrophy) and may reflect an increased requirement for thin filament assembly and integration at the intercalated disk. The intercalated disks display with a broader appearance in DCM hearts (Wilson et al. 2014), similarly to that in aged hearts (Forbes and Sperelakis 1985), and this may be indicative of increased convolution of the structure during cardiomyocyte growth. Indeed, a recent study, which employed volume overloaded rabbits, suggested that cycles of broadening and narrowing of the intercalated disks, resulting in a transient interruption in the signal for intercalated disk proteins, allowed for insertion of sarcomeres at the ends of cardiomyocytes and accordingly resulted in the proposition of the 'weaving sarcomere hypothesis' (Yoshida et al. 2010). During cardiac development, similar insertion of sarcomeres was noted in regions of increased membrane convolution (Wilson et al. 2014). Such observations would support the idea of the transitional junction as proposed by Bennett and colleagues (Bennett et al. 2006). During instances of cardiomyopathy, as ascertained using heart sections of $MLP^{-/-}$ mice, cΔex3 mice (overexpress a cardiac-specific β-catenin mutant (Hirschy et al. 2010)), and idiopathic DCM human samples, controlled insertion of terminal myofibrils at these sites was found to be disrupted (Wilson et al. 2014). Regarding FHOD1, its different sets of potential actin regulating activities could contribute to the abnormalities in actin filament insertion seen in pathological remodelling and therefore may partly explain the phenotypes in DCM (Dwyer et al. 2014).

Another notion that arose in this study is that alterations in the relative levels of formins might be a characteristic of DCM, just as altered ratios in formin levels have been described during different phases of postnatal cardiac development (Rosado et al. 2014).

Studies in MLP$^{-/-}$ mice have indicated differential expression of FHOD1 and FHOD3, possibly suggesting diverging roles for these two FHOD proteins in disease. The precise cause and functional consequences of these changes in expression have yet to be determined, although it may be conserved among human examples of DCM, which have suggested similar alterations in both FHOD1 (Dwyer et al. 2014) and FHOD3 (Iskratsch et al. 2010). In MLP$^{-/-}$ mice, there was also an isoform switch to the non-muscle isoform of FHOD3, which is subject to degradation via p62 (Iskratsch et al. 2010), and may have accounted for the reduction in FHOD3 levels. As to the reason behind the FHOD3 isoform switch, this may have been a consequence of the fetal reprogramming events that partly accompany the transition towards a heart failure phenotype (Machackova et al. 2006; Cappola 2008). The increase in total FHOD1 levels may have reflected a switch to fetal reprogramming in hearts and/or may have resonated an increased requirement for its actin regulatory function. It also remains to be determined if there is an isoform switch relating to FHOD1 in instances of cardiac disease. While the two presently characterised FHOD1 isoforms exhibit similar behaviour in their supposedly inactive state in cardiomyocytes, comparison of their behaviours upon activation remains to be seen. The possibility of different sets of interacting partners, potentially mediated by the alternatively spliced exon 12-13, may also modulate function of the FHOD1 isoforms in healthy and diseased cells.

7.7 Insights from Interacting Partners

7.7.1 Potential Contribution of FHOD3

In our search for novel interacting partners, we found a possible interaction between FHOD1 and FHOD3, which were suggested to directly interact. This interaction could have indicated that FHOD1 and FHOD3 may form heterodimers. This would not be the first report of heterodimerisation between two different DRFs. mDia1 has been reported to dimerise with mDia2 as the full-length variants of both proteins bound each other in co-immunoprecipitation assays (Copeland et al. 2007). However, this interaction was ascribed to contribute to an inhibitory cross-regulation of these formins. Binding was dependent on the presence of the DAD regions and it was also found that the DID of mDia2 inhibited the activity of mDia1. Furthermore, cross-regulation did not extend to the formin DAAM-1 implying that this mechanism was restricted to closely related members (Copeland et al. 2007). The portions of FHOD3 that were

revealed in the interaction screen would argue against a cross-regulatory mechanism like the one seen between mDia1 and mDia2. Perhaps FHOD1 could sterically block association between FHOD3 and actin by binding part of its actin polymerising module (FH1-FH2), thus providing a new means of negative regulation of FHOD3 besides autoinhibitory regulation. This interaction could also be indicative of a new mechanism of activation for FHOD1. Perhaps the exposed FH1-FH2 region of activated FHOD3 could bind the N-terminus of FHOD1 to sterically displace the FHOD1 autoinhibitory interaction. Alternatively, FHOD1 and FHOD3 could work synergistically to aid in the assembly or reorganisation of actin-based strictures. However, one can only speculate into the functional consequences of association between FHOD1 and FHOD3 until functional studies have been performed in cells.

7.7.2 Potential Contribution of Src

The present study may have uncovered evidence in support of a physical interaction between the FHOD1 N-terminus and Src kinase, which could have a number of functional consequences if it is indeed present in muscle cells. A large proportion of the research efforts into Src have largely focused on the role of this protein in the context of cancer cell biology. Although extensive data are lacking, there is some evidence that Src may play a role in both healthy and diseased striated muscle. For instance, Src has been suggested to have roles in skeletal muscle development. In C2C12 cells Src activation was shown to be required for differentiation into multinucleated myotubes (Lu et al. 2002). However, the role of Src in muscle differentiation remains somewhat controversial since other reports have suggested that inhibition of Src activity actually stimulates skeletal muscle differentiation (Lim et al. 2007). In the heart, there have been some indications, although somewhat scarce, that SFKs accumulate at the intercalated disks between cardiomyocytes (Tsukita et al. 1991). However, a role for SKFs at the intercalated disks has been described and they may play a role in the regulation of gap junctions (Toyofuku et al. 1999). Src was suggested to be a potent inhibitor of gap junction communication by phosphorylating connexin43 and that this may have contributed to the deficits in gap junction communication noted in cardiomyopathic hamsters (Toyofuku et al. 1999; Palatinus et al. 2012). Src activity can also exhibit changes during different pathological states in the heart and it has been suggested that

increased Src activity is involved in mediating the signal transduction events that contribute to cardiac hypertrophy (Takeishi et al. 2001).

In terms of the known functions of Src with respect to muscle and FHOD1, a number of roles could be proposed for how Src could modulate the function of FHOD1 in muscle. One of the previously proposed roles for Src is that it mediates the localisation of FHOD1 in cells. Src seemed to regulate translocation of FHOD1 to the plasma membrane and to mediate its association with ROCK-I (Hannemann et al. 2008). In MEFs, Src mediated targeting of FHOD1 to early integrin clusters upstream of activation by ROCK-1 (Iskratsch et al. 2013b). In the present study we noted FHOD1 localising to specific cardiomyocyte compartments. Given the previous role of Src in mediating the localisation of FHOD1 and the potential physical interaction between FHOD1 and Src, Src could conceivably be involved in targeting FHOD1 to some of these sites in cardiomyocytes. One such mode of translocation between the two proteins could involve a shuttling mechanism by which Src binds FHOD1 and delivers it to its subcellular destination. The functional relevance of the FHOD1-Src interactions remains to be fully elucidated but current lines of thinking suggest that Src mediates targeting of FHOD1 to the plasma membrane where FHOD1 is subsequently phosphorylated by ROCK-I (Hannemann et al. 2008; Iskratsch et al. 2013b).

7.7.3 Potential Contribution of NRAP

The potential FHOD1-NRAP interaction also poses interesting possibilities by which these proteins could contribute to regulation of actin filaments. Knock down of NRAP has so far been associated with impaired myofibrillogenesis but we have not been able to show the same so far with FHOD1. Furthermore, it is unclear whether NRAP is required for myofibrillar maintenance since experiments have primarily employed embryonic mouse cardiomyocytes to study its function. Overall, both proteins may play a role in regulation of the myofibrillar apparatus at the level of actin. Perhaps their roles also extend to regulation of the intercalated disk, which may represent a major site of localisation of both proteins in adult cardiac muscle. The main function ascribed to NRAP in striated muscle is that of a scaffolding role. Interestingly, FHOD1 may have interacted with an SR region of NRAP, which has been found to be essential in organising actin filaments for myofibril assembly in embryonic chick cardiomyocytes

(Carroll et al. 2004). Thus, a number of possibilities arise with respect to the functional consequences that an FHOD1-NRAP interaction may pose. If there is indeed a physical interaction between NRAP and FHOD1, NRAP could serve to tether FHOD1 within a given subcellular localisation and/or reinforce the interaction between FHOD1 and actin so that FHOD1 may fulfil one or more of its putative actin regulatory functions. The notion that these proteins are concomitantly increased in DCM could suggest greater cooperation between them to fulfil their actin regulating roles. Nevertheless, although an FHOD1-NRAP interaction could represent an exciting possibility, conformation of the interaction will be required and the functional consequences of the possible association between them would need to be explored.

7.8 Conclusion

The present study attempted to characterise the formin protein FHOD1 in striated muscle. Analysis of the expression pattern of FHOD1 suggested that it is expressed in striated muscle at the protein level. It was also apparent that FHOD1 was more abundantly expressed in the heart than in skeletal muscle, where it was preferentially expressed in fast rather than slow skeletal muscle. Work exploring the localisation of FHOD1 in cultured muscle cells may have indicated sarcomeric targeting of endogenous FHOD1 but will require further exploration because of the technical issues relating to the commercial antibodies. Nevertheless, in sections of adult mouse heart tissue, FHOD1 may exhibit a prominent signal at the intercalated disks although it may have been present in some of the Z-disks. Overexpression of GFP-tagged human FHOD1 resulted in diffuse cytoplasmic distribution, accumulation at the cell peripheries, and some myofibrillar targeting. It would also seem that targeting of the full-length human FHOD1 construct was not mediated by the presence of the alternatively spliced exons 12-13. Although the precise mechanisms guiding the localisation of FHOD1 require further elucidation, a construct lacking its N-terminal GBD fail to target in a similar way to full-length FHOD1. In trying to dissect the function of FHOD1 it was revealed that overexpression of constitutively active versions of this formin could induce cytoskeletal rearrangements. While there was a possibility that FHOD1 activation may have increased the F-actin content in cells, the precise mechanism by which this occurred by remains to be determined. Although pending validation by confirming knockdown of FHOD1, loss-of-function experiments

suggested that FHOD1 may have been involved in maintenance of muscle cytoarchitecture in both NRCs and C2C12 cells. If the effects of the shRNA constructs were indeed due to FHOD1 depletion, the mechanisms by which the cellular defects arose remain to be explored given the various actin regulating roles that have been proposed for FHOD1. General inhibition of formin activity with the inhibitor SMIFH2 also resulted in perturbation of the myofibrillar apparatus and the intercalated disks in cardiomyocytes, suggesting a broad role for formins in muscle cells.

In trying to establish potential regulatory interactions for FHOD1, possibly mediated by the alternatively spliced exons 12-13, it was suggested that the N-terminal half of FHOD1 did not bind some of the classical Rho family small GTPases or the Rho effector molecule ROCK. However, the FHOD1 N-terminus may have interacted physically with the cytoskeletal regulator Src. A set of potential novel interactions were also described with the FHOD1 N-terminus, which included FHOD3 and NRAP. FHOD1 may have weakly bound one of the SR repeats of NRAP and both proteins may have co-localised at the intercalated disk in frozen sections of adult mouse hearts. FHOD1 levels were also suggested to increase dramatically in the $MLP^{-/-}$ mouse model of DCM and this was associated with a greater signal for FHOD1 at the intercalated disk. Overall, functional studies and potential interactions with well-known cytoskeletal regulators, like Src and proteins involved in myofibril assembly, like NRAP may have implicated FHOD1 in regulation of the myofibrillar apparatus and cytoskeleton at the level of actin in striated muscle.

In conclusion, the regulation and turnover of actin in striated muscle is continuously being revealed as a dynamic process and the involvement of the formin family of proteins is increasingly being shown. The current study supported the notion that FHOD1 may represent a crucial regulator of myogenic cytoarchitecture at the level of F-actin and that this may occur in healthy and diseased muscle.

7.9 Future Directions

The current work involving FHOD1 has highlighted this formin protein as a possible regulator of actin-based structures in striated muscle. Although FHOD1 was found to

be involved in myofibrillar maintenance, its role in myofibrillogenesis remains to be explored. The expression and localisation of FHOD1 should thus be investigated in different models of myofibrillogenesis. Embryonic mouse samples can be used to provide a clearer picture about the role of FHOD1 in developing skeletal muscle and heart. Developing chicken muscle samples could also provide an excellent platform to look at FHOD1 expression and localisation at specific stages of development as gauged by number of somites. Eventually, it will be necessary to have a complete spatio-temporal expression and localisation profile for FHOD1 in developing, post-natal, and diseased muscle samples.

The mechanisms governing regulation of FHOD1 in muscle have yet to be elucidated. While we may have identified novel sets of binding partners for FHOD1, it remains to be seen how they could modulate the function of FHOD1 in muscle cells. While, the direct physical interaction between FHOD1 and some of these interacting partners remains to be confirmed, functional studies by way of co-expression experiments and RNAi could help paint a picture of where these proteins interact in cells and if they can modulate each other's behaviour. In terms of known regulators of FHOD1, such as Rac and ROCK-I, it would also be of interest to examine the relevance of these protein interactions in muscle.

Further functional studies will also eventually shed light on the actual role of FHOD1. One way of visualising FHOD1's effect on actin could involve live imaging studies using Lifeact, which fluorescently labels F-actin in cells without altering its dynamics (Riedl et al. 2008). Live imaging studies in cultured cells and *ex vivo* samples would also allow one to study the behaviour of FHOD1, when tagged with a fluorescent protein and could be done under different stimuli, such as IGF-1 treatment to induce actin assembly. Ultimately, work involving FHOD1 should converge at the creation of knock-out and transgenic animals. Global and muscle-specific depletion and overexpression of FHOD1 *in vivo* would paint a clearer picture of the function of this formin. In summary, FHOD1 may be a crucial regulator of the myofibrillar apparatus and cytoskeleton in cardiac and skeletal muscle as suggested by work involving its expression, localisation, function, regulation, and interacting partners. Future work involving the formin protein FHOD1 will hopefully further elucidate how actin is regulated in striated muscle.

References

8. References

Abmayr, S. M. and G. K. Pavlath (2012). "Myoblast fusion: lessons from flies and mice." Development **139**: 641-656.

Adachi, S., H. Ito, et al. (1998). "Skeletal and smooth muscle alpha-actin mRNA in endomyocardial biopsy samples of dilated cardiomyopathy patients." Life Sci **63**: 1779-1791.

Agarkova, I. and J. C. Perriard (2005). "The M-band: an elastic web that crosslinks thick filaments in the center of the sarcomere." Trends Cell Biol **15**: 477-485.

Agarkova, I., D. Auerbach, et al. (2000). "A novel marker for vertebrate embryonic heart, the EH-myomesin isoform." J Biol Chem **275**: 10256-10264.

Agrawal, P. B., R. S. Greenleaf, et al. (2007). "Nemaline myopathy with minicores caused by mutation of the CFL2 gene encoding the skeletal muscle actin-binding protein, cofilin-2." Am J Hum Genet **80**: 162-167.

Agrawal, P. B., M. Joshi, et al. (2012). "Normal myofibrillar development followed by progressive sarcomeric disruption with actin accumulations in a mouse Cfl2 knockout demonstrates requirement of cofilin-2 for muscle maintenance." Hum Mol Genet **21**: 2341-2356.

Ahn, A. H. and L. M. Kunkel (1993). "The structural and functional diversity of dystrophin." Nat Genet **3**: 283-291.

Ahuja, P., E. Perriard, et al. (2004). "Sequential myofibrillar breakdown accompanies mitotic division of mammalian cardiomyocytes." J Cell Sci **117**: 3295-3306.

Ahuja, P., E. Perriard, et al. (2006). "Probing the role of septins in cardiomyocytes." Exp Cell Res **312**: 1598-1609.

Ahuja, P., E. Perriard, et al. (2007). "Re-expression of proteins involved in cytokinesis during cardiac hypertrophy." Exp Cell Res **313**: 1270-1283.

Alberts, A. S., N. Bouquin, et al. (1998). "Analysis of RhoA-binding proteins reveals an interaction domain conserved in heterotrimeric G protein beta subunits and the yeast response regulator protein Skn7." J Biol Chem **273**: 8616-8622.

Alvarez, D. E. and H. Agaisse (2013). "The formin FHOD1 and the small GTPase Rac1 promote vaccinia virus actin-based motility." J Cell Biol **202**: 1075-1090.

Andrianantoandro, E. and T. D. Pollard (2006). "Mechanism of actin filament turnover by severing and nucleation at different concentrations of ADF/cofilin." Mol Cell **24**: 13-23.

Arber, S., G. Halder, et al. (1994). "Muscle LIM protein, a novel essential regulator of myogenesis, promotes myogenic differentiation." Cell **79**: 221-231.

Arber, S., J. J. Hunter, et al. (1997). "MLP-deficient mice exhibit a disruption of cardiac cytoarchitectural organization, dilated cardiomyopathy, and heart failure." Cell **88**: 393-403.

Auerbach, D., S. Bantle, et al. (1999). "Different domains of the M-band protein myomesin are involved in myosin binding and M-band targeting." Mol Biol Cell **10**: 1297-1308.

Bähler, M., T. Wallimann, et al. (1985). "Myofibrillar M-band proteins represent constituents of native thick filaments, frayed filaments and bare zone assemblages." J Muscle Res Cell Motil **6**: 783-800.

Balasubramanian, S., S. K. Mani, et al. (2010). "Hypertrophic stimulation increases beta-actin dynamics in adult feline cardiomyocytes." PLoS One **5**: e11470.

Baldassarre, M., Z. Razinia, et al. (2009). "Filamins regulate cell spreading and initiation of cell migration." PLoS One **4**: e7830.

Balza, R. O., Jr. and R. P. Misra (2006). "Role of the serum response factor in regulating contractile apparatus gene expression and sarcomeric integrity in cardiomyocytes." J Biol Chem **281**: 6498-6510.

Bamburg, J. R. and B. W. Bernstein (2010). "Roles of ADF/cofilin in actin polymerization and beyond." F1000 Biol Rep **2**: 62.

Bang, M. L., X. Li, et al. (2006). "Nebulin-deficient mice exhibit shorter thin filament lengths and reduced contractile function in skeletal muscle." J Cell Biol **173**: 905-916.

Bantle, S., S. Keller, et al. (1996). "Tissue-specific isoforms of chicken myomesin are generated by alternative splicing." J Biol Chem **271**: 19042-19052.

Bartles, J. R. (2000). "Parallel actin bundles and their multiple actin-bundling proteins." Curr Opin Cell Biol **12**: 72-78.

Bartolini, F., J. B. Moseley, et al. (2008). "The formin mDia2 stabilizes microtubules independently of its actin nucleation activity." J Cell Biol **181**: 523-536.

Bartolini, F. and G. G. Gundersen (2010). "Formins and microtubules." Biochim Biophys Acta **1803**: 164-173.

Bear, J. E., T. M. Svitkina, et al. (2002). "Antagonism between Ena/VASP proteins and actin filament capping regulates fibroblast motility." Cell **109**: 509-521.

Bearer, E. L. (1991). "Direct observation of actin filament severing by gelsolin and binding by gCap39 and CapZ." J Cell Biol **115**: 1629-1638.

Bennett, P. M. (2012). "From myofibril to membrane; the transitional junction at the intercalated disc." Front Biosci **17**: 1035-1050.

Bennett, P. M., A. M. Maggs, et al. (2006). "The transitional junction: a new functional subcellular domain at the intercalated disc." Mol Biol Cell **17**: 2091-2100.

Bentzinger, C. F., Y. X. Wang, et al. (2012). "Building muscle: molecular regulation of myogenesis." Cold Spring Harb Perspect Biol **4**.

Benz, P. M., C. J. Merkel, et al. (2013). "Mena/VASP and alphaII-Spectrin complexes regulate cytoplasmic actin networks in cardiomyocytes and protect from conduction abnormalities and dilated cardiomyopathy." Cell Commun Signal **11**: 56.

Berry, F. B., Y. Miura, et al. (2001). "Positive and negative regulation of myogenic differentiation of C2C12 cells by isoforms of the multiple homeodomain zinc finger transcription factor ATBF1." J Biol Chem **276**: 25057-25065.

Beuckelmann, D. J. and W. G. Wier (1988). "Mechanism of release of calcium from sarcoplasmic reticulum of guinea-pig cardiac cells." J Physiol **405**: 233-255.

Bione, S., C. Sala, et al. (1998). "A human homologue of the Drosophila melanogaster diaphanous gene is disrupted in a patient with premature ovarian failure: evidence for conserved function in oogenesis and implications for human sterility." Am J Hum Genet **62**: 533-541.

Blanchoin, L. and T. D. Pollard (2002). "Hydrolysis of ATP by polymerized actin depends on the bound divalent cation but not profilin." Biochemistry **41**: 597-602.

Block, J., T. E. Stradal, et al. (2008). "Filopodia formation induced by active mDia2/Drf3." J Microsc **231**: 506-517.

Block, J., D. Breitsprecher, et al. (2012). "FMNL2 drives actin-based protrusion and migration downstream of Cdc42." Curr Biol **22**: 1005-1012.

Boateng, S. Y. and P. H. Goldspink (2008). "Assembly and maintenance of the sarcomere night and day." Cardiovasc Res **77**: 667-675.

Boateng, S. Y., R. J. Belin, et al. (2007). "Cardiac dysfunction and heart failure are associated with abnormalities in the subcellular distribution and amounts of oligomeric muscle LIM protein." Am J Physiol Heart Circ Physiol **292**: H259-269.

Boateng, S. Y., S. E. Senyo, et al. (2009). "Myocyte remodeling in response to hypertrophic stimuli requires nucleocytoplasmic shuttling of muscle LIM protein." J Mol Cell Cardiol **47**: 426-435.

Boehm, M. B., T. J. Milius, et al. (2005). "The mammalian formin FHOD1 interacts with the ERK MAP kinase pathway." Biochem Biophys Res Commun **335**: 1090-1094.

Braga, V. (2000). "Epithelial cell shape: cadherins and small GTPases." Exp Cell Res **261**: 83-90.

Braga, V. M. (2002). "Cell-cell adhesion and signalling." Curr Opin Cell Biol **14**: 546-556.

Braga, V. M., L. M. Machesky, et al. (1997). "The small GTPases Rho and Rac are required for the establishment of cadherin-dependent cell-cell contacts." J Cell Biol **137**: 1421-1431.

Bravo-Cordero, J. J., M. A. Magalhaes, et al. (2013). "Functions of cofilin in cell locomotion and invasion." Nat Rev Mol Cell Biol **14**: 405-415.

Breitsprecher, D. and B. L. Goode (2013). "Formins at a glance." J Cell Sci **126**: 1-7.

Brieher, W. (2013). "Mechanisms of actin disassembly." Mol Biol Cell **24**: 2299-2302.

Broderick, M. J. and S. J. Winder (2005). "Spectrin, alpha-actinin, and dystrophin." Adv Protein Chem **70**: 203-246.

Bruckner, A., C. Polge, et al. (2009). "Yeast two-hybrid, a powerful tool for systems biology." Int J Mol Sci **10**: 2763-2788.

Brummelkamp, T. R., R. Bernards, et al. (2002). "A system for stable expression of short interfering RNAs in mammalian cells." Science **296**: 550-553.

Bulgheresi, S., E. Kleiner, et al. (2001). "Inscuteable-dependent apical localization of the microtubule-binding protein Cornetto suggests a role in asymmetric cell division." J Cell Sci **114**: 3655-3662.

Burattini, S., P. Ferri, et al. (2004). "C2C12 murine myoblasts as a model of skeletal muscle development: morpho-functional characterization." Eur J Histochem **48**: 223-233.

Buyandelger, B., K. E. Ng, et al. (2011). "MLP (muscle LIM protein) as a stress sensor in the heart." Pflugers Arch **462**: 135-142.

Caldwell, J. E., S. G. Heiss, et al. (1989). "Effects of CapZ, an actin capping protein of muscle, on the polymerization of actin." Biochemistry **28**: 8506-8514.

Camelliti, P., T. K. Borg, et al. (2005). "Structural and functional characterisation of cardiac fibroblasts." Cardiovasc Res **65**: 40-51.

Campbell, I. D. and M. J. Humphries (2011). "Integrin structure, activation, and interactions." Cold Spring Harb Perspect Biol **3**.

Cappola, T. P. (2008). "Molecular remodeling in human heart failure." J Am Coll Cardiol **51**: 137-138.

Carlier, M. F. and D. Pantaloni (1986). "Direct evidence for ADP-Pi-F-actin as the major intermediate in ATP-actin polymerization. Rate of dissociation of Pi from actin filaments." Biochemistry **25**: 7789-7792.

Carlier, M. F., V. Laurent, et al. (1997). "Actin depolymerizing factor (ADF/cofilin) enhances the rate of filament turnover: implication in actin-based motility." J Cell Biol **136**: 1307-1322.

Carroll, S. L., A. H. Herrera, et al. (2001). "Targeting and functional role of N-RAP, a nebulin-related LIM protein, during myofibril assembly in cultured chick cardiomyocytes." J Cell Sci **114**: 4229-4238.

Carroll, S., S. Lu, et al. (2004). "N-RAP scaffolds I-Z-I assembly during myofibrillogenesis in cultured chick cardiomyocytes." J Cell Sci **117**: 105-114.

Castillo, A., R. Nowak, et al. (2009). "A nebulin ruler does not dictate thin filament lengths." Biophys J **96**: 1856-1865.

Chang, F., D. Drubin, et al. (1997). "cdc12p, a protein required for cytokinesis in fission yeast, is a component of the cell division ring and interacts with profilin." J Cell Biol **137**: 169-182.

Chang, J., M. Xie, et al. (2006). "Activation of Rho-associated coiled-coil protein kinase 1 (ROCK-1) by caspase-3 cleavage plays an essential role in cardiac myocyte apoptosis." Proc Natl Acad Sci U S A **103**: 14495-14500.

Chang, W., E. S. Folker, et al. (2013). "Emerin organizes actin flow for nuclear movement and centrosome orientation in migrating fibroblasts." Mol Biol Cell **24**: 3869-3880.

Chen, L., G. Liao, et al. (2007). "Rac1 controls the formation of midline commissures and the competency of tangential migration in ventral telencephalic neurons." J Neurosci **27**: 3884-3893.

Chereau, D., M. Boczkowska, et al. (2008). "Leiomodin is an actin filament nucleator in muscle cells." Science **320**: 239-243.

Cherepanova, O., A. Orlova, et al. (2006). "Xin-repeats and nebulin-like repeats bind to F-actin in a similar manner." J Mol Biol **356**: 714-723.

Chesarone, M. A. and B. L. Goode (2009). "Actin nucleation and elongation factors: mechanisms and interplay." Curr Opin Cell Biol **21**: 28-37.

Chhabra, E. S. and H. N. Higgs (2006). "INF2 Is a WASP Homology 2 Motif-containing Formin That Severs Actin Filaments and Accelerates Both Polymerization and Depolymerization." Journal of Biological Chemistry **281**: 26754-26767.

Chhabra, E. S. and H. N. Higgs (2007). "The many faces of actin: matching assembly factors with cellular structures." Nat Cell Biol **9**: 1110-1121.

Chlopcikova, S., J. Psotova, et al. (2001). "Neonatal rat cardiomyocytes--a model for the study of morphological, biochemical and electrophysiological characteristics of the heart." Biomed Pap Med Fac Univ Palacky Olomouc Czech Repub **145**: 49-55.

Choi, S., E. A. Gustafson-Wagner, et al. (2007). "The Intercalated Disc Protein, mXinα, Is Capable of Interacting with β-Catenin and Bundling Actin Filaments." Journal of Biological Chemistry **282**: 36024-36036.

Conley, C. A. (2001). "Leiomodin and tropomodulin in smooth muscle." Am J Physiol Cell Physiol **280**: C1645-1656.

Conley, C. A., K. L. Fritz-Six, et al. (2001). "Leiomodins: larger members of the tropomodulin (Tmod) gene family." Genomics **73**: 127-139.

Cooper, J. A. and D. Sept (2008). "New insights into mechanism and regulation of actin capping protein." Int Rev Cell Mol Biol **267**: 183-206.

Copeland, J. W. and R. Treisman (2002). "The diaphanous-related formin mDia1 controls serum response factor activity through its effects on actin polymerization." Mol Biol Cell **13**: 4088-4099.

Copeland, S. J., B. J. Green, et al. (2007). "The diaphanous inhibitory domain/diaphanous autoregulatory domain interaction is able to mediate heterodimerization between mDia1 and mDia2." J Biol Chem **282**: 30120-30130.

Costa, M. L., R. Escaleira, et al. (2004). "Desmin: molecular interactions and putative functions of the muscle intermediate filament protein." Braz J Med Biol Res **37**: 1819-1830.

Costandi, P. N., L. R. Frank, et al. (2006). "Role of diastolic properties in the transition to failure in a mouse model of the cardiac dilatation." Am J Physiol Heart Circ Physiol **291**: H2971-2979.

Cramer, L. P., M. Siebert, et al. (1997). "Identification of novel graded polarity actin filament bundles in locomoting heart fibroblasts: implications for the generation of motile force." J Cell Biol **136**: 1287-1305.

Crowley, M. R., K. L. Head, et al. (2000). "The mouse mammary gland requires the actin-binding protein gelsolin for proper ductal morphogenesis." Dev Biol **225**: 407-423.

Cunningham, C. C., T. P. Stossel, et al. (1991). "Enhanced motility in NIH 3T3 fibroblasts that overexpress gelsolin." Science **251**: 1233-1236.

Delorme, V., M. Machacek, et al. (2007). "Cofilin Activity Downstream of Pak1 Regulates Cell Protrusion Efficiency by Organizing Lamellipodium and Lamella Actin Networks." Dev Cell **13**: 646-662.

Dent, E. W., A. V. Kwiatkowski, et al. (2007). "Filopodia are required for cortical neurite initiation." Nat Cell Biol **9**: 1347-1359.

DeWard, A. D., K. M. Eisenmann, et al. (2010). "The role of formins in human disease." Biochim Biophys Acta **1803**: 226-233.

Dhume, A., S. Lu, et al. (2006). "Targeted disruption of N-RAP gene function by RNA interference: a role for N-RAP in myofibril organization." Cell Motil Cytoskeleton **63**: 493-511.

Djinovic-Carugo, K., P. Young, et al. (1999). "Structure of the alpha-actinin rod: molecular basis for cross-linking of actin filaments." Cell **98**: 537-546.

Dong, Y., D. Pruyne, et al. (2003). "Formin-dependent actin assembly is regulated by distinct modes of Rho signaling in yeast." J Cell Biol **161**: 1081-1092.

Dwyer, J., T. Iskratsch, et al. (2012). "Actin in striated muscle: recent insights into assembly and maintenance." Biophysical Reviews **4**: 17-25.

Dwyer, J., M. Pluess, et al. (2014). "The Formin FHOD1 in Cardiomyocytes." Anat Rec (Hoboken) **297**: 1560-1570.

Eble, D. M., M. Qi, et al. (1998). "Contractile activity is required for sarcomeric assembly in phenylephrine-induced cardiac myocyte hypertrophy." Am J Physiol **274**: C1226-1237.

Edwards, D. C., L. C. Sanders, et al. (1999). "Activation of LIM-kinase by Pak1 couples Rac/Cdc42 GTPase signalling to actin cytoskeletal dynamics." Nat Cell Biol **1**: 253-259.

Ehler, E. and J. C. Perriard (2000). "Cardiomyocyte cytoskeleton and myofibrillogenesis in healthy and diseased heart." Heart Fail Rev **5**: 259-269.

Ehler, E. and M. Gautel (2008). "The sarcomere and sarcomerogenesis." Adv Exp Med Biol **642**: 1-14.

Ehler, E., V. M. Fowler, et al. (2004). "Myofibrillogenesis in the developing chicken heart: Role of actin isoforms and of the pointed end actin capping protein tropomodulin during thin filament assembly." Developmental Dynamics **229**: 745-755.

Ehler, E., B. M. Rothen, et al. (1999). "Myofibrillogenesis in the developing chicken heart: assembly of Z-disk, M-line and the thick filaments." J Cell Sci **112**: 1529-1539.

Ehler, E., R. Horowits, et al. (2001). "Alterations at the intercalated disk associated with the absence of muscle LIM protein." J Cell Biol **153**: 763-772.

Ehler, E., T. Moore-Morris, et al. (2013). "Isolation and culture of neonatal mouse cardiomyocytes." J Vis Exp doi: 10.3791/50154.

Ellis, S. and H. Mellor (2000). "Regulation of endocytic traffic by rho family GTPases." Trends Cell Biol **10**: 85-88.

Essers, L. and R. Kunze (1996). "A sensitive, quick and semi-quantitative LacZ assay for the two-hybrid system." Trends Genet **12**: 449-450.

Estigoy, C., F. Pontén, et al. (2009). "Intercalated discs: multiple proteins perform multiple functions in non-failing and failing human hearts." Biophysical Reviews **1**: 43-49.

Etienne-Manneville, S. and A. Hall (2003). "Cdc42 regulates GSK-3beta and adenomatous polyposis coli to control cell polarity." Nature **421**: 753-756.

Evangelista, M., D. Pruyne, et al. (2002). "Formins direct Arp2/3-independent actin filament assembly to polarize cell growth in yeast." Nat Cell Biol **4**: 260-269.

Evangelista, M., S. Zigmond, et al. (2003). "Formins: signaling effectors for assembly and polarization of actin filaments." J Cell Sci **116**: 2603-2611.

Fay, F. S., K. Fujiwara, et al. (1983). "Distribution of alpha-actinin in single isolated smooth muscle cells." J Cell Biol **96**: 783-795.

Felsenfeld, D. P., P. L. Schwartzberg, et al. (1999). "Selective regulation of integrin--cytoskeleton interactions by the tyrosine kinase Src." Nat Cell Biol **1**: 200-206.

Feng, Y. and C. A. Walsh (2004). "The many faces of filamin: a versatile molecular scaffold for cell motility and signalling." Nat Cell Biol **6**: 1034-1038.

Floyd, S., N. Whiffin, et al. (2013). "Spatiotemporal organization of Aurora-B by APC/CCdh1 after mitosis coordinates cell spreading through FHOD1." J Cell Sci **126**: 2845-2856.

Flynn, K. C., F. Hellal, et al. (2012). "ADF/cofilin-mediated actin retrograde flow directs neurite formation in the developing brain." Neuron **76**: 1091-1107.

Forbes, M. S. and N. Sperelakis (1985). "Intercalated discs of mammalian heart: a review of structure and function." Tissue Cell **17**: 605-648.

Fowler, V. M., M. A. Sussmann, et al. (1993). "Tropomodulin is associated with the free (pointed) ends of the thin filaments in rat skeletal muscle." J Cell Biol **120**: 411-420.

Fowler, V. M., N. J. Greenfield, et al. (2003). "Tropomodulin contains two actin filament pointed end-capping domains." J Biol Chem **278**: 40000-40009.

Frank, E. D. and L. Warren (1981). "Aortic smooth muscle cells contain vimentin instead of desmin." Proc Natl Acad Sci U S A **78**: 3020-3024.

Fritz-Six, K. L., P. R. Cox, et al. (2003). "Aberrant myofibril assembly in tropomodulin1 null mice leads to aborted heart development and embryonic lethality." J Cell Biol **163**: 1033-1044.

Fukata, M., M. Nakagawa, et al. (2003). "Roles of Rho-family GTPases in cell polarisation and directional migration." Curr Opin Cell Biol **15**: 590-597.

Fürst, D. O., M. Osborn, et al. (1988). "The organization of titin filaments in the half-sarcomere revealed by monoclonal antibodies in immunoelectron microscopy: a map of ten nonrepetitive epitopes starting at the Z line extends close to the M line." J Cell Biol **106**: 1563-1572.

Gabella, G. (1984). "Structural apparatus for force transmission in smooth muscles." Physiol Rev **64**: 455-477.

Gardberg, M., K. Kaipio, et al. (2013). "FHOD1, a formin upregulated in epithelial-mesenchymal transition, participates in cancer cell migration and invasion." PLoS One **8**: e74923.

Gasteier, J. E., R. Madrid, et al. (2003). "Activation of the Rac-binding partner FHOD1 induces actin stress fibers via a ROCK-dependent mechanism." J Biol Chem **278**: 38902-38912.

Gasteier, J. E., S. Schroeder, et al. (2005). "FHOD1 coordinates actin filament and microtubule alignment to mediate cell elongation." Exp Cell Res **306**: 192-202.

Gautel, M. (2011). "Cytoskeletal protein kinases: titin and its relations in mechanosensing." Pflugers Arch **462**: 119-134.

Geeves, M. A. and K. C. Holmes (1999). "Structural mechanism of muscle contraction." Annu Rev Biochem **68**: 687-728.

Gehmlich, K., C. Geier, et al. (2004). "Decreased interactions of mutant muscle LIM protein (MLP) with N-RAP and alpha-actinin and their implication for hypertrophic cardiomyopathy." Cell Tissue Res **317**: 129-136.

Gietz, R. D. (2006). "Yeast two-hybrid system screening." Methods Mol Biol **313**: 345-371.

Gill, M. B., J. Roecklein-Canfield, et al. (2004). "EBV attachment stimulates FHOS/FHOD1 redistribution and co-aggregation with CD21: formin interactions with the cytoplasmic domain of human CD21." J Cell Sci **117**: 2709-2720.

Giot, L., J. S. Bader, et al. (2003). "A protein interaction map of Drosophila melanogaster." Science **302**: 1727-1736.

Gluzman, Y. (1981). "SV40-transformed simian cells support the replication of early SV40 mutants." Cell **23**: 175-182.

Goddette, D. W. and C. Frieden (1986). "Actin polymerization. The mechanism of action of cytochalasin D." J Biol Chem **261**: 15974-15980.

Goh, W. I., T. Sudhaharan, et al. (2011). "Rif-mDia1 interaction is involved in filopodium formation independent of Cdc42 and Rac effectors." J Biol Chem **286**: 13681-13694.

Gokhin, D. S. and V. M. Fowler (2011). "Tropomodulin capping of actin filaments in striated muscle development and physiology." J Biomed Biotechnol **2011**: 103069.

Goldspink, D. F. (1991). "Exercise-related changes in protein turnover in mammalian striated muscle." J Exp Biol **160**: 127-148.

Goldstein, M. A., L. H. Michael, et al. (1986). "The Z-band lattice in skeletal muscle before, during and after tetanic contraction." J Muscle Res Cell Motil **7**: 527-536.

Goode, B. L. and M. J. Eck (2007). "Mechanism and function of formins in the control of actin assembly." Annu Rev Biochem **76**: 593-627.

Gordon, A. M., M. A. LaMadrid, et al. (1997). "Calcium regulation of skeletal muscle thin filament motility in vitro." Biophys J **72**: 1295-1307.

Gould, C. J., S. Maiti, et al. (2011). "The Formin DAD Domain Plays Dual Roles in Autoinhibition and Actin Nucleation." Current Biology **21**: 384-390.

Granger, B. L. and E. Lazarides (1979). "Desmin and vimentin coexist at the periphery of the myofibril Z disc." Cell **18**: 1053-1063.

Granzier, H. L. and S. Labeit (2004). "The giant protein titin: a major player in myocardial mechanics, signaling, and disease." Circ Res **94**: 284-295.

Gregorio, C. C., A. Weber, et al. (1995). "Requirement of pointed-end capping by tropomodulin to maintain actin filament length in embryonic chick cardiac myocytes." Nature **377**: 83-86.

Grove, B. K., V. Kurer, et al. (1984). "A new 185,000-dalton skeletal muscle protein detected by monoclonal antibodies." J Cell Biol **98**: 518-524.

Guarino, M. (2010). "Src signaling in cancer invasion." J Cell Physiol **223**: 14-26.

Gunst, S. J. and D. D. Tang (2000). "The contractile apparatus and mechanical properties of airway smooth muscle." Eur Respir J **15**: 600-616.

Guolla, L., M. Bertrand, et al. (2012). "Force transduction and strain dynamics in actin stress fibres in response to nanonewton forces." J Cell Sci **125**: 603-613.

Gupton, S. L., K. L. Anderson, et al. (2005). "Cell migration without a lamellipodium: translation of actin dynamics into cell movement mediated by tropomyosin." J Cell Biol **168**: 619-631.

Gustafson-Wagner, E. A., H. W. Sinn, et al. (2007). "Loss of mXinalpha, an intercalated disk protein, results in cardiac hypertrophy and cardiomyopathy with conduction defects." Am J Physiol Heart Circ Physiol **293**: H2680-2692.

Hall, A. (1998). "Rho GTPases and the actin cytoskeleton." Science **279**: 509-514.

Hamadi, A., T. B. Deramaudt, et al. (2009). "Src activation and translocation from focal adhesions to membrane ruffles contribute to formation of new adhesion sites." Cell Mol Life Sci **66**: 324-338.

Hannemann, S., R. Madrid, et al. (2008). "The Diaphanous-related Formin FHOD1 associates with ROCK1 and promotes Src-dependent plasma membrane blebbing." J Biol Chem **283**: 27891-27903.

Hanson, J. and H. E. Huxley (1953). "Structural basis of the cross-striations in muscle." Nature **172**: 530-532.

Harris, E. S. and H. N. Higgs (2006). "Biochemical analysis of mammalian formin effects on actin dynamics." Methods Enzymol **406**: 190-214.

Harris, E. S., T. J. Gauvin, et al. (2010). "Assembly of filopodia by the formin FRL2 (FMNL3)." Cytoskeleton (Hoboken) **67**: 755-772.

Harris, E. S., F. Li, et al. (2004). "The Mouse Formin, FRLα, Slows Actin Filament Barbed End Elongation, Competes with Capping Protein, Accelerates Polymerization from Monomers, and Severs Filaments." Journal of Biological Chemistry **279**: 20076-20087.

Harris, E. S., I. Rouiller, et al. (2006). "Mechanistic differences in actin bundling activity of two mammalian formins, FRL1 and mDia2." J Biol Chem **281**: 14383-14392.

Hart, M. C. and J. A. Cooper (1999). "Vertebrate isoforms of actin capping protein beta have distinct functions In vivo." J Cell Biol **147**: 1287-1298.

Hayakawa, K., H. Tatsumi, et al. (2008). "Actin stress fibers transmit and focus force to activate mechanosensitive channels." J Cell Sci **121**: 496-503.

Heasman, S. J. and A. J. Ridley (2008). "Mammalian Rho GTPases: new insights into their functions from in vivo studies." Nat Rev Mol Cell Biol **9**: 690-701.

Heath, J. P. (1981). "Arcs: curved microfilament bundles beneath the dorsal surface of the leading lamellae of moving chick embryo fibroblasts." Cell Biol Int Rep **5**: 975-980.

Heath, J. P. (1983). "Behaviour and structure of the leading lamella in moving fibroblasts. I. Occurrence and centripetal movement of arc-shaped microfilament bundles beneath the dorsal cell surface." J Cell Sci **60**: 331-354.

Hein, S., S. Kostin, et al. (2000). "The role of the cytoskeleton in heart failure." Cardiovasc Res **45**: 273-278.

Herrera, A. H., B. Elzey, et al. (2000). "Terminal regions of mouse nebulin: sequence analysis and complementary localization with N-RAP." Cell Motil Cytoskeleton **45**: 211-222.

Higashida, C., T. Miyoshi, et al. (2004). "Actin polymerization-driven molecular movement of mDia1 in living cells." Science **303**: 2007-2010.

Higgs, H. N. (2005). "Formin proteins: a domain-based approach." Trends Biochem Sci **30**: 342-353.

Hilfiker-Kleiner, D., U. Landmesser, et al. (2006). "Molecular Mechanisms in Heart FailureFocus on Cardiac Hypertrophy, Inflammation, Angiogenesis, and Apoptosis." Journal of the American College of Cardiology **48**: A56-A66.

Hingtgen, S. D., X. Tian, et al. (2006). "Nox2-containing NADPH oxidase and Akt activation play a key role in angiotensin II-induced cardiomyocyte hypertrophy." Physiol Genomics **26**: 180-191.

Hirschy, A., F. Schatzmann, et al. (2006). "Establishment of cardiac cytoarchitecture in the developing mouse heart." Dev Biol **289**: 430-441.

Hirschy, A., A. Croquelois, et al. (2010). "Stabilised beta-catenin in postnatal ventricular myocardium leads to dilated cardiomyopathy and premature death." Basic Research in Cardiology **105**: 597-608.

Hotulainen, P. and P. Lappalainen (2006). "Stress fibers are generated by two distinct actin assembly mechanisms in motile cells." J Cell Biol **173**: 383-394.

Husson, C., L. Renault, et al. (2011). "Cordon-Bleu uses WH2 domains as multifunctional dynamizers of actin filament assembly." Mol Cell **43**: 464-477.

Huveneers, S. and E. H. J. Danen (2009). "Adhesion signaling – crosstalk between integrins, Src and Rho." J Cell Sci **122**: 1059-1069.

Huxley, H. E. (1953). "Electron microscope studies of the organisation of the filaments in striated muscle." Biochim Biophys Acta **12**: 387-394.

Huxley, A. F. and R. Niedergerke (1954). "Structural changes in muscle during contraction; interference microscopy of living muscle fibres." Nature **173**: 971-973.

Huxley, H. and J. Hanson (1954). "Changes in the cross-striations of muscle during contraction and stretch and their structural interpretation." Nature **173**: 973-976.

Huxley, H. E. and M. F. Perutz (1951). "Polypeptide chains in frog sartorius muscle." Nature **167**: 1054.

Iskratsch, T. and E. Ehler (2011). "Formin-g muscle cytoarchitecture." Bioarchitecture **1**: 66-68.

Iskratsch, T., S. Lange, et al. (2010). "Formin follows function: a muscle-specific isoform of FHOD3 is regulated by CK2 phosphorylation and promotes myofibril maintenance." J Cell Biol **191**: 1159-1172.

Iskratsch, T., S. Reijntjes, et al. (2013a). "Two distinct phosphorylation events govern the function of muscle FHOD3." Cell Mol Life Sci **70**: 893-908.

Iskratsch, T., C.-H. Yu, et al. (2013b). "FHOD1 Is Needed for Directed Forces and Adhesion Maturation during Cell Spreading and Migration." Dev Cell **27**: 545-559.

Jaiswal, R., D. Breitsprecher, et al. (2013). "The formin Daam1 and fascin directly collaborate to promote filopodia formation." Curr Biol **23**: 1373-1379.

Jansen, S., A. Collins, et al. (2011). "Mechanism of actin filament bundling by fascin." J Biol Chem **286**: 30087-30096.

Jelinek, T., P. Dent, et al. (1996). "Ras-induced activation of Raf-1 is dependent on tyrosine phosphorylation." Mol Cell Biol **16**: 1027-1034.

Ji, P., S. R. Jayapal, et al. (2008). "Enucleation of cultured mouse fetal erythroblasts requires Rac GTPases and mDia2." Nat Cell Biol **10**: 314-321.

Joung, J. K., E. I. Ramm, et al. (2000). "A bacterial two-hybrid selection system for studying protein-DNA and protein-protein interactions." Proc Natl Acad Sci U S A **97**: 7382-7387.

Jurmeister, S., M. Baumann, et al. (2012). "MicroRNA-200c represses migration and invasion of breast cancer cells by targeting actin-regulatory proteins FHOD1 and PPM1F." Mol Cell Biol **32**: 633-651.

Kaiser, D. A., V. K. Vinson, et al. (1999). "Profilin is predominantly associated with monomeric actin in Acanthamoeba." J Cell Sci **112 (Pt 21)**: 3779-3790.

Kan-o, M., R. Takeya, et al. (2012a). "Mammalian formin Fhod3 plays an essential role in cardiogenesis by organizing myofibrillogenesis." Biol Open **1**: 889-896.

Kan-o, M., R. Takeya, et al. (2012b). "Expression and subcellular localization of mammalian formin Fhod3 in the embryonic and adult heart." PLoS One **7**: e34765.

Kanaya, H., R. Takeya, et al. (2005). "Fhos2, a novel formin-related actin-organizing protein, probably associates with the nestin intermediate filament." Genes Cells **10**: 665-678.

Katoh, M. (2004). "Identification and characterization of human FHOD3 gene in silico." Int J Mol Med **13**: 615-620.

Kee, A. J., P. W. Gunning, et al. (2009). "Diverse roles of the actin cytoskeleton in striated muscle." J Muscle Res Cell Motil **30**: 187-197.

Kim, J. R., H. J. Kee, et al. (2009). "Enhancer of polycomb1 acts on serum response factor to regulate skeletal muscle differentiation." J Biol Chem **284**: 16308-16316.

Kislinger, T., A. O. Gramolini, et al. (2005). "Proteome dynamics during C2C12 myoblast differentiation." Mol Cell Proteomics **4**: 887-901.

Kitzing, T. M., A. S. Sahadevan, et al. (2007). "Positive feedback between Dia1, LARG, and RhoA regulates cell morphology and invasion." Genes Dev **21**: 1478-1483.

Klietsch, R., J. M. Ervasti, et al. (1993). "Dystrophin-glycoprotein complex and laminin colocalize to the sarcolemma and transverse tubules of cardiac muscle." Circ Res **72**: 349-360.

Knaus, U. G., Y. Wang, et al. (1998). "Structural requirements for PAK activation by Rac GTPases." J Biol Chem **273**: 21512-21518.

Knöll, R., M. Hoshijima, et al. (2002a). "The cardiac mechanical stretch sensor machinery involves a Z disc complex that is defective in a subset of human dilated cardiomyopathy." Cell **111**: 943-955.

Knöll, R., M. Hoshijima, et al. (2002b). "Muscle LIM protein in heart failure." Exp Clin Cardiol **7**: 104-105.

Knöll, R., S. Kostin, et al. (2010). "A common MLP (muscle LIM protein) variant is associated with cardiomyopathy." Circ Res **106**: 695-704.

Kobielak, A., H. A. Pasolli, et al. (2004). "Mammalian formin-1 participates in adherens junctions and polymerization of linear actin cables." Nat Cell Biol **6**: 21-30.

Koch, P. J. and W. W. Franke (1994). "Desmosomal cadherins: another growing multigene family of adhesion molecules." Curr Opin Cell Biol **6**: 682-687.

Koka, S., C. L. Neudauer, et al. (2003). "The formin-homology-domain-containing protein FHOD1 enhances cell migration." J Cell Sci **116**: 1745-1755.

Koka, S., G. T. Minick, et al. (2005). "Src regulates the activity of the mammalian formin protein FHOD1." Biochem Biophys Res Commun **336**: 1285-1291.

Konieczny, P., P. Fuchs, et al. (2008). "Myofiber integrity depends on desmin network targeting to Z-disks and costameres via distinct plectin isoforms." J Cell Biol **181**: 667-681.

Konno, T., M. Shimizu, et al. (2003). "A novel missense mutation in the myosin binding protein-C gene is responsible for hypertrophic cardiomyopathy with left ventricular dysfunction and dilation in elderly patients." J Am Coll Cardiol **41**: 781-786.

Kothakota, S., T. Azuma, et al. (1997). "Caspase-3-generated fragment of gelsolin: effector of morphological change in apoptosis." Science **278**: 294-298.

Koubassova, N. A. and A. K. Tsaturyan (2011). "Molecular mechanism of actin-myosin motor in muscle." Biochemistry (Mosc) **76**: 1484-1506.

Kovac, B., J. L. Teo, et al. (2013). "Assembly of non-contractile dorsal stress fibers requires alpha-actinin-1 and Rac1 in migrating and spreading cells." J Cell Sci **126**: 263-273.

Kovar, D. R. (2006). "Molecular details of formin-mediated actin assembly." Curr Opin Cell Biol **18**: 11-17.

Kovar, D. R., J. R. Kuhn, et al. (2003). "The fission yeast cytokinesis formin Cdc12p is a barbed end actin filament capping protein gated by profilin." J Cell Biol **161**: 875-887.

Kovar, D. R. and T. D. Pollard (2004). "Insertional assembly of actin filament barbed ends in association with formins produces piconewton forces." Proc Natl Acad Sci U S A **101**: 14725-14730.

Krainer, E. C., J. L. Ouderkirk, et al. (2013). "The multiplicity of human formins: Expression patterns in cells and tissues." Cytoskeleton (Hoboken) **70**: 424-438.

Kueh, H. Y., G. T. Charras, et al. (2008). "Actin disassembly by cofilin, coronin, and Aip1 occurs in bursts and is inhibited by barbed-end cappers." J Cell Biol **182**: 341-353.

Kühn, S. and M. Geyer (2014). "Formins as effector proteins of Rho GTPases." Small GTPases **5**: e29513.

Kulke, M., S. Fujita-Becker, et al. (2001). "Interaction between PEVK-titin and actin filaments: origin of a viscous force component in cardiac myofibrils." Circ Res **89**: 874-881.

Kumar, S., I. Z. Maxwell, et al. (2006). "Viscoelastic retraction of single living stress fibers and its impact on cell shape, cytoskeletal organization, and extracellular matrix mechanics." Biophys J **90**: 3762-3773.

Kureishy, N., V. Sapountzi, et al. (2002). "Fascins, and their roles in cell structure and function." BioEssays **24**: 350-361.

Kutscheidt, S., R. Zhu, et al. (2014). "FHOD1 interaction with nesprin-2G mediates TAN line formation and nuclear movement." Nat Cell Biol **16**: 708–715.

Kwiatkowski, D. J. (1999). "Functions of gelsolin: motility, signaling, apoptosis, cancer." Curr Opin Cell Biol **11**: 103-108.

Labeit, S. and B. Kolmerer (1995). "Titins: giant proteins in charge of muscle ultrastructure and elasticity." Science **270**: 293-296.

Labeit, S., M. Gautel, et al. (1992). "Towards a molecular understanding of titin." EMBO J **11**: 1711-1716.

Lammermann, T. and M. Sixt (2009). "Mechanical modes of 'amoeboid' cell migration." Curr Opin Cell Biol **21**: 636-644.

Lammers, M., R. Rose, et al. (2005). "The regulation of mDia1 by autoinhibition and its release by Rho*GTP." EMBO J **24**: 4176-4187.

Lammers, M., S. Meyer, et al. (2008). "Specificity of interactions between mDia isoforms and Rho proteins." J Biol Chem **283**: 35236-35246.

Lange, S., D. Auerbach, et al. (2002). "Subcellular targeting of metabolic enzymes to titin in heart muscle may be mediated by DRAL/FHL-2." J Cell Sci **115**: 4925-4936.

Lange, S., M. Himmel, et al. (2005). "Dimerisation of myomesin: implications for the structure of the sarcomeric M-band." J Mol Biol **345**: 289-298.

Langley, S. R., J. Dwyer, et al. (2012). "Proteomics - From Single Molecules to Biological Pathways." Cardiovasc Res **97**: 612-22.

Le Clainche, C. and M. F. Carlier (2008). "Regulation of actin assembly associated with protrusion and adhesion in cell migration." Physiol Rev **88**: 489-513.

Leach, R. N., J. C. Desai, et al. (2005). "Effect of cytoskeleton disruptors on L-type Ca channel distribution in rat ventricular myocytes." Cell Calcium **38**: 515-526.

Lebrand, C., E. W. Dent, et al. (2004). "Critical role of Ena/VASP proteins for filopodia formation in neurons and in function downstream of netrin-1." Neuron **42**: 37-49.

Lee, H.-J. and J. Zheng (2010). "PDZ domains and their binding partners: structure, specificity, and modification." Cell Communication and Signaling **8**: 8.

Lee, S. H. and R. Dominguez (2010). "Regulation of actin cytoskeleton dynamics in cells." Mol Cells **29**: 311-325.

Lewis, S. E., F. J. Kelly, et al. (1984). "Pre- and post-natal growth and protein turnover in smooth muscle, heart and slow- and fast-twitch skeletal muscles of the rat." Biochem J **217**: 517-526.

Li, D., M. A. Hallett, et al. (2011). "Dishevelled-associated activator of morphogenesis 1 (Daam1) is required for heart morphogenesis." Development **138**: 303-315.

Li, F. and H. N. Higgs (2003). "The mouse Formin mDia1 is a potent actin nucleation factor regulated by autoinhibition." Curr Biol **13**: 1335-1340.

Li, F. and H. N. Higgs (2005). "Dissecting requirements for auto-inhibition of actin nucleation by the formin, mDia1." J Biol Chem **280**: 6986-6992.

Li, F., X. Wang, et al. (1996). "Rapid transition of cardiac myocytes from hyperplasia to hypertrophy during postnatal development." J Mol Cell Cardiol **28**: 1737-1746.

Lieleg, O., M. M. A. E. Claessens, et al. (2010). "Structure and dynamics of cross-linked actin networks." Soft Matter **6**: 218-225.

Lim, M. J., Y. H. Seo, et al. (2007). "Suppression of c-Src activity stimulates muscle differentiation via p38 MAPK activation." Arch Biochem Biophys **465**: 197-208.

Littlefield, R., A. Almenar-Queralt, et al. (2001). "Actin dynamics at pointed ends regulates thin filament length in striated muscle." Nat Cell Biol **3**: 544-551.

Littlefield, R. S. and V. M. Fowler (2008). "Thin filament length regulation in striated muscle sarcomeres: pointed-end dynamics go beyond a nebulin ruler." Semin Cell Dev Biol **19**: 511-519.

Loisel, T. P., R. Boujemaa, et al. (1999). "Reconstitution of actin-based motility of Listeria and Shigella using pure proteins." Nature **401**: 613-616.

Lorenz, M. and K. C. Holmes (2010). "The actin-myosin interface." Proc Natl Acad Sci U S A **107**: 12529-12534.

Lozano, E., M. A. Frasa, et al. (2008). "PAK is required for the disruption of E-cadherin adhesion by the small GTPase Rac." J Cell Sci **121**: 933-938.

Lu, H., P. Shah, et al. (2002). "The differentiation of skeletal muscle cells involves a protein-tyrosine phosphatase-alpha-mediated C-Src signaling pathway." J Biol Chem **277**: 46687-46695.

Lu, M., W. Witke, et al. (1997). "Delayed retraction of filopodia in gelsolin null mice." J Cell Biol **138**: 1279-1287.

Lu, S., D. E. Borst, et al. (2005). "N-RAP expression during mouse heart development." Dev Dyn **233**: 201-212.

Lu, S., S. L. Carroll, et al. (2003). "New N-RAP-binding partners alpha-actinin, filamin and Krp1 detected by yeast two-hybrid screening: implications for myofibril assembly." J Cell Sci **116**: 2169-2178.

Lu, S., G. L. Crawford, et al. (2011). "Cardiac-specific NRAP overexpression causes right ventricular dysfunction in mice." Exp Cell Res **317**: 1226-1237.

Lu, X. G., G. Azhar, et al. (1998). "SRF binding to SRE in the rat heart: influence of age." J Gerontol A Biol Sci Med Sci **53**: B3-10.

Luo, G., J. Q. Zhang, et al. (1997a). "Complete cDNA sequence and tissue localization of N-RAP, a novel nebulin-related protein of striated muscle." Cell Motil Cytoskeleton **38**: 75-90.

Luo, G., E. Leroy, et al. (1997b). "Mapping of the gene (NRAP) encoding N-RAP in the mouse and human genomes." Genomics **45**: 229-232.

Luo, G., A. H. Herrera, et al. (1999). "Molecular interactions of N-RAP, a nebulin-related protein of striated muscle myotendon junctions and intercalated disks." Biochemistry **38**: 6135-6143.

Luther, P. K. (2009). "The vertebrate muscle Z-disc: sarcomere anchor for structure and signalling." J Muscle Res Cell Motil **30**: 171-185.

Lynch, E. D., M. K. Lee, et al. (1997). "Nonsyndromic deafness DFNA1 associated with mutation of a human homolog of the Drosophila gene diaphanous." Science **278**: 1315-1318.

Machackova, J., J. Barta, et al. (2006). "Myofibrillar remodeling in cardiac hypertrophy, heart failure and cardiomyopathies." Can J Cardiol **22**: 953-968.

Machesky, L. M., S. J. Atkinson, et al. (1994). "Purification of a cortical complex containing two unconventional actins from Acanthamoeba by affinity chromatography on profilin-agarose." J Cell Biol **127**: 107-115.

Madrid, R., J. E. Gasteier, et al. (2005). "Oligomerization of the diaphanous-related formin FHOD1 requires a coiled-coil motif critical for its cytoskeletal and transcriptional activities." FEBS Lett **579**: 441-448.

Maiti, S., A. Michelot, et al. (2012). "Structure and activity of full-length formin mDia1." Cytoskeleton (Hoboken) **69**: 393-405.

Malone, C. M., R. Domaschenz, et al. (2011). "Hes6 is required for actin cytoskeletal organization in differentiating C2C12 myoblasts." Exp Cell Res **317**: 1590-1602.

Marston, S. B. and C. W. Smith (1985). "The thin filaments of smooth muscles." J Muscle Res Cell Motil **6**: 669-708.

Martinez-Quiles, N., R. Rohatgi, et al. (2001). "WIP regulates N-WASP-mediated actin polymerization and filopodium formation." Nat Cell Biol **3**: 484-491.

Masaki, T. and O. Takaiti (1974). "M-protein." J Biochem **75**: 367-380.

Mass, R. L., R. Zeller, et al. (1990). "Disruption of formin-encoding transcripts in two mutant limb deformity alleles." Nature **346**: 853-855.

Masuelli, L., R. Bei, et al. (2003). "Beta-catenin accumulates in intercalated disks of hypertrophic cardiomyopathic hearts." Cardiovasc Res **60**: 376-387.

Mattila, P. K. and P. Lappalainen (2008). "Filopodia: molecular architecture and cellular functions." Nat Rev Mol Cell Biol **9**: 446-454.

McElhinny, A. S., C. Schwach, et al. (2005). "Nebulin regulates the assembly and lengths of the thin filaments in striated muscle." J Cell Biol **170**: 947-957.

Mejillano, M. R., S.-i. Kojima, et al. (2004). "Lamellipodial Versus Filopodial Mode of the Actin Nanomachinery: Pivotal Role of the Filament Barbed End." Cell **118**: 363-373.

Melki, R., S. Fievez, et al. (1996). "Continuous monitoring of Pi release following nucleotide hydrolysis in actin or tubulin assembly using 2-amino-6-mercapto-7-methylpurine ribonucleoside and purine-nucleoside phosphorylase as an enzyme-linked assay." Biochemistry **35**: 12038-12045.

Menard, I., F. G. Gervais, et al. (2006). "Caspase-3 cleaves the formin-homology-domain-containing protein FHOD1 during apoptosis to generate a C-terminal fragment that is targeted to the nucleolus." Apoptosis **11**: 1863-1876.

Messerli, J. M., M. E. Eppenberger-Eberhardt, et al. (1993). "Remodelling of cardiomyocyte cytoarchitecture visualized by three-dimensional (3D) confocal microscopy." Histochemistry **100**: 193-202.

Mi-Mi, L., S. Votra, et al. (2012). "Z-line formins promote contractile lattice growth and maintenance in striated muscles of C. elegans." J Cell Biol **198**: 87-102.

Mian, I., W. S. Pierre-Louis, et al. (2012). "LKB1 destabilizes microtubules in myoblasts and contributes to myoblast differentiation." PLoS One **7**: e31583.

Miano, J. M., X. Long, et al. (2007). "Serum response factor: master regulator of the actin cytoskeleton and contractile apparatus." Am J Physiol Cell Physiol **292**: C70-81.

Minetti, C., F. Beltrame, et al. (1992). "Dystrophin at the plasma membrane of human muscle fibers shows a costameric localization." Neuromuscul Disord **2**: 99-109.

Mohiddin, S. A., S. Lu, et al. (2003). "Genomic organization, alternative splicing, and expression of human and mouse N-RAP, a nebulin-related LIM protein of striated muscle." Cell Motil Cytoskeleton **55**: 200-212.

Moncman, C. L. and K. Wang (2002). "Targeted disruption of nebulette protein expression alters cardiac myofibril assembly and function." Exp Cell Res **273**: 204-218.

Moseley, J. B., I. Sagot, et al. (2004). "A conserved mechanism for Bni1- and mDia1-induced actin assembly and dual regulation of Bni1 by Bud6 and profilin." Mol Biol Cell **15**: 896-907.

Moza, M., L. Mologni, et al. (2007). "Targeted deletion of the muscular dystrophy gene myotilin does not perturb muscle structure or function in mice." Mol Cell Biol **27**: 244-252.

Mseka, T., M. Coughlin, et al. (2009). "Graded actin filament polarity is the organization of oriented actomyosin II filament bundles required for fibroblast polarization." Cell Motil Cytoskeleton **66**: 743-753.

Mullins, R. D., J. A. Heuser, et al. (1998). "The interaction of Arp2/3 complex with actin: nucleation, high affinity pointed end capping, and formation of branching networks of filaments." Proc Natl Acad Sci U S A **95**: 6181-6186.

Mullins, R. D., J. F. Kelleher, et al. (1998). "Arp2/3 complex from Acanthamoeba binds profilin and cross-links actin filaments." Mol Biol Cell **9**: 841-852.

Nakamura, H., T. Sudo, et al. (1998). "Identification of a novel human homolog of the Drosophila dlg, P-dlg, specifically expressed in the gland tissues and interacting with p55." FEBS Lett **433**: 63-67.

Nakano, K., K. Takaishi, et al. (1999). "Distinct actions and cooperative roles of ROCK and mDia in Rho small G protein-induced reorganization of the actin cytoskeleton in Madin-Darby canine kidney cells." Mol Biol Cell **10**: 2481-2491.

Naumanen, P., P. Lappalainen, et al. (2008). "Mechanisms of actin stress fibre assembly." J Microsc **231**: 446-454.

Nechiporuk, T., T. E. Fernandez, et al. (2007). "Failure of epithelial tube maintenance causes hydrocephalus and renal cysts in Dlg5-/- mice." Dev Cell **13**: 338-350.

Nelson, T. J., R. Balza Jr, et al. (2005). "SRF-dependent gene expression in isolated cardiomyocytes: Regulation of genes involved in cardiac hypertrophy." J Mol Cell Cardiol **39**: 479-489.

Nemethova, M., S. Auinger, et al. (2008). "Building the actin cytoskeleton: filopodia contribute to the construction of contractile bundles in the lamella." J Cell Biol **180**: 1233-1244.

Nicholson-Dykstra, S., H. N. Higgs, et al. (2005). "Actin dynamics: growth from dendritic branches." Curr Biol **15**: R346-357.

Nobes, C. D. and A. Hall (1995). "Rho, rac, and cdc42 GTPases regulate the assembly of multimolecular focal complexes associated with actin stress fibers, lamellipodia, and filopodia." Cell **81**: 53-62.

Nosal, R., V. Jancinova, et al. (1992). "Involvement of arachidonic acid and its metabolites in the inhibitory effect of beta-adrenoceptor blocking drugs on blood platelets." Agents Actions Suppl **37**: 47-52.

O'Neill, A., M. W. Williams, et al. (2002). "Sarcolemmal organization in skeletal muscle lacking desmin: evidence for cytokeratins associated with the membrane skeleton at costameres." Mol Biol Cell **13**: 2347-2359.

Oakes, P. W., Y. Beckham, et al. (2012). "Tension is required but not sufficient for focal adhesion maturation without a stress fiber template." J Cell Biol **196**: 363-374.

Obermann, W. M., M. Gautel, et al. (1997). "Molecular structure of the sarcomeric M band: mapping of titin and myosin binding domains in myomesin and the identification of a potential regulatory phosphorylation site in myomesin." EMBO J **16**: 211-220.

Ochala, J., D. S. Gokhin, et al. (2014). "Pointed-end capping by tropomodulin modulates actomyosin crossbridge formation in skeletal muscle fibers." FASEB J **28**: 408-415.

Ohashi, K., K. Nagata, et al. (2000). "Rho-associated kinase ROCK activates LIM-kinase 1 by phosphorylation at threonine 508 within the activation loop." J Biol Chem **275**: 3577-3582.

Olson, E. N. and D. Srivastava (1996). "Molecular pathways controlling heart development." Science **272**: 671-676.

Ono, S. (2010). "Dynamic regulation of sarcomeric actin filaments in striated muscle." Cytoskeleton (Hoboken) **67**: 677-692.

Ono, S. and K. Ono (2002). "Tropomyosin inhibits ADF/cofilin-dependent actin filament dynamics." J Cell Biol **156**: 1065-1076.

Orchard, C. and F. Brette (2008). "t-Tubules and sarcoplasmic reticulum function in cardiac ventricular myocytes." Cardiovasc Res **77**: 237-244.

Oser, M. and J. Condeelis (2009). "The cofilin activity cycle in lamellipodia and invadopodia." J Cell Biochem **108**: 1252-1262.

Otomo, T., C. Otomo, et al. (2005a). "Structural basis of Rho GTPase-mediated activation of the formin mDia1." Mol Cell **18**: 273-281.

Otomo, T., D. R. Tomchick, et al. (2005b). "Structural basis of actin filament nucleation and processive capping by a formin homology 2 domain." Nature **433**: 488-494.

Otten, J., P. F. van der Ven, et al. (2010). "Complete loss of murine Xin results in a mild cardiac phenotype with altered distribution of intercalated discs." Cardiovasc Res **85**: 739-750.

Pacholsky, D., P. Vakeel, et al. (2004). "Xin repeats define a novel actin-binding motif." J Cell Sci **117**: 5257-5268.

Palatinus, J. A., J. M. Rhett, et al. (2012). "The connexin43 carboxyl terminus and cardiac gap junction organization." Biochimica et Biophysica Acta (BBA) - Biomembranes **1818**: 1831-1843.

Panchenko, M. P., N. Silva, et al. (2009). "Up-regulation of a hydrogen peroxide-responsive pre-mRNA binding protein in atherosclerosis and intimal hyperplasia." Cardiovasc Pathol **18**: 167-172.

Papa, I., C. Astier, et al. (1999). "Alpha actinin-CapZ, an anchoring complex for thin filaments in Z-line." J Muscle Res Cell Motil **20**: 187-197.

Pappas, C. T., N. Bhattacharya, et al. (2008). "Nebulin interacts with CapZ and regulates thin filament architecture within the Z-disc." Mol Biol Cell **19**: 1837-1847.

Pappas, C. T., K. T. Bliss, et al. (2011). "The Nebulin family: an actin support group." Trends Cell Biol **21**: 29-37.

Pardo, J. V., J. D. Siliciano, et al. (1983). "A vinculin-containing cortical lattice in skeletal muscle: transverse lattice elements ("costameres") mark sites of attachment between myofibrils and sarcolemma." Proc Natl Acad Sci U S A **80**: 1008-1012.

Parmacek, M. S. (2007). "Myocardin-related transcription factors: critical coactivators regulating cardiovascular development and adaptation." Circ Res **100**: 633-644.

Parsons, J. T. (2003). "Focal adhesion kinase: the first ten years." J Cell Sci **116**: 1409-1416.

Patel, M. and J. F. Cote (2013). "Ras GTPases' interaction with effector domains: Breaking the families' barrier." Commun Integr Biol **6**: e24298.

Paul, A. S. and T. D. Pollard (2008). "The role of the FH1 domain and profilin in formin-mediated actin-filament elongation and nucleation." Curr Biol **18**: 9-19.

Paul, A. S. and T. D. Pollard (2009). "Review of the mechanism of processive actin filament elongation by formins." Cell Motil Cytoskeleton **66**: 606-617.

Paul, M., A. Poyan Mehr, et al. (2006). "Physiology of local renin-angiotensin systems." Physiol Rev **86**: 747-803.

Paulin, D. and Z. Li (2004). "Desmin: a major intermediate filament protein essential for the structural integrity and function of muscle." Exp Cell Res **301**: 1-7.

Pellegrin, S. and H. Mellor (2005). "The Rho family GTPase Rif induces filopodia through mDia2." Curr Biol **15**: 129-133.

Pellegrin, S. and H. Mellor (2007). "Actin stress fibres." J Cell Sci **120**: 3491-3499.

Peng, J., S. M. Kitchen, et al. (2007). "Myeloproliferative defects following targeting of the Drf1 gene encoding the mammalian diaphanous related formin mDia1." Cancer Res **67**: 7565-7571.

Perriard, J. C., A. Hirschy, et al. (2003). "Dilated cardiomyopathy: a disease of the intercalated disc?" Trends Cardiovasc Med **13**: 30-38.

Petersen, J., O. Nielsen, et al. (1998). "FH3, a domain found in formins, targets the fission yeast formin Fus1 to the projection tip during conjugation." J Cell Biol **141**: 1217-1228.

Pollard, T. D. (1986). "Rate constants for the reactions of ATP- and ADP-actin with the ends of actin filaments." J Cell Biol **103**: 2747-2754.

Pollard, T. D. (2007). "Regulation of actin filament assembly by Arp2/3 complex and formins." Annu Rev Biophys Biomol Struct **36**: 451-477.

Pollard, T. D., L. Blanchoin, et al. (2000). "Molecular mechanisms controlling actin filament dynamics in nonmuscle cells." Annu Rev Biophys Biomol Struct **29**: 545-576.

Ponti, A., M. Machacek, et al. (2004). "Two distinct actin networks drive the protrusion of migrating cells." Science **305**: 1782-1786.

Poole, K. J., M. Lorenz, et al. (2006). "A comparison of muscle thin filament models obtained from electron microscopy reconstructions and low-angle X-ray fibre diagrams from non-overlap muscle." J Struct Biol **155**: 273-284.

Porter, G. A., G. M. Dmytrenko, et al. (1992). "Dystrophin colocalizes with beta-spectrin in distinct subsarcolemmal domains in mammalian skeletal muscle." J Cell Biol **117**: 997-1005.

Price, L. S., J. Leng, et al. (1998). "Activation of Rac and Cdc42 by integrins mediates cell spreading." Mol Biol Cell **9**: 1863-1871.

Price, M. G. (1987). "Skelemins: cytoskeletal proteins located at the periphery of M-discs in mammalian striated muscle." J Cell Biol **104**: 1325-1336.

Price, M. G. and R. H. Gomer (1993). "Skelemin, a cytoskeletal M-disc periphery protein, contains motifs of adhesion/recognition and intermediate filament proteins." J Biol Chem **268**: 21800-21810.

Prins, K. W., J. A. Call, et al. (2011). "Quadriceps myopathy caused by skeletal muscle-specific ablation of βcyto-actin." J Cell Sci **124**: 951-957.

Pruyne, D., M. Evangelista, et al. (2002). "Role of formins in actin assembly: nucleation and barbed-end association." Science **297**: 612-615.

Qualmann, B. and M. M. Kessels (2009). "New players in actin polymerization--WH2-domain-containing actin nucleators." Trends Cell Biol **19**: 276-285.

Quinlan, M. E., S. Hilgert, et al. (2007). "Regulatory interactions between two actin nucleators, Spire and Cappuccino." The Journal of Cell Biology **179**: 117-128.

Ramalingam, N., H. Zhao, et al. (2010). "Phospholipids regulate localization and activity of mDia1 formin." Eur J Cell Biol **89**: 723-732.

Rao, D. D., J. S. Vorhies, et al. (2009). "siRNA vs. shRNA: similarities and differences." Adv Drug Deliv Rev **61**: 746-759.

Rapundalo, S. T. (1998). "Cardiac protein phosphorylation: functional and pathophysiological correlates." Cardiovasc Res **38**: 559-588.

Ridley, A. J. (2001). "Rho GTPases and cell migration." J Cell Sci **114**: 2713-2722.

Ridley, A. J. (2006). "Rho GTPases and actin dynamics in membrane protrusions and vesicle trafficking." Trends Cell Biol **16**: 522-529.

Ridley, A. J. and A. Hall (1992a). "The small GTP-binding protein rho regulates the assembly of focal adhesions and actin stress fibers in response to growth factors." Cell **70**: 389-399.

Ridley, A. J. and A. Hall (1992b). "Distinct patterns of actin organization regulated by the small GTP-binding proteins Rac and Rho." Cold Spring Harb Symp Quant Biol **57**: 661-671.

Ridley, A. J., H. F. Paterson, et al. (1992). "The small GTP-binding protein rac regulates growth factor-induced membrane ruffling." Cell **70**: 401-410.

Riedl, J., A. H. Crevenna, et al. (2008). "Lifeact: a versatile marker to visualize F-actin." Nat Methods **5**: 605-607.

Riento, K., N. Totty, et al. (2005). "RhoE function is regulated by ROCK I-mediated phosphorylation." EMBO J **24**: 1170-1180.

Rivero, F., T. Muramoto, et al. (2005). "A comparative sequence analysis reveals a common GBD/FH3-FH1-FH2-DAD architecture in formins from Dictyostelium, fungi and metazoa." BMC Genomics **6**: 28.

Rizvi, S. A., E. M. Neidt, et al. (2009). "Identification and characterization of a small molecule inhibitor of formin-mediated actin assembly." Chem Biol **16**: 1158-1168.

Rohatgi, R., L. Ma, et al. (1999). "The interaction between N-WASP and the Arp2/3 complex links Cdc42-dependent signals to actin assembly." Cell **97**: 221-231.

Rohatgi, R., H. Y. Ho, et al. (2000). "Mechanism of N-WASP activation by CDC42 and phosphatidylinositol 4, 5-bisphosphate." J Cell Biol **150**: 1299-1310.

Rohr, S. (2004). "Role of gap junctions in the propagation of the cardiac action potential." Cardiovasc Res **62**: 309-322.

Romero, S., C. Le Clainche, et al. (2004). "Formin is a processive motor that requires profilin to accelerate actin assembly and associated ATP hydrolysis." Cell **119**: 419-429.

Rosado, M., C. F. Barber, et al. (2014). "Critical roles for multiple formins during cardiac myofibril development and repair." Mol Biol Cell **25**: 811-827.

Rose, R., M. Weyand, et al. (2005a). "Structural and mechanistic insights into the interaction between Rho and mammalian Dia." Nature **435**: 513-518.

Rose, R., A. Wittinghofer, et al. (2005b). "The purification and crystallization of mDia1 in complex with RhoC." Acta Crystallogr Sect F Struct Biol Cryst Commun **61**: 225-227.

Rothen-Rutishauser, B. M., E. Ehler, et al. (1998). "Different behaviour of the non-sarcomeric cytoskeleton in neonatal and adult rat cardiomyocytes." J Mol Cell Cardiol **30**: 19-31.

Sagot, I., A. A. Rodal, et al. (2002). "An actin nucleation mechanism mediated by Bni1 and profilin." Nat Cell Biol **4**: 626-631.

Samarel, A. M. (2005). "Costameres, focal adhesions, and cardiomyocyte mechanotransduction." Am J Physiol Heart Circ Physiol **289**: H2291-2301.

Sanger, J., S. Kang, et al. (2005). "How to build a myofibril." Journal of Muscle Research & Cell Motility **26**: 343-354.

Sanger, J. M. and J. W. Sanger (2008). "The dynamic Z bands of striated muscle cells." Sci Signal **1**: pe37.

Satoh, M., H. Ogita, et al. (2006). "Requirement of Rac1 in the development of cardiac hypertrophy." Proc Natl Acad Sci U S A **103**: 7432-7437.

Schafer, C., U. Faust, et al. (2011). "The filopodium: a stable structure with highly regulated repetitive cycles of elongation and persistence depending on the actin cross-linker fascin." Cell Adh Migr **5**: 431-438.

Schafer, D. A., J. A. Waddle, et al. (1993). "Localization of CapZ during myofibrillogenesis in cultured chicken muscle." Cell Motil Cytoskeleton **25**: 317-335.

Schafer, D. A., C. Hug, et al. (1995). "Inhibition of CapZ during myofibrillogenesis alters assembly of actin filaments." J Cell Biol **128**: 61-70.

Schaub, M. C., M. A. Hefti, et al. (1998). "Modulation of contractility in human cardiac hypertrophy by myosin essential light chain isoforms." Cardiovasc Res **37**: 381-404.

Scherer, W. F., J. T. Syverton, et al. (1953). "Studies on the propagation in vitro of poliomyelitis viruses. IV. Viral multiplication in a stable strain of human malignant epithelial cells (strain HeLa) derived from an epidermoid carcinoma of the cervix." J Exp Med **97**: 695-710.

Schiaffino, S. and C. Reggiani (1996). "Molecular diversity of myofibrillar proteins: gene regulation and functional significance." Physiol Rev **76**: 371-423.

Schiaffino, S. and C. Reggiani (2011). "Fiber types in mammalian skeletal muscles." Physiol Rev **91**: 1447-1531.

Schmeichel, K. L. and M. C. Beckerle (1994). "The LIM domain is a modular protein-binding interface." Cell **79**: 211-219.

Schonichen, A., M. Alexander, et al. (2006). "Biochemical characterization of the diaphanous autoregulatory interaction in the formin homology protein FHOD1." J Biol Chem **281**: 5084-5093.

Schonichen, A., H. G. Mannherz, et al. (2013). "FHOD1 is a combined actin filament capping and bundling factor that selectively associates with actin arcs and stress fibers." J Cell Sci **126**: 1891-1901.

Schuldt, A. (2005). "Spire: a new nucleator for actin." Nat Cell Biol **7**: 107.

Schulte, A., B. Stolp, et al. (2008). "The human formin FHOD1 contains a bipartite structure of FH3 and GTPase-binding domains required for activation." Structure **16**: 1313-1323.

Schulze, N., M. Graessl, et al. (2014). "FHOD1 regulates stress fiber organization by controlling the dynamics of transverse arcs and dorsal fibers." J Cell Sci **127**: 1379-1393.

Schutt, C. E., J. C. Myslik, et al. (1993). "The structure of crystalline profilin-beta-actin." Nature **365**: 810-816.

Sells, M. A., U. G. Knaus, et al. (1997). "Human p21-activated kinase (Pak1) regulates actin organization in mammalian cells." Curr Biol **7**: 202-210.

Sept, D. and J. A. McCammon (2001). "Thermodynamics and kinetics of actin filament nucleation." Biophys J **81**: 667-674.

Seth, A., C. Otomo, et al. (2006). "Autoinhibition regulates cellular localization and actin assembly activity of the diaphanous-related formins FRLalpha and mDia1." J Cell Biol **174**: 701-713.

Severs, N. J. (2000). "The cardiac muscle cell." Bioessays **22**: 188-199.

Sezaki, T., K. Inada, et al. (2012). "Role of Dlg5/lp-dlg, a membrane-associated guanylate kinase family protein, in epithelial-mesenchymal transition in LLc-PK1 renal epithelial cells." PLoS One **7**: e35519.

Shah, G., R. Brugada, et al. (2002). "The cloning, genomic organization and tissue expression profile of the human DLG5 gene." BMC Genomics **3**: 6.

Silacci, P., L. Mazzolai, et al. (2004). "Gelsolin superfamily proteins: key regulators of cellular functions." Cell Mol Life Sci **61**: 2614-2623.

Sitar, T., J. Gallinger, et al. (2011). "Molecular architecture of the Spire-actin nucleus and its implication for actin filament assembly." Proc Natl Acad Sci U S A **108**: 19575-19580.

Sjoblom, B., A. Salmazo, et al. (2008). "Alpha-actinin structure and regulation." Cell Mol Life Sci **65**: 2688-2701.

Skwarek-Maruszewska, A., P. Hotulainen, et al. (2009). "Contractility-dependent actin dynamics in cardiomyocyte sarcomeres." J Cell Sci **122**: 2119-2126.

Skwarek-Maruszewska, A., M. Boczkowska, et al. (2010). "Different localizations and cellular behaviors of leiomodin and tropomodulin in mature cardiomyocyte sarcomeres." Mol Biol Cell **21**: 3352-3361.

Small, J. V. and M. Gimona (1998). "The cytoskeleton of the vertebrate smooth muscle cell." Acta Physiol Scand **164**: 341-348.

Small, J. V., K. Rottner, et al. (1998). "Assembling an actin cytoskeleton for cell attachment and movement." Biochim Biophys Acta **1404**: 271-281.

Songyang, Z., S. E. Shoelson, et al. (1993). "SH2 domains recognize specific phosphopeptide sequences." Cell **72**: 767-778.

Sonnemann, K. J., D. P. Fitzsimons, et al. (2006). "Cytoplasmic gamma-actin is not required for skeletal muscle development but its absence leads to a progressive myopathy." Dev Cell **11**: 387-397.

Spector, I., N. R. Shochet, et al. (1989). "Latrunculins--novel marine macrolides that disrupt microfilament organization and affect cell growth: I. Comparison with cytochalasin D." Cell Motil Cytoskeleton **13**: 127-144.

Spector, I., N. R. Shochet, et al. (1983). "Latrunculins: novel marine toxins that disrupt microfilament organization in cultured cells." Science **219**: 493-495.

Staus, D. P., A. L. Blaker, et al. (2011a). "Formin homology domain-containing protein 1 regulates smooth muscle cell phenotype." Arterioscler Thromb Vasc Biol **31**: 360-367.

Staus, D. P., J. M. Taylor, et al. (2011b). "Enhancement of mDia2 activity by Rho-kinase-dependent phosphorylation of the diaphanous autoregulatory domain." Biochem J **439**: 57-65.

Steiner, F., K. Weber, et al. (1999). "M band proteins myomesin and skelemin are encoded by the same gene: analysis of its organization and expression." Genomics **56**: 78-89.

Stevenson, R. P., D. Veltman, et al. (2012). "Actin-bundling proteins in cancer progression at a glance." J Cell Sci **125**: 1073-1079.

Struhl, K. and R. W. Davis (1981). "Transcription of the his3 gene region in Saccharomyces cerevisiae." J Mol Biol **152**: 535-552.

Suetsugu, S., H. Miki, et al. (2001). "Identification of another actin-related protein (Arp) 2/3 complex binding site in neural Wiskott-Aldrich syndrome protein (N-WASP) that complements actin polymerization induced by the Arp2/3 complex activating (VCA) domain of N-WASP." J Biol Chem **276**: 33175-33180.

Summy, J. M. and G. E. Gallick (2003). "Src family kinases in tumor progression and metastasis." Cancer Metastasis Rev **22**: 337-358.

Suraneni, P., B. Rubinstein, et al. (2012). "The Arp2/3 complex is required for lamellipodia extension and directional fibroblast cell migration." J Cell Biol **197**: 239-251.

Sussman, M. A., S. Welch, et al. (1998). "Myofibril degeneration caused by tropomodulin overexpression leads to dilated cardiomyopathy in juvenile mice." J Clin Invest **101**: 51-61.

Suurmeijer, A. J., S. Clement, et al. (2003). "Alpha-actin isoform distribution in normal and failing human heart: a morphological, morphometric, and biochemical study." J Pathol **199**: 387-397.

Suzuki, T., H. Mimuro, et al. (2000). "Rho family GTPase Cdc42 is essential for the actin-based motility of Shigella in mammalian cells." J Exp Med **191**: 1905-1920.

Svitkina, T. M. and G. G. Borisy (1999). "Arp2/3 complex and actin depolymerizing factor/cofilin in dendritic organization and treadmilling of actin filament array in lamellipodia." J Cell Biol **145**: 1009-1026.

Svitkina, T. M., E. A. Bulanova, et al. (2003). "Mechanism of filopodia initiation by reorganization of a dendritic network." J Cell Biol **160**: 409-421.

Takano, K., H. Watanabe-Takano, et al. (2010). "Nebulin and N-WASP cooperate to cause IGF-1-induced sarcomeric actin filament formation." Science **330**: 1536-1540.

Takeishi, Y., Q. Huang, et al. (2001). "Src and multiple MAP kinase activation in cardiac hypertrophy and congestive heart failure under chronic pressure-overload: comparison with acute mechanical stretch." J Mol Cell Cardiol **33**: 1637-1648.

Takeya, R. and H. Sumimoto (2003). "Fhos, a mammalian formin, directly binds to F-actin via a region N-terminal to the FH1 domain and forms a homotypic complex via the FH2 domain to promote actin fiber formation." J Cell Sci **116**: 4567-4575.

Takeya, R., K. Taniguchi, et al. (2008). "The mammalian formin FHOD1 is activated through phosphorylation by ROCK and mediates thrombin-induced stress fibre formation in endothelial cells." EMBO J **27**: 618-628.

Tamura, K., D. Peterson, et al. (2011). "MEGA5: molecular evolutionary genetics analysis using maximum likelihood, evolutionary distance, and maximum parsimony methods." Mol Biol Evol **28**: 2731-2739.

Tang, N. and W. F. Marshall (2012). "Centrosome positioning in vertebrate development." J Cell Sci **125**: 4951-4961.

Taniguchi, K., R. Takeya, et al. (2009). "Mammalian formin fhod3 regulates actin assembly and sarcomere organization in striated muscles." J Biol Chem **284**: 29873-29881.

Taylor, J. M., J. D. Rovin, et al. (2000). "A role for focal adhesion kinase in phenylephrine-induced hypertrophy of rat ventricular cardiomyocytes." J Biol Chem **275**: 19250-19257.

Thomas, S. G., S. D. Calaminus, et al. (2011). "G-protein coupled and ITAM receptor regulation of the formin FHOD1 through Rho kinase in platelets." J Thromb Haemost **9**: 1648-1651.

Thurston, S. F., W. A. Kulacz, et al. (2012). "The ability to induce microtubule acetylation is a general feature of formin proteins." PLoS One **7**: e48041.

Tojkander, S., G. Gateva, et al. (2012). "Actin stress fibers--assembly, dynamics and biological roles." J Cell Sci **125**: 1855-1864.

Tojkander, S., G. Gateva, et al. (2011). "A molecular pathway for myosin II recruitment to stress fibers." Curr Biol **21**: 539-550.

Tojo, H., I. Kaieda, et al. (2003). "The Formin family protein, formin homolog overexpressed in spleen, interacts with the insulin-responsive aminopeptidase and profilin IIa." Mol Endocrinol **17**: 1216-1229.

Tokuyasu, K. T. (1989). "Use of poly(vinylpyrrolidone) and poly(vinyl alcohol) for cryoultramicrotomy." Histochem J **21**: 163-171.

Tominaga, T., E. Sahai, et al. (2000). "Diaphanous-related formins bridge Rho GTPase and Src tyrosine kinase signaling." Mol Cell **5**: 13-25.

Tondeleir, D., D. Vandamme, et al. (2009). "Actin isoform expression patterns during mammalian development and in pathology: insights from mouse models." Cell Motil Cytoskeleton **66**: 798-815.

Tonino, P., C. T. Pappas, et al. (2010). "Reduced myofibrillar connectivity and increased Z-disk width in nebulin-deficient skeletal muscle." J Cell Sci **123**: 384-391.

Toure, F., G. Fritz, et al. (2012). "Formin mDia1 mediates vascular remodeling via integration of oxidative and signal transduction pathways." Circ Res **110**: 1279-1293.

Toyofuku, T., M. Yabuki, et al. (1999). "Functional role of c-Src in gap junctions of the cardiomyopathic heart." Circ Res **85**: 672-681.

Trinick, J. (1994). "Titin and nebulin: protein rulers in muscle?" Trends Biochem Sci **19**: 405-409.

Tseng, Y., T. P. Kole, et al. (2005). "How actin crosslinking and bundling proteins cooperate to generate an enhanced cell mechanical response." Biochem Biophys Res Commun **334**: 183-192.

Tseng, Y. and D. Wirtz (2001). "Mechanics and Multiple-Particle Tracking Microheterogeneity of α-Actinin-Cross-Linked Actin Filament Networks." Biophys J **81**: 1643-1656.

Tsukada, T., C. T. Pappas, et al. (2010). "Leiomodin-2 is an antagonist of tropomodulin-1 at the pointed end of the thin filaments in cardiac muscle." J Cell Sci **123**: 3136-3145.

Tsukita, S., K. Oishi, et al. (1991). "Specific proto-oncogenic tyrosine kinases of src family are enriched in cell-to-cell adherens junctions where the level of tyrosine phosphorylation is elevated." The Journal of Cell Biology **113**: 867-879.

Uetz, P., S. Fumagalli, et al. (1996). "Molecular interaction between limb deformity proteins (formins) and Src family kinases." J Biol Chem **271**: 33525-33530.

Vaillant, D. C., S. J. Copeland, et al. (2008). "Interaction of the N- and C-terminal autoregulatory domains of FRL2 does not inhibit FRL2 activity." J Biol Chem **283**: 33750-33762.

Vallen, E. A., J. Caviston, et al. (2000). "Roles of Hof1p, Bni1p, Bnr1p, and myo1p in cytokinesis in Saccharomyces cerevisiae." Mol Biol Cell **11**: 593-611.

Vallenius, T. (2013). "Actin stress fibre subtypes in mesenchymal-migrating cells." Open Biol **3**: 130001.

Van Criekinge, W. and R. Beyaert (1999). "Yeast Two-Hybrid: State of the Art." Biol Proced Online **2**: 1-38.

Vavylonis, D., D. R. Kovar, et al. (2006). "Model of formin-associated actin filament elongation." Mol Cell **21**: 455-466.

Vinzenz, M., M. Nemethova, et al. (2012). "Actin branching in the initiation and maintenance of lamellipodia." J Cell Sci **125**: 2775-2785.

Wakabayashi, M., T. Ito, et al. (2003). "Interaction of lp-dlg/KIAA0583, a Membrane-associated Guanylate Kinase Family Protein, with Vinexin and β-Catenin at Sites of Cell-Cell Contact." Journal of Biological Chemistry **278**: 21709-21714.

Wakatsuki, T., B. Schwab, et al. (2001). "Effects of cytochalasin D and latrunculin B on mechanical properties of cells." J Cell Sci **114**: 1025-1036.

Wallar, B. J. and A. S. Alberts (2003). "The formins: active scaffolds that remodel the cytoskeleton." Trends Cell Biol **13**: 435-446.

Wallar, B. J., A. D. Deward, et al. (2007). "RhoB and the mammalian Diaphanous-related formin mDia2 in endosome trafficking." Exp Cell Res **313**: 560-571.

Wang, J., D. K. Dube, et al. (2012). "Clock is not a component of Z-bands." Cytoskeleton **69**: 1021-1031.

Wang, J., Y. Fan, et al. (2014). "Jasplakinolide reduces actin and tropomyosin dynamics during myofibrillogenesis." Cytoskeleton (Hoboken) **71**: 513-529.

Wang, J., J. M. Sanger, et al. (2005). "Differential effects of Latrunculin-A on myofibrils in cultures of skeletal muscle cells: insights into mechanisms of myofibrillogenesis." Cell Motil Cytoskeleton **62**: 35-47.

Wang, K. and C. L. Williamson (1980). "Identification of an N2 line protein of striated muscle." Proc Natl Acad Sci U S A **77**: 3254-3258.

Wang, Q., J. L. Lin, et al. (2010). "Essential roles of an intercalated disc protein, mXinbeta, in postnatal heart growth and survival." Circ Res **106**: 1468-1478.

Wang, Y., M. R. El-Zaru, et al. (2004). "Formin homology domain protein (FHOD1) is a cyclic GMP-dependent protein kinase I-binding protein and substrate in vascular smooth muscle cells." J Biol Chem **279**: 24420-24426.

Wang, Y. L. (1984). "Reorganization of actin filament bundles in living fibroblasts." J Cell Biol **99**: 1478-1485.

Ware, C. B., A. M. Nelson, et al. (2003). "Late gestation modulation of fetal glucocorticoid effects requires the receptor for leukemia inhibitory factor: an observational study." Reprod Biol Endocrinol **1**: 43.

Watanabe, N., T. Kato, et al. (1999). "Cooperation between mDia1 and ROCK in Rho-induced actin reorganization." Nat Cell Biol **1**: 136-143.

Watanabe, N., P. Madaule, et al. (1997). "p140mDia, a mammalian homolog of Drosophila diaphanous, is a target protein for Rho small GTPase and is a ligand for profilin." EMBO J **16**: 3044-3056.

Webb, R. C. (2003). "Smooth muscle contraction and relaxation." Adv Physiol Educ **27**: 201-206.

Weber, A., C. R. Pennise, et al. (1994). "Tropomodulin caps the pointed ends of actin filaments." J Cell Biol **127**: 1627-1635.

Welch, M. D., A. H. DePace, et al. (1997). "The Human Arp2/3 Complex Is Composed of Evolutionarily Conserved Subunits and Is Localized to Cellular Regions of Dynamic Actin Filament Assembly." J Cell Biol **138**: 375-384.

Wen, Y., C. H. Eng, et al. (2004). "EB1 and APC bind to mDia to stabilize microtubules downstream of Rho and promote cell migration." Nat Cell Biol **6**: 820-830.

Weng, Z., S. M. Thomas, et al. (1994). "Identification of Src, Fyn, and Lyn SH3-binding proteins: implications for a function of SH3 domains." Molecular and Cellular Biology **14**: 4509-4521.

Westendorf, J. J. (2001). "The formin/diaphanous-related protein, FHOS, interacts with Rac1 and activates transcription from the serum response element." J Biol Chem **276**: 46453-46459.

Westendorf, J. J. and S. Koka (2004). "Identification of FHOD1-binding proteins and mechanisms of FHOD1-regulated actin dynamics." J Cell Biochem **92**: 29-41.

Westendorf, J. J., R. Mernaugh, et al. (1999). "Identification and characterization of a protein containing formin homology (FH1/FH2) domains." Gene **232**: 173-182.

Wheeler, A. P. and A. J. Ridley (2004). "Why three Rho proteins? RhoA, RhoB, RhoC, and cell motility." Exp Cell Res **301**: 43-49.

Wheeler, M. A., A. Warley, et al. (2010). "Identification of an emerin-beta-catenin complex in the heart important for intercalated disc architecture and beta-catenin localisation." Cell Mol Life Sci **67**: 781-796.

Williams, M. W. and R. J. Bloch (1999). "Extensive but coordinated reorganization of the membrane skeleton in myofibers of dystrophic (mdx) mice." J Cell Biol **144**: 1259-1270.

Wilson, A., R. Schoenauer, et al. (2014). "Cardiomyocyte growth and sarcomerogenesis at the intercalated disc." Cellular and Molecular Life Sciences **71**: 165-181.

Witke, W., W. Li, et al. (2001). "Comparisons of CapG and gelsolin-null macrophages: demonstration of a unique role for CapG in receptor-mediated ruffling, phagocytosis, and vesicle rocketing." J Cell Biol **154**: 775-784.

Wooten, E. C., V. B. Hebl, et al. (2012). "Formin Homology 2 Domain Containing 3 (FHOD3) Variants Associated with Hypertrophic Cardiomyopathy." Circ Cardiovasc Genet **6**:10-8.

Woychik, R. P., R. L. Maas, et al. (1990). "'Formins': proteins deduced from the alternative transcripts of the limb deformity gene." Nature **346**: 850-853.

Xu, Y., J. B. Moseley, et al. (2004). "Crystal structures of a Formin Homology-2 domain reveal a tethered dimer architecture." Cell **116**: 711-723.

Yaffe, D. and O. Saxel (1977). "A myogenic cell line with altered serum requirements for differentiation." Differentiation **7**: 159-166.

Yagi, R., F. Mayer, et al. (2010). "Refined LexA transactivators and their use in combination with the Drosophila Gal4 system." Proc Natl Acad Sci U S A **107**: 16166-16171.

Yamaguchi, M., R. M. Robson, et al. (1982). "Nemaline myopathy rod bodies. Structure and composition." J Neurol Sci **56**: 35-56.

Yamana, N., Y. Arakawa, et al. (2006). "The Rho-mDia1 pathway regulates cell polarity and focal adhesion turnover in migrating cells through mobilizing Apc and c-Src." Mol Cell Biol **26**: 6844-6858.

Yamashiro, S., D. S. Gokhin, et al. (2012). "Tropomodulins: pointed-end capping proteins that regulate actin filament architecture in diverse cell types." Cytoskeleton (Hoboken) **69**: 337-370.

Yanazume, T., K. Hasegawa, et al. (2002). "Rho/ROCK Pathway Contributes to the Activation of Extracellular Signal-regulated Kinase/GATA-4 during Myocardial Cell Hypertrophy." Journal of Biological Chemistry **277**: 8618-8625.

Yang, C., L. Czech, et al. (2007). "Novel roles of formin mDia2 in lamellipodia and filopodia formation in motile cells." PLoS Biol **5**: e317.

Yang, C. and T. Svitkina (2011). "Filopodia initiation: focus on the Arp2/3 complex and formins." Cell Adh Migr **5**: 402-408.

Yang, N., O. Higuchi, et al. (1998). "Cofilin phosphorylation by LIM-kinase 1 and its role in Rac-mediated actin reorganization." Nature **393**: 809-812.

Yang, S., F. K. Huang, et al. (2013). "Molecular mechanism of fascin function in filopodial formation." J Biol Chem **288**: 274-284.

Yayoshi-Yamamoto, S., I. Taniuchi, et al. (2000). "FRL, a novel formin-related protein, binds to Rac and regulates cell motility and survival of macrophages." Mol Cell Biol **20**: 6872-6881.

Yoshida, M., E. Sho, et al. (2010). "Weaving hypothesis of cardiomyocyte sarcomeres: discovery of periodic broadening and narrowing of intercalated disk during volume-load change." Am J Pathol **176**: 660-678.

Yoshizaki, H., Y. Ohba, et al. (2003). "Activity of Rho-family GTPases during cell division as visualized with FRET-based probes." J Cell Biol **162**: 223-232.

Young, K. G. and J. W. Copeland (2010). "Formins in cell signaling." Biochim Biophys Acta **1803**: 183-190.

Yu, C.-h., J. B. K. Law, et al. (2011). "Early integrin binding to Arg-Gly-Asp peptide activates actin polymerization and contractile movement that stimulates outward translocation." Proceedings of the National Academy of Sciences **108**: 20585-20590.

Yue, J., S. Huhn, et al. (2013). "Complex roles of filamin-A mediated cytoskeleton network in cancer progression." Cell Biosci **3**: 7.

Zalevsky, J., L. Lempert, et al. (2001). "Different WASP family proteins stimulate different Arp2/3 complex-dependent actin-nucleating activities." Curr Biol **11**: 1903-1913.

Zamudio-Meza, H., A. Castillo-Alvarez, et al. (2009). "Cross-talk between Rac1 and Cdc42 GTPases regulates formation of filopodia required for dengue virus type-2 entry into HMEC-1 cells." J Gen Virol **90**: 2902-2911.

Zhang, J. Q., B. Elzey, et al. (2001). "Ultrastructural and biochemical localization of N-RAP at the interface between myofibrils and intercalated disks in the mouse heart." Biochemistry **40**: 14898-14906.

Zhang, X., G. Azhar, et al. (2001). "Cardiomyopathy in transgenic mice with cardiac-specific overexpression of serum response factor." Am J Physiol Heart Circ Physiol **280**: H1782-1792.

Zigmond, S. (2004). "Formin' adherens junctions." Nat Cell Biol **6**: 12-14.

Zigmond, S. H., M. Evangelista, et al. (2003). "Formin leaky cap allows elongation in the presence of tight capping proteins." Curr Biol **13**: 1820-1823.

Zolk, O., P. Caroni, et al. (2000). "Decreased expression of the cardiac LIM domain protein MLP in chronic human heart failure." Circulation **101**: 2674-2677.

Zuniga, A., O. Michos, et al. (2004). "Mouse limb deformity mutations disrupt a global control region within the large regulatory landscape required for Gremlin expression." Genes Dev **18**: 1553-1564.